Stratigraphy and petrogenesis of the Parana continental flood basalts, southern Brazil

Thesis

Stratigraphy and Petrogenesis of the Paraná Continental Flood Basalts, Southern Brazil.

A thesis presented for the degree of

Doctor of Philosophy

by

DAVID WILLIAM PEATE

B.A. (Hons.) *Cantab.* 1985

Department of Earth Sciences,

The Open University.

July 1989

thesis preface

Abstract.

The Early Cretaceous (~130 Ma) Paraná lavas of South America represent the largest preserved example of a continental flood basalt (CFB) province, with a present area in excess of 1.2 x 10^6 km^2. Magmatism is dominated by tholeiitic basalts (> 90 %), with minor rhyolites as a late-stage feature along the continental margin. The basaltic magmas show a wide diversity in trace element and isotope composition, and a revised scheme of distinct magma types is proposed, based on new geochemical data plus a review of literature analyses, which retains the previously established overall classification into high- and low-Ti varieties; *viz.* high-Ti (> 2 wt%) - {Urubici, Pitanga, Paranapanema}, low-Ti (< 2 wt%) - {Gramado, Esmeralda, Ribeira}.

A preliminary regional picture of the internal north-south structure of the lava pile is presented, constrained largely by analyses of borehole drillcore chippings which have provided a window to the otherwise inaccessible deeper stratigraphical levels. Within this central/north Paraná region, the dominant magma type has evolved from Gramado to Pitanga to Paranapanema with time. The stratigraphical pattern of overlapping geochemical units which dip towards the north suggests a northward migrating source for the Paraná magmatism, and this was probably related to the rapid northward propagation of initial rifting of the South Atlantic ocean rather than any motion relative to an underlying hot-spot.

Detailed stratigraphical investigations on the coastal Serra Geral escarpment (Santa Catarina state, Brazil) showed complex interbedding of Urubici- and Gramado- type flows. Division of the Urubici-type flows into locally correlated sub-units has allowed the effects of polybaric fractionation to be resolved. The Gramado magma type is dominated by AFC (assimilation / fractional crystallisation), and the geochemical variations are consistent with taking an average Palmas rhyolite composition (the best estimate of a local crustal melt) to be the contaminant. Within the southern Paraná region, the composition of the Gramado parental magma prior to AFC is regionally variable (in terms of Ba/Nb, $(^{87}Sr/^{86}Sr)_i$, SiO_2).

The Urubici and Gramado magma types can not be related to a single mantle source by varying degrees of partial melting, and require distinct source regions. The 'enriched' isotopic and trace element signatures inferred for uncontaminated Gramado- and Urubici-type magmas are distinct from MORB-OIB and it is suggested that at least the trace elements (and therefore the isotopic characteristics) of the Paraná CFB were largely derived from sources within a heterogeneous lithospheric mantle.

The sharp stratigraphical transition from the 'lithospheric'-dominated Gramado magma type to more 'depleted' trace element and isotope compositions (the minor Esmeralda magma type) can not be accommodated on trace element grounds by a decrease in the amount of crustal assimilation. Instead, these late-stages of magmatism show a significant asthenospheric component, consistent with such material being available during the advanced stages of lithospheric attenuation and rifting.

For my parents,

David and Lilian.

"Go, my sons, buy stout shoes, climb the mountains, search the deep recesses of the earth. In this way, and in no other, will you arrive at a knowledge of the nature and properties of things."

Severinus, 7th C.

Frontispiece

Photograph of the 'GB' road section near São Joaquim, Santa Catarina state, Brazil, showing the spectacular exposure of the Paraná continental flood basalts (and rhyolites) along the Atlantic coastal margin Serra Geral escarpment.

Acknowledgements.

Many people have contributed in some form or other to this project, and I owe a large debt of gratitude to the following:

- my supervisor, Chris Hawkesworth, for guidence through this project, keeping me on the straight and narrow, and for very rapid and pertinent comments on this manuscript.
- Marta Mantovani, without whom this project would not have been possible; for smoothing the path through the inevitable Brazilian bureaucracy, and for many fruitful discussions on the Paraná
- my drivers Elio and Nei in Brazil are thanked for their careful negotiation of the Brazilian highways, and I am also grateful for the hospitality shown by all at IAG-USP in São Paulo, especially Vladimir, and Miguel at IG-USP.
- the many individuals who have helped (hindered ?) me in the pursuit of those all important numbers: Peter van Calsteren, Mabs Kunka, and Zenon Palacz (in the isotope lab), Nick Rogers (INAA), John Watson (XRF), and Tim Brewer (Nottingham XRF).
- Nick Rogers, for numerous games of GO, and more recently, squash, and being a friendly testing ground for my more unorthodox ideas.
- Andy Tindle and Dave Ormerod, for initiation into the world of Apple Macintosh, and the original 'Mac-crew' of Rob Ellam, Cherry Lewis, Jim Miller.
- downstairs, John Holbrook is acknowledged for creative accounting beyond the call of duty, and use of the Ian Chaplin car hire service was much appreciated, not forgetting of course the occasional thin section.
- fellow inmates of room Z107 - Simon[2] and Gavin for putting up with the ideosyncracies of a geochemist.
- to all and sundry in the department (I'm sorry I haven't got time to mention you all) for all their kind words of encouragement - 'no, I haven't *quite* finished yet'.
- all the residents at Towan Avenue {Graham, Matthew, Jacqui, Leon and Sara}, including all the temporary lodgers too numerous to mention, that have all helped me survive the Milton Keynes experience.
- NERC for funding this project, and the OU overseas travel fund that enabled to migrate south for a third time.
- Lamport and Holt shipping company for kindly transporting my samples back to the U.K. freight-free.

...and the final thanks must go to my parents for their continued support throughout my education - 'but when are you going to get a proper job, David ?'.

Table of Contents.

List of Figures.

Chapter Three.

Chapter Four.

Chapter Five.

Chapter Six.

List of Tables.

List of Plates.

Chapter 1
Introduction and thesis objectives.

1.1 Continental flood basalt magmatism.

Continental flood basalt provinces represent some of the greatest ever manifestations of terrestrial magmatism, with the exception of the ocean floors. They are characterised by thick accumulations of sheet-like sub-horizontal lava flows which have flooded vast areas of the continental surface, often in excess of 10^6 km^2, and they are commonly associated with extensive intrusive activity in the form of dolerite sills and dyke swarms. Historically such lavas have been referred to as 'Plateau basalts' (Geike, 1903) or 'Traps' (Woodworth, 1912), though the current, widely accepted nomenclature uses the term 'Continental Flood Basalts' (adapted from Tyrrell, 1937) which is commonly abbreviated to CFB. The magmatism is generally of subaerial lava flows fed almost exclusively by fissure eruptions, with only the occasional occurrence of any pyroclastic debris. Magmatic compositions are dominantly tholeiitic basalts; hence the alternative name of 'continental tholeiite' provinces.

A striking feature of most CFB provinces is the eruption of huge volumes of magma within a relatively short time interval. For example, the Columbia River basalts have a total volume of at least 200 x 10^3 km^3 and over 95% of this was erupted in less than 3 Myrs (Hooper, 1982), and recent $^{40}Ar/^{39}Ar$ and palaeomagnetic studies of the Deccan basalts have indicated that the duration of the main magmatic episode which covers an area of at least 0.5 x 10^6 km^2 was probably less than 1 Myr. There is increasing evidence from other CFB provinces that the magmatic activity was similarly of a short duration on the order of a few million years or so, although the accuracy of the dating of many of these provinces (*e.g.* Paraná, Karoo, Siberia) requires considerable improvement. This leads to high eruption rates for CFB magmatism, and Thompson (1977) has shown that average magma production rates for the Columbia River and Snake River provinces were similar to those of

comparable length segments of the mid-ocean ridge system, although the eruption rates of individual flows might be several orders of magnitude greater than even the fastest spreading sections of mid-ocean ridges (Swanson *et al.*, 1975).

Continental flood basalts have not been restricted to any specific period of earth history and examples are known throughout the geological record from the Archaean to Recent times. A list of the location and age of the worlds' major CFB provinces is given in table 1.1. The bias towards Mesozoic-Tertiary ages is probably an artifact of preservation since most CFB provinces have been uplifted to form elevated plateaus which are susceptible to rapid dissection and erosion. Thus, the list could be extended to include many of the great Archaean and Proterozoic tholeiitic dyke swarms {*e.g.* Nipissing dykes (~2.22 Ga) of the Canadian Shield; Scourie dykes (~2.39 Ga) of the Scottish Lewisian}

Columbia River	(U.S.)	6-17 Ma.
Snake River	(U.S.)	1-15 Ma.
Ethiopia	(N.E. Africa)	15-30 Ma.
Aden/Yemen	(Arabia)	20-30 Ma.
North Atlantic province		53-63 Ma.
(British Tertiary province, Faeroes, East/West Greenland)		
Deccan	(India)	60-65 Ma.
Rajmahal	(India)	108-128 Ma.
Paraná	(S. America)	115-135 Ma.
Etendeka	(Namibia)	120-130 Ma.
Maranhão	(N.E. Brazil)	170-200 Ma.
Ferrar dolerites	(Antarctica)	165-180 Ma.
Tasmanian dolerites	(Australia)	~175 Ma.
Karoo	(Southern Africa)	178-193 Ma
Siberian	(U.S.S.R.)	220-250 Ma.
Keweenawan	(Canada/U.S.)	1190 Ma.
Huronian	(Canada)	2450 Ma.
Ventersdorp	(S. Africa)	2700 Ma.
Fortesque	(Australia)	2700 Ma.
Dominion	(S. Africa)	3000 Ma.

Table 1.1 Location and age of some of the major terrestrial continental flood basalt provinces. Data taken from: Basaltic Volcanism Study Project (1981); Hooper (1982); Erlank *et al.*, (1984); Fitch and Miller (1984); Kyle *et al.*, (1981); Jolly (1987); Baksi *et al.*, (1987); Bristow (1988); Bellieni *et al.*, (1988); White and McKenzie (1989).

since it is probable that they represent the deeply eroded feeder systems of former flood basalt provinces (Basaltic Study Volcanism Project, 1981; Weaver and Tarney, 1983).

The Mesozoic era appears to have been a time of exceptional continental flood basalt activity which was in some way linked to the tensional regime associated with the disruption of the Gondwana supercontinent. This produced three of the worlds' largest and best known examples of CFB provinces (Paraná, Karoo and Deccan) as well as numerous more minor occurrences stretching right across the former Gondwana landmass from South America (Paraná, Maranhão), Southern Africa (Karoo, Etendeka), Antarctica (Ferrar dolerites, Kirkpatrick), Australia (Tasmanian dolerites, Bunbury) to India (Deccan, Rajmahal).

1.2 Current areas of interest in CFB magmatism.

1.2.1 Geochemical aspects.

A brief mention should be made as to the status of primary magmas within CFB provinces since this has often been the subject of much discussion. A striking characteristic of the major element composition of most CFB is the bias towards Fe-rich compositions (Mg-poor basalts and tholeiitic andesites) relative to MORB (Dupuy and Dostal, 1984; MacDougall, 1988), and this lies at the core of the long-standing argument as to whether CFB (and MORB for that matter) represent primary mantle melts or are derived from a more Mg-rich picritic melt. This saga has been reviewed by Cox (1980) and Thompson *et al.*, (1983) who both concluded that the available evidence pointed towards a picritic precursor to continental flood basalts, and two points that favoured this hypothesis were:

(i) The magnesium-iron ratio of the erupted flood basalts are generally too low to have been in equilibrium with the apparent dominant olivine composition of the upper mantle (Cox, 1980). To circumvent this problem, Wilkinson and Binns (1977) postulated an iron-rich lherzolitic upper mantle as a possible direct source for the basaltic primary magma, but

nodules of such material are rare among the kimberlite xenolith suites and are thought to be unrepresentative of the upper mantle.

(ii) Thompson *et al.*, (1983) considered the results from experimental petrology on the phase relations of natural CFB samples and the melting of peridotite material, and demonstrated that most CFB are too Mg-poor and/or silica saturated to be primary magmas from an anhydrous lherzolitic mantle. Predicted melt compositions at appropriate depths are picritic, although melting under hydrous conditions might account for the high SiO_2.

The availability of such picritic liquids is demonstrated by the extensive picritic lavas found in West Greenland/Baffin Island and Lebombo monocline in the Karoo, and locally in the Deccan, although as yet none have been recorded from the Paraná. Cox (1980) argued that the apparent major element uniformity of many CFB lava sequences is a consequence of low-pressure fractional crystallisation of a gabbroic assemblage of olivine+clinopyroxene+plagioclase which can essentially buffer the concentration of many key elements such as SiO_2 and Al_2O_3. Thus the Fe-rich nature of many CFB compared to MORB is largely imposed by their crystallisation history rather than being a source feature. In this respect, many CFB samples are compositionally very similar to the more extreme ferro-basalts of the East Pacific Rise which are thought to be the product of large amounts of fractional crystallisation (MacDougall, 1988).

A more fundamental, and yet still perplexing, geochemical question posed by basaltic magmatism is the precise nature and location of the magmatic source region. Within the oceanic environment, mid-ocean ridge basalts (MORB) and ocean island basalts (OIB) apparently both have their origins within the convecting upper mantle (*i.e.* the asthenosphere). However, in the case of continental magmatism there are two potential candidates available to act as mantle source regions, *viz.* the asthenosphere and the sub-continental lithospheric mantle. It is this possible role for continental lithosphere, both in the generation and subsequent evolution of continental flood basalt (CFB) magmas, that has been the underlying theme of many studies into CFB in recent years.

CFB have an enriched Sr and Nd isotopic signature with respect to MORB, and on a ε_{Sr} - ε_{Nd} diagram they are displaced to higher ε_{Sr} and lower ε_{Nd} (the ε notation represents the deviation of a sample from the isotopic parameters deduced for bulk earth; DePaolo and Wasserburg, 1976). CFB exhibit a range in Sr, Nd (and Pb) isotope ratios far greater than that reported for OIB and, although the field for CFB data overlaps with that for OIB, it extends well into the 'enriched' quadrant (denoted by positive ε_{Sr} and negative ε_{Nd}). This implies at least a contribution to CFB from sources that were enriched in incompatible elements (*i.e.* high Rb/Sr, low Sm/Nd) relative to bulk earth estimates (and consequently to MORB / OIB also) for geologically long periods of time. Many workers (*e.g.* Carlson *et al.*, 1981; Thompson *et al.*, 1983; Mahoney *et al.*, 1982) have placed this 'enriched' component within the crustal portion of the continental lithosphere and invoked various contamination mechanisms to modify the composition of asthenosphere-derived magmas during the passage through the crust. This was the view also taken by Dupuy and Dostal (1984) and Campbell (1985) who considered that the relative enrichment in SiO_2 and K_2O of continental tholeiites with respect to their oceanic counterparts reflected the assimilation of significant amounts of continental crust *en route* to the surface. Unfortunately life is not this simple, and it is becoming increasingly apparent from studies of mantle xenoliths (*e.g.* Menzies and Murthy, 1980; Erlank *et al.*, 1987) that these 'enriched' isotopic characteristics are not unique to the continental crust but can also develop, given sufficient time, within the underlying sub-continental lithospheric mantle in response to certain trace element enrichment processes (Hawkesworth *et al.*, 1984a), *i.e.* the continental mantle lithosphere shares many of the isotopic and trace element features generally only attributed to the continental crust.

The mantle portion of the continental lithosphere, which may be up to 300 km thick, is relatively rigid with respect to the convecting upper mantle from which it is presumably isolated from active convection (Jordan, 1978,1988). It is thought that the lithospheric mantle was stabilised after the last major thermal event in the overlying crust (Oxburgh and Parmentier, 1978; Hawkesworth *et al.*, 1983), and developed largely by the accretion of asthenospheric material onto the base of the crust by conductive cooling (except in the

Archaean; Richter, 1988). Thus much of the sub-continental lithosphere is likely to be old enough for ancient trace element heterogeneities, produced by regional injections of fluids or melts derived from the asthenosphere or over subduction zones, to have sufficient time to be mirrored by variations in radiogenic isotope ratios.

Evidence for the various types of trace element enrichment processes that have occurred within the lithospheric mantle has been derived largely from textural and geochemical studies of mantle xenoliths brought up in kimberlites and alkali basalts. These have been reviewed by Hawkesworth *et al.*, (1984a) who recognised two dominant styles of mantle enrichment process. One style, exhibited by garnet-free, phlogopite ± K-richterite (PP and PKP) peridotites, has low Ti/K, high Rb/Sr and is thought to reflect mantle metasomatism by H_2O-rich fluids, whereas the other style, displayed by the garnet-bearing peridotites (garnet ± phlogopite; GP and GPP), has high Ti/K, low Rb/Sr and has been attributed to the migration of small volume silicate (basanitic) melts. Both styles show similar LREE enrichment (low Sm/Nd) and with time, the isotopic composition of these now modified mantle sources should evolve to high ε_{Sr}, low ε_{Nd} and low ε_{Sr}, low ε_{Nd} respectively. Similar trace element and isotope enrichment trends have been seen in lamproites and kimberlites (Fraser *et al.*, 1985), which are believed to represent small degree lithospheric melts, and also in some CFB, as shown by Hawkesworth *et al.*, (1983) who compared xenoliths from South African kimberlites to the Karoo CFB lavas. In detail on an ε_{Sr} - ε_{Nd} diagram, the global CFB data 'fan-out' from the so-called mantle array defined by MORB / OIB, forming either a shallow trend towards high ε_{Sr}, low ε_{Nd} or a steeper trend with low ε_{Sr}, low ε_{Nd}. Workers who favour the contamination hypothesis would previously have automatically assigned such trends to the assimilation of high Rb/Sr upper crustal material and low Rb/Sr lower crustal granulite-facies rocks respectively (*e.g.* Carter *et al.*, 1978), whereas they could equally be derived from within an enriched heterogeneous sub-continental lithospheric source (*e.g.* Hawkesworth *et al.*, 1984a).

Herein lies the crux of the current controversy regarding CFB magmatism. The presence of a strong lithospheric component in many CFB is generally accepted but opinion is divided as to whether this is of crustal or mantle origin, and discussions have become

polarised into arguing the relative merits of contamination processes versus mantle enrichment processes. As has been stressed by Hawkesworth *et al.*, (1983); "The debate is not over whether these processes take place, for the evidence for both is surely overwhelming, but over the criteria by which they might best be recognised". Mantle derived melts, whether asthenospheric or lithospheric, may be affected by crustal assimilation on their way to the surface, and therefore the effects of contamination could be superimposed on those produced by mantle enrichment processes. Clearly the isotopic signature on its own is ambiguous, and a better approach is to look at the isotopic variations in conjunction with other geochemical parameters. A combined trace element and isotope approach can be used to characterise the various petrogenetic process that have modified the composition of a magma subsequent to leaving its source region, as distinct from features inherited from the source itself. This technique relies on using the different behaviour of certain elements, both within and between, the crust and mantle environments in an effort to distinguish the dominant source of the trace element and isotope variation in CFB.

One factor in this debate is that unlike MORB and OIB, there is not really any 'typical' CFB composition (or province), and the trace element and isotopic diversity seen within an individual province is virtually the same as the total range displayed by all CFB. This diversity is highlighted by the failure of tectonic disciminant diagrams based on geochemical criteria (*e.g.* Pearce and Cann, 1973) to distinguish a specific field for CFB. Duncan (1987) has shown for example that using such an approach the Karoo CFB lavas would actually classify within a wide spectrum of tectonic settings {'within-plate' basalts, 'calc-alkaline' basalts, 'oceanic' basalts} despite the whole Karoo province having a similar tectonic environment.

Thompson *et al.*, (1983) concluded on the basis of trace element abundance patterns that most CFB had compositions consistent with a derivation from a sub-lithospheric OIB-type mantle source. The remainder had distinctive geochemical features (*i.e.* enrichment in LIL-elements Rb, Ba, K etc., and a trough at Nb, Ta) that could be attributed to the addition of crustal material to an OIB-type magma during its ascent through, and residence within, the continental crust, although importantly Thompson *et al.*, (1983) did not

discount the possibility that this trace element signature might represent a subducted sediment component within the mantle source. The availability of an OIB-type mantle source beneath the continents has been elegantly demonstrated by Fitton and Dunlop (1985) in a study of the Cameroon line volcanics which straddle the continental margin of West Africa. Alkali basalts from the oceanic and continental sectors had identical compositions in terms of trace elements and Sr isotopes and the implication of this is that they must have originated from the same mantle source, the asthenosphere, and cannot have interacted to any significant extent with the continental lithosphere.

Geochemical modelling techniques using a combined trace element and isotope approach to account for the modifying effects of crustal level processes on CFB magmas has led to an increased confidence that estimated trace element and isotope ratios of inferred uncontaminated basalts reflect those of the mantle source region. Uncontaminated basalts from the Columbia River (*e.g.* Carlson *et al.*, 1981) and Deccan (*e.g.* Mahoney *et al.*, 1982; Lightfoot, 1985) CFB provinces have trace element and isotopic signatures which strongly suggest an origin from 'depleted' sub-lithospheric OIB-type mantle source (*c.f.* Thompson *et al.*, 1983). Problems begin when the extensive CFB magmatism (*i.e.* Paraná, Karoo, Antarctica, Tasmanian provinces) generated within the Gondwana super-continent during the Mesozoic era is considered, since the majority of these lavas have an 'enriched' isotopic signature (positive ε_{Sr}, negative ε_{Nd}). This holds true for the samples believed to have been unaffected by crustal contamination as well as those for which the effects of crustal contamination are thought to have been accounted for (Hawkesworth *et al.*, 1984b; Erlank *et al.*, 1984). A few samples with 'depleted' isotopic and trace element characteristics do occur {*e.g.* Rooi Rand dolerites, Karoo (Duncan *et al.*, 1984); Horingbaai dolerites, Etendeka (Erlank *et al.*, 1984)}, but they are a minor feature, restricted to the later phases of activity and it has proved difficult to model them as uncontaminated versions of the other magma types (*e.g.* Erlank *et al.*, 1984). Marsh (1987) argued that these were asthenospheric melts, unrelated to the earlier lithospheric-dominated lavas, that were emplaced only after pronounced lithospheric attenuation or rifting had taken place. Thus it is difficult to escape the conclusion (Hawkesworth *et al.*, 1984b,1988;

Duncan *et al.*, 1988; Kyle, 1980; Hergt *et al.*, 1989) that the CFB over this huge region of Gondwana are dominated by a strong lithospheric influence.

A marked feature of these Gondwana CFB provinces is the existence of two major geochemical provinces within the lavas that was first noted by Cox *et al.*, (1967). The magmas can be sub-divided into two distinct groups with contrasting minor/trace element and isotopic characteristics which have been termed the 'High-Ti' and 'Low-Ti' types (*e.g.* Bellieni *et al.*, 1984a; Erlank *et al.*, 1988). The trace element signatures of both types are sufficiently different from OIB (*e.g.* low Nb,Ta) to require a different source. Several authors have therefore concluded that at least the minor and trace elements of these Gondwana CFB were largely derived from the sub-continental lithospheric mantle, and that the difference between the two groups reflected different processes within the lithosphere (*e.g.* Hawkesworth *et al.*, 1984b; Erlank *et al.*, 1987). The 'High-Ti' group are characterised by high HFS (high field strength) element abundances and relatively low LIL/HFS ratios, and such features are thought to reflect enrichment of the source region by the migration of small volume silicate melts. The 'Low-Ti' group have several features in common with recent subduction related magmas, such as their low Ti, Ta, Zr, and P contents, and high LIL/HFS ratios, which might suggest that previous subduction episodes contributed to the mantle source region. On the basis of the high Rb/Sr (Hawkesworth *et al.*, in prep.) and Pb contents (Hergt *et al.*, 1989) of the 'Low-Ti' group, it has been suggested that this subduction component might reflect the contribution of subducted sediments rather than a 'slab fluid' to the mantle source.

The contribution of sub-continental lithospheric mantle to CFB magmatism is increasingly becoming a more accepted scenario within the literature (Hawkesworth *et al.*, 1984b, 1988; Duncan *et al.*, 1984; Marsh, 1987; Allègre *et al.*, 1987; Thompson and Morrison, 1988) although attention is now focussed on the exact nature of this process. This participation might be achieved either by the scavenging of low-temperature lithospheric components by asthenospheric melts during their ascent, or alternatively the lithospheric mantle could be remobilised by wholesale melting, and deciding between these possibilities is tricky and still an unresolved question. Postulating direct melting of

lithosphere to produce CFB magmas is a highly contentious issue and the dominant argument against this notion is the prevailing conception of the continental lithospheric mantle as cold and compositionally depleted in basaltic constituents. Richter (1988) has proposed that there was a major change in the mechanism of lithospheric stabilisation around the time of the Archaean/Proterozoic boundary. In tandem with this, Hawkesworth *et al.*, (in prep.) have argued that Archaean and post-Archaean lithospheric mantle are compositionally distinct, and this has implications for the potential of the lithosphere to act as a magma source for CFB. They propose that lithosphere during the Archaean (as sampled today as garnet peridotite xenoliths in kimberlites) was stabilised as a result of komatiite extraction which left a depleted, Fe-poor residue which was intrinsically less dense than the surrounding asthenosphere. In contrast, the post-Archaean lithosphere is believed to have stabilised by conductive cooling and therefore it should be compositionally similar to the asthenosphere at that time. Spinel peridotite xenoliths from alkali basalts are thought to be representative of such post-Archaean lithospheric material, and their more fertile composition would make it a more acceptable source for CFB magmas than the Archaean lithosphere. The fact that no CFB have been found that preserve source ages older than the Proterozoic (*e.g.* Paraná - ~1.8 Ga, Hawkesworth *et al.*, 1986; Nuanetsi picrites, Karoo - ~1.1 Ga, Ellam and Cox, 1989) is consistent with this notion.

1.2.2 Geodynamical origins of CFB provinces.

The origin of mid-ocean ridge basalts is reasonably clear; they are generated by decompression melting of rising asthenospheric mantle at relatively shallow depths (< 100 km) as a passive response to rifting at the oceanic ridges. The underlying tectonic reason for the eruption of continental flood basalts on the other hand remains largely a mystery, especially in the absence of any convincing modern day analogues. The only theme that is apparently common to all CFB provinces is a 'tensional tectonic setting'. The Proterozoic Keweenawan province near Lake Superior on the Canada-U.S. border is associated with with a major intra-continental rift zone (Basaltic Volcanism Study Project, 1981), and the Miocene Columbia River basalts of the north-western U.S. were apparently extruded into a 'back-arc'-like environment (*e.g.* Hooper, 1982). Most of the other large CFB provinces

seem to be in some way connected with the break-up of continents and the development of continental margins by lithospheric thinning and rifting; for example, the Deccan province is related to the detachment of the Seychelles platform from the western margin of the Indian sub-continent (*e.g.* Devey and Lightfoot, 1986), the North Atlantic province (consisting of the British Tertiary province, East and West Greenland, Faeroes, Jan Mayen) is related to the initiation of the North Atlantic ocean (*e.g.* Basaltic Volcanism Study Project, 1981), and the Mesozoic CFB activity of the Paraná and Karoo provinces is related to the disruption of the Gondwana supercontinent (*e.g.* Duncan *et al.*, 1984).

This close association of CFB provinces with rifts begs the question as to why all rifts and continental margins are not characterised by flood basalts. A favoured candidate has been to invoke the presence of a deep mantle thermal plume or 'hot-spot' beneath the rift, although several different interpretations have been suggested as to the actual mechanisms of how such plumes can contribute to the generation of CFB magmatism. Morgan (1981) extrapolated the locations of currently active 'hot-spots' (h/s) to their palaeopositions via plate reconstruction models and demonstrated that for most continental flood basalt provinces there was a 'hot-spot' in the general vicinity of the province either just before or during the major episode of volcanism; *e.g.* Paraná (Tristan da Cunha h/s), Columbia River (Yellowstone h/s), Deccan (Reunion h/s), North Atlantic (Iceland h/s), Karoo (Crozet h/s). This close coincidence of flood basalts and 'hot-spots' led Morgan (1981) to argue for a plume origin for CFB magmatism, and he envisaged a scenario in which a 'hotspot' that was initiated beneath the continental interior would produce a gradual heating of the sub-continental lithosphere over a period of 10 to 30 Myrs resulting in the generation of CFB magmatism as the 'hot-spot' moved away.

In a variation of the 'hot spot' theme, White and McKenzie (1989) investigated the consequences of rifting the continental lithosphere above a 'hot-spot' or mantle plume. Mantle plumes produce thermal anomalies beneath the lithosphere, typically 2000 km in diameter, where the potential temperature is about 150-200°C above that of normal asthenosphere (1280 ± 30°C). When continental lithosphere is stretched, partial melt is generated by the decompression melting of asthenospheric mantle upwelling beneath the

rift, and McKenzie and Bickle (1988) have demonstrated that the volume of melt that is produced depends critically on the asthenospheric potential temperature (the temperature the asthenosphere would have if it were brought to the surface adiabatically without melting) and also on the amount of lithospheric extension. Therefore if a rift is initiated above the wide thermal anomaly associated with a mantle plume, the elevated mantle temperature will lead to more than double the normal amount of melt being generated. As well as explaining the voluminous extent of CFB provinces, this model has also addressed several other important aspects of CFB magmatism in relation to continental rifting. For example, the rapid eruption of the lavas, the relative timing of magmatism and rifting, and the subsidence history and uplift of the continental margin, and these might offer a means of assessing the viability of this scenario for individual CFB provinces.

Despite the clear spatial and temporal relationship between mantle plumes and CFB provinces, there are no convincing examples (except perhaps for the Deccan) where the geochemical signature of the plume (as identified from the present-day manifestation of the plume) has been recognised as contributing to the CFB magmatism. This suggests that the plume was probably only responsible for the additional thermal input into the melting regime, although the plume geochemical signature might have been obscured by complex mixing processes involving 'depleted' asthenosphere and 'enriched' lithospheric mantle and crustal components.

Several alternative models that do not require the presence of mantle plumes have been proposed, specifically to explain the large Mesozoic CFB provinces of Gondwana (*i.e.* Paraná, Karoo, Antarctica, Tasmanian), and these include the 'subduction related' model of Elliot (1975) and Cox (1978), and the 'insulation melting' model of Anderson (1982) and Marsh (in prep.). Elliot (1975) and Cox (1978) noted the alignment of the Paraná, Karoo, Antarctica and Tasmanian flood basalt provinces forming a broad band parallel to, and about 2,000-4,000 km behind, the Pacific margin of a reconstructed Gondwana along which subduction had occurred, at least since the Devonian. The tectonic setting of the basalts is unlikely to have been directly analogous to a 'back-arc'-like situation (*c.f.* Columbia River) since this environment is believed to be restricted to within a

few hundred km of the subducted region. Froidvaux and Nataf (1981) have shown that large convective 'rolls' will develop on the continental side of a subduction zone. The upwelling limb of these subduction-induced rolls would lie about 3,000-4,000 km inland of the subduction zone and take about 200 Myrs to establish, and this is consistent with time delay of volcanism which happened about 200-300 Myrs after subduction is known to have been active. This is the view favoured by Duncan *et al.*, (1984) to explain the Karoo magmatism, since the upwelling limb would lead to large scale heating of the sub-continental lithosphere over a large area parallel to the Pacific subduction zone. Anderson (1982) argued that the former presence of the large Pangea supercontinent had an insulating effect on the underlying mantle, allowing an increase in temperature of the sub-continental mantle, because of the lack of nearby mid-ocean ridges to dissipate the heat. This could lead to pervasive melting of the lithospheric mantle that, according to Marsh (in prep.), is more consistent with the large scale extent of these CFB provinces. This would also initiate continental rifting, and once sea-floor spreading was established, the magmatism in the continental interiors would decrease due to the increased role of the asthenospheric mantle in convecting the heat away through the mid-ocean ridges.

The variety in postulated geodynamic models emphasizes the need for good age control and stratigraphical control on the lavas so that the magmatic development of individual provinces can be linked to the transition from lithospheric thinning/rifting to ocean initiation. This thesis will investigate the extensive Paraná CFB of South America, in order to assess the viability of these alternative geodynamic models for a specific CFB province.

1.3 The Paraná CFB province.

1.3.1 General introduction.

The Paraná continental flood basalt province of South America must rank as one of the largest extant CFB provinces in the world since the present day extent of the lavas is at

least 1.2 x 10^6 km^2 (Maack, 1952). It lies predominantly in southern Brazil (Rio Grande do Sul, Santa Catarina, Paraná, São Paulo and Mato Grosso do Sul states) although it does extend into Uruguay, eastern Paraguay and northern Argentina (Misiones and Corrientes states). The 'Serra Geral Formation' is the accepted stratigraphical term for the lava sequences themselves (Zalan *et al.*, 1987) but when the whole magmatic event which includes both extrusive and intrusive activity is being considered, it is generally referred to as the Paraná CFB province. The lava sequences are dominated by tholeiitic basalts (> 90% by volume), restricted to fairly evolved compositions with less than 8 wt% MgO, and significantly, no picritic magmas have yet been encountered within the Paraná lavas (*c.f.* Deccan and Karoo). The basalts are accompanied by significant quantities of acidic rocks (rhyolites and rhyodacites), including scarce intermediate lavas, which cover an area of about 0.15 x 10^6 km^2 (Marimon *et al.*, 1983). This silicic magmatism typically forms the uppermost units of the lava sequences and is concentrated towards the continental margin, particularly in the south-east where the rhyolites are up to 400 m thick. The lavas reach a maximum known thickness of 1723 m in the 'CB' borehole at Cuiaba Paulista, São Paulo state (this study), and an estimate of 660 m for the average thickness over the province (Leinz *et al.*, 1966) yields a minimum volume of about 0.8 x 10^6 km^3 for the Paraná lavas.

The Paraná is quite a youthful province in terms of the level of erosion since the lava coverage is continuous over this large area. It did not escape the effects of erosion altogether, and the abundant dykes, especially along the coastal margins, and basaltic outliers, largely lying to the north-west in Mato Grosso do Sul state in Brazil, suggest that the original area might have been nearer 2 x 10^6 km^2 (Basaltic Study Volcanism Project, 1981). This is in contrast to the appearance of the formerly adjacent and earlier Karoo province of southern Africa where erosion has reduced the province to a vestige of its former glory leaving a collection of scattered lava field remnants and exposed the underlying intrusive sill and dyke complexes. Remains of the Karoo magmatism are spread over an area of about 2 x 10^6 km^2, but the present day lava coverage is only 0.14 x 10^6 km^2 in total.

In any palaeogeographical reconstruction of Gondwana, the Etendeka lavas of northern Namibia would have been adjacent to the south-east corner of the Paraná lavas in Brazil prior to the development of the South Atlantic ocean, and Erlank *et al.*, (1984) have addressed this coincidence with a reconnaissance study of the Etendeka province. The remnants of the Etendeka volcanics are scattered along the coastal margin over an area of about 78,000 km^2, with a maximum preserved thickness of about 900 m in the main lava field at Tafelberg. They consist of a series of interbedded basalts and rhyolites (quartz latites), accompanied by several phases of intrusive dolerites, and these stratigraphical sequences are reminiscent of the Paraná lavas on the southern Brazil coastal margin. The Etendeka lavas are distinguished from the main Karoo volcanism by their Lower Cretaceous age (see section 1.4.2), and Erlank *et al.*, (1984) has shown that the Etendeka quartz latites and basalts show strong compositional similarities with rhyolites and low TiO_2 basalts from the Paraná (this will be illustrated in the discussion on magma types in chapter two). Although the Etendeka lavas are generally treated as a younger phase of the widespread Karoo magmatism, their stratigraphy, chemical composition, and age all point to the conclusion that the Etendeka volcanics should really be considered as a continuation of the Paraná magmatic event, that became stranded on the African continent on the opening of the South Atlantic ocean.

1.3.2 Historical outline of Paraná research.

Research into the Paraná magmatism can be divided into three main phases of activity; (i) the initial discovery and field descriptions (1870's-1950's), (ii) palaeomagnetic and K-Ar dating studies in the context of the emerging continental drift hypotheses (1960's), (iii) major geochemical investigation (1980's).

The lavas were first described by Derby (1878) as 'Paraná Trapp' after studying sections in the Serra da Esperança, near Guarapuava, Paraná state. In the stratigraphical classification of the Paraná basin sequences by White (1908), the formation name 'Serra Geral' was assigned to the lavas, named after the coastal escarpment that marks their eastern margin in southern Brazil in such a spectacular fashion (see frontispiece). The first

description of the Paraná lavas in English was given in an expedition account by Woodworth (1912), and this was followed by a more comprehensive treatment in Baker (1923). Even these earliest published studies had realised the true extent and scale of the Paraná lava field. Numerous papers dealing with the petrography and general geological setting of the Paraná magmatism were published by Brazilian workers over the ensuing decades (see review in Cordani and Vandoros, 1967).

The 1960's were the heyday of the continental drift debate that was to culminate in the 'revolution in Earth Science' in the form of plate tectonic theory, and this also led to a period of renewed interest in the Paraná lavas. Du Toit (1937) had already noted the general similarities of stratigraphical successions between the Paraná basin in South America and the Karoo basin of southern Africa, which was further evidence for the postulated Gondwana supercontinent, and in 1965 Cambridge, A.N.U. and the newly established São Paulo laboratory initiated a major programme to date the Paraná lavas using the K-Ar method in an effort to correlate the major southern hemisphere Mesozoic CFB provinces and investigate their relationship to the break-up of Gondwana (see section 1.4.2). Palaeomagnetic studies of the Paraná lavas were also carried out (*e.g.* Creer, 1962) and these had an important role to play, both in aiding possible continental reconstructions of South America and Africa, and in constraining the polar wander curve for the South American continent during the Cretaceous (see section 1.5).

CFB provinces around the world were the subject of extensive geochemical studies during the 1970's and 1980's; *e.g.* Karoo (South African Geodynamics - Karoo project, ed. Erlank, 1984), Deccan (Mahoney *et al.*, 1982; Cox and Hawkesworth, 1984; Beane *et al.*, 1986), Columbia River (Swanson and Wright, 1980; Hooper, 1982), British Tertiary (Thompson *et al.*, 1982; Thirlwall and Jones, 1983), Keewenawan (Basaltic Study Volcanism Project, 1981), amongst others. The success of these studies, which had recognised the compositional diversity both within and between the different CFB provinces, was the incentive to initiate several major geochemical investigations of the Paraná magmatism during the early 1980's, involving various collaborations between workers from Brazilian, Italian, British and American universities {*e.g.* Bellieni *et al.*,

1983; Mantovani *et al.*, 1985a; Hawkesworth *et al.*, 1986; Fodor *et al.*, 1985a}. A special mention should be given to the joint Italian/Brazilian group under E.M. Piccirillo (Trieste) who in 1981 began a systematic study of the entire province including borehole sills and the coastal dyke swarms, since their work, soon to be collated into a book entitled "The Mesozoic flood volcanism of the Paraná basin: petrogenetic and geophysical aspects" edited by E.M. Piccirillo and A.J. Melfi, established much of the groundwork in describing the variety of geochemical types within the Paraná magmas.

Preliminary geochemical data allowed the Paraná basalts to be sub-divided into two geochemical groups based on their Ti contents (Bellieni *et al.*, 1984a; Mantovani *et al.*, 1985a), with the low-Ti group having $TiO_2 < 2$ wt% and the high-Ti basalts with $TiO_2 > 3$ wt%. Intriguingly, this difference is apparently controlled by the geographical location, since the high-Ti rocks are dominant in the northern part of the lava field whereas the low-Ti rocks are concentrated in the south. The geochemical distinction is also reflected in certain incompatible element contents with the high-Ti group enriched in LREE, Sr, Ba, P, Zr and Nb over the low-Ti rocks. The two groups also have consistently different radiogenic isotope compositions; high-Ti rocks have lower and more restricted $(^{87}Sr/^{86}Sr)_i$ (0.705-0.706), ε_{Nd} (-2.5 to -4.6) and less radiogenic $^{206}Pb/^{204}Pb$ (16.63-17.73) than the low-Ti which have 0.707-0.719, -3.7 to -7.9, and 17.90-19.11 respectively (Hawkesworth *et al.*, 1986). In terms of a Sr-Nd isotope diagram, this places the high-Ti rocks on an extension of the so-called 'mantle array', with the low-Ti samples displaced from this towards high ε_{Sr}. The rhyolites also reflect the high-Ti/low-Ti division seen within the basalts, and Bellieni *et al.*, (1986b) recognised two types, the Palmas rhyolites (low-Ti) and the Chapecó rhyolites (high-Ti).

Major element modelling has shown that the chemical variations within each group are consistent with low-pressure fractional crystallisation of the observed phenocryst phases olivine, augite, pigeonite, plagioclase, magnetite) although crustal interaction was important in the evolution of the low-Ti rocks. Trace element arguments illustrate the need for distinct parental magmas for the two geochemical groups, and these could have been derived either by varying degrees of partial melting of a homogeneous mantle source

(Fodor, 1987) or by appealing to mantle heterogeneities (Bellieni *et al.*, 1984a; Mantovani *et al.*, 1985a). The latter authors pointed to the high-Ti and low-Ti geochemical provinces within the Paraná as being more suggestive of the presence of large scale lateral variations within the lithospheric mantle beneath Brazil. The geochemical classification of the Paraná lavas into two groups is a rather simplistic scheme, and more recent work has highlighted several anomalies such as distinct geographical variations within both the low-Ti and high-Ti groups as well as a significant intermediate-Ti group with 2-3 wt% TiO_2 (Piccirillo *et al.*, 1988a). The recognition of different geochemical sub-groups and their spatial distribution forms a central part of this thesis and is developed in chapter two.

1.4 Age constraints on the Paraná magmatism.

1.4.1 Stratigraphical evidence.

Precise stratigraphical control on the age of the Paraná lavas is lacking. In Rio Grande do Sul state in southern Brazil the lavas locally lie unconformably on sediments of the Santa Maria Formation which has been dated from its reptilian fauna as Upper Triassic. Over most of the basin, the lavas lie directly on the essentially unfossiliferous sandstones of the Botucatu Formation, which in turn overlies the Santa Maria Formation, and this constrains the lavas to be younger than Upper Triassic. Towards the north, in Mato Grosso do Sul, Paraná and São Paulo states, sediments of the Bauru Formation overlie an irregular erosional surface cut into the lavas, and its abundant vertebrate fossil fauna has been assigned to the Upper Cretaceous (Huene, 1933; Oliveira, 1956).

Therefore, on the basis of their stratigraphical position and fossil evidence, the age of Paraná lavas can be constrained to between Upper Triassic and Upper Cretaceous. Most workers (*e.g.* Oliveira, 1956; Sandford and Lange, 1960) preferred an Early Jurassic age by appealing to the coincidence of widespread Mesozoic flood basalt volcanism in South America, southern Africa, Antarctica and Australia, and the likelihood that these represented a contemporaneous event throughout Gondwana.

1.4.2 Radiometric dating.

There have been numerous studies since the mid 1960's to determine K-Ar ages for the Paraná magmatic activity, {Creer *et al.*, (1965); Amaral *et al.*, (1966); McDougall and Rüegg, (1966); Vandoros *et al.*, (1966); Melfi *et al.*, (1967); Minioli *et al.*, (1971); Comte and Hasui, (1971); Sartori *et al.*, (1975); Pacca and Hiodo, (1976), Fodor *et al.*, (1985a); Mantovani *et al.*, (1985b); Piccirillo *et al.*, (1987)}, and over 140 dates are available on samples, both whole rock and mineral separates, from throughout the province (southern Brazil, Paraguay, Uruguay and Argentina). The results are summarised in a histogram on Figure 1.1 which shows the 5 Myr grouped frequency distribution of K-Ar ages for both Paraná lavas and intrusives. This diagram illustrates that there is no significant age

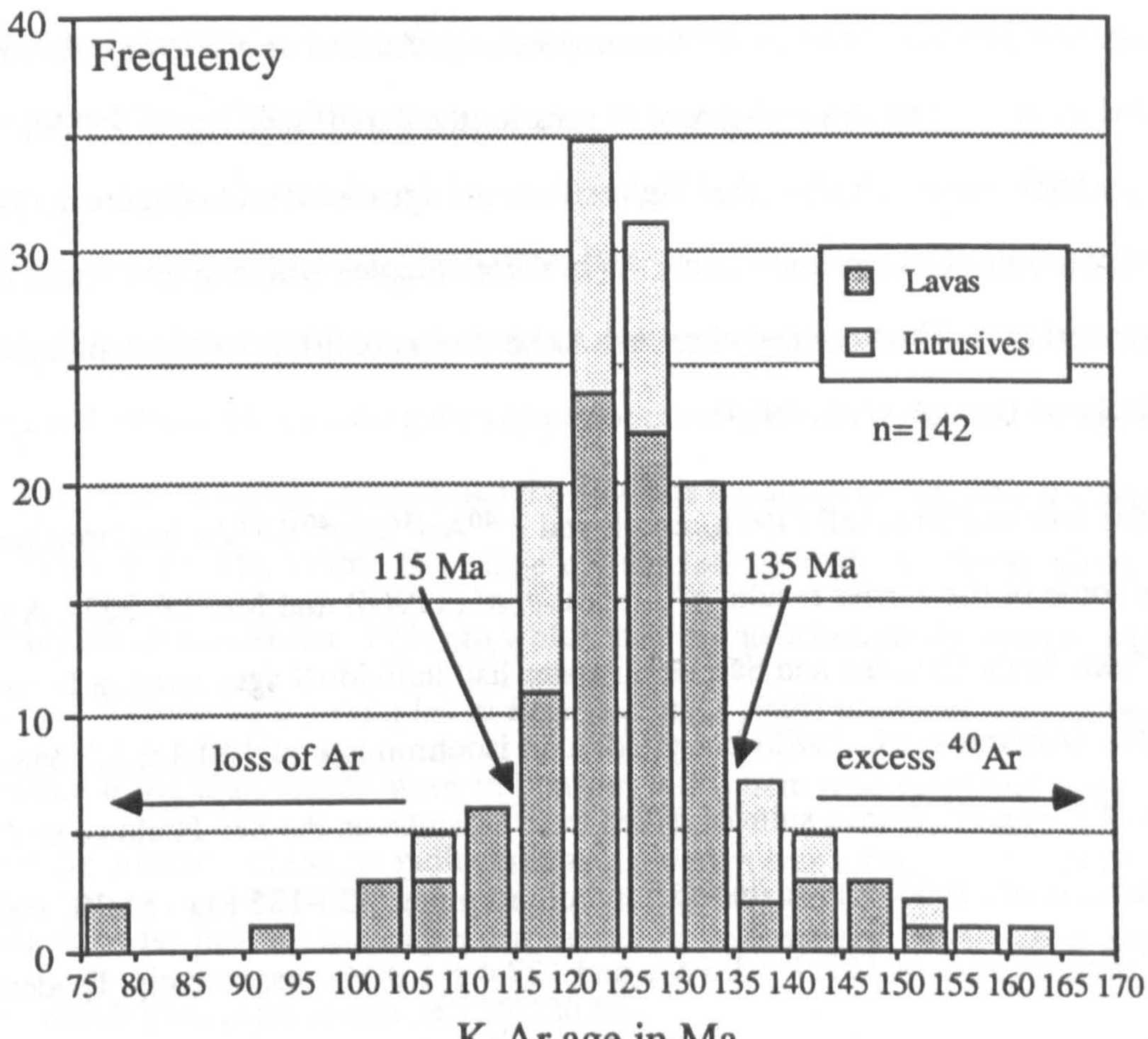

Figure 1.1 Histogram showing the grouped frequency distribution of conventional K-Ar ages for 142 samples of both Paraná lavas and intrusives. Errors quoted on most individual age determinations is about ± 5 Myrs. Data sources - {Creer *et al.*, (1965), Amaral *et al.*, (1966), McDougall and Rüegg (1966), Vandoros *et al.*, (1966), Melfi (1967), Minioli *et al.*, (1971), Comte and Hasui (1971), Pacca and Hiodo (1976), Cordani *et al.*, (1980), Mantovani *et al.*, (1985b), Piccirillo *et al.*, (1987)}.

difference between the basalt lava flows and the numerous dykes and sills, and hence, using the K-Ar method, the intrusive and extrusive Paraná activity appears to have been contemporaneous. The majority of the samples (> 70%) yielded ages in the range 115 Ma to 135 Ma which would clearly place them in the Early Cretaceous (144 Ma to 98 Ma; Harland *et al.*, 1982). As stated by Creer *et al.*, (1965) among others, this implies that the Paraná event was not contemporaneous with the other areas of Mesozoic Gondwana tholeiitic magmatism as had been previously thought, since these all have Jurassic ages {Karoo, southern Africa - 178 ± 5 Ma and 193 ± 5 Ma (Fitch and Miller, 1984); Ferrar, Antarctica - 165 ± 2 Ma and 179 ± 7 Ma (Kyle *et al.*, 1981); Tasmania - 175 ± 8 Ma (Schmitt and McDougall, 1977)}.

Loss of Ar, usually attributed to alteration effects, can account for the anomalously young ages (< 115 Ma) of some of the samples (*e.g.* Amaral *et al.*, 1966). Amaral *et al.*, (1966) believed there to be a real spread in ages for the Paraná lavas up to 150 Ma, whereas a more probable explanation of this 'high tail' on the age distribution (figure 1.1) could be the incorporation of excess radiogenic Ar in these samples which would result in higher than expected ages. The presence of excess Ar has been confirmed in the contemporaneous Etendeka lavas (Erlank *et al.*, 1984).

Siedner and Mitchell (1976) employed a $^{40}Ar/^{36}Ar$-$^{40}K/^{36}Ar$ isochron method to reassess some of the earlier results of Amaral *et al.*, (1966) and Melfi (1967). A group of basalts from Santa Catarina and São Paulo states had individual ages ranging from 110 Ma to 123 Ma (Amaral *et al.*, 1966) but yielded an isochron age of 120.3 ± 1.2 Ma. Similar analysis of the results from a suite of dykes from Ubatuba on the São Paulo coast (129-138 Ma, Amaral *et al.*, 1966) and scattered borehole samples (120-135 Ma - Melfi, 1967) gave similar isochron ages of 127.9 ± 3.6 Ma and 127.4 ± 1.0 Ma respectively. Evidence for a systematic variation in the age of the lavas over the province is not however very convincing. Melfi (1967) noticed a tendency for older ages to be towards the west, since the samples in Amaral *et al.*, (1966) were concentrated in the eastern portion of the province and gave ages of about 120 Ma whereas those of Melfi (1967) came mainly from the centre of the basin and generally had slightly older ages of about 130 Ma.

Cordani *et al.*, (1980) attempted to use the Rb-Sr method on whole-rock samples to date the Palmas-type rhyolites of southern Paraná and produced an errorchron of 118 ± 17 Ma. Mantovani *et al.*, (1985b) obtained internal Rb-Sr isochrons on three samples of the Chapecó-type rhyolites from the central Paraná that had already been dated by K-Ar. The Rb-Sr ages for each sample were systematically about 7 Myrs older than those determined by the K-Ar method {PR01 131.8 ± 5.9 Ma vs. 123.8 ± 1.6 Ma; SC06 138.4 ± 3.5 Ma vs. 126.0 ± 2.4 Ma; RS67 135.2 ± 2.3 Ma vs. 129.9 ± 1.6 Ma}. If it is assumed that all three samples were contemporaneous and cogenetic, the individual results can be combined to give an Rb-Sr isochron age of 135.4 ± 3.5 Ma and, since the rhyolites represent one of the last stages of the magmatic activity, this would constrain the underlying basalts to be older than about 130 Ma.

Several studies have obtained K-Ar ages on the Etendeka lavas and intrusives, (Siedner and Miller, 1968; Gidskehaug *et al.*, 1975; Erlank *et al.*, 1984), which have given a similar age range to that found for the Paraná lavas. Siedner and Mitchell (1976) reinterpreted the earlier results using the $^{40}Ar/^{36}Ar$-$^{40}K/^{36}Ar$ isochron method and gave an age of 121.0 ± 1.2 Ma for the Etendeka lavas and some regional intrusives. Several of the other regional intrusives, including the Doros complex, gave a slightly earlier age of 134 ± 0.9 Ma. The other Mesozoic igneous activity towards the south of Namibia produced older ages of 183.5 ± 3.4 Ma, within the range quoted for the main southern African Karoo magmatism (Fitch and Miller, 1984) to which they are geochemically similar (Marsh and Eales, 1984). Several of the samples in Erlank *et al.*, (1984) produced anomalously high conventional K-Ar ages which were in conflict with their stratigraphical position. This suggested the presence of excess radiogenic argon which was subsequently confirmed by a $^{40}Ar/^{39}Ar$ stepwise heating technique carried out on two mineral separates of Horingbaai dolerites, which gave plateau ages of 125-130 Ma.

Allsopp *et al.*, (1984a) used Rb/Sr studies to try and date the acidic rocks of the Etendeka but could only produce an errorchron age of 154 ± 21 Ma, with the scatter attributed to the effects of zeolitisation and a heterogeneous crustal source. A more successful result was achieved for the Messum igneous complex that intrudes the

Gobobosebberge remnant of the Etendeka lavas which yielded an Rb/Sr isochron age of 132 ± 2.2 Ma (Allsopp *et al.*, 1984b).

In view of the fact that both the Horingbaai dolerites and Messum complex are intrusive into the Etendeka lava sequences, Erlank *et al.*, (1984) suggested 130 Ma as a minimum age for the Etendeka lavas. Therefore, taking into consideration the age information available from both the Paraná lavas in Brazil, and their formally adjacent counterparts, the Etendeka lavas in Namibia, an age of 130 Ma has been assumed for the purpose of calculating initial Sr and Nd isotope ratios.

1.5 Palaeomagnetic studies on the Paraná CFB.

The first palaeomagnetic study in the Paraná was a preliminary regional survey carried out by Creer (1962). A more detailed approach was undertaken by workers from São Paulo University (Pacca and Hiodo, 1976; Ernesto *et al.*, 1979) who went to the well exposed coastal sections through the Serra Geral escarpment in southern Brazil and sampled every flow within particular sections. The magnetic inclination, declination and polarity were measured to assess the natural remenant magnetism of each sample

The results from these palaeomagnetic studies have been applied to three distinct problems; (i) to establish a magnetostratigraphy within each section which might then be used as a tool for regional correlations, (ii) to address the wider context of plate motions by calculating palaeopole positions, and (iii) to constrain ideas of eruption rates for the lavas via palaeosecular variations and reversal time scales. Only the latter two points will be considered in this section since the stratigraphical implications of the palaeomagnetic data are dealt with in chapter two.

Prior to the opening of the South Atlantic ocean, the sampled sections of Pacca and Hiodo (1976) and Ernesto *et al.*, (1979) from the Serra Geral escarpment would have been adjacent to the Etendeka province of northern Namibia. The palaeomagnetic poles calculated from these sections can be compared with the pole determined by Gidskehaug *et al.*, (1975) for the Etendeka lavas on a pre-drift reconstruction map of Gondwana, and this is

illustrated in figure 1.2 which shows them to be almost indistinguishable. This coincidence of palaeomagnetic poles is further evidence that, prior to continental break-up, the Paraná and Etendeka plateaus formed one large lava field. More recent work on the Paraná (Piccirillo *et al.*, 1988b) has considered the magmatic activity further to the north and observed that the northern lavas gave similar palaeopoles as the southern lavas, though more scattered. The palaeomagnetic poles determined on sills and dykes of the northeastern basin on the other hand were significantly displaced from those calculated from the lavas and suggested that this intrusive activity might have been a distinct event separate from the main lava eruptions.

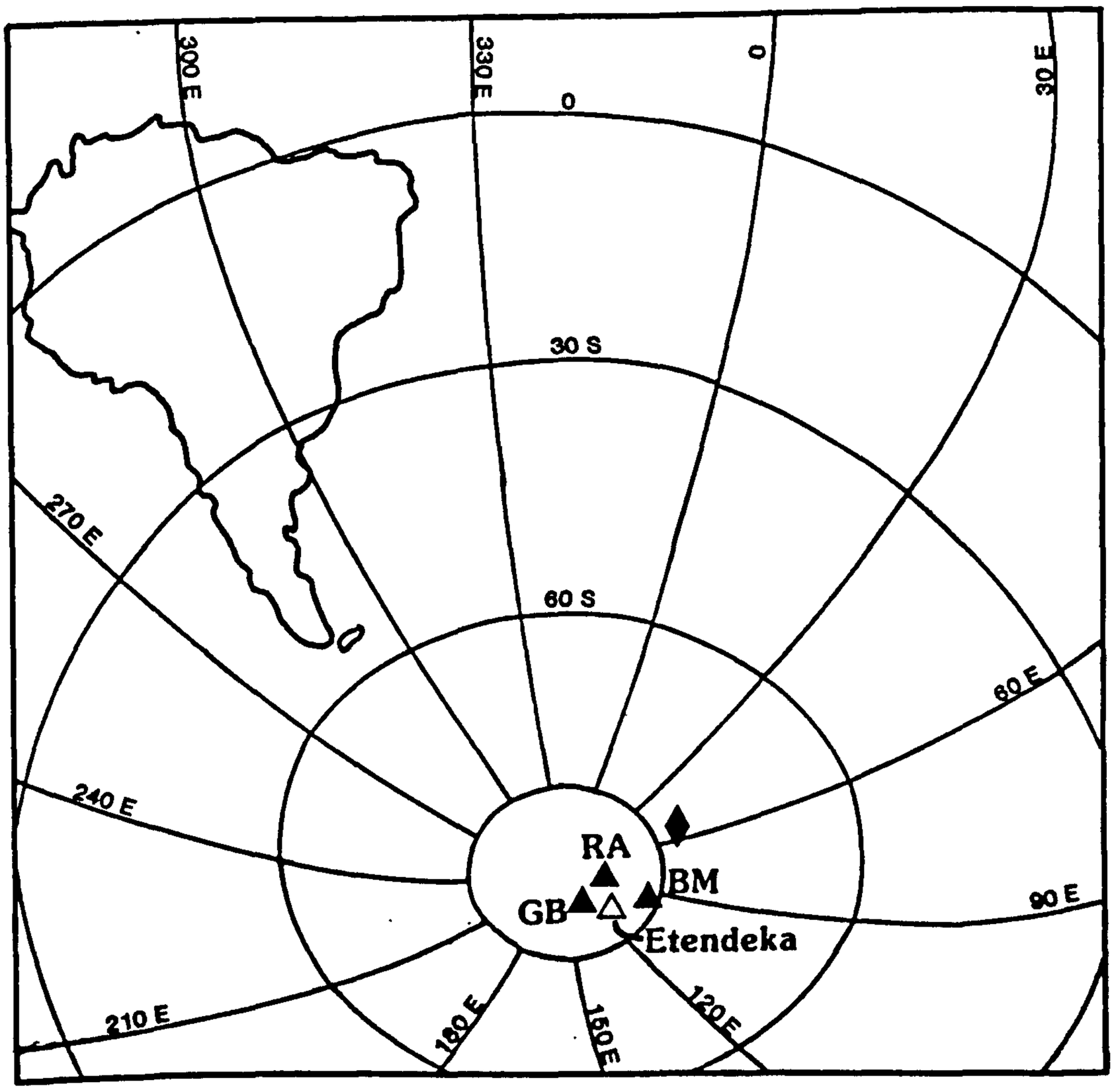

Figure 1.2 Comparison of palaeomagnetic poles of lavas from the Paraná and Etendeka provinces, after Ernesto *et al.*, (1979). Filled triangles are the three southern Paraná road sections RA, GB, BM of Ernesto *et al.*, (1979) - (for field locations, see figure 2.15), filled diamond is Paraná palaeomagnetic pole from Creer *et al.*, (1962), and open triangle is that obtained by Gidskehaug *et al.*, (1975) for the Etendeka lavas (corrected for a rotation of 57° around a pole at 44°N 30.6°W to take account of the subsequent opening of the South Atlantic ocean).

Bellieni *et al.*, (1983) attempted to equate changes in magnetisation direction to geomagnetic secular variations. Several flow sequences show regular and slow changes in both magnetic inclination and declination which might suggest that they were erupted during a single secular variation cycle. If the Mesozoic geomagnetic secular variation was of a similar periodicity as in the Quaternary, this would imply an individual cycle was of the order of a few thousand years. Bellieni *et al.*, (1983) suggested that sequences containing several polarity reversals would include several secular cycles but that the total time interval would not exceed a few hundred thousand years. Caution is needed in such an approach since any discontinuities in the variation of magnetisation direction might represent a temporary cessation of magmatism of unknown duration.

A slightly more rigorous approach has been to compare the polarity reversal pattern recorded in the lava sequences to those obtained from oceanic studies. It appears that the Early Cretaceous was a period of relatively rapid polarity reversals, with the mean duration of a polarity event on the order of 0.4 Myrs (Kent and Gradstein, 1985). Therefore, since the majority of the sampled sequences through the Paraná lava pile seem to record only two or three reversals, this would suggest a maximum period of lava eruption of less than a few million years. The possibility that the low resolution of polarity stripes on the ocean floors might miss reversal events of shorter duration, perhaps on the order of 5000 years, would considerably reduce this estimate for the duration of the magmatic activity in any one location (Piccirillo *et al.*, 1988b).

1.6 Regional geology and structure.

1.6.1 Introduction.

The three main aspects of the regional geology to be considered in this section are; (i) the age and structural trends of the regional crystalline basement rocks, (ii) the subsequent development of the sedimentary basin underlying the lavas, and (iii) the extent and diversity of the Mesozoic igneous activity.

1.6.2 Tectonic provinces within the regional basement.

The structure and age of the regional basement rocks have been discussed by several workers, and the summary given here is largely based on the review by Bernasconi (1987). Figure 1.3 is an attempt to summarise the salient tectonic and chronological features of the basement rocks. Knowledge of the nature of the basement rocks directly beneath the lava field is poorly known and can only be inferred by extrapolation between the basement exposures that occur right along the Atlantic coast as well as to the north-east and north-west of the lava field. The Archaean São Francisco craton, which lies to the north-east of the Paraná lavas, consists of low-grade granite-greenstones with ages in the range 2.8-3.2 Ga. This is surrounded by the Goias mobile belt, a late-Archaean high-grade granulite-gneiss terrain, produced by extensive crustal reworking during the ~2.7 Ga Jequié event (the Brazilian equivalent of the Limpopo-Liberia event in Africa), and the Paraná lavas lie directly on this unit along their north-eastern margin. The evolution of the whole region during the Proterozoic was dominated by three major orogenic episodes. The earliest was the Transamazonian event (1.8-2.2 Ga) that was largely characterised by reworking of Archaean crust, and the Amazonian and Rio de la Plata tectonic provinces, which lie to the north-west and south of the Paraná region respectively, were stabilised after this event. Much of this terrain is now obscured by the Chaco basin of western Paraguay, and the extensive Quaternary alluvium cover of the Brazilian Pantanal and northern Argentina. The middle Proterozoic (1.1-1.6 Ga) Uraçuano episode was restricted in this area to a regional overprint of the Goias mobile belt, although this is also believed to have been a period of new crust generation further south since the later Brasiliano granites of the Dom Feliciano belt yield model Nd ages of about 1.4 Ga (M. Basai, pers. comm., 1989). The last major event across the region was the Brasiliano or Pan-African event (0.5-0.7 Ga) and this produced the Ribeira-Mantiqueira belt of the Paraná-São Paulo coast and the Paraguai-Araguaia belt running through Mato Grosso state. These two features might possibly link up beneath the Paraná basin to form a single continuous belt (see figure 1.3). The Dom Feliciano Brasiliano-age) belt, which is exposed in Uruguay and along the coastline of Rio Grande do Sul and Santa Catarina states in Brazil, is separated from the Ribeira-

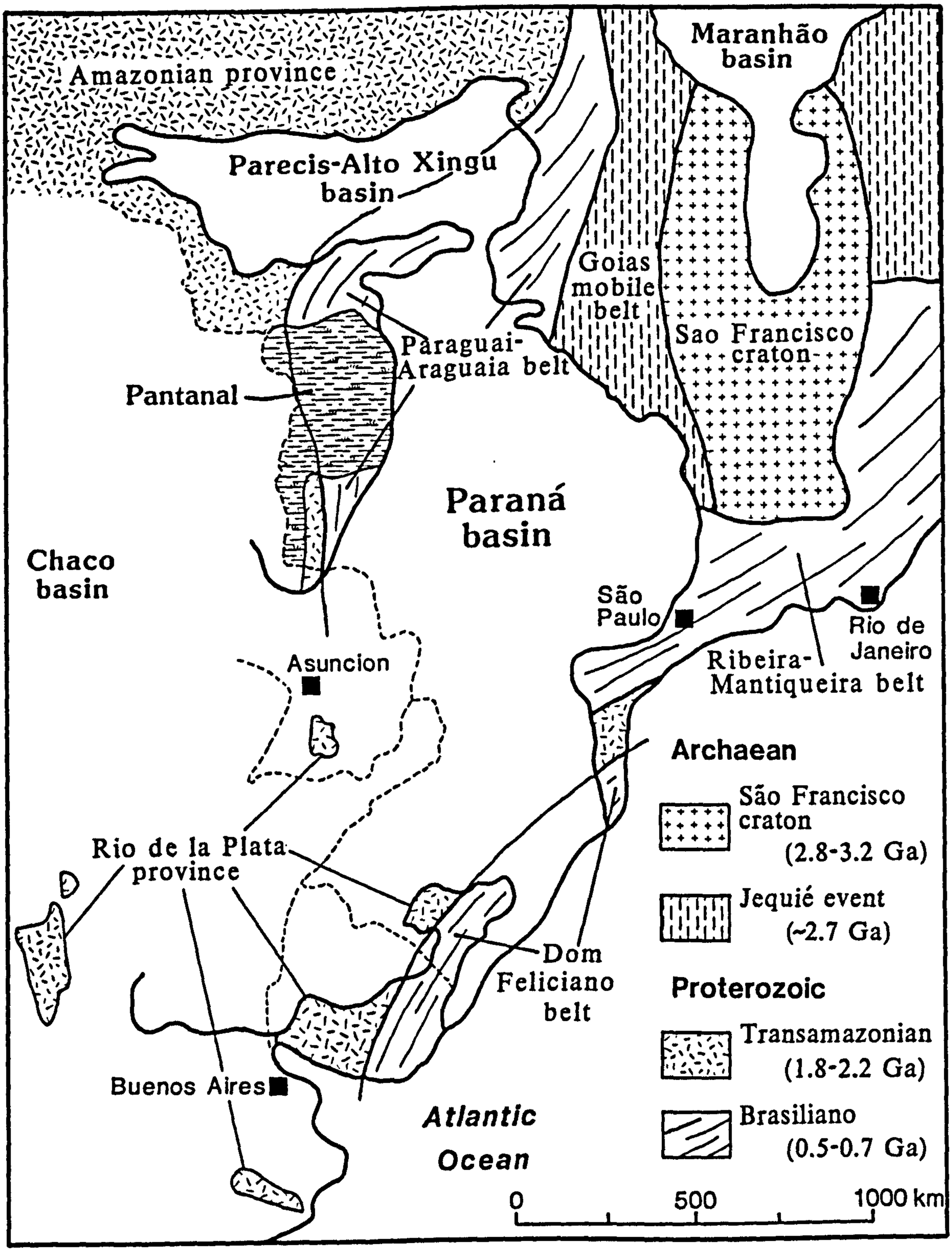

Figure 1.3 Schematic map of the basement geology, illustrating the crustal provinces and their age of stabilisation (after Bernasconi, 1987), and the sedimentary basins that developed subsequently during the Palaeozoic (adapted from Asmus and Baisch, 1983).

Mantiqueira and Paraguai-Araguaia belts, and is thought to represent an accreted terrane onto the Rio de la Plata province (S. May, pers. comm., 1989).

1.6.3 Evolution of the Palaeozoic Paraná sedimentary basin.

The Paraná lavas were erupted during the Early Cretaceous, largely covering the pre-existing Paraná sedimentary basin that had been initiated during the Late Ordovician / Early Silurian. The presence of this sedimentary basin beneath the lavas and its possible potential for petroleum deposits has led to an extensive investigation by several oil companies, involving both geophysical studies and drilling boreholes. Although much of this work is hidden in internal company reports, several general summaries have been published (*e.g.* Sandford and Lange, 1960; Zalan *et al.*, 1987) which has resulted in a clearer picture of the overall structure of both the basin and the overlying lavas. Figure 1.4 gives a map of the depth to the pre-Ordovician basement rocks beneath the basin, and illustrates the overall shape and areal extent of the Paraná basin (from Zalan *et al.*, 1987). The basin is aligned roughly NE-SW paralleling the structural trends in the underlying basement, and at its deepest point reaches over 5 km below sea level. The origin of the Paraná sedimentary basin is still the subject of conjecture, and Zalan *et al.*, (1987) has suggested that it either developed in response to a period of crustal stretching in the manner of McKenzie (1978) or from thermal subsidence induced by cooling after the intense magmatic activity of the Brasiliano-Pan African event. There is no clear evidence of a precursor central rift under the basin though the isopach map for the earliest sedimentary formation (Rio Ivai) showed a marked linear depocentre suggestive of a rift-type structure. The extent and shape of the basin have been variable throughout its history and this is thought to have been in response to changing intraplate stresses, since there is a close temporal correlation between major regional unconformities within the sedimentary sequences of the basin and the main Andean orogenic events happening further to the west. The basin infill is dominated by siliciclastic material, and minor limestones and evaporites are only found in the Permian Irati Formation. The Palaeozoic sedimentary sequences

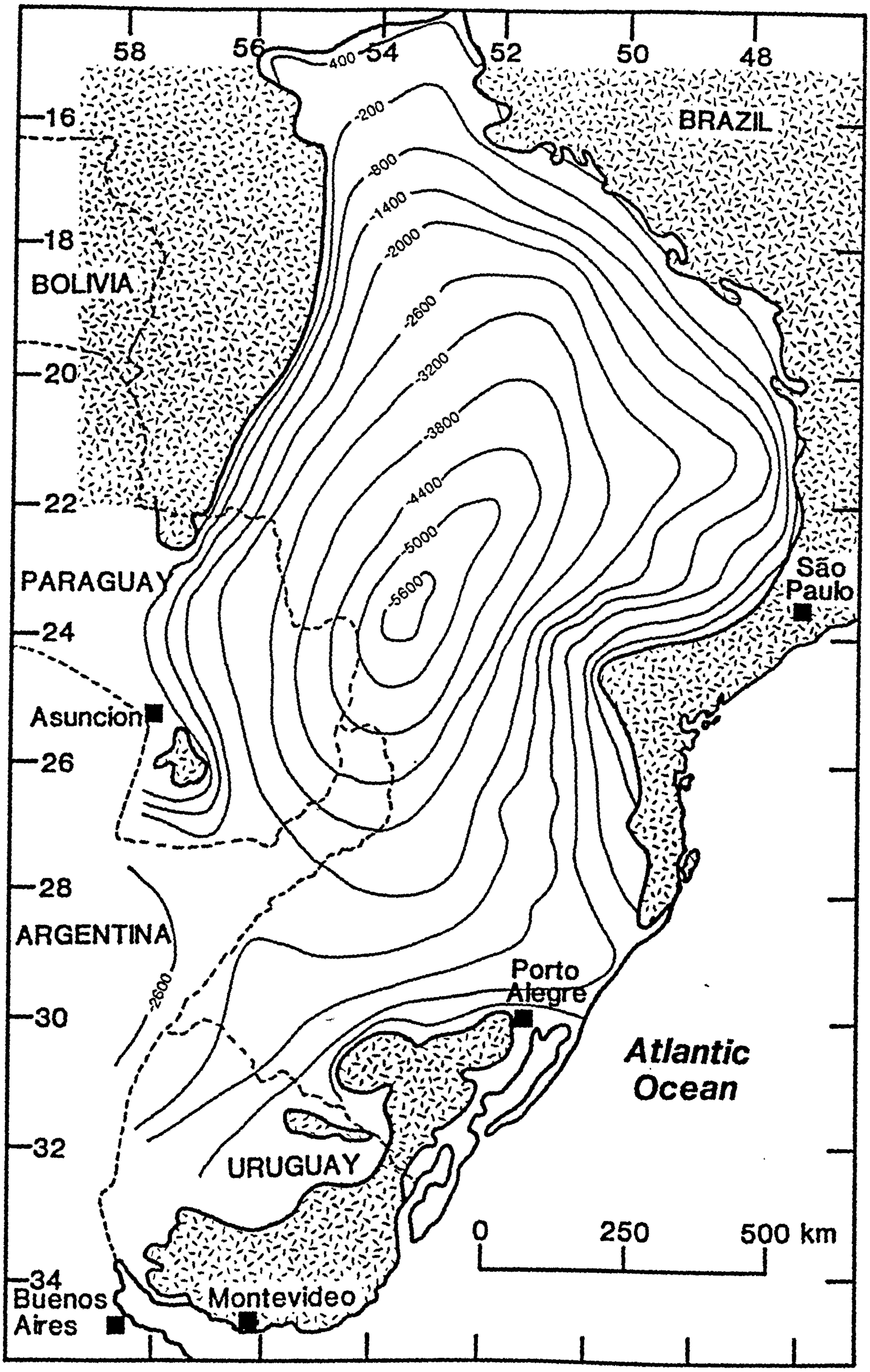

Figure 1.4 Map showing the areal extent of sediments of the Paraná basin and the depth to basement (*i.e.* pre-Ordovician) rocks (after Zalan *et al.*, 1987). Contours are at 600 m intervals.

represent several marine transgression-regression cycles, though the tillites of the Itararé formation reflect the widespread Gondwana glaciation event during the Early Carboniferous.

With the onset of the Mesozoic era, the sediments were exclusively continental, consisting of alternations of lacustrine and fluvial sequences and culminating in the aeolian dune crossbedded sandstones of the Jurassic Botucatu Formation. These sandstones persist as intercalations within the lava sequences indicating the continuation of desert conditions during the eruption of the Paraná lavas, and similar aeolian sandstones (Caiurá Formation) also occur overlying the more northerly lavas. A large proportion of the northern half of the lava field is obscured by the Late Cretaceous Bauru Formation, a fluvial and lacustrine sequence of siltstones, sandstones and conglomerates (Schobbenhaus *et al.*, 1984). To the south, isolated exposures of unconsolidated Tertiary sandstones and conglomerates of the Tupanciretã Formation locally overlie the Paraná lavas in Rio Grande do Sul state in Brazil, whereas in northern Argentina the lavas are covered by extensive Quaternary alluvium derived from the Uruguay, Paraguay and Paraná rivers (Schobbenhaus *et al.*, 1984).

Reactivation of regional structural trends within the basement has been an important control on the tectonic and sedimentary evolution of the Paraná basin. The structural framework of the basin is dominated by two major groups of tectonic elements, trending NE-SW and NW-SE respectively. The NE-SW trending fault zones have been inherited from the Brasiliano basement of the coastal Dom Feliciano and Ribeira-Mantiqueira belts and have been the site of extensive dyke emplacement and alkaline igneous complexes, as seen along the São Paulo-Rio de Janeiro coastline. More importantly, these regional NE-SW zones of weakness within the basement appear to have influenced the eventual location of the South Atlantic ocean. The NW-SE trending structures are represented by several antiform structures, the Rio Grande, Ponta Grossa and Goiânia 'Arches', which have had an important role in the present configuration of the basin. The Ponta Grossa and Rio Grande 'Arches' are believed to have been active during the Triassic to Jurassic sedimentation and have resulted in two large semi-elliptical reentrants into the eastern margin of the basin. The Ponta Grossa 'Arch' also acted as a locus for igneous activity in

the form of dyke swarms and alkaline intrusions. The Goiânia 'Arch', which marks the north-eastern margin of the Paraná basin, is though to represent the peripheral bulge that developed as a flexural response to the sedimentary and volcanic load of the Paraná basin. During the Tertiary, the Paraná basin has been dominated by extensive alkaline magmatism, including kimberlites. The basin is marked on its western margin by the Asuncion 'Arch', an antiform structure initiated during the Devonian that represents the peripheral bulge of the Chaco basin, a sub-Andean foreland basin. The southeastern margin of the basin was affected later by a phase of uplift which produced the impressive coastal range in southern Brazil known as the Serra do Mar, and its southerly extension, the Serra Geral escarpment. According to Zalan *et al.*, (1987) this uplift began in the Turonian (Cretaceous, 91-88.5 Ma; Harland *et al.*, 1982) although the evidence on which this age was based was not stated. The Ponta Grossa and Rio Grande 'Arches' were subsequently reactivated during this Serra do Mar uplift.

1.6.4 Structure of the Paraná lava field and intrusive activity.

Despite the general lack of extensive erosion exposing the deeper levels of the lava pile, a great deal is known of the general layout of the province and its external 3-D structure from oil company boreholes. Figure 1.5 is an isopach map for the Paraná lavas (Serra Geral Formation, taken from Zalan *et al.*, 1987) and shows how the variation in lava thickness over the province mirrors the overall structure of the underlying sedimentary basin. The thickest preserved accumulation of lavas (> 1.5 km) is in the northern half of the province, beneath the Paraná River, coinciding with the deepest part of the sedimentary basin, and the main axis of lava thickness (> 1 km) runs down the central area, roughly parallel to the northeast-southwest elongation of the basin. There is an anomalously thick sequence in the south-east corner onshore of the Rio Grande Rise and coincident with the Torres-Posadas synform.

The extent of the Paraná lavas to the south-west in northern Argentina is difficult to establish because of the extensive cover of Quaternary alluvial sediments. Although several boreholes have been drilled in this region, access to the well data is generally lacking. Leinz

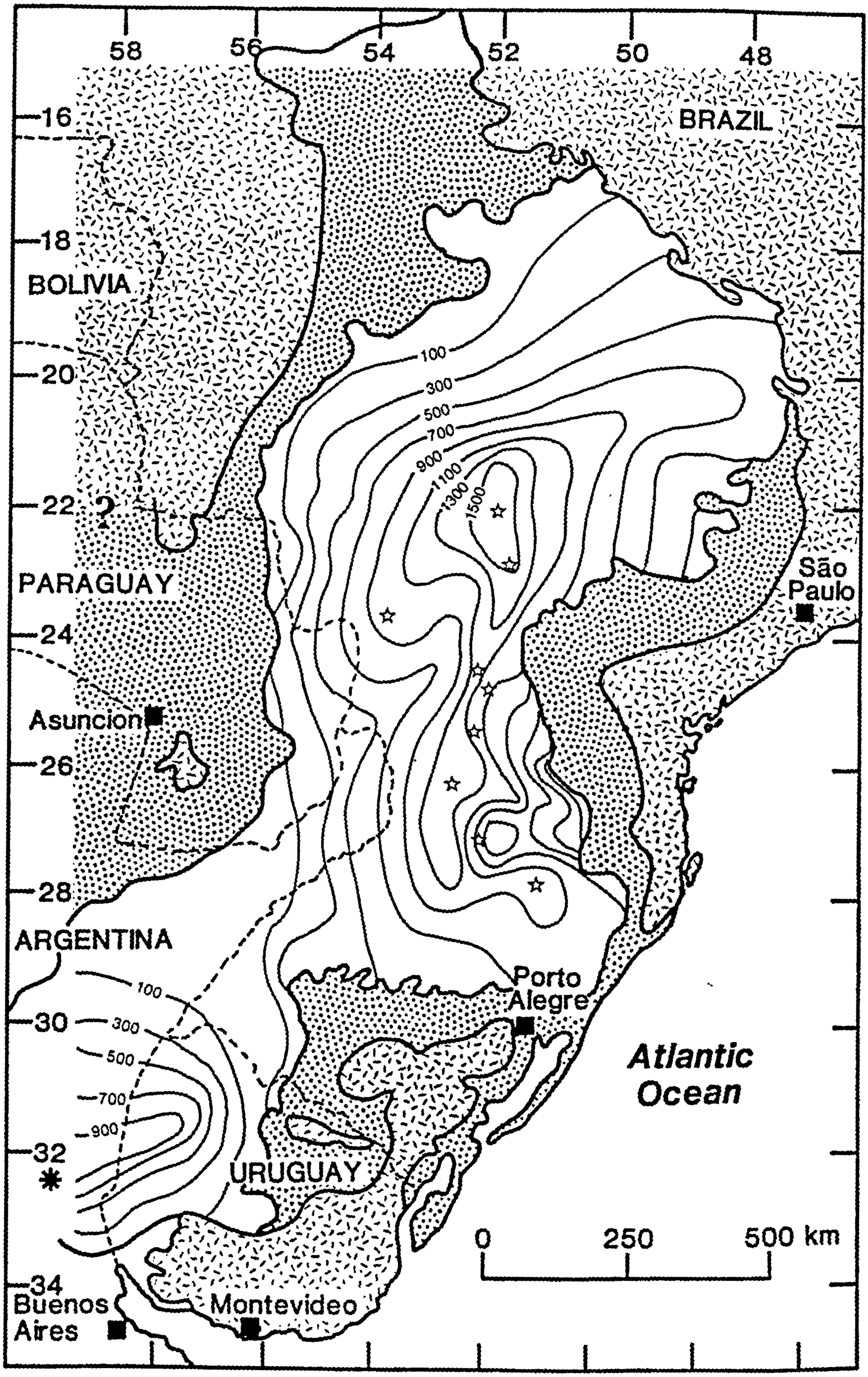

Figure 1.5 Isopach map of the Paraná lavas, with 200 m thickness intervals (after Zalan *et al.*, 1987; except for the south-west of the lava field in Argentina and Uruguay where the isopachs have been adapted from Leinz *et al.*, 1968). The star symbols indicate the location of the boreholes studied in this thesis, and the asterisk symbol in Argentina marks the position of the Nogoyá borehole mentioned by Leinz *et al.*, (1968).

et al., (1968) state that over 1000 m of lava were encountered in the borehole at Nogoyá (about 250 km NNW of Buenos Aires), indicating that this is another area of exceptional lava thickness (*i.e.* > 1 km) within the Paraná lava field. Zambrano and Urien (1974) noted the presence of pre-Middle Cretaceous basalts in a well drilled near Samborombon bay in the River Plate, about 300 km south-east of Buenos Aires (35°41' S, 57°19.5' W) which they assumed were correlated with the Paraná magmatism, but seismic evidence suggested that the basalts, although covering an area of about 250 km x 200 km, were restricted to just the narrow, approximately east-west trending, Salado basin and were isolated from the main Paraná basin. Emery and Uchupi (1984) stated that the Serra Geral volcanism extended to the Salado basin south of Buenos Aires, and as far to the south-west as the Cuyo basin, an Andean marginal basin close to Córdoba which lies about 750 km west of Buenos Aires. Apart from the surface exposures of north-eastern Argentina that are part of the main Paraná lava field, no geochemical analyses are available from the more southerly basalt occurrences which could verify their true relationship to the Paraná magmatism.

Evidence for the former extension of the Paraná lava field right into Mato Grosso state, to the north-west of the present exposure marked on figure 1.5, is given by the numerous basalt outliers lying on Paraná basin sediments on the Planalto de Mato Grosso between Cuiaba and Goias (Schobbenhaus *et al.*, 1984). Moving north-west, in the Serra dos Parecis that lie close to the Brazilian-Bolivian border, Schobbenhaus *et al.*, (1984) noted the presence of two substantial basalt exposures, the Tapirapuã and Anari Formations, which outcropped along the main Cuiaba to Porto Velho road. The Tapirapuã Formation lies about 150 km north of Cuiaba in Mato Grosso state, covering an area of approximately 130 km x 30 km with up to 310 m of lavas. K-Ar ages lie in the range 112 Ma to 126 Ma, similar to that for the Paraná (Serra Geral Formation) lavas (see section 1.4.2). The Anari Formation is exposed further to the north-west, just west of Vilhena, in Rondonia state. They cover an area of about 110 km x 40 km, and the limited K-Ar data available suggests ages of 140 Ma to 210 Ma, slightly older than the Tapirapuã Formation. Schobbenhaus *et al.*, (1984) correlated the Anari and Tapirapuã Formations which lie at the south-western margin of the Parecis-Alto Xingu basin, a northern continuation of the

Paraná basin (see figure 1.3), with the Serra Geral Formation of the Paraná basin. So far, these two formations have largely been ignored, probably as a result of their assignment to separate stratigraphical formations from the main Serra Geral Formation, and they need to be investigated geochemically so that a direct comparison with the main Paraná lava compositions can be made.

Borehole evidence has shown that sills between 2 m and 200 m in thickness occur throughout the Paraná basin, emplaced mainly within the Palaeozoic sediments, although examples are known within the Botucatu Formation and from the lava pile itself. The sills are concentrated in the northern half of the basin where they reach a total thickness of over 1000 m, coinciding with the maximum thickness of the volcanics (Piccirillo *et al.*, 1988b). Their petrography and geochemistry have been considered by Bellieni *et al.*, (1984b) who showed that they were all tholeiitic magmas and had evolved by low-pressure (< 1 kb) *in situ* crystallisation of olivine+pyroxene+plagioclase+magnetite. Compositionally they reflected the nature and distribution of magma types seen in the surface lavas, with low-, intermediate- and high-Ti varieties.

Lower Cretaceous tholeiitic dykes are also concentrated in the north-east of the basin, occurring in two main dyke swarms, but are very scarce in the southern Paraná. Dykes are widespread in the basement rocks of the Serra do Mar along the coastline of São Paulo and Rio de Janeiro states, well to the east of the main Paraná lava field. They trend NE-SW sub-parallel to the regional structural lineament within the basement rocks, and are all high-Ti (>3 wt%) magmas (Comin-Chiaramonti *et al.*, 1983). The Ponta Grossa 'Arch' is characterised by numerous dykes about 20-50 m wide trending NW-SE along the crest of the antiform. Their compositions, while covering the full spectrum from low-, intermediate-, and high-Ti, are similar only to the northern basalt magma types (Ribeira, Paranapanema, Pitanga of this study) and cannot be considered as feeders to the southern lavas.

1.6.5 Alkaline igneous complexes

Numerous intrusive ring-complexes are found scattered around the rim of the Paraná basin (see figure 1.6), and they represent several pulses of alkalic-carbonatitic magmatic activity that occurred during, or subsequent to, the Paraná CFB magmatism, spanning a period from about 140 Ma to 40 Ma (see review by Ulbrich and Gomes, 1981). Several have ages that overlap with the 115-135 Ma age range determined by K-Ar for the Paraná, and these include the Jacupiranga province (122-130 Ma, Ulbrich and Gomes, 1981; Roden *et al.*, 1985 give an Rb/Sr age of 131 ± 3 Ma) which lies along the coast of São Paulo state, and Anitopolis (129 Ma; Ulbrich and Gomes, 1981) which lies about 85 km NE of São Joaquim in Santa Catarina state and is only 40 km from the studied lava road sections of this thesis. Intrusive complexes with similar ages have also been reported from north-eastern Paraguay (Cêrro Corá, ~140 Ma; Comte and Hasui, 1971) and the Uruguayan coast (Mariscala, 120 Ma; Marsh, 1973). The younger alkalic activity seems to have been preferentially located along the three main NW-SE antiform structures mentioned earlier. The Piratini phonolite complex (85 Ma; Barbieri *et al.*, 1987) was controlled by the Rio Grande 'Arch', the Tunas alkaline province (80 Ma; Gomes *et al.*, 1987) is aligned with the Ponta Grossa 'Arch', but the Goiânia 'Arch' along the north-eastern edge of the Paraná basin was the locus of the most extensive post-Paraná alkalic magmatism with a belt of igneous complexes, varying from nepheline-syenites, phonolites, carbonatites and kimberlites, that stretched from Mato Grosso state to the Rio de Janeiro coastline and with an age range of 40-90 Ma (Ulbrich and Gomes, 1981). Activity in Paraguay was localised within the Asuncion graben, and included the Sapucai province and the Nemby nephelinites which give ages of 80-120 Ma and 45 Ma respectively (Palmieri and Velazquez, 1982).

This alkaline activity was not restricted to South America, and intrusive complexes yielding Paraná (or Etendeka) ages also occur in three regions on the western coast of Africa; the Lüderitz province of southern Namibia (~130 Ma; Marsh, 1973), the Angolan province (~112 Ma; Marsh, 1973) and the Damaraland province of northern Namibia (~130 Ma; Marsh, 1973; Erlank *et al.*, 1984). Several of the complexes (Cape Cross, Messum, Brandberg) within the Damaraland province are intrusive into the Etendeka lava sequences

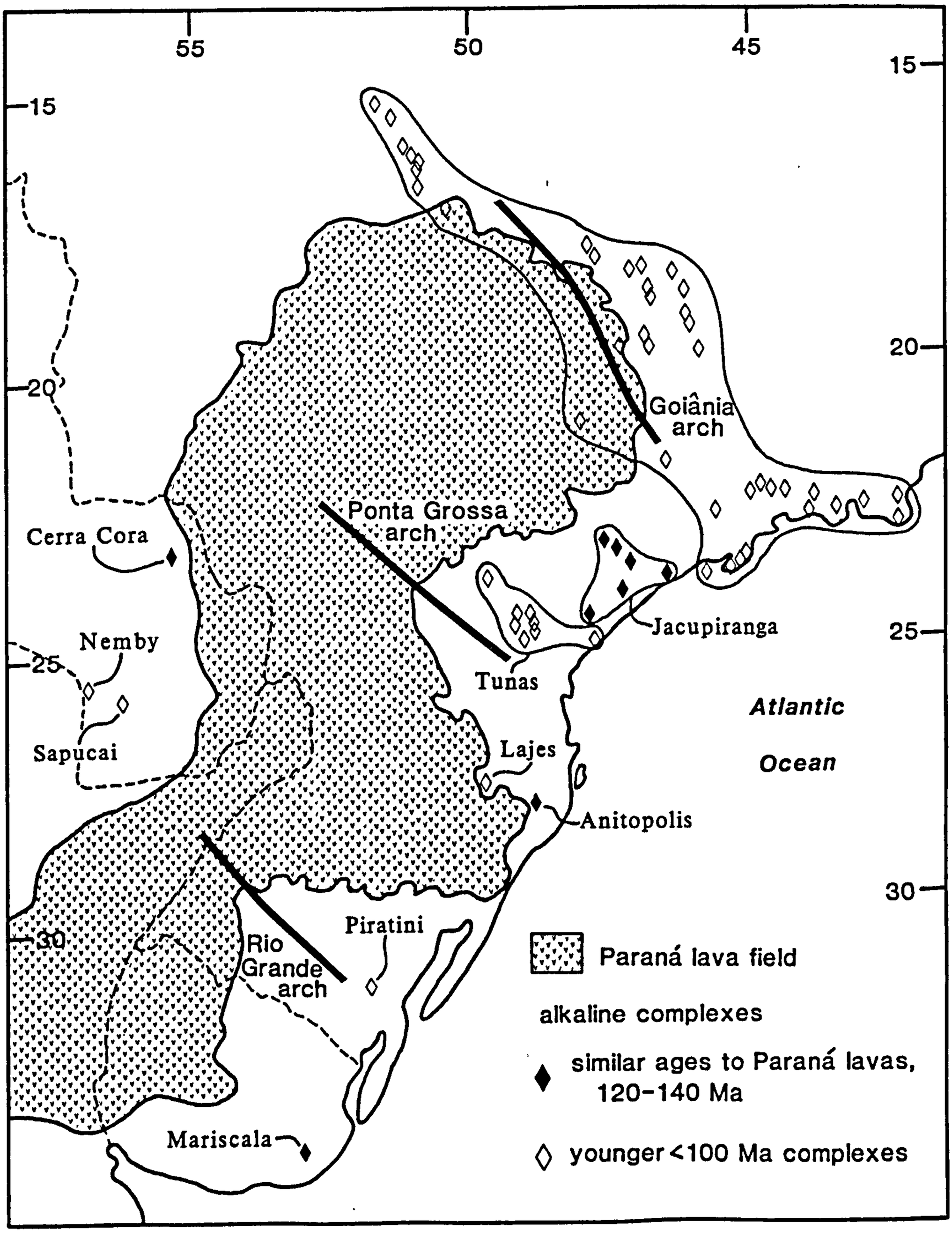

Figure 1.6 Location map of the alkaline magmatism relative to the Paraná lava field and regional tectonic structures.

(Erlank *et al.*, 1984), clearly demonstrating that they post-dated the CFB magmatism, and a similar situation has also been shown for the tholeiite flood lavas and alkaline rocks of the Deccan province (Beane, 1988). The close spatial and temporal association of tholeiitic CFB's with varied alkaline magmatism is seen in several CFB provinces, including the

Paraná, Deccan and Karoo, but the underlying tectonic and petrogenetic links between the two styles of magmatism have rarely been addressed in this context and are still poorly understood.

1.7 Aims and structure of this thesis.

As its title suggests, this thesis is not only concerned with unraveling the petrogenesis of the various Paraná magma types but also in outlining their distribution within the lava pile. Stratigraphical studies are important in providing spatial and temporal constraints on any proposed petrogenetic models, and these were carried on two different scales. A localised study, based on road sections cutting through the coastal Serra Geral escarpment in Santa Catarina state, was first undertaken to look at the detailed chemical variations within individual magma types. The scope of the study was then broadened to view the whole lava field and assess the lava stratigraphy on a regional scale. This was achieved by a survey and re-evaluation of the available data in the literature as well as a rather unique approach using borehole samples. Over 150 samples of drillcore chippings from nine boreholes along a 650 km north-south section through the central area of the basin were analysed to provide information on the otherwise inaccessible and unexposed deeper portions of the lava pile.

The thesis is structured so as to outline the classification and stratigraphy of the Paraná lavas prior to discussing their petrogenetic origins. The importance of stratigraphical studies within CFB provinces is emphasized in chapter two, and this chapter also establishes the scheme of magma types that will be followed in the rest of the thesis for the Paraná lavas, as well as outlining their regional distribution. The discussion of the petrogenesis of the Paraná lavas focuses mainly on the magma types that have been recognised in the road sections studied in Santa Catarina state on the Serra Geral escarpment. The high-Ti types (Urubici basalts, Chapecó rhyolites) are the subject of chapter three, and the low-Ti types (Gramado and Esmeralda basalts, Palmas rhyolites) are discussed in chapter four. Chapter five considers the petrogenetic relationships that link the

various magma types on a regional scale, and then expands the discussion to consider the Paraná province in the wider context of the other Gondwana continental flood basalt provinces. The concluding remarks in chapter six are accompanied by a short discussion on the possible geodynamical origins of the Paraná-Etendeka CFB province.

The objectives of this thesis can be summarised as follows;

(i) To recognise and establish a series of magma types, and then use them to define a geochemical stratigraphy for the Paraná CFB province.

(ii) To investigate the petrogenetic relationships within, and between, these magma types.

(iii) To link the temporal variations in magmatic composition, as highlighted by the stratigraphical framework, to the changing regional tectonic environment.

Chapter 2
Stratigraphy of the Paraná lavas.

2.1 Importance of stratigraphical studies in CFB provinces.

It is now generally accepted that the establishment of a reliable stratigraphy is of paramount importance in the investigation of CFB provinces. Stratigraphical studies have proved fruitful because they can reveal both the structure and sequential evolution of the lava pile as well as providing a framework in which to base any petrogenetic interpretations of the magmatism.

On a local scale, detailed sections through the lavas can highlight the temporal variations in magmatic composition and provide information on processes such as crystallisation, mixing, and assimilation that might have occurred within the magma chamber environment. Expanding this to the province as a whole, a regionally-based stratigraphy can outline the structure of the whole lava pile and allow the effects of syn- and post-eruption uplift and deformation to be assessed. This approach should also provide an insight into the poorly understood geodynamic mechanisms responsible for the generation and emplacement of large flood basalt provinces via the pattern of the lithostratigraphical units, and help towards understanding how magma sources and processes have varied in response to changes in the tectonic environment during the evolution of the province.

2.2 Development of a flow stratigraphy.

2.2.1 Introduction.

To develop a stratigraphical classification scheme, it is necessary to be able to characterise and distinguish individual flows or groups of flows, despite the apparently

monotonous layer-cake field appearance of most flood basalt lava sequences. Many attributes of the lavas (physical characteristics, palaeomagnetic polarity, chemical composition) have been considered by workers in other provinces, chiefly those in the Columbia River and Deccan. The usefulness of these criteria in defining a coherent regional stratigraphy, as well as their applicability to the lava sequences of the Paraná, will be reviewed in the following sections.

2.2.2 Physical characteristics of flows.

A wide variety of physical attributes can be recorded in the field but if they are to be of any use in stratigraphical correlations, the flows must display sufficient variation within a sampled section to ensure that there are at least a few distinctive flows that will allow the lava pile to be subdivided.

Typical characteristics of the lava flows include jointing habit, weathering colour, flow thickness, abundance and size of vesicles, and the presence or absence of flow-top rubble. The ability to recognise and utilise such features depends on the quality and extent of the exposure which in several of the studied Paraná sections was rather discontinuous and left a lot to be desired. These physical features are often not unique to an individual flow since they largely reflect factors such as the distance from the vent source and variations in both palaeotopography and the local cooling regime. It is not surprising therefore that they are known to change markedly within a single flow over a few kilometres laterally (Swanson and Wright, 1980), which limits their usefulness for anything except purely local correlations.

Intraflow structures formed during the cooling of individual subaerial basaltic flows are characterised by laterally persistent joint patterns known as 'entablature' and 'colonnade'. The colonnade has a well-defined columnar structure normally developed perpendicular to the flow-base. The entablature structure has smaller column diameters and a more irregular pattern of fractures than the underlying colonnade. Long (1978) developed a classification scheme for flows in the Columbia River based on the type of entablature development; Type I had no entablature, Type II had repeated entablature and colonnade

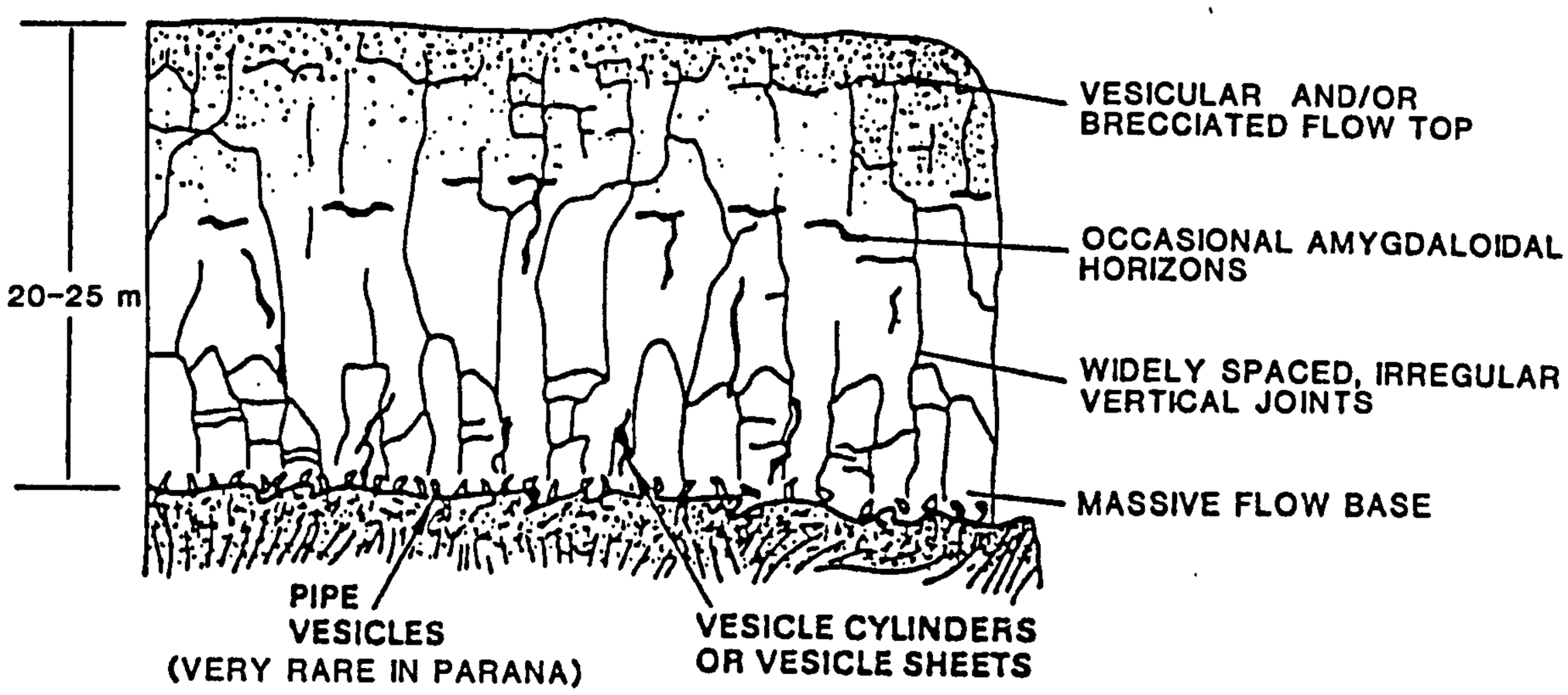

Figure 2.1 Sketch of a typical Paraná lava flow (adapted from Long and Wood, 1986), which is equivalent to the type I flow of Long (1978), showing no entablature development.

tiers, and Type III had a single colonnade/entablature unit. The Columbia River basalts appear to be unusual in that a high proportion of the flows exhibit entablatures, a feature not common in other flood basalt provinces, the Paraná included. The Paraná flows seen in the São Joaquim area correspond exclusively to the Type I flows of Long (1978) which consist entirely of highly irregular colonnade and lack an entablature (see figure 2.1). Thus for the majority of CFB suites this rules out using the morphological flow structures of individual flows as a criterion for developing a flow stratigraphy.

Sequences of basaltic flows can be classified into simple or compound flows, after Walker (1972). Simple flows are single cooling units which often display well-developed jointing perpendicular to the flow-base and an increase in vesicularity towards the oxidised flow-top or flow-top breccia. Compound flows by contrast form massive poorly-jointed horizons comprising numerous thin (a few cm to a few m) laterally discontinous flow units which are each picked out by thin oxidised surfaces and highly vesicular zones. The distinction between these two flow morphologies is thought to result from differences in the surface extrusion rate, and the critical extrusion rate below which a compound lava rather than a simple one forms is probably viscosity dependent (Walker, 1972). Most of the flows in the studied road sections in the Paraná appeared to be simple flows although there were the occasional compound flows. This was not considered to be a reliable means of

correlation because the more restricted exposure in the Paraná often made it difficult to follow a whole eruptive unit from its base to the flow top at outcrop. Whereas compound flows appear to be more susceptible to weathering, simple flows often tend to weather out as prominent bands across the hillsides and this proved to be useful in tracing flows between sections in the southern Deccan traps (Lightfoot, 1985). Unfortunately for the Paraná lavas, the nature of the local topography, the climate and the extensive vegetation cover in the Santa Catarina region all conspired to make it difficult to observe the lava sequences from a distance and thereby ruled out a similar visual correlation of distinctive flows along the escarpment.

The petrography of flood basalts has also proved to be of limited value in making stratigraphical correlations because of; (i) the broad similarities between successive flows, and (ii) the variability found within individual flows in terms of the degree of vesicularity and phenocryst population. Care must be taken when considering the texture of a sample since this will reflect the variable post-eruption cooling history encountered within an individual flow. As with the Columbia River basalts (Swanson and Wright, 1980), the majority of the Paraná basalts are virtually aphyric, having < 5% phenocrysts, and very few flows have any unique petrographical features. Occasionally certain flows within a flood basalt sequence do have a characteristic phenocryst assemblage, and a good example are the Giant Plagioclase Basalts (GPB) units that occur within the Kalsubai subgroup in the Deccan basalts (Beane *et al.*, 1986), containing large (1-5 cm) plagioclase phenocrysts. Each GPB flow has a distinctive field appearance and their widespread distribution qualifies them as useful marker horizons with which to subdivide the lava pile.

The overwhelming consensus from studies in the Columbia River (*e.g.* Swanson and Wright, 1980) and the Deccan provinces (*e.g.* Cox and Hawkesworth, 1984; Lightfoot, 1985) is that it is not possible to subdivide the flood basalt sequence using the physical characteristics of the lavas alone, although such features might be of importance in the local correlation of flows, and this view has been borne out by these field studies in the Santa Catarina road sections through the Paraná lavas.

2.2.3 Palaeomagnetism.

Detailed palaeomagnetic studies involving laboratory determinations of the natural remanent magnetic polarity of the lava flows can be used to establish regional magnetostratigraphic units. The number of these units will depend on the frequency of reversals of the earths magnetic field during the eruption of the whole lava sequence. Certain flows occasionally record unusual dipole field directions and can sometimes be used as marker horizons throughout the region. Unfortunately such studies are expensive and time consuming, and a rapid field-based method is preferable. Workers in the Columbia River province had considerable success in mapping out the established magnetostratigraphic units on the basis of magnetic polarity determined using a portable fluxgate magnetometer in the field, provided that suitable care was taken as to which parts of the flows were tested (Swanson and Wright, 1980).

Several detailed palaeomagnetic studies (Pacca and Hiodo, 1976; Ernesto *et al.*, 1979) have been carried out on the Paraná lavas though their main emphasis has been on determining palaeomagnetic pole positions to aid Gondwana reconstructions, and in

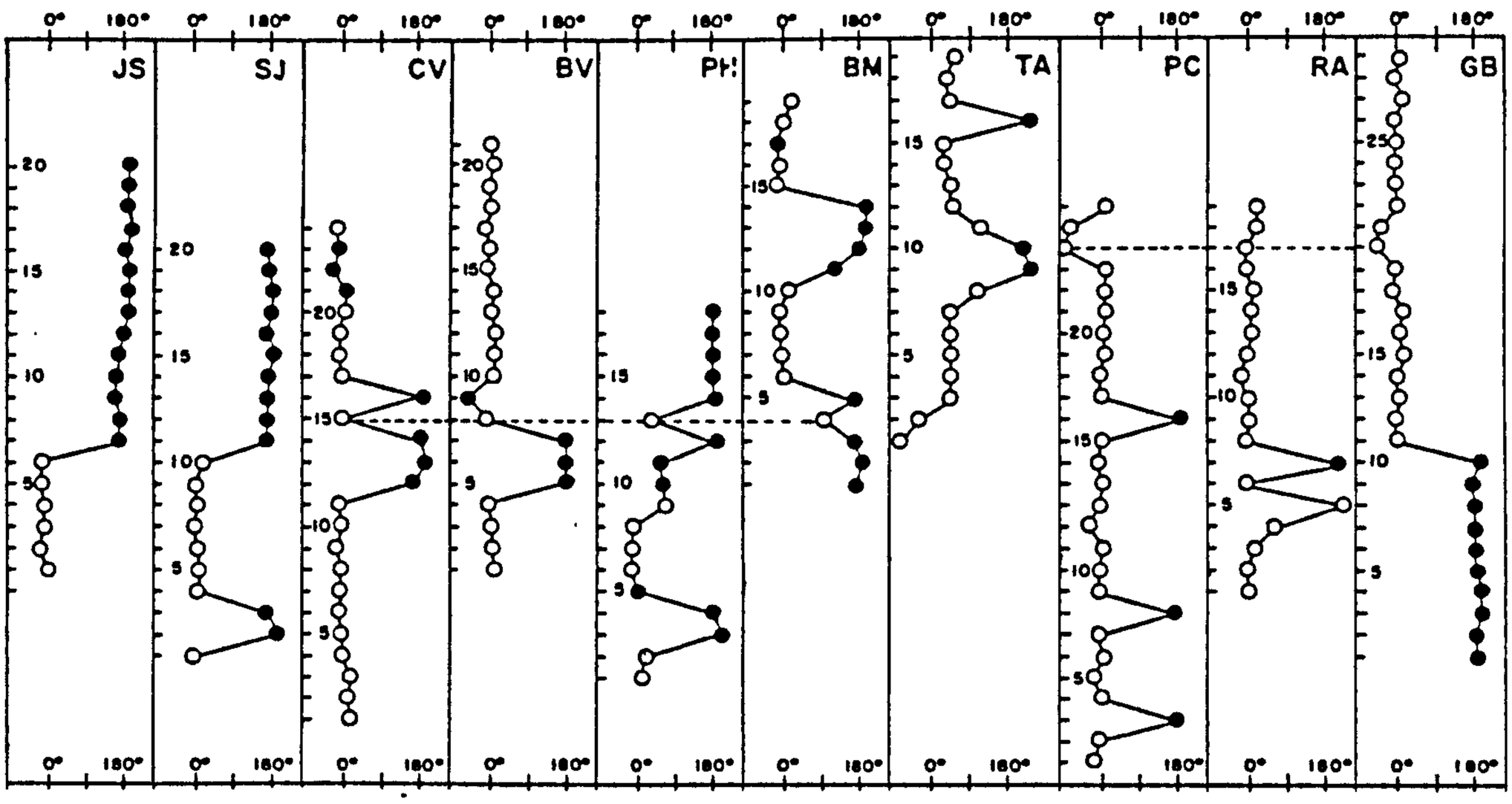

Figure 2.2 Variation in declination through lava sequences of southern Paraná, from Piccirillo *et al.*, (1988b). Profile localities are shown on figure 2.15. N.B. the vertical axis is the flow number within a particular sequence and not the absolute stratigraphical height. Sequences have been aligned in an attempt to match polarity events. Normal polarities (open circles), reversed polarities (filled circles).

assessing the secular variations in an attempt to constrain eruption rates, as outlined in chapter one. The most extensive studies have concentrated on road sections down in the south-east corner of the province, along the Serra Geral escarpment (see figure 2.15), for which there is also a considerable amount of chemical data available (Piccirillo *et al.*, 1988a). Most of the lava sequences contain at least one, and in some cases up to seven, polarity reversals but there are difficulties in assigning each reversal to a specific polarity event and hence in defining magnetostratigraphic units. An obvious feature illustrated by the palaeomagnetic profiles in figure 2.2 is that the volcanic activity did not start simultaneously over the Southern Paraná region. Some clear correlations do exist between the sections; for instance, the four adjacent profiles CV, BV, PH, BM all show a sole normal flow, probably related to a very short normal polarity event, that can be used as a stratigraphical marker. The declination and inclination for successive flows in the reversed sequences at the top of the GB, RA, and PC profiles show a remarkably good match suggesting that they are all from the same polarity event, and this is interesting as it implies that rhyolitic flows at RA were contemporaneous with basaltic lavas at GB. There has not been much detailed effort to directly correlate the magnetostratigraphy with the chemical variations, especially those of the rhyolitic eruptions, and this is certainly an avenue that needs to be pursued in the future.

2.2.4 Age determinations.

K-Ar age determinations for most CFB provinces yield a considerable range in ages and these are often not consistent with the stratigraphical succession of the lavas. The range in K-Ar ages for the Paraná lavas is 75-165 Ma, as shown previously in figure 1.1, though much of this range is just apparent since the younger ages can be attributed to the effects of variable Ar loss during post-eruptive cooling and alteration. The majority of Paraná samples have ages between 115-135 Ma, but the K-Ar method is clearly not sufficiently precise to distinguish between successive flows. Recent determinations for the Deccan basalts using the more precise $^{40}Ar/^{39}Ar$ technique have considerably tightened the range in reported ages. A review of K-Ar ages for the Deccan by Courtillot *et al.* (1986) gave a range from 55-71 Ma with a peak between 60-67 Ma. Duncan and Pyle (1988) showed that $^{40}Ar/^{39}Ar$

ages were indistinguishable throughout a 2 km thick composite section through the lavas and gave a mean age of 67.4 ± 0.7 Ma. This means that the $^{40}Ar/^{39}Ar$ method is also of little use in defining a stratigraphy, but if the stratigraphy can be established by independent means, then $^{40}Ar/^{39}Ar$ studies might have a future role to play as the best chance to provide sufficient resolution to date these stratigraphical events.

2.2.5 Chemical stratigraphy.

The advances made in analytical techniques to determine major and trace element contents of lavas have shattered the long-held belief that CFB provinces were comprised of monotonous sequences of indistinguishable basalt flows, and have demonstrated that systematic compositional differences exist within the lava sequences. The magnitude of these differences is too large to be ascribed solely to the effects of post-solidification alteration of the basalts and must therefore reflect processes that acted prior to eruption. Such chemical diversity, coupled with the ability to perform rapid geochemical analyses, has allowed detailed stratigraphical successions to be established in several flood basalt suites, especially the Columbia River and Deccan provinces. The compositional data tend to cluster and to define a certain number of chemical groups which are referred to as magma-types (or chemical types). From this, each magma type can be delineated using a range of elemental abundances and ratios to enable flows to be assigned to a specific magma type. The underlying causes for the major chemical changes between the magma types, {*e.g.* variations in mantle source region, degree of crustal assimilation, etc.}, are not the immediate concern in developing a chemical stratigraphical succession.

Assessing the possible resolution of the stratigraphical classification requires a clearer understanding of the extent of inter- and intra- flow chemical variations and of the effects of post-eruption alteration on the lavas. Subdivision on a flow-by-flow basis will only be possible if the compositional differences between successive flows exceeds the combined effect of intraflow heterogeneity and imprecisions inherent in the analytical methods, and if the original inter-flow differences were minor then alteration will act to obscure this. Hence the level down to which a particular sequence can be subdivided will

be a function of the degree of alteration, the magnitude of the pristine compositional diversity and the nature of the exposure.

In conclusion, only chemical criteria perhaps in conjunction with palaeomagnetic data are likely to produce a reliable method of sub-dividing flood basalt lava sequences. The exact methodology of stratigraphical classification adopted for each CFB province has varied slightly in response to the particular local conditions.

(a) *Deccan Traps.*

The lava sequences of the Deccan Traps have been divided into at least ten stratigraphical formations illustrated in figure 2.3(a) (from Beane *et al.*, 1986). A 'Formation' is defined as "a packet of flows characterised by, though not necessarily entirely made up of, a given magma type", (Cox and Hawkesworth, 1984), *i.e.* "a regionally mappable group of stratigraphically adjacent flows", (Beane, 1988). Cox and Hawkesworth (1984) did not attempt to correlate individual flows or groups of flows between sections, but lower down in the stratigraphical succession, Beane *et al.* (1986) could occasionally recognise locally mappable groups of identifiable flows, termed 'Members', within a particular formation. There is a certain amount of interbedding of flows of different magma types near the formation boundaries and in addition, several flows show transitional characteristics. This means that fixing the position of the formation boundary in a particular section relies either on deciding at what stratigraphical level a specific magma type becomes dominant or alternatively in having a formation definition that is based on the first appearance of a certain magma type.

(b) *Columbia River.*

The Columbia River basalts are one of the youngest CFB provinces and their accessibility, freshness and extent of exposure have made them one of the world's most comprehensively studied provinces. A combination of detailed field mapping plus extensive chemical analyses and palaeomagnetic determinations by

Subgroup	Formation	Members and Chemical Types (CT)
WAI	Mahabaleshwar	(Incomplete)
	Ambenali	Ambenali CT
	Poladpur	Main Poladpur
		Ambavne
LONAVALA	Bushe	Bushe CT
		Pingalvadi
		Bushe CT
		Shingi Hill
		Bushe CT
		Picrite basalt
		Bushe CT
	Khandala	Rajmachi basalt
		Kp (2)
		Kaf_3 (2)
		Boyhare basalt (Kb)
		Kaf_2 (2)
		Kp (2)
		Kp (2)
		Kaf_1 (2)
		Dhak Dongar basalt
		Kcg (2)
		Monkey Hill GPB
		Giravali GPB
KALSUBAI	Bhimashankar	Bhimashankar CT
		Manchar GPB
	Thakurvadi	Thakurvadi CT
		Water Pipe Member
		Thakurvadi CT
		Picrite basalt
		Jammu Patti Member 3
		Jammu Patti Member 2
		Jammu Patti Member 1
	Neral	Tunnel 5 GPB
		Picrite basalt
		Neral CT
		Tembre basalt
		Ambivili picrite basalt
	Igatpuri	Kashele GPB
		Igatpur CT
		Thal Ghat GPB
	Jawhar (Incomplete)	Jawhar CT
		Kasara phyric basalt

(a) Lava stratigraphy of the **Deccan** basalts.

(b) Lava stratigraphy of the **Columbia River** basalts.

Formation	Member	Magnetic Polarity	K/Ar Dates
Saddle Mountains Basalt	Lower Monumental	N	6 my
	Ice Harbor	N,R	8.5 my
	Buford	R	
	Elephant Mountain	N,T	10.5 my
	Pomona	R	12 my
	Esquatzel	N	
	Weissenfels Ridge	N	
	Asotin	N	
	Wilbur Creek	N	
	Umatilla	N	13.5 my
Wanapum Basalt	Priest Rapids	R	
	Roza	T,R	
	Frenchman Springs	N	
	Eckler Mountain	N	14.5 my
Picture Gorge Basalt R_2 / N_1	Grande Ronde Basalt	N_2	
		R_2	
		N_1	
		R_1	16.5 my
Imnaha Basalt		T	
		N_0	
		R_0	17.5 my

Figure 2.3 Examples of chemical stratigraphical schemes developed in other CFB provinces; (a) Deccan (Beane *et al.*, 1986), (b) Columbia River (Hooper, 1988).

numerous workers (*e.g.* Swanson *et al.*, 1979; Mangan *et al.*, 1986) has established a detailed stratigraphical succession within the basalts. In total, five formations have been recognised, with two being further subdivided into numerous members as shown in figure 2.3(b) (from Hooper, 1988). In several cases, individual flows have been correlated across the whole basin back to their feeder dykes allowing a reconstruction of the magnitude of the eruption. The Grande Ronde Formation comprises the vast bulk (~85% by volume) of the Columbia River basalts. During their eruption there were three polarity reversals which leads to four well defined magnetostratigraphic units. A detailed study by Mangan *et al.* (1986) delineated chemical sub-units within these magnetostratigraphic units. Five main chemical groupings could be recognised within the Grande Ronde basalts, and flows or packets of flows of each chemical type were correlated between field sections to define specific chemical stratigraphic sub-units. Each sub-unit was about 30 m to 150 m thick made up of several flows and represented an individual eruptive event ("one or more eruptions closely spaced in time that produced lavas of similar chemistry", Mangan *et al.*, 1986). The sub-units of most chemical types were repeated at irregular intervals and there were no progressive chemical trends through the Grande Ronde formation.

The approach adopted in this thesis for the lava sequences in the Paraná differs from that employed for the Deccan and Columbia River suites in that no attempt has been made to outline stratigraphical formations. Instead, the main aim was to recognise and characterise regionally applicable magma types and then essentially to map out their distribution throughout the basin. In this manner, it was similar to the initial stages of the Deccan studies where magma types were established before the definition of specific formations. This approach was necessitated by the type of exposure found in the Paraná region as well as by the current state of studies on the province which have tended to be of a more basin-wide scale. In areas where several closely spaced sections were investigated, the finer details of stratigraphical variations within a specific magma type could then be considered.

2.3 Stratigraphical studies in the Paraná.

2.3.1 State of play in the Paraná.

Stratigraphical studies of the flood basalt sequences of the Paraná are still in their early stages and, as yet, there is not a complete consensus between the various groups working in the region as to the classification and nomenclature of geochemical units recognised within the lavas.

The basalts exhibit a wide spectrum of major and trace element abundances (*e.g.* TiO_2 - 0.8 to 4.3 wt%, P_2O_5 - 0.10 to 0.65 wt%, Sr - 150 to 1100 ppm, Zr - 70 to 360 ppm), and this diversity has allowed the lavas to be grouped into several geochemical units. The initial classification divided the basalts into two groups based on their Ti and P contents (Bellieni *et al.*,1984a; Mantovani *et al.*, 1985a). The low-Ti or LPT group was characterised by < 2 wt% TiO_2 and < 0.35 wt% P_2O_5 whereas the high-Ti or HPT group had > 3 wt% TiO_2 and > 0.4 wt% P_2O_5. This had significant implications for the understanding of the evolution of the province since there was a distinct geographical bias to their distribution, with the high-Ti rocks dominant in the north of the basin and the low-Ti in the south (Bellieni *et al.*, 1984a).

Continued work over the last few years by several groups (*e.g.* Fodor *et al.*, 1985a; Petrini *et al.*, 1987; Piccirillo *et al.*, 1988a; Peate *et al.*, 1988a) has revealed a more complex story, highlighting subtle but resolvable variations within the two groups of the original simple scheme, as well as proposing other new magma types. The Paraná basin has been arbitrarily subdivided into three main regions separated by two roughly east-west trending tectonic/magnetic lineaments *viz.* Southern Paraná - south of the Rio Uruguai lineament, Central Paraná - between the Rio Uruguai and Rio Piquiri lineaments, Northern Paraná - north of the Rio Piquiri lineament (Bellieni *et al.*, 1986b). This division was initially made, presumably to facilitate the handling of a large data set covering such an extensive area but unfortunately it has become ingrained within the literature as representing a fundamental influence on the chemistry of the lavas even though these lineaments have no obvious control on the nature and distribution of the magma types at the surface. These

factors have all combined to make the present nomenclature of geochemical units within the Paraná lavas very confusing. The chemical definitions for most of the groups are still rather vague and there are uncertainties as to their basin-wide applicability. Therefore one of the principal aims of this chapter is to try and clarify the status of the magma types and tighten up the chemical criteria needed to assign flows to a specific magma type.

2.3.2 Availability of stratigraphical data for the Paraná lavas.

The ease of stratigraphical work within a particular province is dictated largely by the overall physiography of the lava field. In the Paraná region, the greater part of the province is devoid of suitable sections for stratigraphical sampling as sufficient topographic relief is rarely achieved. There is a lack of any major incised rivers, and no escarpment is developed to the west in Paraguay and to the north in Mato Grosso do Sul and São Paulo states. Work is further hampered in the north-west, and to the south in Argentina, by an extensive cover of Late Cretaceous (Bauru formation) and younger sediments that obscures over a third of the total areal extent of the lavas (Schobbenhaus *et al.*, 1984). This has meant that sampling over most of the province has mainly been of surface samples with little or no stratigraphical control. Because of these problems, most detailed studies have concentrated on the extreme south-east of the province where the lavas form a prominent escarpment, the "Serra Geral". This escarpment, reaching a maximum height at Morro da Igreja of 1820 m, is marked by a sudden rise of nearly 1000 m over just a few kilometres laterally, from the coastal plain up to the flat-lying lava plateau. Stratigraphical profiles are restricted to road sections cutting the escarpment because of the problems of accessibility due to the dense vegetation cover and the often precipitous drop, which also prevent the visual tracing of individual flows between sections. Along the coastal segment of the Serra Geral escarpment, in Santa Catarina and Rio Grande do Sul states, lava sequences of up to 750-800 m are exposed although once the escarpment turns inland this thickness decreases to 350-400 m (Bellieni *et al.*, 1986b). Data from fourteen profiles, covering a distance of about 550 km along the escarpment, are available and are summarised in Bellieni *et al.* (1986b), Mantovani *et al.* (1985a) and Hawkesworth *et al.* (1988). Work carried out in this

study has extended the coverage to the north, adding five more stratigraphical profiles in Santa Catarina state, where the Serra Geral escarpment becomes less distinct.

In order to define and map out many of the magma types, reliance will have to be made on the wealth of geochemical data that exists in the literature from samples collected throughout the whole basin (*e.g.* Bellieni *et al.*, 1986a; Petrini *et al.*, 1987). These samples are often only given a generalised location, *i.e.* Northern, Central or Southern Paraná basin, rather than having each analysis accompanied by specific details of its locality, topographic height and relationship to other sampled flows that might assist in the task of mapping out the surface distribution of the magma types and in developing a basin-wide stratigraphy. Considering the huge areal extent of the Paraná magmatic event, the biasing of the available stratigraphical data to just the south-east portion, a restricted area within the province, places severe limitations on any interpretation regarding models for its geodynamic evolution, but the coverage of the rest of the province away from the south-east has been less systematic. A few road sections have been studied from the central regions of the basin, in western Santa Catarina and Paraná states (Nardy, 1988), but apart from these, the data are restricted to scattered surface samples, which as well as literature data include a suite of samples collected from the western and southwestern extremities of the exposed province in Paraguay and Argentina during the course of this study.

A totally new avenue of investigation of the Paraná lava sequences was afforded when access to samples of drill-core chippings from oil exploration boreholes in the central regions of the plateau was obtained. These provided a unique opportunity to develop the stratigraphy of an otherwise inaccessible area. This work has been carried out in conjunction with Prof. M.S.M. Mantovani at São Paulo University, Brazil, to whom the samples had been made available by Petrobrás through Paulipetro, and is still in progress. Representative samples analysed from nine boreholes along a 650 km north-south cross section have provided the first impressions of the stratigraphy of the deeper unexposed portions of the lava pile and have revealed a consistent pattern of distribution of magma types.

2.4 Magma types in the Paraná.

2.4.1 Methodology.

Our aim is to be able to uniquely assign any given unknown Paraná sample to a particular magma type, and in order to carry this out, a set of diagnostic features that describe each magma type need to be established. The choice depends on their ability to resolve the compositional differences between the various magma types. Since stratigraphical studies in the Paraná are still in the 'development-stage', it is important that the criteria chosen should be as widely applicable as possible, and restricting their choice to the elements commonly determined by the XRF-method {majors + certain trace elements, Rb, Ba, Sr, Zr, Y, Ni, Cu, Zn, (Nb), (V)} would allow any published analyses to be re-evaluated in the light of the new magma type definitions. This would then hopefully lead to a rapid expansion in the development of a regional geochemical stratigraphy for the Paraná province. Use of INAA or isotope data might help clarify the definitions of, and highlight important fundamental differences between, the various magma types but such criteria are not realistically employable for any large-scale reconnaissance studies.

The results of surface weathering and hydrothermal alteration are almost inevitably present at outcrop throughout the Paraná lava sequences and hence caution must be exercised when taking an analysed rock sample as being representative of the original erupted magma composition. The geochemical effects of these secondary processes on the Paraná samples are discussed in more detail in sections 2.5.2 and 2.7.2. In keeping with other more extensive studies, (*e.g.* Marsh and Eales, 1984; Wood *et al.*, 1976) certain elements, especially the alkali and alkaline-earth elements Rb, Ba, K, are known to be more susceptible to mobilisation during alteration. Therefore to recognise and discriminate between the various magma types more reliance will be placed on the more immobile elements such as the high-field strength (HFS) elements Ti, Zr, Y that give a truer reflection of the pristine magmatic composition.

The lavas defining a given magma type will all have enjoyed varying degrees of crystal fractionation, and for magma types where some of their geochemical characteristics

are similar then the results of this shallow level fractionation on lava chemistry must be considered. For example, a sample with 250 ppm Zr could either be an evolved low-Ti magma or a primitive high-Ti magma, and using Zr as the sole classification criterion will be ambiguous. To minimise these fractional crystallisation effects, ratios of incompatible elements or isotopic ratios may be more useful in 'fingerprinting' magma types.

Unfortunately, for many of the elements that can be used as discriminants because they show relative depletions and enrichments between different magma types, the compositional range of such an element within a particular magma type often has a certain amount of overlap with that in another magma type. This can lead to ambiguities, and caution is needed if the composition of an unknown sample lies close to the defined boundary between two magma types. This further emphasizes the need to consider several characteristics when delineating magma types, and ultimately when classifying flows. An additional point to be wary of is flows possessing truly transitional characteristics, that is, flows whose compositions consistently lie between the fields defining two magma types, a feature that could possibly be a result of high-level magma mixing.

Examination of the chemical composition of the Paraná lavas by surveying numerous bivariate element or elemental ratio plots allows the initial recognition of the different magma types including which elements and/or ratios best discriminate between the types. As part of this process of defining magma types, as well as in the subsequent assignment of unknown samples, it is important to take into consideration the geographical location and stratigraphical position of the sample otherwise subtle regional differences hidden away within the overall compositional field for a particular magma type might be missed.

The above methodology, outlining the process of setting up of the magma types to be used in this thesis, has produced a preliminary set of proposed limits on compositional range for specific elements and/or ratios within each magma type. This has demonstrated the existence of distinct magma types but in order to further clarify problems of overlap between types, it is desirable that the next step should be to use a computer-based system

capable of dealing with a large number of variables and employ some form of multivariate analysis which allows all elements within the data set to be considered simultaneously, an advancement on the restrictions of using bivariate diagrams. This will be necessary to be able to handle the large amounts of data on the Paraná lavas now becoming available, especially with the near completion of our borehole sample suite (~300+ analyses) and the imminent release of the large (~1500 analyses) data set generated by the group working under E.M. Piccirillo at Trieste, Italy (Piccirillo and Melfi, 1988). Discriminant function analysis (DFA) was used in a similar study of the Karoo basalts by Duncan *et al.*, (1984), as this produced an effective means of recognising multivariate differences between groups of samples and also of indicating which elements were the most effective discriminants. It is important to emphasize that DFA can not be used as a primary classification tool but requires the data to be pre-defined into groups prior to use. DFA works by attempting to find a function that is a linear combination of the variables (*i.e.* elements) in the data set such that it produces the maximum difference between the classified groups of samples. This method should improve the resolution between magma types and hopefully allow a more successful allocation of unknown samples to the defined magma types.

2.4.2 Background to Paraná lavas.

The products of the Paraná magmatic event show a marked bimodal distribution in terms of SiO_2, and as a generalisation can be thought of as either 'Basaltic' (< 60 wt% SiO_2) or 'Acidic' (> 60 wt% SiO_2). The following sections will concentrate on the basalt (*sensu lato*) magma types, returning to consider the rhyolites in section 2.4.5. In keeping with the current literature nomenclature, the Paraná basalts will be initially screened by their TiO_2 content and divided into either 'High-Ti' (> 2 wt% TiO_2) or 'Low-Ti' (< 2 wt% TiO_2), although it is important to note that the 'High-Ti' lavas fall naturally into two sub-groups, one with truly high-Ti contents (> 3 wt% TiO_2) and the other with more intermediate Ti contents (2-3 wt% TiO_2), a point that will be elaborated on in the following section. Care must be exercised when dealing with evolved basaltic samples since these might have fractionated Fe-Ti oxides and therefore could have lower than expected TiO_2

Basalt magma types **(SiO_2 < 60 wt%)**

High-Ti (> 2 wt% TiO_2)

Urubici	HTiB[1], HTi(S)[2], HPT[5,7], Khumib[11]
Pitanga	HTiB[1], HTi(N)[2], HPT[8]
Paranapanema	HTiB[1], ITi[6], IPT[8], sector III[9]
Votuverava	HPTen[8]

Low-Ti (< 2 wt% TiO_2)

Gramado	LTiB[1], LTi(S)[2], LPT[5,7], sector II[9], Tafelberg[10], Albin[10]
Esmeralda	LTiB[1], LPTupper[7], sector I[9]
Ribeira	LTi(N)[2], group A[4]

Rhyolite magma types **(SiO_2 > 60 wt%)**

Palmas	PAV[3], LPT rhyolite[8], Tafelberg quartz latites[10]
Chapecó	CAV[3], HPT rhyolite[8], Sarusas quartz latites[11]

1	Bellieni *et al.*, (1984a).
2	Marques *et al.*, (1988).
3	Bellieni *et al.*, (1984a).
4	Petrini *et al.*, (1987).
5	Mantovani *et al.*, (1985a).
6	Mantovani *et al.*, (1988).
7	Peate *et al.*, (1988a).
8	Hawkesworth *et al.*, (1988).
9	Fodor *et al.*, (1985a).
10	Erlank *et al.*, (1984).
11	Duncan *et al.*, (1988).

Table 2.1 Proposed new nomenclature scheme for the magma types of the Paraná-Etendeka CFB province, together with their synonyms from the literature sources given.

contents. The details of these 'High-Ti' and 'Low-Ti' groups are discussed in sections 2.4.3 and 2.4.4 respectively, and within both of these groups at least three distinct magma types can be recognised. As well as combining a survey of the Paraná literature information and the new data from this thesis, studies of the Etendeka sequences in Namibia will also be considered since these all effectively form part of the same magmatic episode. The preliminary data on the Etendeka lavas has similarly recognised distinct magma types and these will be integrated into the Paraná scheme.

The literature has spawned a multitude of names to describe the various groups and sub-groups within the lavas, often with several names to cover essentially the same magma type; for example, the Gramado magma type as used in this study has also been called 'LPT' by Mantovani *et al.*, (1985a), 'LTi(S)' by Marques *et al.*, (1988), 'Sector II' by Fodor *et al.*, (1985a), and in the Etendeka, 'Tafelberg' and 'Albin' by Erlank *et al.*, (1984). Table 2.1 is an attempt to clear up the magma type nomenclature. It summarises all of the pre-existing names used in the literature and their equivalents, and lists the proposed new names to be used in this thesis for the magma types as defined in table 2.2. It is hoped that that this scheme will become by agreement adopted (or adapted) by other workers in this area. Table 2.2 gives a list of the diagnostic features for each of the main magma types and their average compositions taken from the data in this study are listed in table 2.3.

	(a) 'High-Ti' magma types			(b) 'Low-Ti' magma types			(c) Rhyolites	
	Urubici	Pitanga	Paranapanema	Gramado	Esmeralda	Ribeira	Chapecó	Palmas
TiO_2 (wt%)	> 3.3	> 2.9	1.8 - 3.2	< 1.8	1.3 - 2.2	1.5 - 2.1	0.9 - 1.5	0.6 - 1.1
P_2O_5 (wt%)	> 0.45	> 0.35	0.2 - 0.7	< 0.35	< 0.35	0.2 - 0.4	> 0.3	< 0.35
SiO_2 (wt%)	> 50	47 - 52	49 - 51.5	> 51	50.5 - 53	49.5-51.5	63 - 68	65 - 72
Fe_2O_3 (wt%)	< 14.2	> 14.0	> 13.5	< 14.5	13 - 16	12 - 15		
Sr (ppm)	> 600	400 - 600	< 430	< 430	< 250	> 250	> 250	< 170
Ba (ppm)	> 450	340 - 700	< 410	< 540	< 350	250 - 500	> 900	< 800
Zr (ppm)	> 270	200 - 440	< 250	< 250	< 200	< 170	> 500	< 400
Sr/Y	> 10.5	> 10	> 10.5	< 11	< 7	> 8		
Ba/Y	> 11.5	9.0 - 14.5	4.5 - 13	7.5 - 14.5	< 8	> 8.5		
Zr/Y	> 7	5.5 - 8	4.5-6	4.0 - 5.5	3.0 - 4.5	4.0 - 7.0		
Ti/Y	> 500	350 - 700	300 - 500	< 300	< 300	300 - 500		
Ti/Zr	> 60	> 50	> 65	< 60	> 60	> 70		

Table 2.2 Geochemical criteria defining the proposed new Paraná magma types of this study, based on XRF analytical data only.

	(a) High-Ti magma types						(b) Low-Ti magma types				(c) Rhyolites			
	Urubici n=59		Pitanga n=53		Paranapanema n=30		Gramado n=49		Esmeralda n=16		Palmas n=50		Chapecó n=3	
	mean	s.d.	mean	s.d.	mean	s.d.	mean	s.d.	mean	s.d.	mean	s.d.	mean	s.d.
SiO_2	51.71	0.79	50.40	1.06	50.23	0.64	53.81	1.35	51.17	1.19	67.84	0.77	65.89	0.94
TiO_2	3.76	0.28	3.55	0.24	2.34	0.31	1.55	0.18	1.63	0.29	1.00	0.06	1.13	0.13
Al_2O_3	13.28	0.32	12.82	0.35	13.13	0.50	13.88	0.51	13.82	0.90	13.06	0.33	12.75	0.11
Fe_2O_3	13.28	0.52	15.29	0.71	15.05	0.93	13.25	0.89	14.14	1.04	6.38	0.51	7.80	0.17
MnO	0.17	0.01	0.22	0.02	0.22	0.02	0.20	0.02	0.24	0.09	0.11	0.01	0.12	0.03
MgO	4.56	0.34	4.41	0.55	5.24	0.72	4.59	0.79	5.44	0.83	1.26	0.24	1.75	0.13
CaO	8.19	0.50	8.36	0.77	9.25	1.03	8.40	1.03	9.89	1.19	3.11	0.37	3.49	0.34
Na_2O	2.80	0.28	2.98	0.43	3.28	1.00	2.72	0.27	2.78	0.32	3.18	0.34	3.22	0.11
K_2O	1.70	0.35	1.41	0.44	0.97	0.38	1.37	0.58	0.68	0.31	3.79	0.52	3.50	0.30
P_2O_5	0.54	0.04	0.58	0.22	0.33	0.10	0.23	0.04	0.22	0.06	0.29	0.03	0.34	0.03
Mg#	44.4	2.2	40.1	3.2	44.7	4.7	44.4	4.9	47.1	5.6	31.3	4.8	34.3	2.0
Ni	55	14	32	14	51	19	39	14	58	17	10	2	3	
V	355	21	391	59	391	47	306	41	354	49	80	10	55	
Cu	162	30	172	63	198	52	150	30	191	39	88	19	118	
Zn	118	9	131	19	122	14	108	10	107	14	79	8	141	
Ga	26	2	25	3	20	2	21	2	21	2	17	2	26	
Rb	38	11	33	14	22	9	47	23	25	14	161	28	94	
Sr	773	105	481	61	304	62	263	53	206	49	141	17	514	
Y	39	3	42	8	37	8	37	5	36	6	50	9	70	
Zr	319	28	280	50	182	34	181	31	132	35	271	10	560	
Nb	28.0	3.1	24.8	4.5	15.4	2.7	14.8	2.9	8.5	2.5	21	1	46	
Ba	638	92	470	70	301	74	402	75	235	72	701	110	1115	
La	41.3	4.10	34.9	8.81	22.0	5.35	22.3	6.15	11.6	4.64	44.8	2.92	81.0	
Ce	89.7	10.2	80.3	21.8	51.1	10.9	51.0	8.31	28.2	9.83	90.0	6.15	175	
Nd	51.0	5.66	44.9	8.47	29.2	6.32	25.9	6.28	17.6	5.31	44.4	5.07	92.2	
Sm	10.8	1.14	7.12	-	6.24	1.55	6.06	0.98	4.58	0.85	9.06	0.72	19.5	
Eu	3.46	0.31	3.10	0.69	2.09	0.39	1.66	0.27	1.56	0.24	1.87	0.15	5.35	
Tb	1.51	0.16	1.47	0.32	1.15	0.25	1.08	0.13	0.97	0.12	1.46	0.13	2.53	
Yb	2.92	0.27	3.76	0.50	3.58	0.72	3.25	0.63	3.18	0.40	4.67	0.87	5.24	
Lu	0.45	0.04	0.57	0.07	0.60	0.13	0.51	0.09	0.53	0.06	0.71	0.11	0.82	
Th	4.51	0.58	3.89	0.85	3.17	1.19	5.58	1.77	2.66	1.18	13.7	1.19	8.91	
U	1.26	0.31	1.12	0.11	1.08	0.49	1.71	0.26	0.83	0.35	4.57	0.57	1.89	
Ta	1.92	0.22	1.79	0.44	1.08	0.26	0.91	0.21	0.51	0.17	1.71	0.18	3.17	
Hf	7.73	0.73	7.00	1.59	4.75	0.94	4.13	1.02	3.16	0.72	6.97	0.46	13.9	
		n=12		n=4		n=10		n=9		n=6		n=14		n=2

Table 2.3 Average magma type compositions from the samples in this study.

2.4.3 'High-Ti' magma types.

'High-Ti' as used in most of the Paraná literature refers to samples having in excess of 2 wt% TiO_2. In the first basin-wide geochemical study of the Paraná lavas, Bellieni *et al.*, (1984a) noted that the 'very scarce' high-Ti rocks from the south were chemically distinct from those in the north. For a similar MgO content, the southern high-Ti samples

had higher P, K, Ba, Sr, Rb, Zr, La, Ce and lower Fe than their northern counterparts. T(°C) and f(O_2) data obtained on coexisting groundmass Ti-magnetite/ilmenite pairs also indicated different oxygen fugacities between the areas, with the northern high-Ti basalts forming a trend close to the NNO-QFM buffer at higher f(O_2) values than both low-Ti and high-Ti rocks from the south, which scattered around the QFM-MW buffer. The southern high-Ti rocks of Bellieni *et al.*, (1984a) all had TiO_2 > 3 wt% whereas the northern data covered a wider compositional range and included samples with 2-3 wt% TiO_2. This was noticed by Piccirillo *et al.*, (1988a) who distinguished two groups within the 'High-Ti' magmas; the high-Ti proper or HTi with > 3 wt% TiO_2, and the intermediate or ITi group with 2-3 wt% TiO_2 and contents of other incompatible elements intermediate between 'Low-Ti' and HTi. Marques *et al.*, (1988) assessed the regional variation in just the HTi group, clarifying the earlier observations of Bellieni *et al.*, (1984a), and found that at a similar MgO content, the southern HTi or HTi(S) contained higher amounts of SiO_2, K_2O, Rb, Ba, U, Th, Sr than the northern samples, HTi(N). This north-south difference in the HTi rocks was picked up during this study since the high-Ti samples from the São Joaquim road sections corresponded exclusively to the HTi(S) type whereas the boreholes contained many samples akin to the HTi(N) type. It is proposed that these are treated as independent magma types and have been given more eloquent names; the HTi(S) group is termed the Urubici magma type, and the HTi(N) is called the Pitanga magma type.

Major element variation diagrams with both the Urubici and Pitanga magma types plotted, show that the most diagnostic major elements for distinguishing between the two types are Si and Fe. For similar MgO contents, the Urubici-type lavas have higher SiO_2 and lower Fe_2O_3(t) contents than the Pitanga-type {see figures 2.4(a)and 2.4(b)}, and in addition there is a tendency for the Urubici-type to have higher TiO_2, Al_2O_3, K_2O and lower CaO contents. Both groups have the same average MgO content, but the difference in total Fe between them means that the Urubici magmas have higher Mg# (mg number, see appendix C) than the Pitanga magmas. The high Fe_2O_3(t) of the Pitanga-type (>14.2 wt%) is also accompanied by a higher Mn and V content. From the 'primitive mantle'-normalised trace element abundance plot of figure 2.9, it can be seen that on the whole the trace element

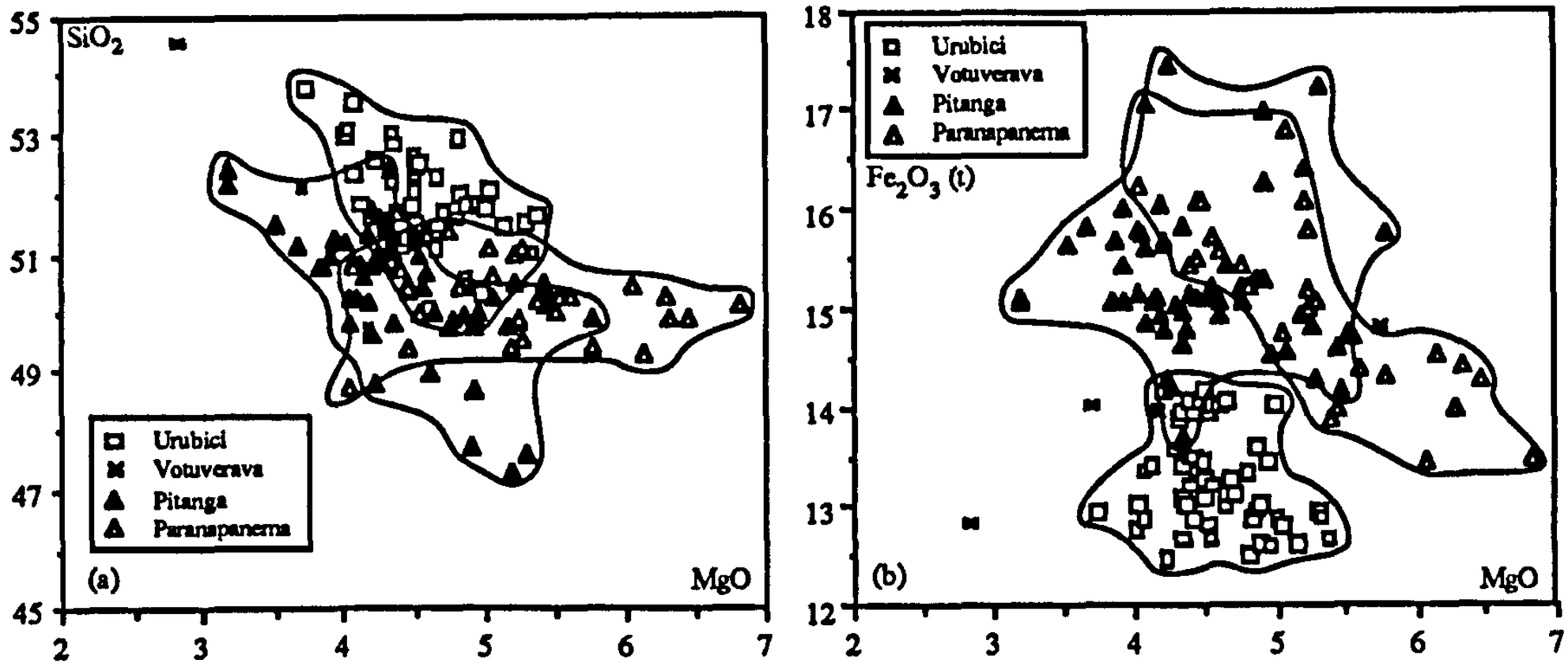

Figure 2.4 Major element variation diagrams for the Paraná high-Ti magma types: (a) MgO vs. SiO_2 - note the higher SiO_2 content of the Urubici magma type relative to the other high-Ti magmas, (b) MgO vs. $Fe_2O_3(t)$ - this shows the high $Fe_2O_3(t)$ of the northern magma types (Pitanga and Paranapanema) compared to the Urubici magma type.

signatures for the Urubici and Pitanga magma types are similar over a wide incompatability range (Rb to Ti), though with the Urubici pattern lying at higher abundances. One notable deviation from this is the abundance of Sr in the Pitanga lavas which appears to be anomalously depleted thus making it a very diagnostic feature to distinguish the two magma types; Pitanga-type has < 600 ppm Sr, Urubici-type has > 600 ppm Sr, (see figure 2.5). Because both trace element patterns are anchored at the same Y and Yb abundances, indicating that these elements have a similar distribution in the two magma types, the relative enrichment in incompatible trace elements in the Urubici-type over the Pitanga-type will be reflected in element ratios including Y or Yb, and such ratios will minimise any crystal fractionation effects within each group; *e.g.* Zr/Y and Ba/Y are both higher in the Urubici magmas. The overall similarity in the trace element patterns implies that most inter-element ratios between the elements illustrated, except those involving Sr, Y and Tb, will be the same in both magma types; *e.g.* Th/Ta is about 2.5 in both Urubici and Pitanga samples.

The basal four samples in the 'CB' borehole form a unit about 200 m thick and have a distinctive composition to that of the overlying Pitanga-type magmas. They have higher Ba, Rb, and K and are distinguished from the Pitanga magmas by having Rb/Y > 1.2 and

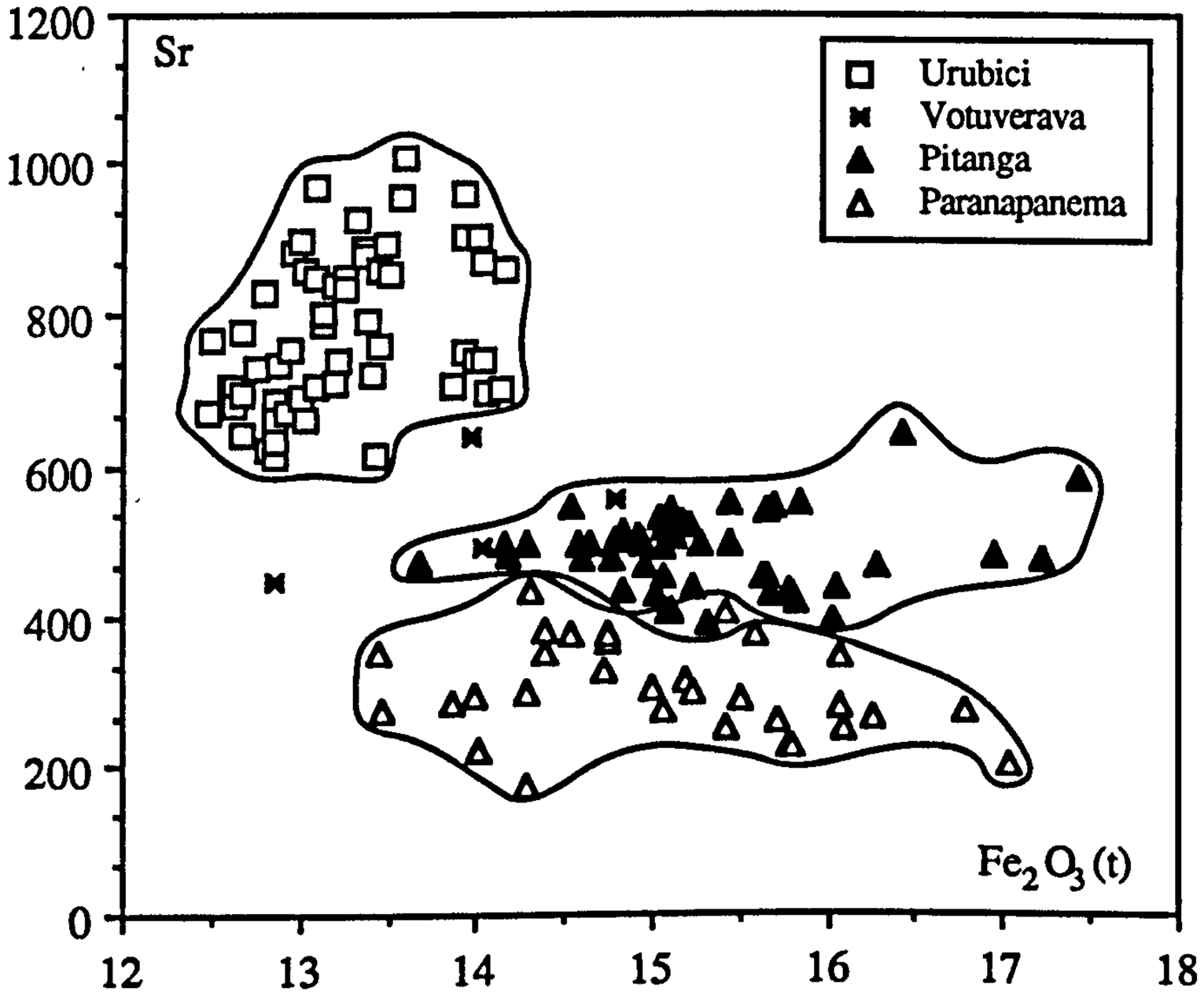

Figure 2.5 Variation of Sr vs. $Fe_2O_3(t)$ to discriminate between the various high-Ti magma types. The Urubici magma type is characterised by high Sr content (> 600 ppm) and low (< 14.2 wt%) $Fe_2O_3(t)$. The Pitanga and Paranapanema magma types both have high $Fe_2O_3(t)$ but can be distinguished from each other by Sr content greater than or less than 400 ppm respectively.

Ba/Y > 15. In this respect, as well as $Fe_2O_3(t)$ contents less than 14.8 wt%, they are similar to lavas of the Urubici magma type but important differences include their lower Sr contents (< 600 ppm) (see figure 2.5). In a preliminary report on the borehole samples, this group of samples was referred to as the 'HPT LIL-enriched' or 'HPTen' (Peate *et al.*, 1988b). Rocks of similar geochemical affinity have been reported from the north-east margin of the lava field in São Paulo state where they have been termed the Votuverava-type (M.S.M. Mantovani, pers. comm., 1989). Their temporary status as an independent magma type awaits further clarification.

Lavas of the Urubici magma type appear to have a more restricted spatial distribution than those of the Pitanga type which occur extensively throughout the basin north of about 27° S. The Urubici rocks are best exposed in the road sections at the northern end of the coastal Serra Geral escarpment, north of 29° S. They occur within the central region as far north as the Rio Iguaçu but only along the eastern margin of the province, east of 52° W (Piccirillo and Melfi, 1988). Their furthest inland extent known at

present is in the 'ES' borehole, and further to the west in the exposures of Paraguay and Argentina any HTi rocks are exclusively of Pitanga type, having < 500 ppm Sr and > 14.5 wt% Fe_2O_3(t) (Bellieni *et al.*, 1986a). The borehole data (see section 2.7) indicates that there is no direct stratigraphical link between the Urubici and Pitanga magma types and hence they are not just the result of geographical variation within a single stratigraphical unit as defined by the same magma type.

High-Ti lavas, known as the Khumib basalts, have recently been found within the Etendeka lava sequences of Namibia, and are restricted to the exposures north of 20° S (Duncan *et al.*, 1988). If Africa and South America are juxtaposed to their pre-Atlantic Ocean positions then this boundary is in an equivalent latitude to the incoming of Urubici-type magmas north of 29° S along the Brazilian Serra Geral escarpment. The average Khumib basalt, taken from Milner *et al.*, (1988) has low Fe_2O_3(t) of 12.8 wt% (*c.f.* Urubici - 13.3 wt%, Pitanga - 15.3 wt%) and high Sr of 703 ppm (*c.f.* Urubici - 773 ppm, Pitanga - 481 ppm). Figure 2.10(a) is a plot of trace element abundances normalised to primitive mantle values (Sun and McDonough, 1989) and illustrates the almost identical trace element signature displayed by both the Khumib and Urubici magmas. This geochemical equivalence between the Khumib and Urubici lavas means that they can be considered as belonging to essentially the same magma type.

Samples with intermediate Ti contents, the ITi group, have made several fleeting appearances in the literature but their existence has generally only been briefly acknowledged. The data set of Mantovani *et al.*, (1985a) included two samples from boreholes in Paraná and São Paulo states (PR-110 and SP-511) which had 2.1 wt% TiO_2, and the sector III samples (RS-73 and RS-68) in Fodor *et al.*, (1985a) from the west of Rio Grande do Sul state were also of this ITi type. The occurrence of samples with 2-3 wt% TiO_2 was noted by Piccirillo *et al.*, (1988a) but they considered them to be largely a feature of the Central region, reflecting the transition between HTi in the north and LTi in the south. Studies of the borehole samples (see section 2.7) have firmly established the ITi group as an independent magma type that forms the uppermost stratigraphical unit over most of the Paraná lava field, largely in the north but as well, the data in Bellieni *et al.*,

(1986a) and samples collected during this study also reveals extensive exposures of ITi to the west in Paraguay. It is now referred to as the Paranapanema magma type.

The Paranapanema-type lavas are clearly separated from the HTi magma types (Urubici and Pitanga) and the 'Low-Ti' magma types (see next section) on an MgO vs. TiO_2 diagram (figure 2.6), which also shows that the Paranapanema-type tend to have higher MgO contents than the HTi groups and some of these more primitive samples have TiO_2 contents down to 1.75 wt %, overlapping with the overall range of the low-Ti magma

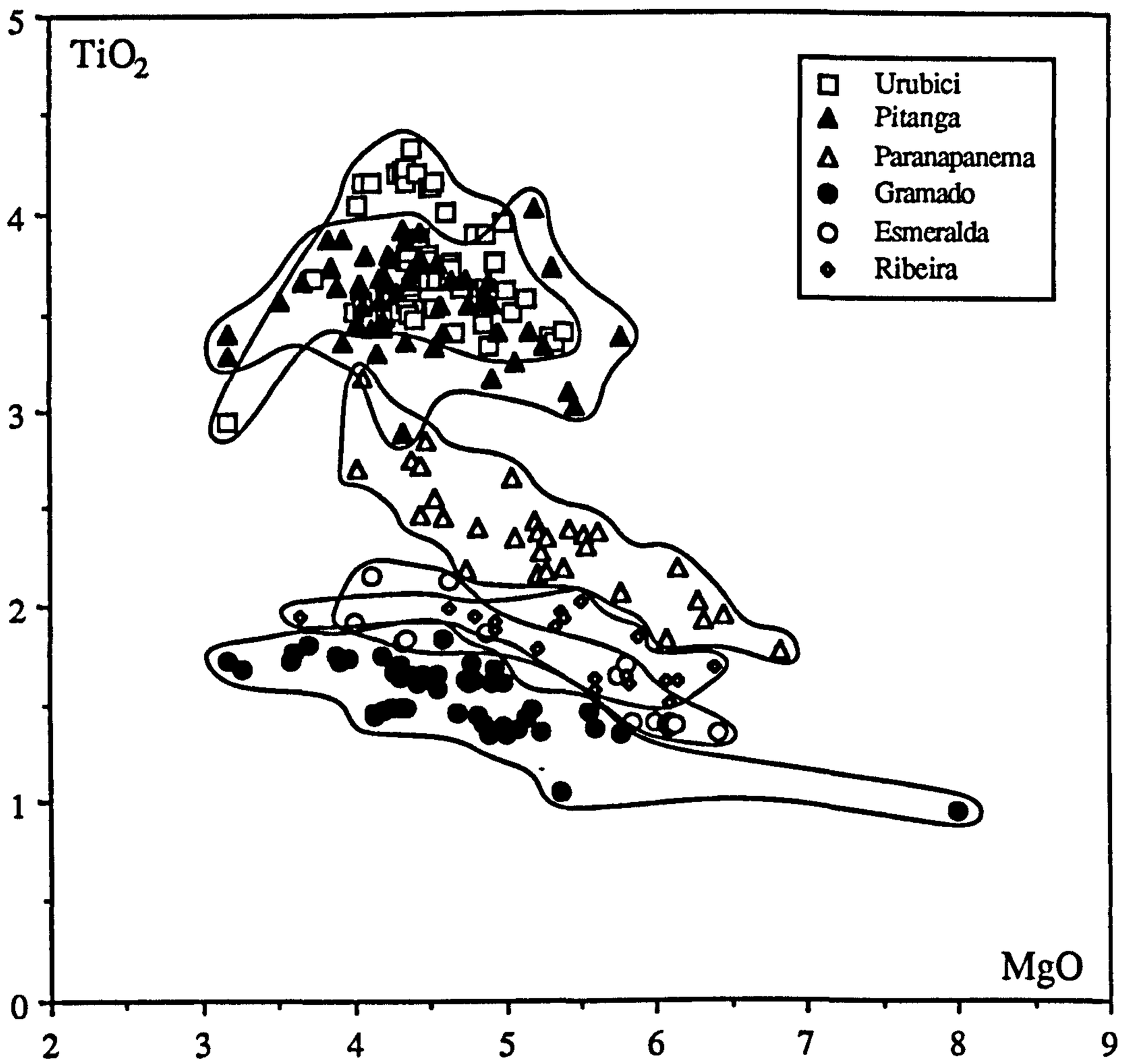

Figure 2.6 MgO vs. TiO_2 variation for all the 'basic' Paraná magma types. The Paranapanema magma type is clearly separated from the higher TiO_2 (> 3 wt%) of the Urubici and Pitanga magma types, and from the three low-Ti (< 2 wt%) magma types. All data is from this study {Urubici / Gramado / Esmeralda - São Joaquim road sections; Pitanga / Paranapanema - boreholes} except for Ribeira-type (Petrini *et al.*, 1987). The Ribeira and Esmeralda low-Ti magma types are displaced to higher TiO_2 contents relative to the Gramado magma type.

types. The Paranapanema-type share some of the major element features of the Pitanga-type, namely higher $Fe_2O_3(t)$ {see figure 2.4(b)} and lower K_2O relative to the Urubici magma type. Most of the incompatible elements have generally lower abundances in the Paranapanema-type lavas than those of the HTi types, *i.e.* lower Ba, Sr, Zr, Nb, P, but similar Y contents. This difference is reflected by the low Zr/Y < 6.0 and low Sr < 430 ppm of the Paranapanema-type lavas. All the high-Ti magmas are characterised by having the same Th/Ta ratio of about 2.5 but at different Ta/Yb values, (Urubici > 0.58, Pitanga 0.41-0.55, Paranapanema 0.25-0.33).

From out present knowledge, the isotopic abundances of Sr, Nd and Pb do not uniquely discriminate between the three high-Ti magma types, though more subtle differences do exist. The ranges in these isotopes are generally more restricted than those found in the low-Ti magmas. Extensive isotopic studies have been carried on samples of the Urubici magma type (this study; Mantovani *et al.*, 1985a; Hawkesworth *et al.*, 1986). The Urubici-type lavas have; $(^{87}Sr/^{86}Sr)_i$ 0.7048-0.7062, $(^{143}Nd/^{144}Nd)_i$ 0.51219-0.51242, and $^{206}Pb/^{204}Pb$ 17.06-18.23. Assessing the isotope data for the northern high-Ti magma types is more problematical because in the literature the Pitanga and Paranapanema groups have generally been considered together as one group. The review of Sr isotopic data in Cordani *et al.*, (1988) indicates a total range in $(^{87}Sr/^{86}Sr)_i$ from 0.7054 to 0.7082 for the high-Ti rocks from the northern half of the lava field, with a mean value of 0.7062, which contrasts with the average of the Urubici magma type of 0.7052. Piccirillo *et al.*, (1987) looked at the high-Ti basalts from near Piraju, São Paulo state, which had initial Sr ratios of 0.7058-0.7078. Using the criteria of table 2.2 these samples can be assigned to either the Pitanga or Paranapanema magma type, and it is apparent that whilst the Pitanga magmas have almost constant $(^{87}Sr/^{86}Sr)_i$ of 0.7059-60, the Paranapanema-type span a wide range from 0.7058-0.7078. Samples of the Paranapanema magma type taken from both the boreholes, and surface exposures in Paraguay, and including those in the data sets of Mantovani *et al.*, (1985a) and Fodor *et al.*, (1985b), had a range in $(^{87}Sr/^{86}Sr)_i$ of 0.7055-0.7068, whereas Pitanga-type samples from the boreholes gave a narrower range of 0.7055-0.7058. From this survey it appears that whilst

the Pitanga magma type is characterised by quite a narrow range in $(^{87}Sr/^{86}Sr)_i$ of 0.7055-60, in the Paranapanema type there is a more considerable variation from 0.7055-0.7078. The only Nd data on the northern rocks is given in Cordani *et al.*, (1988) as measured $^{143}Nd/^{144}Nd$ ratios. If a realistic average Sm/Nd of 0.22 is assumed for these samples then the range of initial $^{143}Nd/^{144}Nd$ ratios is 0.51216-0.51227. This lies to the less radiogenic end of the range found for the Urubici magma type, and together with the average $(^{87}Sr/^{86}Sr)_i$ data outlined above, indicates that the Urubici magma type appear to have more depleted isotopic compositions than the other high-Ti magma types. Pb isotopic information on the northern magma types is sorely lacking. A few of the Paranapanema-type samples collected from Paraguay were determined for Pb isotopes and, together with unpublished Paranapanema analyses (Cordani *et al.*, 1988), give a range in $^{206}Pb/^{204}Pb$ of 17.8-18.15. Selected Paranapanema-type and Pitanga-type samples from the boreholes were also analysed but these gave rather anomalous results (see section 2.7.2). Thus at present the Pitanga type is uncharacterised for Pb isotopes, a situation that should be remedied in view of its role as the most voluminous high-Ti magma type.

2.4.4 'Low-Ti' magma types.

Rocks with less than 2 wt% TiO_2, 'Low-Ti', are generally concentrated in the southern half of the basin, though there are a few isolated examples in the north (Petrini *et al.*, 1987). In a study of lavas from Southern Brazil, Fodor *et al.*, (1985a) recognised three distinct sub-groups within their data set, which also corresponded to a specific geographical location, denoted by sectors I, II and III. The relatively minor sector III samples were characterised by higher Ti, Sr, Ba, and P contents and in fact actually classify with flows of the Paranapanema magma type. The other two sub-groups were distinguished largely due to differences in Fe, K, Rb and Ba; the sector I rocks had higher total Fe and lower K, Rb, and Ba than the sector II rocks. Examination of the data acquired during this study on the lavas and dykes of the São Joaquim area also showed two sub-groups within the low-Ti rocks, recognised on both trace element and isotopic grounds, and these had compositional characteristics consistent with the two sub-groups of Fodor *et al.*, (1985a). In Peate *et al.*, (1988a) these were referred to as the LPT and LPTupper groups. These new data have

allowed stricter definitions of these groups and have also shown that they form stratigraphically coherent units. Hence they are considered here as two separate and distinct magma types; (i) the sector I and LPTupper samples are now being called the Esmeralda-type, and (ii) the volumetrically more significant sector II and LPT lavas are termed the Gramado magma type.

Two papers recently have dealt with variations within the low-Ti magmatism throughout the whole of the Paraná lava field. Marques *et al.*, (1988) outlined the marked differences in low-Ti basalts from the northern {LTi(N)}, and southern {LTi(S)} Paraná respectively; at similar MgO, the LTi(N) have higher P, Ti, Fe, Sr, Ta and lower Si, K, Rb, Ba, U, Th relative to the LTi(S), LPT or Gramado-type. Petrini *et al.*, (1987) divided the low-Ti basalts into sub-groups based primarily on initial Sr ratios, and also trace element characteristics. The samples with $(^{87}Sr/^{86}Sr)_i < 0.706$ fell into two groups A and B which were relatively enriched in incompatible elements (*e.g.* av. K_2O 0.85%, Ba 346 ppm, Sr 289 ppm, Rb 16 ppm, Zr 132 ppm) or relatively depleted (*e.g.* av. K_2O 0.31%, Ba 178 ppm, Sr 179 ppm, Rb 11 ppm, Zr 93 ppm) respectively. The group A samples were restricted to the northern half of the basin, north of about 26° S and are the equivalent of the LTi(N) group of Marques *et al.*, (1988). They will now be referred to as the Ribeira magma type.

Considering rocks with a similar MgO content, those of the Esmeralda magma type have higher TiO_2 (figure 2.6) and $Fe_2O_3(t)$ and lower SiO_2 and Al_2O_3, relative to the Gramado-type lavas {figures 2.7(a) and 2.7(b)}. The behaviour of V is analogous to that of $Fe_2O_3(t)$, and Y is also slightly enriched in the Esmeralda-type samples. In contrast, the majority of the incompatible elements *e.g.* Zr, Nb, Ba are all depleted though with K, Rb, Sr to a lesser extent, and consequently ratios such as Zr/Y, Nb/Y, Ba/Y are all lower in the Esmeralda samples. For example, Zr/Y: Gramado 4.0-5.5 vs. Esmeralda 3.0-4.5. The ratios Ti/Zr and Ti/Nb proved to be the clearest discriminant between the groups, with the Esmeralda-type characterised by Ti/Zr > 60 and Ti/Nb > 750 {see figure 2.8(a); Ti/Zr vs. Zr/Y}. Another notable feature of the Esmeralda-type is the high Zr/Nb which on the whole

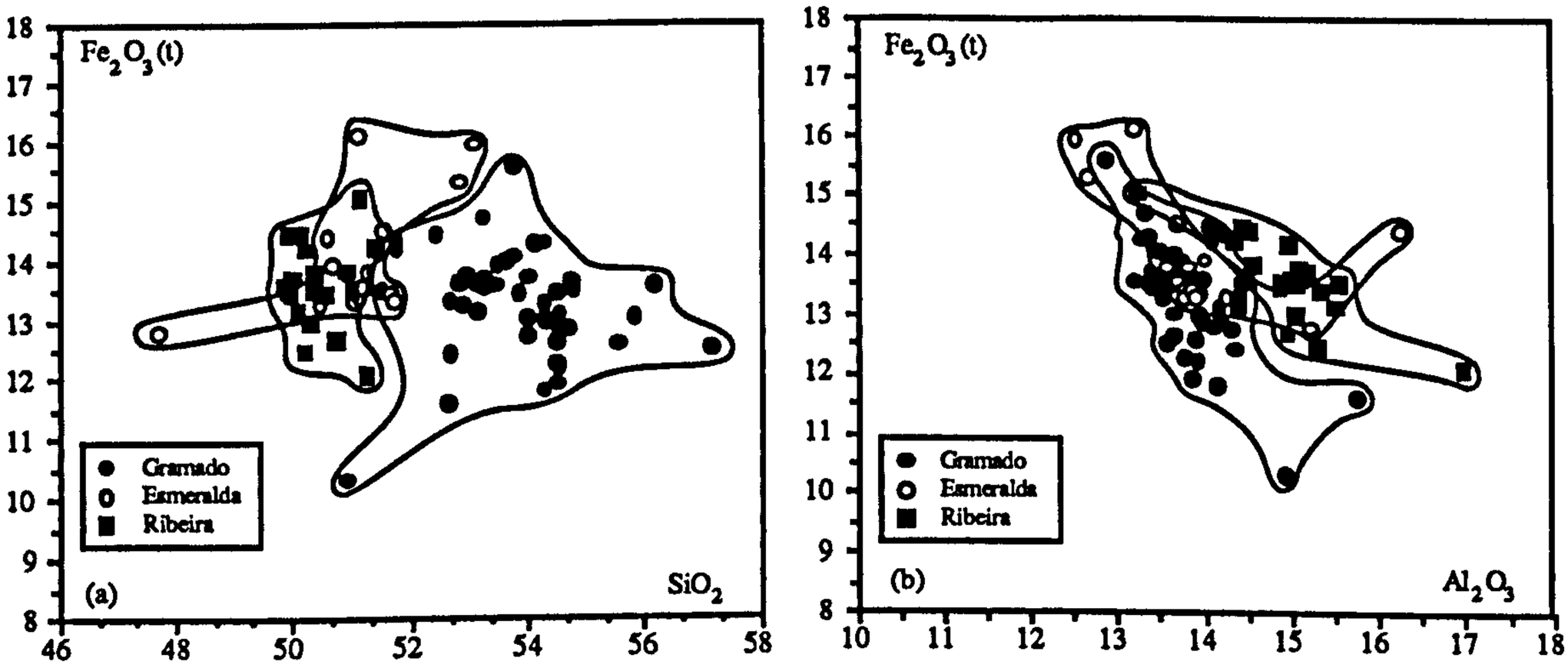

Figure 2.7 Major element variation diagrams for the Paraná low-Ti magma types: (a) $Fe_2O_3(t)$ vs. SiO_2 - this illustrates the lower $Fe_2O_3(t)$, higher SiO_2 of the Gramado magma type relative to the Esmeralda and Ribeira magma types, (b) $Fe_2O_3(t)$ vs. Al_2O_3 - the Gramado magma type is displaced from the Esmeralda and Ribeira magma types to lower $Fe_2O_3(t)$ and Al_2O_3. Note that on both diagrams the Esmeralda and Ribeira magma types are indistinguishable.

varies between 14 and 19 compared with the range in all other Paraná magma types of 10 to 14. The Esmeralda magma type is also distinctive for the range it displays in certain incompatible trace element ratios, ratios that maintain virtually constant values within all the other magma types. For instance, Sm/Nd, which is relatively restricted in the Gramado magma type (0.21-0.23), has a considerable range of 0.22-0.29 in the Esmeralda magma type.

The Ribeira and Esmeralda magma types share several similar geochemical features, and it is worth contrasting the different behaviour of elements in Ribeira and Esmeralda relative to the Gramado magma type. For major elements, both magma types are enriched in TiO_2 (figure 2.7) and depleted in SiO_2 but, whereas Al_2O_3 is lower and $Fe_2O_3(t)$ higher in the Esmeralda-type magmas, the reverse is true for the Ribeira-type {see figures 2.7(a) and 2.7(b)}. The extent of LREE enrichment in both types is less than in the Gramado-type, though the Ribeira-type is notable amongst the low-Ti rocks in having Eu/Eu* generally in excess of 1 (1.03 ± 0.06), (Marques *et al.*, 1988). The difference between the Ribeira and Esmeralda magma types is clearly illustrated on figures 2.8(a) and 2.8(b). Figure 2.8(a) shows that, although both the Esmeralda and Ribeira magma types have similar $Ti/Zr > 60$ which distinguishes them from the Gramado magma type, the Ribeira-type magmas have

higher Zr/Y. Similarly on figure 2.8(b), the difference between the Esmeralda and Ribeira magma types is highlighted by the low Ba/Y (< 8) and low Sr/Y (< 7) of the Esmeralda magma type compared to the higher and more variable ratios in the Ribeira-type magmas.

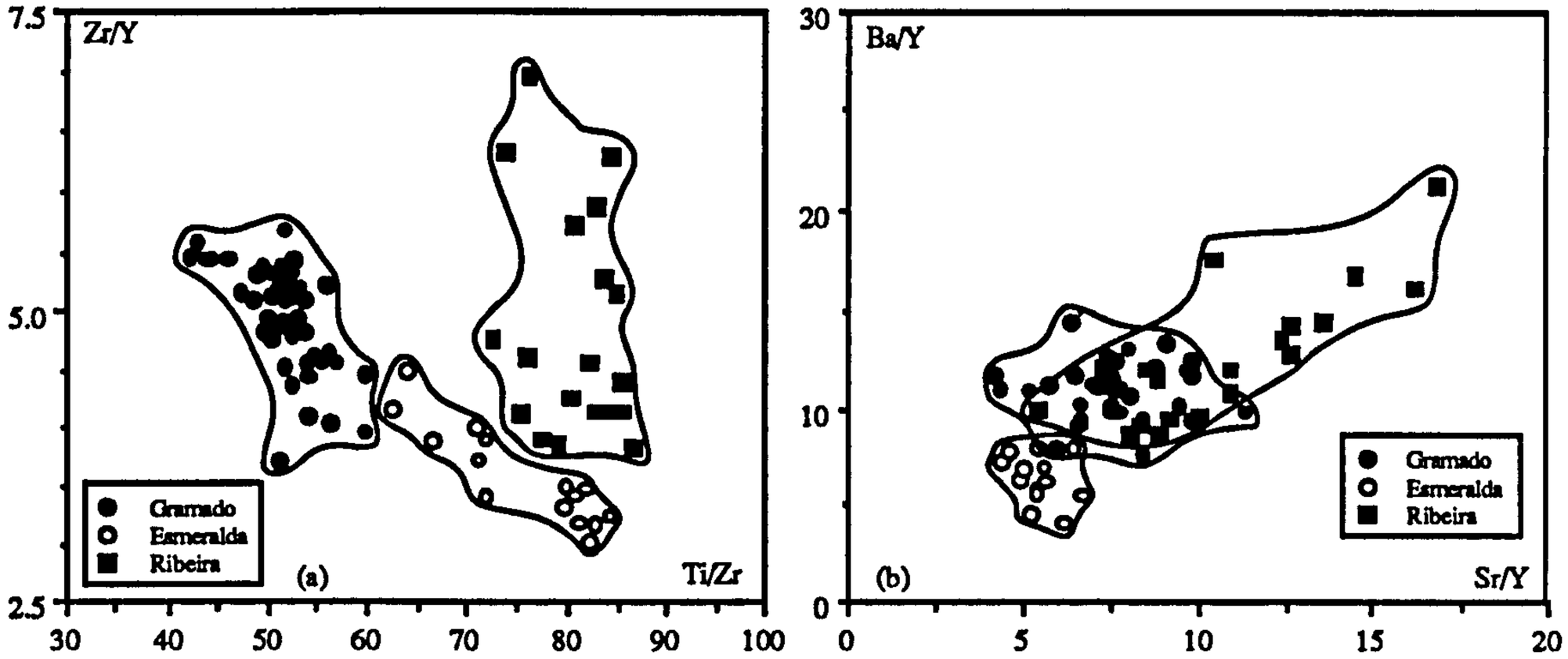

Figure 2.8 Trace element discriminants for the Paraná low-Ti magma types: (a) Zr/Y vs. Ti/Zr - all three low-Ti magma types are clearly resolved on this figure; the Ribeira magma type has high and almost constant Ti/Zr (~75-90) for a wide range in Zr/Y; Ti/Zr of 60 acts as a division between the Gramado and Esmeralda magma types, {Gramado - Ti/Zr < 60, high Zr/Y; Esmeralda - Ti/Zr > 60, low Zr/Y}, (b) Ba/Y vs. Sr/Y - the Esmeralda magma type has lower Ba/Y and Sr/Y than the Ribeira and Gramado magma types and shows a relatively restricted variation; the Ribeira magma type shows a large range in Ba/Y and Sr/Y, overlapping with the Gramado magma type.

These 'Low-Ti' magma-types have different isotopic characteristics. In terms of Sr and Nd isotope systematics, the Esmeralda-type lie at more depleted compositions relative to those of the Gramado-type. For the Esmeralda magma type, $(^{87}Sr/^{86}Sr)_i$ varies between 0.7059 and 0.7076, and $(^{143}Nd/^{144}Nd)_i$ likewise from 0.51255 to 0.51233, and this isotopic trend is related to the variation in incompatible trace element ratios mentioned above. The Gramado magma type has $(^{87}Sr/^{86}Sr)_i$ from 0.7075 to 0.715 and $(^{143}Nd/^{144}Nd)_i$ between 0.51210 and 0.51230, and the wide range of initial Sr ratios which correlates with SiO_2 and Rb has been attributed to the effects of crustal interaction (*e.g.* Mantovani *et al.*, 1985a; Fodor *et al.*, 1985a; Hawkesworth *et al.*, 1988). The underlying cause for this variation in low-Ti composition in the southern Paraná is discussed extensively in chapter four. The data from Petrini *et al.*, (1987) indicated that the

Ribeira magma type has a rather restricted Sr and Nd isotopic composition, with $(^{87}Sr/^{86}Sr)_i$ 0.7055-0.7060 (lower than in the Gramado magma type) and $(^{143}Nd/^{144}Nd)_m$ 0.51240-0.51248; no Pb data are available yet. This range intriguingly is very similar to that found for the northern high-Ti magmas, the Pitanga-type, and of interest in the context of the comment by Marques *et al.*, (1988) that the trace element distribution pattern for the Ribeira and Pitanga magma types were also very similar.

Difficulties were encountered when trying to relate the other two groups of Petrini *et al.*, (1987) {group B and the samples with $(^{87}Sr/^{86}Sr)_i > 0.706$)} that cover the central and south basin to the Esmeralda / Gramado magma type scheme. The choice of 0.706 seems a rather arbitrary division since there is an equally natural break in the data set between 0.7066 and 0.7076 similar to that between the Gramado and Esmeralda magma types of this study. If all these samples are considered together, it is interesting that the eight southernmost samples conformed nicely to the scheme outlined here, classifying as either Esmeralda-type or Gramado-type. This leaves just the few group B samples within the central region as being problematical, and it is uncertain as to how much of this could be due to regional variations within a particular magma type. It is especially frustrating since a few of the samples have interesting isotopic compositions {$(^{87}Sr/^{86}Sr)_i$ ~0.7046 and $(^{143}Nd/^{144}Nd)_m$ ~0.5128} and could be related to the Esmeralda-type in this respect.

The Gramado magma type is similar to the Paranapanema-type in many respects, for example in Sr content and ratios such as Zr/Y, Ta/Yb and Tb/Yb. On the primitive-mantle normalised abundance plot of figure 2.9, both have similar patterns from Nb to Yb, with the distinctive differences being the higher P, Eu, Ti and lower LIL-elements (Rb to K) in the Paranapanema-type. Therefore the Paranapanema-type are clearly distinguished from the Gramado magma type by higher Ti/Zr (> 60) and low LIL/HFS ratios such as Ba/Nb or Th/Ta.

Low-Ti basalts have been described from the main Etendeka lava field by Erlank *et al.*, (1984), and the dominant group has been termed the Tafelberg basalt type. A second

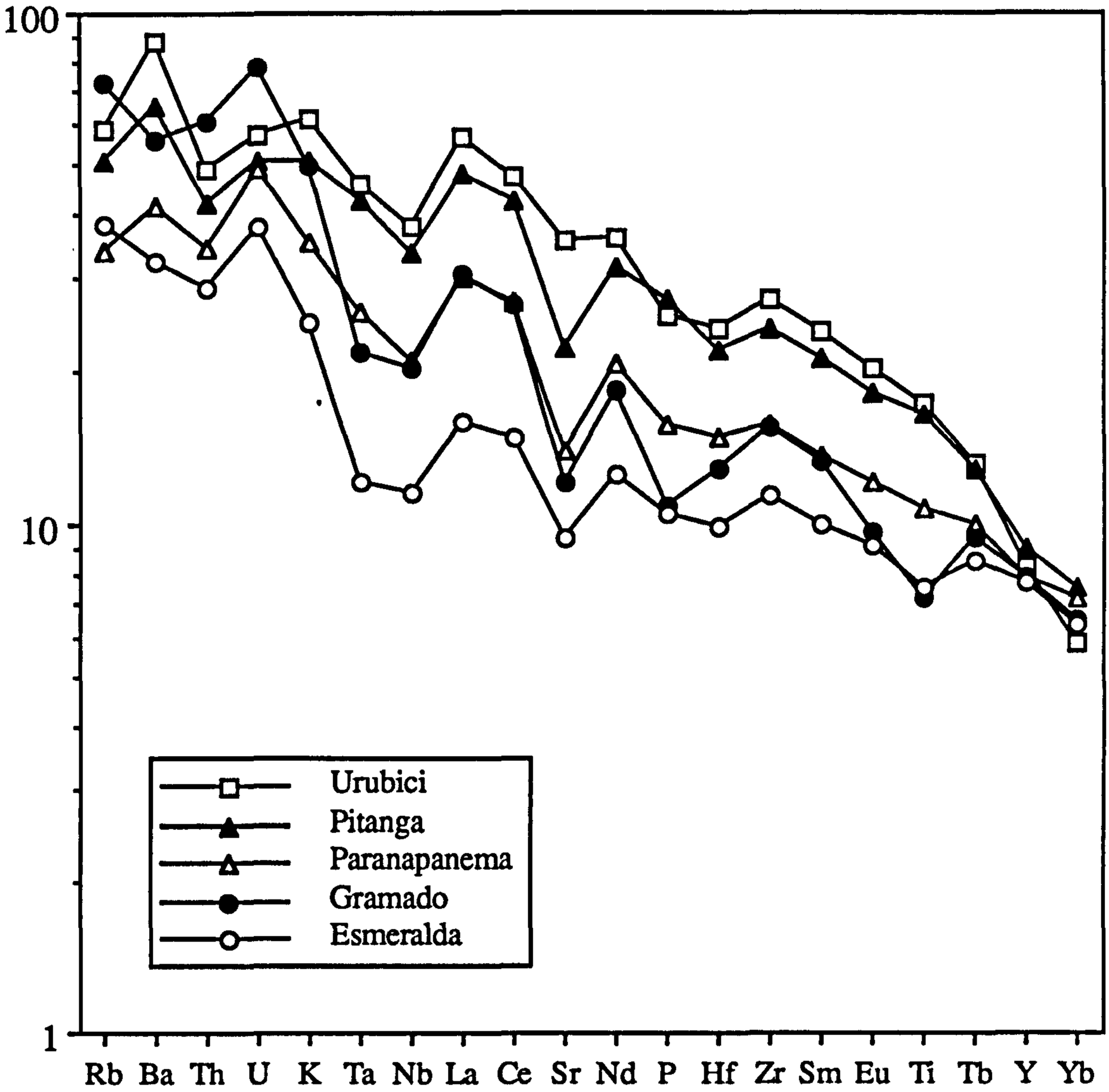

Figure 2.9 Comparison of average Paraná magma type compositions (taken from table 2.3) on a 'primitive-mantle' normalised trace element diagram. Normalising values are from Sun and McDonough (1989) (see appendix C).

group known as the Albin basalt type, minor in volume compared with the Tafelberg type, are petrographically distinct being plagioclase phyric. The geochemical evidence suggests that the Albin basalts are plagioclase-enriched variations of the less evolved Tafelberg basalts which had not undergone marked olivine fractionation, and therefore both basalt groups can be considered as belonging to the same magma type. The Tafelberg magma type has similar isotopic characteristics as the Gramado magma type of the Paraná with $(^{87}Sr/^{86}Sr)_i$ 0.7081-0.7133 and $(^{143}Nd/^{144}Nd)_i$ 0.51210-0.51226. The geochemical equivalence between the Gramado and Tafelberg magma types is demonstrated on the

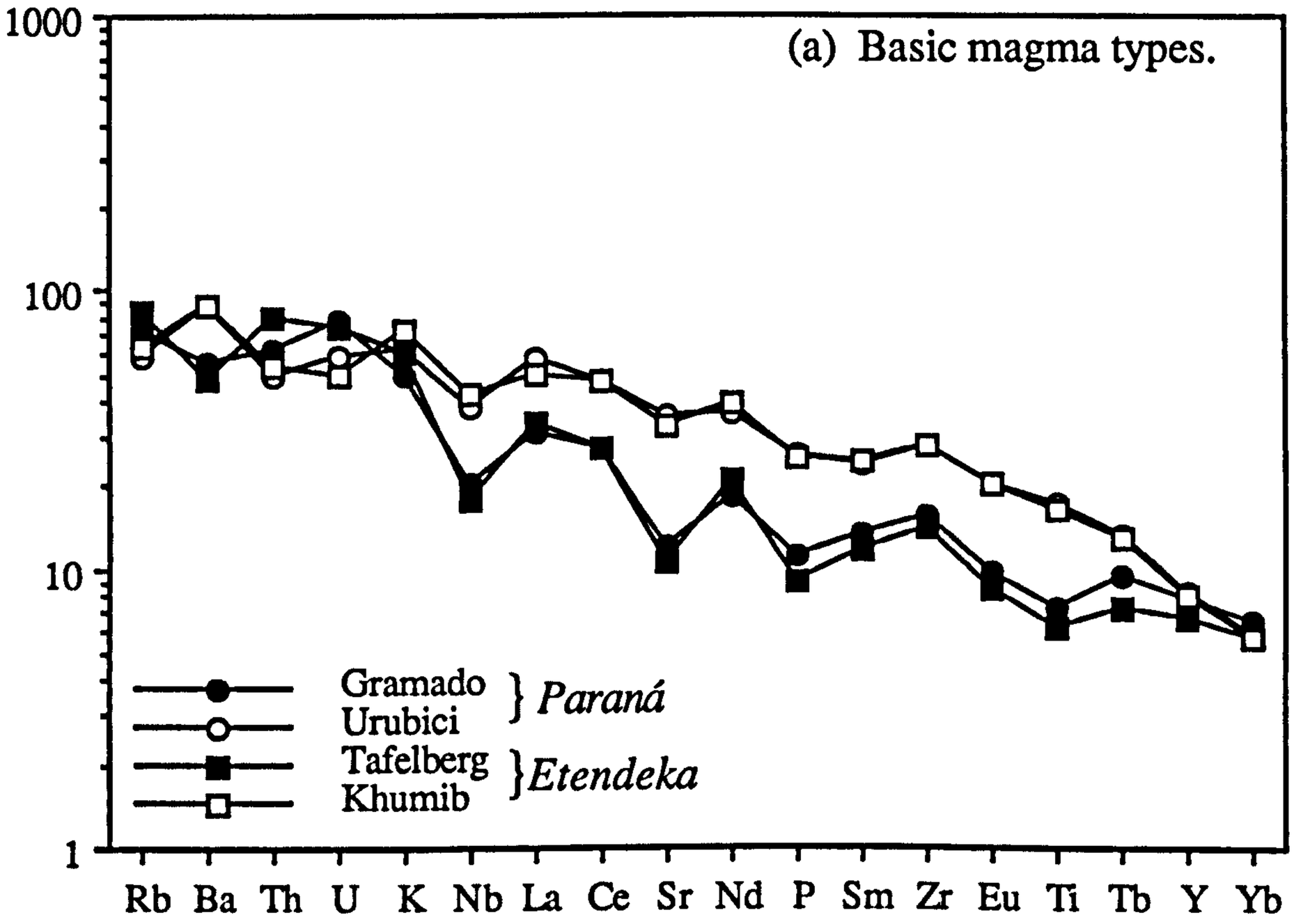

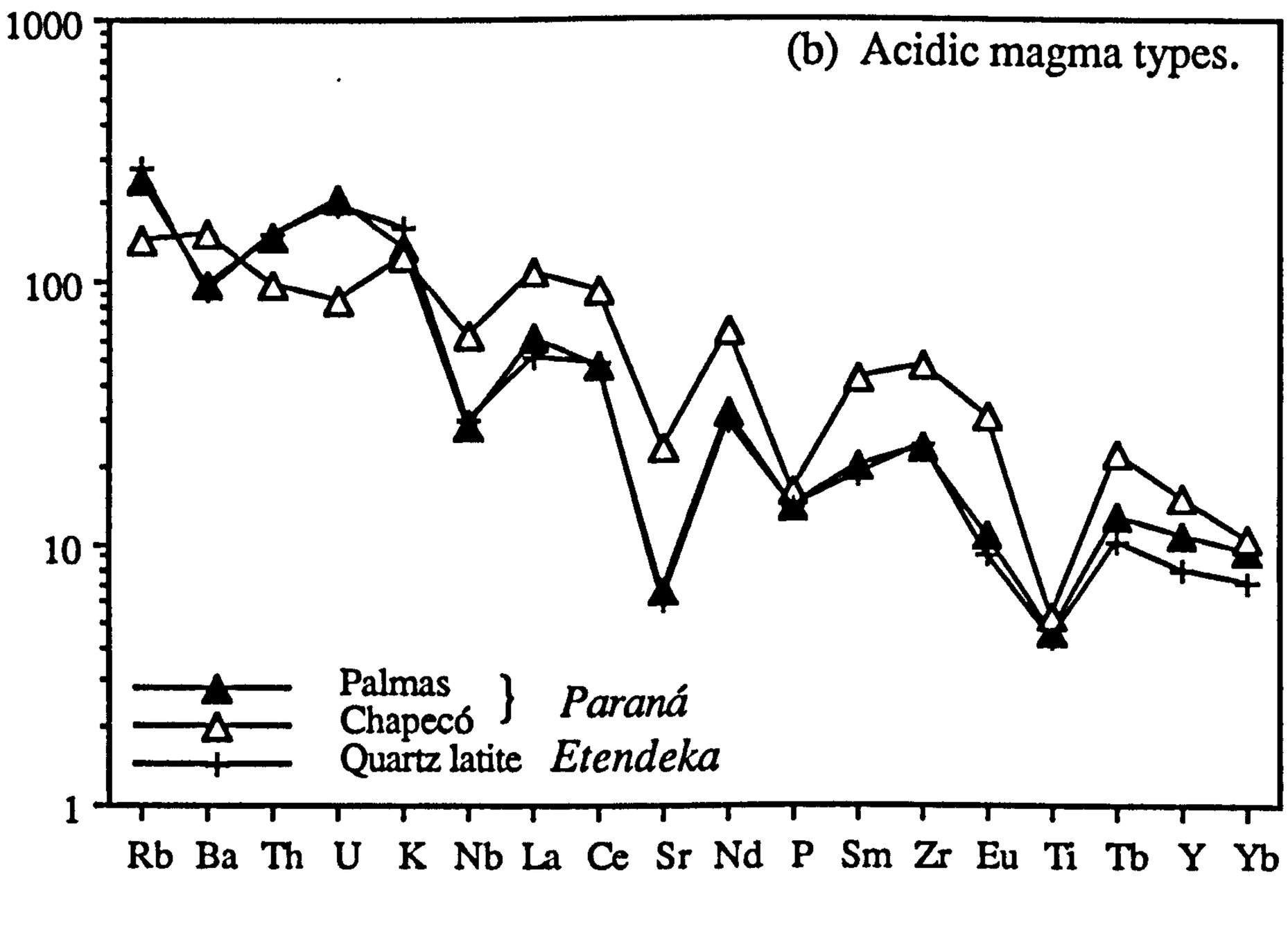

Figure 2.10 Direct comparison of average compositions of magma types from the Paraná and Etendeka provinces: (a) Basic magma types - (i) high-Ti - Urubici (Paraná) vs. Khumib (Etendeka), and (ii) low-Ti - Gramado (Paraná) vs. Tafelberg (Etendeka); (b) Acidic magma types. Trace element abundances are normalised to primitive mantle values (Sun and McDonough, 1989). Paraná average compositions are taken from table 2.3, this study. For the Etendeka lavas, the Tafelberg and quartz latite averages are from Erlank *et al.*, (1984) and the Khumib average composition is from Milner *et al.*, (1988).

primitive mantle normalised patterns illustrated in figure 2.10(a).

2.4.5 Rhyolite magma types.

Mantovani *et al.*, (1985b) first recognised two chemically distinct groups within the silicic volcanics on the basis of their relatively low or high contents of Ti, P and other incompatible elements (Zr, Nb, LREE, etc.), analogous to the high-Ti / low-Ti division of the basaltic rocks. Following the terminology of Bellieni *et al.*, (1986b) the incompatible element 'poor' group, largely concentrated in the southern part of the basin, are known as the Palmas-type, and the incompatible element 'rich' group, restricted to the north and central regions, are called the Chapecó-type.

The two rhyolite types are easily distinguished in the field by their contrasting petrographical features (Bellieni *et al.*, 1986b). The Palmas-type are only slightly porphyritic in character, with less than 5 % of phenocrysts that include plagioclase, augite, pigeonite, Ti-magnetite and orthopyroxene. The Chapecó-type on the other hand are markedly porphyritic (> 5-10 % phenocrysts), carrying large phenocrysts (2-20 mm) of plagioclase and augite as well as smaller crystals of pigeonite and Ti-magnetite; orthopyroxene is a notable absentee in the Chapecó rocks.

For major elements, the Chapecó-type tend to have lower SiO_2 contents relative to the Palmas-type, 63-68 wt% vs. 65-72 wt%, but are enriched in both TiO_2 (0.9-1.5 wt% vs. 0.6-1.1 wt%) and P_2O_5 (0.3-0.6 wt% vs. 0.15-0.35 wt%). The most striking differences are in the abundances of certain incompatible elements, with the compositional fields for Sr, Ba and Zr contents not overlapping between the groups. The Palmas-type are characterised by Zr < 400 ppm, Ba < 800 ppm and Sr < 170 ppm whereas the Chapecó-type have Zr > 500 ppm, Ba > 900 ppm and Sr > 250 ppm The contrasting trace element characteristics of the two rhyolites types is illustrated in the primitive mantle normalised abundance diagram of figure 2.10(b). This shows the higher Rb, Th and U of the Palmas-type. Comparing figure 2.10(a) and (b) the close similarity of the Chapecó rhyolites and Urubici basalts can be seen, notably both have fractionated HREE compared to all other Paraná magma types; Tb/Yb in Chapecó rhyolites is 0.47-0.50, and is 0.45-0.55 in the

Urubici-type magmas, whereas in the Gramado, Esmeralda, Paranapanema and Palmas magma types Tb/Yb is 0.28-0.38

The Chapecó-type have a relatively restricted range in Sr, Nd and Pb isotopic compositions, with values notably similar to the high-Ti magma types; $(^{87}Sr/^{86}Sr)_i$ 0.7056-0.7059, $(^{143}Nd/^{144}Nd)_i$ ~0.51227, $^{206}Pb/^{204}Pb$ 18.15-18.23. These data were obtained from samples from the central region (see Mantovani *et al.*, 1985b), and Piccirillo *et al.*, (1987) report that Chapecó-type rhyolites further north near Piraju in São Paulo state had more radiogenic initial Sr ratios of 0.7075-0.7080. The Palmas-type are characterised by markedly enriched isotopic characteristics, with $(^{87}Sr/^{86}Sr)_i$ 0.715-0.721, $(^{143}Nd/^{144}Nd)_i$ 0.51204-0.51219 and $^{206}Pb/^{204}Pb$ 19.0-19.2 (Hawkesworth *et al.*, 1988; Cordani *et al.* 1988).

The rhyolites occur flanking the eastern margin of the lava field. The Palmas rhyolites are by far the most abundant variety of acidic volcanics with widespread exposures over large portions of the southeast corner of the Paraná province. There is no sharp transition between the surface distribution of the rhyolite types from south to north since in the central region samples of the Chapecó rhyolites lie on either side of the Rio Uruguai with Palmas rhyolites between there and the Rio Iguaçu to the north. Further north of this, the Chapecó outcrop as just a few scattered remnants in the region of the Ponta Grossa 'arch'.

The dominant acidic rock-type within the main Etendeka lava field are the Tafelberg quartz latites (Erlank *et al.*, 1984) which are the equivalents of the Paraná Palmas rhyolites {see figure 2.10(b)}. Isotopically they have similar $(^{87}Sr/^{86}Sr)_i$ 0.718-0.727 and $(^{143}Nd/^{144}Nd)_i$ 0.51204-0.51209 (Hawkesworth *et al.*, 1984). To the north of the province within the coastal Sarusas remnant, quartz latites of enriched trace element character similar to the Chapecó-type have recently been found (Milner *et al.*, 1988). These Sarusas quartz latites are enriched in Ba, Sr, Zr, LREE, Ti, Y over the Tafelberg quartz latites and have notably lower $(^{87}Sr/^{86}Sr)_i$ 0.707-0.711.

2.4.6 Application of magma types in stratigraphical studies.

The previous sections have been concerned with the recognition of distinct magma types and the establishment of a range of geochemical criteria that uniquely define them. Now that we have the ability to assign unknown flows to one of several magma types, the remainder of this chapter will concentrate on assessing the regional distribution of these magma types. Section 2.5 is a detailed study of local stratigraphical relationships between magma types within a restricted area. Section 2.6 expands on this to view the magma type distribution on a more regional scale over the south-east portion of the province. The final section introduces the results from the borehole study and summarises the stratigraphical picture now available for the whole Paraná CFB province.

2.5 Detailed study of the São Joaquim region, Santa Catarina State.

2.5.1 Introduction to area.

A detailed investigation of the lava stratigraphy of eastern Santa Catarina state was carried out in an area to the northeast of São Joaquim over two field seasons in Oct/Nov 1985 and Nov/Dec 1986. Six new road sections, lying about 20 km to the north of the Guatá-Bom Jardim (GB) section previously studied by Bellieni *et al.*, (1983) and Mantovani *et al.*, (1985b), were surveyed and extensively sampled, and the 'GB' section itself was reinvestigated and extended as there was new exposure resulting from recent road improvements. An altimeter was used to provide vertical stratigraphical control on samples and flow contacts (details of altimetry are given in appendix C).

The stratigraphical sections given in Bellieni *et al.*, (1983) revealed that there was an increasing influence of high-Ti rocks moving north along the Serra Geral escarpment. The Rocinha-Encruzilhada (RA) section contained a single high-Ti flow in 930 m of lavas whereas in the 'GB' section, 50 km to the northeast, there were several packets of high-Ti flows preserved within the 740 m thick lava sequence. This region was chosen for a

detailed study in order to constrain the nature of the contact between the high- and low-Ti magmas types in this 'transition zone' and to investigate any fine-scale stratigraphical variations within each magma type.

The physical layout of the field area and the location of sampled sections are illustrated in figure 2.11. The dominant physical feature is the Serra Geral escarpment which produces an abrupt rise of over 1000 m in under 3 km moving from east to west, though this is less well defined in the north-east of the area. The area is drained by three river systems (Rio Pelotas, Rio Lava-Tudo and Rio Canoas) which all flow inland to the west and north-west away from the Serra Geral into the Rio Uruguai and ultimately into the Atlantic ocean at the River Plate. To the north of the São Joaquim to Orleães road, which contains the 'GB' section, there are few roads that traverse the true Serra Geral escarpment down to the coast. The escarpment becomes much less distinct to the north of Morro da Igreja and coupled with this is the progressive increase in elevation of the basal contact of the lavas moving north through the area. The basal contact at 'RA' is at 240 m a.s.l.(above sea level), at 'GB' it is at 760 m a.s.l. and at 'SM' at 1230 m a.s.l.. Hence on the Urubici to Aiure road which crosses the Serra Geral in a spectacular manner at the Corvo Branco pass, only 35 m of basalt are encountered (the 'CV' section). Sampled profiles relied on the more undulating roads to the west of the escarpment but it was still possible to find 350 m to 400 m sections through the lavas, the 'SM' section being exceptional at over 600 m. In this region, the surface outcrop of the lavas turns inland towards Lajes, except for a few minor isolated outliers to the north, and any future extension of this work would have to concentrate on the area to the north-west.

Exposure was rarely continuous, except in the 'GB' section, and usually consisted of scattered isolated outcrops with lush dense vegetation obscuring the areas in between and thus preventing direct field correlation of individual prominent flows between sections. Within each lava flow, the vesicles generally increased in size and frequency from the base towards the flow-top and so sampling of the flows was biased towards the flow bases in an effort to obtain non-amygdaloidal samples. There was no apparent pattern in the nature and

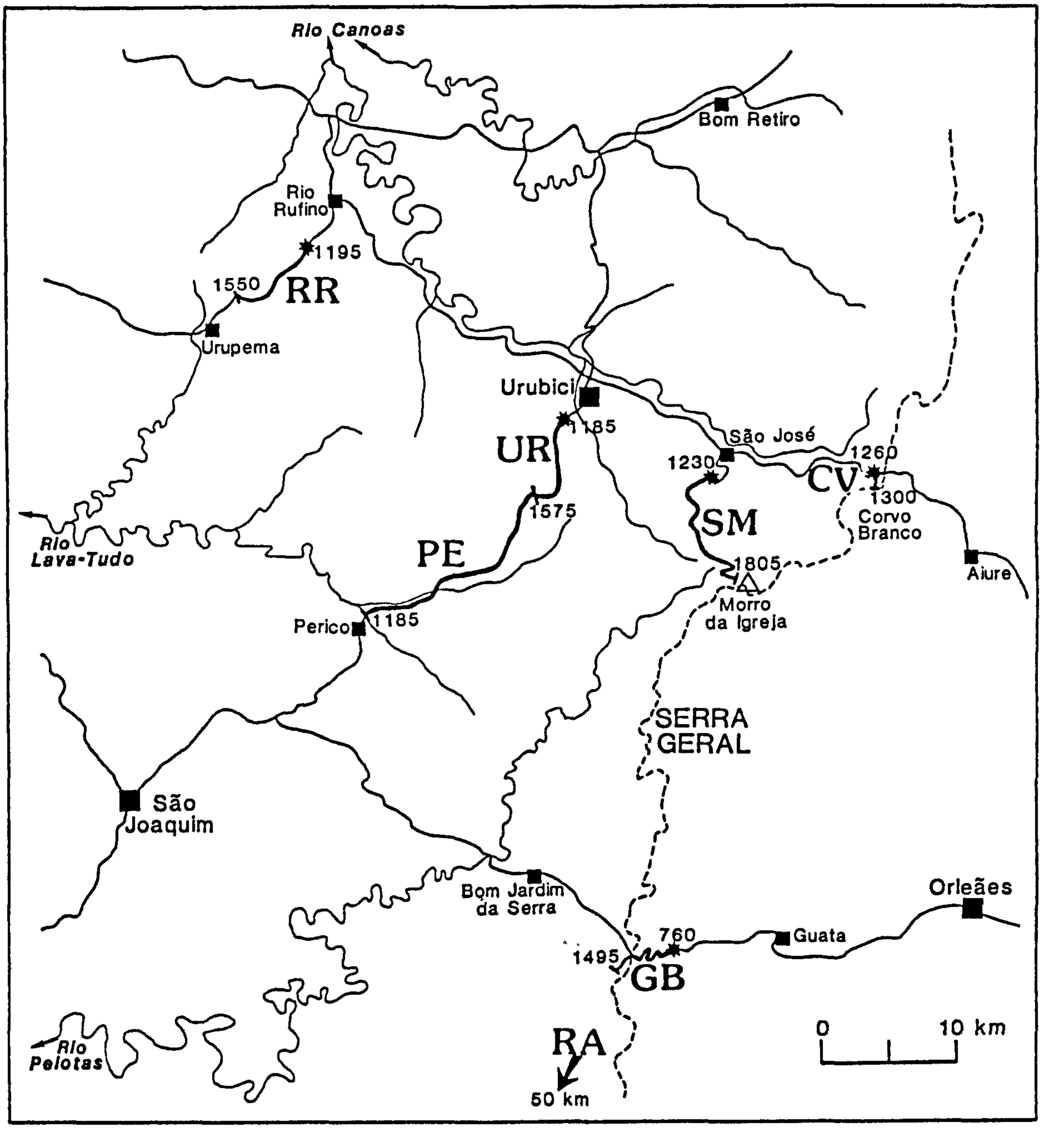

Figure 2.11 Field map of the São Joaquim study area, showing the location of the sampled road sections and the local physiography. The altitude of the top and base of each road section are marked, in metres above sea level (a.s.l.). The basal contact of the lavas with the sandstones of the Botucatu Formation, if encountered, is indicated by an asterisk. The position of the Serra Geral escarpment is marked by the dotted line, with the coastal plain on the right hand side and the elevated lava plateau to the left.

distribution of the amygdaloidal infilling which were usually a random selection from; zeolite, calcite, quartz (often as amethyst) and agate. As an aside, Sanford and Lange (1960) also mention the occurrence of asphaltic infilling of vesicles within the Paraná lavas. Murata *et al.*, (1987) has studied the distribution of zeolites with depth within the lava pile exposed about 200 km to the south of this field area near Caxias do Sul, and recognised three distinct zeolite zones. The contrast between the type of zeolites found within the upper rhyolite zone (low-calcium zeolites - mordenite) and within the lower basalts (high-calcium zeolites - laumontite, scolecite) suggested that the zeolite mineralogy was controlled by the composition of the host lavas. Two zones with the basalts were defined by the presence or absence of laumontite, and its restriction to the most deeply buried lavas reflected the high temperature (> 100 °C) necessary for its formation, which suggested that here the zeolite mineralogy was controlled by the ambient temperature. Heulandite, which can contain high (> 3 wt%) contents of Sr, was found throughout the lava sequence, as was seen in the Etendeka lavas (Erlank *et al.*, 1984). The lavas with the São Joaquim study area changed from a massive, well jointed colonnade habit upwards into a very vesicular and often brecciated upper zone. Field criteria for distinguishing flow/flow contacts was based essentially on the presence of a vesicular, 'aa'-type rubbly flow-top and the sharp transition to the more massive base of the subsequent flow (see plate 2.1). If weathering had been particularly intense, the vesicular flow-top had usually been transformed to a purple/orange-brown clayey soil though often with the amygdales, and zeolites surrounding brecciated blocks, still preserved *in situ*. This proved useful in locating flow/flow contacts in the poorly exposed areas between rock outcrops. A common feature displayed by most flows was weathering concentrated along the joint planes which had obviously also acted as fluid channels during hydrothermal alteration of the basalts. This led to a distinctive pattern of *in situ* blocks surrounded by a clay matrix that marked the old joint surfaces (see plate 2.2). Despite the intense alteration on the outside these blocks were usually quite fresh internally.

Plate 2.1

Well exposed flow-flow contact in the 'SM' road section near Morro da Igreja, showing almost 2 to 3 m relief. It illustrates the sharp contrast between the massive flow base of the top flow and the reddish-brown highly altered brecciated top of the flow beneath.

Plate 2.2

Example of typical 'blocky' weathering pattern in the basalts, with alteration concentrated along the joint planes leaving *in situ* blocks of internally quite fresh basalt.

2.5.2 Extent of within-flow variations and effects of weathering and alteration.

To undertake detailed stratigraphical correlations between sections it is important to assess the variability of analysed samples within individual lava flows. A combination of different processes could have acted to produce flow heterogeneities; (i) magmatic processes - flow differentiation, migration and concentration of late-stage residual fluids during cooling, cumulus enrichment, and/or (ii) secondary low-temperature processes - surface weathering, hydrothermal alteration, amygdale formation.

The ubiquitous presence of amygdales and evidence of extensive zeolitisation throughout the lava pile suggests that the circulation of hydrothermal fluids could have modified the original magma compositional characteristics of the Paraná basalts. The effects of surface weathering and hydrothermal alteration were avoided as much as possible during sample collection but, despite this, many samples still showed visible signs of some alteration; sericitisation of plagioclase phenocrysts and alteration of augite phenocrysts, olivine phenocrysts if present were completely replaced by secondary minerals, glass and groundmass crystals were variably replaced by brown clay minerals. Therefore the geochemical effects of alteration on the composition of the basalts need to be evaluated.

Closely spaced samples (< 5 m) taken from the same outcrop can be used to test for possible element mobility during alteration, and on a larger scale, samples collected at intervals along a single lava flow can allow the extent of within-flow heterogeneity to be assessed. This could only be carried out on a very limited scale up to 1 km within the field area because of the problems of tracing individual flows laterally with any confidence. Four of these data sets are given in table 2.4, with two examples (sets A and B) of samples from a single outcrop and two of samples collected over 500 m to 1000 m within an individual flow (sets C and D). Inspection of the data in sets A and B shows the general uniformity of measured sample compositions for most analysed elements. For the samples of set A the most obviously variable elements are Na, K, Rb, Sr and Ba. Sr and Ba are again highly variable in set B together with, though to a lesser extent, K_2O, Na_2O, CaO and MgO.

	SET A		SET B		SET C				SET D			SET C		SET D		XRF	SET D		
	DSM17a	*DSM17b*	*DUP05*	*DUP06*	*DRR02*	*DRR23*	*DRR22*	*DRR25*	*DSM05b*	*DSM07*	*DSM09*	*mean*	*C.V.*	*mean*	*C.V.*	*C.V.*	*INAA*	*DSM05b*	*DSM07*
SiO_2	51.83	52.35	52.20	53.52	54.69	54.28	55.53	54.53	51.56	51.61	51.43	54.76	1.0	51.53	0.2	0.4	La	39.8	40.7
TiO_2	4.16	4.15	3.55	3.56	1.44	1.49	1.45	1.47	3.51	3.48	3.49	1.46	1.4	3.49	0.4	1.0	Ce	87.5	88.5
Al_2O_3	13.07	13.10	13.39	13.26	13.98	14.16	13.88	14.12	13.24	13.32	13.32	14.04	0.9	13.29	0.3	1.0	Nd	49.0	50.8
Fe_2O_3	13.39	13.36	13.09	12.87	12.86	13.02	12.56	12.77	13.87	14.15	14.05	12.80	1.5	14.02	1.0	0.7	Sm	10.3	10.2
MnO	0.16	0.17	0.18	0.17	0.19	0.19	0.18	0.19	0.19	0.17	0.17	0.19	2.8	0.18	6.5	0.0	Eu	3.41	3.37
MgO	4.12	4.06	4.35	4.06	4.14	4.31	4.14	4.19	4.30	4.21	4.37	4.19	1.9	4.29	1.9	4.4	Tb	1.47	1.45
CaO	7.62	7.85	8.05	7.45	7.51	7.87	7.76	7.02	8.01	7.93	8.04	7.54	5.0	7.99	0.7	0.7	Tm	0.61	0.63
Na_2O	2.91	2.50	2.68	2.49	3.13	2.73	2.51	3.25	3.01	2.72	2.94	2.90	11.9	2.89	5.2	7.9	Yb	3.12	3.11
K_2O	2.11	1.84	1.92	2.06	1.87	1.76	1.80	2.26	1.80	1.87	1.71	1.92	12.1	1.79	4.5	1.5	Lu	0.47	0.48
P_2O_5	0.61	0.62	0.60	0.54	0.20	0.20	0.20	0.20	0.51	0.53	0.50	0.20	0.7	0.51	3.0	7.3			
L.O.I.	0.91	0.91	0.75	0.86	0.22	1.24	0.28	0.32	0.75	1.65	0.86	-	-	-			Th	5.02	5.20
Mg#	41.8	41.5	43.6	42.4	42.9	43.5	43.4	43.3	41.9	40.9	42.0	43.3	0.7	41.6	1.4		U	1.08	1.37
Ni	51	55	35	32	26	24	36	25	39	37	40	28	20.0	39	4.0	6.0	Hf	7.30	7.44
V	363	352	323	332	n/a	n/a	n/a	n/a	387	373	407	-	-	389	4.4	4.6	Pb (I.D.)	7.35	7.31
Cu	169	181	118	125	141	155	137	140	188	200	165	143	5.6	184	9.6	5.2	Cs	0.62	0.62
Zn	114	116	123	124	110	108	107	101	107	123	117	107	3.6	116	7.0	3.5	Sc	27	27
Ga	24	24	24	27	21	19	22	21	27	26	27	21	6.1	27	2.2	6.6	Co	40	41
Rb	43	32	32	35	68	56	52	83	46	48	43	65	21.5	46	5.5	1.9			
Sr	789	885	850	682	220	219	250	186	706	699	692	219	12.0	699	1.0	1.8	$^{87}Sr/^{86}Sr_i$	0.70557	0.70555
Y	40	42	38	40	36	36	46	34	37	40	37	38	14.3	38	4.6	3.9	$^{143}Nd/^{144}Nd_i$	0.51235	0.51236
Zr	345	354	333	341	171	175	170	174	276	283	269	173	1.4	276	2.5	1.9	$^{206}Pb/^{204}Pb$	18.152	18.134
Nb	30.0	29.8	31.6	31.7	14.3	14.9	14.3	14.1	24.7	24.0	23.4	14.4	2.4	24.0	2.7	3.3	$^{207}Pb/^{204}Pb$	15.591	15.562
Ba	713	759	746	690	n/a	n/a	n/a	n/a	595	570	563	-	-	576	2.9	4.4	$^{208}Pb/^{204}Pb$	38.496	38.437

Table 2.4 Geochemical variation within four sample sets to assess the extent of within-flow variation and the effects of alteration processes. Set A - same outcrop, ~ 1 m apart; set B - same outcrop, ~ 3 m apart vertically; set C - same flow (Rio Rufino, 'RR'), sampled over ~ 500 m; set D - same flow (Morro da Igreja, 'SM') sampled over 1 km. Figures in bold highlight the anomalous values referred to in the text. C.V. is the coefficient of variation, which is defined as 100 x (standard deviation)/mean. The C.V. obtained by repeated analyses of international standard rock powders (see appendix B) is included for comparison, as an estimate of the accuracy of the XRF technique.

High variability for an element for an element must either be a consequence of mobility during alteration processes or due to poor analytical precision at low levels of concentration. The variability of individual data set should be compared to the analytical precision of the XRF method which is determined by repeated analyses of standards. This can be monitored using the coefficient of variation (C.V.) which is defined as 100 x standard deviation / mean. The C.V. has been calculated for the sets C and D and can be compared to the mean C.V. for XRF analyses (also given in table 2.4, details in appendix B) that was obtained by combining the results from a number of standards covering a range of compositions. The samples of set C were all collected over 500 m along the col in the 'RR' section from the uppermost flow exposed. The variation in Rb, K and Sr were well outside possible analytical error, and Ca, Na and Y were also affected to a lesser degree. The samples of set D were all taken from a flow in the 'SM' section near to the summit of Morro da Igreja that had been fortuitously exposed in three separate localities over a distance of 1 km. Variations in composition between these samples are not as marked as in set C, and only K, Rb and Cu are significantly affected.

Sets A to D also illustrate the immobile behaviour of the HFS elements (Ti, Zr, Hf, Nb and Y), and SiO_2, Al_2O_3 and Fe_2O_3(t) are similarly invariant. Set D is the only example where neutron activation analysis and isotope data are available on samples from the same flow, and these results, though not extensive, were favourable. Except for U, the abundances of REE, Th, Ta, Hf, Cs, Sc, and Co (plus Pb determined by isotope dilution) were remarkably similar. Th, being a LIL (large ion lithophile) element, might be expected to be highly variable akin to the behaviour of other LIL-elements such as Rb and K but its mobility appears to be limited in view of the good correlation with HFS elements such as Ta and Hf, for all samples. The isotopic ratios of Sr, Nd and Pb have been determined on two of the samples in set D and, reassuringly, in each case the ratios are within analytical error.

Although these studies have been limited, the results are in general agreement with more extensive studies on basalts elsewhere. The work of Wood *et al.* (1976) on the Tertiary basalts of Iceland showed that the degree of zeolitisation varied rapidly on a local

scale and that during this process SiO_2, MgO, Na_2O, K_2O, Rb, Sr, and LREE were variably modified within a single flow, with for instance Sr being preferentially enriched in hydrothermally altered flows. A similar study by Marsh and Eales (1984) on the Central Area rocks of the Karoo concluded that Na, K, Rb, Sr, Ba and Cu were all highly variable but the patterns of variation displayed by these elements were not mutually sympathetic. The effect of secondary processes on the trace element geochemistry of the basalts is predictable in terms of which elements are likely to have been affected but not as to the individual extent. This is highlighted by individual studies (Cox and Hawkesworth, 1985; Lightfoot, 1985) on basalts from within the same region of the Deccan province, who both reached differing conclusions as to the relative mobility of elements within this group of expectedly mobile elements. Cox and Hawkesworth (1985) found that Rb and K were most variable, with Ba and Sr remarkably constant, whereas Lightfoot (1985) found that Rb and Ba were very highly mobile, with Sr and K showing less variation.

In all the cases above (*e.g.* Wood *et al.*, 1976; Marsh and Eales, 1984) the HFS (high field strength) elements Ti, Zr, Hf, Nb, Ta, Y as well as V, Co, Zn and some REE were unaffected by secondary processes and thus greater significance is attached to the variations in these elements. The conclusion from this section is that most of the chemical variation is not the result of post-solidification alteration and the compositional characteristics of the flows have primary significance in terms of petrogenetic models for their ultimate origin.

2.5.3 Stratigraphical variations and flow correlations.

The quality of the available material within a sampled road section was very uneven, and away from the road exposure any suitable material was virtually non-existent. Whereas only the freshest samples were selected for full geochemical analysis, an effort was made to sample, and analyse by XRF, every flow irrespective of the degree of alteration in order to build up a complete stratigraphy. Admittedly some samples were of limited use in assessing the fine-scale variations within a magma type but it was possible to pigeonhole each sample

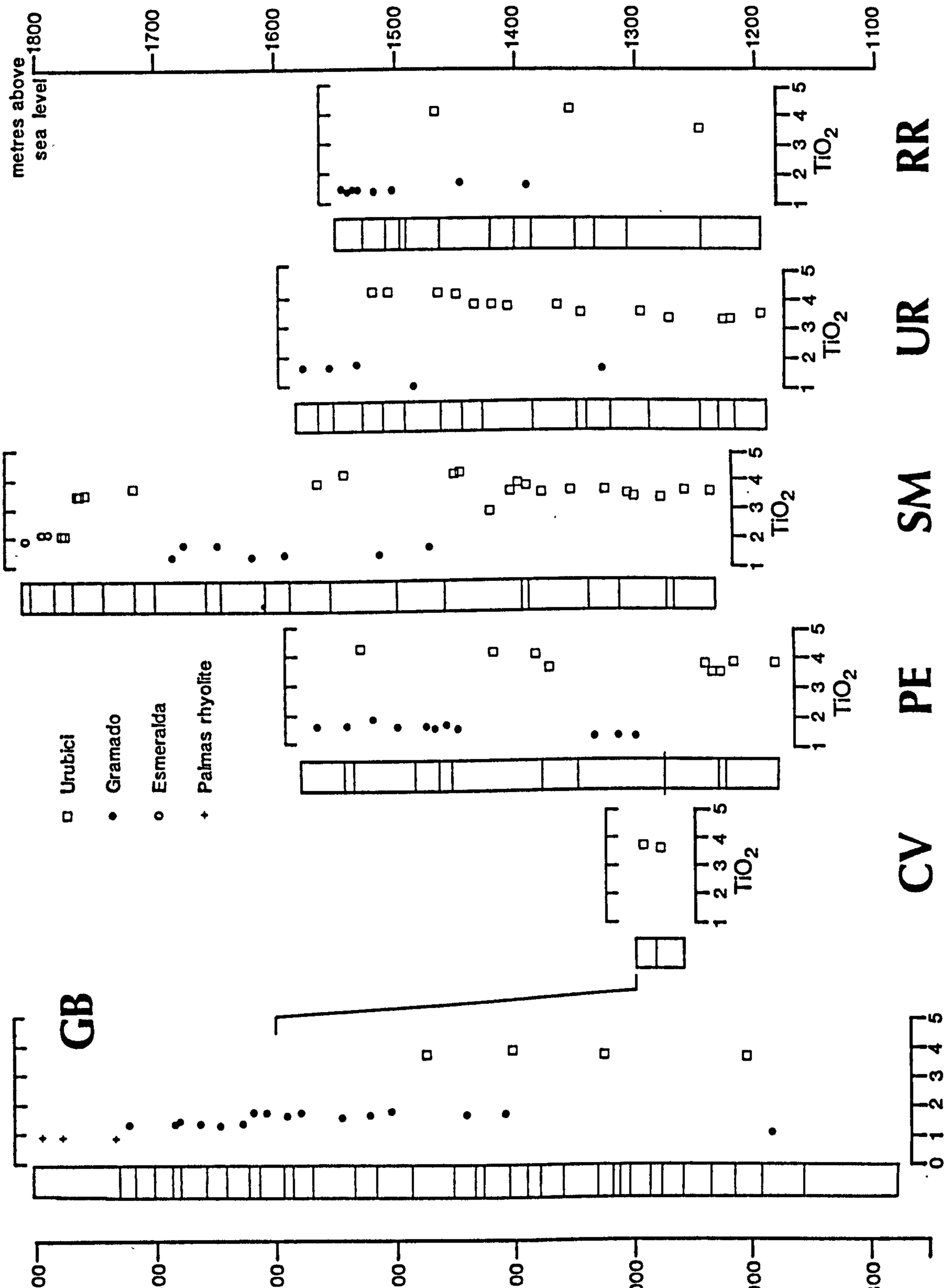

Figure 2.12 Variation of TiO_2 (wt%) with elevation for the sampled road sections in the São Joaquim area. Interbedded flows of the Urubici and Gramado magma type dominate the lava sequence. NB the 'GB' profile has been displaced upwards by 300 m from its true position.

to a particular magma type by virtue of their abundances of the more immobile elements (*e.g.* HFS elements).

The chemical stratigraphy of the lava pile is illustrated in figure 2.12, highlighted by using the variation of TiO_2 with elvation within each of the studied road sections. The lava sequences of the area are clearly dominated by flows of just two magma types; the Urubici type and the Gramado type, with only minor occurrences of flows of other compositions. Rocks of the Esmeralda magma type form the two uppermost flows in the 'SM' section at Morro da Igreja the highest locality in the area, and the sequence at 'GB' is capped by 70 m of Palmas-type rhyolites. The road sections are characterised by alternations of groups of flows of Urubici and Gramado magma types on the order of 50 m to 150 m in thickness, with packets of each magma type repeated on average three times within a lava sequence.

Correlation of the lava sequences between sections was initially attempted on a flow-by-flow basis, with flows considered to match if their compositions lay within analytical errors, determined via duplicate analyses and repeated analyses of standards (see appendix B), but in detail this proved to be difficult. Similar problems were encountered by Devey (1986) in the Deccan who suggested two possible reasons for the lack of correlateable flows; either the basalt pile consisted mainly of small flows whose horizontal dimensions were less than the distance between sections, or the individual flows had a large lateral extent but were inhomogenous with respect to the degree of fractionation and/or contamination. This again exposes the poor knowledge of within-flow heterogeneity over the length scale of typical basaltic lava flows (*i.e.* generally in excess of 10 km). No suitable candidate for study was found in the field area in the Paraná, but Lightfoot (1985) managed to follow one distinctive flow for over 50 km in the Deccan which in this case showed no significant compositional variations outside of the limits of analytical error.

The next stage was to move up a level from looking at individual flows and consider correlating groups of flows. An obvious choice would be to utilise the natural division caused by the alternations of groups of flows of the different magma types. This approach does not take into account the possibility of flows being laterally discontinuous and hence

not being 'picked up' in all the studied stratigraphical sections, as was the case for the evolved Gramado-type flow DUP38, which occurred as a single flow interrupting lavas of the Urubici magma type at 'UR' but was not found in the adjacent 'SM' or 'PE' sections. Within each group of flows of one magma type there is often considerable chemical variation, and it was soon realised that these groups were not easily correlated across the area. A more successful approach involved considering all the flows of a particular magma type, initially in this case the Urubici-type flows, and ignoring the positions of the intervening flows of other magma types and any sedimentary horizons. Small packets of flows could then be matched up visually from variation diagrams after also taking account of their relative position in the stratigraphical succession. Flows within individual packets formed distinct chemical groupings which were distinguished primarily on small but significant variations in MgO and TiO_2 (*c.f.* a similar approach by Mangan *et al.*, 1986 to subdivide the Grande Ronde formation in the Columbia River basalts) and the compositions of the individual flow packets of the Urubici-type magmas are shown in figure 2.13.

Individual flow packets could be correlated between sampled sections over at least 40 km as illustrated in figure 2.14, and they defined distinct sub-units within the sequence. Sub-units comprised several flows collectively 25 m to 80 m thick (*c.f.* 30 m to 150 m in the Columbia River; Mangan *et al.*, 1986). There was a non-systematic variation in the thickness of a specific sub-unit from section to section, with the number of individual flows recognised also varying between one and three, and this could well have been imposed by the local palaeotopography. Basin-wide correlations in the Columbia River basalts allowed the areal extent and volume of many of the sub-units to be estimated and these varied by almost two orders of magnitude, illustrating the vastly different scales possible even for successive eruptions. Occasionally flows of very distinctive composition within the Paraná lavas have a localised distribution and are not encountered in any of the surrounding profiles, for instance, DSM24, an evolved Urubici-type flow with 55 wt% SiO_2 is only found at 'SM'.

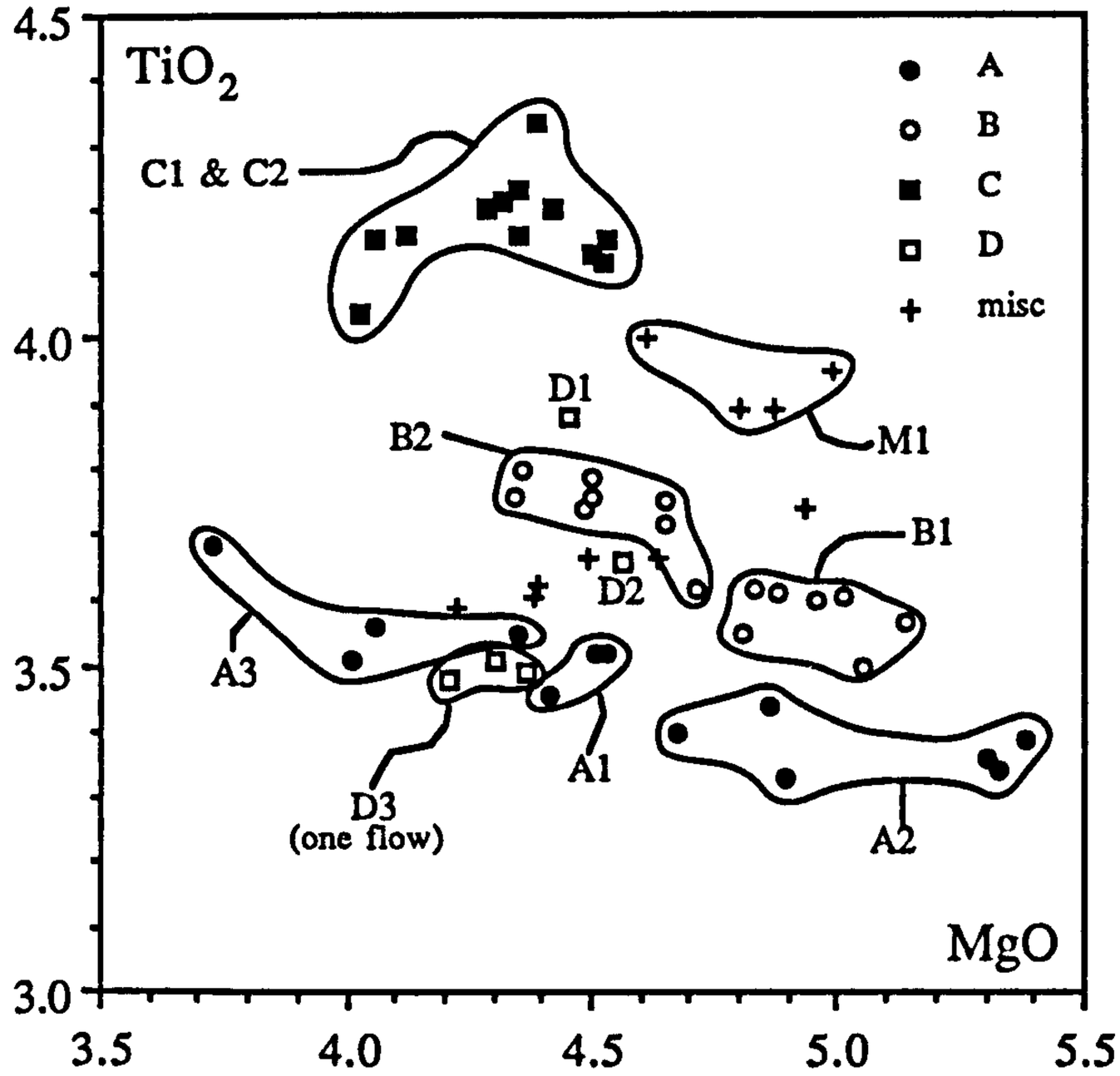

Figure 2.13 TiO_2 vs. MgO variation for samples of the Urubici magma type from the São Joaquim road sections. This illustrates the compositional similarity between packets of two or three stratigraphically adjacent flows, which allows distinct chemical sub-units to be recognised. These sub-units could be combined into larger-scale stratigraphically coherent units, denoted by A, B, C and D.

The variation between the various Urubici sub-units was semi-systematic through the lava sequences and they could be grouped into larger stratigraphically defined units, which were denoted by A, B, and C. Reasonable trends are produced on variation diagrams when all the samples of the Urubici magma type are grouped together but the three stratigraphical units A, B, and C highlight systematic sub-parallel trends within the overall pattern. The underlying causes producing these stratigraphical variations, and the implications for the petrogenesis of the Urubici magma type, will be considered in chapter three. Two-thirds of all Urubici-type flows from the area have been assigned to one of these three units. The remainder include the uppermost flows at 'SM' which are at a higher stratigraphical level of the lava sequence not encountered elsewhere, plus the more problematical flows of both the 'GB' section and the base of the 'PE' section. The few flows of the Urubici magma type found within the lavas of the 'GB' section were more difficult to include in the correlation scheme. The upper flows appeared to correlate with

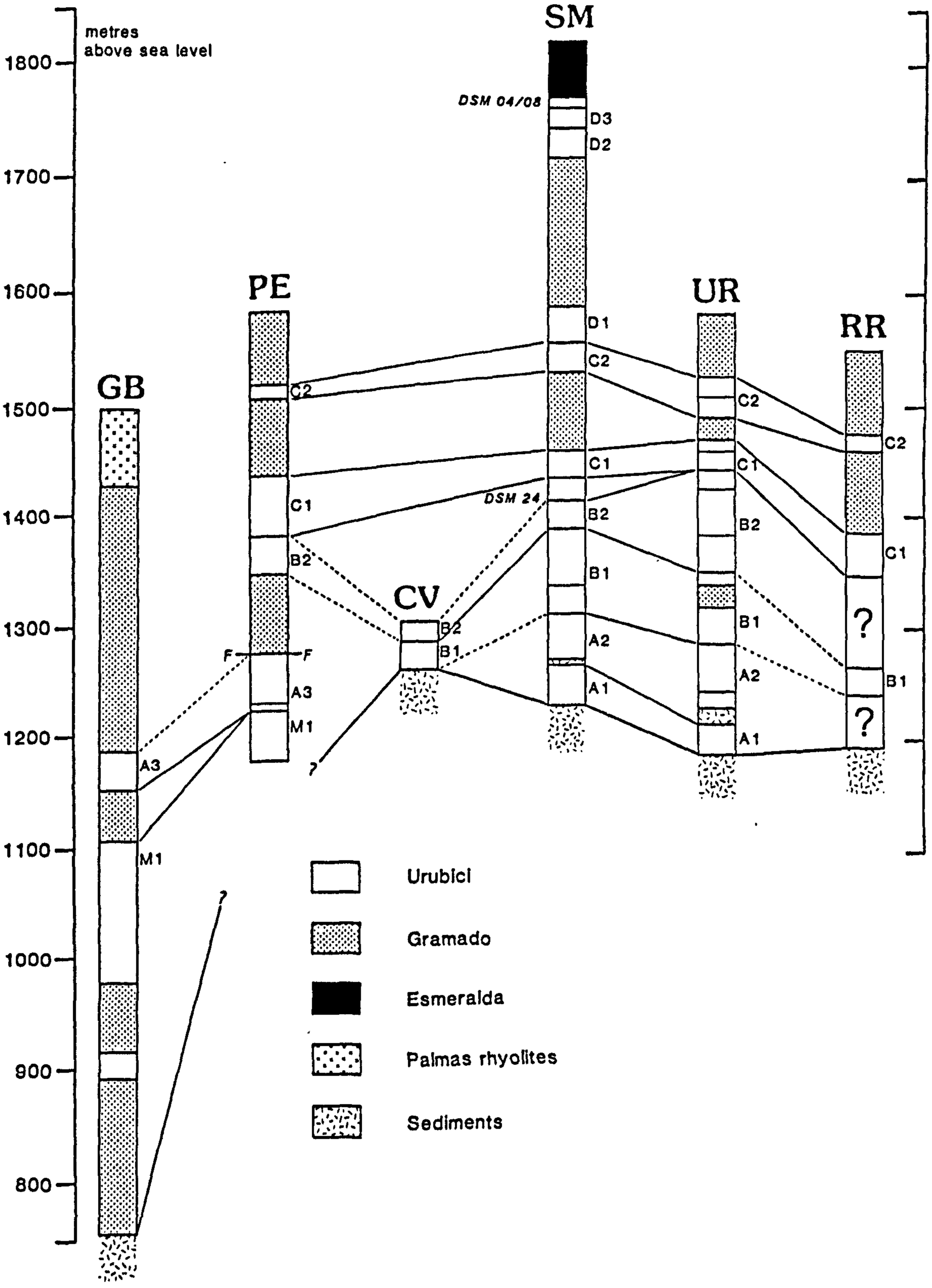

Figure 2.14 Local correlation between the sampled São Joaquim road sections of compositionally distinct packets of Urubici-type flows, as recognised in figure 2.13.

those at the lowest exposed levels of the 'PE' section but these latter flows were separated from flows of the sub-units described above by the fault at Lajeado Liso, and their connection to the main lava sequences was uncertain. It is possible that they underlie unit A since the top sub-unit of these flows shows certain chemical characteristics akin to the unit A flows. They lie on an extension of the trend defined by the unit A flows on figure 2.13 and also share similar isotopic features, with both having higher $^{87}Sr/^{86}Sr$ than the unit B or C lavas.

Unit C is a very distinctive unit characterised by flows with very high (> 4 wt%) TiO_2 contents. This unique composition might allow it to be used as a more widespread stratigraphical marker especially in tracing the distribution of the Urubici magma type further inland to the west and north-west. The two sub-units C1 and C2 are chemically indistinguishable (see figure 2.13), and are only considered as individual sub-units as they are separated in all sections by flows of the Gramado magma type.

Correlating packets of Gramado-type flows proved less successful. The correlations of packets of Urubici-type flows as outlined above were used to delineate possibly related groups of flows of the Gramado magma type, and these were then investigated by viewing a number of elemental variation diagrams. Several flows possessed a rather unique composition and yet were only encountered in one of the sampled sections. For example, the primitive flow DUP30 (8 wt% MgO) was found between the C1 and C2 Urubici sub-units at 'UR' but this flow had a very different composition to the other Gramado-type flows that separated the C1 and C2 sub-units in the 'PE', 'RR' and 'SM' sections. As mentioned previously, the evolved Gramado flow, DUP38 (56 wt% SiO_2), which interrupted the B1 Urubici unit at 'UR', was not found within this sub-unit in any of the other sections, and the only other similar flows were found in the upper portions of the 'GB' section (samples DGB15/17/18) between 1270 m and 1315 m. From figure 2.14 it can be seen that this group of flows was not picked-up in the 'PE' section, despite its location between the profiles of 'GB' and 'UP', because of the complications caused by the fault at Lajeado Liso. This would suggest that there had been at least 100 m of throw on this fault.

2.5.4 Implications of local stratigraphy.

Flows of Urubici and Gramado magma types occur intimately interbedded in the field area with the proportion of Urubici-type flows within a given section increasing to the north. There is no evidence for mixing between magmas of the different types as no samples were found that had compositions transitional between the two. From these points it is inferred that separate storage and/or vent systems existed for the two magma types, with the source of the Gramado lavas to the south and that for the Urubici to the north, erupting essentially simultaneously to produce the observed interfingering of flows. The fact that flows of very similar chemical composition are interrupted by lavas of a different magma type, as seen within unit C of the Urubici-type lavas, could imply relatively fast eruption rates in that the magma has not had time to evolve further along the liquid line of descent.

It is difficult to discern any clear stratigraphical transition from one magma type to the other, that is, whether or not there is a progressive overstepping of either type over the other. Interbedding of both magma types occurs throughout each sampled section, although there is a tendency for the lavas of the Urubici-type to be concentrated towards the lower half of the lava pile. Similarly to the south in the 'GB' section where there are only a few Urubici-type flows, these are found towards the basal portions. Preliminary studies in the northern exposures of the Khumib remnant within the Etendeka province, which in a Gondwana reconstruction would lie adjacent to this area, show a transition from 400 m of Khumib (= Urubici-type) lavas to the top flow which is low-Ti (= Gramado-type), (A.J. Erlank, pers. comm., 1988), consistent with the generalised stratigraphy outlined above for the Paraná lavas in the São Joaquim region.

If the assumption in section 2.5.3 is correct, that the correlated Urubici flows at 'GB' and 'PE' lie stratigraphically below the Urubici unit A flows, then there is a suggestion that in moving north-east from 'GB' and 'PE' towards 'SM' and 'CV' the lavas progressively overstep the underlying sediments. The first lava flows at 'SM' belong to the Urubici unit A and this unit then 'pinches-out' before the 'CV' section where flows of the

Urubici unit B lie directly on the sandstones of the Botucatu formation. This would imply that the lavas in this region had 'ponded-up' against pre-existing topographic highs.

2.6 Distribution of magma types in south-east Paraná.

2.6.1 Introduction.

The previous section looked at the local variations in magma type of the lavas from a relatively restricted area. This section widens the area of interest and is concerned with the distribution of magma types on a more regional scale over the south Paraná. The region considered forms the southeast corner of the lava province, lying within the states of Santa Catarina and Rio Grande do Sul, and covers an area of 500 x 250 km, almost one tenth of the total Paraná lava field.

The data was obtained from three main sources; (i) road sections taken from this study (section 2.5), Bellieni *et al.*, (1986b) and Hawkesworth *et al.*, (1988), (ii) borehole samples (this study, section 2.7) and (iii) scattered surface samples from Fodor *et al.*, (1985a). The location of all available road sections through the lava sequences are illustrated in figure 2.15 together with the stratigraphical distribution of magma types within each profile. The lavas are dominated by low-Ti magma types (Gramado and Esmeralda basalts, Palmas rhyolites), with only minor amounts of high-Ti types found towards the north and west of the area. The two main magmatic features displayed by the lava sequences of the region are; (i) the extensive rhyolitic magmatism, and (ii) a temporal change in low-Ti basalt magma type. An important structural feature to consider in the area is the relationship between the coastal escarpment and the basal contact of the lavas.

2.6.2 Rhyolite distribution.

The bimodality in silica content of the Paraná lavas is well displayed in this region. Despite comprising much less than 10% by volume of the total Paraná magmatism,

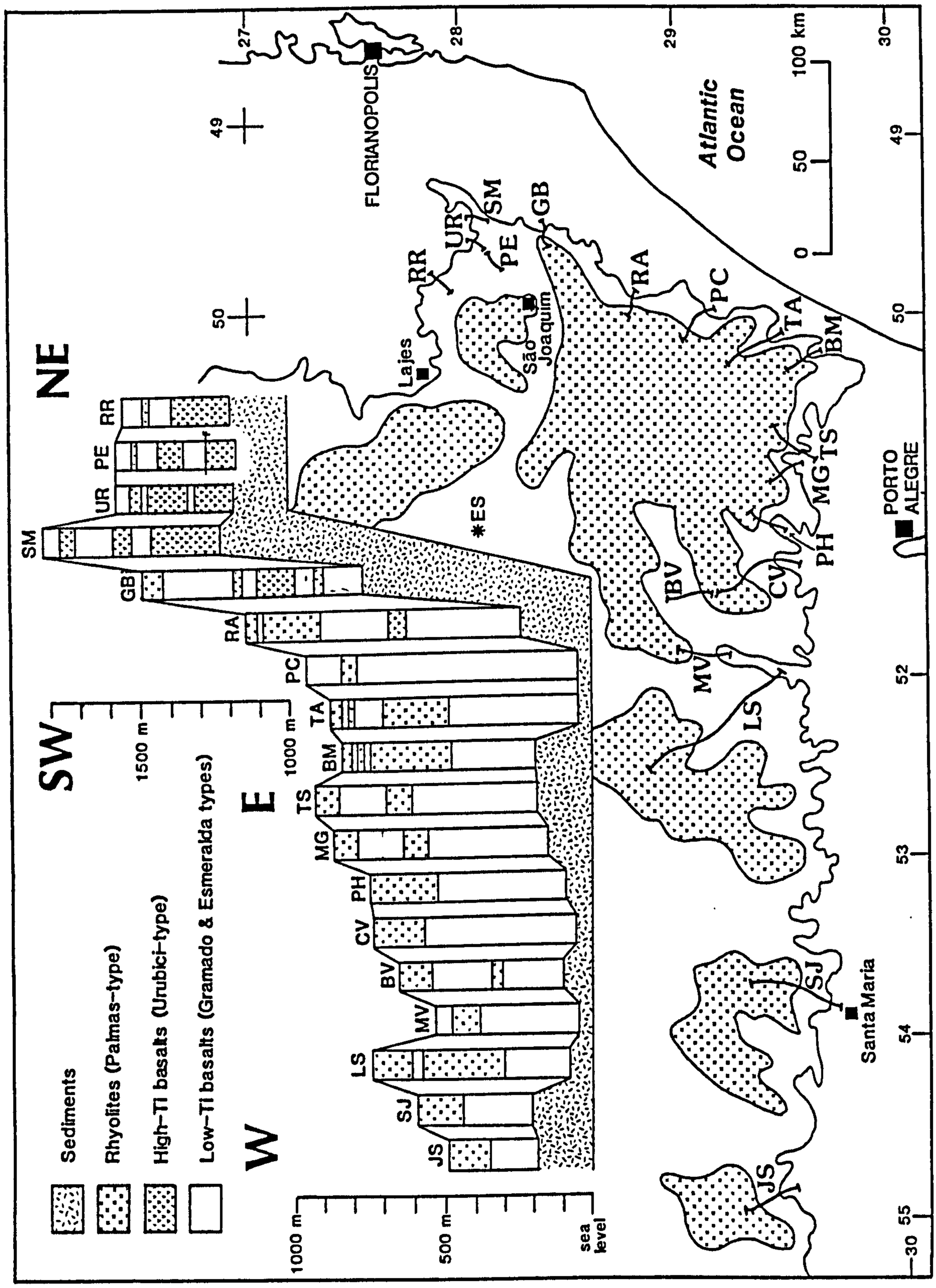

Figure 2.15 Compilation of all available sampled road sections through the southern Paraná lava sequences in Rio Grande do Sul and Santa Catarina states, south Brazil. The main map shows the surface distribution of the rhyolites and the location of each profile. The inset gives stratigraphical details for each profile, and illustrates that; (i) rhyolites form several distinct units and are concentrated in the upper half of the sequence, (ii) flows of the Urubici magma type only occur north of ~29°S, where they dominate the lower portion of the lava pile, and (iii) the sharp increase (1 km) in elevation of the base of the lava pile to the north along the coastal Serra Geral escarpment. Data sources; - [this study, Bellieni *et al.*, (1986b), Hawkesworth *et al.*, (1988)].

rhyolites form a significant proportion of the lava sequences of south-east Paraná. The surface distribution of the rhyolites (Bellieni *et al.*, 1986b; Hawkesworth *et al.*, 1988) shows that they are restricted towards the present day continental margin where they attain thicknesses of almost 400 m (Barra do Ouro-Morrinhos 'BM' section). Away from the sampled profiles, to the west and north, there is a significant decrease in thickness of the acidic volcanics (Bellieni *et al.*, 1986b). The rhyolites are also concentrated towards the upper parts of the lava pile and, especially in the uppermost portions, there is often some interbedding with basaltic flows. The acidic rocks of this region are almost exclusively of the Palmas type, with the Chapecó type only occurring in the extreme north-west.

Bellieni *et al.*, (1986b) noted the laterally persistent sheet-like nature of the acidic volcanics, with individual Palmas-type flows traceable over 60 km, which suggested that the Paraná rhyolites might be ignimbrites, considering the high viscosity of acidic magma. This view was in conflict with the apparent lack of pyroclastic textures typical of ignimbrites and Bellieni *et al.*, (1986b) suggested that the high temperatures (>1000 °C) and low volatile content had led to strong welding thus producing their lava-like appearance. A detailed study of the volcanological features of equivalent acidic rocks in the contemporaneous Etendeka province in Namibia by Milner (1986) showed that the rhyolites preserved features common to both acid lavas and ignimbrites. The extensive sheet-like form of the rhyolitic units and local preservation of pyroclastic features were all evidence pointing towards an ignimbritic origin and Milner (1986) interpreted them as high-temperature ash flows or rheo-ignimbrites. In the final stages of emplacement, such flows can still maintain sufficient heat and momentum to induce viscous lava-like flowage, producing the autobrecciation and flow banding more commonly associated with rhyolitic lavas.

Studies by Milner and Duncan (1987) have shown that individual rhyolitic units have extremely uniform chemical compositions with no significant lateral variation even over 150 km. Even though the Etendeka rhyolites as a whole have a rather uniform composition, small but significant compositional differences especially of TiO_2, $Fe_2O_3(t)$ and Cu exist between some units, which allowed a stratigraphical subdivision of the

Etendeka lava sequences, and Milner and Duncan (1987) recognised six distinct rhyolite units that could be correlated across the province.

A similar approach is needed for the Paraná rhyolites and has recently been initiated by workers at Oxford University. If individual rhyolite units can be recognised and characterised on the basis of their chemical composition, then their widespread nature and internally uniform composition makes them ideal marker horizons to be used to correlate the acidic volcanics between road sections. The compilation of road section profiles illustrated in figure 2.15 hints at the existence of at least three rhyolite units along the southern margin of the province. The lowest unit lies in the five westernmost sections at an elevation of between 300-550 m, the middle unit occurs between 500-700 m capping the sections at 'LS', 'BV', 'CV', 'PH' and towards the central parts of the 'MG', 'TS', 'BM', 'TA' sequences, and the upper unit lies between 750-900 m in the sections from 'MG' eastwards. These speculative units could be confirmed by consideration of their composition and by linking them to the palaeomagnetic variations already established (see figure 2.2), which would also allow a better correlation of individual polarity events. The palaeomagnetic data of figure 2.2 has already established that the first rhyolite units at the 'RA' section were contemporaneous with basaltic lavas at 'GB' and therefore must be due to an earlier eruptive event than that responsible for the rhyolites capping the 'GB' section which is only 50 km to the northeast. Thus the basalt - rhyolite contact is not a chronostratigraphical boundary over the area. The rhyolites offer the best hope in constraining the internal structure of the lava pile in this region and thus in assessing any possible west to east migration of magmatism as suggested by the palaeomagnetic data, especially in light of the possible large scale rhyolite units postulated above for this southern area. An ultimate aim must be to attempt a direct geochemical correlation between the Paraná and Etendeka rhyolites especially since most of the Etendeka units thicken westwards indicating a source area towards the Paraná (Milner and Duncan, 1987).

2.6.3 Temporal change in low-Ti basaltic magma type.

Within this region, Fodor *et al.*, (1985a) recognised distinct subgroups of the low-Ti basalts and in section 2.4 above, this classification was expanded and two separate magma types were established, *viz.* Gramado and Esmeralda. The aim of this section is to unravel the field relations between rocks of these two magma types, and consideration of their petrogenetic relationship is left until chapter four.

In all sections through the lavas where rocks of the Esmeralda magma type have been recognised, they either occur as the uppermost flows, as in the road sections at Morro da Igreja (SM) and Muçum-Vespasiano Correia (MV) and in the Esmeralda borehole (ES), or interbedded with Palmas-type rhyolites near the top of the lava sequence as found in the Rocinha-Encruzilhada (RA) road section (see figure 2.16). This suggests that over the south-east corner of the lava field at least, the Esmeralda magma type represents the last magmatic episode recognised, prior to initiation of the South Atlantic ocean. This is consistent with the observation that the sills and dykes crosscutting the lava sequences in the São Joaquim region were almost exclusively of the Esmeralda magma type.

The conclusion that the Gramado and Esmeralda magma types are sequentially related seems to be in contradiction with the original observation of Fodor *et al.*, (1985a) that rocks of the two magma types lay in adjacent geographical sectors (there was a slight overlap of samples between the sectors, with sample MRO-3 in sector II but having the characteristics of the sector I rocks) and that they just represented geographical variations within the low-Ti group (see figure 2.16). It is important to verify the spatial relationship of the two magma types, whether they are in stratigraphical succession or just geographically side-by-side, as this has a bearing on establishing the underlying cause for the difference between the magma types. Either the difference was imposed by the geographical location which might suggest control by a differing magmatic plumbing system that allowed variable amounts of contamination/mixing/crystallisation to affect the lavas in different areas, or there was a temporal change over the whole region from the Gramado to the Esmeralda

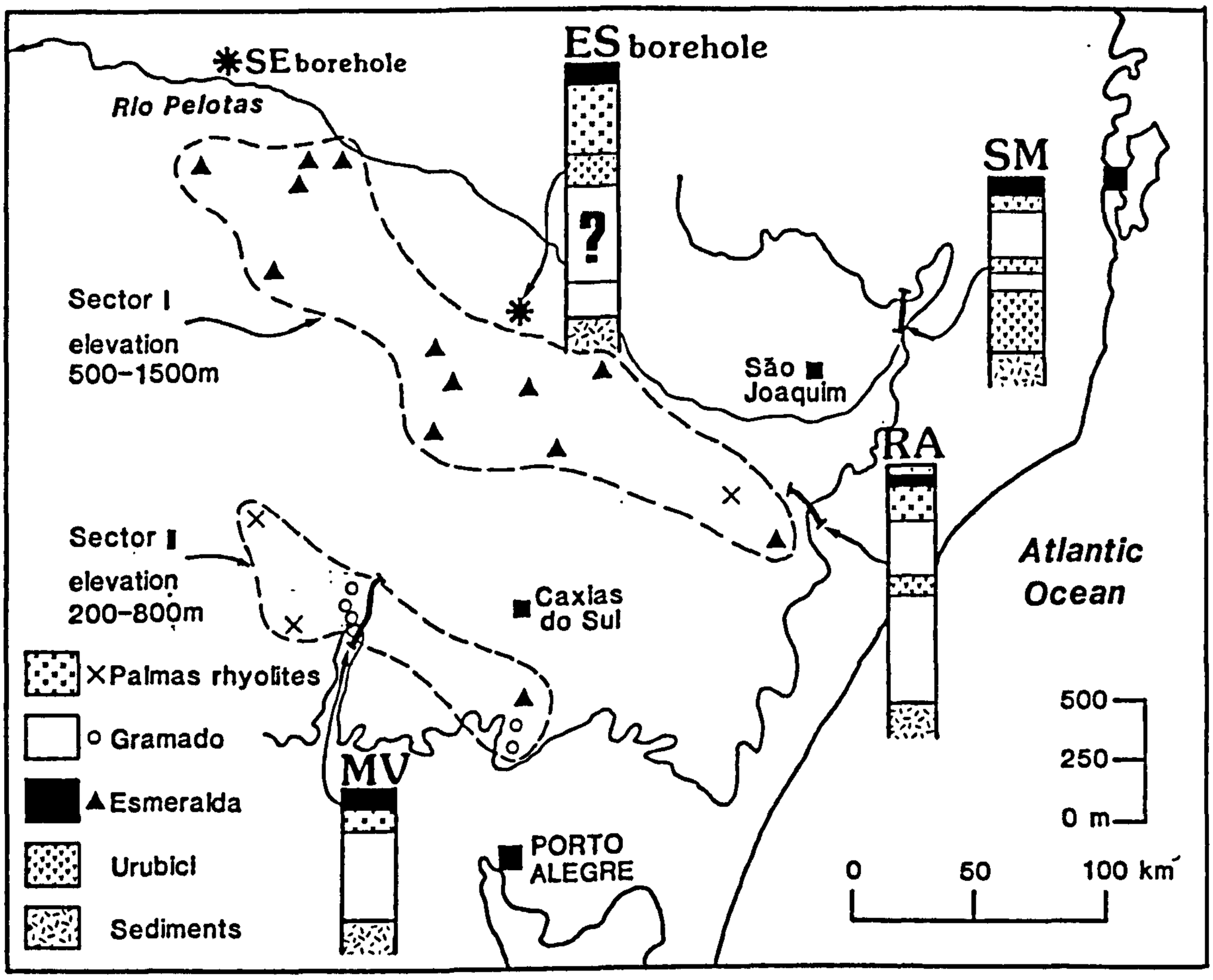

Figure 2.16 Map of the southern Paraná region (adapted from Fodor *et al.*, 1985a), showing the spatial relationship between the low-Ti magma types. The scattered symbols denote sample localities in Fodor *et al.*, (1985a), and are grouped into two compositionally distinct geographical sectors, sector I (= Esmeralda magma type) and sector II (= Gramado magma type). The sampled sections through the lava pile indicate that the two magma types actually define stratigraphical units, and demonstrate a temporal change in low-Ti magmatism from Gramado- to Esmeralda- type magmas (see text for discussion). Stratigraphical sections are from this study ('SM', 'ES' borehole), Bellieni *et al.*, (1984c) ('RA') and Hawkesworth *et al.*, (1988) ('MV').

magma type. Comparison of the average elevation of the two areas from Fodor *et al.*, (1985a) shows that topographic heights within sector I (Esmeralda type) lie between 500 m and 1500 m and are generally over 1000 m whereas the elevation of sector II (Gramado type) falls in the range 200 m to 1000 m with most of the area between 500 m and 800 m (all heights were taken from 'The Times' atlas 1:5,000,000 map). In view of the sub-horizontal dip of the lavas, it seems reasonable therefore to assume that the sector I or Esmeralda-type rocks overlie those of sector II or Gramado magma type, in keeping with the stratigraphical profiles from around the edge of the lava field, and hence the

geographical domains of Fodor *et al.*, (1985a) were purely a function of the present-day erosional surface.

The stratigraphical profiles shown in figure 2.16 imply that the eruption of the Esmeralda lavas was contemporaneous with, or post-dated, the rhyolitic magmatism. An important aspect is the areal extent of the Esmeralda lavas since, if this mirrors the distribution of the rhyolites and is concentrated towards the present day continental margin, then this might demonstrate a direct association with the rhyolitic magmatism and possibly indicate a related tectonic processes for the origin of both. The extent of the Esmeralda rocks inland, and outside the area depicted in figure 2.16, is uncertain, and boils down to the problems of interpreting the low-Ti basalts of Petrini *et al.*, (1987) from the central area.

2.6.4 Relationship of lavas to underlying sediments.

From figure 2.15 it is clear that moving from east to west along the southern margin of the lava field, the height of the base of the lavas remains roughly constant, undulating between 50 m and 150 m a.s.l., over a distance of 300 km inland. In contrast, along the Serra Geral escarpment parallel to the Atlantic coast, the basal contact of the basalts with the sediments rapidly cuts up section being much higher in the north, though over this distance there is only a gradual increase in elevation of the escarpment itself from about 1000 m in the south to about 1500 m in the north. The contact of the lavas on the underlying Botucatu sandstones progressively climbs from near sea level in the south (at Torres, the lavas actually reach the shoreline) to in excess of 1000 m in the area near São Joaquim (at 'TA' and 'PC' 50 m, 'RA' 240 m, 'GB' 760 m, 'SM' 1230 m).

There are three possible options to explain this phenomenon; (i) it could have been formed as a result of pre-Paraná topography controlling the local distribution of the lavas, (ii) it could be a tectonic feature produced by epeirogenic uplift subsequent to the eruption of the basalts, or (iii) it could be a more localised disturbance produced by the intrusion of the Lajes alkaline complex. The presence of an escarpment in the first place suggests that a certain amount of post-eruptional uplift has occurred which might have been more extensive to the north, but the fact that the present escarpment forms the watershed for the south

Paraná region and is parallel to the coastal margin suggests that this can not be the whole story. The marked variation in elevation of the base of the lava pile runs parallel not perpendicular to the escarpment which suggests that it was present to some extent before any epeirogenic uplift. On a local scale within the field area in the São Joaquim region (see section 2.5.4) the rather limited data indicates that the lavas successively overstep sediments to north-east and have essentially 'ponded-up' against the original topographic features. How representative this is of the more regional-scale variations is uncertain since the internal structure of lava pile along the rest of the Serra Geral escarpment is still poorly defined. There is a need to integrate palaeomagnetic and chemical data on basalts and rhyolites for the profiles to the south of 'GB' before this can be further evaluated. It is noteworthy in light of this scenario that the lavas do not cut down into sediments and in all sections lie directly on sandstones of the Botucatu formation. The Lajes alkaline complex is situated about 50 km to the east of the São Joaquim study area and is younger than the Paraná lavas, having an age of 100-40 Ma (L.F. Scheibe, pers. comm., 1988). A 'doming' process related to the intrusion of the massif has exposed a concentric arrangement of Carboniferous to Cretaceous sediments of the Paraná sedimentary basin sequences, lying higher than the surrounding basaltic lavas, and forming an embayment into the present surface extent of the lava field. The 'RR' section lies midway between the 'SM' section and Lajes and yet the basal contact of the lavas is virtually horizontal in both sections, hence the Lajes intrusion does not seem to have had a marked effect in disturbing the lavas except in its immediate locality, within a radius of about 40 km.

2.7 Borehole Stratigraphy.

2.7.1 Sample selection and preparation.

Between 1979 and 1982, thirty-three new oil exploration boreholes were drilled in the Paraná basin, penetrating the Paraná lavas through into the underlying sedimentary sequences (Paulipetro, 1982). Ten of these recently drilled boreholes were chosen in order to give a north-south profile roughly parallel to the main axis of lava thickness (see figure

1.5). Unfortunately the lavas were not cored during drilling due to the high cost and time involved (for oil exploration, the basalts are rather an inconvenience), and the only available samples are the rock chips collected by the mudloggers.

Initial selection of samples from a given borehole was made by Prof. M.S.M. Mantovani (São Paulo University) in Brazil after an assessment of the quality of the collected material and a detailed analysis of the geophysical well-log data which gave an estimate of the position of contact between successive lava flows. The nature of the available material as small rock chips 0.1 cm to 1 cm in size, the limited quantity of each sample, and its collection over a certain thickness range within the borehole, all conspired to make it difficult to assess the extent of within-flow variation caused by *in situ* differentiation and/or varying degrees of alteration. Each sample is the result of the accumulation of rock fragments from at least a 3 m to 4 m depth range in the drillhole and thus any analysis will represent an average over this range of lava thickness. Because of these problems, each sample of rock chips was carefully handpicked under optical magnification, firstly to avoid any fragments with vesicular infillings or that showed any visible signs of mineralisation or alteration, and secondly to try and ensure that all of the sample to be analysed came from the same lithological unit. Once 30 g to 50 g had been sorted, the selected fragments were washed several times with distilled water in an ultrasonic bath to remove any surface dust and drilling mud, and the final product was then crushed in an agate satellite ball-mill.

2.7.2 Reliability of geochemical data.

Clearly the first concern is whether samples collected and prepared in this manner yield reliable geochemical data that is consistent with those obtained on the surface lavas. Figure 2.17 gives the variation of TiO_2 vs. MgO for the main basaltic magma types (Gramado, Paranapanema and Pitanga) recognised from the borehole data. This shows the good agreement between the data from the borehole samples and average compositions of surface lavas of the three magma types sampled in the central area of the Paraná province

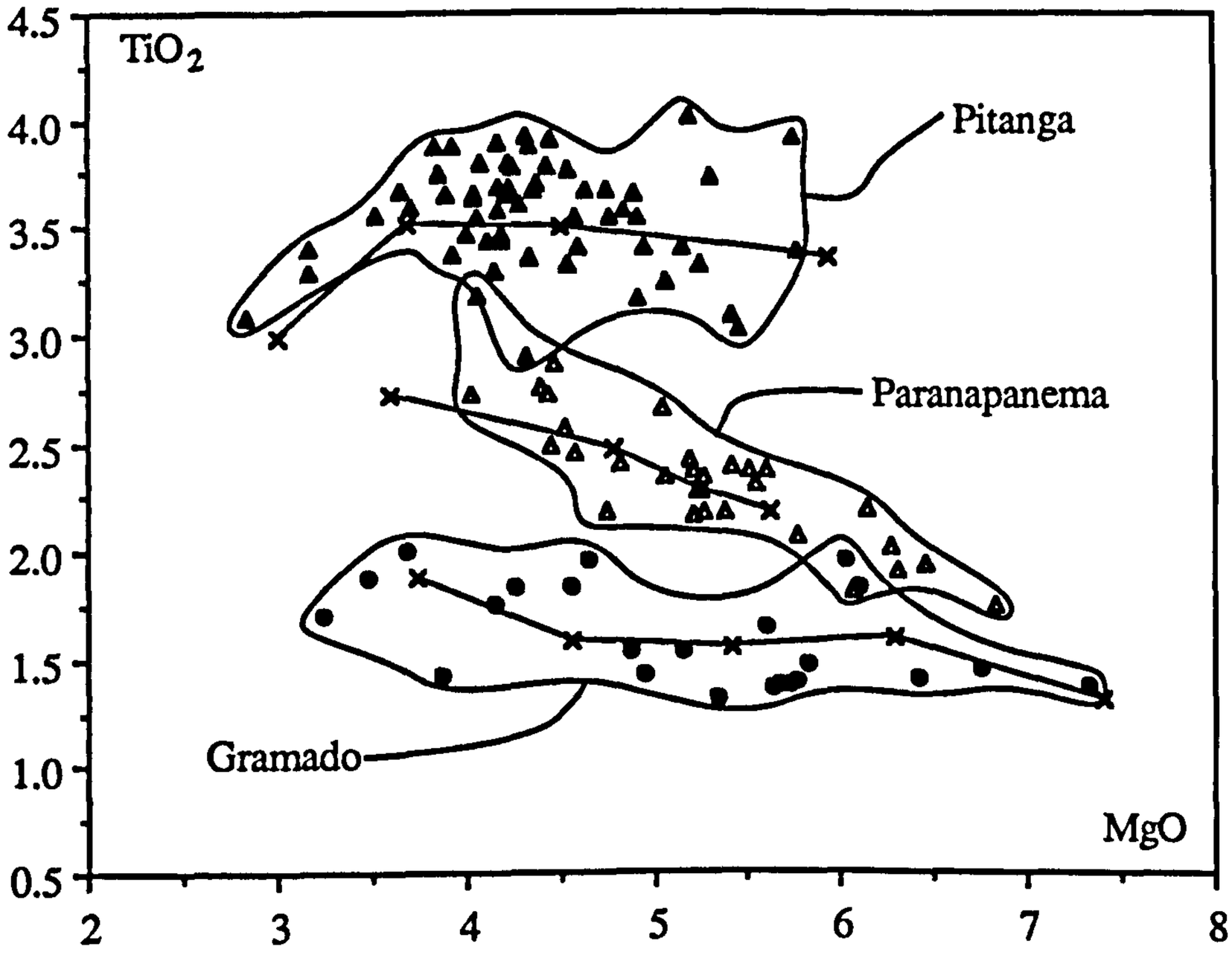

Figure 2.17 TiO_2 vs. MgO variation for analyses on borehole drill chippings (n=??? samples), showing the clear division into three groups; the Gramado, Paranapanema and Pitanga magma types. The joined-up 'crosses' within each group are average analyses taken fron Piccirillo *et al.*, (1988a) and demonstrate the good agreement between surface samples and this borehole material.

(Piccirillo *et al.*, 1988a). On the whole the major element variations within each magma type encountered in the boreholes show remarkably good trends with a scatter similar to that found for analyses of surface lavas though for some elements, namely Na and Ca, a few samples lie significantly off these trends. There is no petrographical control to assess the reasons for this but these samples do have noticeably higher loss on ignition (L.O.I.) values and appear to have gained Na at the expense of Ca. Since L.O.I. gives an approximation of volatile loss, it can be used as a crude indication of the degree of post-solidification alteration of the sample. For fresh samples no correlation is expected between elemental abundance and L.O.I.. This is illustrated in figure 2.18 using the Na_2O contents of borehole samples of just the Paranapanema magma type. The majority of the samples form a cloud of data at low L.O.I. values, but for the more altered samples, reflected by their higher L.O.I. values generally greater than 1 %, there is a marked positive correlation between Na_2O and L.O.I.. It is worth noting how this also affects the normative classification of the basalts, and the data points on figure 2.18 are marked according to their

normative character. Unaltered lavas of the Paranapanema magma type are dominantly quartz tholeiites though probably straddling the plane of silica saturation into the olivine tholeiite field. Samples with high L.O.I. show normative olivine and most are also nepheline-normative which would classify them as alkali basalts, obviously not a characteristic of the original lava composition.

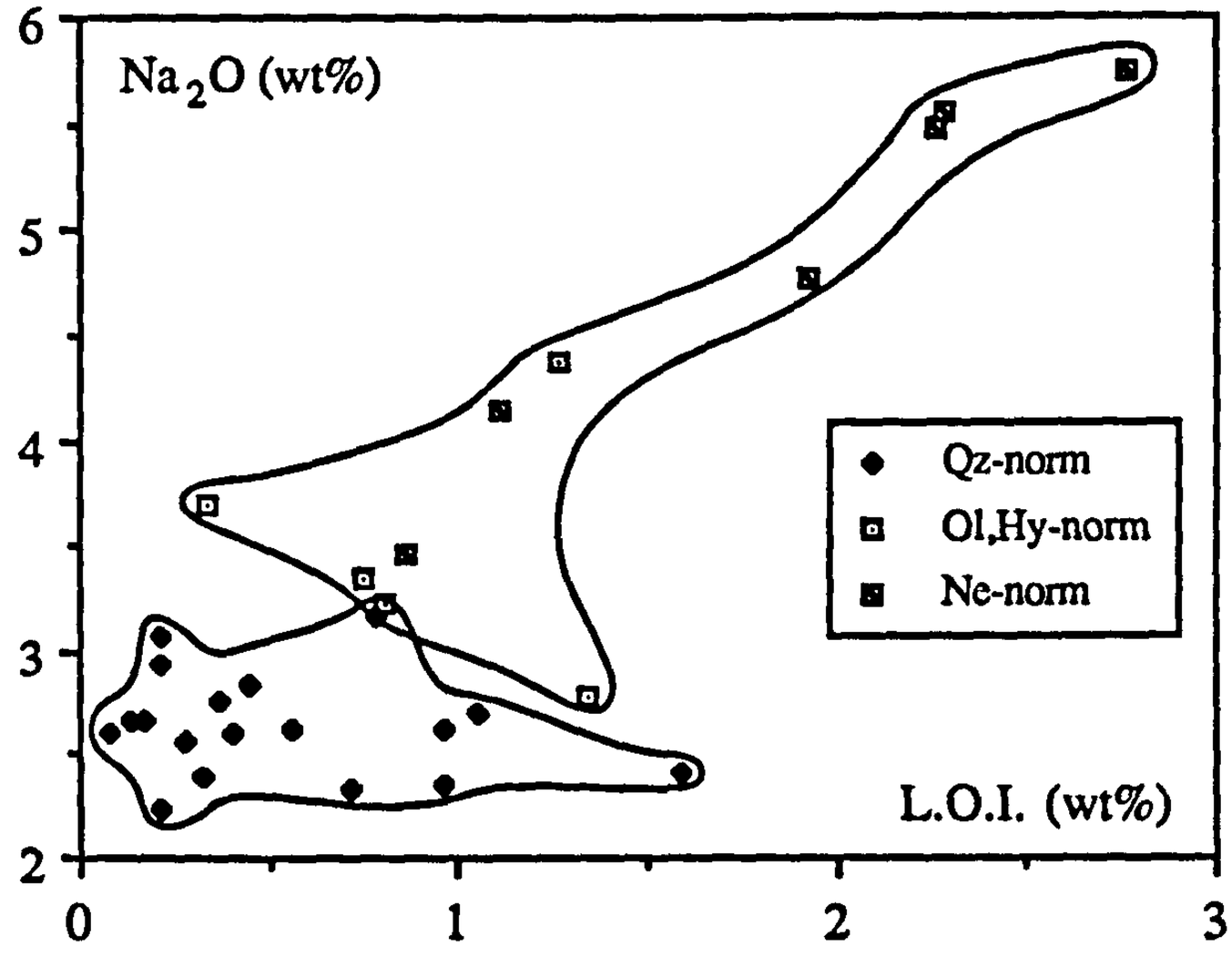

Figure 2.18 Na_2O vs. L.O.I. (loss on ignition at 1000°C) variation, illustrating the effects of alteration on borehole samples of the Paranapanema magma type. Samples with L.O.I. > ~1 wt% show a positive correlation with Na_2O content, and have high Na_2O > 3 wt%. Note the change in normative character of the altered lavas towards Ne-normative compositions (*i.e.* alkali basalts).

The extent of alteration processes can only be assessed qualitatively because of the nature of the samples. Marsh and Eales (1984) demonstrated that Na, K, Rb, Sr and Ba were particularly susceptible to mobilisation during hydrothermal alteration. Although Rb and K_2O vs. MgO is fairly scattered, good positive trends are observed for Ba vs. Rb and K_2O. Thus while some 'noise' may have been introduced by alteration and this method of sample preparation, the bulk chemical trends and particularly those for the less mobile elements, are similar to the trends observed in the surface rocks.

Several borehole samples of the Paranapanema and Pitanga magma types were analysed for Sr and Pb isotopic composition. The validity of such results from this borehole material can be assessed by a comparison with isotopic analyses of surface samples. The borehole Sr isotope data were reasonably consistent with the limited data available from this study and the literature. For the Paranapanema magma type, the borehole samples give a range in $(^{87}Sr/^{86}Sr)_i$ of 0.7055-0.7065 compared with 0.7058-0.7078 obtained on surface samples (this study; Mantovani *et al.*, 1985a; Piccirillo *et al.*, 1987), and for the Pitanga magma type the borehole samples give slightly lower values of $(^{87}Sr/^{86}Sr)_i$ than surface samples (Piccirillo *et al.*, 1987), 0.7055-0.7058 versus 0.7059-0.7060. For the surface samples, Pb isotope analyses are only available for the Paranapanema magma type (this study; Cordani *et al.*, 1989). The borehole Paranapanema-type samples had a similar range in $^{207}Pb/^{204}Pb$ (15.5-15.6) to that found for the surface samples but at generally lower $^{206}Pb/^{204}Pb$ values (17.5-18.0 vs.17.8-18.2), and this is shown on figure 2.19(a). Figure 2.19(b) illustrates that the decrease in $^{206}Pb/^{204}Pb$ was accompanied by large decrease in $^{208}Pb/^{204}Pb$ (37.4-38.4 vs. 38.3-38.5) which trended below the overall Paraná data, as defined by the Gramado and Urubici magma types. Since the few Pitanga-type borehole samples also showed a similar trend on the $^{208}Pb/^{204}Pb$ vs.

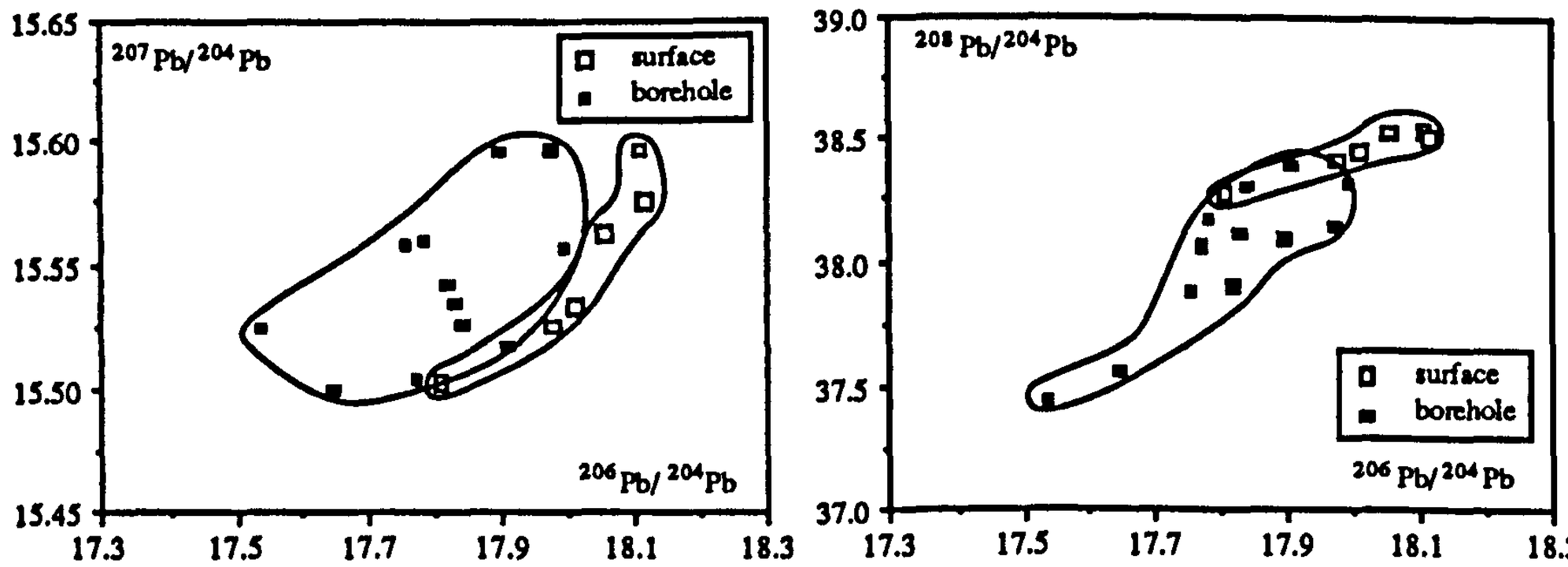

Figure 2.19 Comparison of Pb isotope data for the Paranapanema magma type samples between surface samples and borehole material, showing that the borehole analyses should be treated with suspicion: (a) $^{207}Pb/^{204}Pb$ vs. $^{206}Pb/^{204}Pb$ - borehole samples have a similar range in $^{207}Pb/^{204}Pb$ to the surface samples but at lower $^{206}Pb/^{204}Pb$ values; (b) $^{208}Pb/^{204}Pb$ vs. $^{206}Pb/^{204}Pb$ - borehole samples are displaced below the surface samples to low $^{208}Pb/^{204}Pb$ and low $^{206}Pb/^{204}Pb$.

$^{206}Pb/^{204}Pb$ diagram, this suggests that the borehole data should be treated with caution as regards Pb isotope analyses.

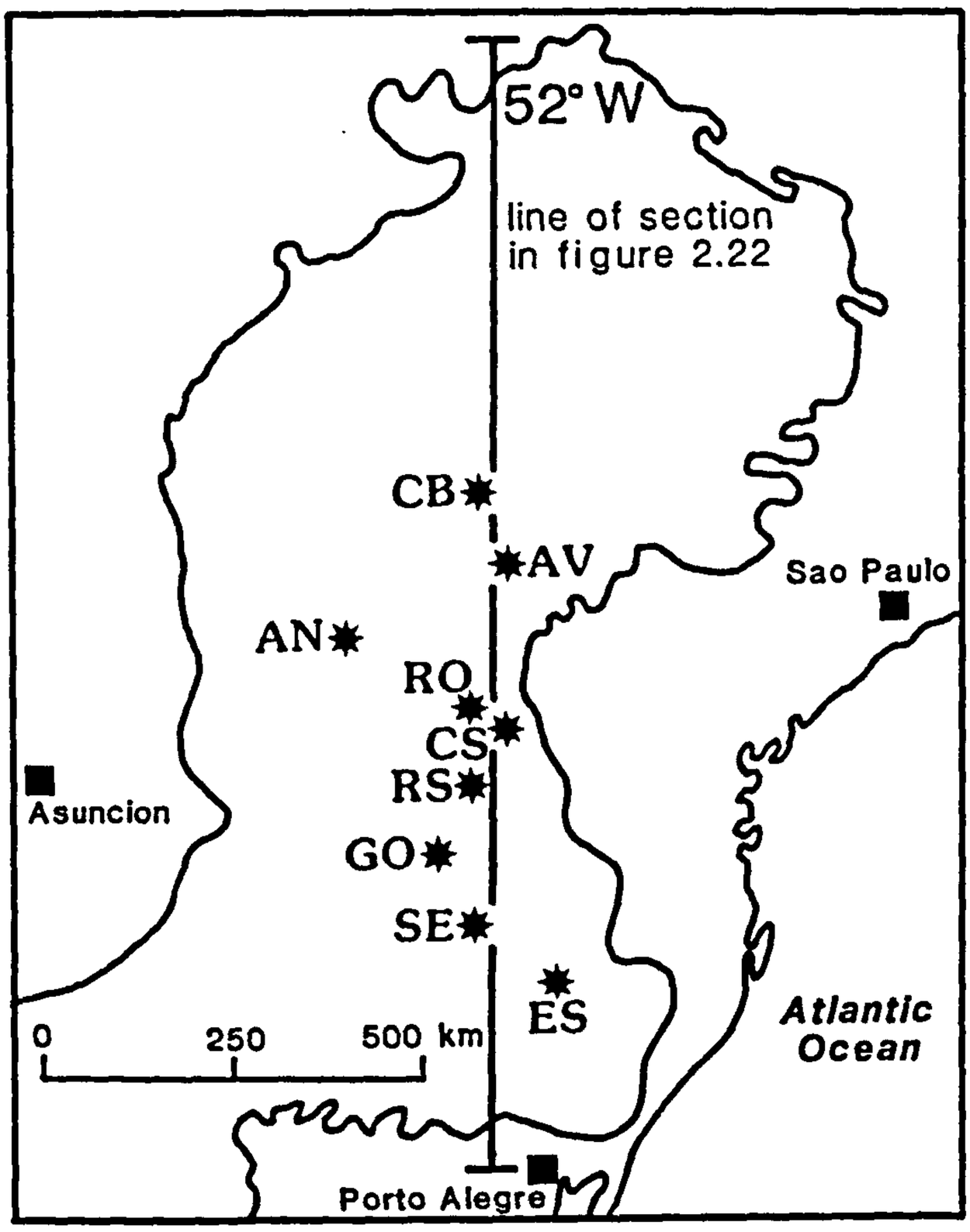

Figure 2.20 Location map of the nine studied boreholes. They span a roughly N-S direction along longitude 52° W; the line of section in figure 2.22.

2.7.3 Chemical variation within boreholes.

The boreholes studied span a north-south distance of about 650 km from 22° S to 28° S and are spaced on average roughly 100 km apart. Figure 2.20 shows the location of the studied boreholes, and further details of the borehole locations are given in table C.2 in appendix C. At the current state of this study, which is still in progress, geochemical data are available from nine of the boreholes, including the 'CB' borehole which is important in view of its location over the deepest known and thickest part of the lava pile. The 'CB' hole cuts through 1723 m of basalts down to the basal contact with the sandstones of the

Botucatu formation that was encountered at a depth of 1534 m below sea level. As yet, sampling and analysis within each borehole is not complete, and the sampling interval also depends on the quality of the recovered material. The average interval between analysed samples taking all the boreholes into account is about 65 m, though for some of the studied boreholes this spacing is much closer (*i.e.* 'RS' average of 34 m, 'CB' average of 43 m). For comparison, lava flows exposed in road sections on the Serra Geral escarpment in the São Joaquim area (see section 2.5 above) had an average thickness of 20 m to 25 m.

Figures 2.21(a) and 2.21(b) show the chemical variation of TiO_2 and Zr/Y respectively with depth for the nine boreholes. Each sample has been assigned to a particular magma type using the criteria outlined in section 2.4 above, and the magma type is indicated on the figures by the appropriate symbol. The lava sequences penetrated by these boreholes are dominated by three main magma types; Gramado, Paranapanema, Pitanga. Minor amounts (< 10% of samples) of other magma types have been found in some boreholes; Chapecó rhyolites towards the top of the 'RS' hole, both Palmas rhyolites and Esmeralda basalts form the upper third of the 'ES' hole, and Urubici-type lavas occur within the 'ES' hole as well as at the base of the 'RO' hole.

An encouraging feature of figures 2.21(a) and 2.21(b) is the coherent compositional variations with depth down each borehole. Lavas of a given magma type occur as packets of sequential flows so that each magma type forms a discrete stratigraphical unit. Within an individual borehole a consistent stratigraphy is observed and the same pattern or order of stratigraphical units can be traced between the boreholes. Samples from the three main magma types can be used to delineate three geochemical units within the lava pile, and in general, lavas of Paranapanema-type overlie sequences of Pitanga flows which in turn overlie Gramado-type lavas to the south. Therefore, for the borehole sequences, the magma types have become approximate or preliminary stratigraphical units. Employed in this sense, a 'stratigraphical unit' is analogous in nomenclature terms to the 'stratigraphical formations' used to subdivide the Deccan lavas, although with our current knowledge of the regional lava stratigraphy it is somewhat premature to begin to define individual formations.

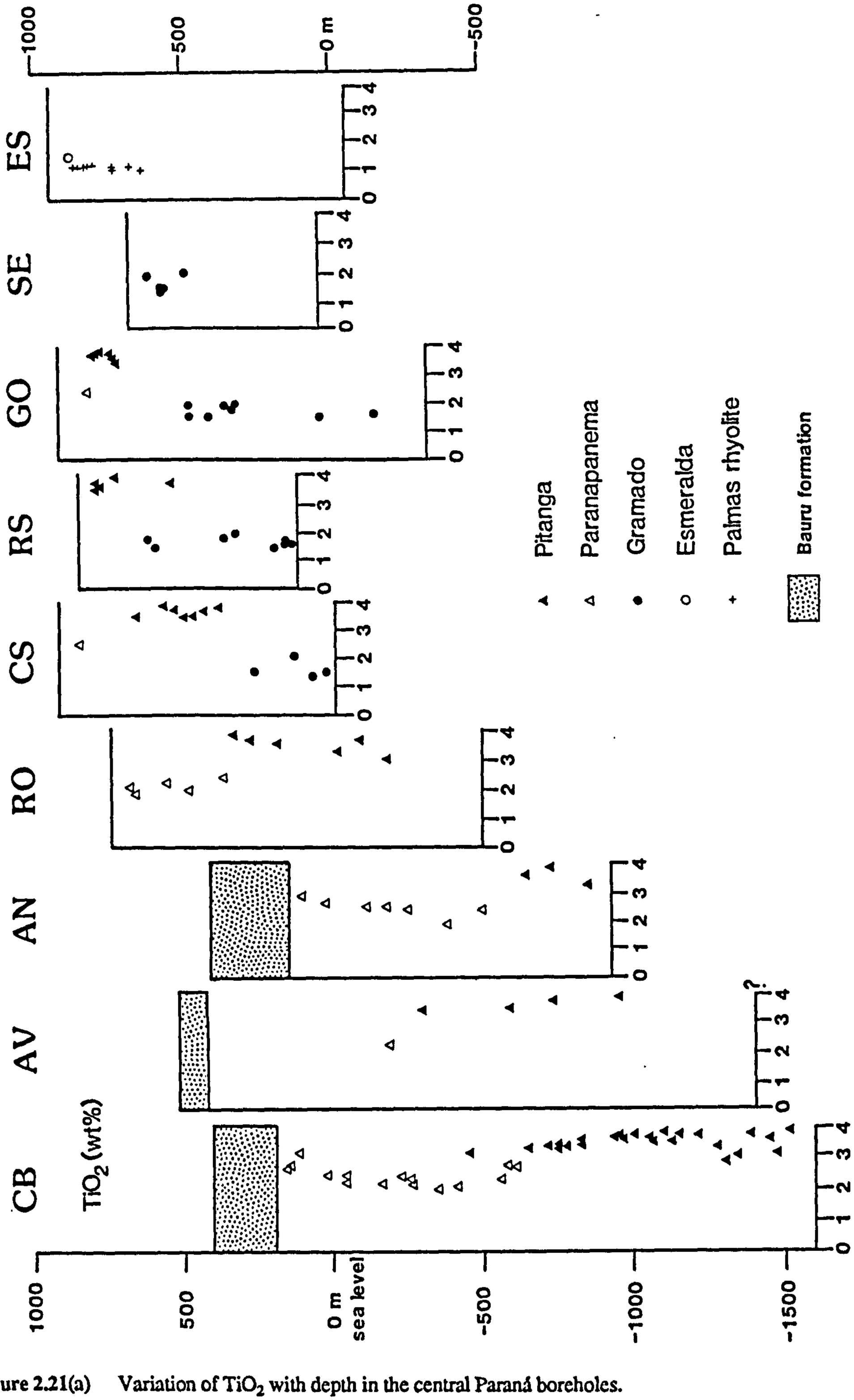

Figure 2.21(a) Variation of TiO_2 with depth in the central Paraná boreholes.

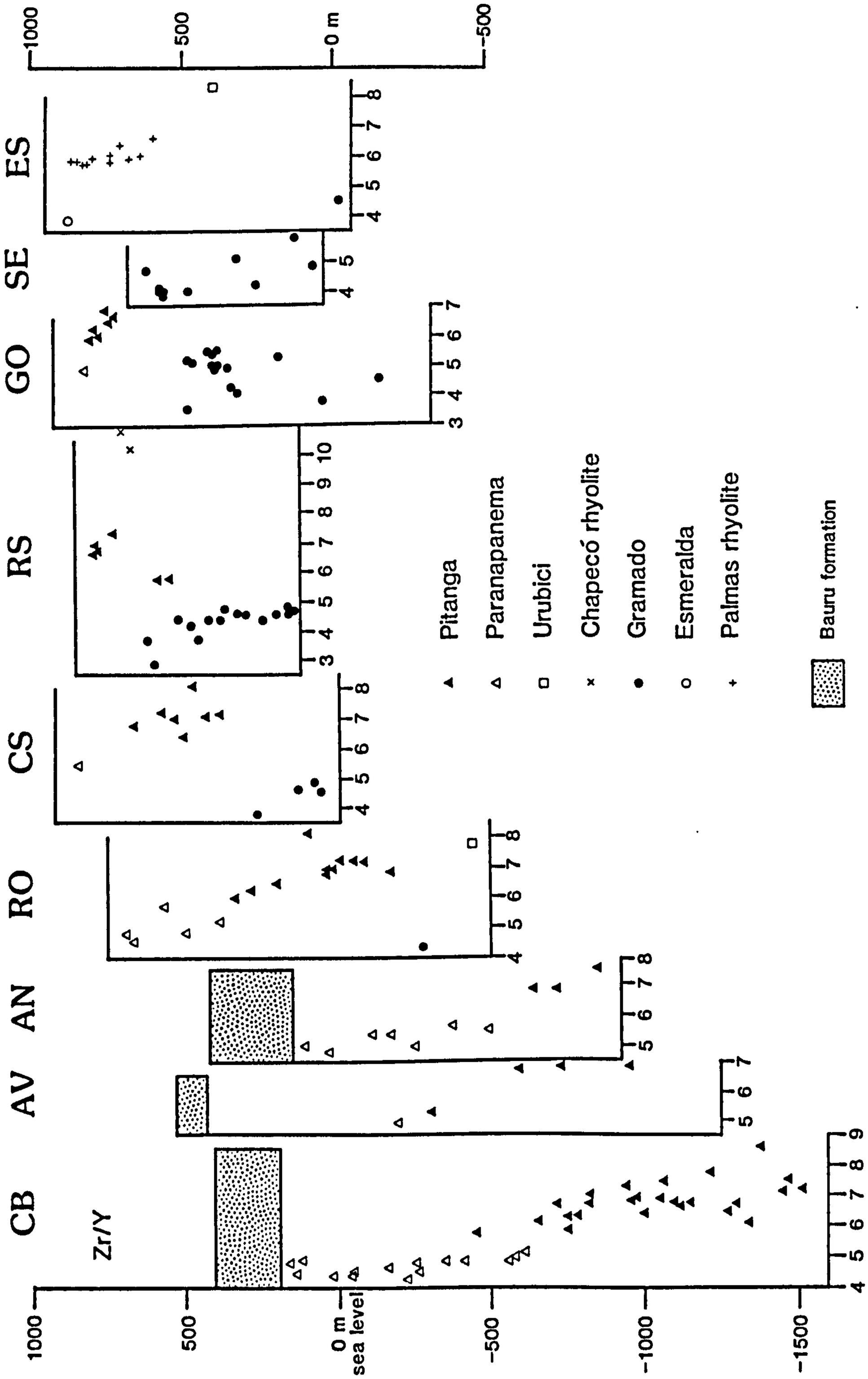

Figure 2.21(b) Variation of Zr/Y with depth in the central Paraná boreholes.

Within the northern boreholes, the contact between the lava packets defined by the Pitanga and Paranapanema magma types occurs at successively lower heights in each borehole moving north, suggesting a northerly regional dip of about 0.25°, ('CS' 751 ± 96 m, 'RO' 351 ± 17 m, 'AV' -242 ± 57 m, 'CB' -629 ± 22 m). In the 'AN' borehole which lies significantly further west than the other holes, the contact is deeper (-564 ± 74 m) than might have been expected if it was extrapolated onto the north-south profile through the other boreholes, implying a westerly component of dip for this boundary. Similarly in the central area, the transition in magma type from Gramado to Pitanga occurs at greater depths towards the north, ('GO' 586 ± 111 m, 'RS' 526 ± 15 m, 'CS' 319 ± 63 m, 'RO' -229 ± 47 m).

As well as considering the absolute depth of the contacts between the stratigraphical units, their position within the lava pile and relationship to the base of the lavas are also of importance since these can indicate whether the units 'pinch-out' or 'expand' down-dip, features which have implications for the emplacement history of the province. Consideration of figures 2.21(a) and 2.21(b) indicates that the Gramado unit thins rapidly down-dip to the north in contrast to the Pitanga unit that pinches-out as it overlaps the Gramado unit southwards. There is no clear picture for the Paranapanema unit since it forms the uppermost unit and the quantity removed through surface erosion is uncertain.

In the boreholes where the sample spacing approaches the typical dimensions of individual lava flows, as in the 'RS' and 'CB' holes, a more detailed picture emerges, and the contact zone between successive units is shown to be more complex. Within the 'RS' borehole the contact between the Gramado unit and the overlying Pitanga unit is marked by a zone 187 ± 28 m thick, as defined by six samples, where the two magma types are interbedded. This transition zone is further complicated by the presence of 50 m to 100 m of Chapecó rhyolites. The boundary between the Paranapanema and Pitanga units in the 'CB' hole is also not clearly defined, and over a distance similar to that of the transition zone in the RS' hole (198 ± 41 m), flows of the two magma types are interbedded (CB846 is of Pitanga-type, CB954 is of Paranapanema-type) and in addition several flows show transitional characteristics between the two types. The samples CB975/1002 have

intermediate TiO_2 contents (2.75-2.85 wt%) and yet have several features more characteristic of the Pitanga magma type including high P_2O_5 (0.65 wt%) and higher LREE and Th. This is analogous to the problems described by Cox and Hawkesworth, (1985) in defining formation boundaries in the Deccan sequences where flows of different magma types are interbedded in the contact zones and can show transitional compositions.

2.7.4 Regional stratigraphy.

These borehole results may be integrated with data on the surface lava exposures and the depth to the base of the lavas to construct a north-south section across the Paraná basin along longitude 52° W. The diagram given in figure 2.22 is a schematic profile intended to give a synopsis of the general features of the lava field stratigraphy. The borehole samples have shown a stacking of units of different magma types all stepping up towards the north. The sequence has Paranapanema-type flows overlying lavas of the Pitanga magma type which in turn overlie Gramado-type flows in the more southerly boreholes. This lithostratigraphical pattern of units defined by specific magma types has several implications for the development of this part of the magmatic province.

Firstly it indicates that the dominant magma type has evolved from Gramado (low-Ti) to Pitanga (high-Ti) to Paranapanema (intermediate-Ti) with time. This can be compared to the Karoo lava sequences in the Lebombo monocline in southern Africa, where there is a similar provinciality with low-Ti rocks to the south and high-Ti to the north. At the boundary between the two provinces in the Sabie River area, the two magma types overlap over a distance of 60 km laterally with the high-Ti dominant at the base of the sequence and overlain by low-Ti magmas (Erlank *et al.*, 1988). This is a similar sense of overlap to that deduced for the Urubici and Gramado magma types in the coastal sequences of the southern Paraná/Etendeka lava field, but opposite to that revealed in the main Paraná lava field from the boreholes where the Pitanga (high-Ti) magmas overlie the Gramado (low-Ti) magmas over about 200 km.

Secondly the overlapping sequence of units dipping towards the north might

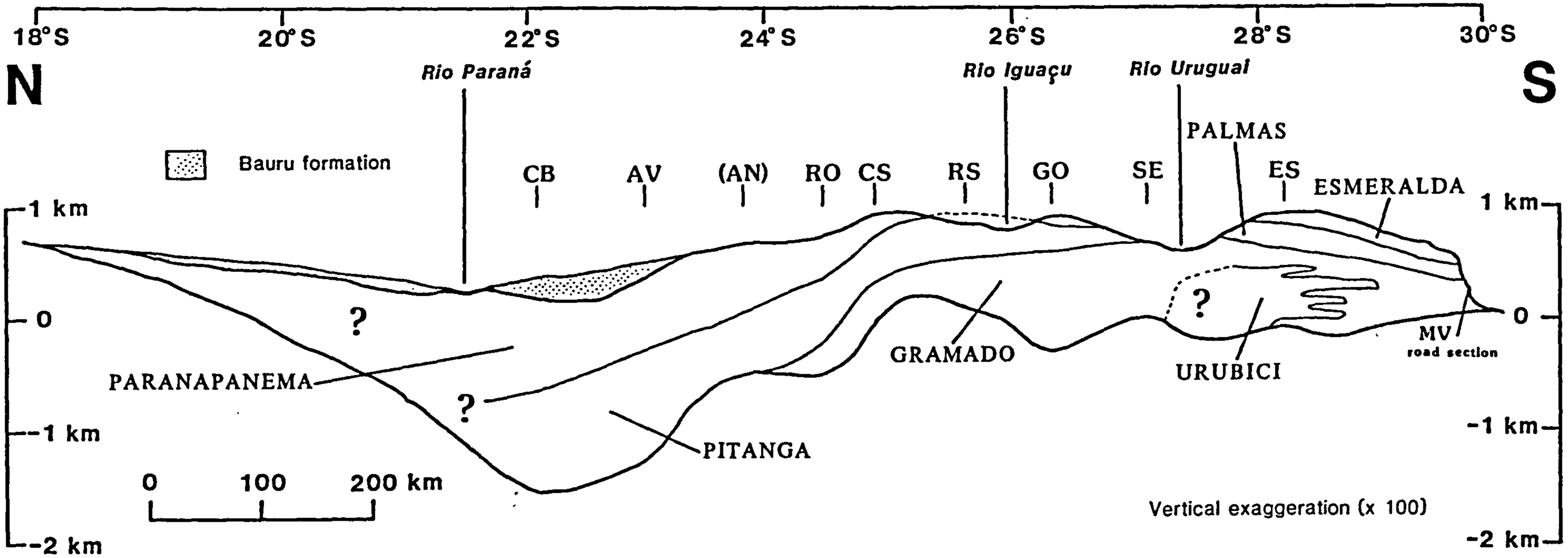

Figure 2.22 Summary north-south cross section through the Paraná lava sequences, along longitude 52° W (see figure 2.20), based primarily on borehole data, but including information from the literature on the surface distribution of the various magma types. It is a schematic profile, intended to highlight the salient features of the lava stratigraphy: (i) within the central-north region, Paranapanema-type flows overlie Pitanga-type flows which in turn overlie Gramado-type lavas, (ii) there is a progressive overstepping of geochemical units, as defined by individual magma types, towards the north, (iii) within the high-Ti magma types, the Urubici-type have a relatively restricted geographical distribution close to the south-east margin compared to the wide extent of the Pitanga-type. The positions of the studied boreholes, and the three major rivers of the basin (Rio Paraná, Rio Iguaçu, Rio Uruguai) are also shown. Vertical exaggeration is x 100.

Notes.

(i) The Urubici/Gramado contact is very schematic, and has been extrapolated inland from the coastal escarpment road sections.

(ii) The area between the 'RS' and 'SE' boreholes is complicated by rhyolitic units (not shown). Chapecó-type rhyolites outcrop at the surface near 'SE' and this is probably the same unit as found at 600 m in 'RS' borehole since there is a large gap in sample coverage at the expected depth in the 'GO' borehole.

suggest a northward-migrating source for the Paraná magmatism in this central-north region. Independent evidence for this conjecture is sparse, but there is a suggestion from the published K-Ar ages (Bellieni *et al.*, 1983) that in the basin as a whole there was a migration of volcanism from the south-west to the north-east but this is not well constrained. This migration could be related to the northward propagation of rifting during the initiation of the South Atlantic ocean.

The profile illustrated in figure 2.22 does not follow exactly the main axis of lava thickness (see isopach map of lavas, figure 1.5) and towards the south it cross-cuts up the edge of the basin structure. The relatively exaggerated dips of unit boundaries as well as the lava/sediment interface itself could be partly a later post-eruptional feature imposed by epeirogenic uplift, a process that appears to have been restricted to the area parallel to the coastal margin. But the northward migration of volcanism is indicated not just by the northerly dip of unit boundaries but more explicitly by the fact that units thin down-dip in this direction and pinch-out against the basal contact, as displayed by the Gramado unit. These features are well established from stratigraphical studies of the Deccan lava pile (Beane *et al.*, 1986; Devey and Lightfoot, 1986) that have revealed an en-echelon pattern of individual units, each thinning down-dip and progressively overstepping the basement rocks to the south. This has been attributed to the southwardly migration of volcanism arising from the northward drift of the Indian continent over the Reunion hotspot. Watts and Cox (1989) have compared the observed lava stratigraphy to the predictions of a geophysical model that evaluated the flexural response of the continental lithosphere to the migrating load imposed by the lava pile. The structurally lowest parts of the modeled sections were in good agreement with the observed Deccan stratigraphy which demonstrated the down-dip thinning of individual units. The model predicted that individual units should have a cross-sectional shape similar to a 'hysteresis-loop' in that the dips of the unit boundaries should shallow-out towards the top of the sequence with the unit thinning out up dip as well. This upper part of the model is not observed in the Deccan but agrees within the structure of the upper, southern end of the Pitanga unit in the Paraná. Developing this model any further for the Paraná sequences firstly requires a realistic

driving mechanism analogous to the Reunion hotspot proposed for the Deccan, and further information of the internal structure of the lava pile to the north of the 'CB' borehole especially on the behaviour of the Pitanga unit against the basal contact as the depth of the lava pile decreases northwards.

Piccirillo *et al.*, (1988b) considered the Paranapanema (or ITi) magma type as a transitional type between what are now termed the Gramado (LTi) and Pitanga (HTi) groups, and proposed a 'transition-zone' in the central Paraná where all three were closely associated. The borehole data has shown the Paranapanema-type to have a similar spatial distribution to the Pitanga-type which they overlie, and both in turn overlie the Gramado-type flows. Therefore the relationship between the different units is temporal rather than geographical, and since the Paranapanema-type magmas are not restricted to the central parts of the basin the concept of a geographical 'transition-zone' is not borne out.

There are still some problems in tying-in the details of the lava stratigraphy, as revealed by the borehole samples, with the external knowledge of the lavas previously gathered from surface samples. Comparisons with the borehole stratigraphy can be made on two levels. On a local scale, detailed stratigraphical variations from nearby road sections (if available) can be used to elaborate on certain portions of the stratigraphy. On a regional scale, predictions from the borehole results can be checked for their consistency with the broad surface distribution of magma types.

The 'ES' borehole is the furthest south and provides a link to the well-studied road sections of southern Paraná in Santa Catarina and Rio Grande do Sul states (see figure 2.15). The upper half of the sequence is dominated by Palmas rhyolites, but of the two basalt samples so far analysed from lower down the borehole, one is Gramado-type and the other is Urubici-type, similar to the interbedded stratigraphy of the coastal road sections. Nardy (1988) has studied several road sections in the central region of the basin between 25° and 27° S and from 53° W to the eastern margin of the lava field. This covers the same area as the boreholes 'CS', 'RS', 'GO' and 'SE'. The topographic relief is not developed to the same extent as on the Serra Geral escarpment, and many of the profiles required over

30 km laterally to achieve vertical sections through the lava pile approaching 300 m. The lowest elevation sampled was about 500 m a.s.l. and since the borehole data shows the basal contact of the lavas to be between 100 m and -300 m a.s.l. in this area, at least 500 m of basalts that are not exposed in the road section can be picked up through the borehole samples. The sections in Nardy (1988) do not show a neat stratigraphical picture for this area, partly due to the nature of the constructed vertical sections which could easily have been affected by any regional dip in the lavas across the lateral distance sampled, but even the upper portions of the boreholes in this area also show a more complex stratigraphy. The 'PCV' section of Nardy (1988) lies directly adjacent to the 'RS' borehole and reassuringly both have similar stratigraphical sequences, with low-Ti rocks overlain by Chapecó rhyolites (at 'PCV' 540-640 m a.s.l., at 'RS' 630-710 m a.s.l.) which in turn are overlain by high-Ti rocks of the Pitanga-type. This Chapecó rhyolite unit at 'RS' can be traced 'through' the gap that exists in the data coverage of the 'GO' hole between 475 m and 697 m a.s.l., to the exposures either side of the Rio Uruguai (samples RS-67 and SC-06 of Mantovani *et al.*, 1985b). The data set of Nardy (1988) considers all rocks with > 2 wt% TiO_2 as one geochemical group, high-Ti, and they have not been sub-divided into the Pitanga and Paranapanema types as recognised here. This is important if the stratigraphy of this central area is to be developed since the borehole data shows that the contact between the Pitanga and Paranapanema magma types is between 500 m and 800 m a.s.l. in this region, an elevation traversed by most of the road sections.

There is also the difficulty of relating the gross stratigraphy of the boreholes to the broad regional surface distribution of magma types. The borehole stratigraphy indicates that the uppermost lava flows over most of the northern half of the basin should be of Paranapanema affinity. This is clearly not the case as extensive Pitanga-type lava sequences and also the occasional Ribeira-type flows have been recorded in this region (Petrini *et al.*, 1987). This highlights the lack of three dimensional control over the stratigraphy. The east-west structure within the lava pile is poorly understood, since the boreholes are constrained to a narrow north-south axis and only the 'AN' borehole lies sufficiently away from this profile, being about 200 km to the west. As mentioned earlier, the results from this

borehole imply a westerly component of dip which would be consistent with the outcrop of Paranapanema-type flows along the western margin of the province in Paraguay (this study; Bellieni *et al.*, 1986a), and suggesting the the overall dip of units is to the north-west. This still leaves the problem of the Ribeira magma type. Lavas of the Ribeira-type have not yet been encountered in the boreholes though according to Petrini *et al.*, (1987) such flows are found at the surface to the north, east and west of the 'CB' borehole. As yet there are no constraints on the magma types and stratigraphy within the sizeable sub-outcrop lava thickness that exists down in the Argentinian 'Mesopotamia' region since there is an absence in the literature of any geochemical data on Argentinian borehole samples.

2.8 Conclusions.

In common with studies of other CFB provinces, geochemical data are considered to be the best means of establishing a reliable stratigraphical sub-division of the Paraná lava pile. From a combination of new geochemical data acquired during this study plus a review of available literature data, a new revised scheme of distinct geochemical magma types has been proposed for the Paraná magmas, together with a more rigorous set of geochemical criteria by which they can be recognised. These definitions have clarified, and improved on, the previously mentioned geochemical groups in the literature, and the new nomenclature scheme will be used throughout this thesis. The scheme maintains the gross division into high-Ti and low-Ti groups of previous studies, but within both of these groups, three distinct basaltic magma types have been recognised: 'High-Ti' (> 2 wt% TiO_2) - {Urubici, Pitanga, Paranapanema}, 'Low-Ti' (< 2 wt% TiO_2) - {Gramado, Esmeralda, Ribeira}.

In the second half of the chapter, the internal stratigraphy of the Paraná lava pile was surveyed at three scales. A detailed flow-by-flow analysis of a restricted area near São Joaquim revealed the intimate association of lavas of both the Gramado and Urubici magma types. The Urubici-type flows tended to be concentrated in the lower half of each sampled section, and their overall proportion within the lava pile increased towards the north. The

absence of any hybrid magmas suggested that separate storage and vent systems existed for the two magma types (Gramado-type to the south, Urubici-type to the north) which were essentially simultaneously active in order to account for the interfingering of flows of the different magma types. There was sufficient compositional variation within flows of the Urubici magma type to locally correlate packets of two or three flows. The stratigraphical variations between these flow packets or sub-units were semi-coherent through the lava pile, and this might provide information on changing magmatic conditions for the Urubici magma type, which requires further consideration.

Integration of the above results with other road section data over the south-east corner of the Paraná lava field has highlighted an important temporal change in the low-Ti magma type, from the dominant Gramado-type to the minor Esmeralda-type which occurs as the final basaltic magmatism (lavas and dykes) over most of the area. Within the south-east Paraná, the Palmas rhyolites form an important part of the magmatic sequence, occurring as a number of discrete sheets across the area, and their future correlation might offer the best hope of any further local sub-division of the lava pile which is almost exclusively of the low-Ti Gramado magma type in this region.

On a more regional scale, the coherent compositional variations provided by samples of borehole drilling chips instills confidence in the use of such material to establish the lava stratigraphy in an otherwise inaccessible part of the lava pile. Two main conclusions have emerged from the borehole studies. Firstly, the dominant magma type within the central and northern regions of the lava province has evolved from Gramado (low-Ti) to Pitanga (high-Ti - > 3 wt% TiO_2) to Paranapanema (high-Ti - 2-3 wt% TiO_2) with time. Secondly, the magma types in this region define an overlapping sequence of units dipping towards the north, which suggests a northward migrating source for the Paraná magmatism.

Chapter 3
The Urubici Magma Type (High-Ti).

3.1 The Urubici magma type: an introduction.

The lavas of the Urubici magma type are all quartz tholeiites being both hypersthene and quartz normative. The samples from the Santa Catarina road sections all had SiO_2 contents between 49.7% and 53.5% with the exception of two intermediate flows, DSM24 (55% SiO_2) and DSM04/08 (60% SiO_2). The complex classification schemes rife throughout the Paraná literature tend to just divert attention from the more important continuous nature of the chemical variation within the lavas, and so to emphasize this here, all flows with less than 55% SiO_2 are simply referred to as basalts (*sensu lato*).

None of the basalts found can be considered as direct primary melts since any magma in equilibrium with presumed mantle olivine (Fo-92) should have an Mg# (Mg-number, see appendix C) in the range 68-72 (Frey *et al.*, 1978), and the most primitive Urubici flow has an Mg# of just 50. Their evolved nature is not unique to this small area, but is a widespread feature of the high-Ti magmas within the Paraná, with no published analyses of the Urubici or other high-Ti basaltic magma types having an Mg# greater than 50 (*c.f.* some low-Ti magmas with Mg#'s in excess of 65). Samples with higher MgO contents of about 7 wt% have been noted from the equivalent Khumib magma type in the Etendeka by Duncan *et al.*, (1988), although the two samples that had even higher MgO > 10 wt% were interpreted as partial cumulates.

As with most of the Paraná lavas, the Urubici-type flows are virtually aphyric, the majority having less than 5% phenocrysts by volume. The phenocrysts are dominantly of plagioclase, which have a maximum size of about 3-4 mm and do not show strong zoning. Smaller, subhedral augite crystals form the other common phenocryst phase, occasionally

asociated with plagioclase in glomerocrysts. Plagioclase, augite and opaques occur as microphenocrysts, together with minor amounts of olivine as rounded grains which are always highly altered to iddingsite and similar products. The groundmass consists of a fine- to medium-grained matrix of small plagioclase laths set in a granular groundmass of augite, opaques and occasionally iddingsitised olivine. Minor amounts of glassy material, now as a brown alteration product, are sometimes found interstitial to the groundmass plagioclase laths. The evolved flow (DSM04/08) is significantly more porphyritic (~20-30 %) than the more basic Urubici-type flows, and plagioclase and augite make up the phenocryst assemblage. Notably, it also contains small euhedral crystals of apatite, often associated with the phenocryst aggregations.

The petrogenesis of the Urubici magmas has generally been considered to be a relatively straightforward story. The coherent variations in the major and trace element data coupled with a narrow range in radiogenic isotope compositions (Bellieni *et al.*, 1984a) are consistent with a low-pressure fractional crystallisation process with no evidence of interaction with crustal material (Hawkesworth *et al.*, 1986). The following sections will look at the major and trace element variations and how successful simple crystal fractionation models are at explaining such data, and then see how these models stand up to the rigours of the more precise INAA data and new Sr, Nd and Pb isotope analyses.

Another aspect to be considered is the relationship between the Urubici basalts and the Chapecó rhyolites. Bellieni *et al.*, (1986b) noticed that the variation diagrams for the high-Ti basalts and the Chapecó suite were consistent with liquid lines of descent and that mass balance calculations indicated a possible role for crystal fractionation in the petrogenesis of the acidic rocks. This was in conflict with the absence of any intermediate rocks; the series having a 'silica gap' from 55 % to 63 % SiO_2. The more evolved Urubici flows will be compared to the Chapecó rhyolites to see if they might represent an intermediate fractionation stage between the basalts and rhyolites.

3.2 Geochemical Variations within the Urubici magma type.

3.2.1 Major Element Variations.

When compared to the low-Ti magma types, the Urubici lavas have a rather restricted compositional range with, for example, MgO only varying between 4.0 wt% and 5.5 wt%. Figure 3.1 shows the major element variations for the Urubici magma type, using Mg# as an indication of the degree of magmatic evolution. Most of the oxides plotted show consistent correlations with Mg# and the most obvious feature shown is the inflection in most of the fractionation trends at about Mg# 40, between the basalt suite and the more evolved compositions. SiO_2 shows a slight tendency to increase (51 % to 52 %) with decreasing Mg#, and this is very pronounced for the two intermediate flows. Overall Al_2O_3 is fairly constant (12.7 % - 14.1 %), whereas CaO shows a marked decline through the whole sequence. Both $Fe_2O_3(t)$ and TiO_2 increase within the basalts, with a sharp fall as Mg# drops below 40. Na_2O and K_2O show considerable scatter (Na_2O 2.2 % - 3.6 %, K_2O 0.9 % - 2.3 %) with no overall trends discernible within the basalt data though both become enriched in the intermediate flows, K_2O especially. P_2O_5 increases from 0.45 % to 0.6 % as Mg# decreases from 50 to 40, but is buffered in the intermediate samples at about 0.7 %.

The major element characteristics displayed by the Urubici basalts exhibit many of the features of gabbroic crystal fractionation. Cox (1980) has shown that fractionation of an assemblage of olivine, clinopyroxene and plagioclase often leads to a buffering of SiO_2 and Al_2O_3, a marked sympathetic decrease of CaO with MgO, and the development of the typical tholeiitic iron-enrichment trend. The change in slope at about Mg# 40 is probably the effect of Fe-Ti oxides playing a larger role in the fractionating extract, producing the strong decrease in $Fe_2O_3(t)$ and TiO_2, and contributing to the increase in SiO_2. The change in behaviour of P_2O_5 from acting as an incompatible element throughout the basalt suite to being constant at low Mg# (< 38) could be due to the magma becoming saturated in P_2O_5 and crystallising minor amounts of apatite which would be in accord with the petrography of DSM04/08.

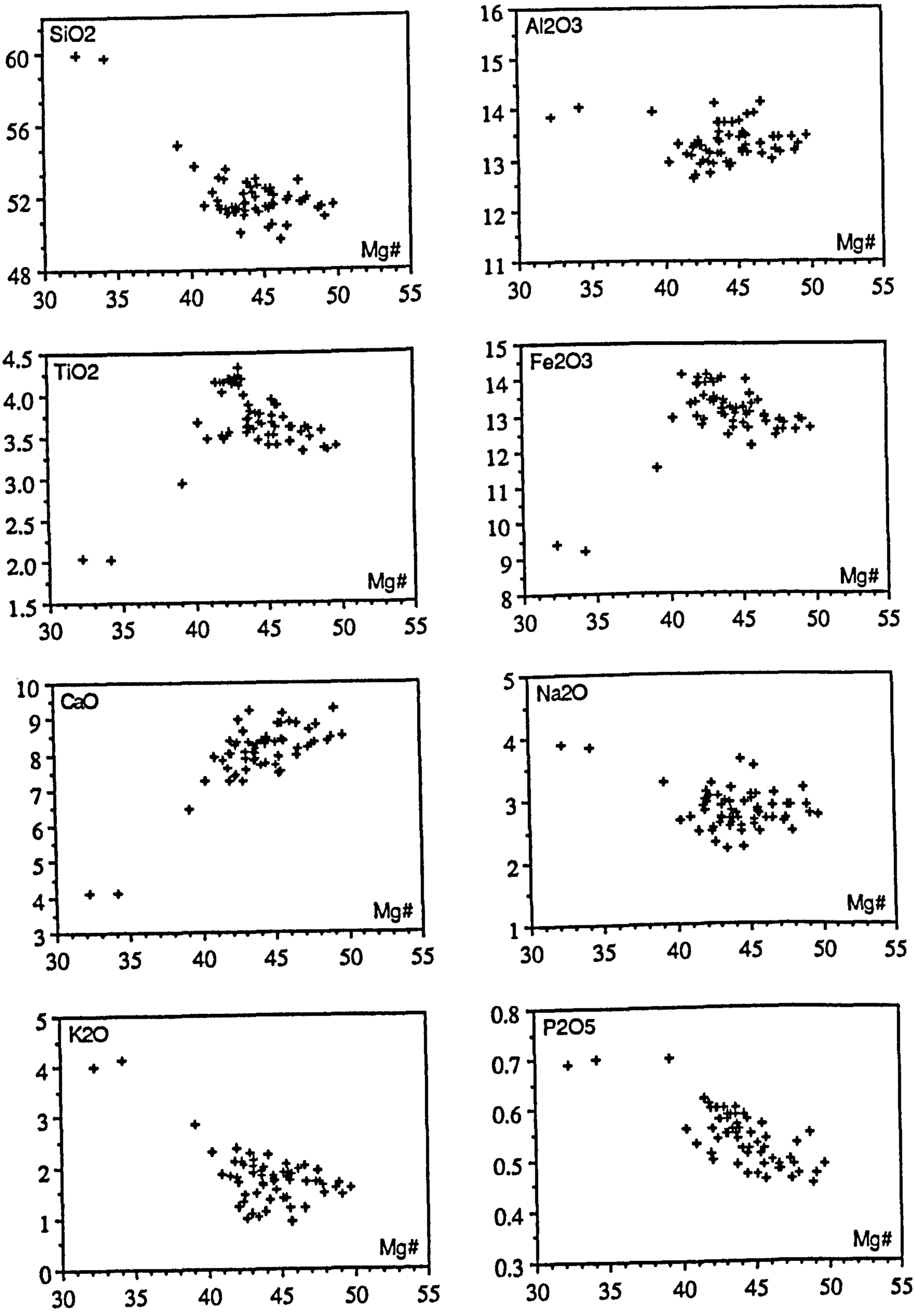

Figure 3.1 Major element variation diagrams for the Urubici magma type.

3.2.2 Trace Element Variations.

Variations in the trace element contents of the Urubici magmas, as determined by XRF analysis are illustrated in figure 3.2. These are discussed in relation to the sample Mg# so as to be consistent with the major element data presented in the previous section. All samples have <100 ppm Ni which again emphasizes their evolved nature. The rapid decrease of Ni with falling Mg# reflects olivine fractionation, for the more primitive samples at least, and Cr (not illustrated) shows a similar, though more scattered, trend. The behaviour of V mirrors that of Fe_2O_3(t) with a slight increase (330 to 380 ppm) within the basalts and then a sharp fall in the evolved flows down to 120 ppm in DSM04/08, indicative of the role of Fe-Ti oxides during the later stages of crystal fractionation. Cu shows a large scatter in the basalts, varying from 80 to 250 ppm, but in general showing an increase with decreasing Mg#. Zn is similar to Cu though with less variation (100 to 130 ppm). In the evolved flows Cu is low at about 50 ppm compared to a Zn content of 110 ppm. Sr contents show a large amount of scatter but remain roughly constant throughout the whole sequence which is consistent with a large plagioclase component in the fractionating extract. Zr and Nb behave as typical incompatible trace elements showing strong enrichment with increasing fractionation; Zr increasing from 270 to 500 ppm and Nb from 24 to 45 ppm. Three data points (DSM05b/07/09) all from the same flow (D3; figure 2.14), sampled over 1 km laterally, have noticeably low Zr and Nb contents, lying below the otherwise tight data trend. The trend of the Y data is similar to Zr and Nb but not as tightly constrained varying from 33 to 45 ppm, and becomes constant in the evolved flows at 50 ppm, probably reflecting a large amount of clinopyroxene fractionation. Ba and Rb also act as incompatible elements but the trends within the basalts, especially for Rb, show excessive scatter.

Selected samples were also analysed by INAA (instrumental neutron activation analysis) at the Open University (details in appendix B) for the rare earth elements (REE) and Th, U, Ta, Hf. For comparison, two analyses of the Chapecó rhyolite magma type are plotted on figures 3.3 and 3.4. These are the samples RS-67 and SC-06 from Mantovani *et al.*, (1985b) and samples were provided for analysis by Prof. M.S.M Mantovani.

Urubici (high-Ti) magma type

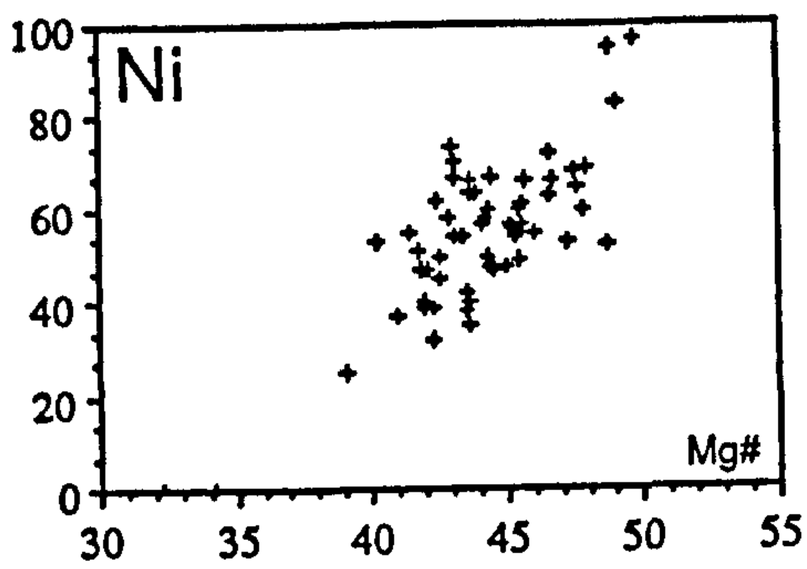

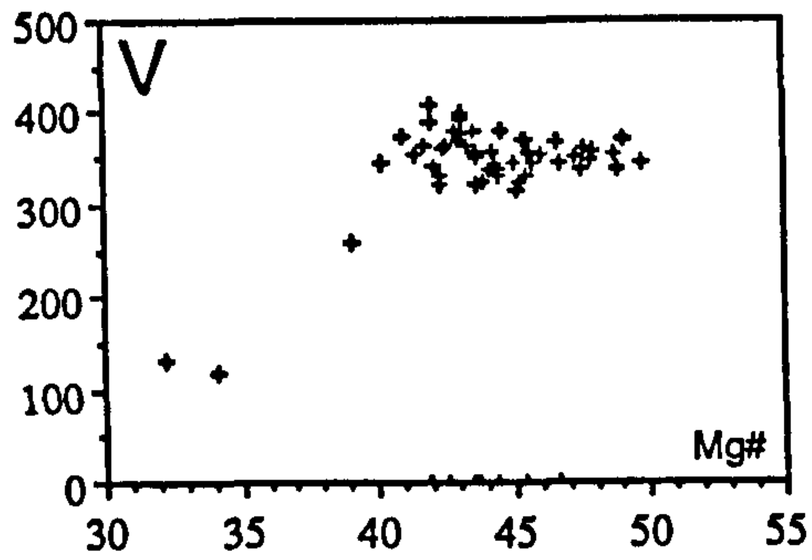

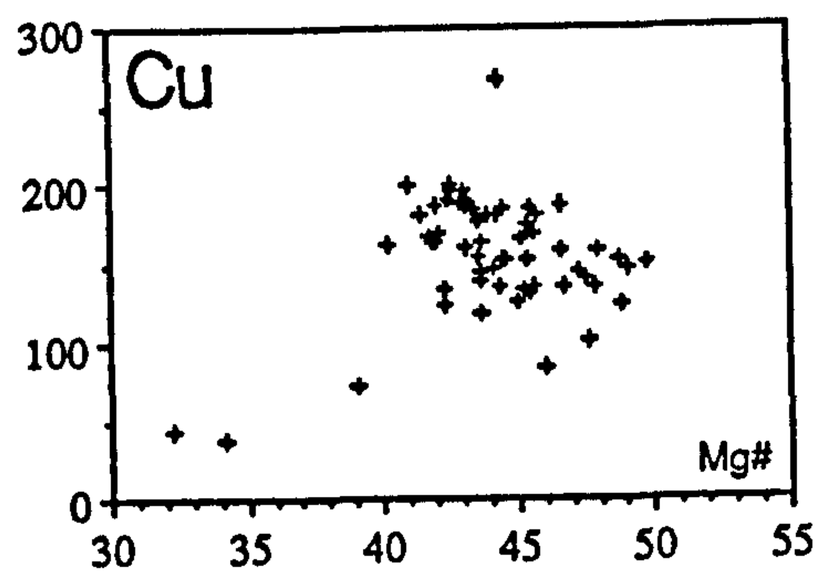

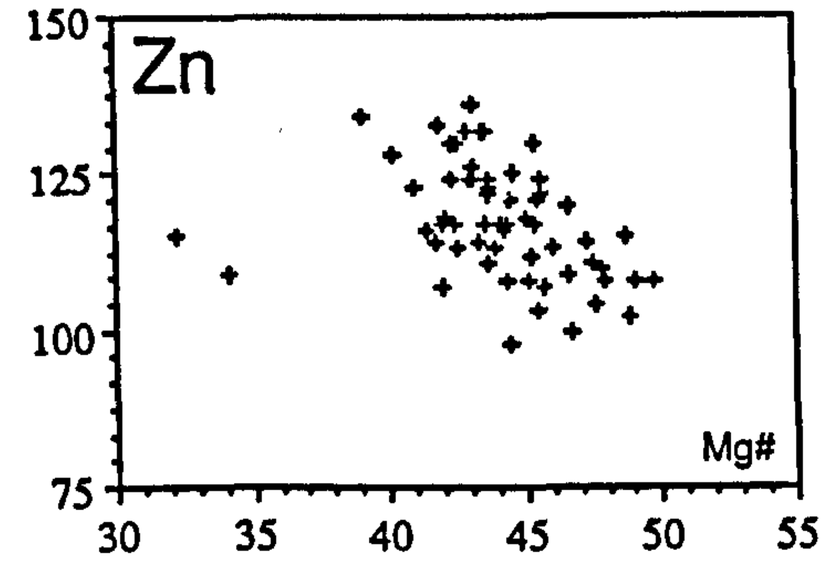

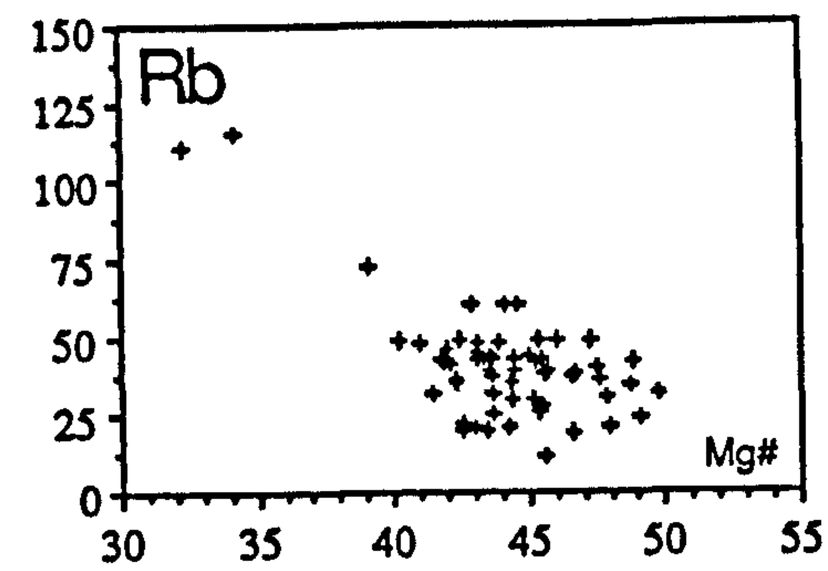

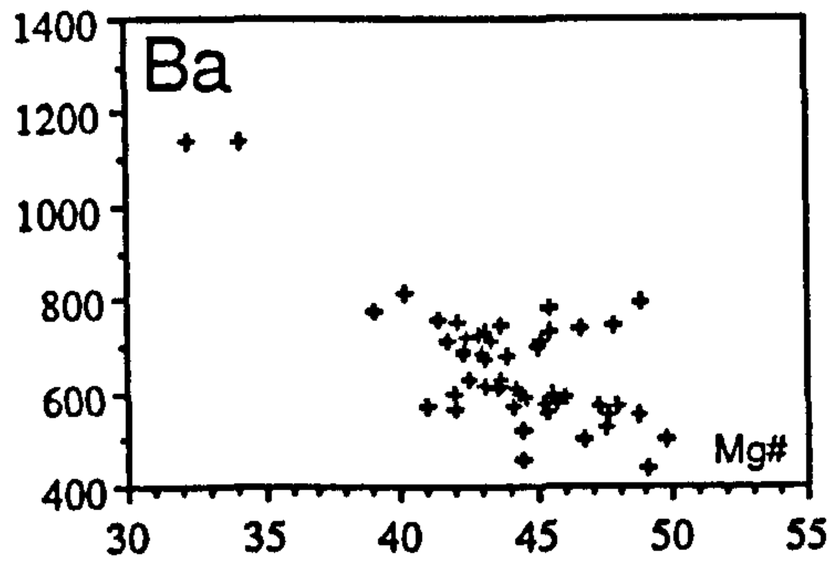

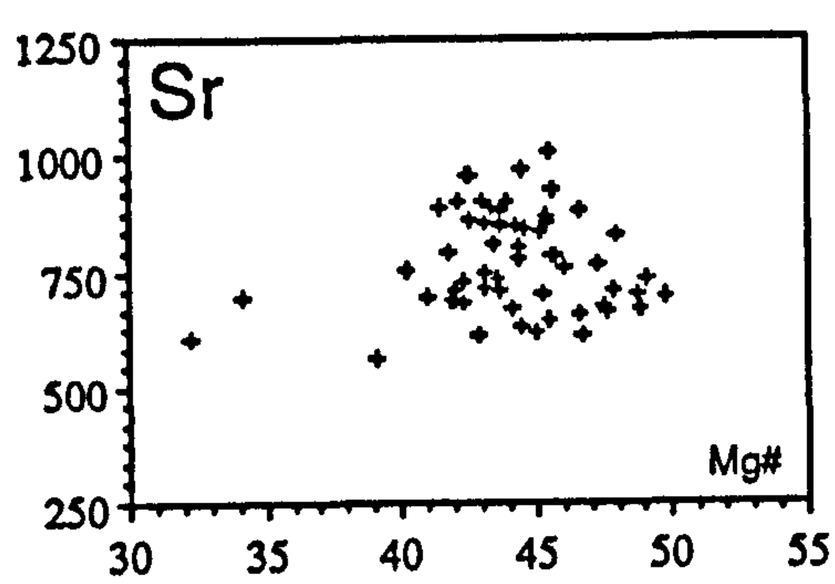

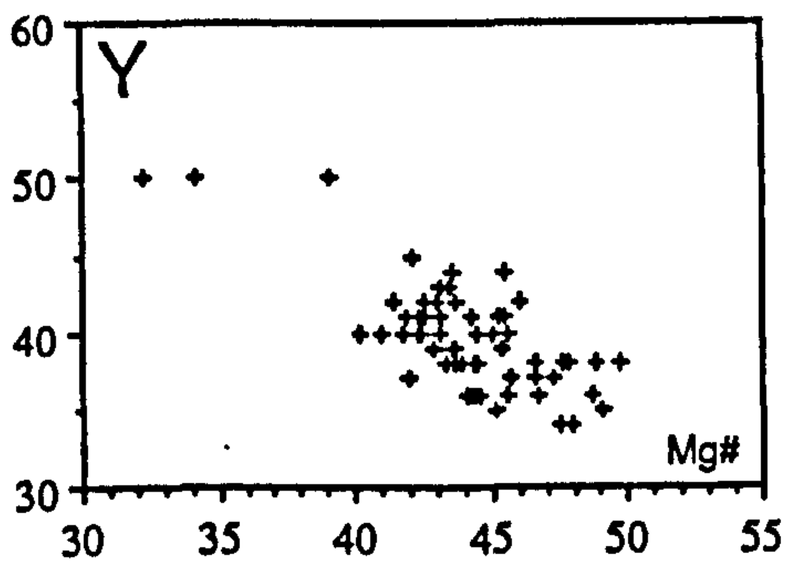

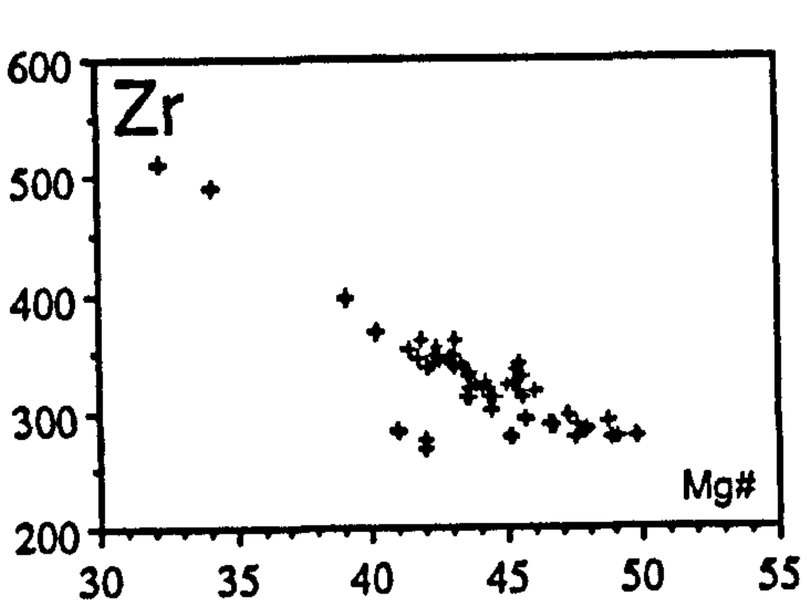

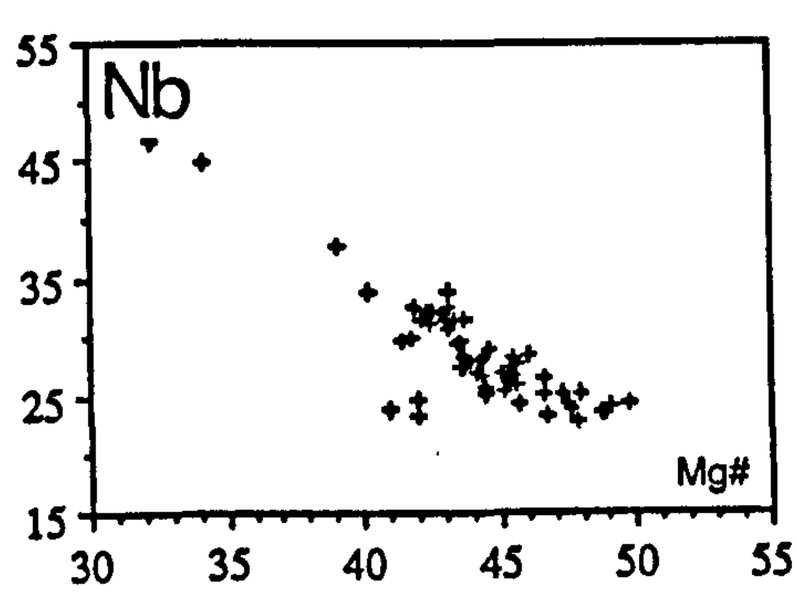

Figure 3.2 Trace element variation diagrams for the Urubici magma type.

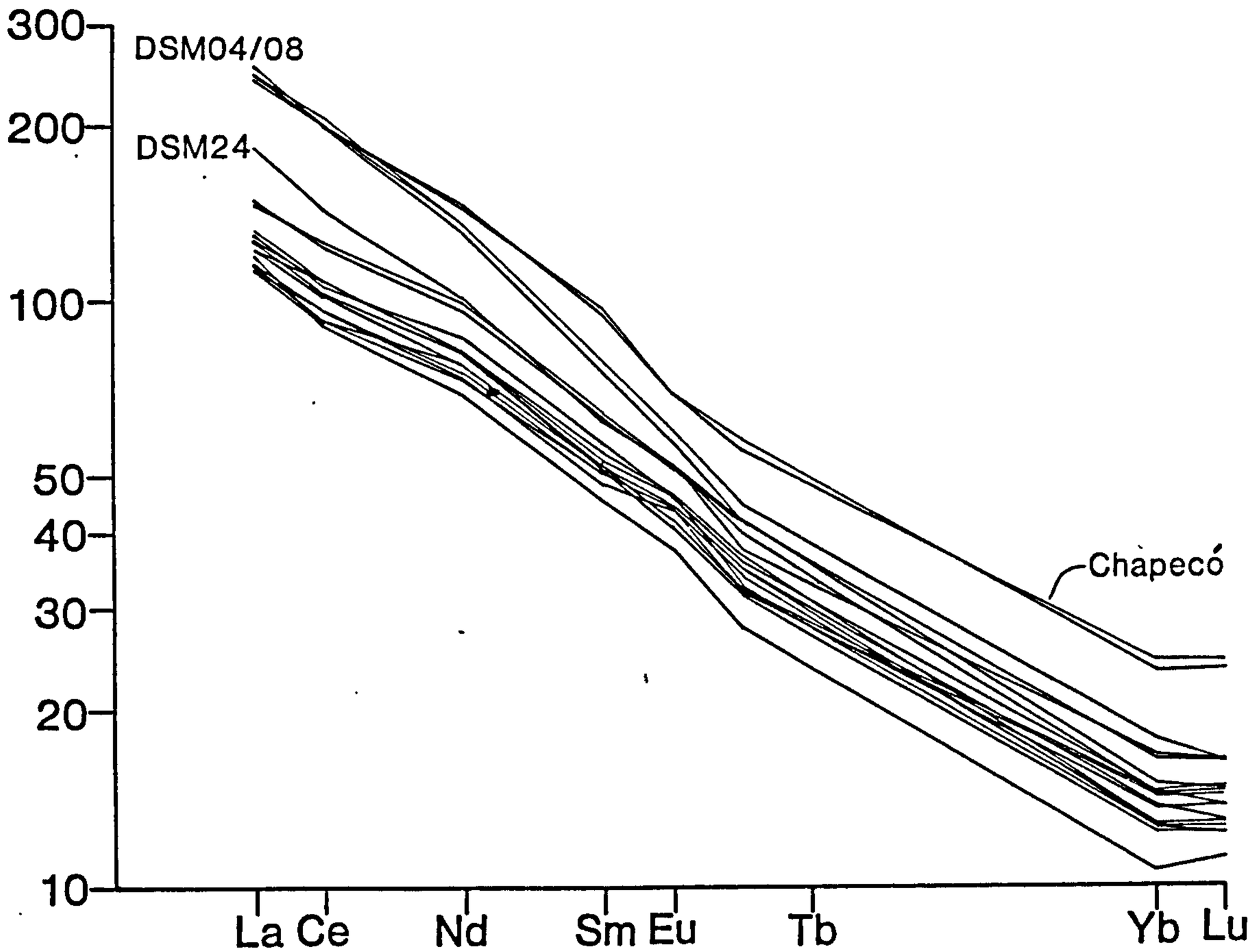

Figure 3.3 Chondrite-normalised REE abundance patterns for the Urubici and Chapecó magma types.

The REE data for the Urubici magmas are presented in figure 3.3 which is a standard Masuda-Coryell diagram where the REE abundances have been normalised to chondrite values (Nakamura, 1974; appendix C) and plotted against increasing atomic number. The patterns show markedly steep linear profiles characterised by $(La/Yb)_N$ ratios of 8.5 to 15. Increasing fractionation within the basalt suite maintains the overall shape of the REE profiles, with $(La/Yb)_N$ virtually constant at 8.5-11, but just displaced to higher REE abundances. One noticeable feature is that the two intermediate (> 55% SiO_2) flows show an increased LREE (light rare earth element) enrichment over the basalts. $(La/Sm)_N$ in the basalts lies in the range 2.2 to 2.6 but in the evolved flows it increases up to 3.2. The Chapecó rhyolites have similar La and Ce abundances to DSM04 and DSM08 but are enriched in the heavier REE. Their overall pattern is similar to the Urubici basalts though at higher abundances, and contrasts with the Urubici evolved lavas that have greater LREE enrichment {$(La/Sm)_N$ - Urubici 'evolved' ~3.2 vs. Chapecó ~2.5}.

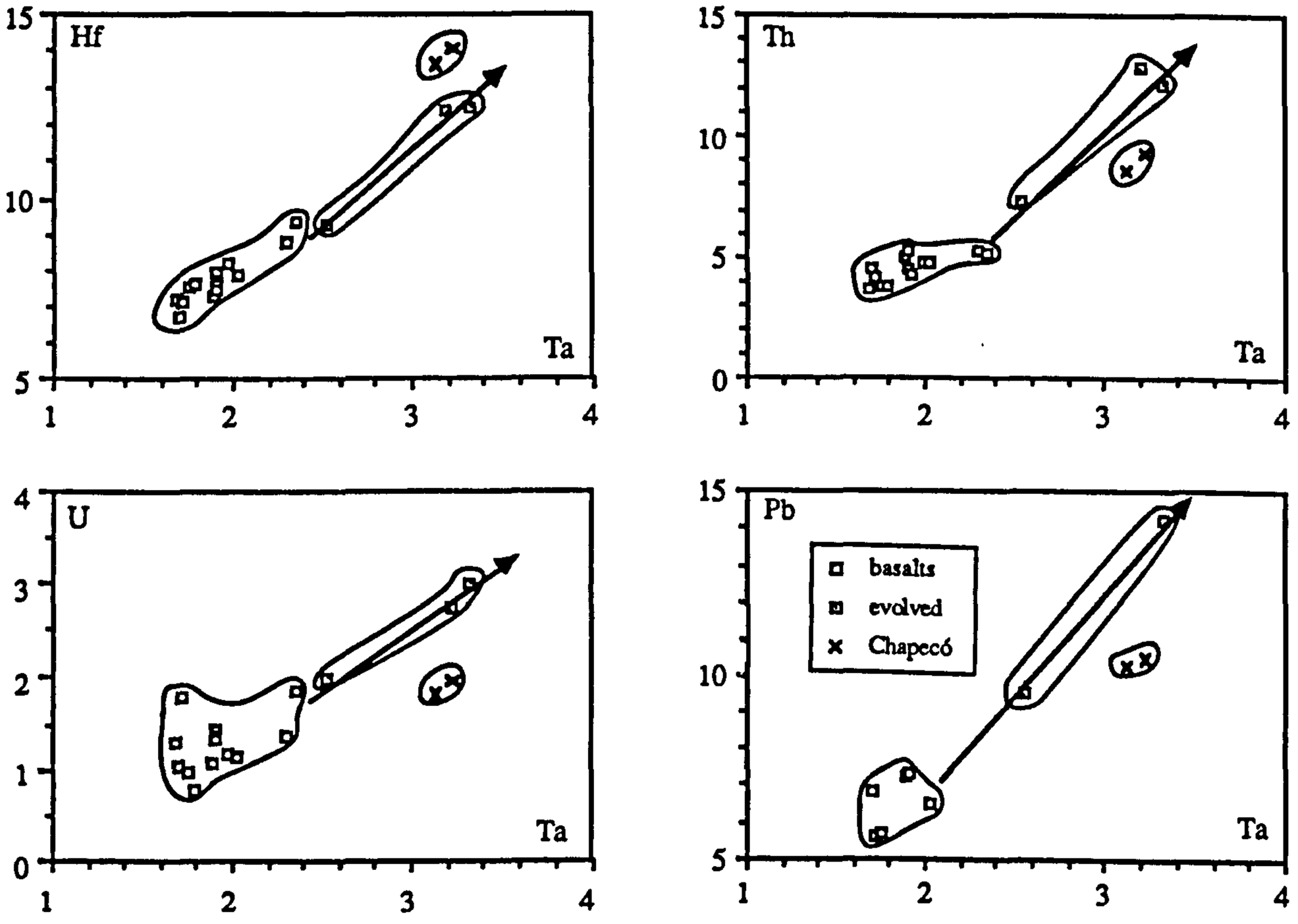

Figure 3.4 Variation of Hf, Th, U, Pb vs. Ta for the Urubici (squares) and Chapecó (crosses) magma types.

The variations encountered in the Ta, Hf, Th, U and Pb data are illustrated in figure 3.4, using Ta as the variable against which the other elements are plotted. Ta was chosen as it is precisely determined by the INAA method and is relatively invariant during alteration processes. All of the elements are highly incompatible, showing good positive inter-element correlations, and reach a maximum abundance in the intermediate flow DSM04/08. The behaviour of Ta and Hf mirrors that of Nb and Zr to which they are geochemically similar, respectively, in terms of ionic charge and radius. The Th vs. Ta diagram is intriguing since there is a change in slope of the trend, between the basaltic and intermediate samples, with Th more enriched over Ta than would be expected if the trend through the basaltic suite is extrapolated to the evolved flows. This observation will be returned to, later. The expected mobility of U as a result of alteration processes does not seem to have been an important factor, except in a few of the basaltic flows, and the data shows a remarkably consistent trend with the relatively immobile Ta. A few samples were analysed for Pb contents by isotope dilution (details in appendix B). There is a slight hint

of Pb being enriched over Ta in the evolved flows, as was seen for Th, since Pb/Ta is 3.2-4.0 in the basalts and increases to 3.8-4.3 in the evolved flows. The Chapecó rhyolites have similar Ta contents to the evolved Urubici flows, but show an enrichment in Hf. For Th, U and Pb, the rhyolites lie on an extension of the basaltic trends and have lower abundances of these elements than in DSM04/08.

3.2.3 Isotopic data.

The Urubici basalts have a relatively restricted range in initial Sr isotopic ratios (calculated back to 130 Ma) with $(^{87}Sr/^{86}Sr)_i$ in the range 0.7048 to 0.7059. This is similar to the range previously reported by Mantovani *et al.*, (1985a) of 0.7048-0.7062, based on rocks taken largely from the GB road section. The evolved flow DSM04/08 has a slightly more radiogenic $(^{87}Sr/^{86}Sr)_i$ of 0.7065. Hawkesworth *et al.*, (1986) quoted a range in ε_{Nd} of -2.5 to -4.6 for the half dozen Urubici flows sampled, equivalent to

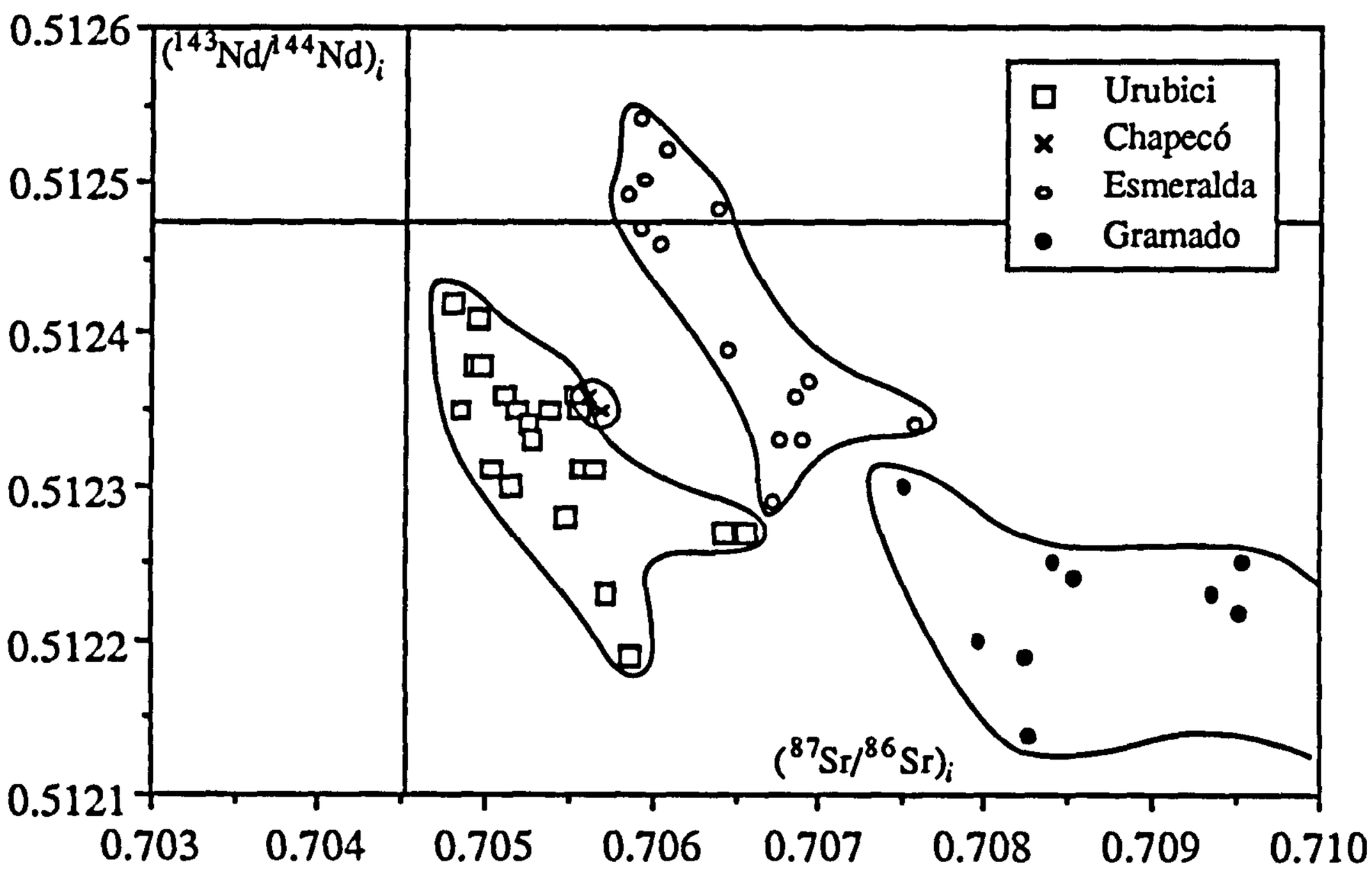

Figure 3.5 Sr and Nd isotopic variation in the Urubici and Chapecó magma types, (data for the low-Ti Gramado and Esmeralda magma types are included for comparison). The Urubici magma type lie on an extension of the MORB-OIB 'mantle array'. Note the Chapecó rhyolite compositions lie within the field for the Urubici magma type.

$(^{143}Nd/^{144}Nd)_i$ of 0.51223-0.51235. This range has now been extended with new data to ε_{Nd} of -1.0 to -5.5 {$(^{143}Nd/^{144}Nd)_i$ of 0.51219-0.51242}. The coherent variation of Sr and Nd isotopic compositions for the Urubici rocks is illustrated on figure 3.5, where they lie on an extension of the so-called 'mantle array'. Notably, the Chapecó rhyolites have initial Sr (Mantovani *et al.*, 1985b) and Nd (this study) isotopic ratios of 0.7056-0.7059 and 0.51235-0.51236 respectively, that lie within the range of the Urubici basalts.

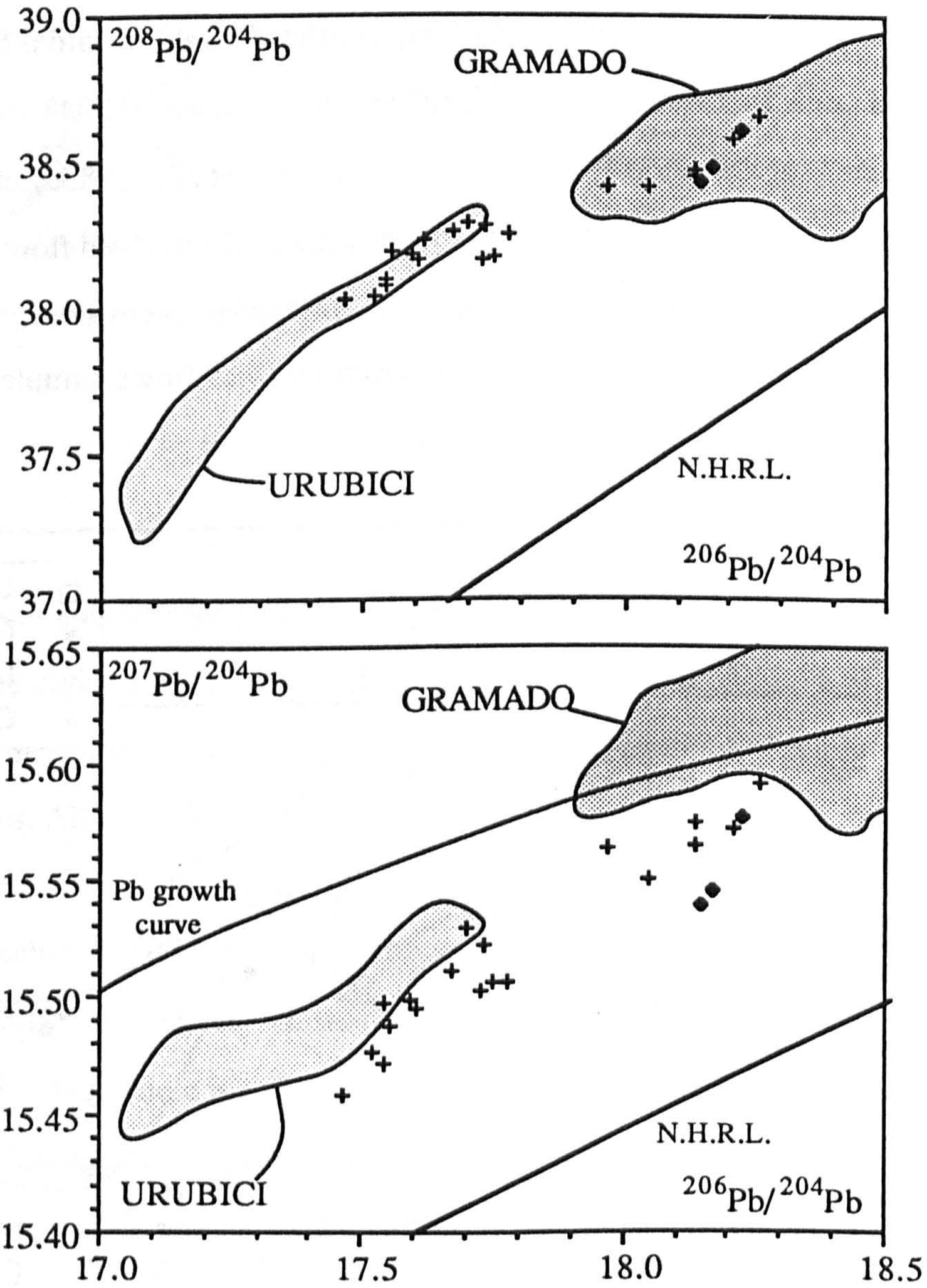

Figure 3.6 Pb isotope variations in the Urubici (crosses) and Chapecó (solid circles) magma types, obtained in this study: (a) $^{208}Pb/^{204}Pb$ vs. $^{206}Pb/^{204}Pb$, (b) $^{207}Pb/^{204}Pb$ vs. $^{206}Pb/^{204}Pb$. For reference, fields for the Urubici (light shading) and Gramado (dark shading) from previous work {Hawkesworth *et al.*, 1986; Cordani *et al.*, 1988} are shown. N.H.R.L. - Northern Hemisphere Reference Line of Hart (1984), Pb ore growth curve of Stacey and Kramers (1975).

The only previous Pb isotope study of the Paraná lavas was by Hawkesworth *et al.*, (1986) on powders taken from the sample set of Mantovani *et al.*, (1985a). This listed six Pb isotope analyses of Urubici magmas from the GB road section, and a further four unpublished analyses have been provided by Prof. M.S.M. Mantovani. These studies gave a range in $^{206}Pb/^{204}Pb$ of 17.06 to 17.72 and these data, together with 24 new analyses, are plotted on figures 3.6(a) and 3.6(b). The new data show a distinct bimodal distribution in $^{206}Pb/^{204}Pb$. The group at lower radiogenic values has a similar range in $^{206}Pb/^{204}Pb$ (17.46-17.77) to that noted for the previous data on the Urubici magma type. The group at higher $^{206}Pb/^{204}Pb$ values, which varies from 17.97 to 18.23, comprises of the evolved magmas together with the uppermost basaltic flows (D2 and D3 on figure 2.14) from the Morro da Igreja section (DSM10 and DSM05b/07). It is interesting to note that the Chapecó rhyolites also have Pb isotopic values that lie within this second group. The age implications of the Pb data will be considered later, in chapter five.

3.3 Fractional Crystallisation.

3.3.1 Major element modelling.

Despite the widespread belief (*e.g.* Bellieni *et al.*, 1984a) that the variations in the Paraná high-Ti lavas are essentially controlled by fractional crystallisation of a gabbroic mineral assemblage (olivine/plagioclase/clinopyroxene±Fe-Ti-oxides), models in the literature have been restricted to dealing with the low-Ti lavas with the added statement that these are also reasonable for the high-Ti lavas (*e.g.* Piccirillo *et al.*, 1988a). The aim of this section therefore is to assess the extent to which low pressure fractional crystallisation can satisfactorily account for the major element variations seen in the Urubici magma type. This was tested by relating representative compositions, chosen along the liquid line of descent, by extraction of the observed phenocryst phases using mineral compositions taken from the literature. Table 3.1 lists the mineral compositions used for the major element modelling, and the footnotes give the reasoning behind the choice of mineral analyses and their sources.

Urubici (high-Ti) magma type

	Olivine	Plagioclase			Augite	Pigeonite	Magnetite	Ilmenite
	Fo 76	An 70	An 64	An 56				
SiO_2	38.20	50.48	51.97	53.97	50.52	51.12	0.96	0.87
TiO_2	0.06	-	-	-	1.39	0.54	19.97	45.39
Al_2O_3	0.18	31.66	30.64	29.28	2.26	0.08	1.61	0.09
Fe_2O_3	23.14	-	-	-	13.53	25.71	76.37	52.00
MnO	0.20	-	-	-	0.43	0.68	0.79	0.56
MgO	37.84	-	-	-	14.46	17.59	0.29	1.09
CaO	0.39	14.34	13.15	11.56	17.70	4.28	-	-
Na_2O	-	3.17	3.80	4.68	0.14	0.01	-	-
K_2O	-	0.34	0.43	0.52	-	-	-	-

Notes.

(i) Olivine. This phase is rarely fresh enough for analysis (Bellieni *et al.* 1984a), and so an olivine composition was calculated using the Fe/Mg distribution equation of Roeder and Emslie (1970). This produces an olivine with Fo-76 composition that is in equilibrium with a 'primitive' Urubici magma having an Mg# of 50.

(ii) Plagioclase. With increasing magmatic evolution, the amount of anorthite component in the plagioclase decreases. [Piccirillo *et al.* (1988a): basalts An 87-60 av. An-76, andesi-basalts An 77-43 av. An-68, andesites An 68-40 av. An-55] Anorthite contents suitable for the whole rock compositions modelled have been estimated from this aproximate relationship. Since the whole rock K_2O content is reflected by the orthoclase component (Piccirillo *et al.* 1988b), this has been taken to be Or 2-3 for whole rock K_2O from 1.5 to 4.0 % in the calculated plagioclase compositions.

(iii) Pyroxenes. There is a reasonable correlation between TiO_2 (wt%) in both augite and pigeonite to that in the host rock (Bellieni *et al.* 1986a).
TiO_2 (aug) = 0.3872.TiO_2 (whole rock) + 0.0785
TiO_2 (pig) = 0.1436.TiO_2 (whole rock) + 0.1037
For a 'primitive' Urubici magma with about 3.4 % TiO_2, these equations suggest TiO_2 (aug) of ~1.4 % and TiO_2 (pig) of ~0.6 %. Clinopyroxenes with the appropriate Ti contents were taken from Bellieni *et al.* (1984a).

(iv) Fe-Ti oxides. There are no systematic differences in the compositions of magnetite and ilmenite between basaltic and andesitic rocks (Piccirillo *et al.* 1988a). Typical analyses were found in Piccirillo *et al.* (1988a).

Table 3.1 Mineral compositions used in major element modelling of the Urubici magma type, and the data sources.

Investigation of major element fractional crystallisation models was carried out using the SUPERMIX program. This is based on the combined linear programming and least squares analysis approach of Wright and Doherty (1970), adapted for the O.U. VAX-mainframe by D.W. Wright. This program attempts to match the composition of a parental

liquid by adding varying amounts of possible fractionating mineral compositions to an evolved liquid composition. The phases present in the fractionating mineral assemblage are input and the program then adjusts the proportions of these phases required to minimise the difference between the observed and calculated 'parental' magma. A measure of the suitability of the calculated model is given by Σr^2 - the sum of the squares of the residuals -

	PRIM obs.	calc. (1)	calc. (2)	EVOL1 obs.	calc. (3)	DSM24 obs.	calc. (4)	DSM04/08 obs.
SiO_2	51.37	51.39	51.42	52.22	52.20	54.93	54.92	59.87
TiO_2	3.36	3.09	3.06	3.51	3.27	2.95	2.51	2.02
Al_2O_3	13.32	13.33	13.29	13.30	13.29	13.94	13.94	13.96
Fe_2O_3	12.83	12.90	12.82	13.54	13.60	11.53	11.65	9.26
MnO	0.18	0.18	0.18	0.17	0.21	0.17	0.19	0.14
MgO	5.34	5.28	5.29	4.19	4.10	3.18	3.11	1.99
CaO	8.77	8.74	8.69	7.76	7.88	6.44	6.47	4.11
Na_2O	2.80	2.59	2.60	2.84	2.85	3.29	3.34	3.87
K_2O	1.56	1.62	1.63	1.91	2.28	2.86	2.91	4.06
ol		11.5	12.5		-		-	
plag	An_{70}	40.3	39.9	An_{64}	30.5	An_{56}	44.3	
aug		47.0	47.5		51.0		39.9	
mag		1.2	-		18.5		15.8	
100-F		16.4	15.7		21.4		30.0	
Σr^2		0.14	0.15		0.22		0.22	

	PRIM obs.	calc. (5)	EVOL2 obs.		PRIM obs.	calc. (6)	EVOL3 obs.
SiO_2	51.37	51.27	51.49		51.37	51.37	51.97
TiO_2	3.36	3.67	4.18		3.36	3.24	3.48
Al_2O_3	13.32	13.44	12.98		13.32	13.31	13.40
Fe_2O_3	12.83	12.97	13.65		12.83	12.86	12.90
MnO	0.18	0.18	0.18		0.18	0.18	0.17
MgO	5.34	5.36	4.35		5.34	5.32	4.53
CaO	8.77	8.90	8.08		8.77	8.77	7.83
Na_2O	2.80	2.64	2.82		2.80	2.92	3.20
K_2O	1.56	1.46	1.67		1.56	1.52	1.75
ol		15.0				6.6	
plag	An_{70}	47.1			An_{70}	35.8	
aug		37.9				52.5	
mag		-				5.1	
100-F		14.2				14.0	
Σr^2		0.19				0.03	

Table 3.2 SUPERMIX linear programming and least squares mixing models for selected averaged magma compositions, chosen in order to cover the full compositional range of the Urubici-type magmas. The mineral compositions used are from table 3.1. The results for six models are given; (1) EVOL 1 to PRIM (with magnetite), (2) EVOL 1 to PRIM (without magnetite), (3) DSM24 to EVOL 1, (4) DSM04/08 to DSM24, (5) EVOL 2 to PRIM, 6) EVOL 3 to PRIM. (see text for discussion of individual models).

where the residual, r, is the difference between the inferred parental liquid and the modelled liquid composition, calculated for each element. The compositions of the magmas used are given in table 3.2, as well as the percentage and make-up of the fractionating mineral assemblage removed for each model.

In a suite of rocks such as these where there is a certain amount of scatter within data trends largely as a result of weathering effects, it is often more meaningful to use average compositions, and in table 3.2 'PRIM' and 'EVOL' represent average primitive and evolved basalts. Looking at Ti, a HFS (high field strength) element which is generally considered immobile during alteration processes, even this shows a wide variation at the evolved end of the basalt suite from 3.3 % to 4.3 % (figure 3.7) which can not be attributed to weathering, hence the need to consider two evolved basalt compositions, EVOL1 and EVOL2, which have higher and lower Ti contents respectively.

The trend towards relatively low Ti ('PRIM' to 'EVOL1') can be modelled by extracting about 16% of olivine/plagioclase/augite in the proportions 12/40/48 though the solutions allow up to 1% magnetite in the crystal extract. These phase proportions are within the range of values given in Bellieni *et al.*, (1986a) as reasonable for all the Paraná basaltic rocks in Argentina/Paraguay. The average trend within the basalts to higher Ti ('PRIM' to 'EVOL2') is consistent with 14% fractionation of olivine/plagioclase/augite in the proportions 15/47/38, comparable with the values used in Cox (1980) of 15/50/35, with no Fe-Ti oxides necessary (negative solutions are obtained for magnetite if it is included in the extract). It is difficult to link this group of Ti-enriched evolved basalts, represented by 'EVOL2', to the intermediate flows, DSM24 and DSM04/08. Models have very high $\Sigma r^2 > 1.5$ and the solutions are only improved by using large percentages of ilmenite to reduce the TiO_2 residuals. The transition from the lower Ti evolved basalt 'EVOL1', to the high SiO_2 flows (DSM24 and DSM04/08) can be produced by more extensive fractionation of a plagioclase/augite/magnetite assemblage. If pigeonite is used in the models then negative solutions are avoided only if, again, ilmenite is also included, and this improves Σr^2 to values below 0.1. The exact composition of the opaque phases in these rocks is not known (the literature contains microprobe compositions of magnetite and

ilmenite but no modal analyses), but whether or not ilmenite is present does not make any difference to the total percentage of opaques required in the modelled fractionating assemblages. The major element models have not included P_2O_5 concentration data. The variation diagram (figure 3.1) showed that P could be considered as an incompatible trace element, having an insignificant concentration in any of the fractionating minerals. It is only in the advanced stages of fractionation when apatite becomes stable and precipitates out that P_2O_5 is important for modelling. SUPERMIX calculations between DSM24 and DSM04/08 predict about 0.9% apatite in the crystal extract to explain the P_2O_5 contents. {29.2% crystallisation of plag/aug/mag/ap in the proportions 44/39/16/1 Σr^2=0.24}.

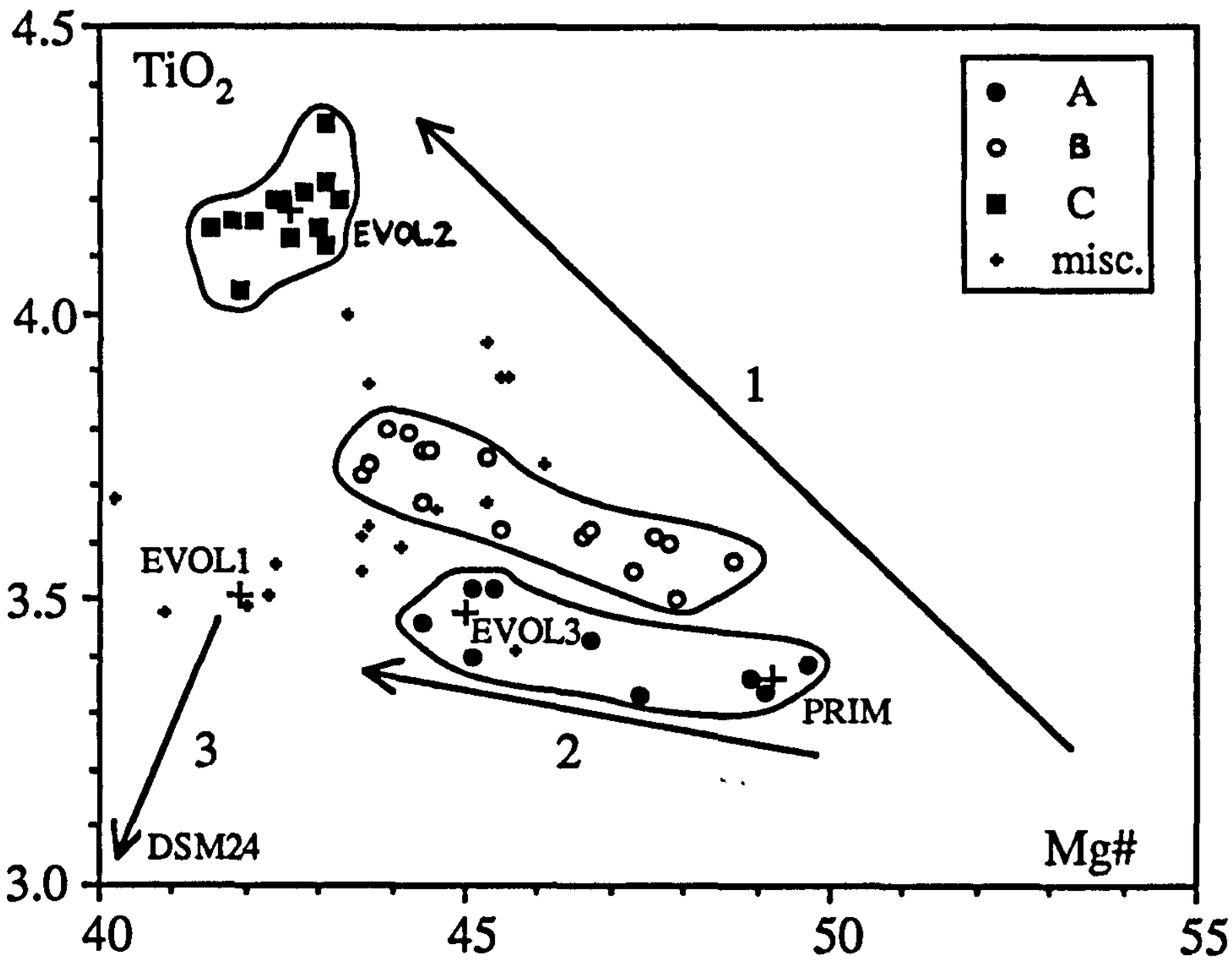

Figure 3.7 TiO_2 vs. Mg# highlighting the three main stratigraphical packets of flows (*i.e.* sub-units within the Urubici magma type); unit A (solid circles), unit B (open circles) and unit C (solid squares). Samples labelled misc. are from minor unrelated flow packets or were not assigned. Large crosses represent the averaged compositions used in the SUPERMIX models. Trend 1 is the variation between the primitive end-members of each sub-unit, trend 2 is the variation within each sub-unit, and trend 3 is the variation towards the evolved flows DSM24 and DSM04/08.

For a more rigorous treatment, allowance can be made of analytical errors in determining major element compositions and their susceptibility to alteration processes, and the SUPERMIX program allows individual elements to be weighted to reflect this. Not surprisingly, strongly weighted elements such as TiO_2 were better fitted at the expense of the more mobile Na_2O and K_2O, but this made little overall difference to the phase proportions and degree of crystallisation required and so this approach was not pursued.

Major element modelling within the basalts, between an average 'primitive' and 'evolved' composition as in table 3.2, gives an idea of the average proportions of mineral phases likely to have been involved in the fractional crystallisation process during the eruption of the whole lava sequence, but are these representative of the low pressure processes that have affected individual eruptions ? Whereas the overall trend within the Urubici basalts is one of increasing TiO_2, the individual stratigraphical flow packets recognised in chapter 2 define coherent sub-parallel trends within the overall data cloud which show only a slight increase in TiO_2, as seen in figure 3.7. It is interesting to note that for the three main stratigraphical packets, each successive flow packet is displaced to higher TiO_2 contents, *viz.* unit A has 3.3 - 3.55 %, unit B has 3.5 - 3.8 %, then unit C has 4.1 - 4.3 %, so that the overall trend of increasing TiO_2 with falling Mg# is largely a temporal feature. To model these secondary, shallow trends, an increased role for a Ti-rich phase must be invoked so that TiO_2 in the liquid becomes almost buffered. One possible SUPERMIX model, given in table 3.2, to account for the variations within the lowest stratigraphical flow packet ('PRIM' to 'EVOL3') required 14 % crystallisation of ol/aug/plag/mag in the proportions 10/53/33/5 - note the high percentages of both augite and especially magnetite. Bellieni *et al.*, (1984c) commented that the absence of magnetite in calculated crystallising sequences (using Nathan and Van Kirk 1978) was difficult to reconcile with sample petrography and they suggested that this could be explained if the Fe_2O_3/FeO ratio used in their modelling was too low. The ubiquitous presence of Fe-Ti oxides in the basalts is consistent with the high proportion (~5 %) of magnetite in major element models and suggests that the shallow trends of individual flow packets are due to low-pressure crystallisation just prior to eruption which has been superimposed on the

steeper trend that was considered by Bellieni *et al.*, (1984c). This steeper trend is more problematical - it could possibly result from crystallisation at higher pressures of a different phase assemblage possibly under different $f(O_2)$ conditions, or as a result of variations in the degree of partial melting, although it also seems to be time dependent as noted above. It is hoped that the trace element and isotope data in the following sections will shed some light on the origin of this trend.

3.3.2 Trace element modelling.

Trace element abundances can be used to evaluate the results of the major element modelling given in the previous section. The behaviour of trace components in a magmatic system undergoing closed system crystal fractionation is described by the Rayleigh fractionation law (Rayleigh 1896).

$$\frac{C_l}{C_o} = F^{(D-1)}$$

where; C_l concentration of element in derivative liquid.

C_o concentration of element in parental magma.

F mass fraction of residual liquid.

D bulk crystal/liquid distribution coefficient for that element.

D is defined as $\sum_{i=1}^{n} w_i.K_{Di}$ where w_i is the weight fraction of each phase *i*, and K_{Di} is the partition coefficient for the element between phase *i* and liquid.

The SUPERMIX results (table 3.2), based on the major element data, give possible values for the degree of crystallisation (*i.e.* 1 - F) and the make-up of the fractionating mineral assemblage. Bulk distribution coefficients (D) can then be obtained using these phase proportions together with reasonable K_D values. This allows the composition of a derivative liquid (C_l) to be calculated from these parameters and an initial liquid composition (C_o), which can then be compared to the observed trace element contents for that magma. One drawback in using the Rayleigh law equation, given above, directly in this manner is that it requires an accurate set of mineral partition coefficients (K_D's) and

these are often poorly known, especially for the minor phases such as magnetite and apatite. Many partition coefficients show large variations with liquid compositions and are also temperature dependent. The values used in this thesis are listed in appendix C, together with their sources, and they are considered reasonable for the low pressure regime of basaltic evolution.

Modelling has been carried out on the same pairs of averaged magma compositions given previously in table 3.2. The results are outlined in table 3.3 which compares the calculated and observed trace element contents in the derivative liquid for each model, using the parameters obtained from the major elements together with the mineral/melt partition coefficients in appendix C. In all the models, the observed and predicted concentrations of the elements Ni, V, Cu, Zn, Rb and Sr are in reasonable agreement, considering the analytical precision of the XRF data and the uncertainties in the K_D values used, and this verifies the phase assemblage indicated by the major elements. The contents of the incompatible elements Ti, Zr, Nb, Y and Ba on the other hand, are consistently either all under- or all over-estimated when compared to the observed abundances which suggests that the F values derived from the major element modelling are incorrect. Although Ti (as TiO_2) was included with the major elements in the earlier models from which these F values were obtained, it was generally poorly fitted producing high residuals, and was the largest contributor to Σr^2. If it is assumed that the phase assemblages used are reasonable, suitable F values can be estimated from the incompatible trace elements and then checked against the major elements to see if this new extent of crystallisation can be accommodated. This can be done by direct forward modelling, mixing (100 - F) % of the previously calculated composition of the crystal extract to F% of the evolved liquid composition.

For example, for the transition from 'PRIM' to 'EVOL3', the SUPERMIX major element model calculated a degree of crystallisation of 14 % and this was inconsistent with the trace element contents which required a lower value of about 11 %. Recalculation of the primitive liquid major element composition by mixing 89 % of 'EVOL1' with 11 % of the

	PRIM obs.	EVOL1 calc. (1)	EVOL1 calc. (2)	EVOL1 obs.	DSM24 calc. (3)	DSM24 obs.	DSM04/08 calc. (4)	DSM04/08 obs.
Ti	3.36	3.90	2.82	3.51	3.07	2.95	2.38	2.02
Zr	279	331	328	303	379	397	533	500
Nb	24	28	28	27	33	38	49	46
Y	37	42	42	39	46	50	52	50
Rb	33	39	39	42	53	73	102	114
Ba	578	676	671	621	770	776	1048	1138
Sr	700	727	725	702	769	564	593	654
Ni	92	64	66	37	22	25	14	2
V	351	369	361	364	232	257	159	125
Cu	141	154	150	162	103	72	45	41
Zn	106	120	117	120	85	134	92	112

	PRIM obs.	EVOL2 calc. (5)	EVOL2 obs.	PRIM obs.	EVOL3 calc. (6)	EVOL3 obs.
Ti	3.36	3.84	4.18	3.36	3.59	3.48
Zr	279	323	346	279	321	308
Nb	24	28	32	24	28	26
Y	37	42	41	37	41	39
Rb	33	38	41	33	38	40
Ba	578	660	702	578	660	663
Sr	700	711	829	700	730	683
Ni	92	67	58	92	70	51
V	351	375	369	351	335	330
Cu	141	154	176	141	140	144
Zn	106	119	121	106	108	107

Table 3.3 Calculated and observed trace element abundances, for the same magma pairs used in major element modelling, using F values and mineral proportions derived from table 3.2 and partition coefficients given in appendix C.

known crystal extract still produces an acceptable match for 'PRIM', having a Σr^2 of 0.13 (*c.f.* Σr^2 of 0.03 for the original SUPERMIX model.).

The main problem in the choice of partition coefficients seems to be those assumed for magnetite, and this becomes especially important in modelling the more evolved flows that require over 15 % Fe-Ti oxides in the modelled fractionating crystal assemblage. As well, it is known that certain partition coefficients show a marked compositional dependence and this must be considered when modelling magmas of more intermediate composition, especially if this could make a significant difference to the bulk D value and alter the behaviour of the element from being incompatible to compatible. This is best illustrated by the behaviour of Y between augite and melt, since in basaltic melts K_D is 0.5

whereas for intermediate compositions this increases to 1.5 (Pearce and Norry, 1979). This difference should be apparent when modelling the transition between the intermediate compositions represented by DSM24 and DSM04/08 since major element modelling shows a large calculated percentage of augite (~40 %) in the crystal extract. If the 'basaltic' K_D value is used then the calculated D_Y is 0.42 with a predicted Y content for DSM04/08 of 61 ppm. By contrast, taking the 'intermediate' K_D value, the bulk D_Y increases to 0.88 and consequently the calculated abundance in DSM04/08 falls to 52 ppm, close to the observed Y content of 50 ppm.

The results of the above modelling have shown that the trace element contents approximately conform with the results of the major element modelling, accepting the limitations imposed by our current knowledge of partition coefficients, but it seems that the major element modelling is more sensitive to the mineral proportions in the crystal extract rather than the exact degree of crystallisation, F.

To obtain better constraints on the value of F, one can use the method first proposed by Anderson and Greenland (1969) and expounded by Allègre *et al.*, (1977). This relies on choosing elements whose bulk D values are very small (*i.e.* $<< 0.1$), termed hygromagmatophile by Treuil and Varet, (1973). For these elements, D can be assumed to be equal to zero without introducing significant errors, and so the equation given above reduces to; $\frac{C_l}{C_o} \approx \frac{1}{F}$ This concept of hygromagmatophile (H) elements, therefore, allows us to use C_l and C_o values to estimate F directly, without reliance on an accurate set of K_D's for each element between every phase and melt. Suitable H elements to use are those that are precisely determined by INAA and are not susceptible to alteration, *e.g.* Th, Ta, Hf, La, Ce.

Table 3.4 looks at the generalised sequence for the whole Urubici suite of PRIM-EVOL1-DSM24-DSM04/08, and compares the F values derived from major element SUPERMIX models (Table 3.2) to those calculated for these H elements, assuming D=0. Values predicted from La, Ce and Ta are in general agreement with the major element figures, within the limits discussed for the other trace elements above. The Hf data

consistently predicts lower degrees of crystallisation which suggests that D_{Hf} is actually greater than 0 and that the approximation used is not valid. Th, the most incompatible element here, shows large discrepancies with the major elements (and Ta, La, Ce) for the evolved flows.

	PRIM	EVOL1	DSM 24	DSM 04/08	PRIM	EVOL2
Majors	100	84	66	46	100	86
Th	100	85	52	31	100	75
La	100	89	62	47	100	77
Ce	100	88	64	46	100	74
Ta	100	86	68	52	100	74
Hf	100	92	78	59	100	81

Table 3.4 Comparison of F values (in %) predicted by SUPERMIX major element models (table 3.2) and those calculated from abundances of hygro-magmatophile (H) elements (bulk D assumed to be 0).

The sequence PRIM-EVOL2 attempts to model the strong-Ti enrichment (trend 2 in figure 3.7) seen between the stratigraphical packets of flows. All trace elements show similar enrichments that give an average F of about 75 % *i.e.* 25 % crystallisation, and this contrasts with the much lower value of 14 % crystallisation required by the major element models. Thus it appears to be difficult to accommodate this steep Ti-enrichment trend on major element grounds and suggests that if simple closed system fractionation is responsible for this trend, then PRIM is not a realistic starting (parental) magma to EVOL2. A more suitable parental magma composition might be obtained by extrapolating the shallow trend (trend 1 on figure 3.7) within the lowest flow packet to a more primitive composition, although this problem will be returned to in the next section.

The above two sections have demonstrated that the gross features of the Urubici magmas are dominated by the action of closed system fractional crystallisation, but several features stand out as requiring further investigation; (i) the fine-scale variations within the basalt sequence, as picked out by the compositional contrast between individual flow

packets, (ii) the relationship between the Urubici basalts and intermediate flows, and these points are considered in the following sections.

3.4 Urubici basalts: role of polybaric fractionation and/or contamination.

The Urubici basalts, when considered as a whole, do not preserve tight, well constrained arrays on the major element variation diagrams (figure 3.1). The general trend through the data has been shown to be consistent, to a first order approximation, with the action of fractional crystallisation, but even taking into account the ubiquitous effects of post-eruption alteration, the range in concentration of a relatively immobile element such as Ti suggests that there must have been an additional process(es) acting to cause the scatter on the variation diagrams, *i.e.* consider the contrast between the steep versus shallow trends on figure 3.7.

It was demonstrated in chapter two that the basalt sequence in this region could be divided into several distinct stratigraphical packets of flows. These were best characterised by their TiO_2 contents, as illustrated in figure 3.7, with each flow packet defining a coherent trend within the overall spread of TiO_2 data. The discussion of this in section 3.3.1 above concluded that the variation displayed within each flow packet could be modelled in terms of extraction of a gabbroic mineral assemblage that included magnetite. Because each packet shows a similar, sub-parallel trend of shallow Ti enrichment with increasing fractionation, this suggests that they all evolved under similar conditions with a similar fractionating assemblage, and that the composition of the parental magma being input to this shallow level environment was varying. Therefore another earlier process was responsible for the strong Ti-enrichment seen throughout the sequence as a whole, onto which a later-stage low-pressure fractionation event, as highlighted by the trends within the stratigraphical groups, was superimposed.

An obvious candidate to consider is high-pressure crystal fractionation in accord with Cox (1980) who emphasized that much of the variation seen in basaltic rocks is likely

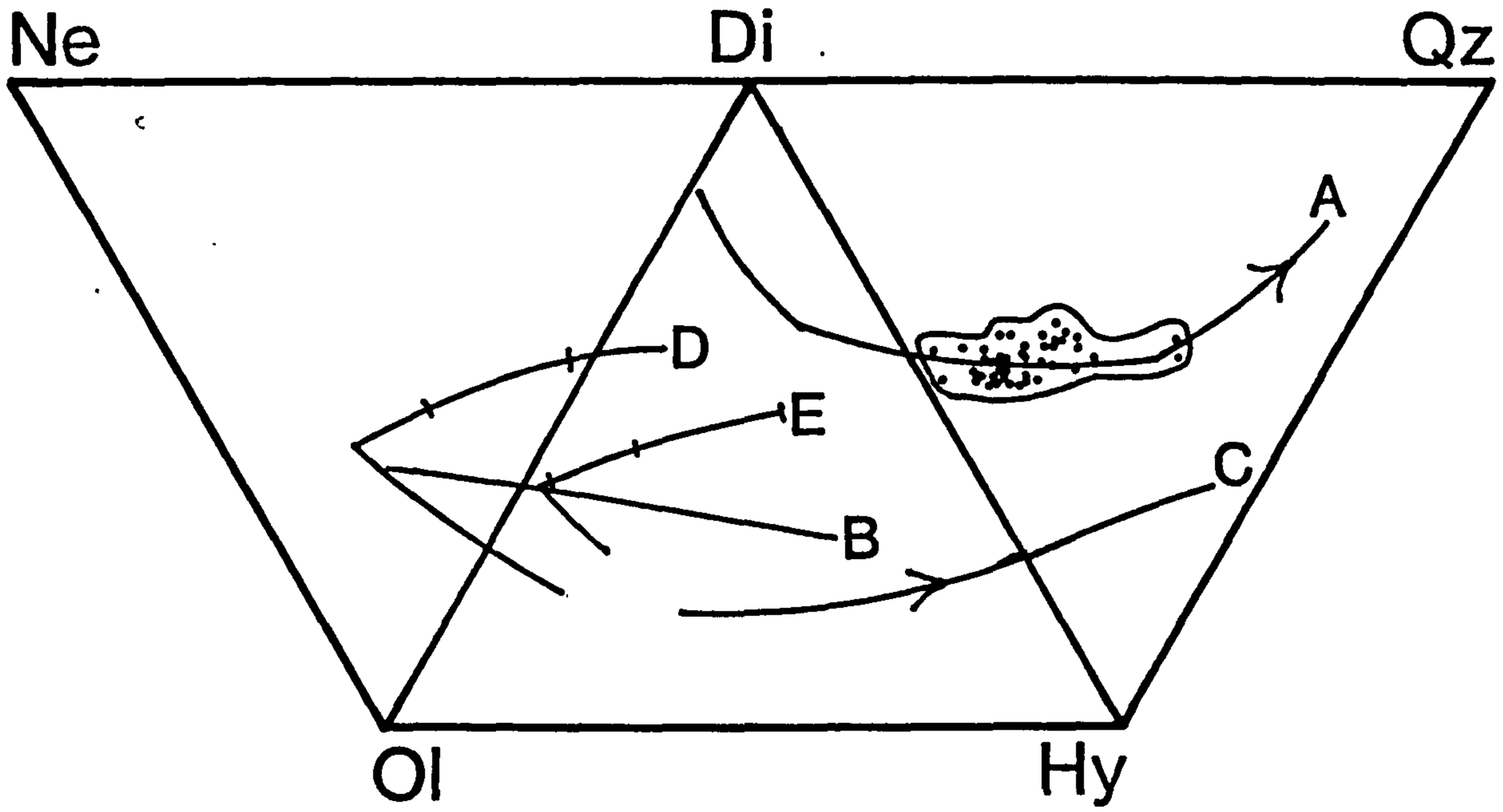

Figure 3.8 Projection of the basalt tetrahedron, with normative olivine, diopside, hypersthene, and nepheline or quartz (CIPW, wt%), showing various equilibria relevent to CFB genesis (after Thompson *et al.*, 1983).
A, B - cotectics for olivine+clinopyroxene+plagioclase+liquid at; (A) 1 atm., (B) 9 kb.
C - tentative cotectic for olivine+clinopyroxene+plagioclase+titanomagnetite 'deep in the continental crust'.
D - locus of initial melts from fertile anhydrous lherzolite mantle.
E - locus of initial melts from depleted (or MORB source) mantle.
Note the position of the Urubici-type samples clustering around the 1 atm cotectic (curve A).

to have been imposed by fractionation over a range of pressures. Evaluating the role of fractionation at high-pressure in the Urubici magmas, as with many lava sequences, is not straightforward. Figure 3.8 is a normative plot (CIPW wt%) of olivine, diopside, hypersthene and quartz or nepheline, together with various equilibria relevant to CFB genesis in general (Thompson *et al.*, 1983). The Urubici magmas all lie close to the 1 atm. cotectic and have clearly evolved to their final lava composition by extensive low-pressure crystal fractionation. The nature of high-pressure liquidus phases and their composition is uncertain since the vast majority of phenocrysts within the lavas would presumably reflect the latest fractionation event, but typical minerals expected for tholeiitic liquids are olivine, clinopyroxene, orthopyroxene and plagioclase (see Marsh and Eales, 1984). Garnet can be ruled out for the Urubici magma type since the HREE are not fractionated.

Urubici (high-Ti) magma type

The SUPERMIX model ('PRIM' to 'EVOL2', table 3.2) discussed above involved extraction of just olivine/augite/plagioclase *i.e.* no magnetite, and gave a reasonable fit. This modelling can only be qualitative since; (i) the mineral compositions used are not necessarily valid at high-pressure, and (ii) the parental magma to each low-pressure fractionation trend is not well constrained (*i.e.* how far back can each trend be extrapolated ?). This second point was highlighted by the modelling of the H elements (table 3.4), which illustrated the discrepancies between the major, and the trace, element models for this trend. Direct modelling of the trace element data also leads to problems since the pressure, temperature and compositional dependence of partition coefficients are poorly known.

Figure 3.9 shows the variation in Ti and Zr for the Urubici basalts. Ti and Zr have similar K_D's for olivine, clinopyroxene, orthopyroxene and plagioclase but differ

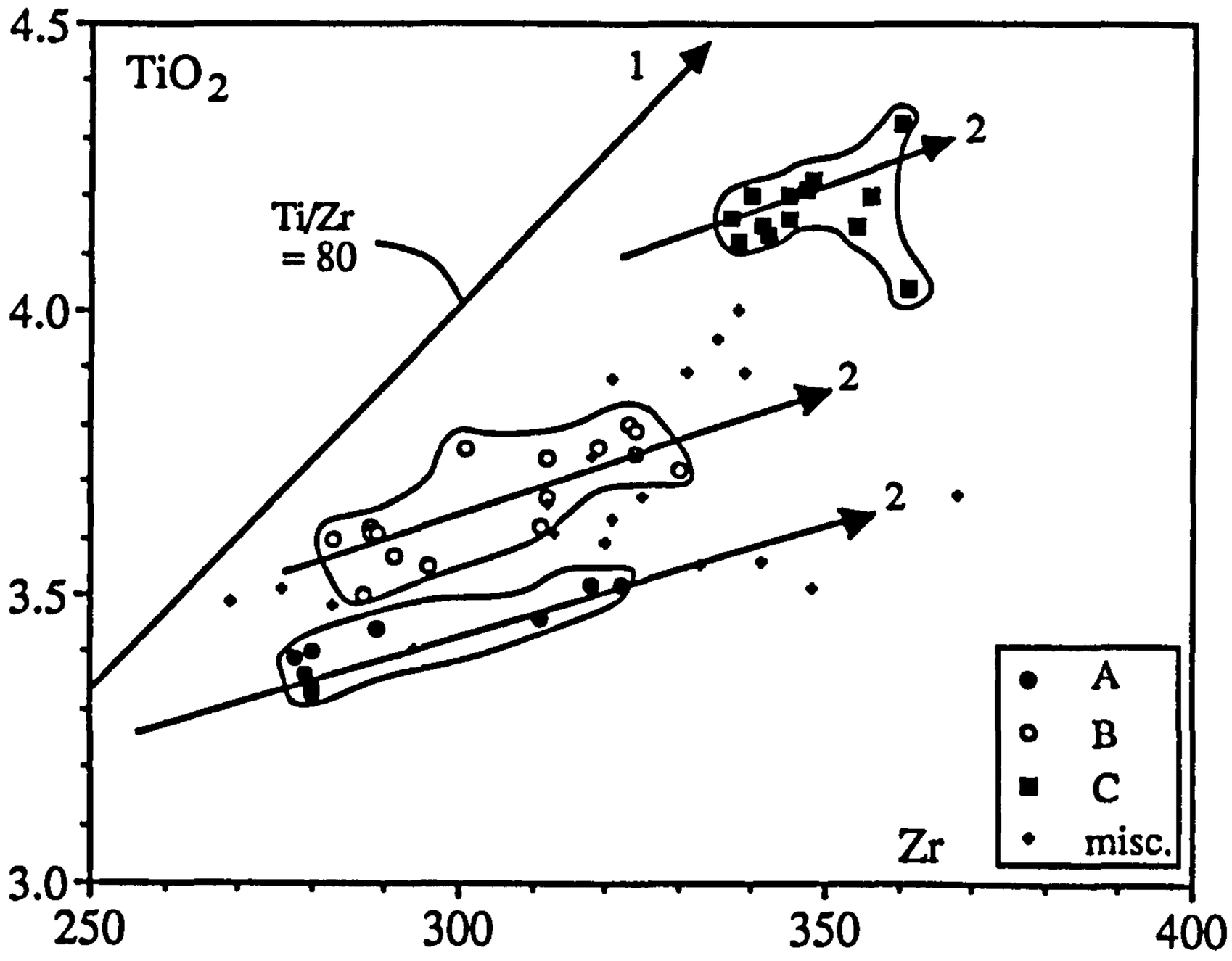

Figure 3.9 Variation of TiO_2 vs. Zr for the three main stratigraphical Urubici sub-units (symbols as in figure 3.7). The steep Ti-enrichment trend (trend 1) represents the inferred magnetite-free high-pressure fractionation at constant Ti/Zr, and the shallow, sub-parallel arrays (trend 2) defined by each flow packet result from low-pressure fractionation of gabbro+magnetite.

markedly for magnetite {K_D (Ti)=7.5, K_D (Zr)=0.1} (Pearce and Norry, 1979). The 'primitive' end members of each flow packet have similar Ti/Zr, consistent with high-pressure fractionation of a magnetite-free assemblage, but this ratio decreases within each packet as a result of low-pressure removal of magnetite.

Consideration should be given to the possibility that the variation in magma composition input to the higher level chambers could result from varying degrees of partial melting. The increase in TiO_2 and other incompatible elements with stratigraphical height would then imply a waning in the percentage of melting with time. The process identification methodology of Allègre and Minster (1978) suggested possible tests to discriminate between fractional crystallisation and partial melting. Plots of a compatible element (Ni, Cr, *etc.*) against an highly incompatible, H, element (Th, Ta, Zr, *etc.*) should distinguish the two processes. During crystallisation, the abundance of a compatible element decreases rapidly compared to the increase in incompatible element content, and the reverse is true during partial melting. Unfortunately this is difficult to assess for the Urubici because of their evolved nature, as illustrated by their low (< 100 ppm) Ni

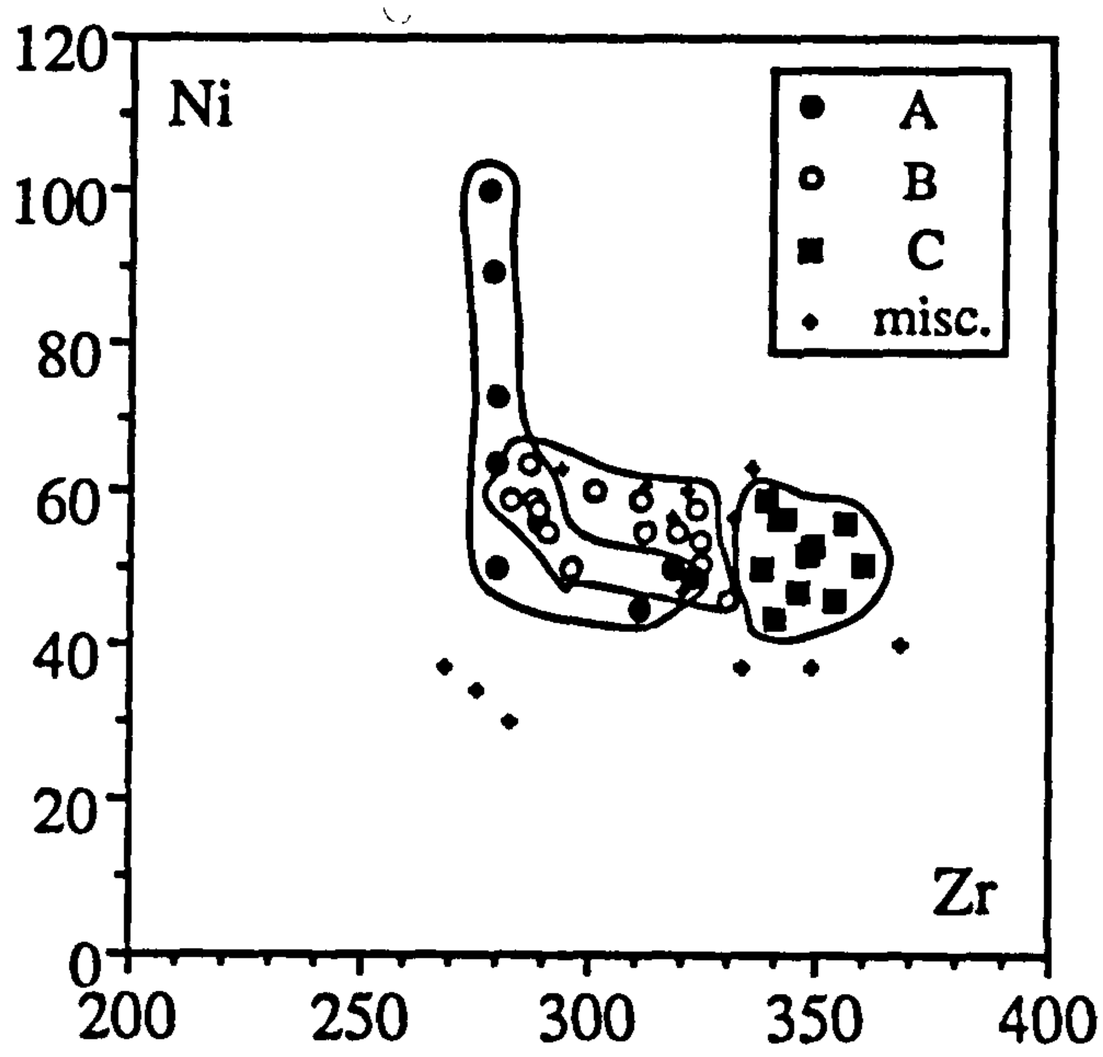

Figure 3.10 Variation of Ni (compatible element) vs. Zr (incompatible element) between the Urubici magma type sub-units.

contents (see figure 3.10). They are far removed from any plausible mantle derived melts and even the most primitive end members to each fractionation trend have already seen extensive fractionation to cause their Ni contents to be so low. A further complication on such a diagram (*e.g.* figure 3.10, Ni vs. Zr) is the possible effects of open system behaviour; the operation of an RTF (replenishment, tapping, fractionation) magma chamber would act to decouple compatible and incompatible elements (O'Hara and Matthews, 1981), and this might lead to some of the scatter seen. It is difficult to quantify conclusively the effects of small variations in the degree of melting but this has probably only introduced further noise into the data set rather than been the dominant control on magmatic compositions.

If all the variation seen within the basalts is to be attributed solely to the effects of polybaric fractionation then this should be reflected in their isotopic compositions since crystal fractionation on its own will have no effect on isotopic ratios. The basalts show a range in $(^{87}Sr/^{86}Sr)_i$ from 0.7048 to 0.7062, and this is partly correlated with their stratigraphical position. Figure 3.11 is a histogram showing the frequency distribution of initial Sr isotopic compositions of the Urubici basalts, and includes data taken from Mantovani *et al.*, (1985a) on samples from the GB section that lies within the field area of this study. It shows that the majority of the basalts have relatively low $(^{87}Sr/^{86}Sr)_i$ between 0.7048-0.7053. The only flows that show elevated $(^{87}Sr/^{86}Sr)_i$ are the initial few flows across the area (unit A) that have $(^{87}Sr/^{86}Sr)_i$ 0.7054-0.7058, together with the final Urubici flow both at at SM (0.7056) and GB (0.7062), although it is worth noting that this GB flow (A3) was tentatively correlated with the unit A flows from its major element composition in chapter two (see figure 2.14). This difference is emphasized in figure 3.12(a) which shows the variation of $(^{87}Sr/^{86}Sr)_i$ with TiO_2. The dominant trend is one of constant $(^{87}Sr/^{86}Sr)_i$ for a wide range in TiO_2 (3.2 to 4.3 wt%), with only a few points falling at higher $(^{87}Sr/^{86}Sr)_i$, although there is a perceptible negative correlation within the dominant low $(^{87}Sr/^{86}Sr)_i$ group, with the higher TiO_2 samples (> 4 wt%) having the lowest $(^{87}Sr/^{86}Sr)_i$ (< 0.7050).

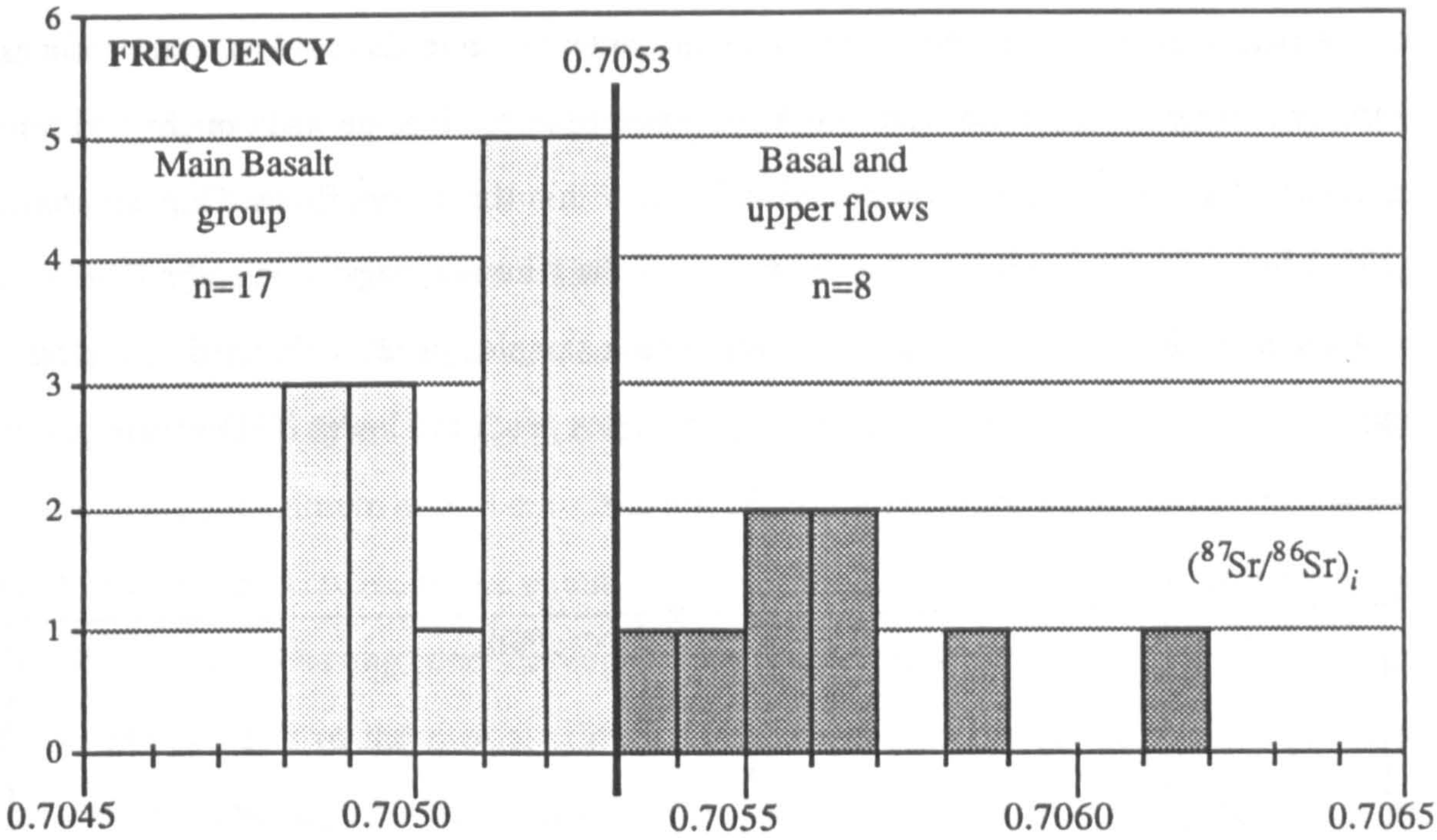

Figure 3.11 Frequency distribution of $(^{87}Sr/^{86}Sr)_i$ for the Urubici-type basalts. Data sources - {this study, Mantovani *et al.*, 1985a}. Main basalt group (sub-units B and C) - light shading, basal flows (sub-unit A) and uppermost flow - dark shading.

Because the total range in $(^{87}Sr/^{86}Sr)_i$ is relatively restricted, it is worth considering certain factors, such as machine precision and the calculation of initial ratios, that might lead to possible errors in these numbers. Machine precision is well constrained and is monitored via repeated analysis of an international standard NBS 987. Late stage weathering has affected both Rb and Sr to some extent, and since the Rb/Sr ratio is needed to correct measured $^{87}Sr/^{86}Sr$ back to initial values at 130 Ma, consideration of the variation within one of the stratigraphical units can give an estimate of the error in the measured Rb/Sr (~35% max.). For the worst case scenario, the combined effect of these factors might lead to errors of ± 0.0002 in $(^{87}Sr/^{86}Sr)_i$, comparable to the variation seen within the main group, but this is certainly not responsible for the difference between the groups. Alteration processes such as zeolitisation might have involved the addition of a Sr component of a different isotopic composition to the host rock. It is hoped that the careful selection and preparation of samples should minimise the effects of this possibility, but there is scope in the future to carry out leaching tests to verify this. This type of alteration

would be expected to follow a more random pattern across the area of over 50 km that is considered here, and the consistent stratigraphic pattern seen tends to rule alteration out as a major cause of the isotopic variation. A combined Sr and O isotope study might also help to assess the extent of alteration on $(^{87}Sr/^{86}Sr)_i$ within these lava flows. Duncan *et al.*, (1988) have obtained $\delta^{18}O$ results on samples of the Khumib magma type; the Etendeka equivalent to the Urubici magma type. Whole rock samples gave an elevated $\delta^{18}O$ in the range 8-11 ‰ whereas plagioclase mineral separates produced lower $\delta^{18}O$ values of 6-7 ‰, this difference was attributed to alteration effects.

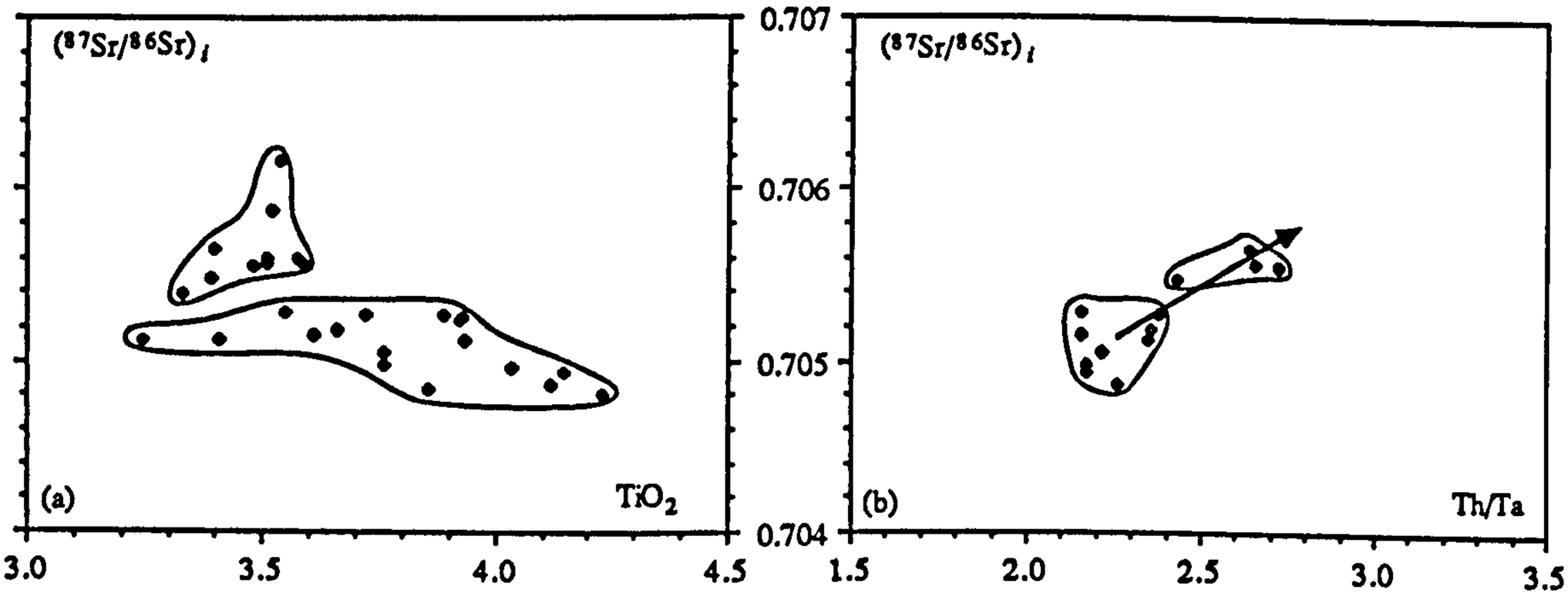

Figure 3.12 Variation of $(^{87}Sr/^{86}Sr)_i$ with; (a) TiO_2, and (b) Th/Ta, within the Urubici magma type. Main basalt group -'uncontaminated' (open symbols), shows little variation in $(^{87}Sr/^{86}Sr)_i$ for a wide range in TiO_2. Basal and upper flows - 'contaminated' (solid symbols), displaced to higher $(^{87}Sr/^{86}Sr)_i$ and higher Th/Ta.

It is interesting that the shift to elevated $(^{87}Sr/^{86}Sr)_i$ is accompanied by an increase in Th/Ta ratio {figure 3.12(b)}, *i.e.* the isotopic change correlates with a change in trace elements. The main basalt sequence has Th/Ta of 2.2-2.4 whereas the few 'anomalous' flows have Th/Ta 2.4-2.8. The most probable cause for this is for the enriched rocks to have suffered from some interaction with crustal material, since this is characterised by high Th/Ta and $(^{87}Sr/^{86}Sr)_i$ (*e.g.* Taylor and McLennan, 1985). It is not easy to resolve the intricacies of this process, as to whether or not it occurred within the magma chamber or during ascent, since the effects of crustal assimilation on the Urubici magmas are expected to be limited because of their trace element enriched character (also true of crustal rocks).

For magmas with high Sr contents, modification of $(^{87}Sr/^{86}Sr)_i$ by assimilation of crustal Sr will not be extensive (*c.f.* the Gramado magma type in the next chapter). There is no simple relationship between isotopic composition and extent of fractionation, within the basal flow packet for example, that would be characteristic of the AFC (assimilation and fractional crystallisation) process within the chamber (DePaolo, 1981). Huppert and Sparks (1985) considered the effects of temperature-controlled assimilation by the turbulent ascent of magmas through dykes and showed that a magma containing 7 % MgO had the potential to assimilate a maximum of 5 % crust. The decrease in $(^{87}Sr/^{86}Sr)_i$ with stratigraphic height might suggest a decrease in the extent of contamination with time, with all the readily mobilised material having been scavenged from the conduit walls by the earlier flows. This leaves the problem of the two last flows. These might result from the initiation of new pathways to the surface but the D3 flow at SM (DSM05b/07/09) is noticeably anomalous in terms of its major and trace element, as well as isotopic composition. It is evolved, having Mg# of 40 and low Ni, but has low Ti, P and Zr, and high V and $^{206}Pb/^{204}Pb$ compared to the rest of the Urubici magmas, and its relationship to these is uncertain.

Despite the overprint of some crustal interaction on the Urubici magmas it appears that we can still 'see-through' this, back to source heterogeneities. Figure 3.13 shows the covariation of $(^{87}Sr/^{86}Sr)_i$ vs.$(^{143}Nd/^{144}Nd)_i$, highlighting the 'uncontaminated' versus 'contaminated' basalts. The main 'uncontaminated' group of basalts, with $(^{87}Sr/^{86}Sr)_i <$ 0.7053, maintains a good negative correlation with $(^{143}Nd/^{144}Nd)_i$. Within this group, there is no change in ratios of highly incompatible elements (*e.g.* Th/Ta, Th/La, Hf/Ta, etc.) for a wide range of abundances. The wide range in from 0.51224 to 0.51242 is unlikely to be a consequence of surface alteration since most studies (*e.g.* Hawkesworth and Morrison 1978) have shown that $^{87}Sr/^{86}Sr$ is more susceptible to alteration by low-temperature processes than $^{143}Nd/^{144}Nd$. The implication therefore, is that this Sr-Nd isotope array is probably a source-inherited feature. Furthermore, this variation is linked to the stratigraphical packets of flows; those at lower $^{87}Sr/^{86}Sr$, higher $^{143}Nd/^{144}Nd$ are from unit C (with $TiO_2 > 4$ wt%) and those at higher $^{87}Sr/^{86}Sr$, lower $^{143}Nd/^{144}Nd$ are from unit B. This can be seen from figure 3.12(a) earlier which shows a slight negative

correlation between $(^{87}Sr/^{86}Sr)_i$ and TiO_2 within the 'uncontaminated' group. The contaminated flows still show a negative correlation between $(^{87}Sr/^{86}Sr)_i$ and $(^{143}Nd/^{144}Nd)_i$ but the array is displaced to higher $(^{87}Sr/^{86}Sr)_i$ and slightly lower $(^{143}Nd/^{144}Nd)_i$ with 0.51219-0.51236.

Evidence of polybaric processes affecting a suite of lavas is found only in favourable geological circumstances. It is often difficult to unravel the effects of fractionation at more than one pressure, since their combined effect often just leads to a scattering of compositional data. It appears that in the case of the Urubici magmas we have been fortunate and can resolve the effects of two fractionation processes at different pressures. Several factors have worked in our favour; (i) only rocks from a relatively restricted area have been considered to minimise complications from possible regional variations, (ii) good stratigraphical control on samples, and (iii) the change in mineral phases in the fractionating assemblage caused a marked change in at least one element (*e.g.* TiO_2).

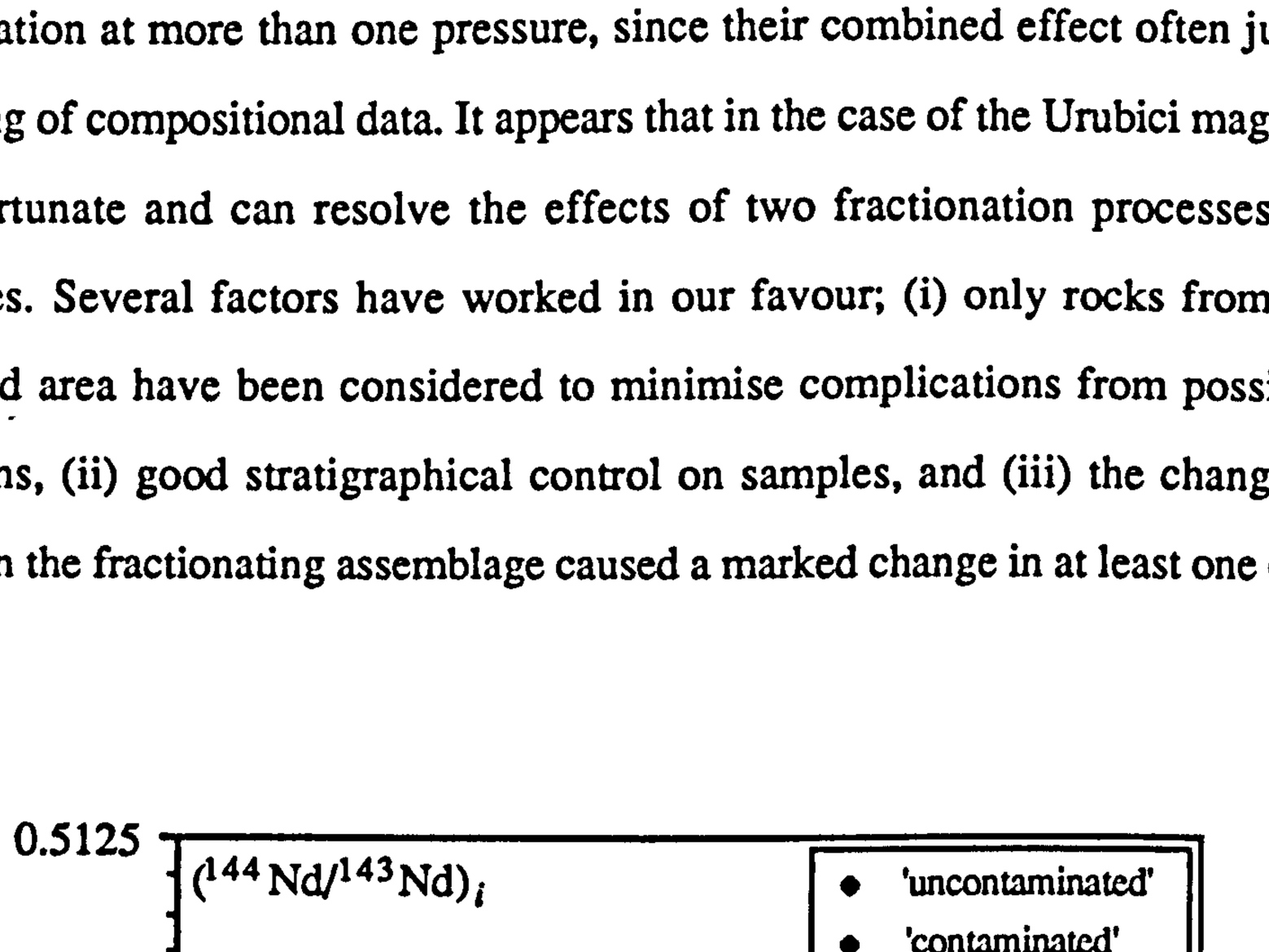

Figure 3.13 Variation of $(^{143}Nd/^{144}Nd)_i$ vs. $(^{87}Sr/^{86}Sr)_i$ for the Urubici and Chapecó magma types. Data sources - {this study, Hawkesworth *et al.*, 1986}. The 'contaminated' flows are displaced to higher $(^{87}Sr/^{86}Sr)_i$ and lower $(^{143}Nd/^{144}Nd)_i$.

3.5 Urubici basalts to intermediate flows: fractionation or contamination ?

For the transition from the basalts to the two intermediate flows, major and trace element models involving crystallisation of augite/plagioclase/magnetite/apatite have produced reasonable matches for the compositions of the evolved flows, but two remaining worries are the change in ratios of certain incompatible trace elements and the accompanying move to higher $(^{87}Sr/^{86}Sr)_i$ with fractionation, summarised in table 3.5 below.

Taking the H elements such as Th, Ta, La, which are generally considered as highly incompatible, crystal fractionation should not change inter-element ratios except in the presence of certain minor phases (*e.g.* Ta is compatible in magnetite). Fractionation of magnetite cannot be used to explain the change in Th/Ta and La/Ta since Hf/Ta is not affected. Figure 3.14(a) illustrates the contrasting behaviour of the REE between the basalts and the intermediate flows (see also figure 3.3). Within the basaltic rocks, the extent of LREE enrichment as monitored by Ce/Sm remains constant over a range of Sm values whereas there is a marked increase in Ce/Sm for the intermediate flows. The results of predicting F values from the H elements, given in table 3.4, showed that Th stood out as behaving much more incompatibly than the other elements. The main feature of the transition from basalt to intermediate magmas seems to be a marked increase in the LILE-abundances (Th, U, Pb, Rb, K) and to a lesser extent, the LREE, and this is shown in figure 3.14(b) using Th/Ta vs. La/Sm. The correlation between Th enrichment and increasing LREE enrichment is also marked by a shift to more radiogenic Sr isotopic compositions, and each group on figure 3.14(b) has been annotated with its range in $(^{87}Sr/^{87}Sr)_i$. In absence of any phases that would retain Ta, Hf, Ce to the exclusion of Th, Pb etc. it seems reasonable to explain the addition of the LIL-elements and ^{87}Sr by crustal assimilation. Since there is a correlation between degree of fractionation and extent of contamination, an AFC style of contamination is envisaged (DePaolo, 1981), although the variations within the basalt suite could have been generated by temperature-controlled assimilation during ascent. It is worth noting that DSM24 and DSM04/08 are not

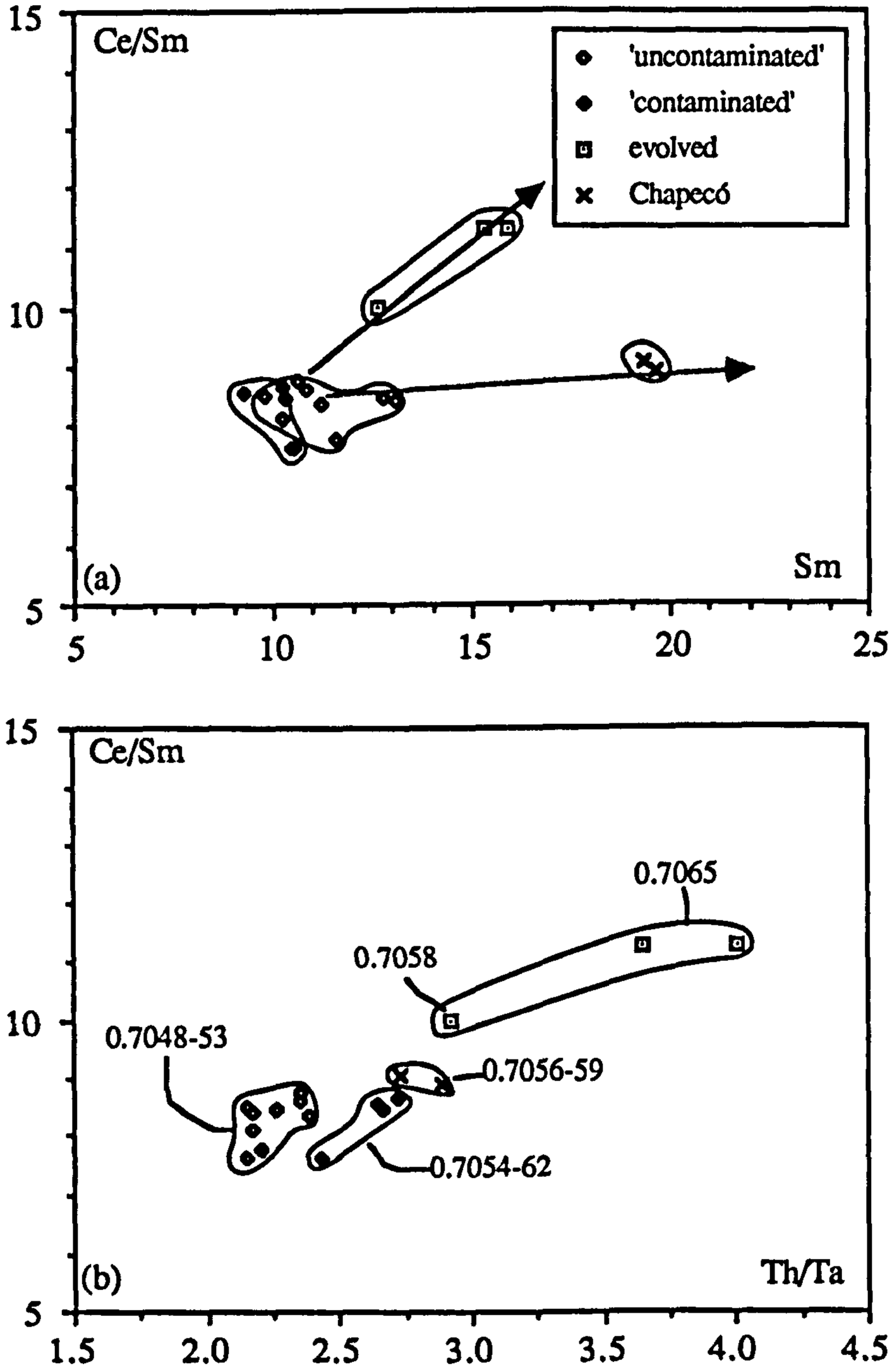

Figure 3.14 Variation of LREE enrichment (Ce/Sm) with; (a) Sm, (b) Th/Ta, for the Urubici and Chapecó magma types. Outlined fields in (b) are labelled with range in $(^{87}Sr/^{86}Sr)_i$.

necessarily directed related to each other, especially since they are not stratigraphically adjacent (see figure 2.14); DSM24 occurred after unit B, and DSM04/08 was the last Urubici flow seen, erupted after the anomalous basalt flow DSM05b/07/09. The operation of an AFC-type process does seem to have been a localised event since there are only two such flows in the area studied and these both lie within the same road section, SM. The trend from the most primitive basalt to the most evolved flow does not show a coherent

increase in the amount of assimilation, and so constraining the parameters of the AFC process and possible contaminant compositions can only be qualitative.

3.6 Urubici and Chapecó magma types : any connections ?

Because the Paraná rhyolites also show, to a first approximation, the high-Ti / low-Ti north / south provinciality seen within the basaltic rocks (Mantovani *et al.*, 1985b), it has been tempting to seek a genetic relationship between the low-Ti basalts and Palmas rhyolites on one hand, and the high-Ti basalts and Chapecó rhyolites on the other. Bellieni *et al.*, (1986b) attempted to relate the high-Ti basalts to the Chapecó rhyolites by a fractional crystallisation process. Major element models using a crystal extract of augite+plagioclase+pigeonite+magnetite+apatite yielded relatively low Σr^2 values, and were supported by their calculated trace elements contents. One major drawback to this model was the lack of any rocks of intermediate composition, and Bellieni *et al.*, (1986b) invoked the early extraction of substantial amounts of magnetite that would cause a rapid increase in SiO_2 to possibly get around this problem. The models used can only be an approximation since there are likely to be changes in mineralogy and mineral proportions of the fractionate as crystallisation proceeds, and therefore in the absence of any intermediate samples, modelling 'across the silica gap' might be fraught with problems. This illustrates the possible importance of the two intermediate Urubici flows found during the course of this fieldwork in resolving this issue.

The question now is whether they represent an intermediate fractionation stage between the basalts and the rhyolites. Using similar mineral compositions to those employed by Bellieni *et al.*, (1986b) in their modelling, exploratory SUPERMIX major element models between DSM04/08 and a Chapecó rhyolite composition taken from Mantovani *et al.*, (1985b) produced poor fits for a variety of possible phase assemblages. All solutions had high residuals ($\Sigma r^2 > 1.5$) and most produced negative solutions for augite. For this scenario, the evolved Urubici flows should lie on fractionation trends towards the rhyolites and this is patently not the case (see figures 3.3 and 3.4), perhaps

understandable since the previous section showed that many of the features of these evolved rocks could not be explained in terms of crystal fractionation alone, and that some crustal assimilation was necessary to explain their elevated $^{87}Sr/^{86}Sr$, Th/Ta, La/Sm *etc.* The abundances of the HREE and Y in the Chapecó seem to be too high to result from fractionation from the Urubici basalts, if ideas of plausible phase assemblages and partition coefficients are reasonable. The average Urubici basalt has 320 ppm Zr and 40 ppm Y compared to 560 ppm Zr and 70 ppm Y in the Chapecó rhyolites. This means that both have the same Zr/Y ratio of about 8, implying a similar bulk distribution coefficient for both Zr and Y during crystallisation. The major element data indicates that to produce the Chapecó rhyolites from the basalts about 50 % fractionation is necessary and that any postulated crystal extract must include at least 30 % clinopyroxene plus a few percent of apatite. From Pearce and Norry (1979), the partition coefficients for Zr and Y are similar for most phases, but Y is noticeably more compatible than Zr in clinopyroxene and especially apatite. Therefore the transition from basalt to rhyolite would be expected to

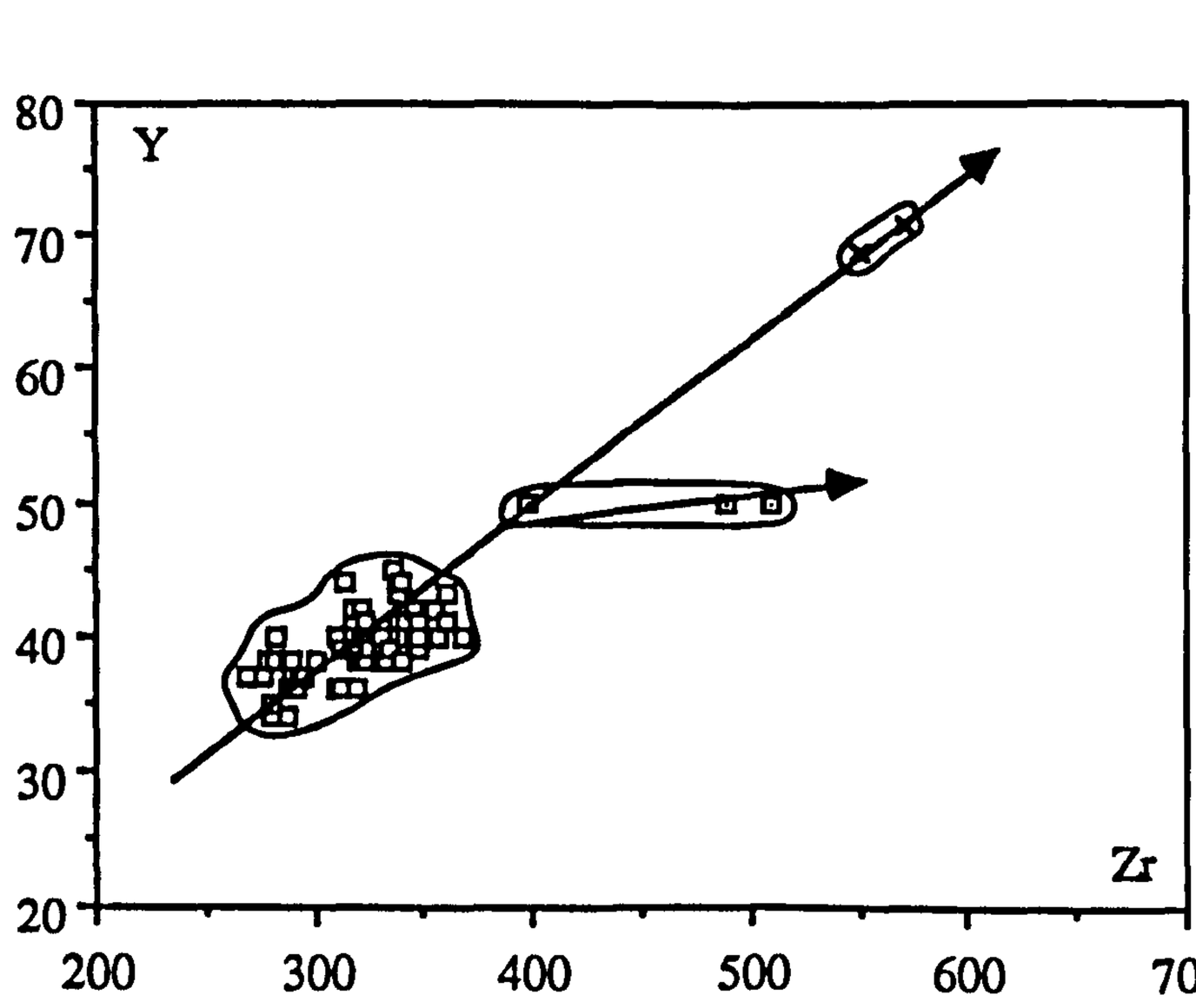

Figure 3.15 Variation of Y vs. Zr for the Urubici basalts (open squares), evolved Urubici flows (open squares + dot), and Chapecó rhyolites, illustrating the constant Zr/Y between the Urubici basalts and the Chapecó rhyolites, in contrast to the evolved Urubici flows.

fractionate Zr from Y and this is not seen (figure 3.15), the Chapecó rhyolites having higher Y contents than expected.

To explain the 'silica gap' and the confinement of acidic rocks to the continental margin, Bellieni *et al.*, (1986b) suggested partial melting of crustal material as an alternative mechanism for the derivation of the Chapecó rhyolites. They were uncertain as to the nature of this source material proposing either (i) lower crustal mafic/intermediate granulites, similar to the Pre-Cambrian granulites now exposed between 15-31°S in the São Francisco, Tocatins and Paraná provinces, or (ii) underplated high-Ti rocks. The second of these hypotheses might explain many of the geochemical similarities between the Chapecó and Urubici magmas, both in terms in terms of incompatible trace element ratios (see table 3.5) and especially the reasonable agreement of Sr, Nd and Pb isotopic compositions illustrated on figures 3.5 and 3.6, without having to resort to extremes of crystal fractionation. This is akin to the model proposed by Betton and Cox (1979) to account for the characteristics of the Lebombo rhyolites in the Karoo, where the rhyolites shared similar isotopic compositions to the earlier basalts. Cleverly *et al.*, (1984) modelled the rhyolites as 7-15 % melts of lower crustal sill complexes emplaced during the flood basalt activity. Residual garnet can be ruled out by the high Y contents and lack of HREE depletion in the rhyolites, as noted for the Lebombo rhyolites (Cleverly *et al.*, 1984). Bellieni *et al.*, (1986b) remarked that the resorbed plagioclase phenocrysts, a feature of the

	BASALTS	DSM24	DSM04/08	CHAPECO
La/Sm	3.6-4.2	4.8	5.2	4.1
Th/Ta	2.2-2.4	2.9	3.8	2.8
Th/La	0.10-0.11	0.12	0.16	0.11
La/Ta	21-23	24	25	25
Hf/Ta	3.8-4.3	3.7	3.8	4.4
$^{87}Sr/^{86}Sr$	0.7048-53	0.7057	0.7065	0.7056-59

Table 3.5 Comparison of incompatible trace element and isotopic ratios between the uncontaminated Urubici basalts, the intermediate Urubici flows (DSM24 and DSM04/08), and the Chapecó rhyolites.

Chapecó rhyolites, could represent unmelted restite material.

Because of the many geochemical similarities between the high-Ti basaltic magma types, in terms of isotopic ratios and ratios of highly incompatible trace elements that might reflect those of the source region (*i.e.* the groups were distinguished mainly by their differing elemental abundances), ascertaining which magma type might be the possible source to the Chapecó rhyolites is problematical. The Chapecó rhyolites do show some regional variation in composition in moving from the central to northern sections of the Paraná province, as seen in figures 4 and 5 of Piccirillo *et al.*, (1988b), and this is best illustrated by the Sr contents which average 500 ppm in the central region (Mantovani *et al.*, 1985b) versus 300 ppm in the northern region (Piccirillo *et al.*, 1988b). The details of the northern Chapecó rhyolites are further complicated by their enriched initial Sr ratios (0.7075-0.708) compared to those in the central region (~0.7056, Mantovani *et al.*, 1985b) and this was attributed by Piccirillo *et al.*, (1988b) to contamination during ascent. The underlying cause for this variability has not been considered previously and it is tempting to suggest that it might reflect the nature of the postulated underplated high-Ti basalts, whether Urubici or Pitanga type. A study of the regional geochemical variations within the Chapecó rhyolites plus further trace element and isotopic data are needed to constrain this possibility.

3.7 Conclusions.

As with previous studies on the high-Ti rocks of the Paraná basin, the main conclusion of this chapter is that fractional crystallisation has been the dominant cause of the variations within the Urubici magma type, although because of the good field control on sampling, the general trend through the data has been shown to preserve the effects of multi-stage fractionation; low-pressure fractionation of gabbro+magnetite superimposed on a higher-pressure (*i.e.* deeper) trend, less well constrained but involving no Fe-Ti oxides. Assimilation of crustal material appears to have modified some of the basalt flows, namely the initial batch of magmas across the area as well as the final Urubici flow, but it was not

responsible for the major geochemical characteristics of the lavas. Despite this, it is still possible to see through to source inherited isotopic variations, and it is worth pointing out the similarity between the isotopic composition of the 'pristine' Urubici-type magmas and several South Atlantic magmas, especially those of the Walvis Ridge (Hawkesworth *et al.*, 1986).

The few evolved Urubici-type flows found are consistent with the localised operation of an AFC-type contamination process and do not represent intermediate fractionation stages to the Chapecó rhyolites. Whereas there is no direct relationship between the Urubici basalts and the Chapecó rhyolites, the fact that the Chapecó rhyolites share many geochemical features with the Urubici magma type suggests that these might be source inherited, *i.e.* by melting of underplated Urubici-type material.

Urubici (high-Ti) magma type

Chapter 4

The Gramado and Esmeralda magma types (Low-Ti).

4.1 Introduction.

This chapter is restricted to the low-Ti magma types that occur in the south-east portion of the lava field, in the Santa Catarina and Rio Grande do Sul states of Brazil. Basalts of the Gramado magma type dominate the lava sequences in this area whereas those of the Esmeralda-type are a late stage feature restricted to a few of the upper flows and intrusions cutting the lava pile (see section 2.6.3 above). Aspects of the rhyolitic magmatism, which is exclusively of Palmas-type in southern Paraná, will also be touched upon and, in addition, the conclusions reached from the equivalent lava sequences in Namibia (Erlank *et al.*, 1984) are pertinent to these discussions. The first part is mainly concerned with describing the variations seen within the Gramado and Esmeralda magma types, and then it considers the significance of differences between these two magma types and see how, if at all, they are related.

4.2 Geochemical variations within the Gramado and Esmeralda magma types: Fractional crystallisation ?

Lavas of the Gramado and Esmeralda types are almost exclusively quartz tholeiites, in common with the Urubici basalts, although a few of the more mafic samples are slightly olivine normative. In general, the average degree of evolution of the Gramado- and Esmeralda-type samples is similar to that found for the Urubici magma type (see table 2.3), but Gramado-type flows with Mg# higher than 55 can be found. Even so, these more primitive flows still have Mg# < 65 and therefore can not be considered primary in the

sense that they could have been in equilibrium with mantle olivine (Frey *et al.*, 1978). Their evolved nature is also demonstrated by their generally low Ni (< 130 ppm) contents.

There are no distinguishing petrographical features that can separate the Gramado and Esmeralda magma types. The Gramado- and Esmeralda-type flows, like those of the Urubici magma type, are weakly porphrytic to subaphryic. The observed phenocryst phases are predominantly plagioclase and augite, plus rarer highly altered olivine. These minerals also occur as microphenocrysts along with Fe-Ti oxides and minor pigeonite. The groundmass is fine- to medium-grained and displays a range in texture from intergranular to intersertal. More commonly, anhedral equant crystals of augite, pigeonite and opaques occupy the interstitial spaces between lath-shaped plagioclases, but there are often brownish areas of altered glass enclosing the plagioclase crystals which, if large enough, produce patches with hyalophitic texture. The sills of the Esmeralda magma type had a coarse-grained groundmass of equigranular plagioclase and augite, with occasional olivine (iddingsite) and large irregular grains of interstitial Fe-Ti oxides.

The geochemical trends within the Gramado and Esmeralda magma types are illustrated in figures 4.1, 4.2, 4.3 and 4.4 which show the variation of selected major and trace elements with Mg#, a monitor of the extent of magmatic evolution. The Gramado type in particular, covers a large compositional range. It is important to note that although for the data set collected during this study a large proportion of this range is caused by the presence of a single, primitive sample (DUP30), this sample is similar in composition to other primitive Gramado magmas and analyses given in the literature for the Gramado magma type form a compositional continuum from about Mg# 65 to 30 (Mantovani *et al.*, 1985a).

The geochemical variation within the Esmeralda and Gramado magma types are superficially similar, but often the trends are parallel though displaced from one another. For major elements, within both magma types there is a sympathetic decrease of CaO and, to a lesser extent, Al_2O_3 with Mg#, whilst SiO_2, K_2O and P_2O_5 all increase. Both groups show the typical tholeiitic trend of TiO_2 and $Fe_2O_3(t)$ enrichment as Mg# falls, though once Mg# 40 is reached, the Gramado-type samples show an inflection indicating the removal of

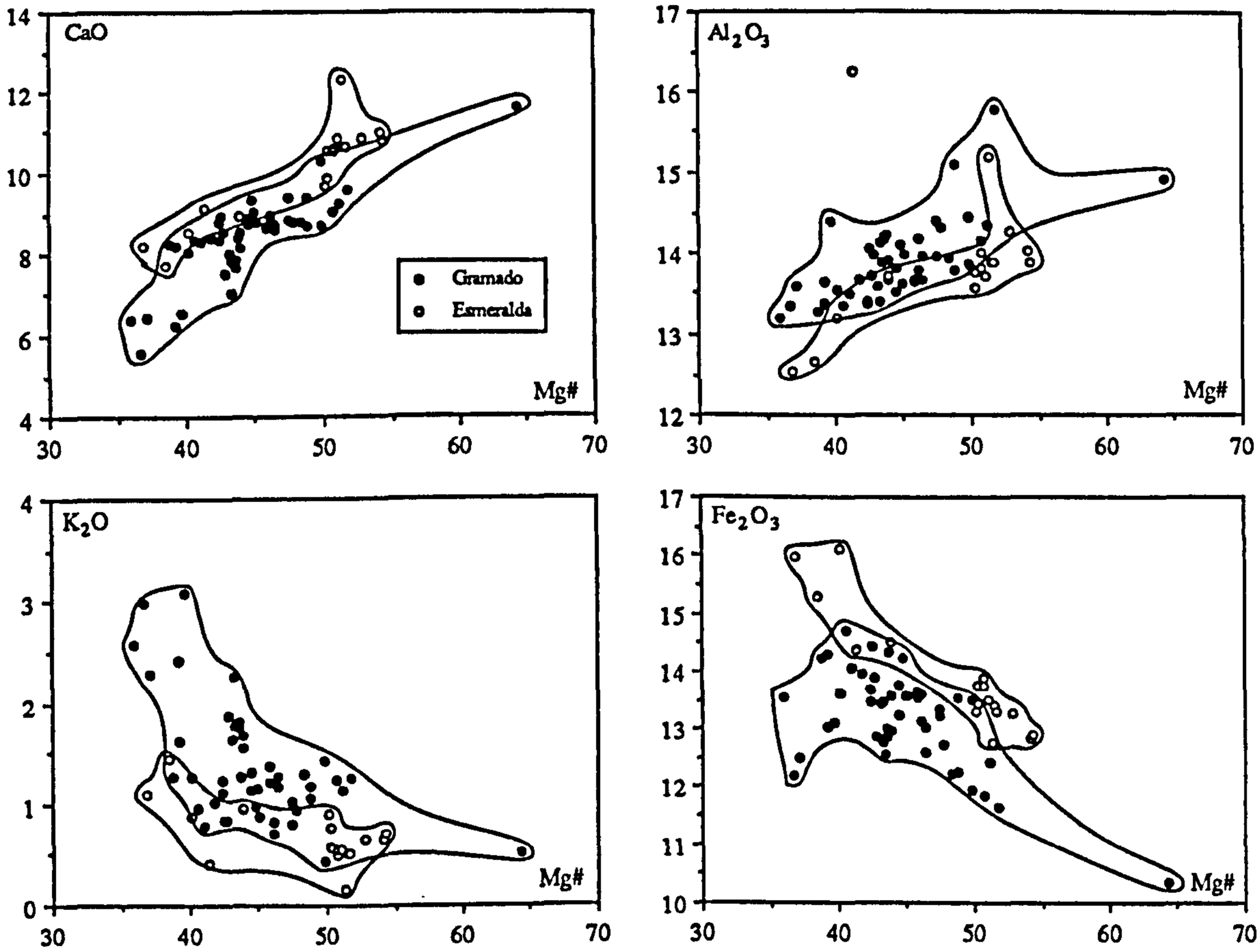

Figure 4.1 Selected major element variation diagrams for the Gramado and Esmeralda magma types.

TiO_2 and Fe_2O_3(t). Looking at the trace element variations, V mirrors the behaviour of Ti and Fe, and Rb, Ba, Zr, Nb, Y all behave as typical incompatible trace elements showing strong enrichment with increasing fractionation. Sr contents, despite a certain amount of scatter, remain roughly constant within each magma type. The elemental variations displayed by both the Gramado-type and Esmeralda-type magmas are suggestive of the effects of crystal fractionation.

Several previous studies have modelled fractional crystallisation processes, concentrating on the Gramado magma type, and have shown that the variations are largely due to the removal of plagioclase and clinopyroxene plus minor amounts of olivine and/or magnetite. These studies have considered both actual samples (Bellieni *et al.*, 1984c; Mantovani *et al.*, 1985a; Fodor *et al.*, 1985a) and average compositions (Bellieni *et al.*, 1984c; Piccirillo *et al.*, 1988a), but they have all yielded similar major element solutions.

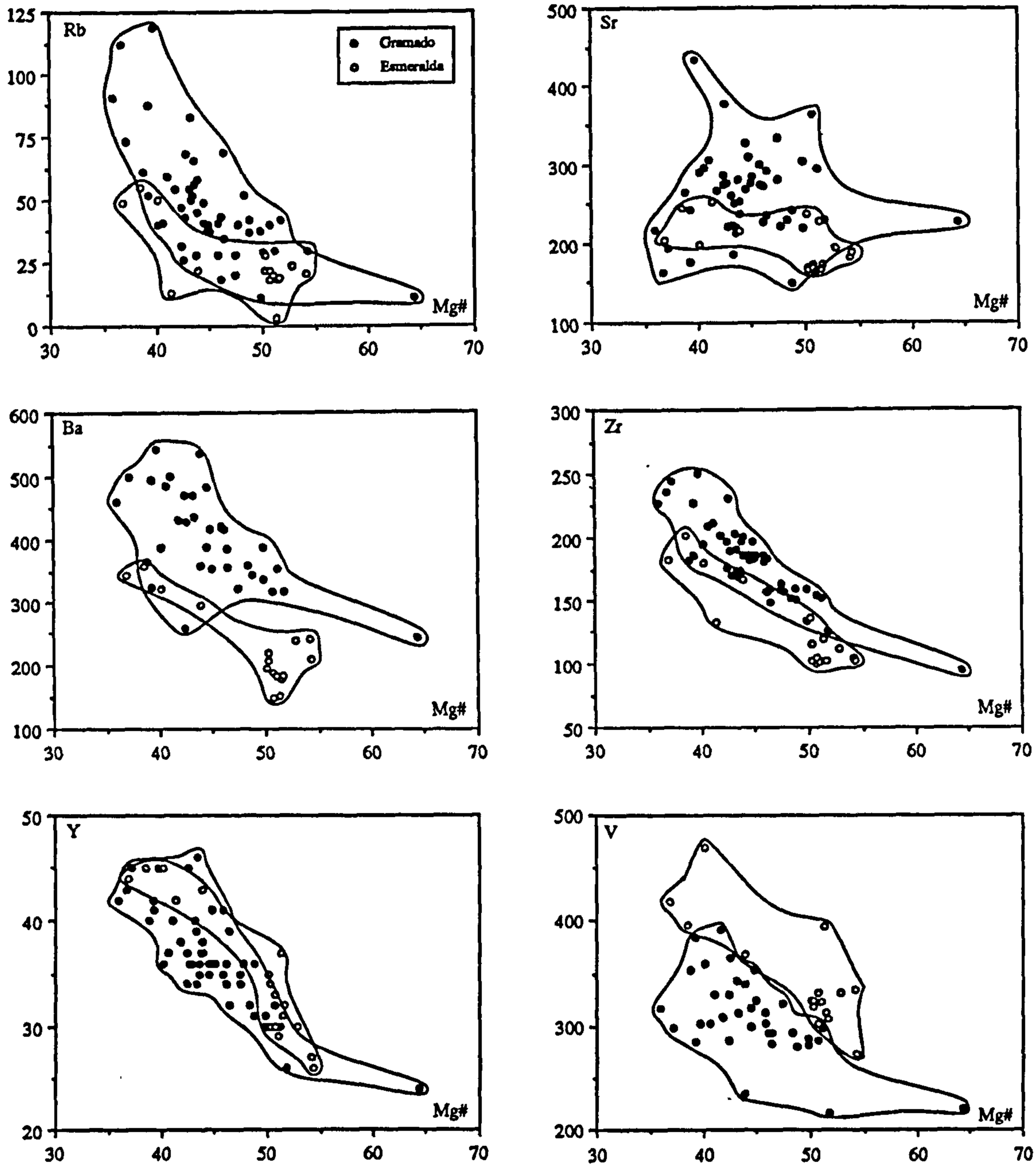

Figure 4.2 Selected trace element variation diagrams for the Gramado and Esmeralda magma types.

On average, the transition from Mg# 65 to 45 could be accommodated by ~35-55 % crystallisation of an olivine+augite+plagioclase+magnetite assemblage in the approximate proportions 12/36/52/2, or 16/30/54/0 if no magnetite was included in the modelling. To reach the more evolved compositions, from Mg# 45 to 35, required the removal of an augite+pigeonite+ plagioclase+magnetite crystal extract in the approximate proportions 24/15/54/7. The Esmeralda magma type was considered by Fodor *et al.*, (1985a) who

modelled the variation from Mg# 55 to 40 with about 20-40 % crystallisation of olivine+augite+plagioclase in the average proportions 4/57/39, with augite dominating over plagioclase in the crystal extract.

Attempts to match the trace element contents of the modelled magmas by fractional crystallisation, using the predicted crystal extract from major element modelling and reasonable partition coefficient data, in most cases proved difficult. For example, certain trace elements in the modelled solutions of Bellieni *et al.*, (1984c) such as Zr were up to 20 % in error. Both Mantovani *et al.*, (1985a) and Fodor *et al.*, (1985a) commented that the geochemical trace element variations could not be completely explained qualitatively by fractional crystallisation using major element modelling predictions and this, together with the dispersion on variation diagrams, suggested that closed system fractional crystallisation was not the only process that had acted on these magmas.

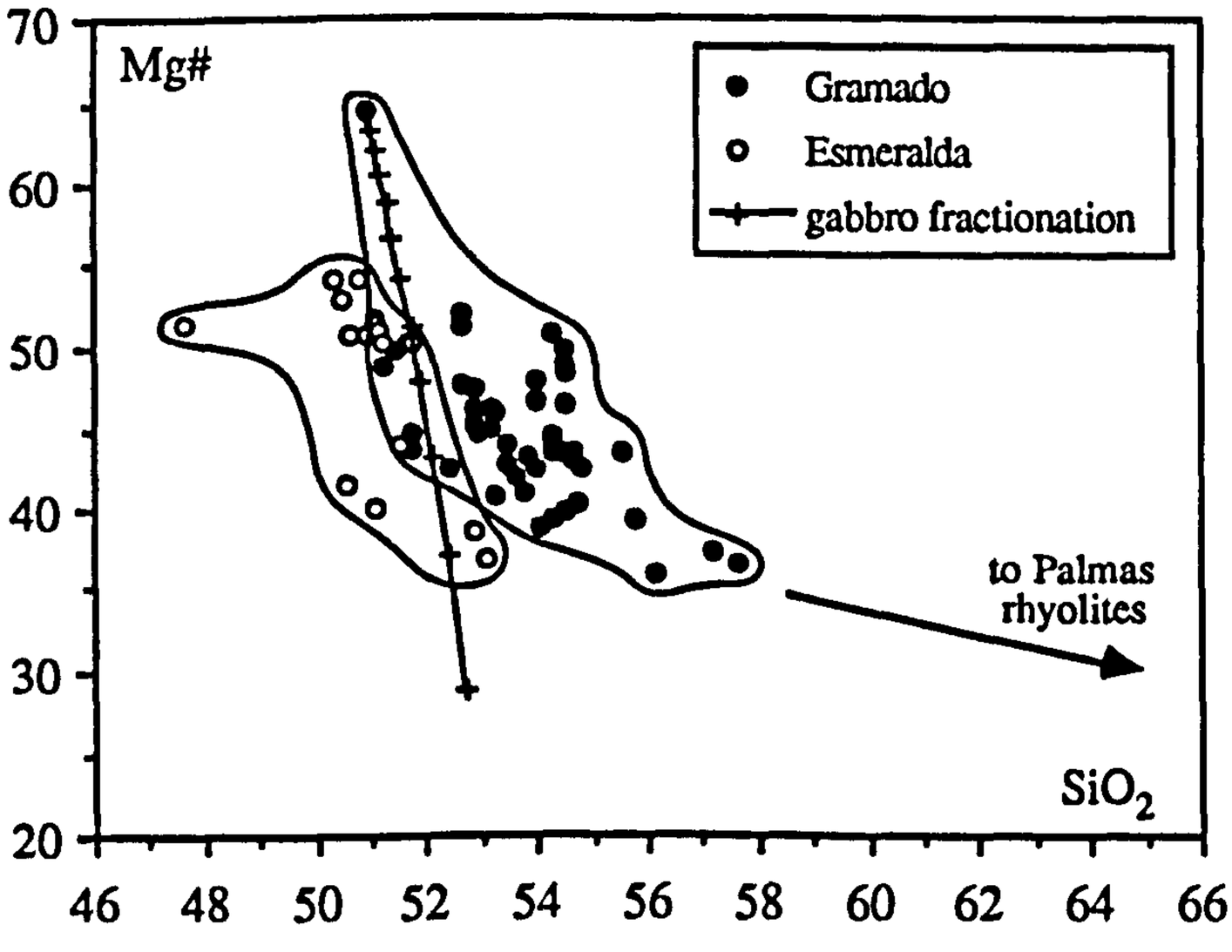

Figure 4.3 Mg# vs. SiO_2 for the Gramado and Esmeralda magma types showing the divergence of the Gramado data field away from a gabbro fractionation vector towards higher SiO_2. Gabbro fractionation vector modelled for olivine/clinopyroxene/plagioclase extract in the proportions 15/35/50 (Cox, 1980). Tick marks indicate 5 % crystallisation intervals.

This is also indicated by the variation of SiO_2 with Mg# illustrated in figure 4.3. The important feature is the marked increase in SiO_2 with decreasing Mg#, with SiO_2 varying from 50 to 58 wt% as Mg# changes from 65 to 35. Cox (1980) has shown that in many tholeiitic suites protracted fractionation of a gabbroic crystal extract of olivine+ clinopyroxene+plagioclase will lead to only a slight increase in SiO_2, provided no Fe-Ti oxides were also precipitating, and a plausible gabbro fractionation vector has been included on figure 4.3 to highlight this. Thus, as pointed out by Erlank *et al.*, (1984) for the Tafelberg basalts in Etendeka, this marked increase in SiO_2 requires further consideration. To model the increase in SiO_2, Bellieni *et al.*, (1984c) and Piccirillo *et al.*, (1988a) included up to 4 % of magnetite in the crystal extract, but this not surprisingly resulted in poorly fitted TiO_2 contents since the strong Ti, Fe enrichment suggested an absence of Fe-Ti oxides in the fractionating crystal extract.

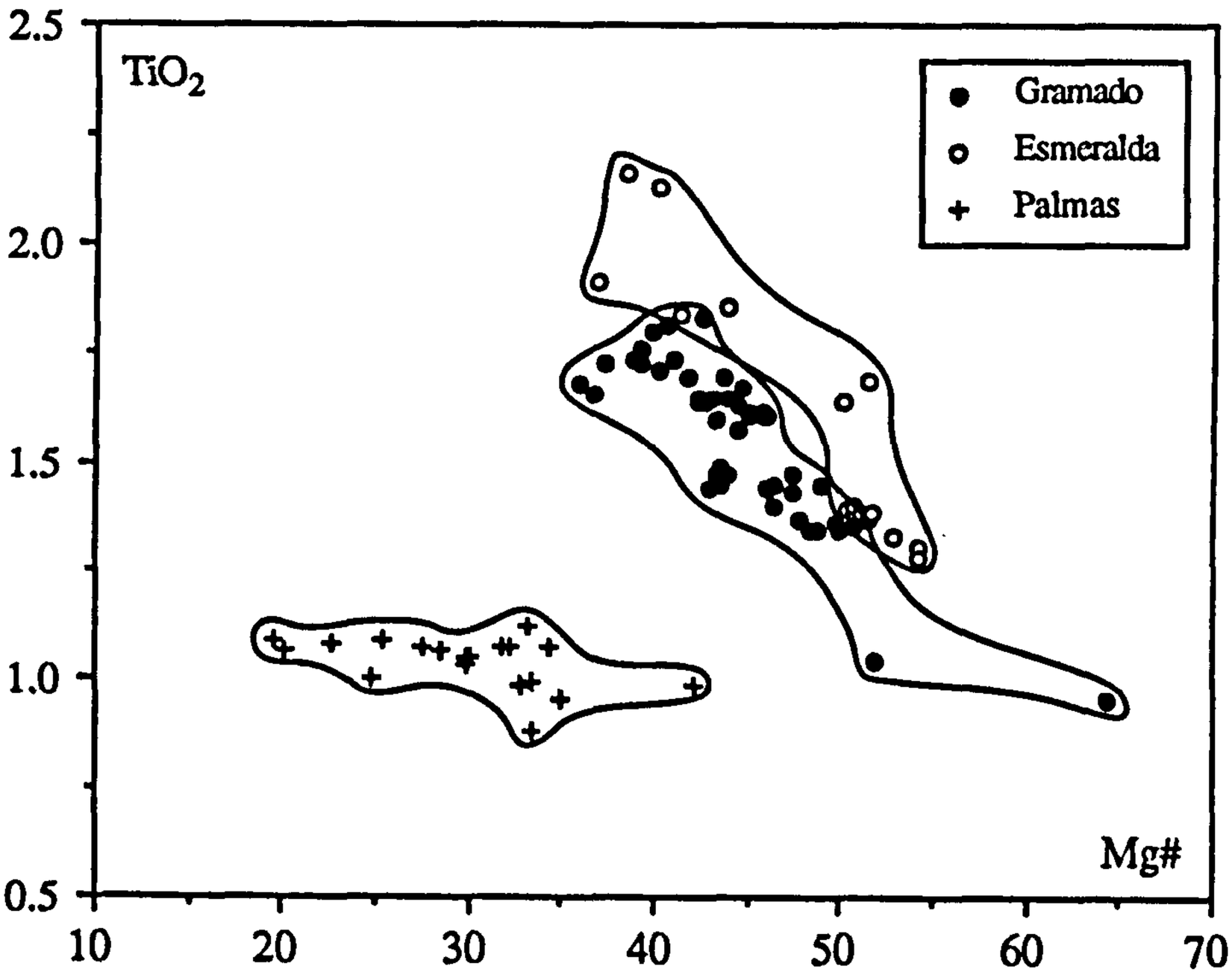

Figure 4.4 Mg# vs. TiO_2 variation in the Gramado, Esmeralda and Palmas magma types. The increase in TiO_2 with decreasing Mg# for the Gramado magma type rules out simple mixing with a Palmas rhyolite liquid in order to explain their increasing high SiO_2 content shown on figure 4.3.

As has been stressed many times, in order to fully understand the nature of petrogenetic processes acting on a suite of magmas, the behaviour of major and trace elements must be considered in conjunction with any isotopic variations. Once isotopic data became available for low-Ti magmas from the southern part of the Paraná province, it was plainly obvious that an additional process had played a role in their evolution since the isotope ratios were highly variable and fractional crystallisation alone could not have been responsible for this.

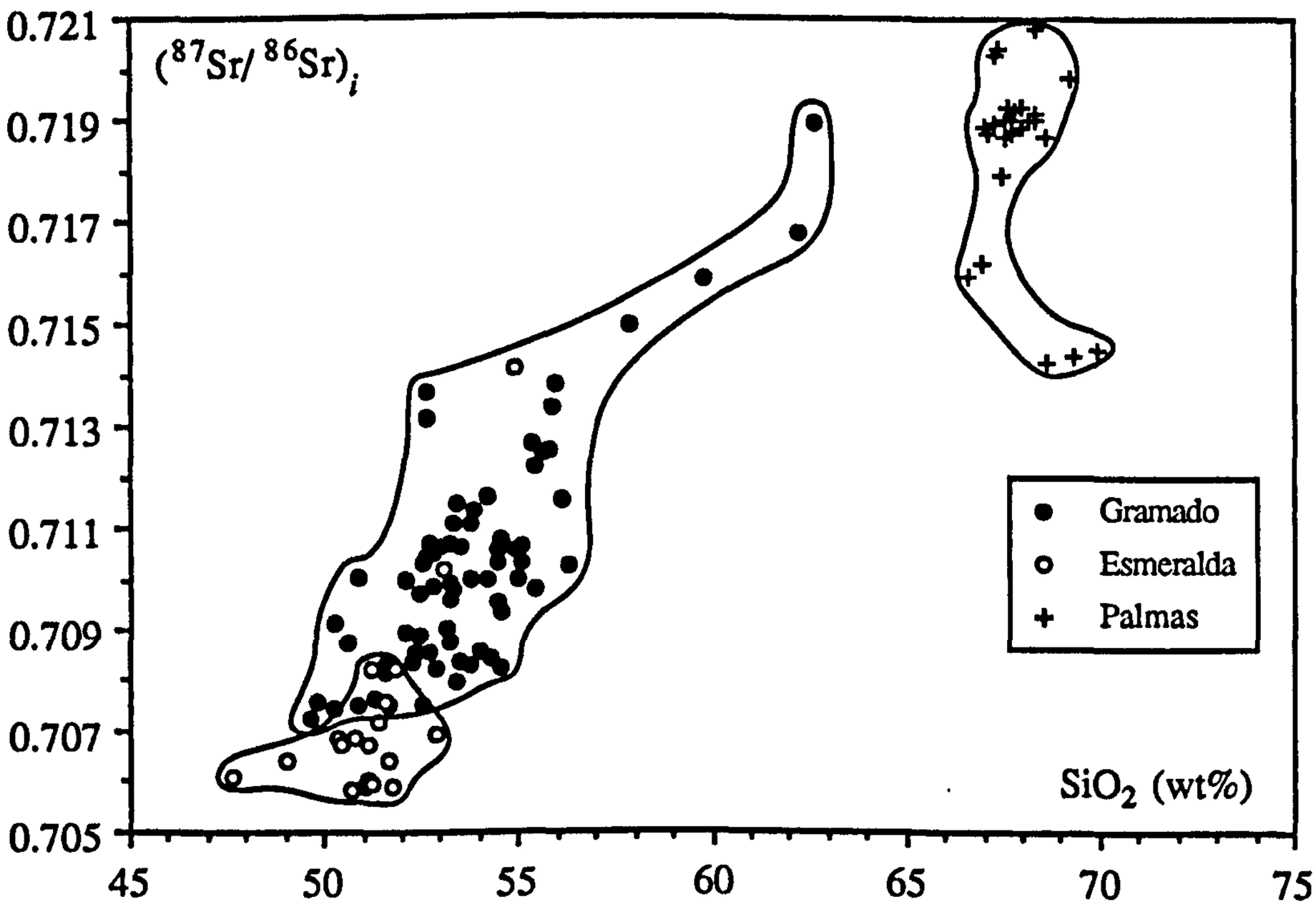

Figure 4.5 Variation of $(^{87}Sr/^{86}Sr)_i$ with SiO_2 for all low-Ti magma types from southern Paraná, {Esmeralda, n=20; Gramado, n=72; Palmas rhyolite, n=27}, showing a general positive corelation. Data sources - {this study, Mantovani *et al.*, 1985a; Fodor *et al.*, 1985b; Petrini *et al.*, 1987; Hawkesworth *et al.*, 1988}.

The Gramado-type magmas are characterised by striking increases in $(^{87}Sr/^{86}Sr)_i$ (Mantovani *et al.*, 1985a; Petrini *et al.*, 1987) and $\delta^{18}O$ (Fodor *et al.*, 1985b) with SiO_2, and such correlations have generally been attributed to crustal contamination. These trends cannot be achieved simply by mixing between a primitive Gramado magma and a Palmas-

type rhyolitic liquid since the Mg# vs. TiO_2 variations of figure 4.4 show TiO_2 increasing with decreasing Mg# within the Gramado magmas whereas the Palmas rhyolites lie at low Mg# and low TiO_2. The covariation of $(^{87}Sr/^{86}Sr)_i$ with SiO_2 for all southern Paraná low-Ti magmas is illustrated in figure 4.5, and similar results have been obtained on the Etendeka sequences by Erlank *et al.*, (1984). This emphasizes that crystal fractionation models cannot be discussed in isolation from the crustal contamination processes that were also operating on the magmas. It is necessary to assess the importance of assimilation in modifying the original magma composition, as well as to evaluate the possible contamination mechanisms, and the next section digresses slightly to consider, and review, our knowledge of contamination processes and modelling techniques.

4.3 Contamination processes.

A magma *en route* to the surface has the potential to interact with the surrounding wall rocks. The process of assimilation requires a considerable input of heat since the wall rock material must first be raised to its solidus temperature and then be provided with the latent heat necessary for melting. As Bowen (1928) pointed out, ascending magmas are unlikely to be superheated and the most plausible alternative heat source for assimilation is the latent heat released by simultaneous crystallisation. Hence crystallisation and assimilation must be considered together. The actual physical mechanism of assimilation is often not well constrained, and possibilities include bulk assimilation, incorporation of a crustal partial melt and contamination by a crustally derived fluid (*e.g.* Patchett, 1980). This latter process can lead to selective contamination of a few elements that are enriched in the fluid phase and has been invoked by Dickin (1981) among others to explain the isotopic characteristics of the Skye lavas. Experimental data by Watson (1982) has shown that selective contamination can also occur during dissolution of minerals into a basaltic magma if the assimilation does not go to completion, because the chemical diffusivities of certain elements, notably the alkalis such as K, are orders of magnitude greater than those for silica.

The geochemical consequences of assimilation accompanied by fractional crystallisation were first investigated by Taylor (1980), and numerical models to calculate the isotopic and trace element variations of the resultant magma were developed by DePaolo (1981). The process of simultaneous Assimilation and Fractional Crystallisation has become known as the AFC process, and generates trends where there is a positive correlation between the degree of magmatic evolution and the extent of assimilation such that the more evolved rocks are the more contaminated. AFC is likely to be characteristic of the magma chamber environment where magmas have a certain residence time and are able to undergo fractional crystallisation before eruption.

An alternative scenario involves assimilation of wall rock during ascent through a dyke. Both Campbell (1985) and Huppert and Sparks (1985) have considered this possibility from fluid dynamic and thermal viewpoints, and concluded that whether or not assimilation occurs will largely depend on the nature of the flow regime within the dyke. If the flow is laminar, a chilled margin rapidly develops on the walls of the dyke thus sealing the magma from further assimilation. By contrast, during turbulent flow conditions, mixing maintains a uniform temperature within the magma and the heat transfer to the surroundings is much greater than for laminar flow where heat is lost entirely by conduction. Hence turbulent flow will cause thermal erosion of the dyke wall rocks and result in contamination of the magmas. Turbulent flow is indicated by a high Reynolds number ($Re > 2000$) and dyke width is a key factor in controlling Re. The ascent rate, which is related to dyke width, has an important influence on whether the flow regime is laminar or turbulent. The situation envisaged by Huppert and Sparks (1985) had a deep crustal magma chamber (à la Cox, 1980) where basaltic magmas fractionated to varying degrees before being periodically tapped through fissures. The more primitive magmas would be hotter, because of their higher liquidus temperatures, and therefore more able to assimilate crustal material during ascent. The geological and geochemical consequences touched on by Huppert and Sparks (1985) of this temperature-controlled assimilation process were pursued further by Devey and Cox (1987). Strictly speaking, this process can be described as assimilation accompanied by crystallisation but without loss of crystals, in contrast to the AFC situation

where the emphasis is on crystal fractionation, and Devey and Cox (1987) proposed the term AEC (Assimilation and Equilibrium Crystallisation). The most important point is that geochemical trends will be opposite to those expected for the fractionation dominated AFC process since AEC produces a negative correlation between parameters that reflect contamination {*e.g.* $(^{87}Sr/^{86}Sr)_i$} and those that reflect the extent of fractionation {*e.g.* Mg#}.

Hence the geochemical trends imposed by contamination on the composition of a suite of magmas are largely a function of where the assimilation took place; whether during ascent through a conduit or during residence in a magma chamber. Examples of both styles of contamination have now been recognised in CFB provinces; (i) AFC - assimilation and fractional crystallisation - in Paraná (Mantovani *et al.*, 1985a), Etendeka (Erlank *et al.*, 1984), and Columbia River (Carlson *et al.*, 1981), (ii) AEC or temperature-controlled assimilation - in Skye (Thirlwall and Jones, 1983) and Deccan (Devey and Cox, 1987). Many factors can influence the contamination style, and the extent to which it proceeds, and they include; temperature and composition of magma, flow regime and ascent rate through crust, site of crystallisation, local P,T conditions, fusion temperature of wall rock, and contaminant availability. How these parameters interact to allow a specific contamination style to dominate within a particular CFB province is still the subject of some conjecture (see discussion in Devey and Cox, 1987). There is no reason for AFC or AEC to operate exclusively. The effects of one contamination style could be superimposed on the other, reflecting the changing conditions during the development of a magmatic suite, such that there are no significant correlations between an index of contamination and degree of magmatic evolution, despite the fact that contamination has occurred.

4.4 Review of previous AFC modelling of the Southern Paraná low-Ti magmas.

The SiO_2 - Mg# relationship illustrated in figure 4.3, as well as the positive correlation of SiO_2 with $(^{87}Sr/^{86}Sr)_i$ shown in figure 4.5, emphasise that it is the AFC style

of contamination that seems to predominate within the low-Ti Paraná lavas, in that the more evolved magmas are also the more contaminated. This has generally been the conclusion reached by other workers (*e.g.* Mantovani *et al.*, 1985a; Fodor *et al.*, 1985b; Petrini *et al.*, 1987). It is important to realise that in the literature, the Gramado and Esmeralda magma types have been considered together as a single low-Ti magma type. This may partly explain the discrepancies between the published AFC models especially as regards conclusions for the isotopic and trace element composition of the parental magma. One of the purposes of this chapter will be to convince the reader that, despite first appearances, the Esmeralda magma type does not represent uncontaminated or less contaminated magmas of the Gramado-type, but instead reflects an additional component.

There seems to be agreement among the various groups working in the Paraná province that crustal contamination has played a major role in the evolution of the low-Ti magmas of southern Paraná but there is still a healthy debate as to the nature of the contaminant and the composition of the uncontaminated parental magma. Being able to assess the composition of the initial uncontaminated magma by stripping off the effects of contamination is important in that it allows comparisons to be made with the uncontaminated high-Ti rocks and thus can result in a better understanding of the ultimate origin of the fundamental high-Ti / low-Ti variation within the Paraná lavas.

All published models have assumed that the contamination process was AFC and it is worth briefly reviewing the modelling technique employed as well as their conclusions. The AFC numerical modelling as developed by DePaolo (1981) describes the compositional evolution of an assimilating magma in terms of five parameters;

(i) composition of assimilated material; C_a for elements, ε_a for isotope ratios.

(ii) composition of initial magma; C_o for elements, ε_o for isotope ratios.

(iii) F - mass of magma as a fraction of the original magma mass.

(iv) D - bulk crystal/liquid distribution coefficient of the fractionating crystal extract.

(v) r - ratio of the rate of assimilation to the rate of fractional crystallisation.

Gramado and Esmeralda (low-Ti) magma types

To carry out forward modelling on a suite of magmas, the values of these parameters must be manipulated so as to explain the data trends on the chosen element-isotope or isotope-isotope diagrams. Certain constraints can be put on the choice of values used for these parameters. Minimum estimates for F can be obtained via a least squares analysis of the major element data assuming closed system fractional crystallisation, and a realistic range of values for D for each element can be constrained using reasonable K_D values and the phase assemblage of the calculated crystal extract. Similarly, on thermal grounds it is likely that 'r' is less than 1. The major assumptions necessary therefore are the respective compositions of the uncontaminated parental magma and the contaminant and, as mentioned above, this is where the major disagreements lie. Unlike trends generated by simple mixing, AFC trends do not necessarily point towards the end-member (*i.e.* contaminant) composition, and this emphasizes the problems encountered in trying to characterise the contaminant involved.

The strong increase of SiO_2, K_2O, and Rb accompanying the increase in $(^{87}Sr/^{86}Sr)_i$ is suggestive of a 'granitic' contaminant, and most workers have looked to the Brasiliano-age granites that are presently exposed along the southern Brazilian coastline as possible indicators of the composition of this crustal contaminant. Calculations in Piccirillo *et al.*, (1988a) based on an average composition of basement granites (SiO_2 72.4 wt%, K_2O 4.3 wt%, Rb 127 ppm) implied that the amount of contamination might have been about 7% to 15%. Most studies have attempted to just explain the Sr isotopic data, coupled with a few selected trace elements, and the values of $(^{87}Sr/^{86}Sr)_i$ and Sr used for the contaminant have been; Mantovani *et al.*, (1985a) 0.725 and 200 ppm, Fodor *et al.*, (1985b) 0.735 and 100-330 ppm, Petrini *et al.*, (1987) 0.737 and 250 ppm. The study by Mantovani *et al.*, (1985a) assumed that the initial magma had $(^{87}Sr/^{86}Sr)_i$ of 0.707 and 200-400 ppm Sr and, together with $D_{Sr} \sim 1.0$-1.7 and $r \sim 0.4$, these values fitted the data considered. They considered that assimilation was negligible for the rocks with < 52 wt% SiO_2 and that the relatively high $(^{87}Sr/^{86}Sr)_i$ of 0.707-0.709 of the parental magmas must have been a feature of an enriched and heterogeneous mantle source. Petrini *et al.*, (1987)

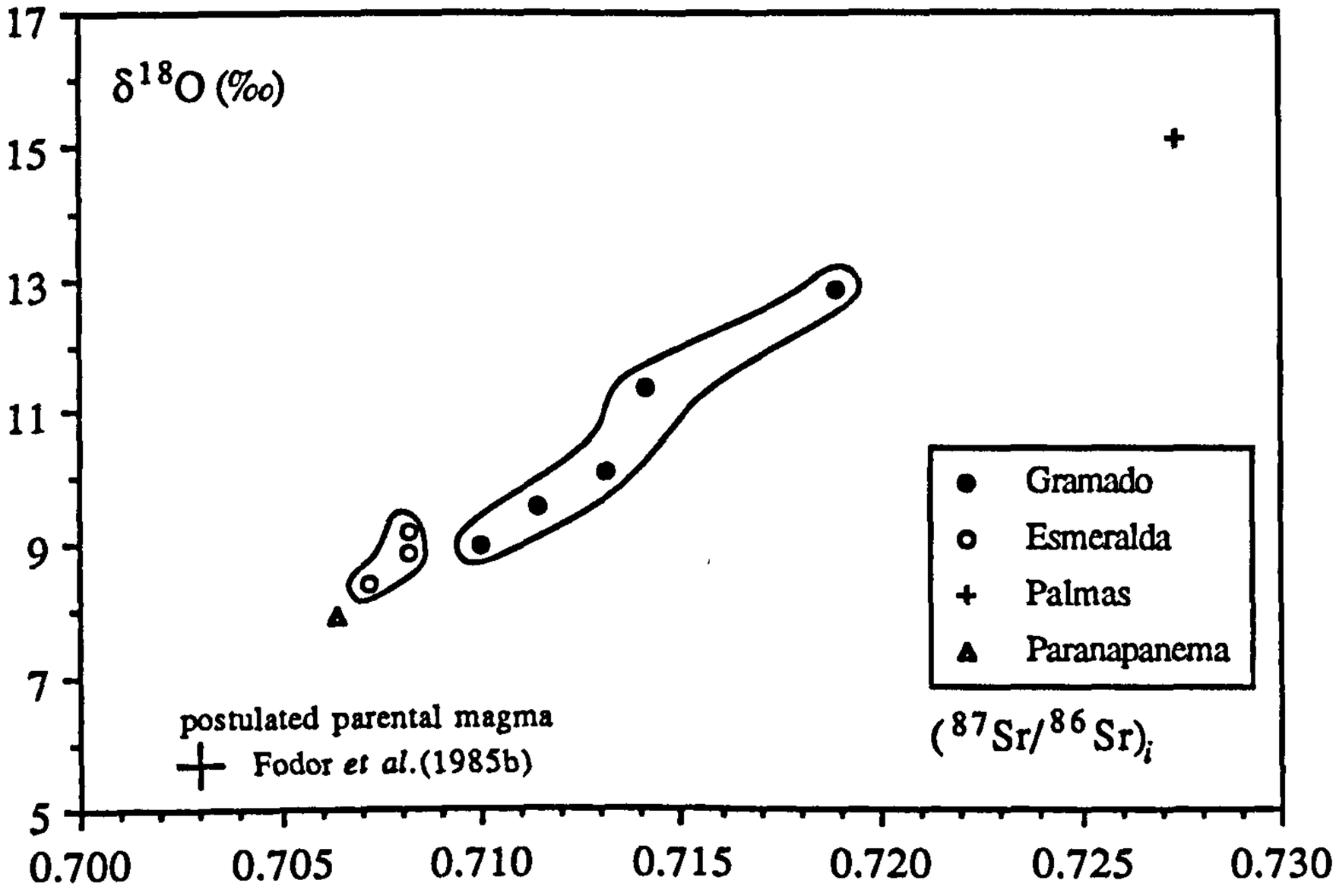

Figure 4.6 Positive correlation between whole rock $\delta^{18}O$ and $(^{87}Sr/^{86}Sr)_i$ for southern Paraná magma types (data form Fodor *et al.*, 1985b).

modelled low-Ti sequences from central Paraná using a parental magma that had $(^{87}Sr/^{86}Sr)_i$ of 0.7046 and 150-200 ppm Sr since such magmas actually existed there, and they suggested that the uncontaminated magmas parental to the southern Paraná lavas might have had similar characteristics. The study by Fodor *et al.*, (1985b) was the first to consider a combined $\delta^{18}O$ - $^{87}Sr/^{86}Sr$ approach, in the manner of Taylor (1980). The good correlation between $\delta^{18}O$ and $(^{87}Sr/^{86}Sr)_i$ is illustrated in figure 4.6 although it is important to note that the modelled data set not only included samples of the Esmeralda, Gramado and Palmas magma types but also a Paranapanema sample which had high Sr (327 ppm) and low $(^{87}Sr/^{86}Sr)_i$ (0.70637). This meant that Fodor *et al.*, (1985b) were obliged to use the more extreme values of 500 ppm Sr and an $(^{87}Sr/^{86}Sr)_i$ of 0.703 for the parental magma. $\delta^{18}O$ for the parental magma was taken to be similar to the typical mantle value of +5.7 ‰, and it was assumed that the crustal contaminant had $\delta^{18}O$ of +15 to +17 ‰.

The above examples illustrate that a choice of plausible parental magma and assimilant compositions can all yield viable AFC models, and it is obvious that the conventional methods of modelling, which attempt to reproduce the observed compositions

essentially by trial and error, produce non-unique solutions. There are problems in handling a large number of variables (*i.e.* elemental and / or isotopic compositions) when using these techniques, and most models are formulated to explain the variations seen on just a restricted number of bivariate element / isotope diagrams. Since there are a large set of solutions for the values of the AFC parameters that can reproduce the observed data trend on any particular variation diagram, a chosen solution might not necessarily explain the data on a different diagram.

An alternative approach is to employ an inverse method that uses the geochemical variations within the data set itself to constrain the initial conditions of the petrogenetic process. Mantovani and Hawkesworth (1988) have developed a computer-based inversion program that allows a large number of trace elements and isotope ratios to be considered simultaneously. Their program calculates the best-fit surface through a multi-dimensional set of data and then provides a range of solutions for the AFC parameters that are consistent with this best fit surface. Preliminary results obtained by this method were presented in Mantovani and Hawkesworth (1988) who used a suite of samples from the MV road section in Rio Grande do Sul state, Brazil (see figure 2.15). They demonstrated that the data were consistent with a crustal contaminant which had the trace element characteristics of an upper crustal melt (syn-collision granite of Pearce *et al.*, 1984) with $(^{87}Sr/^{86}Sr)_i$ of 0.746, as opposed to bulk assimilation of average crust. For elements with a low D value it was found that any changes in D had little corresponding effect on C_a so that the ratios of highly incompatible elements in the contaminant were well constrained by this method. Mantovani and Hawkesworth (1988) added a note of caution to the effect that, as with any non-linear fitting program, different initial conditions could lead to different solutions, each internally consistent with the wide range of trace elements and isotopes considered. Since the selection of input parameters remains critical even using this method, one still has to look to external geological constraints as a means of arriving at a preferred set of initial conditions.

4.5 The role of the Palmas rhyolites.

A common feature to all the studies reviewed above is the inclusion of the rhyolites (Palmas-type) in the modelled sequences Implicit in this is the assumption that the Gramado and Palmas magma types have a common origin, with the transition from basalt to rhyolite dominated by fractional crystallisation coupled with crustal assimilation. Since the Palmas rhyolites have elevated $(^{87}Sr/^{86}Sr)_i$, this necessitates a correspondingly higher $(^{87}Sr/^{86}Sr)_i$ (> 0.730) for the contaminant.

The low-Ti rocks of southern Paraná are characterised by a marked bimodality in terms of SiO_2 (see figure 4.7) and $(^{87}Sr/^{86}Sr)_i$, which was a contributory factor in distinguishing the basaltic and rhyolitic flows as separate magma types in chapter two. This strongly bimodal SiO_2 distribution is difficult to reconcile with the operation of a semi-

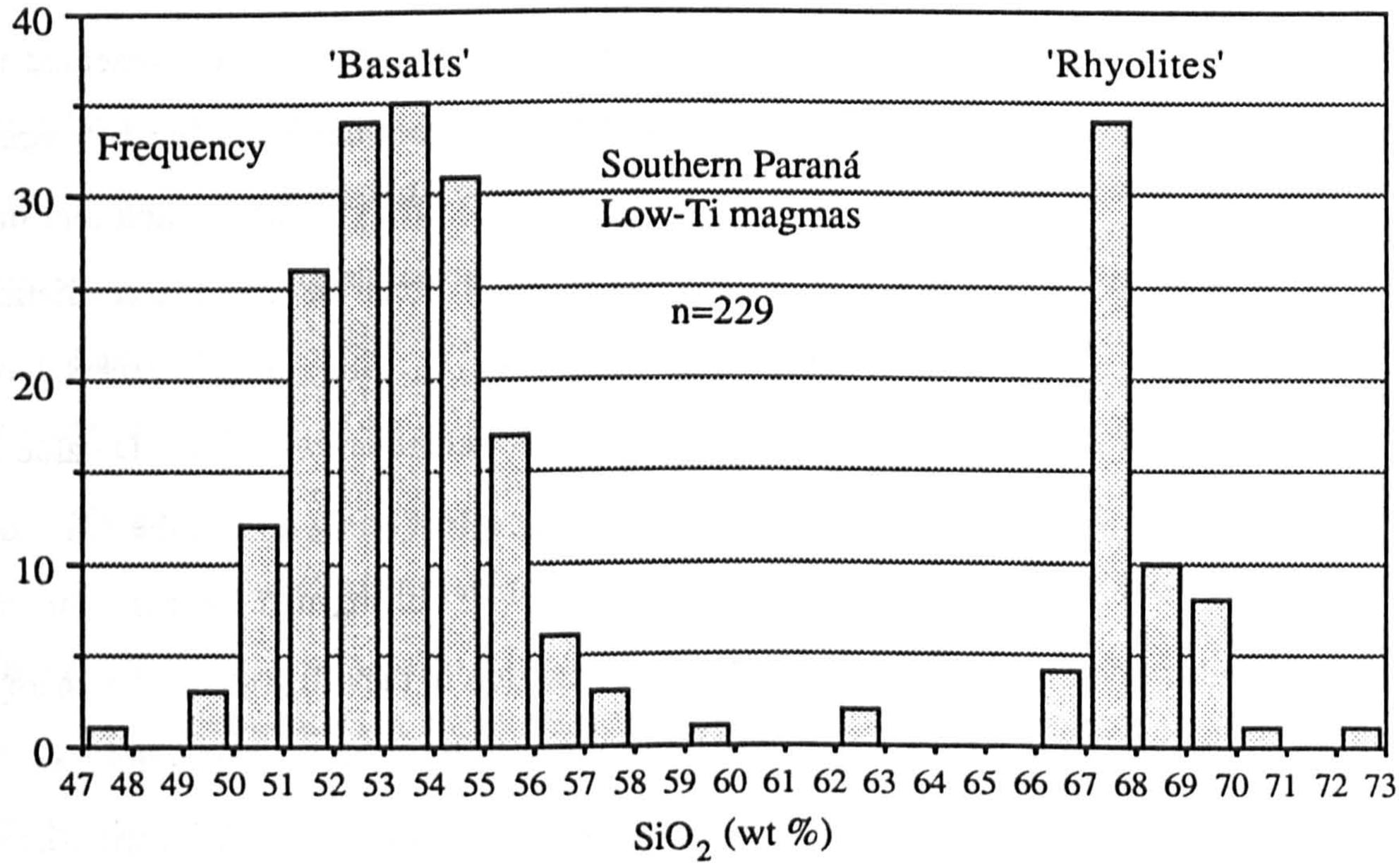

Figure 4.7 SiO_2 frequency diagram of low-Ti magmas (n=229) of southern Paraná {Esmeralda, Gramado, Palmas magma types} illustrating the strongly bimodal nature of the Paraná magmatic suite. Data sources - {this study; Bellieni *et al.*, 1984c; Mantovani *et al.*, 1985a; Fodor *et al.*, 1985a; Petrini *et al.*, 1987; Hawkesworth *et al.*, 1988}.

continuous AFC process. Unless there is some as yet unknown mechanism that can suppress the eruption of magmas of more intermediate andesitic composition, a more plausible model is that the Palmas rhyolites are crustal melts and thus independent of the Gramado-type basalts. A similar situation has been outlined for the high-Ti Paraná rocks in chapter three (Urubici/Pitanga basalts, Chapecó rhyolites), and bimodal basalt-rhyolite associations are also a feature of the Deccan (Lightfoot *et al.*, 1987) and the Karoo (Betton and Cox, 1979; Cleverly *et al.*, 1984) CFB provinces. In these areas, the majority of the rhyolites have similar isotopic ratios to the basalts and are therefore thought to have been derived by partial melting of the intrusive equivalents of the basalts. This is not the case for the Palmas rhyolites since they have different Sr and Pb isotopic ratios to the associated Gramado-type basalts, and it has been suggested that these Palmas rhyolites result from crustal anatexis (Cordani *et al.*, 1980; Hawkesworth *et al.*, 1988).

Thus the origin of the Palmas rhyolites can have a role to play in placing geological constraints on modelling AFC processes. If the rhyolites are produced by crustal anatexis as opposed to being the extreme products of an AFC process then they should not be included in any AFC modelling. This has consequences for the contaminant composition in that it is now constrained by the composition of the most evolved basalt rather than by the rhyolites. For example, $(^{87}Sr/^{86}Sr)_i$ in the contaminant must now only be greater than about 0.715 whereas previously the inclusion of the rhyolites meant that this needed to be in excess of 0.730.

Hawkesworth *et al.*, (1988) appealed to the good correlations between isotopes and elements that are sensitive to crustal contamination {*e.g.* Rb, SiO_2, $(^{87}Sr/^{86}Sr)_i$} found between the Gramado and Palmas magma types to suggest that the Palmas rhyolites might be compositionally similar to the crustal end-member that was involved in the open system evolution of the Gramado basalts. Hawkesworth *et al.*, (1988) used the inversion technique again but in the reverse sense to that outlined above in that they pre-defined the isotope and trace element abundances in the crustal end-member and then used the inversion program, with data from two southern Paraná road sections MV and MG (see figure 2.15), to estimate the composition of the parental magma. Two separate cases were investigated, first

using an average syn-collision granite as the contaminant, which is probably fairly representative of small degree partial melts of continental crust, and then using average Palmas rhyolite. If the problem of the SiO_2 gap (figure 4.7) was ignored, then taking a contaminant akin to a syn-collision granite (Pearce *et al.*, 1984) and with a high $(^{87}Sr/^{86}Sr)_i$ of 0.746 (see Mantovani and Hawkesworth, 1988), the program forced an AFC solution through the data to achieve a parental magma with a low $(^{87}Sr/^{86}Sr)_i$ of 0.704 (*c.f.* ~0.7046, Petrini *et al.*, 1987). For the other case, if it was assumed that the Palmas rhyolites afforded a best estimate as to the composition of the contaminant, with an average $(^{87}Sr/^{86}Sr)_i$ of 0.7195, then a much higher value of $(^{87}Sr/^{86}Sr)_i$ of 0.7086 was calculated for the parental magma. Significantly the trace element pattern of the calculated parental magmas in each case were broadly similar although at different absolute abundances.

The Palmas rhyolites have not received much attention as regards their geochemical variability either locally or on a more regional scale, and the nature of the petrogenetic processes responsible are still poorly understood. Bellieni *et al.*, (1986b) gave a range in SiO_2 from 65 to 72 wt% for the Palmas rhyolites, and several elements show a strong covariation with SiO_2 content. As SiO_2 increases, both K_2O and Rb follow suit, rising from 3.5 to 5.0 wt% and from 150 to 220 ppm respectively. TiO_2, FeO(t), P_2O_5 and Sr all exhibit marked negative correlations with SiO_2 with, for example, TiO_2 falling from 1.1 to 0.6 wt% and Sr from 150 to 80 ppm. Elements such as Zr and LREE show only a slight enrichment. Most of this variation is probably the result of fractional crystallisation: the TiO_2 and FeO(t) depletion suggests fractionation of Fe-Ti oxides, and the declining Sr contents could be the result of a large plagioclase component in the crystal extract. The possibility that variable degrees of partial melting might contribute to the geochemical variability of the rhyolites should also be considered. The only published model for within-suite fractional crystallisation of the Palmas rhyolites is given in Piccirillo *et al.*, (1988a) who explain the variation from 67 to 69 wt% SiO_2 by about 9 % fractionation of a clinopyroxene+plagioclase+ magnetite crystal extract in the proportions 17/70/13, though the decrease in P_2O_5 would imply a certain amount of apatite crystallisation as well. Unfortunately the situation within the Palmas rhyolites is not this straightforward.

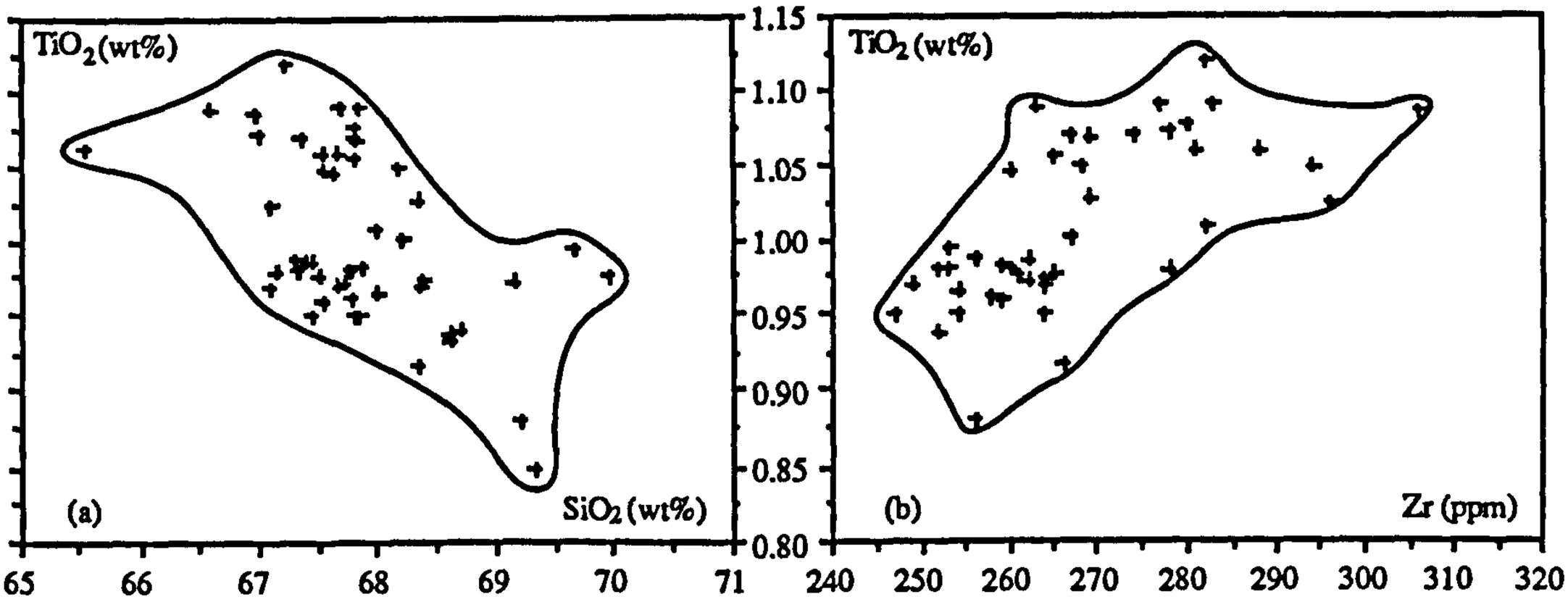

Figure 4.8 Variation of TiO_2 with; (a) SiO_2, (b) Zr, for the Palmas rhyolites of the coastal margin of the southern Paraná region.

Considering data from this study (ES borehole, and GB and RA road sections) and road section analyses from Mantovani *et al.*, (1985a) (RA) and Hawkesworth *et al.*, (1988) (MV and MG) restricts the sample coverage to the eastern half of the southern Paraná region. These samples all have relatively low SiO_2 (< 70 wt%), and TiO_2 decreases from 1.1 to 0.8 wt% as SiO_2 increases from 65 to 70 wt% {see figure 4.8(a)}. In contrast to the average trends for the whole province illustrated by Bellieni *et al.*, (1986b), Zr displays a sympathetic behaviour with TiO_2 {figure 4.8(b)}, also decreasing from 300-245 ppm, which suggests that zircon might have been involved along with magnetite in the fractionating mineral assemblage. N.B. A similar control on the rhyolite composition could have been achieved if magnetite and zircon were residual phases during melting. The presence of minor phases such as zircon can cause elements which are usually regarded as incompatible to become compatible and this could lead to large changes in otherwise invariant trace element ratios. This is illustrated, using the limited INAA data available, in figure 4.9 which shows the negative correlation of Hf and Ta, with Hf behaving compatibly, and this results in a wide range in Hf/Ta of 3.0-5.5.

The compositional variability shown by the Palmas rhyolites has important implications when choosing a rhyolite composition as an estimate of the crustal contaminant that affected the Gramado-type basalts. An average Palmas composition will not necessarily

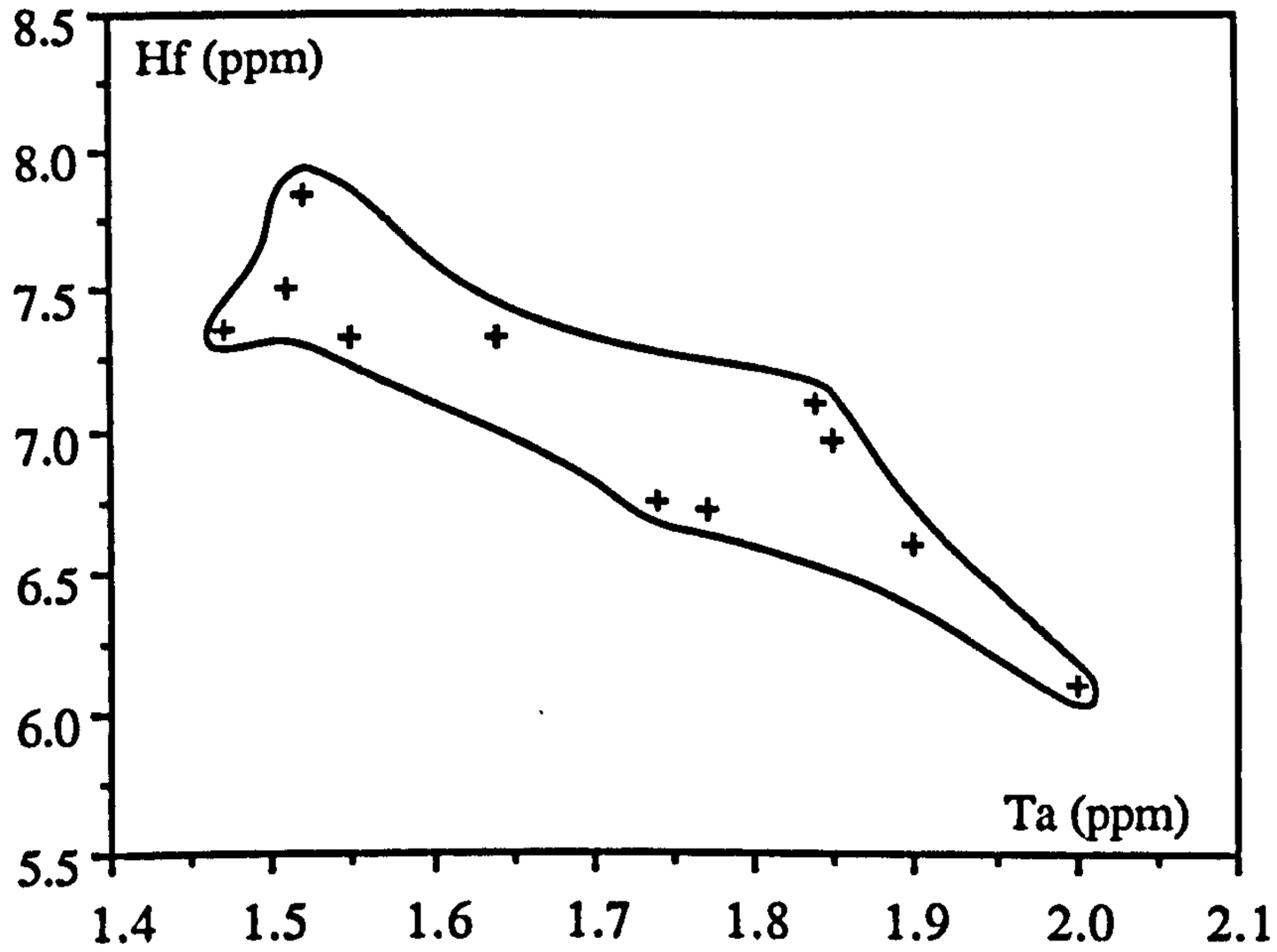

Figure 4.9 Negative correlation of Hf with Ta for the Palmas rhyolites, with Hf behaving compatibly, suggesting control by zircon, either as a minor phase during crystallisation or as a residual phase during partial melting.

represent this contaminant since it would be more evolved than the primary crustal melt. For example, the contaminant used by Mantovani and Hawkesworth (in press) had Hf/Ta of 4.2, whereas the low SiO_2, high TiO_2 rhyolites have Hf/Ta of about 5.5. Crystal fractionation cannot cause any variation of $(^{87}Sr/^{86}Sr)_i$ and yet the $(^{87}Sr/^{86}Sr)_i$ data illustrated in Bellieni *et al.*, (1986b) fall into three groups; (i) 0.714-0.715 (minor), (ii) 0.719-0.721, (iii) 0.725-0.728. There appears to be some regional bias to these groups, with all samples having $(^{87}Sr/^{86}Sr)_i > 0.725$ (and correspondingly high Rb/Sr) located in the south-west of Rio Grande do Sul state near Santa Maria (see Fodor *et al.*, 1985b; Cordani *et al.*, 1988). The group with $(^{87}Sr/^{86}Sr)_i$ of 0.719-0.721 seems to be by far the most dominant, although this might be a reflection of the sample coverage, and they are concentrated along the coastal Serra Geral escarpment. This might arise from regional differences in the crustal source material. Alternatively, Bellieni *et al.*, (1986b) suggested an origin involving melting of basic source material, either lower crustal mafic granulites or the intrusive equivalents of the Gramado-type basalts, followed by crustal interaction during ascent. In this case though, the amount of contamination needed would have to have been considerable in order to raise $(^{87}Sr/^{86}Sr)_i$ up to the value seen in the Palmas rhyolites

of about 0.720, since the invoked source material, granulites with low Rb/Sr or Gramado-type magmas perhaps with $(^{87}Sr/^{86}Sr)_i$ of 0.707, would not be expected to have $(^{87}Sr/^{86}Sr)_i$ close to that observed in the rhyolites.

Fodor *et al.*, (1985b) suggested that once rhyolitic magmas were formed then direct mixing with basaltic magma could be a possibility. Hence the intermediate andesitic compositions could be produced via magma mixing rather than from an AFC process, and this is partly supported by the observation of Piccirillo *et al.*, (1988b) that the intermediate lavas tend to be associated with the rhyolites towards the upper halves of the lava pile.

4.6 New constraints on crustal interaction affecting low-Ti magmas of southern Paraná.

4.6.1 The approach of this study.

From these reviews of the published literature, it is clear that although the role of contamination is not in doubt, there is no consensus as to the nature of the contaminant, whether it is represented by the basement granites or by a Palmas rhyolite composition, and consequently the characteristics of the parental magma are also poorly constrained. The choices for the parental magma seem to be between one with $(^{87}Sr/^{86}Sr)_i$ of 0.704-0.705 and 0.707-0.709. What new light can this study shed on the problems of unravelling the effects of contamination, especially in answering the latter point regarding the parental magma ? This will be addressed in two ways. Firstly, the relationship between the two southern Paraná low-Ti basaltic magma types, Esmeralda and Gramado, will be explored to see whether they can be related to a single parental magma solely by differences in the amount of crustal contamination. Secondly, the regional aspects to this contamination saga will be investigated by comparing data from two well studied areas; the São Joaquim area (this study) and the MV/MG road sections near Caxias do Sul (Hawkesworth *et al.*, 1988) which lie about 200 km to the south-west.

4.6.2 Esmeralda vs. Gramado: different degrees of contamination ?

The Gramado and Esmeralda magma types were distinguished in chapter two primarily on their major and trace element compositions. This section will attempt to evaluate what petrogenetic process(es) gave rise to this distinction. The development of the compositional trend within the Esmeralda magma type itself will be considered in the final section. When discussing the origin of the compositional difference between these two magma types it is important to bear in mind that chapter two also established that the switch in magma type from Gramado to Esmeralda was a stratigraphical feature and hence a temporal change in magmatism.

The difference between the two magma types is also reflected in their Sr and Nd isotopic compositions, and this is illustrated in figure 4.10. The Esmeralda samples have low $(^{87}Sr/^{86}Sr)_i$ and high $(^{143}Nd/^{144}Nd)_i$ relative to the Gramado-type magmas and are displaced towards the so-called 'depleted quadrant' on figure 4.10. The Sr and Nd isotopic composition of the 'uncontaminated' Gramado-type parental magma, as proposed by Petrini *et al.*, (1987), is also shown. This is similar to the Esmeralda samples but lies at a more depleted isotopic composition. Faced with such a data set, it is very tempting to explain all the Esmeralda and Gramado magma type variation seen, in terms of a single curve through the data. A possible, although by no means unique, AFC solution has been superimposed on the data in figure 4.10 to illustrate this point. To calculate this model curve, the initial magma was taken to be the most primitive Esmeralda-type magma and the contaminant was represented by the average Palmas rhyolite composition. D_{Sr} and D_{Nd} were inferred assuming reasonable K_D's and plausible crystal extracts, though D_{Sr} had to be less than 1 to account for the increase in Sr content from the Esmeralda to Gramado magma types; 'r' was arbitrarily set at 0.5.

If it is assumed that the composition of both the initial magma and the contaminant remained constant during the eruption of the whole lava sequence, then the stratigraphical

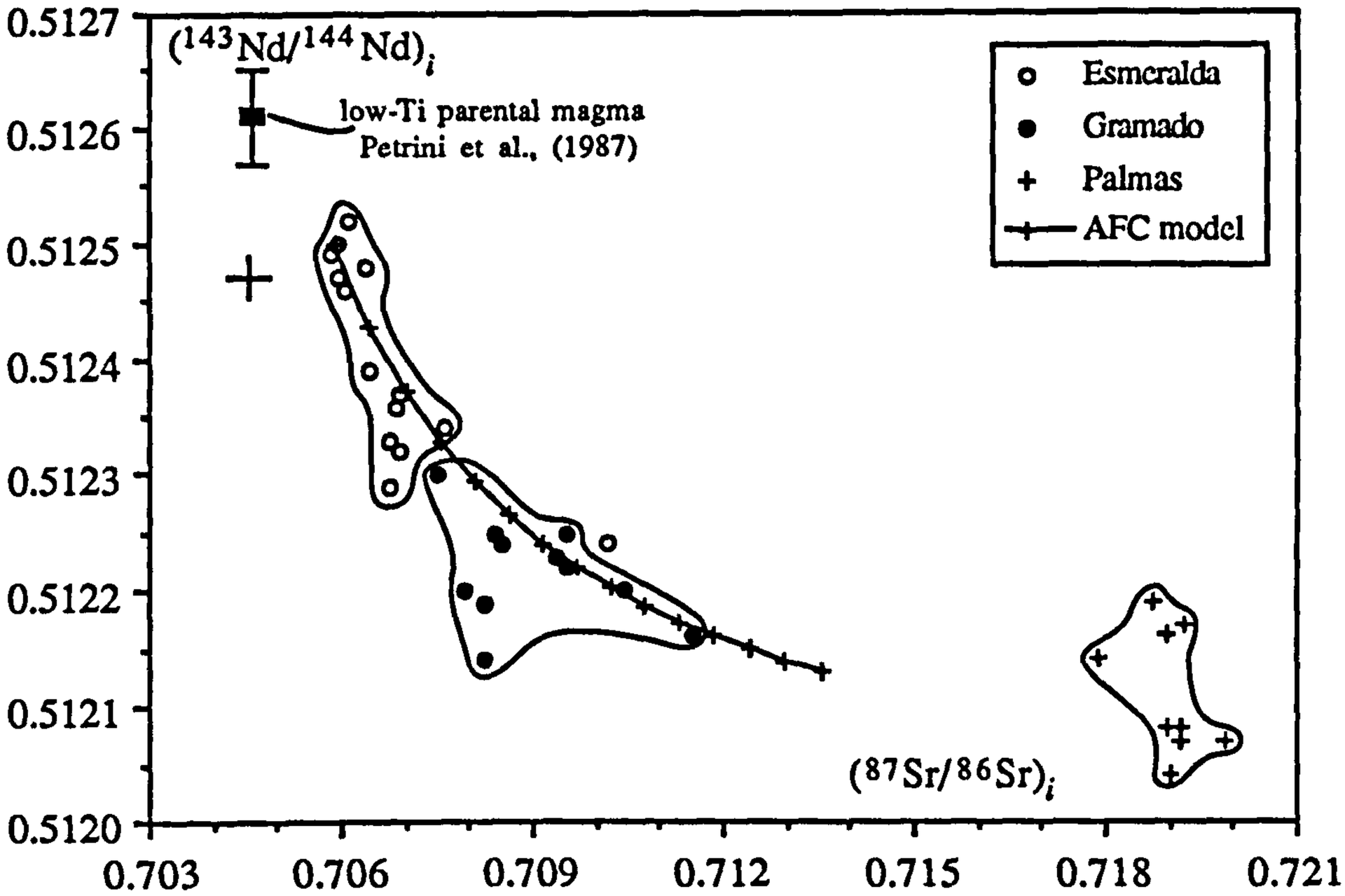

Figure 4.10 Variation in Sr and Nd isotopic composition for the southern Paraná low-Ti magma types. One possible explanation for the relationship between the Gramado and Esmeralda magma types is variable amounts of crustal contamination, and the superimposed curve represents a possible AFC solution. The cross represents bulk earth at 130 Ma {0.70454, 0.51247}. Low-Ti parental magma from Petrini *et al.*, (1987) has {0.7046, 0.51261 (0.51258-64 assuming Sm/Nd of 0.28-0.32)}. Data sources - {Esmeralda, Gramado - this study: Palmas - Mantovani *et al.*, 1985a; Hawkesworth *et al.*, 1988}.
Parameters for AFC model curve;
(a) assimilant composition - Palmas rhyolite (Mantovani and Hawkesworth, in press) {Sr 142 ppm, Nd 44 ppm, $(^{87}Sr/^{86}Sr)_i$ 0.7195, $(^{143}Nd/^{144}Nd)_i$ 0.51206}.
(b) initial magma - primitive Esmeralda 'sill' composition {Sr 170 ppm, Nd 13.5 ppm, $(^{87}Sr/^{86}Sr)_i$ 0.7059, $(^{143}Nd/^{144}Nd)_i$ 0.51250}.
(c) $D_{Sr} = 0.8$, $D_{Nd} = 0.2$, $r = 0.5$.
Tick marks on curve represent F values from 1.0 to 0.3, in intervals of 0.05.

transition from Gramado-type to Esmeralda-type magmas could have been achieved in two possible ways; either (i) more primitive magmas were erupted during the later stages of magmatism, shifting the position of samples along the modelled curve to higher F values, or (ii) there was a decrease in the amount of contamination. *i.e.* a decrease in 'r'. Since there is no significant difference in the average degree of magmatic evolution between the Gramado and Esmeralda magma types (see figures 4.1 to 4.4), the latter possibility would appear more likely, *i.e.* that there was a decrease in the extent of contamination of the low-Ti magmas with time. The low-Ti basalts of southern Paraná do not produce a continuum of compositions. Instead, the Gramado and Esmeralda magma types form distinct groups,

which can be seen from many of the subsequent figures of this chapter (*e.g.* figure 4.12, La/Hf vs. Sm/Nd), and this is why they were recognised as separate magma types in chapter two. This indicates that there must have been a sudden change in conditions rather than a gradual waning in the degree of crustal assimilation.

The scenario outlined above, that the Gramado and Esmeralda magma types can be explained in terms of an AFC-style contamination process from a single parental magma, was postulated solely on the basis of Sr and Nd isotope variations. This must be checked to

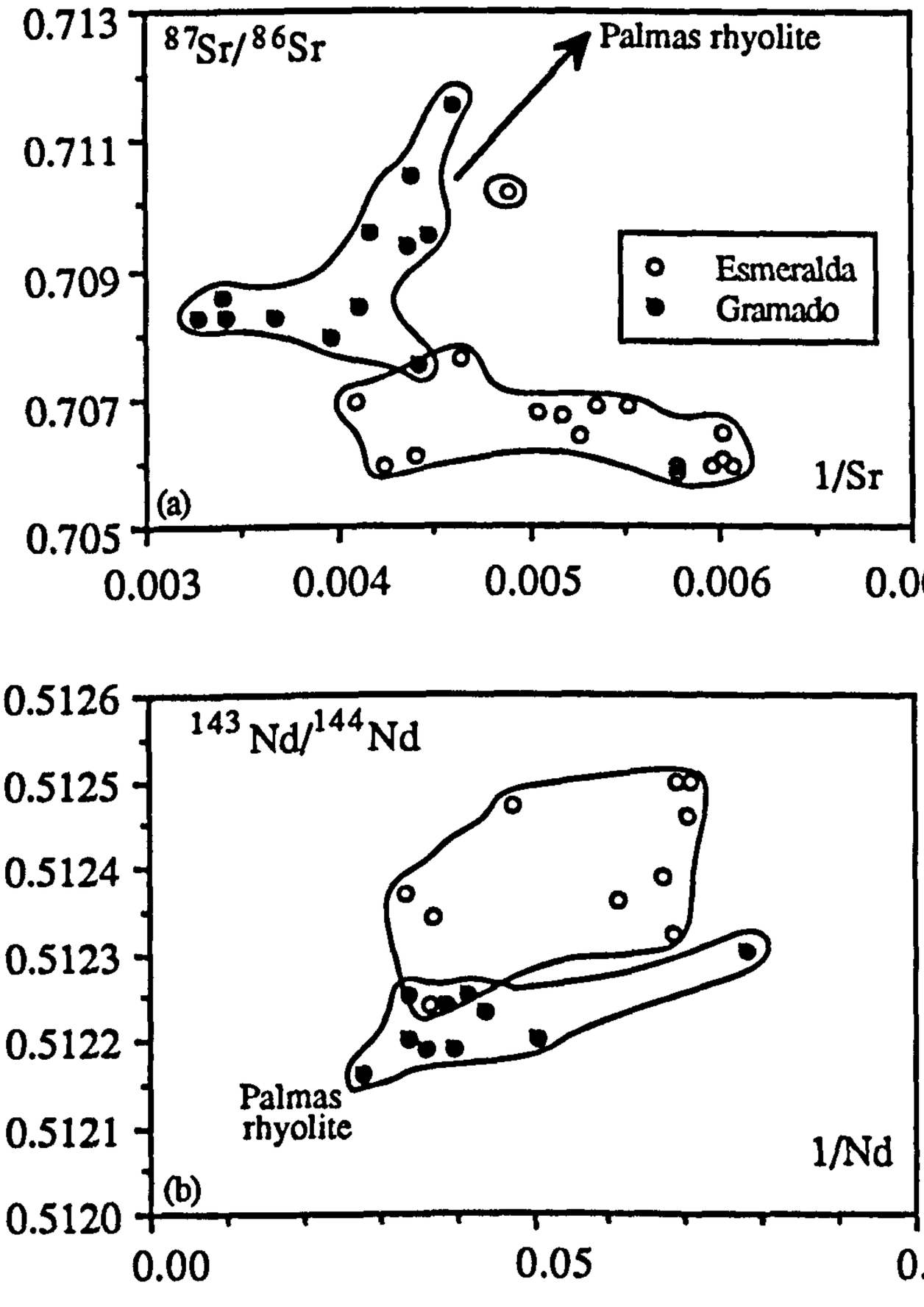

Figure 4.11 (a) 1/Sr vs $(^{87}Sr/^{86}Sr)_i$ for the Gramado and Esmeralda magma types, illustrating the contrasting trends within the Gramado-type samples to both low and high Sr contents with increasing $(^{87}Sr/^{86}Sr)_i$, (b) 1/Nd vs. $(^{143}Nd/^{144}Nd)_i$ shows the similar range in Nd content for the Gramado and Esmeralda magma types at different Nd isotopic composition, and argues against a simple AFC relationship.

see if it is consistent with all the major and trace element data, and unfortunately this is where this simple picture breaks down. This is illustrated in the two diagrams of figure 4.11; (a) 1/Sr vs. $(^{87}Sr/^{86}Sr)_i$, (b) 1/Nd vs. $(^{143}Nd/^{144}Nd)_i$, which both argue against the simple AFC model. There is a difference in the number of samples plotted on these two diagrams because more samples were analysed for $(^{87}Sr/^{86}Sr)_i$. These diagrams link the isotopic compositions of figure 4.10 to their respective elemental abundances, which have been plotted as the reciprocal since the form of such plots is linear for simple mixing and curved, but coherent, for AFC. On figure 4.11(a), the Gramado data shows two distinct trends. One trend has 1/Sr decreasing as $(^{87}Sr/^{86}Sr)_i$ increases, similar to the generally coherent trend within the Esmeralda magmas, and this implies that $D_{Sr} < 1$ (as assumed for the curve on figure 4.10). The other trend shows a marked change in the behaviour of Sr and is more suggestive of direct mixing towards the Palmas rhyolites. On figure 4.11(b), both magma types have a similar range in Nd content but a different isotopic signature. This produces two essentially parallel trends and rules out the possibility of a single AFC solution.

A further problem is the wide range shown in many incompatible trace element ratios which is a characteristic feature of the Esmeralda magma type. These ratios have a noticeably more restricted range within the Gramado magma type and are often similar, or just slightly displaced from, the values shown by the Palmas rhyolites. This is illustrated in figure 4.12 using La/Hf and Sm/Nd. For incompatible elements where $D << 0.1$, crystal fractionation cannot exploit small differences in bulk distribution coefficients and hence any change in ratios of these elements must either result from partial melting variations or more likely be due to some mixing phenomenon. A ratio such as La/Hf maintains an almost constant value within the Gramado magma type over a wide range of magmatic evolution, as shown in figure 4.13 {La/Hf vs. Mg#}, and this is despite the fact that there is a gradual increase in the extent of contamination {$(^{87}Sr/^{86}Sr)_i$ increases from 0.7075 to 0.7115}. This suggests that contamination took place with crustal material which had incompatible element ratios quite similar to, or not far removed from, the parental Gramado-type magma.

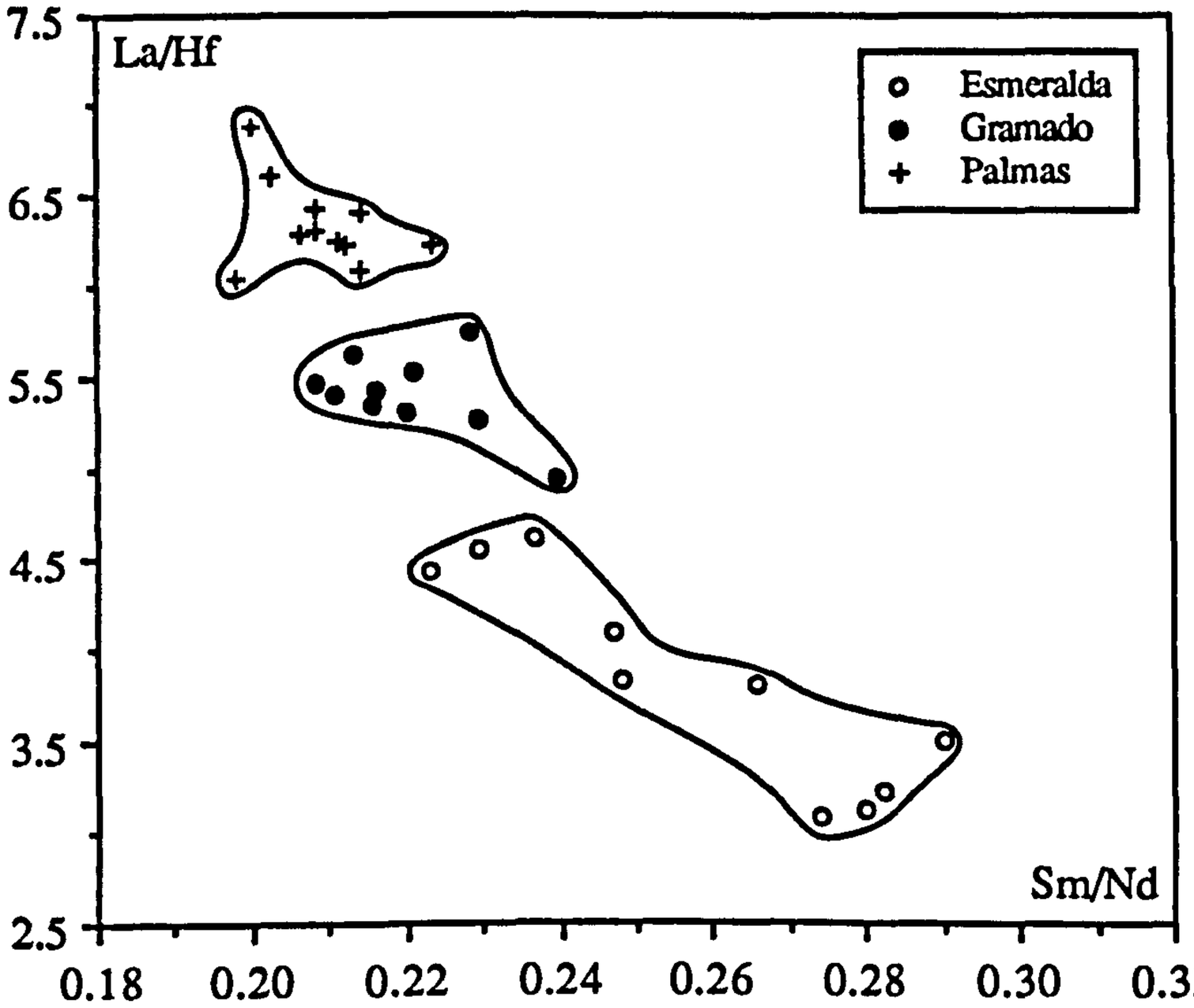

Figure 4.12 Variation of La/Hf vs. Sm/Nd for the southern Paraná low-Ti magma types. The Gramado magma type has a restricted range in both incompatible element ratios whereas they are variable and correlated in the Esmeralda magma type.

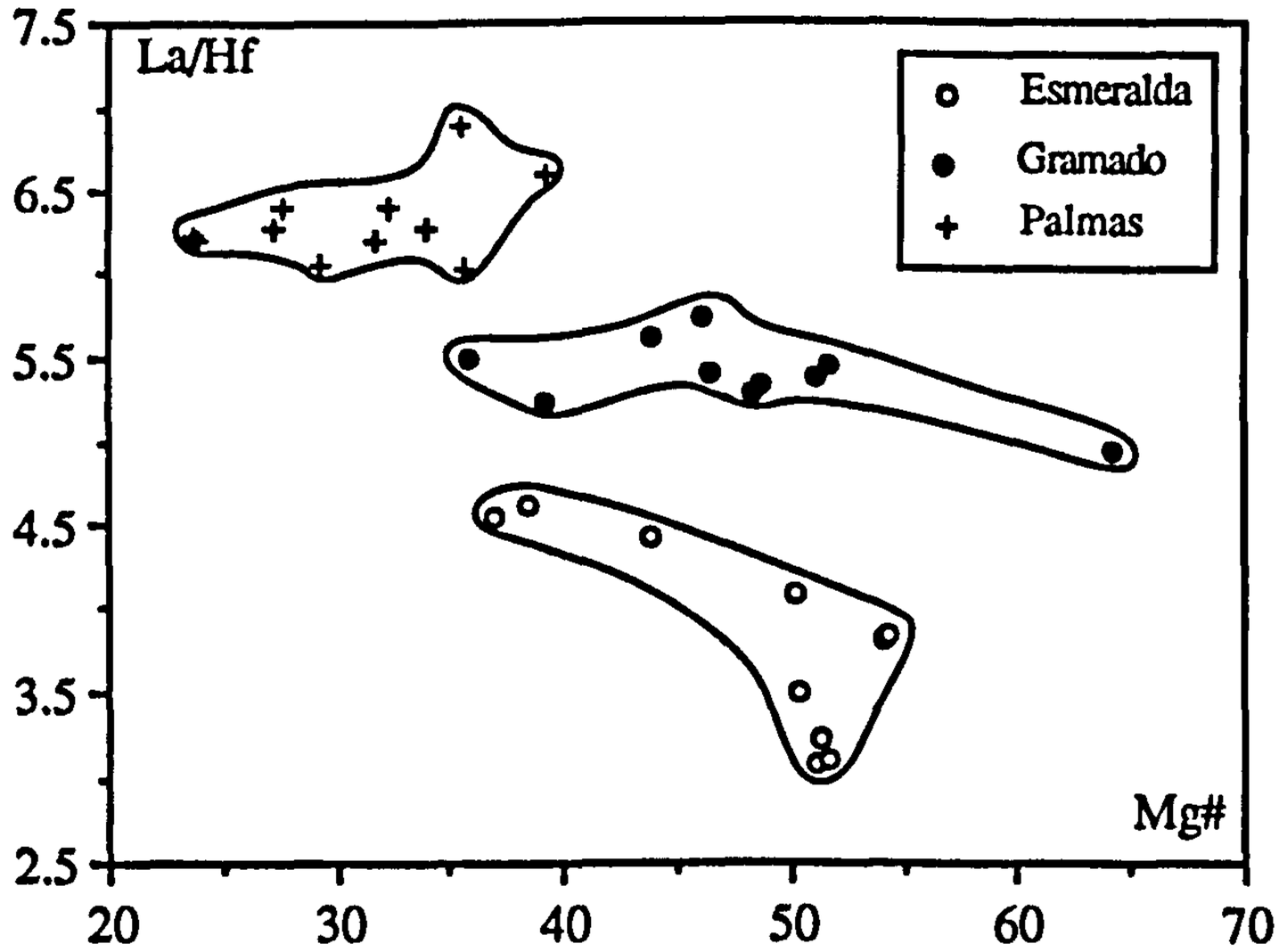

Figure 4.13 Variation of La/Hf vs. Mg# for the Esmeralda, Gramado and Palmas magma types, illustrating the poor correlation of incompatible trace element ratios with major elements for the Esmeralda magma type.

Gramado and Esmeralda (low-Ti) magma types

Even though the Esmeralda magma type has a more restricted range in Mg#, the variation in La/Hf is more pronounced, and the trend emanates from a different primitive composition to that of the Gramado magma type, suggesting a different parent magma to each series.

This is further illustrated by the contrasting behaviour of the REE elements between the two magma types. Figures 4.14(a) and 4.14(b) are Masuda-Coryell diagrams of chondrite-normalised REE abundances for samples of the Gramado and Esmeralda magma types respectively, with an average Palmas rhyolite composition also included for reference. The Gramado magma type samples all have similar REE patterns which just lie at higher or lower absolute abundances depending on their degree of magmatic evolution. The Esmeralda-type magmas all have similar HREE to the Gramado-type magmas but in contrast, they display varying degrees of LREE enrichment with patterns 'fanning-out' at the LREE end from being almost flat to being similar to the Gramado-type samples. This difference in LREE enrichment within, and between, the Esmeralda and Gramado magma types is best illustrated on a graph of $(La/Sm)_N$ vs. La, shown in figure 4.15, where $(La/Sm)_N$ is used as a monitor of LREE enrichment. This graph is also difficult to reconcile with the concept of a single low-Ti parental magma for the southern Paraná. For the Gramado magma type, $(La/Sm)_N$ is almost constant, increasing gradually from about 2.0 to 2.5 as La changes from 10 to 30 ppm, towards the compositional field for the Palmas rhyolites. In marked contrast, $(La/Sm)_N$ sharply increases from about 1.2 to 2.2 with increasing La content within the Esmeralda magma type, reflecting the variable LREE enrichment of figure 4.14. The important feature of this graph (and that of figure 4.13) is that the trends within the two magma types diverge moving away from the contaminant field, here represented by Palmas rhyolites. This shows that it is impossible to force a single AFC solution through all the data, although the individual magma type trends might be explained in terms of an AFC process provided that they each started from a different parental magma composition. The parental Gramado magma would have had $(La/Sm)_N \sim 2$ whereas the parental magma to the Esmeralda magma type would have had a more depleted REE pattern with $(La/Sm)_N \sim 1$.

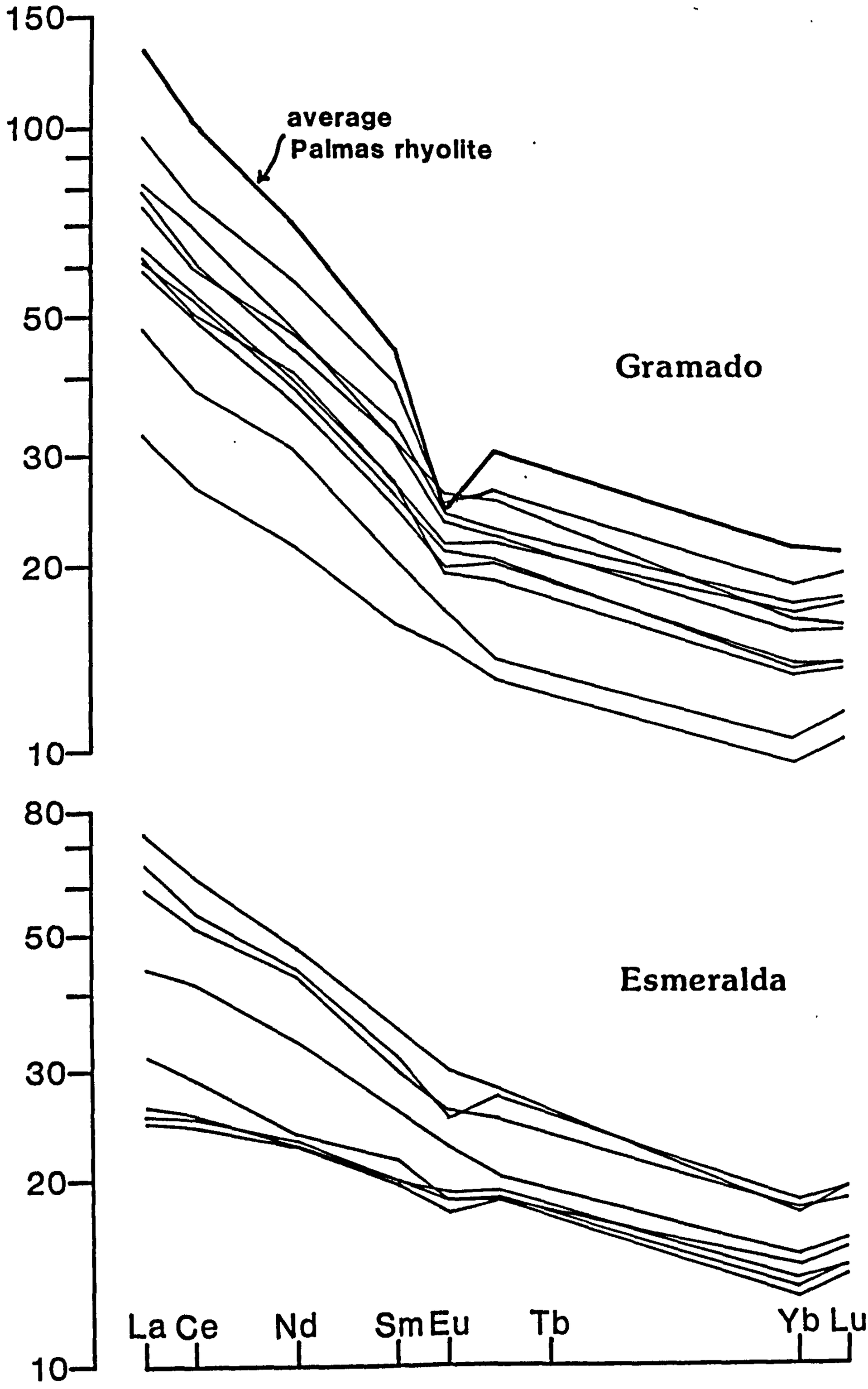

Figure 4.14 Chondrite-normalised REE abundance patterns for; (a) Gramado magma type - similar pattern at different element contents, (b) Esmeralda magma type - strongly variable LREE enrichment. Average Palmas rhyolite composition (Mantovani and Hawkesworth, in press) is also shown for comparison.

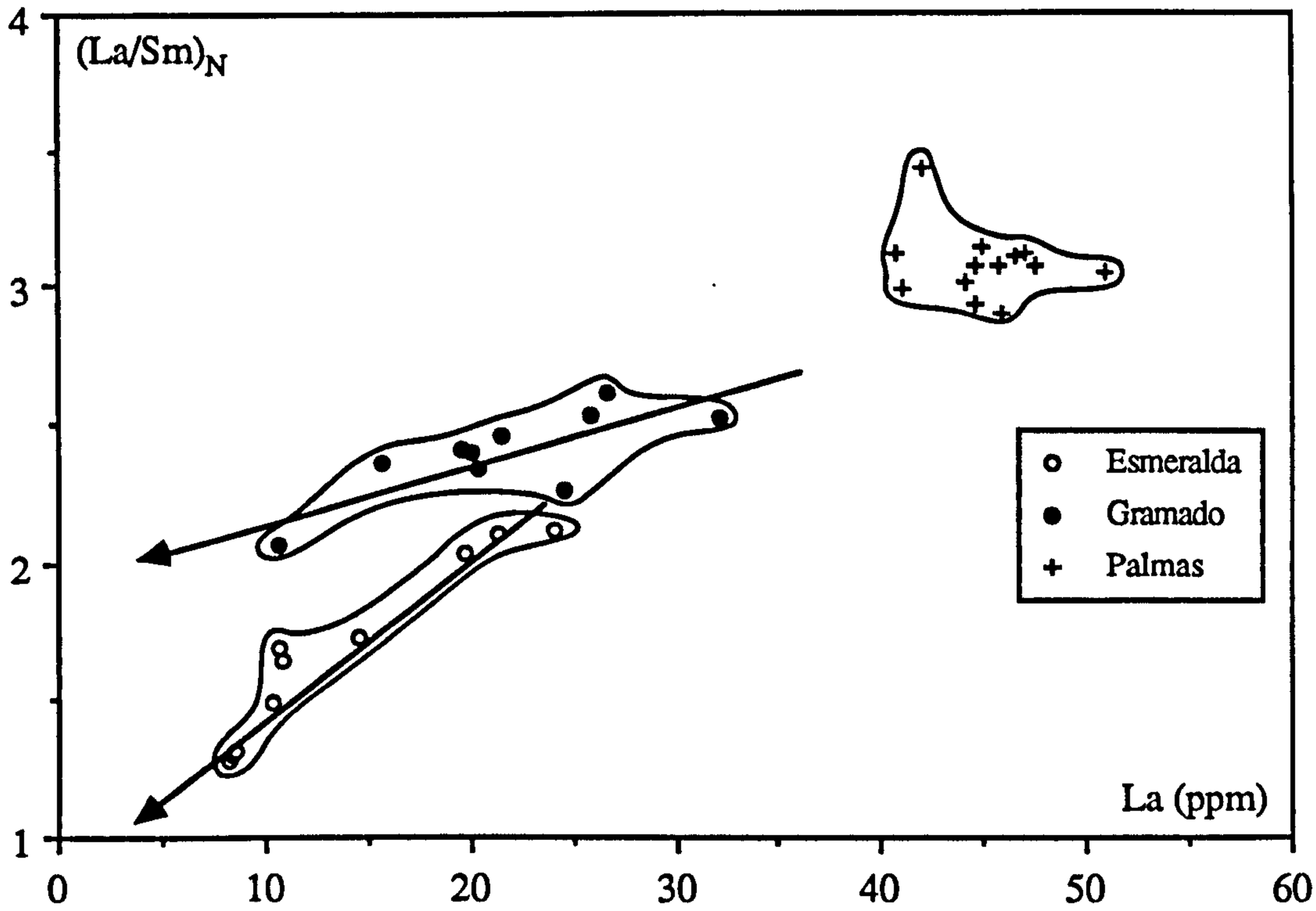

Figure 4.15 Variation of $(La/Sm)_N$ vs. La for southern Paraná low-Ti magmas. The trends for the Gramado and Esmeralda magma types diverge moving to lower La contents (*i.e.* more primitive compositions) suggesting the existence of distinct parental magmas to each magma type; parental Gramado magma with $(La/Sm)_N$~2, and parental Esmeralda magma with $(La/Sm)_N$ ~1.

If both trends were to be explained by AFC under different conditions from a single parental magma as represented by the Esmeralda end-member, then the curve for the Gramado trend would have to have an unrealistically extreme hyperbolic shape to be able to move vertically on this diagram before rapidly flattening out to give the linear Gramado data array itself. To move from a primitive Esmeralda to a primitive Gramado composition would require a change in $(La/Sm)_N$ from 1 to 2 for a slight increase in La content. This could be achieved by bulk mixing with a contaminant of different composition to that of the Palmas rhyolites, that had lower La and probably higher $(La/Sm)_N$. Simple mixing calculations (Langmuir *et al.*, 1978) between a primitive Esmeralda composition and typical syn-collision granite (from Pearce *et al.*, 1984) require the addition of 20 % {La 33 ppm, $(La/Sm)_N$ 4.5} to 45 % {La 15 ppm, $(La/Sm)_N$ 2.6} granite to produce a parental Gramado magma with $(La/Sm)_N$ of 2. It is difficult on thermal grounds to envisage a situation where a primitive magma could absorb 20-45 % of crustal material and then still happily undergo a

separate AFC process; and there are also problems with SiO_2 contents. A typical syn-collision granite has ~73 wt% SiO_2 and if a primitive Esmeralda magma has ~48 wt% SiO_2, then 20-45 % mixing would lead to a parental Gramado magma with 53-59 wt% SiO_2, which is somewhat excessive. Alternatively, the contaminant could have been lower crustal material which is generally less silicic (~54.4 wt% SiO_2, Taylor and McLennan, 1985). According to Taylor and McLennan, (1985), La/Hf is not very variable between average upper crust and average lower crust, being about 5.2. This lies within the range found in the Gramado magma type (4.8-5.7), whereas in the primitive Esmeralda magmas, La/Hf is about 3.0. This would require over 90 % assimilation to raise La/Hf from 3 to 5, and hence the nature of this hypothetical assimilant is still problematical. Also, any mixing would have to have occurred prior to the AFC process responsible for the variation within the Gramado magma type. Since the Gramado-type lavas seen at the surface are unlikely to have been the result of a single magma batch (they show no systematic stratigraphical variations within the lava pile) and the Gramado samples form quite a tight trend, this mixing process would have to have proceeded to the same extent each time before the resultant hybrid was input into the environment where the AFC was taking place. These alternatives all seem to be rather unlikely, and it is difficult to escape the conclusion that two distinct parental magmas existed for the southern Paraná low-Ti magmas.

In terms of trace element signatures, the Gramado parental magma was relatively LREE enriched, with $(La/Sm)_N$ ~2 whereas the parental magma anchoring the Esmeralda magma type trends had a more depleted trace element pattern with $(La/Sm)_N$ ~1. The two parental magmas were also isotopically distinct. The link between trace element and isotope ratios is provided by figure 4.16 which illustrates the coherent covariation of La/Nd and $(^{143}Nd/^{144}Nd)_i$. There is a slight correlation within the Gramado data field and, given the difference in the parental magmas, the lowest La/Nd value corresponds to $(^{143}Nd/^{144}Nd)_i$ of about 0.5123. The Esmeralda-type lavas show a strong negative correlation and the most LREE depleted samples (La/Nd ~0.55) have the most radiogenic $(^{143}Nd/^{144}Nd)_i$ of about 0.51255. Figure 4.10 of $(^{87}Sr/^{86}Sr)_i$ vs. $(^{143}Nd/^{144}Nd)_i$ shown earlier can be used to infer the corresponding Sr isotopic composition for these two parental liquids. The Gramado-

type parental magma probably had $(^{87}Sr/^{86}Sr)_i$ ~0.7075 and $(^{143}Nd/^{144}Nd)_i$ ~0.5123, whereas the Esmeralda-type parental magma had a more depleted isotopic signature with $(^{87}Sr/^{86}Sr)_i$ ~0.7055 and $(^{143}Nd/^{144}Nd)_i$ ~0.51255.

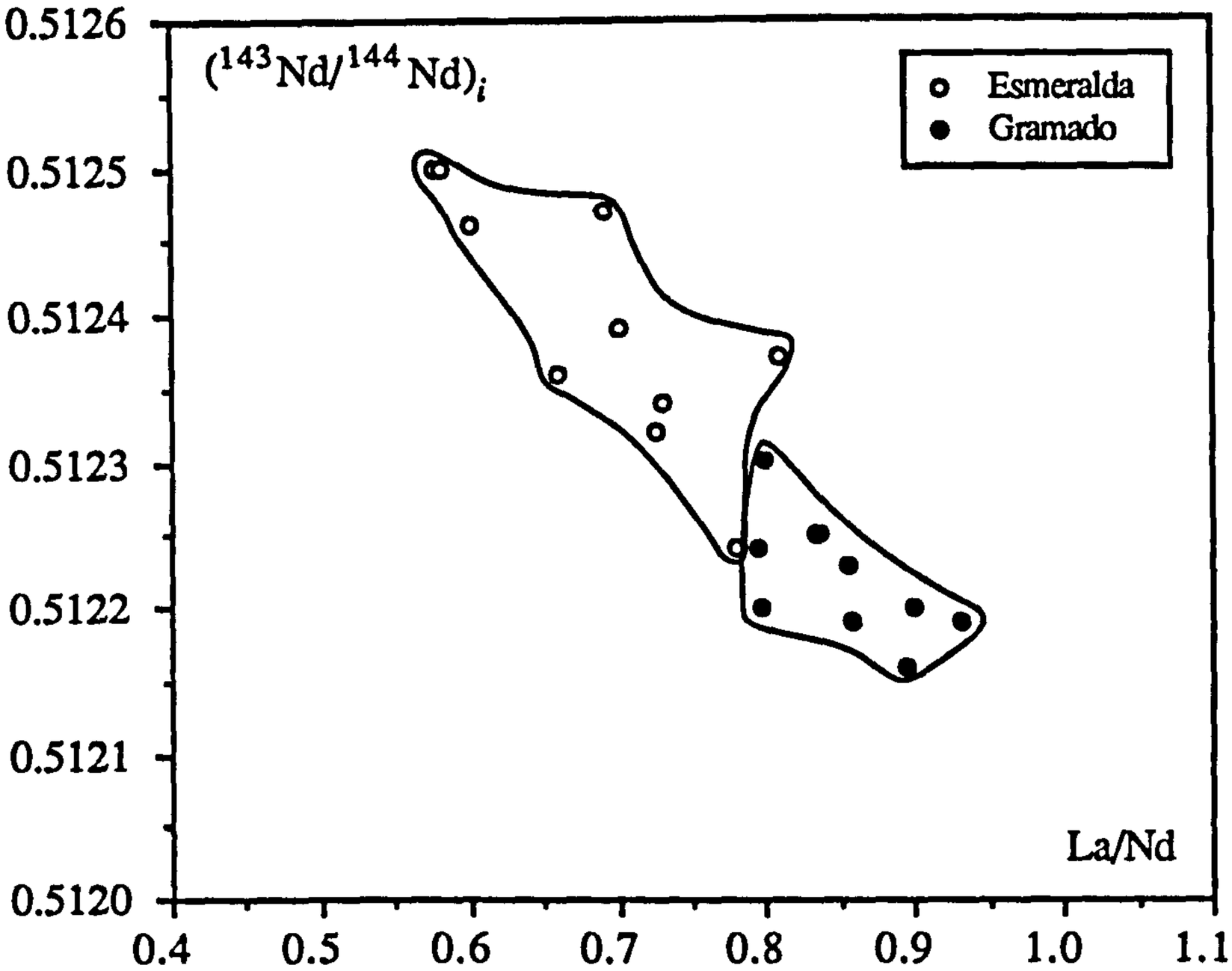

Figure 4.16 Variation of $(^{143}Nd/^{144}Nd)_i$ vs. La/Nd for the Esmeralda and Gramado magma types. Esmeralda-type samples show a good correlation between Nd isotopic composition and an incompatible trace element ratio (La/Nd), and this constrains the parental Esmeralda-type magma to have $(^{143}Nd/^{144}Nd)_i$ ~0.51255. The Gramado-type samples do not show a good correlation, but the data suggest that the parental 'uncontaminated' magma had $(^{143}Nd/^{144}Nd)_i$ ~0.5123.

4.6.3 Regional variation within the Gramado magma type.

Several studies have looked at the Gramado magma type on a regional scale taking lava samples from throughout the southern Paraná (Fodor *et al.*, 1985a/b; Bellieni *et al.*, 1986a/b; Hawkesworth *et al.*, 1986; Petrini *et al.*, 1987; Piccirillo and Cox, 1988). Such studies, whilst giving a feel for the general variations that characterise the magma type, suffer from the inherent problem that any subtle regional effects will be masked by the

averaging nature of this approach. It has already been established that crustal interaction was a major theme of the processes producing the Gramado magma type, and section 4.3 has illustrated the complexities of the contamination process. It is conceivable that both AFC and AEC could have acted on a suite of magmas to produce a series of geochemical relationships not easily interpretable in terms of either contamination style. Devey and Cox (1987) pointed out that in order to resolve this problem, it is best to restrict sampling to a limited area in the hope that within such a localised region, the magmatic evolution maintained a relatively stable pattern. Contamination will be linked to the local thermal regime which must surely have been variable over an area the size of the southern Paraná.

There have been a few published papers that have attempted to assess the contamination process within very localised areas {*e.g.* Mantovani *et al.*, 1985a; Mantovani and Hawkesworth, 1988; Hawkesworth *et al.*, 1988} but as yet there has been no regional comparison of these results. For this investigation two areas have been selected which lie about 200 km apart; (i) São Joaquim area, Santa Catarina state - this study, and Mantovani *et al.*, (1985a), (ii) Caxias do Sul area, Rio Grande do Sul state - MV and MG road sections of Hawkesworth *et al.*, (1988).

The most striking difference between these two areas is the contrast in the distribution of initial Sr isotope ratios. In the Caxias do Sul area, $(^{87}Sr/^{86}Sr)_i$ is relatively elevated and all samples have ratios greater than 0.7088, whereas to the north-east in the São Joaquim area, Gramado-type samples with $(^{87}Sr/^{86}Sr)_i$ down to 0.7073 have been found, and over 50% of the analysed samples there have $(^{87}Sr/^{86}Sr)_i$ less than the minimum value seen at Caxias do Sul. This regional variation in $(^{87}Sr/^{86}Sr)_i$ within the Gramado magma type is best illustrated using a histogram, and figures 4.17(a) and 4.17(b) show the frequency distribution of $(^{87}Sr/^{86}Sr)_i$ for the two areas; (a) São Joaquim and (b) Caxias do Sul. At São Joaquim two-thirds of the samples have $(^{87}Sr/^{86}Sr)_i$ of 0.707 to 0.709 whereas at Caxias do Sul, all samples have $(^{87}Sr/^{86}Sr)_i > 0.7088$ and here, two-thirds lie in the range 0.709 to 0.711.

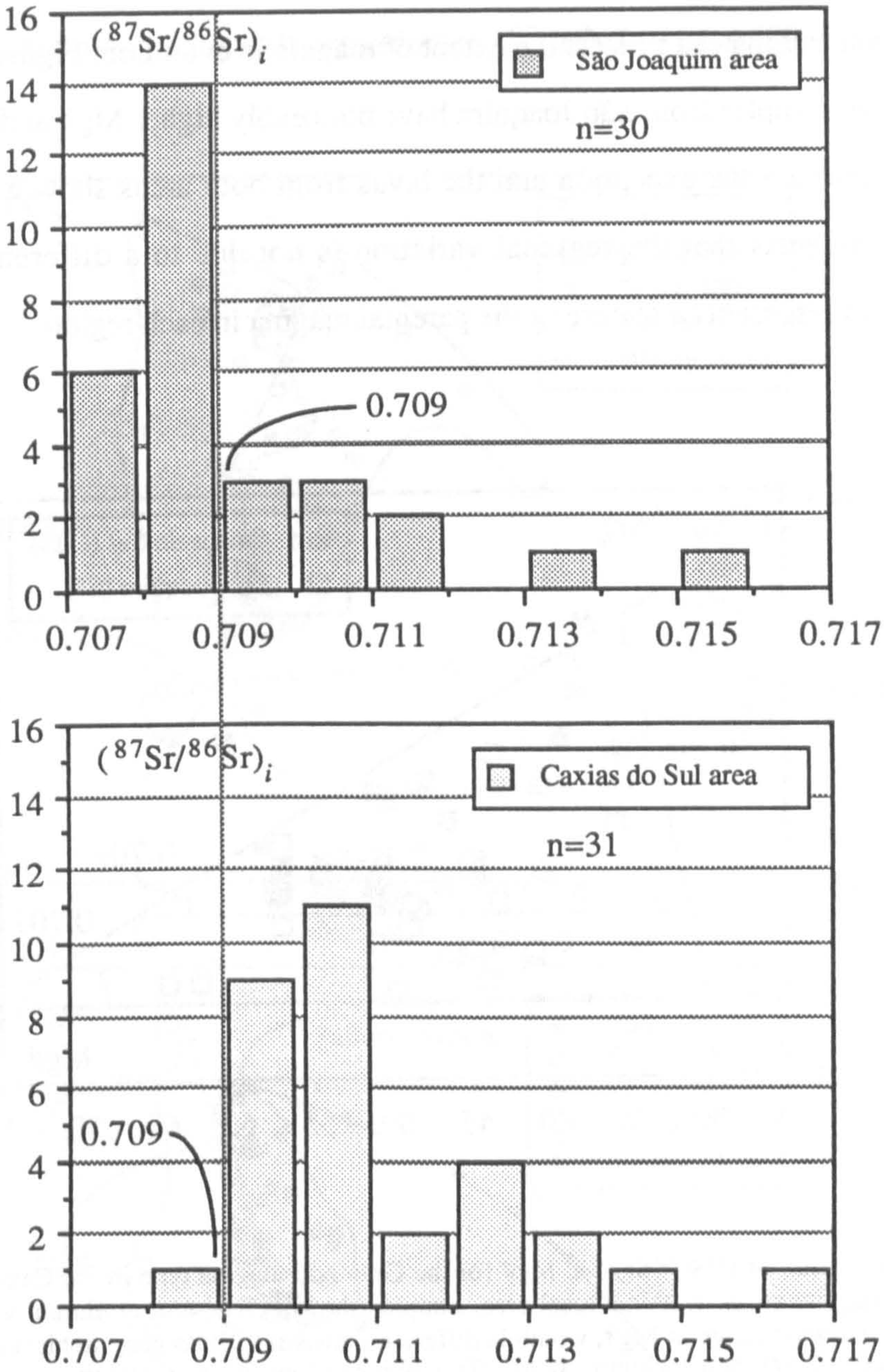

Figure 4.17 Frequency distribution of $(^{87}Sr/^{86}Sr)_i$ for the Gramado magma type in; (a) São Joaquim area, and (b) Caxias do Sul area, about 200 km to the SW. Note the virtual restriction of samples from Caxias do Sul to values > 0.709, in contrast to the São Joaquim area where two-thirds of the samples have $(^{87}Sr/^{86}Sr)_i < 0.709$. Data sources - {São Joaquim - this study; Mantovani *et al.*, 1985a: Caxias do Sul - Hawkesworth *et al.*, 1988; M.S.M. Mantovani, pers. comm., 1988}.

What could have given rise to this difference ? An obvious thought is that, if an AFC process was operating, the magmas at São Joaquim could be more primitive and thus these would be less contaminated and have lower $(^{87}Sr/^{86}Sr)_i$. This can be evaluated by looking at a plot of $(^{87}Sr/^{86}Sr)_i$ against Mg#, since Mg# is relatively insensitive to

contamination and instead reflects the extent of magmatic evolution. Figure 4.18 shows that although three samples from São Joaquim have noticeably higher Mg# and are indeed more primitive, these are the exception and the lavas from both areas show a similar range in Mg#. This suggests that the regional variation is not due to a difference in magmatic evolution, and represents a feature of the parental magma in each region.

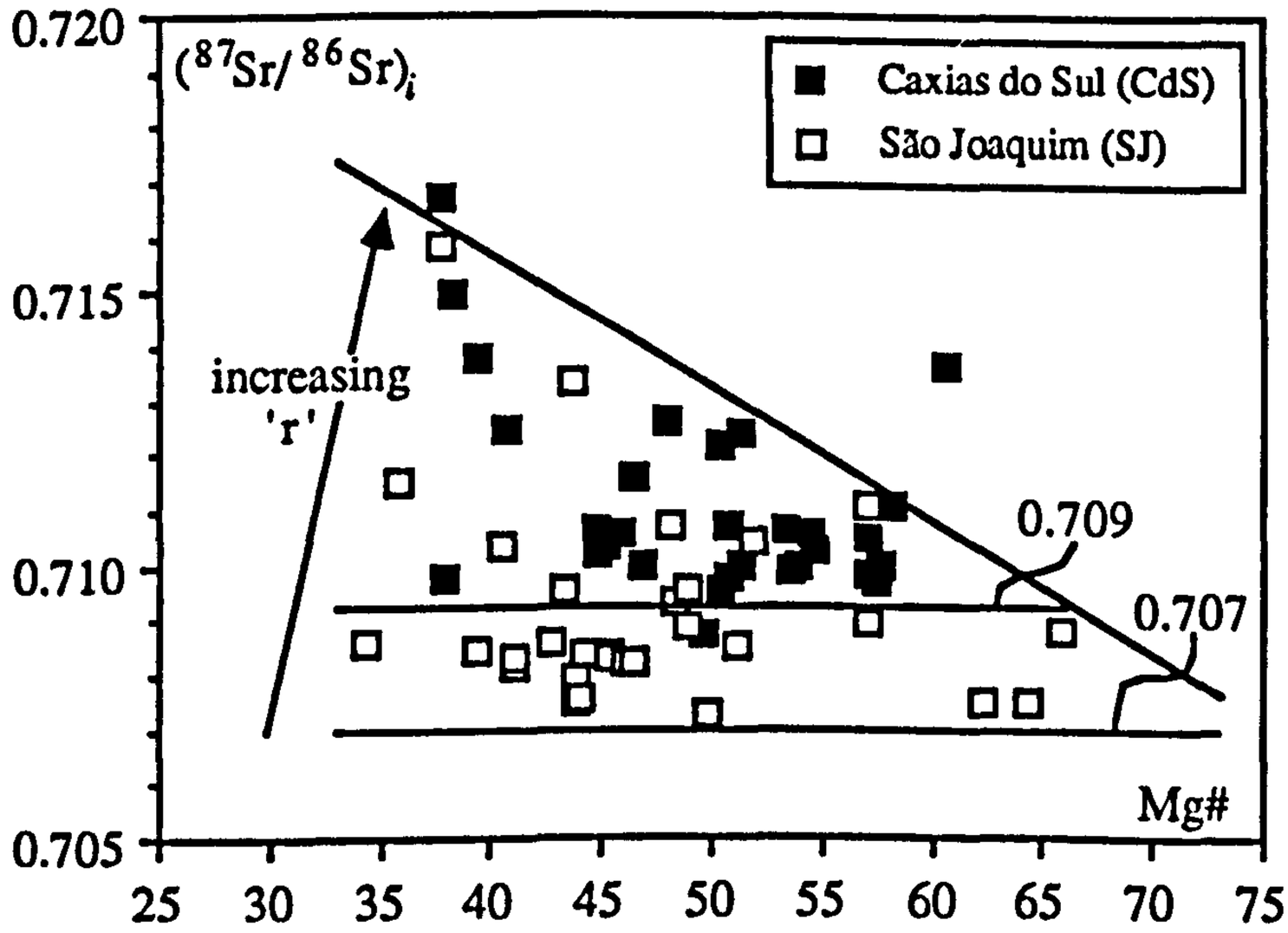

Figure 4.18 Variation of $(^{87}Sr/^{86}Sr)_i$ vs. Mg# for the Gramado magma type in the Caxias do Sul and São Joaquim areas. Within a local area, samples show a consistent minimum value of $(^{87}Sr/^{86}Sr)_i$ for a wide range in Mg#, which is different between the two geographical regions; Caxias do Sul - 0.709, São Joaquim - 0.707. This suggests that the 'uncontaminated' parental Gramado-type magma varied regionally, prior to the operation of an AFC process. The more evolved samples show a wider range in $(^{87}Sr/^{86}Sr)_i$, perhaps reflecting variable 'r'-values during AFC.

The inversion modelling of Hawkesworth *et al.*, (1988) concluded that the Gramado parental magma in the Caxias do Sul area must already have had an elevated $(^{87}Sr/^{86}Sr)_i$ of about 0.7086 prior to the occurrence of the AFC process, and this was backed up by the more rigorous treatment given in Mantovani and Hawkesworth, (in press). This can be seen in figure 4.18 where for a wide range in Mg#, the samples from the Caxias do Sul area reach a base level in $(^{87}Sr/^{86}Sr)_i$ of approximately 0.709 but in the São Joaquim area this minimum level is consistently at about 0.707. This suggests that it was the magma that

has to be addressed is whether this variation in $(^{87}Sr/^{86}Sr)_i$ of 0.707 to 0.709 for the

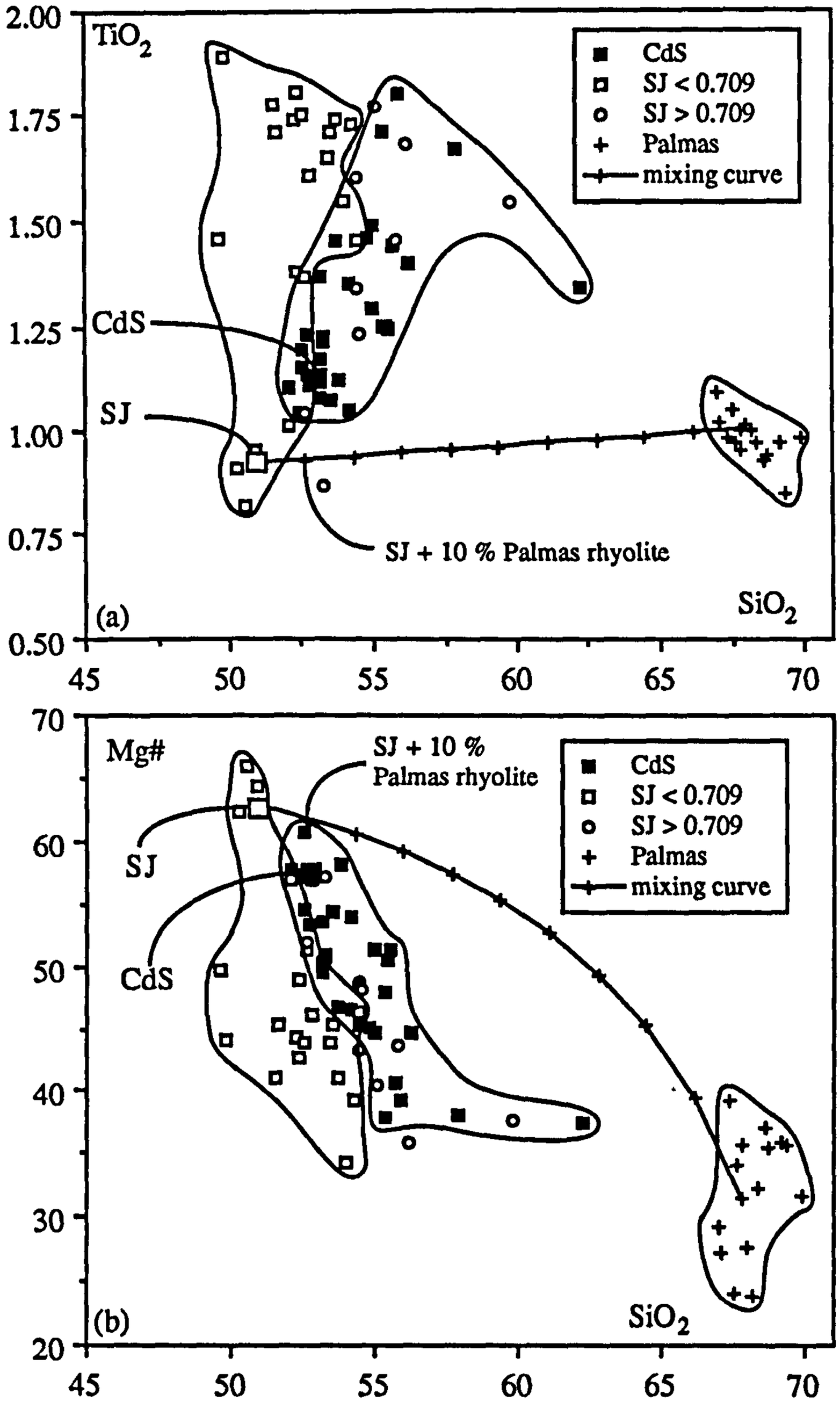

Figure 4.19 SiO_2 vs. (a) TiO_2, (b) Mg#, illustrating the regional variation shown by certain major elements within the Gramado magma type. Samples from Caxias do Sul (CdS) are displaced to higher SiO2 contents. The average primitive compositions, SJ and CdS, from table 4.1 are marked by the large open and filled squares respectively. Mixing curves between SJ and average Palmas rhyolite are shown, tick marks represent 10 % mixing intervals

parental Gramado magma was of mantle origin or whether it was imposed by an additional contamination process in the crust. The difference could have been the result of variable contamination during ascent to the magma chamber, direct mixing with a different component or alternatively a feature inherited from the mantle source.

The regional geochemical variation is not restricted to $(^{87}Sr/^{86}Sr)_i$. There is a major element difference also, and it is argued that this still remains even when the effects of the subsequent AFC are stripped off. This is illustrated in figures 4.19(a) and 4.19(b) which show the variation of SiO_2 with; (a) TiO_2 and (b) Mg#. The São Joaquim samples have been divided into two groups based on $(^{87}Sr/^{86}Sr)_i$ values. The few samples that have $(^{87}Sr/^{86}Sr)_i$ greater than 0.709, the range shown by the Caxias do Sul lavas, have similar major element compositions to those in the Caxias do Sul area. The majority of the São Joaquim lavas, on the other hand, which have lower Sr isotope ratios than any encountered near Caxias do Sul, plot at distinctly lower SiO_2 contents.

The lavas of the Caxias do Sul area are enriched in SiO_2 and $(^{87}Sr/^{86}Sr)_i$ relative to their more northerly counterparts near São Joaquim, suggesting the addition of an SiO_2-rich component with high $(^{87}Sr/^{86}Sr)_i$. A good candidate to investigate for this is the Palmas rhyolites since it was inferred earlier to be similar in composition to the contaminant affecting the Gramado magma type as a whole. Possible mixing vectors between the most primitive Gramado-type samples at São Joaquim and a Palmas rhyolite composition have been marked on figures 4.19(a) and 4.19(b), together with the fractionation trends. These illustrate that the variation within the lavas erupted in a particular area are dominated by fractional crystallisation accompanied by some assimilation (*i.e.* AFC), but the shift in position of the data fields between the two areas could be consistent with mixing with a rhyolitic magma prior to any crystallisation. The major element data can be used to roughly constrain the percentage of rhyolite that would be needed. From figure 4.19(b), it can be seen that the São Joaquim samples are displaced, at a given Mg#, to lower SiO_2 abundances on average by about 2 wt%. The most primitive magmas in the São Joaquim area have about 50 wt% SiO_2 and an average Palmas rhyolite has 68 wt% SiO_2, which

	São Joaquim SJ	Caxias do Sul CdS	Palmas rhyolite	Mixture 10% Palmas + 90 % SJ
SiO_2	50.95	52.77	67.84	52.64
TiO_2	0.92	1.10	1.00	0.93
Al_2O_3	15.84	15.16	13.06	15.56
Fe_2O_3(t)	10.64	10.78	6.38	10.21
MnO	0.17	0.16	0.11	0.16
MgO	7.76	6.25	1.26	7.11
CaO	10.73	9.82	3.11	9.97
Na_2O	2.25	2.61	3.18	2.34
K_2O	0.63	1.16	3.79	0.95
P_2O_5	0.12	0.18	0.29	0.14
Mg#	63.0	57.5	31.3	61.9
Rb	16	40	161	31
Sr	212	199	141	205
Ba	190	376	701	241
Nb	7.4	10	21	8.8
Zr	92	137	271	110
Hf	2.19	3.47	6.97	2.67
Y	20	26	50	23
La	11.4	18.8	44.8	14.7
Ce	22.7	40.0	90.0	29.4
Nd	13.3	21.1	44.4	16.4
Sm	3.17	4.60	9.06	3.76
Eu	0.95	1.34	1.87	1.04
Tb	0.61	0.79	1.46	0.70
Yb	1.97	2.43	4.67	2.24
$(^{87}Sr/^{86}Sr)_i$	0.7082	0.7102	0.7195	0.7089

Table 4.1 Comparison of average primitive Gramado-type samples from the São Jaoquim (SJ) and Caxias do Sul (CdS) areas, and composition of a hybrid magma formed by a mixture of 10 % Palmas rhyolite and 90 % SJ Gramado-type composition. SJ average (n=4) - {DUP30, GB20, GB40, GB18}, CdS average (n=5) - {MV2, MG4, MG5, MG10, MG11}. [GB samples from Mantovani *et al.*, 1985a; MV, MG samples from Hawkesworth *et al.*, 1988].

means that to get a magma with about 52 wt% SiO_2 would require adding about 10 % of the rhyolite. If the enriched end-member was less silicic than the rhyolite, then the percentage necessary to be added would have to be higher.

The addition of a rhyolite component must also be consistent with the trace element and isotope data, and one way to approach this problem is to take an average of the most mafic samples, with the lowest Sr isotopic ratios, in each area. These average 'primitive'

compositions, abbreviated to SJ (São Joaquim) and CdS (Caxias do Sul), are given in Table 4.1, and included on figures 4.19(a) and 4.19(b). The composition of a mixture obtained by adding 10 % Palmas rhyolite to 90 % of the SJ composition, as suggested by the SiO_2 data, is also shown and if the mixing model is correct then this mixture should be directly comparable with the average Caxias do Sul 'primitive' magma. The compositional difference between the 'primitive' magmas of the two geographical areas, as well as the suitability of the mixing model to account for this variation, can be examined in the context of figure 4.20. This shows the trace element patterns for the magmas listed in table 4.1, which have been normalised to the composition of the average São Joaquim primitive magma (SJ). The difference in degree of magmatic evolution for the compositions in table

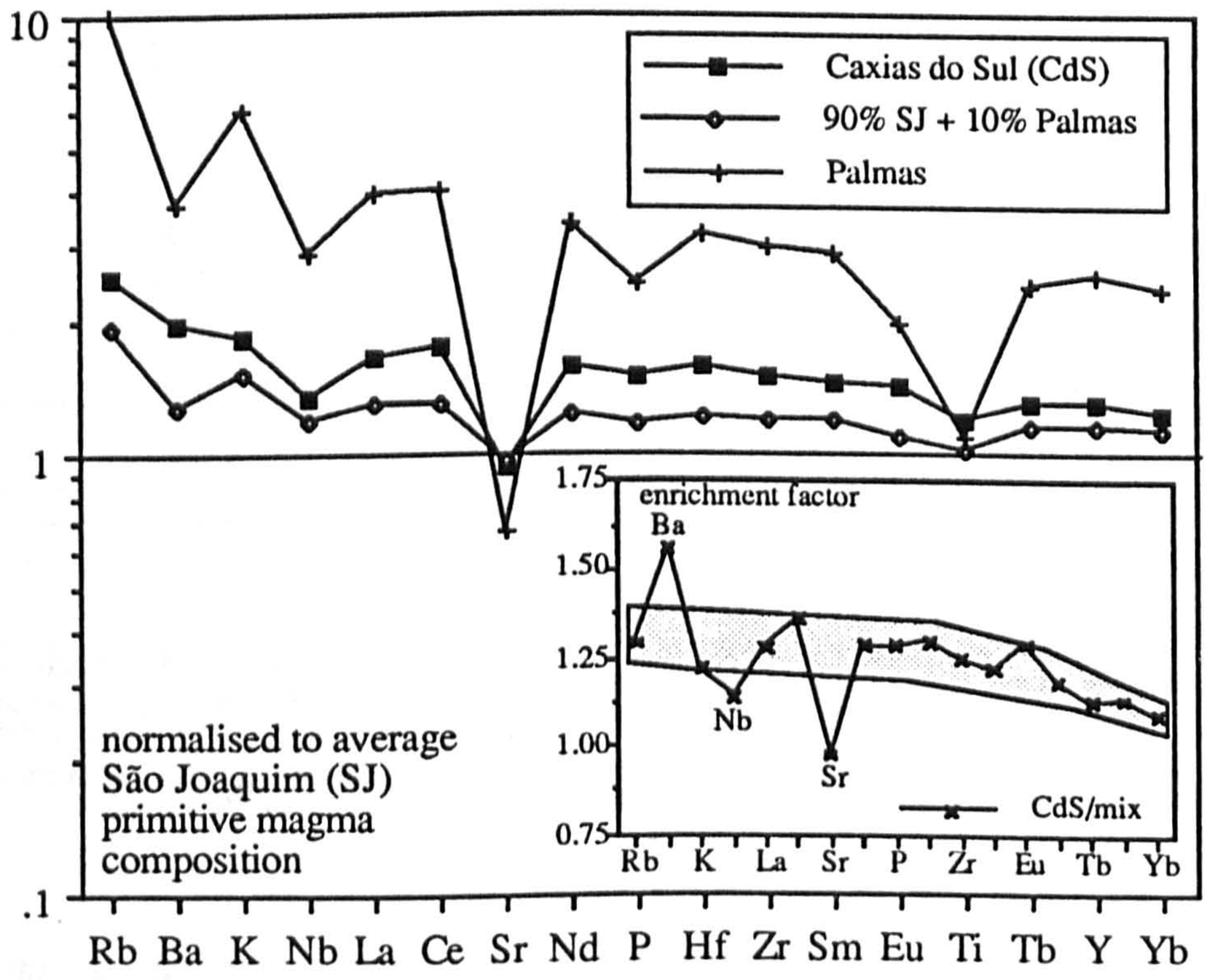

Figure 4.20 Comparison of the trace element contents for the compositions given in table 4.1 {average primitive CdS Gramado-type magma, average Palmas rhyolite, and mixture (10% Palmas/90% SJ)} normalised to SJ, the average primitive Gramado-type magma from Sâo Joaquim. The inset figure examines in more detail the difference between the Caxias do Sul (CdS) composition and the modelled hybrid magma, and shows the CdS composition normalised to the trace element content of the calculated mixture. If these two compositions were related solely by fractional crystallisation, then the calculated enrichment factors should lie within the shaded area (except for Sr which is strongly controlled by plagioclase fractionation). Note the anomalies for Ba and Nb.

4.1 is illustrated by their range of Mg# from 57 to 63, and therefore the trace element patterns of figure 4.20 must partly reflect the role of fractional crystallisation. However, this will only have adjusted the absolute element concentrations and should not have affected the relative abundances of the more incompatible elements, *i.e.* it is the shape of the patterns on figure 4.20 that is important, rather than their actual abundances.

The Caxias do Sul primitive magma has a more evolved composition (Mg# 57.5) than the calculated mixture (Mg# 61.9), and for the mixing hypothesis this implies that the Caxias do Sul primitive magma must have undergone a certain amount of post-mixing crystallisation. The similarity of the trace element patterns on figure 4.20 for the Caxias do Sul composition and the mixture is superficially consistent with this model. The effects of fractional crystallisation can be more easily assessed using the concept of the enrichment factor, E.F. which is the ratio of an element in the more evolved sample (*i.e.* CdS) to the inferred more primitive sample (*i.e.* the SJ+rhyolite mixture). E.F. is equivalent to C_l/C_o in the Rayleigh fractionation equation (see chapter three) and, since F will be the same for all elements in a particular sample, E.F. is only a function of the bulk distribution coefficient, D, during crystallisation. The elements on figure 4.20 are arranged from right to left in order of roughly increasing incompatibility, and so any crystallisation should produce a smooth curve of gradually increasing E.F. values towards the left hand side. The enrichment factors for a range of elements between CdS and the postulated mixture are plotted on the inset diagram of figure 4.20. Most elements conform to the expected trend, with reasonably similar enrichment factors of about 1.25, suggestive of a crystallisation origin from the modelled mixture. The almost constant Sr content between the two compositions (*i.e.* E.F. ~ 1) is probably a consequence of buffering by plagioclase in the crystal extract. This leaves Ba and Nb as being anomalous. Nb is too high and Ba is too low in the mixture to be comparable to the Caxias do Sul composition, and this can not be due to the crystallisation process. This implies that the enriched end-member in the mixing event would need to have higher Ba and lower Nb than in the Palmas composition used here. This distinction in the behaviour of Ba and Nb between the two areas (and in the

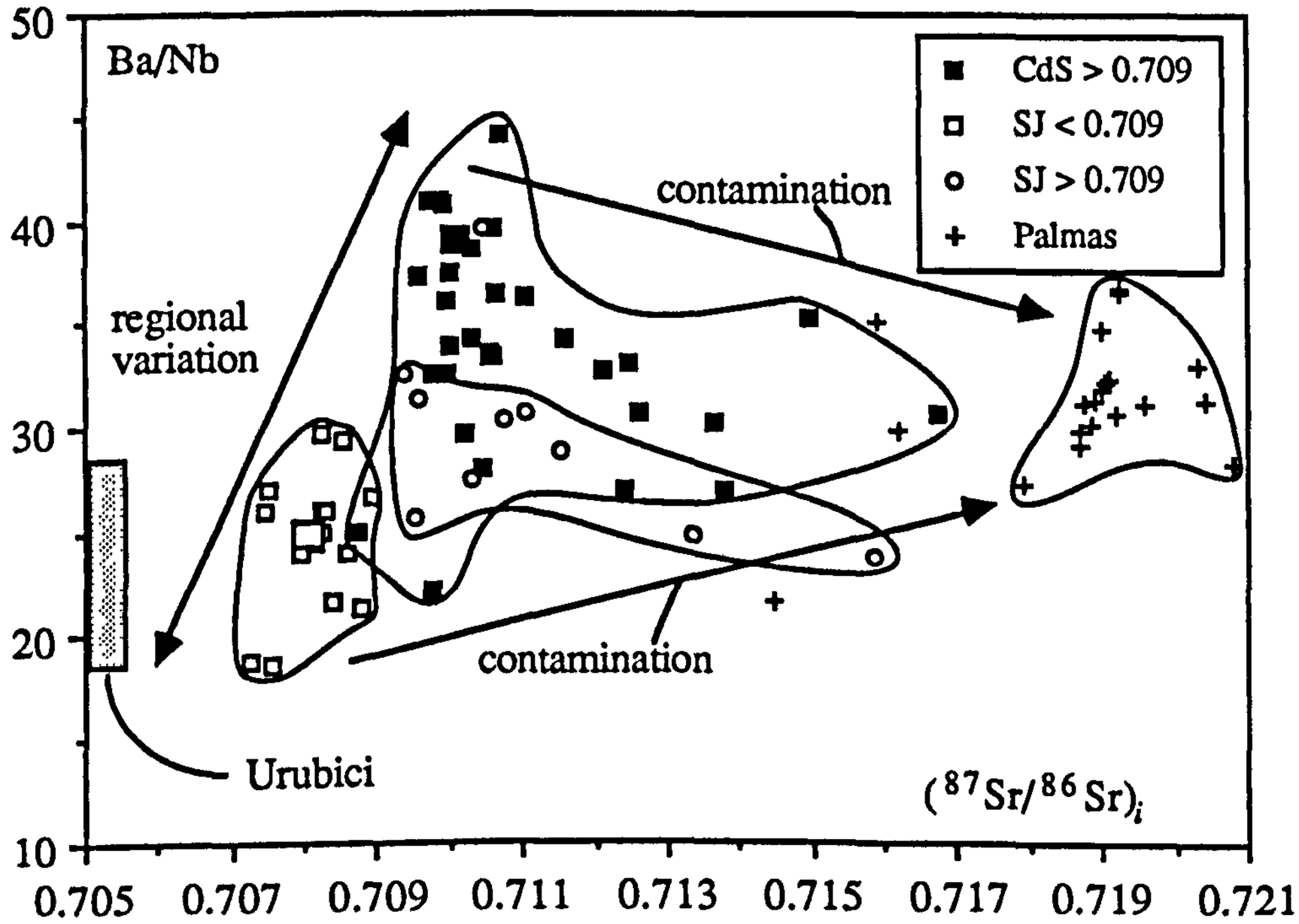

Figure 4.21 Variation of Ba/Nb vs. $(^{87}Sr/^{86}Sr)_i$, highlighting the regional differences within the Gramado magma type. Samples from São Joaquim have Ba/Nb < 30, whereas the majority from Caxias do Sul have Ba/Nb > 30. The Palmas rhyolites have Ba/Nb ~30, midway in the range shown by the Gramado-type basalts, confirming that they were not controlling the regional variation. The displacement of samples from both areas towards the Palmas rhyolite field, and higher $(^{87}Sr/^{86}Sr)_i$, reflects the subsequent effects of an AFC process superimposed on the earlier regional differences. The Urubici magma type has a similar range in Ba/Nb to the Gramado-type samples from São Joaquim but at lower $(^{87}Sr/^{86}Sr)_i$ and is unlikely to be related to the regional variation in the Gramado magma type. The SJ and CdS compositions from table 4.1 are represented by the large open and filled squares respectively.

Palmas rhyolites) is illustrated in figure 4.21 of Ba/Nb vs. $(^{87}Sr/^{86}Sr)_i$, which keeps the same sample groups as in figure 4.19.

A further problem with this model is the difficulty in reconciling the quantity of rhyolite which must be added in order to account for both the major and trace element composition and the observed isotope variations. The effect on $(^{87}Sr/^{86}Sr)_i$ of mixing with a magma of Palmas rhyolite composition can be investigated using the mixing equations from Faure (1986);

$$C_{mix}.\varepsilon_{mix} = F.C_A.\varepsilon_A + (1 - F).C_B.\varepsilon_B \qquad \text{and} \qquad C_{mix} = F.C_A + (1 - F).C_B$$

where A, B represent the two end-members involved, C is the element concentration, ε is the isotopic ratio of that element, and F is the fraction of component A added. Many of the

variables for this equation are poorly constrained. For the two proposed mixing end-members, the São Joaquim (SJ) composition in table 4.1 has 212 ppm Sr and $(^{87}Sr/^{86}Sr)_i$ of 0.7082, and the Palmas rhyolites on average contain 141 ppm Sr and have $(^{87}Sr/^{86}Sr)_i$ of 0.7195. If these values are fed into the equations above, the $(^{87}Sr/^{86}Sr)_i$ calculated for a mixture produced by the addition of 10 % rhyolite is 0.7089, and this is lower than the observed value of 0.7102 in the average Caxias do Sul composition. If instead the Sr isotopic composition of the resultant mixture is assumed to be equal to this observed value of 0.7102, then this produces a value for F of 0.24 which implies the addition of 24 % of the rhyolite composition. This is significantly higher than the 10 % suggested by the major element data above. It is possible that the Sr content in the SJ composition has been affected by crystal fractionation and, by reversing the above problem and keeping the other parameters the same, this can be calculated for an assumed F value of 10 %. In this case the Sr content of the SJ end-member would be expected to be about 73 ppm compared with the observed value of 212 ppm, which is unrealistically low even if the crystal extract was plagioclase-free.

The conclusions from these discussions is that any direct role for the Palmas rhyolites in controlling the regional variation within the Gramado magma type is difficult to sustain, since the models produce inconsistencies between the isotopes, major elements and trace elements. Therefore we are still left with the choice between involvement of a non-rhyolitic crustal component or ascribing the variation to a mantle feature. The Nb and Ba discrepancies apparent from the rhyolite mixing model discussions above are more pronounced between the average 'primitive' magmas for the two areas. This is illustrated on the main figure 4.20 where the CdS composition plotted has a high Ba/Nb ratio relative to the normalised SJ composition. This feature is developed in figure 4.21 which clearly picks out the regional variation. The Gramado magma type over the southern Paraná region has a wide range in Ba/Nb from 18 to 44. Samples from the São Joaquim area with $(^{87}Sr/^{86}Sr)_i < 0.709$ have low Ba/Nb (< 30) whereas the majority of samples from near Caxias do Sul have higher Ba/Nb (> 30), and this defines the steep regionally controlled trend on figure 4.21. The São Joaquim samples with high Sr isotopes (> 0.709), and

samples within the Caxias do Sul group, scatter towards the Palmas rhyolite field to higher $(^{87}Sr/^{86}Sr)_i$, reflecting the crustal assimilation process described earlier in the chapter. The Palmas rhyolites have a Ba/Nb ratio of about 30, which is midway in the range displayed by the basalts and, together with their high $(^{87}Sr/^{86}Sr)_i$, this further confirms that the rhyolites were not responsible for the differences in the Gramado magma type between the two areas. Instead, a contaminant with the composition of the Palmas rhyolites controlled the AFC trends displayed by the lavas, but this was a subsequent event whose effects were superimposed on a regionally variable parental magma. This regional variation reflects the addition of a high Ba/Nb (> 40) component with relatively low $(^{87}Sr/^{86}Sr)_i$, but still in excess of 0.709. Equally, this can not be due to mixing back to a low $(^{87}Sr/^{86}Sr)_i$ Urubici-type magma because Ba/Nb in the Urubici magma type is the same as the range within the São Joaquim area.

The ultimate origin for the pre-AFC regional variation seen within the Gramado magma type is still not clearly understood. It is difficult to place constraints on the nature of the process(es) involved because the variations tend to be masked by the overprinting of subsequent assimilation and crystallisation. It has been possible to establish some geochemical features that characterise this regional difference but these are ambiguous in constraining the underlying petrogenetic process responsible. The Caxias do Sul samples have higher $(^{87}Sr/^{86}Sr)_i$, Ba/Nb, and SiO_2 than their counterparts from São Joaquim. The variation is compatible on a gross scale with the addition of a component with 'crustal' features, as was demonstrated (with the exception of a few trace elements) with the mixing model attempted with the Palmas rhyolite. This leads us to the dilemma introduced in chapter one since such signatures can also be developed within the sub-continental lithospheric mantle in response to trace element enrichment processes (*e.g.* Hawkesworth *et al.*, 1984a), or even via the introduction of a subducted sediment component (Hergt *et al.*, 1989).

If the regional contrast was determined by variable assimilation of a non-rhyolitic component during ascent through the lithosphere, this process must have consistently occurred to a greater extent in the south of the region, around Caxias do Sul. More

importantly, this would leave open the possibility that the magmas sampled near São Joaquim themselves may have also undergone similar assimilation, albeit to a lesser extent, and this would imply that the true Gramado primary magma would have had $(^{87}Sr/^{86}Sr)_i <$ 0.707 and Ba/Nb < 15. Such a model assumes that there was a unique primary magma composition to the Gramado magma type, and that this was variably modified between the regions as a result of interaction with crustal material. An alternative is to suggest that it was the primary magma which varied consistently between the São Joaquim and Caxias do Sul areas, and the difference in $(^{87}Sr/^{86}Sr)_i$ and Ba/Nb reflected subtle variations within the mantle source region. This is consistent with the view of Mantovani *et al.*, (1985a) who noticed that in general, Gramado-type samples with < 52 wt% SiO_2 which they considered to be uncontaminated, still had a range in $(^{87}Sr/^{86}Sr)_i$ of 0.707-0.709, and it was suggested that this reflected derivation from variably enriched mantle source regions. If the high Ba/Nb component also had higher Rb/Sr then, provided the regional characteristics of the mantle source were established at a sufficient time prior to the Paraná magmatism, this would develop the correspondingly higher $(^{87}Sr/^{86}Sr)_i$ that is seen in the Caxias do Sul lavas. The higher SiO_2 content of these high $(^{87}Sr/^{86}Sr)_i$ lavas might therefore reflect melting under hydrous conditions that resulted from the mantle enrichment process.

It has now been shown that two processes were responsible for the geochemical diversity within the Gramado magma type over the southern Paraná region; (i) AFC, and (ii) an earlier regionally-imposed variation. Hence, when considering the later stage AFC process in detail, it will be important to restrict the samples discussed to a limited geographical area, and even then it is found that the AFC trends are still fairly scattered. In published AFC models, it is often assumed that the controlling parameters {*e.g.* C_a, C_o, D, r} remained constant during the eruption of a particular suite of lavas. In the southern Paraná, the variations within the Gramado magma type do not correspond to those produced by the operation of such an ideal AFC process, even when the samples considered are restricted to an individual area, although the gross chemical variations (*e.g.* figure 4.5) demonstrate that AFC did occur. Mantovani and Hawkesworth (in press) recognised that within the MV-MG sections near Caxias do Sul, several flows lay along, or

just slightly displaced from, a gabbro fractionation vector at almost constant $(^{87}Sr/^{86}Sr)_i$ and showed little evidence (< 5%) of crustal interaction, whereas the rest scattered towards the Palmas rhyolite composition with modelled 'r' values of 0.1 to 0.6. Similarly the lava flows of the São Joaquim area also contain a group of samples that show only a slight variation in $(^{87}Sr/^{86}Sr)_i$ for a wide range in Mg# (see figure 4.18). This implies that they have undergone extensive crystal fractionation with little or no accompanying contamination and that the parental magma to this sequence was reasonably constant in composition. Figure 4.18 also shows that for the remainder of the flows the higher $(^{87}Sr/^{86}Sr)_i$ values tend to occur in the rocks with the lower Mg#, and at low Mg# there is a wider range in $(^{87}Sr/^{86}Sr)_i$ than the more primitive flows. The absence of any correlation between $(^{87}Sr/^{86}Sr)_i$ and stratigraphical position within the São Joaquim flow sequences suggests that the array of data on figure 4.18 was the result of random, temporal variations in 'r' rather than any changes in contaminant or parental magma composition.

Powell (1984) commented that AFC trends were rarely well defined (we have now seen that the Gramado magma type is no exception !), which was taken to be a reflection of the complexity of the actual physical processes involved. There has not been much consideration paid as to how the theoretical AFC model links with the physical processes operating within a magma chamber. In the mathematical formulation of the AFC process, DePaolo (1981) assumed a rather simplistic, idealised view of magma chambers by not taking into account the thermal and fluid dynamical behaviour within a magma chamber and the possible effects these might have on assimilation. It is possible that the chemical and thermal systems of igneous bodies are decoupled (Nielsen, 1988) such that only a relatively small fraction of the main mafic magma body which is providing the heat for melting actually mixes with the silicic melt produced from the country rock. Assimilation could occur at the chamber roof and walls driven by heat released by crystallisation within a magma that might not necessarily be able to 'see' this assimilated material, perhaps because of convective layering within the magma chamber. This would not only result in variable 'r' values in the erupted magma but might also allow 'r' values to be higher than that expected for the bulk system from thermal arguments. This is the situation envisaged by Grove and

Baker (1984) to explain the geochemical characteristics of the volumetrically minor andesites at Medicine Lake, since the high amounts of assimilation required ('r' > 1) violated simple heat budget calculations. Thermal arguments constraining the value of 'r' have been outlined by several authors (Taylor, 1980; Nicholls and Stout, 1982; Grove and Baker, 1984) and the consensus is that, for an upper crustal magma chamber and typical continental geotherm, the maximum value of 'r' allowable if heat balance is to be maintained is about 0.3-0.5. The heat required for melting depends on the temperature differential between the magma and wall rock, as well as their respective latent heats of fusion. If the country rock is hotter than in this typical upper crustal environment just mentioned, as is the case for a deeper crustal level chamber or alternatively as a result of a locally raised geothermal gradient, this would allow a greater amount of assimilation for the same extent of crystallisation, placing an upper limit on 'r' of 0.5 (Grove and Baker, 1984) to 1.0 (DePaolo, 1981). Presumably high 'apparent r' values can also be obtained from direct mixing although it is uncertain whether this process will always be recognised if it only occurs in minor amounts and is not the dominant control on the magmatic evolution.

When looking at the problems posed by contamination of the low-Ti magmas in the southern Paraná, most previous studies (*e.g.* Petrini *et al.*, 1987) have tended to view $(^{87}Sr/^{86}Sr)_i$ as an index of contamination and assumed that any samples with $(^{87}Sr/^{86}Sr)_i$ < 0.706 were essentially uncontaminated. Unfortunately other factors such as source mantle heterogeneities could also have affected $(^{87}Sr/^{86}Sr)_i$ and so Piccirillo and Cox (1988) pursued an alternative approach based on the fact that the SiO_2 content of a magma is buffered during the fractionation of a gabbroic crystal extract (Cox, 1980). The data set of low-Ti rocks was 'filtered' by SiO_2 content and all samples with SiO_2 less than 52.5 wt% were considered to be largely uncontaminated by acidic material. This enabled Piccirillo and Cox (1988) to assess the nature of the crystal fractionation process that had affected these 'uncontaminated' magmas. The almost constant Al_2O_3 and Sr with decreasing MgO confirmed the original assumption of gabbroic fractionation, though an inflection shown on a CaO vs. MgO diagram suggested that the evolution of magmas with MgO > 7 wt% was dominated by fractionation of just olivine and plagioclase. The strong

enrichment in TiO_2 and Fe_2O_3 indicated that no Fe-Ti oxide phases were involved, emphasizing that the crystal fractionation occurred with little effect on SiO_2 content and therefore any changes in SiO_2 could then be attributed solely to the assimilation of a rhyolitic contaminant. Because this group of low SiO_2 mafic magmas maintained a wide range in $(^{87}Sr/^{86}Sr)_i$ of 0.7046-0.710, Piccirillo and Cox (1988) postulated that this range of values had been present before contamination with a rhyolitic composition, and suggested that it was either inherited from the mantle source or that a second, non-rhyolitic crustal contaminant was involved.

In view of the work elsewhere in this chapter which has addressed the possibility of having separate, and distinct, low-Ti parental magmas as well as looking at the regional aspects of variability within these different magma types, a different perspective can be placed on the origin of the range in initial Sr isotopic ratios seen in these low-Ti rocks with $SiO_2 < 52.5$ wt%. The bulk of the variation largely reflects the inclusion of samples of both the Gramado and Esmeralda magma types in the data set used. The range in $(^{87}Sr/^{86}Sr)_i$ from 0.707-0.710 represents the regional variation seen within the parental magma of the Gramado magma type that was discussed above. Samples with $(^{87}Sr/^{86}Sr)_i$ of 0.704-0.707 are restricted to those of the Esmeralda magma type, and this is thought to involve interaction with a more depleted component, which will be dealt with in the next section.

4.7 Origin of the variations within the Esmeralda magma type.

Since it has now been established that the parental magma to the Esmeralda magma type was distinct from that of the main Gramado magma type, the final questions left to answer in this chapter are firstly what petrogenetic processes gave rise to the geochemical variation within the Esmeralda magma type, and secondly what is the origin of the Esmeralda parental magma.

Several key geochemical features of the Esmeralda magma type were introduced in section 4.6.2 and these must be accounted for in any petrogenetic model. The most striking

characteristic displayed by the Esmeralda magma type is the large range in ratios of incompatible trace elements {*e.g.* La/Hf, Sm/Nd on figure 4.12; La/Sm on figure 4.15}. These changes in incompatible trace element ratios are also strongly coupled with Sr and Nd isotope variations {*e.g.* La/Nd vs. $^{143}Nd/^{144}Nd$ on figure 4.16}. It is important to note that by contrast, there is only a poor correlation of major and trace element contents with isotope compositions. For trace elements, figure 4.11(b) earlier showed the lack of any systematic correlation between $(^{143}Nd/^{144}Nd)_i$ and 1/Nd, and the poor relationship for the major elements is demonstrated in Figure 4.22 with $(^{87}Sr/^{86}Sr)_i$ and Mg#.

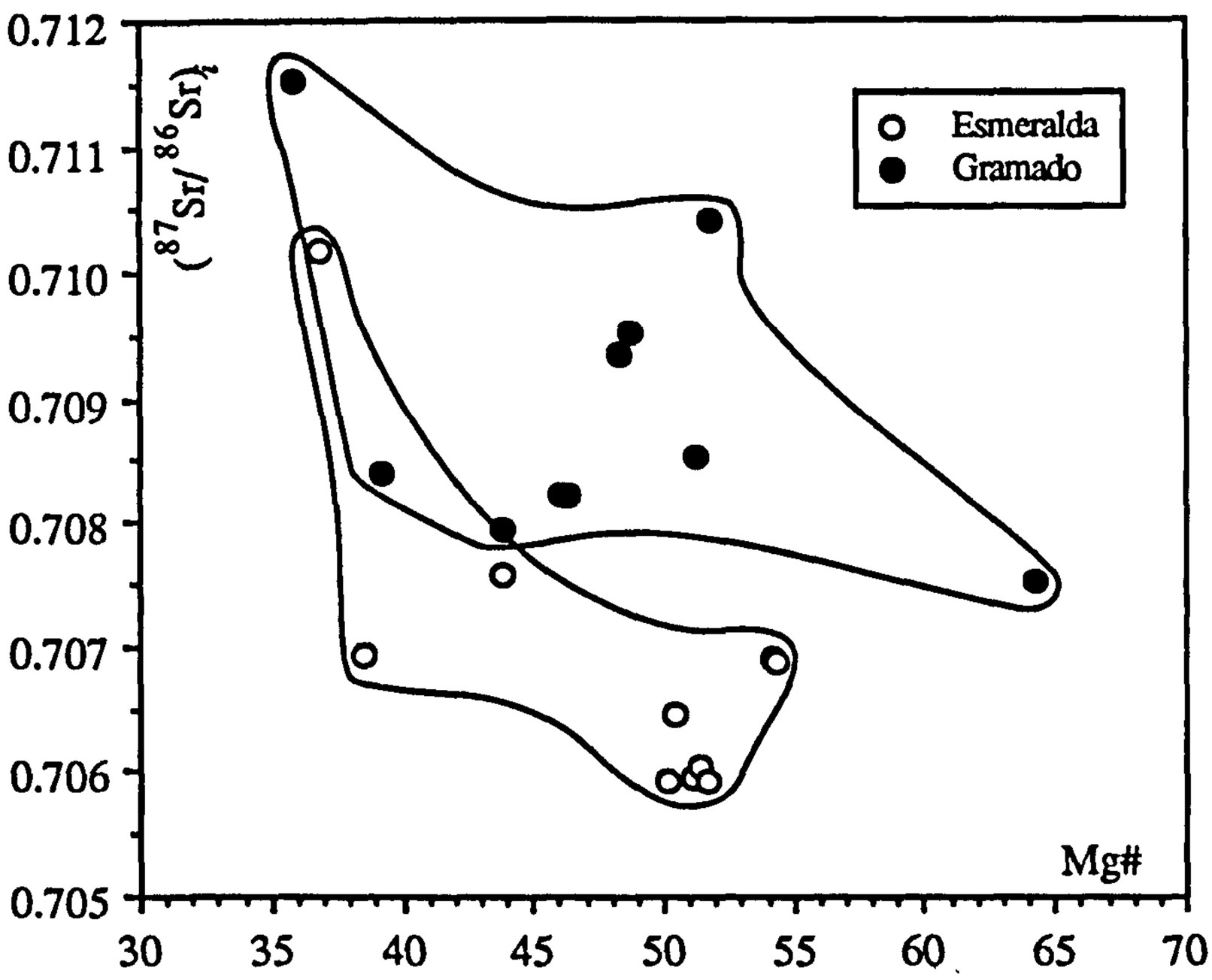

Figure 4.22 Variation of $(^{87}Sr/^{86}Sr)_i$ vs. Mg# for the Gramado and Esmeralda magma types, showing the poor relationship between major elements and isotopes for the Esmeralda-type magmas.

The major and trace element data discussed in section 4.2 above were qualitatively consistent with the effects of fractional crystallisation, but fractional crystallisation on its own cannot account for the large changes in ratios of incompatible trace elements. Although the linear increase in La/Sm with increasing La, shown in figure 4.15 is reminiscent of a partial melting trend (Allègre and Minster, 1978), these magmas are all relatively evolved, and the consistent shift in Sr and Nd isotopic composition along this trend is difficult to

explain by variations in the degree of partial melting. The conclusion to be drawn from this must be that, at least in terms of its isotopic and trace element ratios, the Esmeralda magma type represents some form of mixing array. Since the major and trace element abundances seem to indicate a role for crystal fractionation also, the relative timing of the mixing and fractional crystallisation processes need to be addressed.

The first possibility to consider is that the variations within the Esmeralda magma type are analogous to those of the Gramado magma type and were caused by an AFC-style of contamination, although starting with a different parental magma. The AFC process, from its very definition, involves concurrent crystal fractionation and mixing, and for an AFC-style of contamination, a parameter that reflects the degree of contamination/mixing (*e.g.* highly incompatible trace element or isotope ratio) should correlate with an index of fractionation (*e.g.* Mg# or incompatible trace element abundance). In contrast to the Gramado magma type, it was demonstrated above that there is a lack of any convincing relationship between isotopic composition and major or trace element abundance within the Esmeralda-type magmas, and this rather argues against an origin for the Esmeralda magma type by AFC.

Even if it is assumed that the mixing process was AFC then there are other problems. If the contaminant affecting the Esmeralda magma type is taken to be the same as that for the Gramado magma type which, for this study, has been assumed to be represented by the composition of the Palmas rhyolites, then there are difficulties in reconciling the magnitude of the change in incompatible trace element ratios with the observed isotopic variations within the Esmeralda magma type. Simple mixing calculations should give a minimum estimate of the amount of contaminant needed to be added to a primitive Esmeralda magma to account for the full range in a particular incompatible trace element ratio. For example, to explain the variation in $(La/Sm)_N$ from 1.3 up to 2.1 requires the addition of ~28 % of a Palmas rhyolite composition with $(La/Sm)_N$ of 3.1, but using the Sr contents and $(^{87}Sr/^{86}Sr)_i$ data given in the figure caption of figure 4.10 for the Palmas rhyolite and a primitive Esmeralda magma, this would lead to a calculated $(^{87}Sr/^{86}Sr)_i >$ 0.7093 compared with the observed $(^{87}Sr/^{86}Sr)_i$ of about 0.7070. Using forward

modelling techniques, it is possible to force an AFC curve through the Esmeralda magma type data on the La vs. $(La/Sm)_N$ diagram of figure 4.15. Generally it was found that La increased too fast for the concomitant increase in $(La/Sm)_N$, thus making the model curves lie below the actual data trend, even when allowing for a large difference in bulk distribution coefficients for La and Sm {D_{La} 0.01-0.05; D_{Sm} 0.15-0.20}. This could be remedied by increasing the value of 'r' but reasonable fits to the data were only obtained when 'r' was greater than 0.6 or alternatively if the contaminant had a higher $(La/Sm)_N$ than the Palmas rhyolites. If the contaminant was indeed different to that affecting the Gramado magma type then one would have to appeal to a sudden change in both the parental magma composition and the nature of the contaminant at the transition from the Gramado to the Esmeralda magma type.

A more likely strategy is one of direct magma mixing plus subsequent crystal fractionation. Variable crystal fractionation superimposed on mixing trends will upset incompatible element abundances but leave inter-element ratios largely invariant. Thus, whilst there generally is a good correlation of incompatible trace element ratios with isotope ratios {*e.g.* $(^{143}Nd/^{144}Nd)_i$ vs. La/Nd; figure 4.16}, plotting either against an element abundance results in much poorer correlations. This is illustrated with figure 4.11(b) from earlier which demonstrates that any coherent mixing relationship between 1/Nd and $(^{143}Nd/^{144}Nd)_i$ has been disrupted by variable amounts of later crystal fractionation.

There appear to be three plausible end-members for a primitive Esmeralda magma to mix with; (i) a primitive Gramado magma, (ii) an evolved (and contaminated ?) Gramado magma, and (iii) a Palmas rhyolite. In general, the $(^{87}Sr/^{86}Sr)_i$ and $(^{143}Nd/^{144}Nd)_i$ data on figure 4.10 would be consistent with a mixing array involving any of these three end-member candidates. The curvature of a mixing trajectory on this diagram is controlled by the Sr/Nd ratios in the two end-members (see Langmuir *et al.*, 1978). The apparent linearity of the Esmeralda array on figure 4.10 might suggest similar Sr/Nd ratios in the two end-members, but there is sufficient scatter within the data array to accommodate quite a range in Sr/Nd. The most 'depleted' Esmeralda-type samples have Sr/Nd of about 10-12, although any fractionation of a plagioclase rich crystal extract will have decreased Sr/Nd.

For the Gramado magma type, the least contaminated magmas have Sr/Nd of about 16 compared with values of 7-11 in the more evolved and contaminated lavas. Therefore the Sr and Nd isotope data is rather ambiguous in placing constraints on the nature of the 'evolved' end-member.

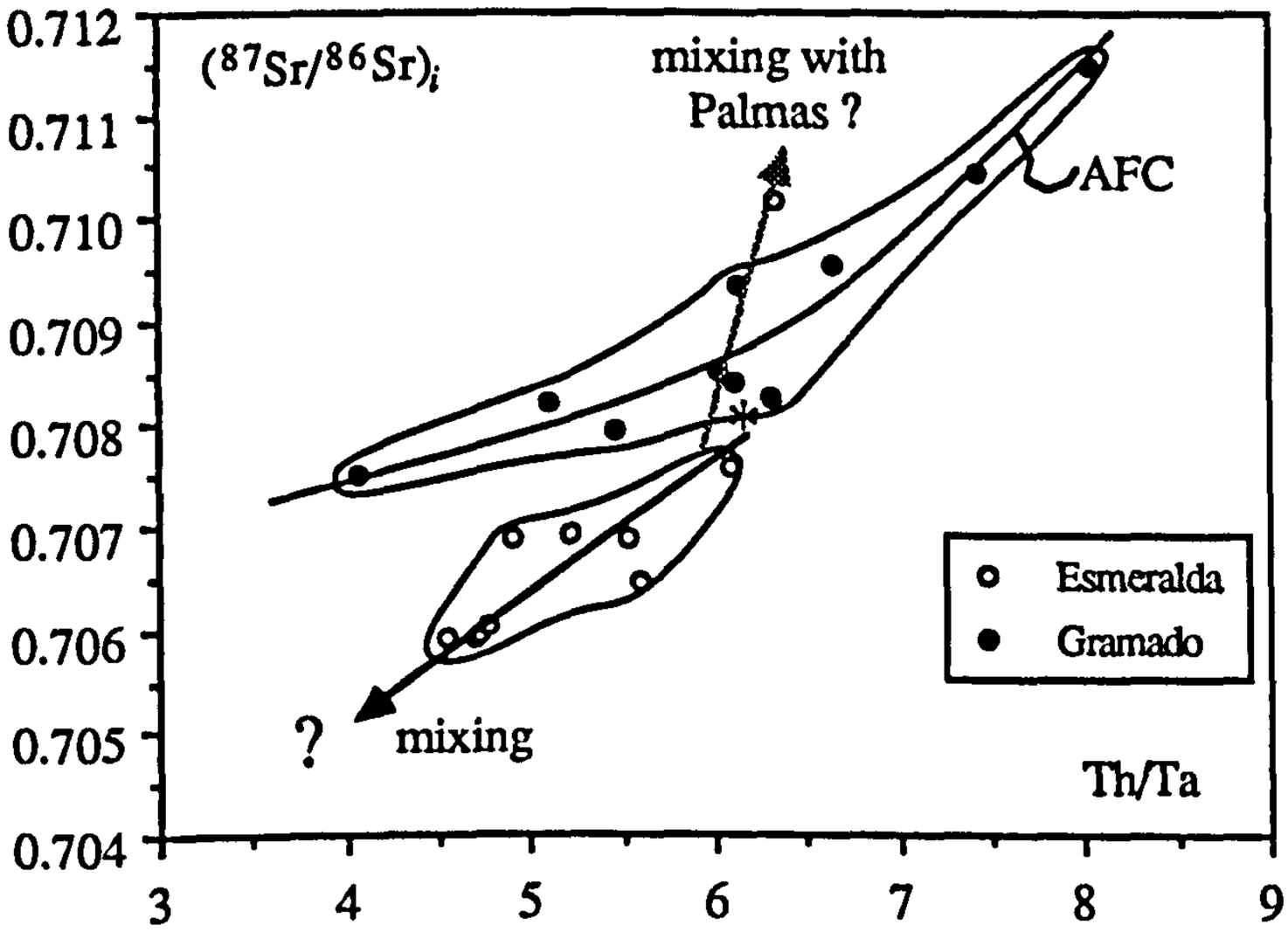

Figure 4.23 Variation of $(^{87}Sr/^{86}Sr)_i$ vs. Th/Ta for the Gramado and Esmeralda magma types. The Esmeralda-type samples show an increase in Th/Ta from 4.5 to 6.0 as $(^{87}Sr/^{86}Sr)_i$ increases from 0.7059 to 0.7075. This implies that the 'enriched' end-member cannot be a primitive 'uncontaminated' Gramado-type magma since this has Th/Ta ~4.0, and is more likely to be a more evolved, and contaminated, Gramado-type magma. The isolated Esmeralda-type sample (DW17) at high $(^{87}Sr/^{86}Sr)_i$ is consistent with simple mixing with a Palmas rhyolite magma.

A better discrimation is given by the $(^{87}Sr/^{86}Sr)_i$ vs. Th/Ta relationships illustrated in figure 4.23. Despite the most 'enriched' samples of the Esmeralda magma type having similar Sr and Nd isotopes to the parental (least contaminated) Gramado-type magma, figure 4.23 rules out the involvement of this parental Gramado magma type composition in causing the Esmeralda mixing array. The Gramado parental magma only has Th/Ta < 4.0 whereas the Esmeralda magma type shows an increase in Th/Ta from 4.5 to 6.0 as $(^{87}Sr/^{86}Sr)_i$ increases from 0.7059 to 0.7075. This constrains the 'enriched' end-member to have Th/Ta > 6.0 and $(^{87}Sr/^{86}Sr)_i$ > 0.7075, and therefore it must be either a contaminated Gramado magma or a crustal melt such as the Palmas rhyolites.

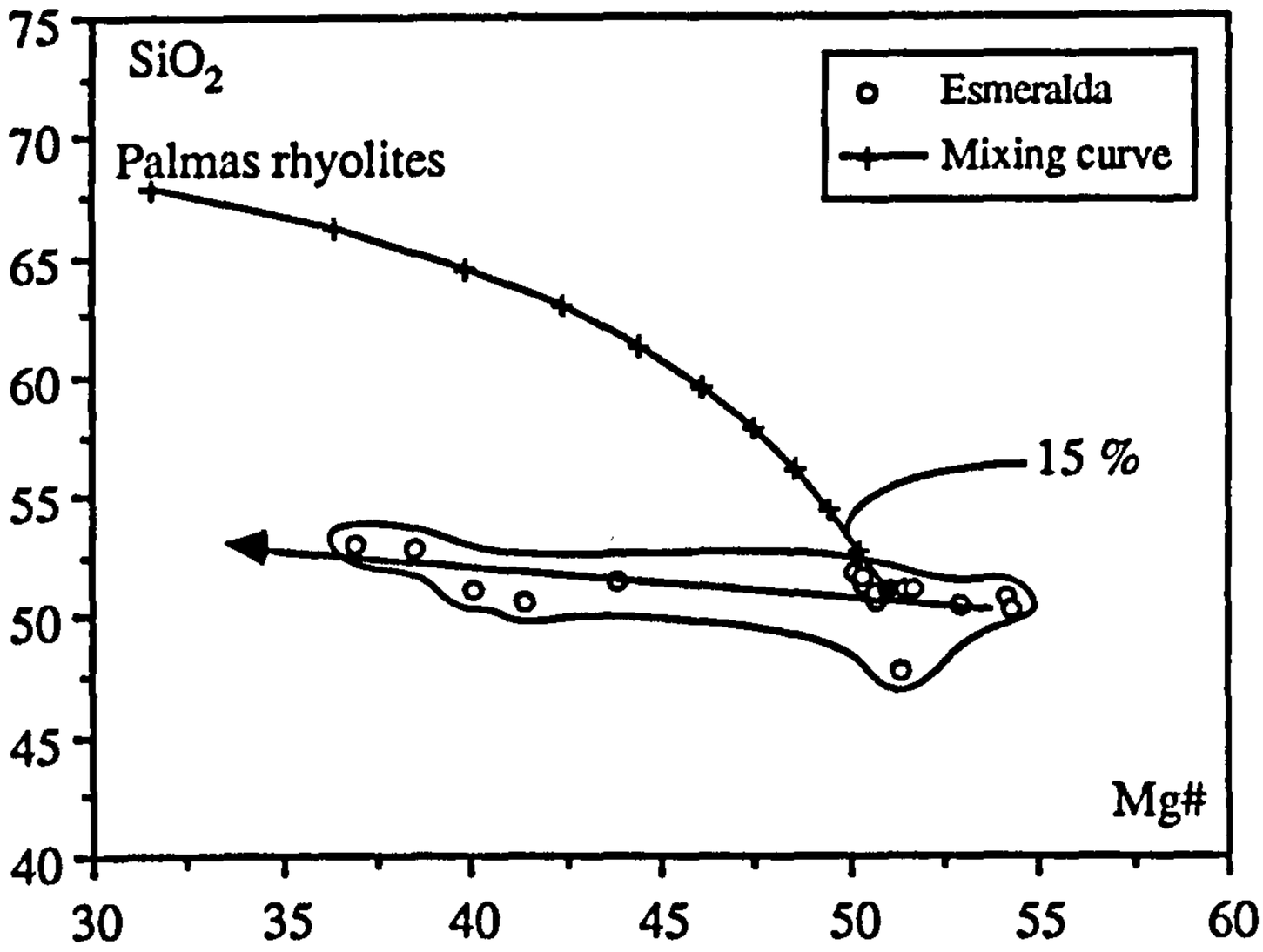

Figure 4.24 Variation of SiO_2 vs. Mg# for the Esmeralda magma type. A mixing curve between a primitive Esmeralda-type magma composition and average Palmas rhyolite has been superimposed; tick marks represent 10 % mixing intervals. The scatter within the Esmeralda data field constrains the maximum possible amount of rhyolite added to be about 15 %.

The general similarity in major element composition between the Gramado and Esmeralda magma types means that any mixing between these two basaltic magma types will not be apparent from major element data. In contrast, the major element data can be used to assess the possibility of mixing with a rhyolitic composition because of the disparity between fractionation vectors and mixing trends. Figure 4.24 of SiO_2 vs. Mg# illustrates the curvature of a mixing trajectory between a primitive Esmeralda composition and average Palmas rhyolite away from the gabbroic fractionation trend exhibited by the Esmeralda magma type as a whole. The scatter within the Esmeralda data set constrains the maximum amount of mixing to about 15 % rhyolite addition. To account for the Sr and Nd isotope data of the Esmeralda magma type by simple mixing with a Palmas rhyolite composition, using the same parameters as for the AFC model on figure 4.10, at least 20 % mixing is needed and this disagrees with the smaller amounts suggested by the major elements. To reach the low Mg# samples requires a large amount of subsequent fractionation since figure 4.24 clearly shows that addition of a rhyolitic composition does not have a great affect on Mg#, and this will not be the case if mixing is with a basaltic

component. The implication from this discussion is that the favoured candidate for the 'enriched' end-member to the Esmeralda array is an evolved and contaminated Gramado-type magma. Since it is unlikely that such a component could maintain a consistent composition over an area the size of the southern Paraná, this might lead to some regional scatter within the Esmeralda mixing trends.

There is some local evidence that Palmas rhyolite liquids might have been directly involved in mixing with Esmeralda-type magmas. Many of the previous diagrams have shown one sample in particular, DW17, which consistently plots away from the main Esmeralda compositional field. It has a notably higher $(^{87}Sr/^{86}Sr)_i$ of 0.71016 and a lower $(^{143}Nd/^{144}Nd)_i$ of 0.51224 than the other Esmeralda-type samples, and is also characterised by a marked Eu-anomaly (see figure 4.14). This suggests that it might have mixed directly with a Palmas rhyolite composition, which would be consistent with its stratigraphical position. DW17, which is from the 'RA' road section (see figure 2.16), is unique among the Esmeralda-type samples collected in this study in that it lies interbedded with Palmas rhyolites.

The composition of the other end-member in this mixing scenario, the so-called 'primitive' Esmeralda magma, is constrained by the samples with the most 'depleted' trace element and isotopic signatures, *i.e.* with $(^{87}Sr/^{86}Sr)_i < 0.7060$, $(^{143}Nd/^{144}Nd)_i > 0.51245$, $(La/Sm)_N < 1.4$, $La/Hf < 3.5$ and, in terms of the more readily available XRF trace elements, low Nb/Y, Ba/Y and high Ti/Zr, Zr/Nb etc. Magmas with these characteristics were widespread throughout the São Joaquim area, although occurring exclusively as sill-like intrusions into the main lava pile. It is unlikely that these magmas left their mantle sources without subsequent modification since their Mg#'s of 50-52 are much lower than the expected Mg# of 68-72 expected for a primary melt in equilibrium with a presumed mantle olivine composition of Fo-92 (Frey *et al.*, 1978). It is worth noting that several Esmeralda-type lava flows (ES 66, a borehole sample from this study; MV1 and MV11, Mantovani and Hawkesworth, 1988) are more primitive in terms of their major element compositions than this Esmeralda 'sill' composition, with Mg#'s of 53-54 but they contain more of the 'enriched' component since isotopically they have $(^{87}Sr/^{86}Sr)_i$ 0.7067-

0.7069 and $(^{143}Nd/^{144}Nd)_i$ 0.51229-0.51236. This is also clear from the diagram of La/Hf vs. Mg# given earlier (figure 4.13) where extrapolation of the Esmeralda trend would suggest that the samples with the lowest La/Hf originally would have had Mg# of at least 60. What is more important is whether the highly incompatible trace element and isotope ratios of these Esmeralda sills (ratios that would have remained invariant during any crystal fractionation or partial melting) were inherited from the mantle source and indeed represent the mixing end-member. The alternative would be that they represent a hybrid composition, with the true end-member lying at an even more 'depleted' composition still.

The Horingbaai dolerites in Namibia have a very distinctive composition compared to other Etendeka magmas, and Erlank *et al.*, (1984) have shown that they bear strong chemical and isotopic similarities to MORB. Since they are intrusive into the Etendeka lava sequences, although similar in radiometric age (see chapter one), they are evidence that such 'depleted' material was available during the Paraná/Etendeka magmatic event. New major and trace element data have recently been added to the initial reconnaissance survey results of Erlank *et al.*, (1984) by Duncan *et al.*, (1988) who show that the Horingbaai dolerites have low SiO_2 (47-49 wt%), TiO_2 (1.0-1.7 wt%) and Zr (50-100 ppm) with a range in Mg# of 65-53. The intricacies of the geochemical variations within the Horingbaai dolerites have not yet been investigated in detail and only the most primitive samples have been studied isotopically. Sample KLS-145 of Erlank *et al.*, (1984), although not the most primitive Horingbaai dolerite, is the most 'depleted' in terms of its trace element and isotopic ratios. These had almost flat chondrite-normalised REE patterns (Sm/Nd 0.29-0.30), with correspondingly radiogenic $(^{143}Nd/^{144}Nd)_i$ of 0.5128-0.5129 (ε_{Nd} +6 to +8) and, coupled with low $(^{87}Sr/^{86}Sr)_i$ of 0.703-0.7073 (ε_{Sr} -17 to -22), this places the Horingbaai dolerites within the MORB / OIB field {isotope data from Hawkesworth *et al.*, (1984) and Bristow *et al.*, (1984)}. Duncan *et al.*, (1988) give a range in $\delta^{18}O$ of +5.9 to +6.3 for the Horingbaai dolerites, similar to that deduced for the primitive mantle (Kyser *et al.*, 1982).

Similar intrusives to the Horingbaai dolerites have not, as yet, been encountered

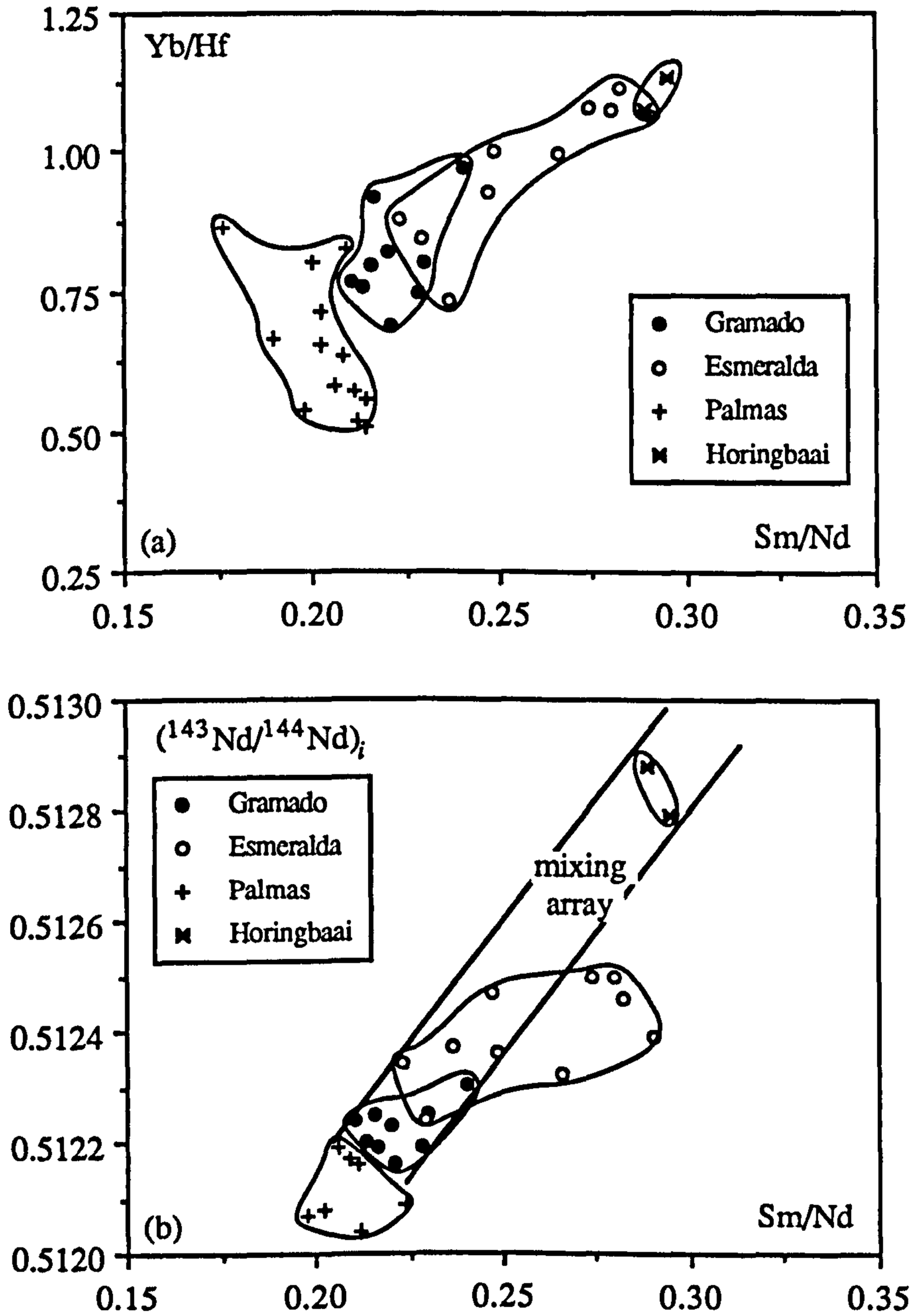

Figure 4.25 Variation of Sm/Nd vs. (a) Yb/Hf, (b) $(^{143}Nd/^{144}Nd)_i$. For incompatible trace element ratios, such as in diagram (a), the Horingbaai dolerites lie at the 'depleted' end of the Esmeralda mixing array. This is not consistent with the isotope data however, and in diagram (b) the Esmeralda type samples fall off a mixing array between the Horingbaai dolerites and the Gramado magma type, and are displaced to higher Sm/Nd.

within the Paraná province. Duncan *et al.*, (1988) state that the Horingbaai dolerites have only been found to the south of latitude 20° 45' S in Namibia and, allowing for closure of the South Atlantic ocean, the equivalent latitude in South America would be about 30° S. This is to the south of the Paraná lava escarpment in Rio Grande do Sul state in Brazil and,

if such dolerites are present in South America, the basement terranes along the coastal margin of Rio Grande do Sul and Uruguay will be the place to look.

Even though the presence of the Horingbaai dolerites demonstrates the local availability of 'depleted' material, it does not follow that they are necessarily representative of the actual 'depleted' component possibly involved in the Esmeralda mixing event. The major problem is the discrepancy between the trace element and isotope data. The Horingbaai dolerites have a trace element signature just slightly more depleted than the Esmeralda 'sill' compositions, and yet the isotope compositions are markedly different, being more akin to typical MORB / OIB asthenospheric values. This is illustrated in figure 4.25 with; (a) Yb/Hf vs. Sm/Nd, and (b) $(^{143}Nd/^{144}Nd)_i$ vs. Sm/Nd. The two Horingbaai samples lie at the end of the Esmeralda mixing array on figure 4.25(a), with Sm/Nd and Yb/Hf displaced to slightly higher values than in the Esmeralda 'sills'. On figure 4.25(b), the Horingbaai dolerites lie at much higher $(^{143}Nd/^{144}Nd)_i$ relative to the primitive Esmeralda 'sills', despite their almost identical Sm/Nd ratios. According to Langmuir *et al.*, (1978), mixing will always produce a linear array on such a ratio-ratio plot since both denominators are the same {*i.e.* $^{143}Nd/^{144}Nd$ and Sm/Nd}. A linear mixing curve has been drawn on figure 4.25(b) from the Gramado magma type, which plots as a restricted field, to the Horingbaai samples, and many of the Emeralda-type samples lie off the curve at higher values of Sm/Nd. If a more 'depleted' end-member to the Esmeralda mixing array really existed then this diagram suggests that it must have had Sm/Nd > 0.30. If this end-member had a similar $(^{143}Nd/^{144}Nd)_i$ to the Horingbaai dolerites then the Esmeralda array on figure 4.25(b) constrains its Sm/Nd ratio to be about 0.36 (*c.f.* Sm/Nd in Horingbaai dolerites of 0.29-0.30), which is in the range of N-type MORB (Sun and McDonough, 1989).

It is possible to account for the Sr, Nd and Pb isotope characteristics of the Esmeralda data trend by mixing between a Gramado-type magma and a component with the isotopic composition of the Horingbaai dolerites, provided that reasonable assumptions are made as to the elemental abundances of the relevent end-members. Figure 4.26 shows

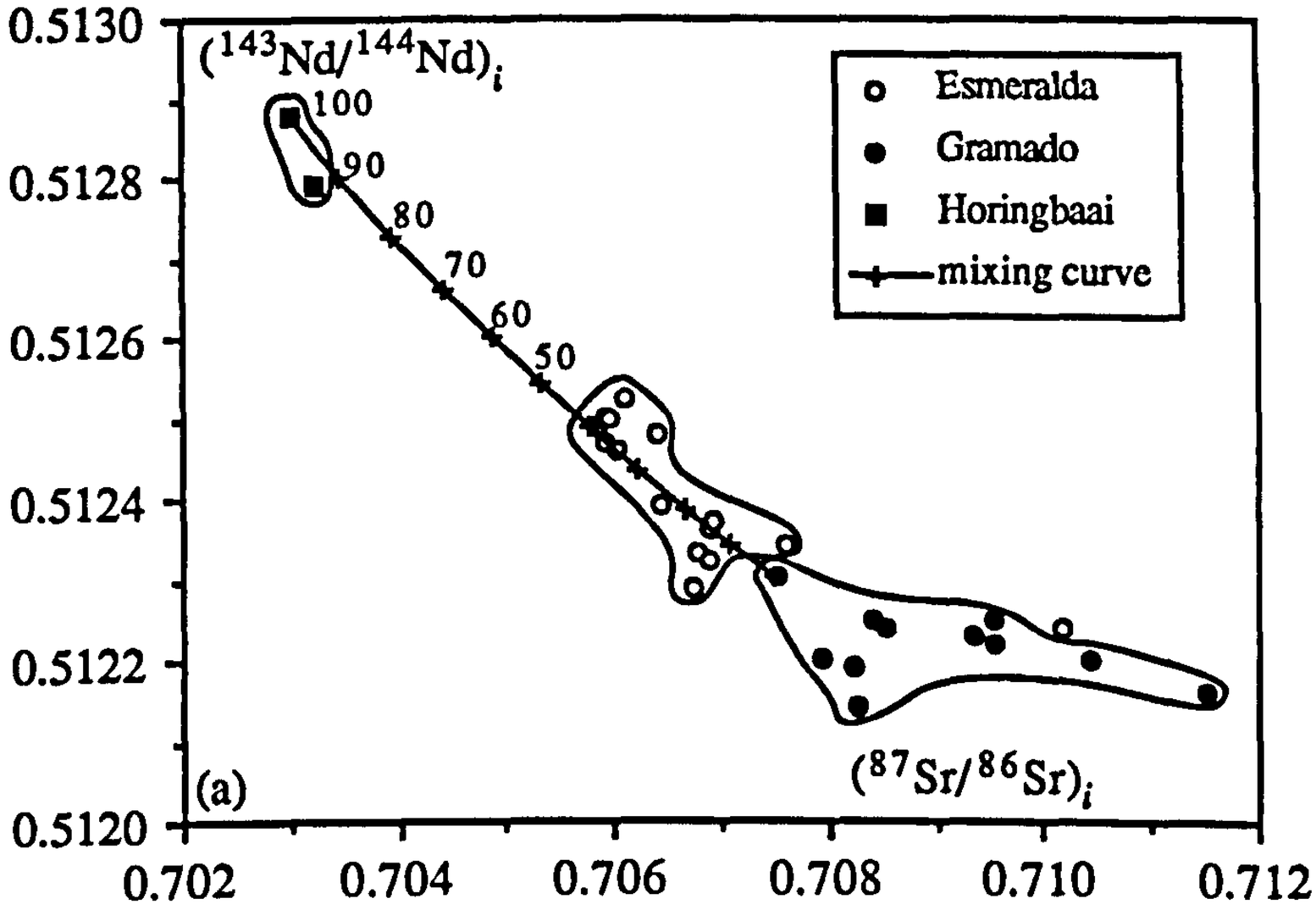

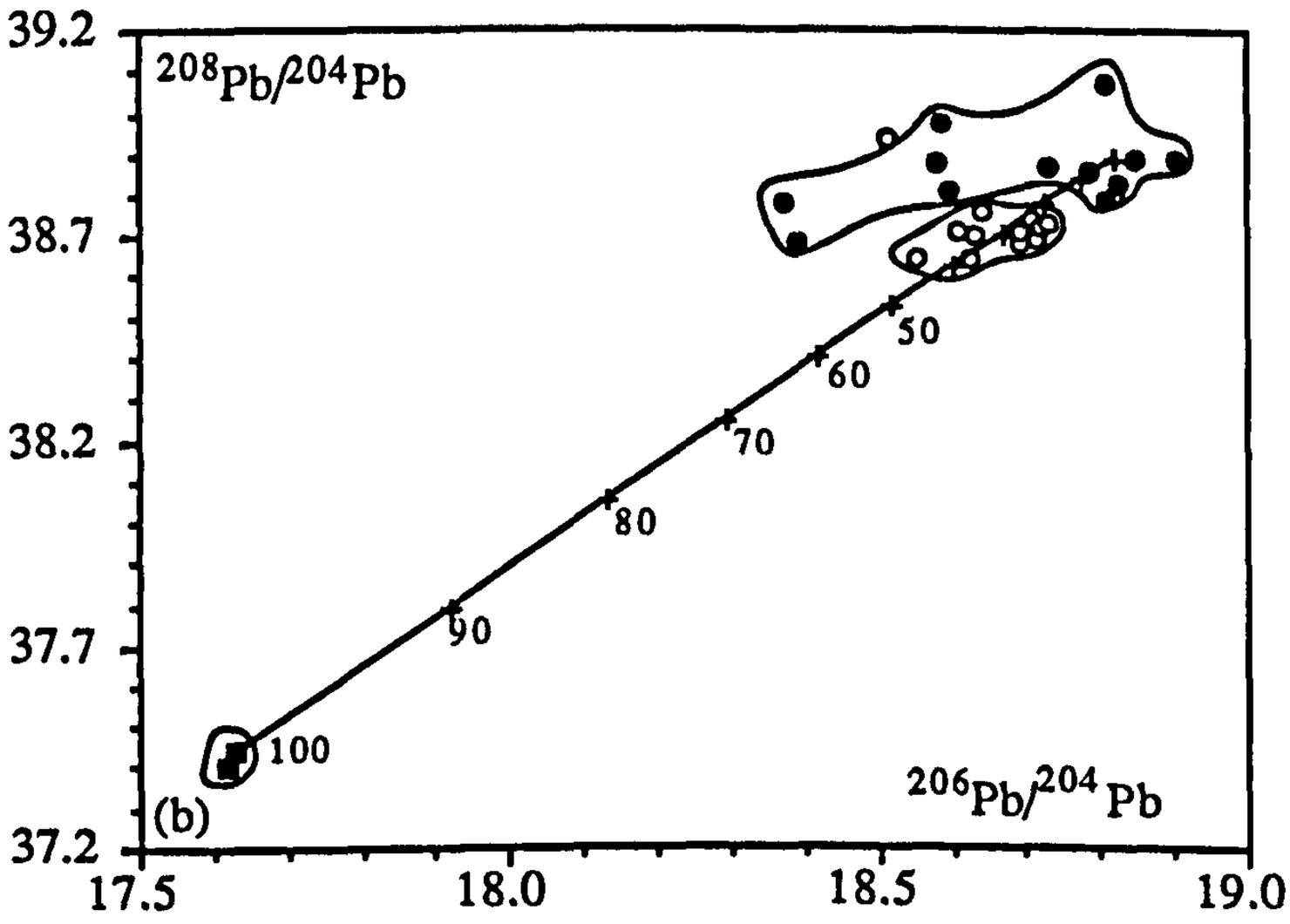

Figure 4.26 Possible mixing model to account for the Sr, Nd and Pb isotope compositions of the Esmeralda magma type. One end-member has the isotopic composition of the Horingbaai dolerites, and the other is a Gramado-type magma.

(a) Horingbaai dolerite - {Sr 193 ppm, $(^{87}Sr/^{86}Sr)_i$ 0.70299, Nd 7.4 ppm, $(^{143}Nd/^{144}Nd)_i$ 0.51288, Pb 1.0 ppm†, $^{206}Pb/^{204}Pb$ 17.62, $^{208}Pb/^{204}Pb$ 37.42}.

(b) Gramado magma type - {Sr 207 ppm, $(^{87}Sr/^{86}Sr)_i$ 0.7075, Nd 10.5 ppm, $(^{143}Nd/^{144}Nd)_i$ 0.51230, Pb 3.0 ppm, $^{206}Pb/^{204}Pb$ 18.82, $^{208}Pb/^{204}Pb$ 38.89}.

† Pb in KLS-145 (Erlank *et al.*, 1984) is 2.7 ppm, but this would imply a Ce/Pb ratio of 5.3 for the Horingbaai (Ce 14.2 ppm), *c.f.* MORB / OIB Ce/Pb is 25 ± 5. Therefore for Ce/Pb > 10, then Pb < 1.4 ppm.

possible mixing models for (a) $^{143}Nd/^{144}Nd$ vs. $^{87}Sr/^{86}Sr$ and (b) $^{208}Pb/^{204}Pb$ vs. $^{206}Pb/^{204}Pb$. Details of the mixing models are given in the figure captions. On figure 4.26(b) the Esmeralda-type samples are only slightly displaced below the Gramado-type compositional trend to lower $^{208}Pb/^{204}Pb$ values. This reflects the large contrast in Pb content between the two end-member compositions, and the low Pb content in the Horingbaai dolerites means that a large proportion of this component must be added in order to significantly affect the Pb isotopic composition.

Therefore, the Esmeralda magma type, which is a late-stage feature of the magmatism in the southern Paraná, appears to represent mixing between a Gramado-type magma and an end-member with a 'depleted' trace element and isotope signature more characteristic of asthenospheric melts.

4.8 Conclusions.

Although fractional crystallisation has played a major part in the evolution of the Gramado and Esmeralda magma types, their trace element and isotopic characteristics especially, are dominated by mixing processes.

The strong increase in SiO_2, K_2O and $^{87}Sr/^{86}Sr$ with the extent of magmatic evolution suggested that an AFC-style of crustal contamination was controlling the compositional variations within the Gramado magma types. From geological considerations, the average Palmas rhyolite composition was considered to be representative of a local crustal melt, and the addition of crustal material with this composition was at least consistent with the observed variations in the Gramado magma type.

A more contentious issue has been the composition of the 'uncontaminated' parental low-Ti (Gramado-type) magma. At first sight, the more 'depleted' Sr and Nd isotope composition of the Esmeralda-type samples might suggest that they represent less contaminated varieties of the Gramado magma type, but this was found to be untenable on

trace element grounds. Therefore, the temporal change in low-Ti magma type over the southern Paraná basin, from Gramado-type to Esmeralda-type magmas, was not caused by a waning in the extent of contamination but instead requires a more fundamental change in process to produce a distinct parental magma to each magma type.

A comparison of the data in this study from the São Joaquim area with those of Hawkesworth *et al.*, (1988) from the Caxias do Sul area ~ 200 km to the south-west, highlighted a marked regional geochemical variation within the Gramado magma type. The more southerly lavas have higher $(^{87}Sr/^{86}Sr)_i$ (> 0.709 vs. 0.707-0.709), SiO_2 and Ba/Nb, and this difference was apparently imposed prior to the AFC process, although the underlying cause for this variation is not well constrained at present. Even within a restricted area, to minimise the effects of this regional variation, the Gramado magma type does not display tight AFC trends. The range shown in $(^{87}Sr/^{86}Sr)_i$ is greater in the more evolved rocks than in the primitive samples, and it is suggested that this behaviour is controlled by a random variation in 'r' during the evolution of the lava sequence, dependent on the magma chamber dynamics.

The Esmeralda magma type is characterised by a wide range in incompatible trace element ratios which show a good correlation with Sr and Nd isotopic composition but not with elemental abundances. The favoured interpretation is one involving direct magma mixing with an evolved and contaminated Gramado-type magma, plus subsequent crystallisation. The 'depleted' end-member in this mixing event has $(^{87}Sr/^{86}Sr)_i < 0.706$, $(^{143}Nd/^{144}Nd)_i > 0.5125$ ($\varepsilon_{Nd} > +1$) and an almost flat chondrite-normalised REE pattern, indicating a strong asthenospheric component in these magmas.

Gramado and Esmeralda (low-Ti) magma types

Chapter 5

Geochemical relationships between magma types.

5.1 Introduction.

The previous two chapters have been restricted to understanding the cause(s) for the compositional variations that are observed *within* individual magma types. This chapter will now concentrate on attempting to assess the nature of the underlying petrogenetic process(es) that were responsible for the diversity *between* magma types. The initial classifications of the lavas (Bellieni *et al.*, 1984a; Mantovani *et al.*, 1985a) subdivided the basalts into high-Ti and low-Ti magma types, as outlined in section 2.3.1. This distinction probably represents the most important compositional difference within the Paraná lavas and its ultimate origin forms the subject for much of the following discussions.

The detailed lava stratigraphy provided by small scale studies within the São Joaquim field area in the southern Paraná (see section 2.5) has revealed the intimate association of high-Ti and low-Ti magmas, with lavas of the Urubici and Gramado magma types occurring as interbedded packets of flows. The petrogenetic origins of the high-Ti versus low-Ti distinction will be explored in this chapter with reference to the Urubici and Gramado magma types, as sampled within this limited study area. This follows the studies of Mantovani *et al.*, (1985a) and Hawkesworth *et al.*, (1986) who also used samples of the Urubici and Gramado magma types from this region as representative of the high-Ti and low-Ti magmas of the Paraná. Most other literature discussions that have considered this problem have tended to look at the province on a regional scale and assumed a rather simplified view of the geographical distribution of magma types. Thus they have generally contrasted the more dominant high-Ti rocks of the northern half of the province, *i.e.* the Pitanga magma type, with the southern low-Ti rocks, *i.e.* the Gramado magma type

(Fodor, 1987; Piccirillo *et al.*, 1988a). The high incompatible trace element contents that characterise the high-Ti magma types relative to the low-Ti magma types, are more pronounced for the Urubici magma type than for the Pitanga magma type, and thus the contrast between low-Ti and high-Ti flows within the road sections studied here is more accentuated than between the north and south of the province.

5.2 The role of shallow level processes.

Chapters three and four have already argued that the principal controlling factor on the compositional variation within each magma type was the operation of fractional crystallisation processes. The evolution of the Gramado magma type was dominated by open system behaviour with the involvement of crustal assimilation, and this had also affected some of the Urubici-type lavas although to a much lesser extent.

Whether or not fractional crystallisation can adequatetly explain the transition from the Gramado (low-Ti) to the Urubici (high-Ti) magma type may be assessed by considering the enrichment of certain trace elements in the Urubici magma type relative to the Gramado lavas, and this can be done by using the average compositions for these two magma types. Table 5.1 presents these averages and a list of enrichment factors for several elements, calculated simply by taking the ratio of the concentration of an element between the Urubici and Gramado magma types. Two factors act to make these estimates of the

	TiO_2	P_2O_5	K_2O	Rb	Sr	Zr	Nb	La	Ce	Ba	Y	Mg#
Gramado	1.55	0.23	1.37	47	263	181	14.8	22.3	51.0	402	37	44.4
Urubici	3.76	0.54	1.70	38	773	319	28	41.3	89.7	638	39	44.4
enrichment factor	2.4	2.4	1.2	0.8	2.9	1.8	1.9	1.9	1.8	1.6	1.1	

Table 5.1 Enrichment factors between the Gramado and Urubici magma types for a selection of minor / trace elements.

degree of enrichment rather conservative, especially for elements like Zr, Nb, La, Ce. Firstly, crystal fractionation from a Gramado parental magma to a primitive Urubici magma would be expected to decrease Mg#, and since the average compositions used had similar Mg#'s, the trace element levels in the average Gramado-type composition are too high relatively speaking. Secondly, removing the influence of crustal contamination from the Gramado-type composition will also reduce certain trace element levels in the average 'uncontaminated' magma composition and thereby increase the calculated enrichment factor. The enrichment factor (E.F.) for a highly incompatible element provides a minimum estimate of the extent of crystallisation if it is assumed that the bulk distribution coefficient for that element equals zero. The Rayleigh fractionation law can then be reduced to E.F.= 1/F, where F is the fraction of residual liquid. To account for trace element enrichment factors of about 2 by fractional crystallisation processes, crystallisation must have been extensive (> 50%, *i.e.* F < 0.5). It is difficult to accommodate such amounts of crystallisation since this would have substantially modified the major element composition, and the Gramado and Urubici magma types in fact have quite similar major element compositions (see table 2.3). The behaviour of Sr, which shows an enrichment factor of 2.9, rules out the extensive involvement of plagioclase in any postulated crystal extract, and similarly, the lack of depletion in the HREE and Y between the Gramado and Urubici magma types suggests the absence of any garnet fractionation.

A further demonstration of the inability of crystal fractionation to account for the compositional difference between the Gramado and Urubici magma types is given in figure 5.1. This shows the contrasting behaviour of a compatible element, Ni, compared with that of an incompatible element, Zr, during crystallisation and melting. The curves shown on figure 5.1 illustrate the marked difference for crystallisation and melting vectors on such a plot. During fractional crystallistion, the Ni concentration in a magma varies strongly relative to the change in Zr content, whereas the reverse is true during partial melting, independent of the residual source mineralogy, because the Ni content of the melt is

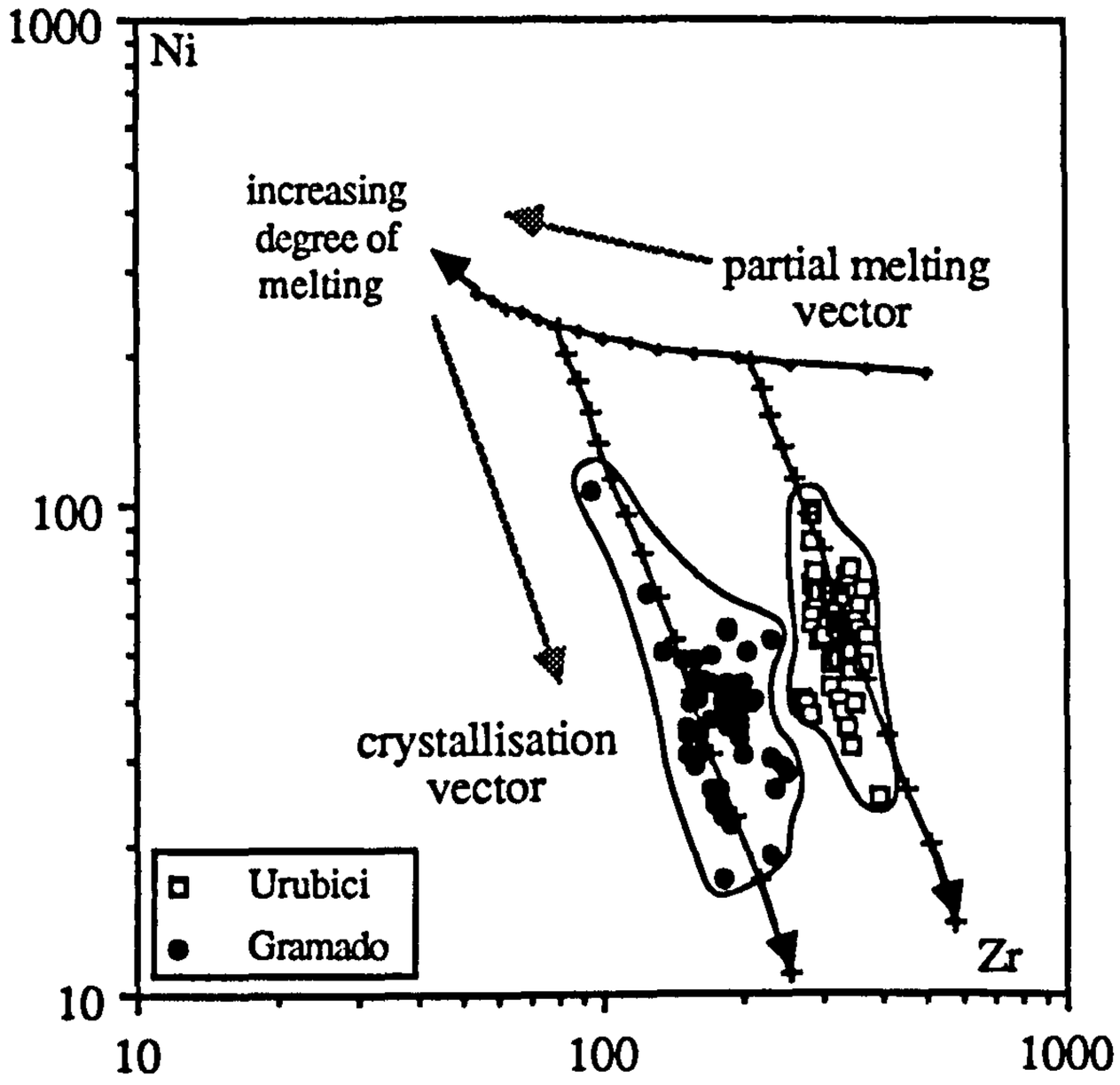

Figure 5.1 Ni vs. Zr variation for the Gramado and Urubici magma types illustrating the marked contrast in partial melting and fractional crystallisation vectors. Source mantle heterogeneities would lie on similar vector to melting curve because of buffering of Ni by olivine.
Melting curve parameters- source composition {Zr 20 ppm, Ni 2000 ppm}, D_{Zr} 0.03, D_{Ni} 10.9, tick marks at 2.5 % intervals
Crystallisation curve parameters - D_{Zr} 0.04, D_{Ni} 3.5, model parental Urubici {Zr 210 ppm, Ni 195 ppm}, model parental Gramado {Zr 80 ppm, Ni 230 ppm}, tick marks at 5% intervals.

buffered by residual olivine (Allègre and Minster, 1978). The displacement of the Urubici data field to higher Zr contents than in the Gramado magma type, for the same range in Ni content, is strongly suggestive of the existence of different parental magmas to each magma type; the Urubici magma type with about 200 ppm Zr and the Gramado magma type with < 100 ppm.

Crustal contamination is unlikely to be the cause of the observed difference between the Urubici and Gramado magma type. To produce a suitable parental Gramado-type magma from a primitive Urubici-type magma, then any contamination process must lead to an increase in SiO_2 and $^{87}Sr/^{86}Sr$, a marked decrease in TiO_2, P_2O_5, Zr, Nb, Ba, and LREE, whilst keeping K_2O and Rb essentially constant. It is difficult to explain these

elemental variations in terms of any realistic contamination models or contaminant compositions (see Duncan *et al.*, 1988).

Thus shallow level processes such as fractional crystallisation and crustal assimilation can be ruled as the major cause of the diversity between the magma types, and instead, these trace element arguments have illustrated the need for distinct parental magmas to the Gramado and Urubici magma types. Therefore the main geochemical difference must be attributed to a deeper level phenomenon, most likely in the mantle source region. The two most obvious suggestions (*e.g.* Bellieni *et al.*, 1984a; Mantovani *et al.*, 1985a; Fodor, 1987) would be to derive these distinct parental magmas either by varying degrees of partial melting of a homogeneous mantle source or by appealing to mantle heterogeneity, and on figure 5.1 both of these mechanisms would produce almost horizontal trends with little effect on Ni. The task of trying to more precisely determine the differences between the two parental magmas in order to address this problem is made more difficult by several factors. The largely non-primary, evolved nature of the Paraná lavas, as seen from their Mg#'s that are too low to have been in equilibrium with presumed mantle olivine {Gramado, Mg# < 65; Urubici, Mg# < 55} and low (< 100 ppm) Ni contents (see figure 5.1), emphasizes that the lavas have all undergone extensive fractionation since leaving their mantle source. Attempts to extrapolate lava compositions back to a possible primary magma composition will be fraught with difficulties since any modelling of this fractionation will be poorly constrained. Additionally, the Gramado magma type is dominated by the effects of crustal contamination, and there is still some disagreement amongst workers in the Paraná as to the composition of the pristine uncontaminated magma that can be inferred from modelling the removal of this crustal influence. Thus any assessment of these two alternative hypotheses will require a judicious choice of elemental and isotopic ratios in order to 'see-through' the modifying effects of shallow level fractionation processes.

5.3 Variable degrees of partial melting of a single mantle source.

5.3.1 Methodology.

The partial melting hypothesis assumes that the average composition of the mantle beneath southern Brazil is homogeneous over the length scale sampled by the melting process, and that melts of differing compositions, *viz.* the Urubici and Gramado magma types, can be derived from this single source just by varying the degree of partial melting. Theoretical partial melting models based on highly idealised assumptions of the melting regime have been developed by several workers to allow a description of the behaviour of trace elements during melting (see review in Wood and Fraser, 1976). The simple cases of fractional melting and equilibrium (batch) melting are two extreme models that represent the limiting conditions for a range of possible intermediate and more realistic melting processes. During fractional melting, infinitesimally small increments of melt are continuously extracted from the solid residue the instant they are formed. In contrast, equilibrium melting requires the partial melt produced to remain interstitially within the source matrix and to undergo continuous re-equilibrium with the residual solid phases until mechanical conditions allow it to be removed as a single batch of primary magma. More complex and physically more realistic models than these have been proposed to try and account for certain trace element characteristics found in specific geological situations. These include incremental batch melting (Wood and Fraser, 1976) which involves the repeated extraction of melts each formed by equilibrium processes from the same source, and dynamic melting (Langmuir *et al.*, 1977) which is a continuous melting process where a certain proportion of the melt at each stage is trapped within the source material to mix with the next formed melt.

With such a wide spectrum of melting models available, it is important to understand to what extent a specific choice of model will influence any conclusions for example as to the inferred degree of melting, especially if the model is too simple in light of the presently understood picture of the physical mechanisms of melting. The melting process, as outlined by McKenzie, (1984, 1987), involves two stages; melt generation and

melt migration. As the melt is produced, it will form an interconnected network, no matter how small the melt fraction may be, and hence any compaction of the matrix will expel the melt from the residual solid phases. The mobility of the melt is governed by its viscosity. Basaltic melt fractions greater than 2 % will rapidly separate from the matrix, which therefore places a constraint on the maximum melt fraction likely to be present in the source during partial melting. A further complication to the whole process in the continuous interaction of the melt with the matrix during segregation which leads to geochemical behaviour analogous to an ion-exchange column. Richter (1986) tackled the problem of the suitability of standard trace element partial melting models by creating a synthetic geochemical data set that was calculated using a dynamic model for melt production and segregation from a deformable matrix (after McKenzie, 1984). This data set was then used to test how well the simple models of equilibrium or fractional melting could recover the actual degree of melting and original source composition. He was surprised that these simple models worked as well as they did, especially when applied to physical situations quite different from those assumed in their derivation. These models assume either that melts do not move relative to their source (equilibrium melting) or that they are instantaneously removed (fractional melting) whereas the real situation is one in which melts migrate at a fixed rate and continuously interact with the matrix as they pass through it.

For the Paraná lavas, the main interest is just to see whether partial melting is a viable means of explaining the gross trace element features that distinguish the high-Ti and low-Ti magma types. The absence of any plausible candidates for primary magma status among the lavas means that there is little point in investigating the fine scale structure of trace element distribution patterns between the two magma types. Thus for the purpose of this study, trace element modelling will be restricted to using the simpler model of equilibrium (batch) melting. For the equilibrium melting model, the variation in the concentration of a trace element in the melt as a function of the initial source composition and degree of partial melting is given by the expression below, taken from Shaw (1970);

$$\frac{C_l}{C_o} = \frac{1}{D + F(1 - P)}$$

where; C_l concentration of element in the melt.

C_o initial concentration of element in the source prior to melting.

F mass fraction of melt formed.

D bulk crystal/liquid distribution coefficient for that element for the initial phase assemblage.

P bulk crystal/liquid distribution coefficient for that element for the minerals entering the melt.

D and P are defined as $\sum_{i=1}^{n} w_i.K_{Di}$ and $\sum_{i=1}^{n} p_i.K_{Di}$ respectively, where

K_{Di} is the partition coefficient for the element between phase *i* and melt, w_i is the weight fraction of each phase *i*, and p_i represents the fraction of liquid contributed by each phase during melting.

The subtle difference in definition between the terms D and P takes account of the fact that the melting will probably be non-modal, *i.e.* the minerals in the source rock will not melt in their modal proportions, and similarly it is also possible that the contribution of each phase to the melt formed (*i.e.* p_i) may vary during melting. Many studies have made the simplifying assumption of modal-melting and this has meant that, since $w_i = p_i$ and therefore D = P, the above equation can be expressed as;

$$\frac{C_l}{C_o} = \frac{1}{D + F(1 - D)}$$

This simplified equation can also be applied to the non-modal melting situation provided that D is calculated in terms of the residual mineralogy at the time of melt removal rather than for the initial source conditions.

The partial melting process, independent of which particular model is used, is able to exploit small differences in bulk distribution coefficient between elements and so produce significant fractionations of trace element ratios that would remain almost invariant during any crystallisation process. A consequence of the partial melting equations is that

large degree melts will inherit incompatible trace element ratios similar to the source material and have relatively low contents of such elements, whereas smaller degree melts can lead to large fractionations of trace element ratios and they are enriched in incompatible elements.

Calculations based on this melting model are strongly dependent on the choices made for the composition and mineralogy of the mantle source, and the relative contribution of the mantle phases to the melt (*i.e.* modal vs. non-modal melting). It is difficult uniquely to constrain the degree of melting that could give rise to a specific melt composition. Trace element modelling using the above equation to explain the compositional difference between two magma types will only lead to a relative difference in the degree of melting responsible and not an absolute value for each one. This arises because the concentration of an element in the source material (C_o) is featured in the equation and is generally an unknown variable (although reasonable guesses can often be made). The form of the equation produces a situation where there is a play-off between having a trace element enriched source and higher degrees of partial melting as opposed to a depleted source coupled with lower degrees of melting. Therefore an independent method of constraining either the degree of melting or the source composition is required.

One avenue of approach has been through experimental petrology. The major element composition of a melt is governed by the source material, the P,T conditions of the melting regime and the extent of melting. These have been extensively investigated using a variety of experimental techniques and conditions, on a number of plausible source compositions. There is a general consensus among the different groups that a degree of melting in excess of 10 % (perhaps up to 40 %) are required in order to produce melts that are tholeiitic in character (*e.g.* Mysen and Kushiro, 1977; Jaques and Green, 1980; Takahashi and Kushiro, 1983). Exactly how such a degree of melting relates to the actual physical mechanism of partial melting is not clear, especially since McKenzie (1987) has shown that, at a maximum, only about 2 % melt can be in equilibrium with its source matrix at a given time. Presumably the 10 % melt represents the integrated effects over a number of accumulated smaller degree melts.

Geochemical relationships

The choice of mineralogy for the proposed mantle source should reflect the observed mineralogy of typical mantle materials such as the abundant mantle xenolith types sampled by kimberlites. In addition, the behaviour of certain trace elements can help to constrain the residual mineralogy of the source if they are controlled by a specific mineral phase (*e.g.* HREE and Y are compatible in garnet). The inversion technique, pioneered by Minster and Allègre (1978) and developed subsequently by Albarède (1983) and Hofmann and Feigenson (1983), uses the variations in trace element concentration in a cogenetic suite of samples to compute the composition and mineralogy of the source. This approach solves the batch melting equation simultaneously for a large number of elements and produces a self-consistent, but not necessarily unique, solution. Unfortunately this method is only really applicable if the suite of lavas are primary or near-primary magmas, a feature sadly lacking for the products of the Paraná magmatism.

5.3.2 Review of previous melting models for the Paraná.

The only published partial melting models have been concerned with trying to explain the gross trace element differences between the low-Ti (Gramado) and high-Ti (Pitanga) magma types. Fodor (1987) investigated a scenario in which the low-Ti and high-Ti magma types were derived from parental picritic melts that had been generated from a common mantle source by different degrees of partial melting. In a detailed treatment that considered both major and trace element data, he suggested that 11 % and 25 % were plausible degrees of melting to produce the high-Ti and low-Ti parental picritic melts respectively, which could then be related to typical high-Ti and low-Ti basalts via extensive (~60-70 %) fractional crystallisation of olivine ± clinopyroxene ± plagioclase. The trace element contents of the picritic melts were modelled using the non-modal equilibrium batch melting equation, with an assumed mantle source mineralogy of just ol / opx / cpx (60 / 25 / 15) and the hypothetical proportions in which these phases contributed to the melt were set at 10 / 10 / 80. The major element contents (SiO_2, Al_2O_3, FeO, MgO, CaO) of the picrites were based on experimental 11 % and 25 % melt compositions from a lherzolite source taken from Jaques and Green (1980), whereas TiO_2, P_2O_5, K_2O were included with the trace elements. The major element compositions of the picrites, and

plausible mineral compositions, were needed for fractional crystallisation least-squares mixing calculations to model the evolution to the erupted basalt compositions, since these results were then used to constrain the trace element compositions of the parental picritic melts. An estimate of the trace element composition of the source was obtained by back-calculation using the assumed percentage of melting and plausible K_D values, and it appeared to be consistent with 'enriched' mantle material of Wood (1979).

As with any such study, the results are model-dependent and although this whole model gave an internally consistent picture for the Paraná magmas considered, there are a number of difficulties with it. The observed and calculated trace element contents for the high-Ti basalts were in reasonable agreement but this was not the case for the low-Ti basalts where Rb, Sr, Ba, K, and Ti all gave poor matches. Fodor (1987) rather casually dismissed this as being the result of crustal assimilation, a process which had already been documented for the Gramado (low-Ti) magma type, although unfortunately this was not given any further detailed consideration. If this is to be attributed to crustal contamination, then it must have been a separate, and earlier, event to the AFC process that dominates the compositional variation within the erupted Gramado-type lavas, following the discussions in chapter four of the contamination affecting the Gramado magma type. The likelihood of such an event will be considered in the next section. A more critical observation is that the chosen parameters of the melting model are flawed, since they lead to clinopyroxene being exhausted in the source after 18.75 % melting. Therefore the trace element composition of the low-Ti picrites, which Fodor (1987) suggested had been produced by 25 % melting, could only have been controlled by the residual phases of olivine and orthopyroxene alone, which would alter the modelled composition given in the paper. The lack of residual clinopyroxene control on the melts required a LREE enriched source composition in order to achieve the LREE enrichment seen in the magmas.

The study of Piccirillo *et al.*, (1988a) which expanded on the earlier investigation of Bellieni *et al.*, (1984a) considered the consequences of two different possible residual mantle mineralogies, and used the equilibrium melting model to attempt to account for the enrichment factor for La/Y, Ba/Y, Zr/Y of about two between the low-Ti and high-Ti

magma types. The first case assumed a residual mantle mineralogy of spinel peridotite with ol / opx / cpx / spinel in the proportitions 60 / 25 / 10 / 5 and from this it was inferred that the high-Ti basalts were related to parental melts produced by very low (~3 %) degrees of melting compared to the higher percentage melts (~25 %) parental to the low-Ti basalts. The second case looked at a garnet-bearing residual mantle source with ol / opx / cpx / garnet in the proportitions 60 / 25 / 10 / 5 and suggested values of about 12 % and about 40 % melting for the high-Ti and low-Ti magma types respectively. Since the difference in partition coefficient (K_D values) between Y and La, Ba, Zr is greater for garnet than spinel, this meant that the melting scenario which involved residual garnet rather than residual spinel did not require such low degrees of melting.

Piccirillo *et al.*, (1988a) took the view that, if it was accepted that tholeiitic melts required degrees of melting in excess of 10 % (*e.g.* Mysen and Kushiro, 1977; Jaques and Green, 1980; Takahashi and Kushiro, 1983) then the origin of high-Ti and low-Ti primary melts appeared to be more compatible with a garnet peridotite source which left garnet as a residual phase. Because of this difference in percentage melting required for the generation of the two magma types, it was argued that the original source material must have been quite different in terms of initial modal mineralogy. This is a result of the melting process being non-modal since the melting coefficients (*i.e.* p_i, a measure of the contribution of a particular mineral to the melt) for the various mantle phases are substantially different (Mysen, 1976). In the end, Piccirillo *et al.*, (1988a) therefore concluded that the high-Ti and low-Ti magma types were derived from different mantle material.

The next section will see whether any fresh insights into the plausibility of the partial melting hypothesis can be obtained by looking at the new trace element and isotopic data generated during this study.

5.4 New isotopic and trace element constraints on partial melting models.

5.4.1 Radiogenic isotopes.

Studies of radiogenic isotope compositions can place important constraints on the feasibility of a single mantle source to the Urubici and Gramado magma types because under closed system conditions, these isotopic ratios will remain invariant during any partial melting process and subsequent evolution of the melt. The Sr, Nd and Pb isotopic compositions of the main southern Paraná magma types are illustrated in figure 5.2 and 5.3, using data from this study, Mantovani *et al.*, (1985a) and Hawkesworth *et al.*, (1986, 1988).

Figure 5.2 shows the coupled variation of $(^{143}Nd/^{144}Nd)_i$ with $(^{87}Sr/^{86}Sr)_i$, expressed in the epsilon notation which represents the sample deviation from bulk earth estimates (DePaolo and Wasserburg, 1976). The Urubici-type samples have a relatively

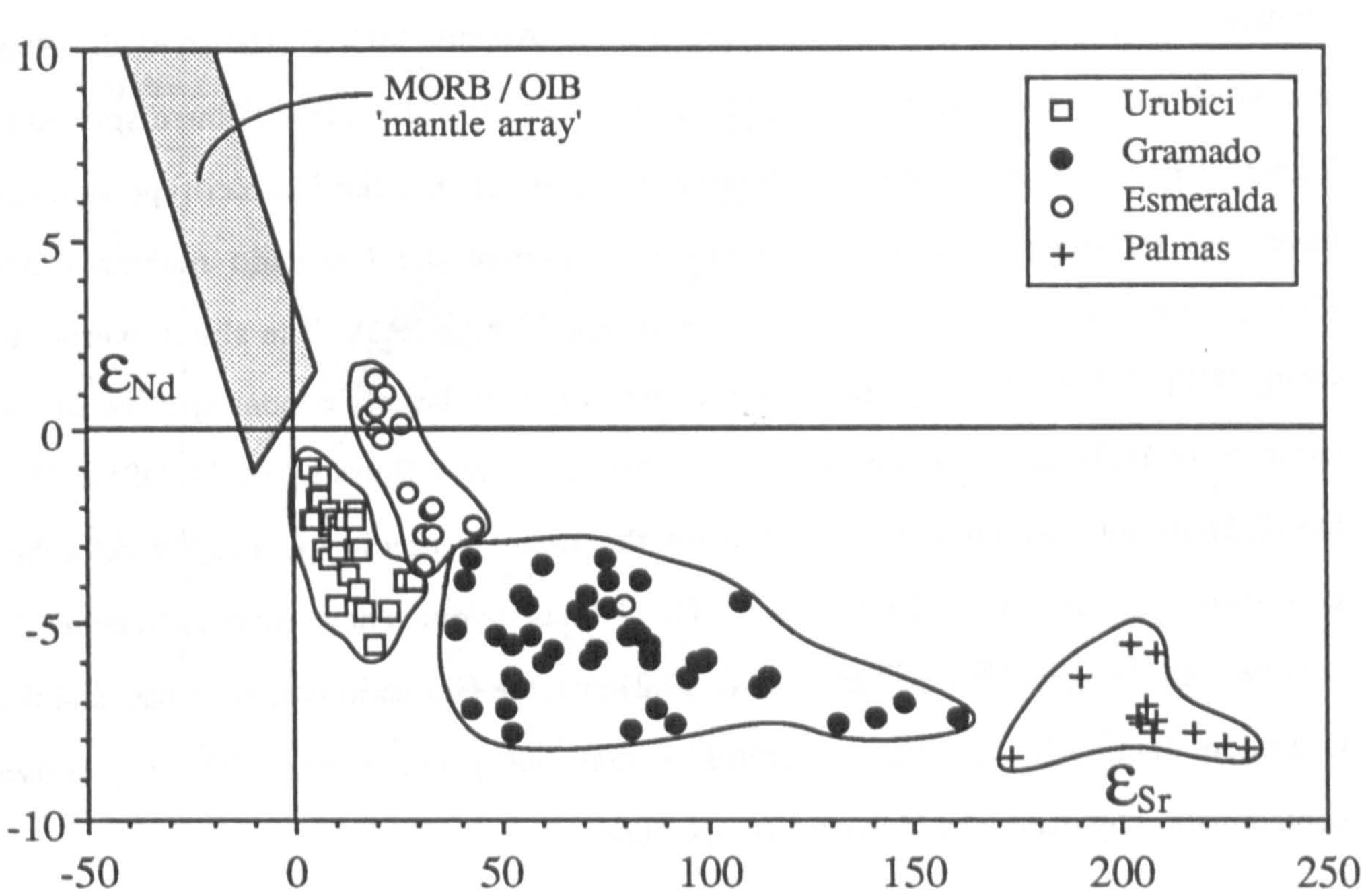

Figure 5.2 ε_{Sr} vs. ε_{Nd} diagram for the main Paraná magma types. Data sources - {this study, Hawkesworth *et al.*, 1986, 1988}.

restricted range in both ε_{Sr} (4 to 29) and ε_{Nd} (-1.0 to -5.5) and plot on an extension of the so-called 'mantle-array' which is loosely defined by the MORB / OIB data. The Gramado-type samples are displaced to the right of the Urubici data field on figure 5.2, with slightly lower ε_{Nd} (-2.5 to -7.8) and higher, and more variable, ε_{Sr} (40 to 160). They define a relatively flat-lying trend which reflects the progressive crustal contamination by material similar in composition to the Palmas rhyolites (ε_{Sr} 160 to 230; ε_{Nd} -5.5 to -8.4). Samples of the minor late-stage Esmeralda magma type define a linear trend from the least contaminated Gramado-type samples towards the MORB / OIB field, and have a range in ε_{Sr} of 18 to 43 and ε_{Nd} of 1.4 to -3.5. It was argued in chapter four that this was not a crustal contamination trend but instead it was controlled by mixing of a Gramado-type magma with more 'depleted' asthenospheric material.

Figures 5.3(a) and 5.3(b) show the variation in $^{207}Pb/^{204}Pb$ vs. $^{206}Pb/^{204}Pb$ and $^{208}Pb/^{204}Pb$ vs. $^{206}Pb/^{204}Pb$ respectively. The Pb isotope data for the Paraná lavas as a whole, define reasonable linear arrays on both diagrams which are sub-parallel to the MORB data field {represented by analyses of South Atlantic MORB (Hanan *et al.*, 1986) and the N.H.R.L.- northern hemisphere reference line, from Hart (1984)} but displaced to higher $^{207}Pb/^{204}Pb$ and $^{208}Pb/^{204}Pb$ respectively. In general, the Urubici-type samples have less radiogenic Pb isotopic compositions than the Gramado magma types {$^{206}Pb/^{204}Pb$ - Urubici 17.1 to 18.3 vs. Gramado 17.9 to 19.1}. The slight overlap in $^{206}Pb/^{204}Pb$ values between these two magma types is largely a consequence of the inclusion of analyses on samples from just three Urubici-type flows {DSM24, DSM04/08, DSM05b/07/09} which are distinct from the main Urubici-type basalts on other geochemical grounds (see chapter three). The Palmas rhyolites have more radiogenic Pb isotope compositions ($^{206}Pb/^{204}Pb$ 19.0 to 19.2) than the Gramado-type magmas, and the Gramado data array on both diagrams is reasonably consistent with progressive contamination by material with such a composition.

The importance of crustal interaction in determining the compositions of the Paraná magmas has been a constant theme running through chapters three and four. It was

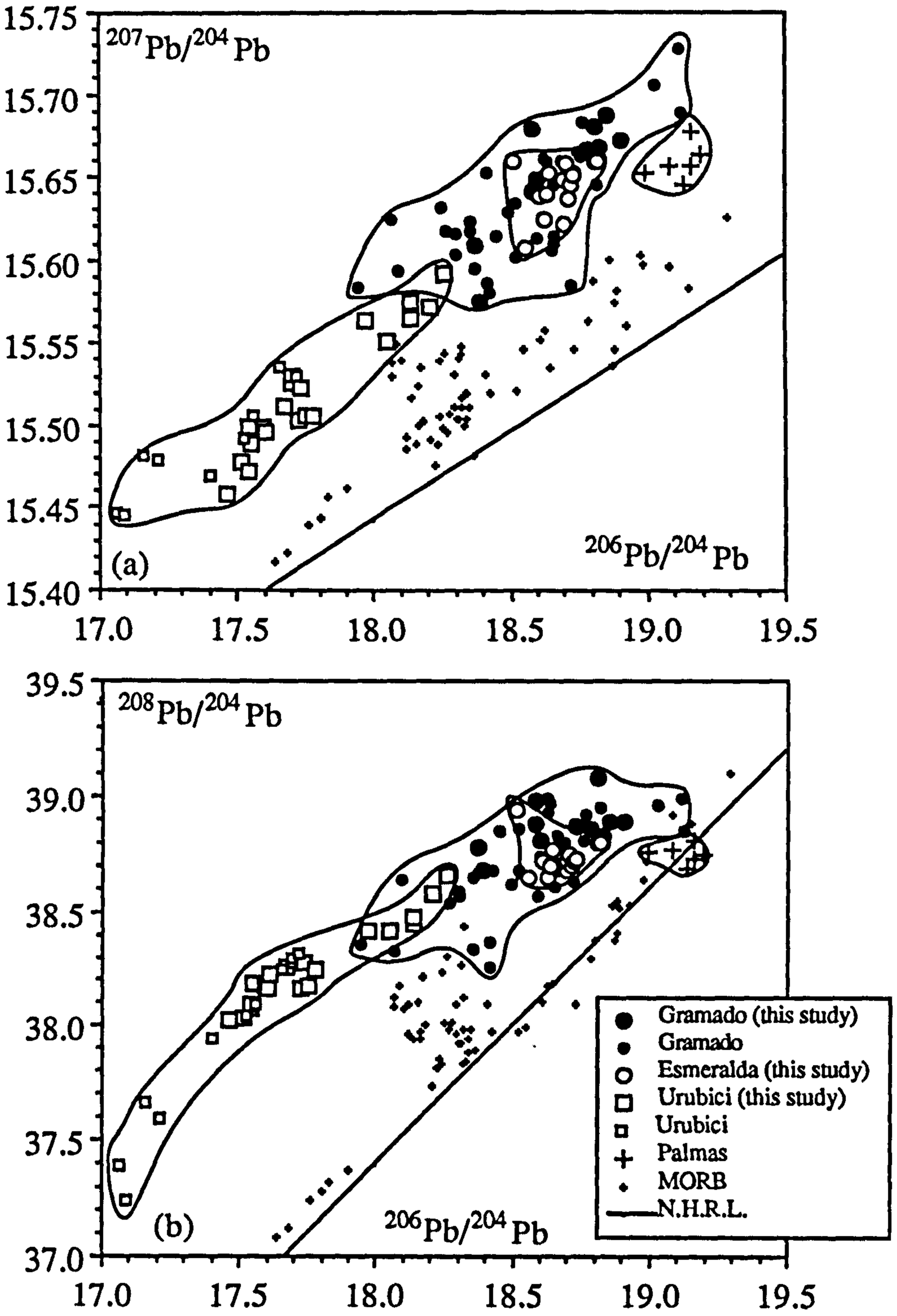

Figure 5.3 Pb isotope variation for the main Paraná magma types; (a) $^{207}Pb/^{204}Pb$ vs. $^{206}Pb/^{204}Pb$, (b) $^{207}Pb/^{204}Pb$ vs. $^{206}Pb/^{204}Pb$. Data sources - {this study, Hawkesworth *et al.*, 1986, 1988}. MORB data is from the South Atlantic Ridge (Hanan *et al.*, 1986), and N.H.R.L. is the Northern Hemisphere Reference Line of Hart (1984).

concluded in chapter three that the Urubici magma type samples had not undergone significant contamination, mainly as a result of their high incompatible element contents. Although some of the scatter within the Urubici data field, for instance on figure 5.2, was attributed to the effects of crustal interaction, such a process was not responsible for the position of this data field. Similarly for the Gramado magma type, even though crustal contamination has played a major role in the evolution of this magma type, it was argued in chapter four that the parental Gramado-type magma in the São Joaquim area had $(^{87}Sr/^{86}Sr)_i$ of about 0.7075 (ε_{Sr} ~40) which is still higher than any of the Urubici-type samples.

Two important points may be inferred from the Sr, Nd and Pb isotope data available on the Paraná magmas:

(i) Since both main basaltic magma types, *viz.* Urubici and Gramado, have negative ε_{Nd} values, this implies derivation from a source region(s) which had a time-integrated LREE enrichment, *i.e.* low Sm/Nd. This point will be discussed further in the next section, as a possible constraint on partial melting modelling of the REE data.

(ii) Both the Urubici and Gramado magma types have consistently different Sr, Nd and Pb isotopic compositions which suggests that they were actually derived from different mantle source regions.

5.4.2 REE elements.

Rare earth element (REE) data can provide additional constraints on any partial melting schemes, especially since the behaviour of the HREE offers the best means of recognising whether or not garnet participated in their fractionation. REE partition coefficients (K_D) for the expected mantle mineral phases {olivine, orthopyroxene, clinopyroxene, garnet, spinel} are comparatively well known (*e.g.* Prinzhofer and Allègre, 1985). If it is assumed that tholeiite compositions require degrees of melting greater than 10 %, then significant relative fractionation of the REE can only be achieved if garnet and / or clinopyroxene remain as residual phases during melting, since the K_D values for other

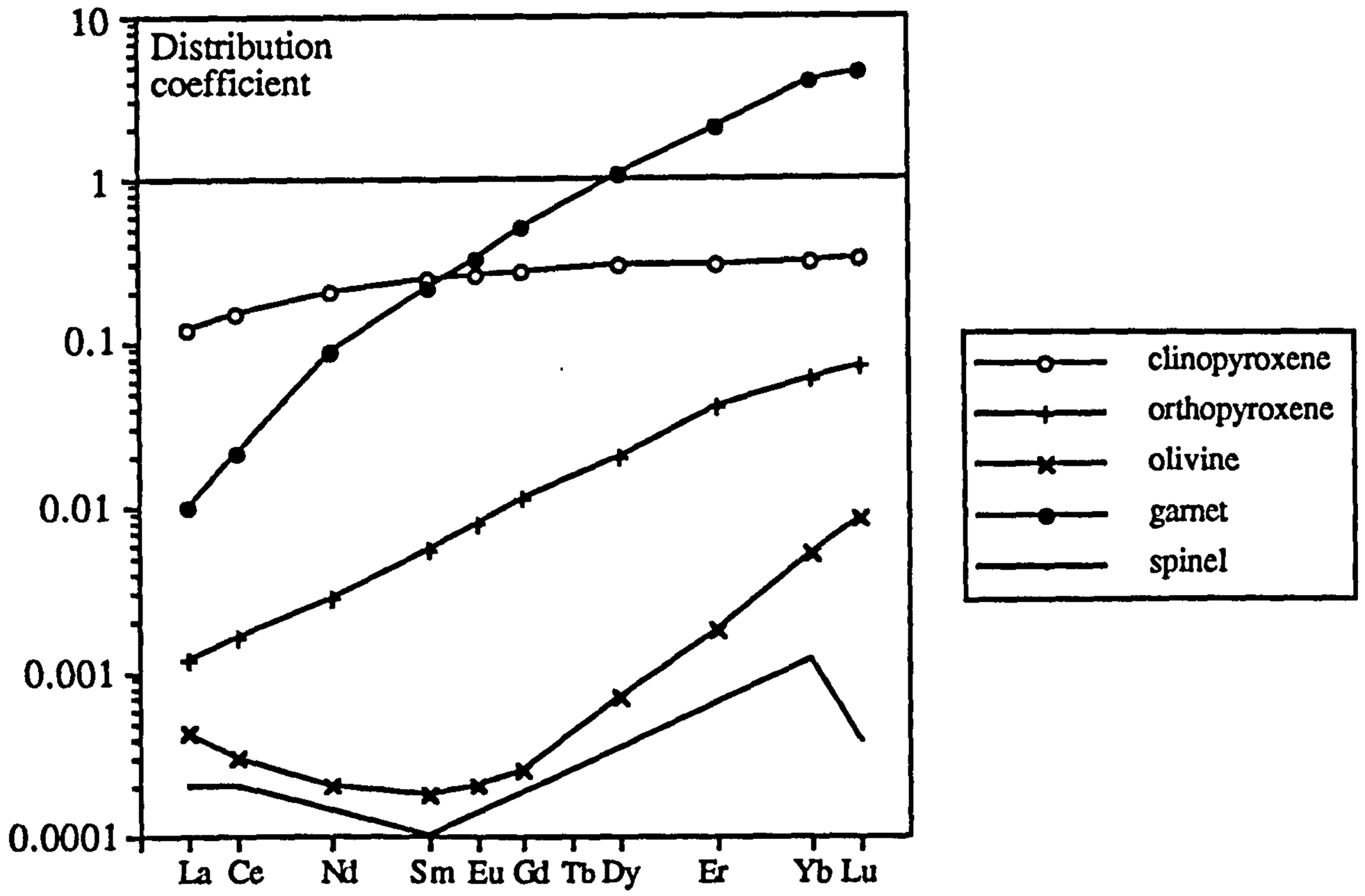

Figure 5.4 REE distribution coefficient data for common mantle mineral phases (data from Prinzhofer and Allègre, 1985).

phases are all << 0.1 (see figure 5.4). It is presumed that any minor phases such as phlogopite, K-richterite, apatite, and ilmenite will have been consumed at lower degrees of melting. The K_D values for the REE in garnet indicate that the presence of residual garnet during melting can cause significant relative fractionation between the slightly incompatible MREE (*e.g.* Tb) and the strongly compatible HREE (*e.g.* Yb). Any fractionation of the LREE will be influenced by the proportion of residual clinopyroxene and / or garnet.

The general features of the chondrite-normalised REE patterns of the Urubici and Gramado magma types from the São Joaquim area are compared in figure 5.5. The details of the REE behaviour within each magma type are discussed separately in chapters three and four (see figures 3.3 and 4.14). Both magma types have similar average LREE enrichments; $(La/Sm)_N$ in the Urubici magma type is 2.36 ± 0.11 which is virtually identical to the $(La/Sm)_N$ of 2.39 ± 0.15 shown by the Gramado magma type. The most noticeable difference between the two magma types is in the extent of HREE fractionation,

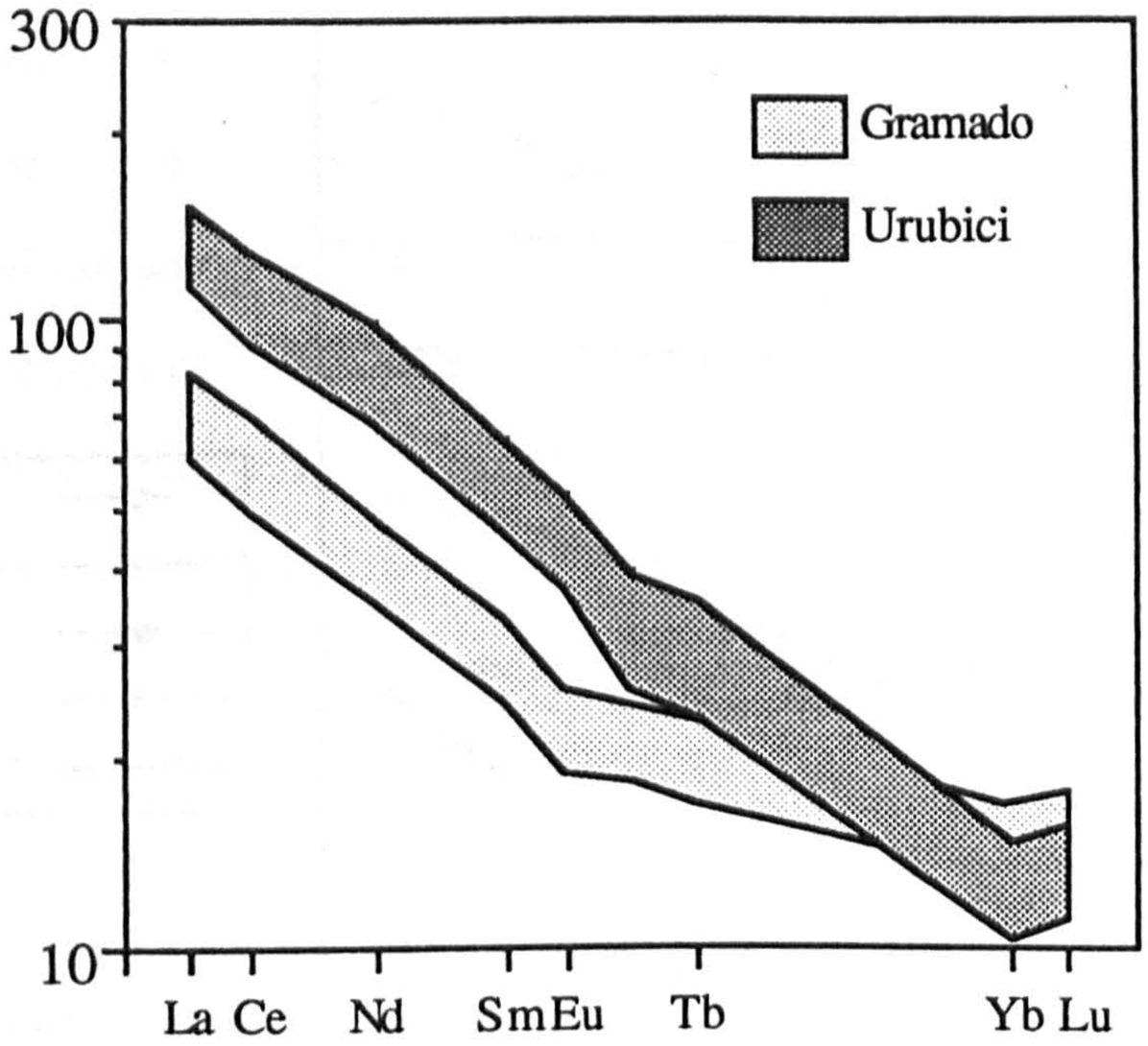

Figure 5.5 Chondrite-normalised REE abundances in the Gramado and Urubici magma types, demonstrating their similar LREE enrichment but markedly different HREE behaviour.

which can be measured by $(Tb/Yb)_N$. In the Urubici magma type $(Tb/Yb)_N$ is 2.20 ± 0.13 compared with $(Tb/Yb)_N$ of 1.32 ± 0.06 in the Gramado magma type. $(Tb/Yb)_N$ remains virtually constant within both the Urubici and Gramado magma types for a wide range in any index of the extent of fractional crystallisation (Mg# or incompatible element content). This implies that Tb/Yb is unaffected by gabbroic fractional crystallisation, as is expected from our knowledge of the relevent K_D values (*e.g.* Frey *et al.*, 1978). Despite the fact that the trace element and isotope composition of the Gramado magma type has been variably modified by assimilation of crustal material, this contamination process must have shared a similar $(Tb/Yb)_N$ ratio to the Gramado magma type, which is consistent with this having a similar composition to the Palmas rhyolites. Figure 5.6 shows the relationship between $(La/Sm)_N$ (*i.e.* LREE enrichment) and $(Tb/Yb)_N$ (*i.e.* HREE enrichment) for the Urubici and Gramado magma types. It also illustrates the similar $(Tb/Yb)_N$ for a number of low-Ti magma types {Horingbaai, Esmeralda, Gramado, Palmas} that span a wide range in $(La/Sm)_N$, which is in keeping with the mixing relationships outlined earlier.

Since the shallow level processes of crystallisation and contamination have not affected $(Tb/Yb)_N$ to any great extent, the marked contrast seen in HREE behaviour

between the Urubici and Gramado magma types must have been present in the distinct parental magmas to each magma type. The conclusion must be that either garnet was a residual phase during melting in order to 'hold-back' Yb with respect to Tb, or two distinct mantle sources were involved, with the the enrichment of MREE over HREE an inherent feature of the Urubici mantle source. This suggests that the melting model of Fodor (1987) involving a mantle source of just olivine+orthopyroxene+clinopyroxene is not valid, and neither is the model of Piccirillo *et al.*, (1988a) which used a residual source of spinel peridotite, since spinel is a negligible phase for REE partitioning in the mantle (Prinzhofer and Allègre, 1985). If the source regions were different, then partial melting of a spinel peridotite source could then be a possibility.

The similarity in LREE enrichment for the two magma types, if derived from different degrees of melting, suggests that the LREE were not extensively fractionated during melting, and furthermore that LREE enrichment might well be a source feature. Given time, this LREE enrichment (*i.e.* low Sm/Nd) would lead to a negative ε_{Nd} signature

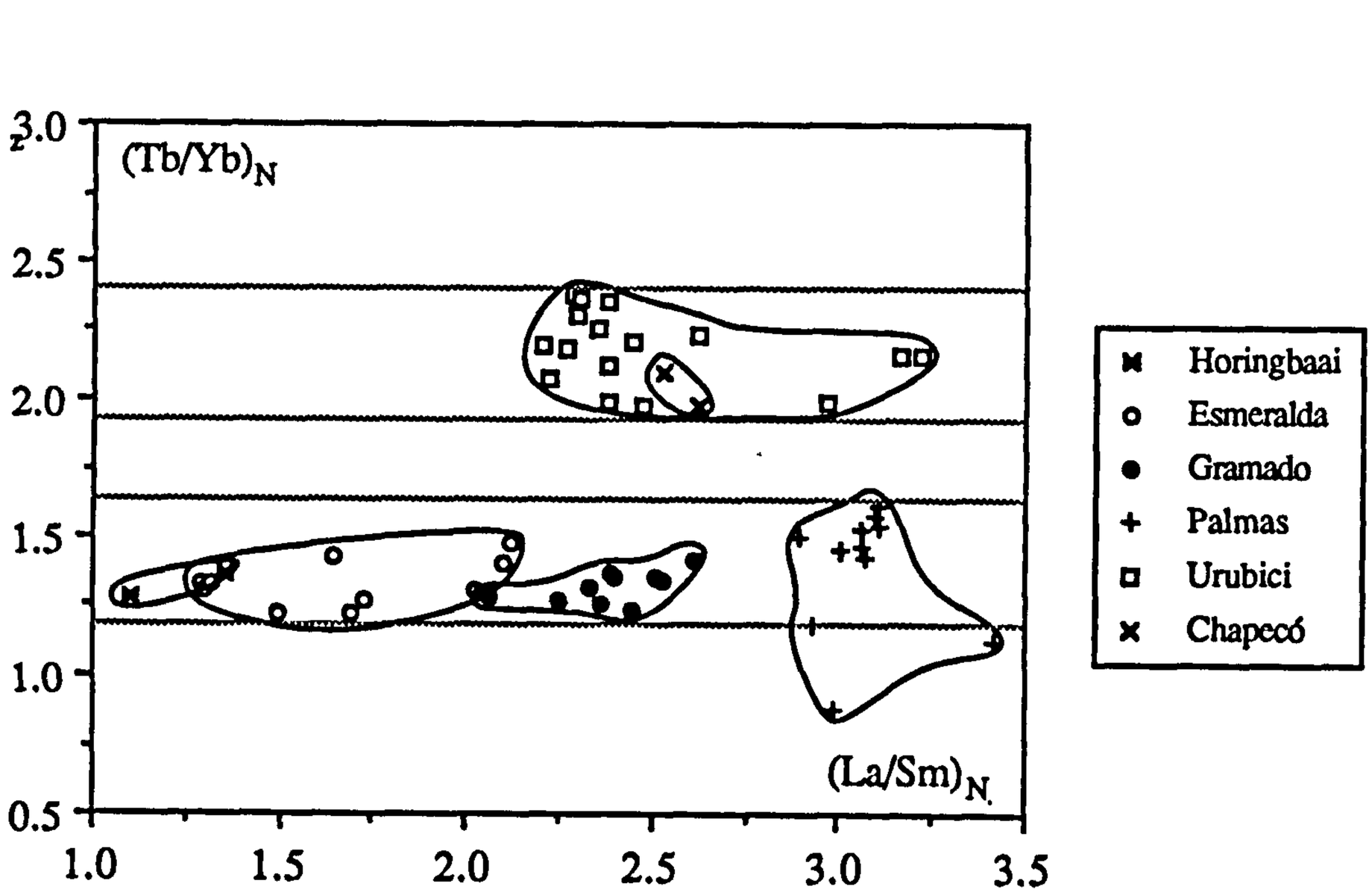

Figure 5.6 Variation of $(La/Sm)_N$ vs. $(Tb/Yb)_N$, used as monitors of LREE and HREE enrichment respectively. The 'low-Ti' magma types {Horingbaai, Esmeralda, Gramado, Palmas} maintain a constant Tb/Yb ratio for a wide range in LREE enrichment {$(La/Sm)_N$ 1.0-3.5} consistent with the mixing relationships outlined in chapter four. The 'high-Ti' magma types {Urubici, Chapecó} are distinctive because of their greater HREE fractionation {*i.e.* higher $(Tb/Yb)_N$}.

for the source and, as was shown in the previous section, both the Urubici and Gramado magma types are indeed characterised by negative ε_{Nd}. If different source regions were involved, then the REE patterns in figure 5.5 would still suggest that the extent of LREE enrichment was similar in the two sources. Hence if a similar age is assumed for both regions, they would develop a similar Nd isotopic signature and this would also be consistent with the observed ε_{Nd} in the Urubici and Gramado magma types.

The features displayed in figure 5.5 by the REE patterns of the Gramado and Urubici magma types can be investigated more quantitatively by using the equilibrium batch melting equation. The behaviour of the LREE and HREE in each magma type can be monitored by $(La/Sm)_N$ and $(Tb/Yb)_N$ respectively, and the modelling will aim to reproduce these ratios. Several assumptions about the parameters of the melting model need to be made. The residual source mineralogy is taken to be a garnet lherzolite following the arguments above, and the source is further assumed to have chondritic relative abundances of the REE. This latter assumption is unlikely to be true, given that the negative ε_{Nd} in both magma types indicates a time-integrated LREE enrichment of the source, but it will be used for the sake of convenience to illustrate this point. An advantage is that the term C_l/C_o in the melting equation can be replaced by C_N, the chondrite normalised abundance for the element, and hence the equations for two elements, for example Tb and Yb, can be combined to give;

$$\frac{Tb_N}{Yb_N} = \frac{D_{Yb} + F(1 - D_{Yb})}{D_{Tb} + F(1 - D_{Tb})}$$

This can be rearranged to get the expression,

$$D_{Yb} = (Tb/Yb)_N.D_{Tb} + F[(Tb/Yb)_N - 1]$$

The degree of melting, F, required to produce each of the magma types is unknown, but for the purposes of this model, it is assumed that the Urubici magma type was derived from a 10 % melt in equilibrium with this residual mantle source material. Although the choice of 10 % is somewhat arbitrary, this value lies at the minimum end of the range suggested by experimental petrology to be necessary to generate tholeiitic melts. Thus, for

the Urubici magma type, F = 0.1 and $(Tb/Yb)_N$ is about 2.2, which reduces the above equation to a simple relationship between the bulk distribution coefficients of Tb and Yb;

$$D_{Yb} = 2.2.D_{Tb} + 0.12.$$

D_{Yb} and D_{Tb} vary as a function of the source mineralogy and the partition coefficients for each mineral phase. Partition coefficient data for the REE (see table 5.2) have been taken from Prinzhofer and Allègre (1985), with values for Tb (not given) estimated by interpolation. It has already been shown that olivine and orthopyroxene are not important phases as a 'sink' for the REE in the mantle, and their role is limited to diluting the effects of clinopyroxene and garnet. The proportions of the mineral phases in the model source were adjusted within plausible limits, to produce a range of possible residual mantle compositions that obeyed the above relationship between D_{Yb} and D_{Tb}. The proportion of garnet in the residue, which controls $(Tb/Yb)_N$, is quite well constrained by this method. For a combined olivine and orthopyroxene content of 70 - 85 %, 6 - 8 % of residual garnet was required to produce $(Tb/Yb)_N$ of 2.2 in a 10 % melt. In all these solutions, the modelled $(La/Sm)_N$ was about 1.2 - 1.3 which is much lower than the observed value of about 2.35 for the Urubici magma type. The observed LREE enrichment could be caused either if the Urubici magma type was related to a considerably smaller degree melt than 10 % (accompanied by a much reduced level of residual garnet), or an appreciably greater proportion of residual clinopyroxene (any more garnet would affect the Tb/Yb ratio). The

	olivine	orthopyroxene	clinopyroxene	garnet
La	0.00044	0.0012	0.12	0.01
Nd	0.00020	0.0028	0.20	0.087
Sm	0.00018	0.0054	0.24	0.212
(Tb)	0.00042	0.0148	0.276	0.727
Yb	0.00522	0.060	0.30	4.03

Table 5.2 Partition coefficient data for selected REE, from Prinzhofer and Allègre (1985). Tb values were estimated by interpolation between the values given for Gd and Dy.

solutions already contained 9 - 22 % clinopyroxene in the modelled residual mantle source, and any marked increase in this amount would be in conflict with experimental phase equilibria of melting (*e.g.* Mysen and Kushiro, 1977; Jaques and Green, 1980) and the modal compositional data for refactory mantle xenoliths (*e.g.* Harte, 1983). A more reasonable resolution of this discrepancy is that the source was already LREE enriched, and for this model, $(La/Sm)_N$ in the source must have been about 1.8 - 2.0. This solution is consistent with the Nd isotope data, since it has already been stressed that the negative ε_{Nd} of uncontaminated Urubici and Gramado magmas implies that both magma types were derived from a source(s) which had experienced a long history of LREE enrichment.

If the primary melt to the Gramado magma type was also in equilibrium with a similar mantle source (which would require melting to have been modal), then the observed $(Tb/Yb)_N$ of about 1.3 can only be matched if the degree of melting was 40 % or more, which is approaching unreasonably high values. For such a high percentage of melting, incompatible trace element ratios in the Gramado magma type should approximate those of the source, and in chapter four, $(La/Sm)_N$ in 'uncontaminated' Gramado parental magma was about 2.0 (*c.f.* 1.8 - 2.0 suggested above for the source).

The Nd isotope data can provide further infomation on the source characteristics if the age of the source region and its Nd isotopic composition at that time are known. Hawkesworth *et al.*, (1986) interpreted the Pb isotope data for the Urubici-type samples {see figure 5.4(a)} in terms of a secondary isochron and obtained an age of about 1.8-2.0 Ga. They suggested that this represented the age of stabilisation of the lithospheric mantle beneath Brazil. This new lithospheric material was presumably derived from the surrounding asthenospheric mantle, and its Nd isotopic composition is inferred to be that of 'depleted mantle' at 1.8-2.0 Ga (see Ben Othman *et al.*, 1984). If it is assumed that the LREE source enrichment dates from that time, the Sm/Nd ratio required in the source in order to produce the observed ε_{Nd} in the Paraná lavas may be calculated as follows:

$$\left\{\frac{^{147}Sm}{^{144}Nd}\right\}_{source} = \frac{\left\{\frac{^{143}Nd}{^{144}Nd}\right\}_{130\ Ma}^{Urubici} - \left\{\frac{^{143}Nd}{^{144}Nd}\right\}_{T}^{DM}}{e^{\lambda(T-130)} - 1}$$

λ (the ^{147}Sm decay constant) is 6.54×10^{-12} yr^{-1} and T (the source age) is 1800-2000 Ma. Within the Urubici magma type, the average Nd isotope composition was ε_{Nd} ~ -2.8 {$(^{143}Nd/^{144}Nd)_i$ ~0.51233}. The Nd isotopic composition of 'depleted mantle' is calculated from the equations given in Ben Othman *et al.*, (1984); at 1.8 Ga $(^{143}Nd/^{144}Nd)_{DM}$ = 0.51053, at 2.0 Ga $(^{143}Nd/^{144}Nd)_{DM}$ = 0.51025. Using these parameter values and converting $(^{147}Sm/^{144}Nd)$ to the elemental ratio, it is calculated that the source had an Sm/Nd ratio of 0.27-0.28. A comparison with the measured Sm/Nd ratio in the Urubici magma type (Sm/Nd range of 0.20-0.23, average 0.212 ± 0.006, n=13) would suggest that for this model, Sm/Nd was on average reduced by about 23 % during partial melting, and this would imply a degree of melting << 10 %. A value for $(La/Sm)_N$ in the source of about 1.5 can be inferred from this value (*c.f.* 1.8 - 2.0 suggested from the partial melting model). This result is entirely model dependent, and if the timing of the LREE enrichment event was younger than 1.8-2.0 Ga, then the source would have to have lower Sm/Nd {and higher $(La/Sm)_N$}.

5.4.3 Other trace elements.

It has already been stressed that the Urubici magma type has an enriched inventory of most incompatible trace elements relative to the Gramado magma type. The LIL-elements, K and Rb, are expected to be more incompatible than the HFS-elements, Ti and Zr, during melting of any realistic mantle phase assemblage, from the partition coefficient data in table 5.3 {data sources - Henderson (1982) and Pearce and Norry (1979)}. Thus the enrichment displayed for TiO_2 and Zr between the Gramado and Urubici magma types should be even more pronounced for K_2O and Rb, but this is not the case as is seen in figures 5.7 (a) TiO_2 vs. K_2O, and (b) Zr vs. Rb. Despite the marked difference in TiO_2 and Zr contents for the two magma types, both share a similar range in K_2O and Rb abundance, which is at odds with any model that seeks to relate the two by different degrees of partial melting from similar source compositions.

	olivine	orthopyroxene	clinopyroxene	garnet
K	0.007	0.01	0.03	0.01
Rb	0.006	0.01	0.04	0.01
Ba	0.006	0.01	0.07	0.01
Ti	0.01	0.1	0.3	0.3
Zr	0.001	0.03	0.1	0.3

Table 5.3 Partition coefficient data for selected trace elements. K, Rb, Ba from Henderson (1982), and Ti, Zr from Pearce and Norry (1979).

Partition coefficients for Ti and Zr are similar for all the main mantle phases, although the values in table 5.3 consistently have Ti slightly more compatible than Zr, which would suggest that during melting $D_{Ti} \geq D_{Zr}$. This would imply that the Gramado primary melt should have the same, or greater, Ti/Zr ratio than the Urubici magma type, but the opposite is actually true. The Urubici magma type has Ti/Zr of 70.8 ± 3.6 compared with the much lower average value of 51.4 ± 3.9 for the Gramado magma type. The Ti/Zr of the Gramado-type magmas might have been lowered during the assimilation of Palmas-type crustal material which has Ti/Zr of 22.4 ± 1.8, but even the most

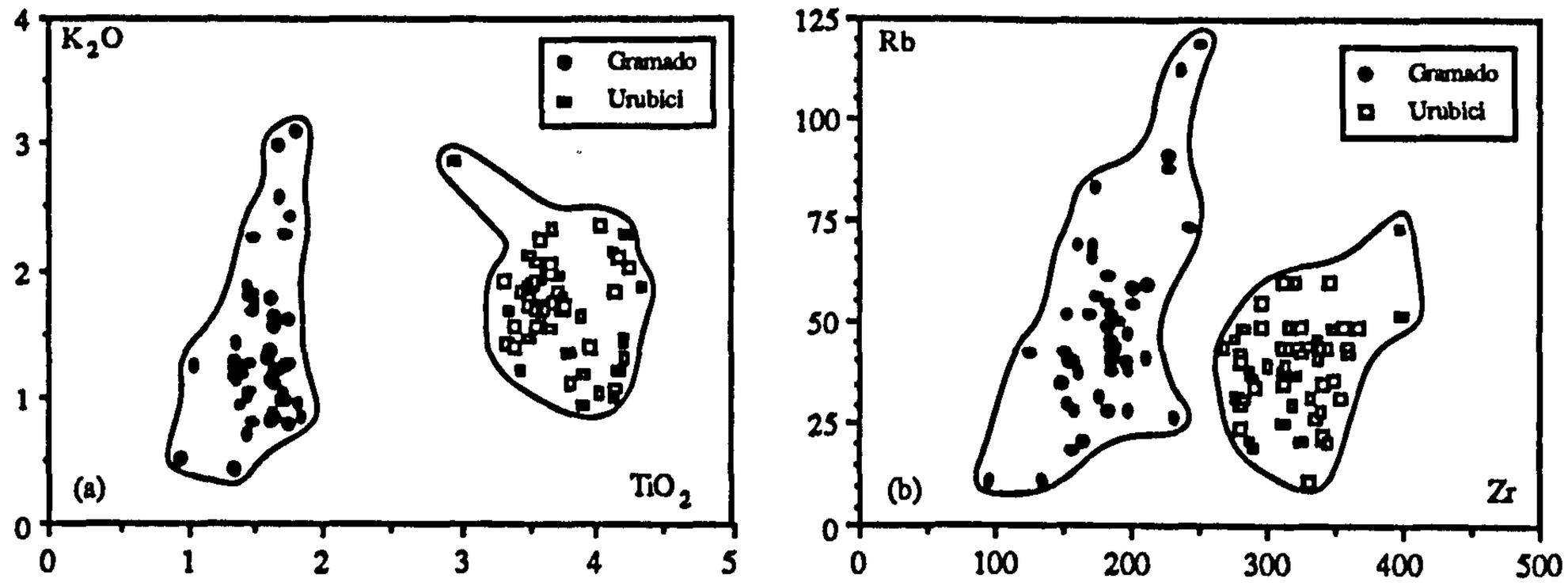

Figure 5.7 (a) K_2O vs. TiO_2, (b) Rb vs. Zr. Despite the strong enrichment in TiO_2 and Zr between the Gramado and Urubici magma types, both magma types have similar range in K_2O and Rb which is not consistent with predictions from partial melting modelling.

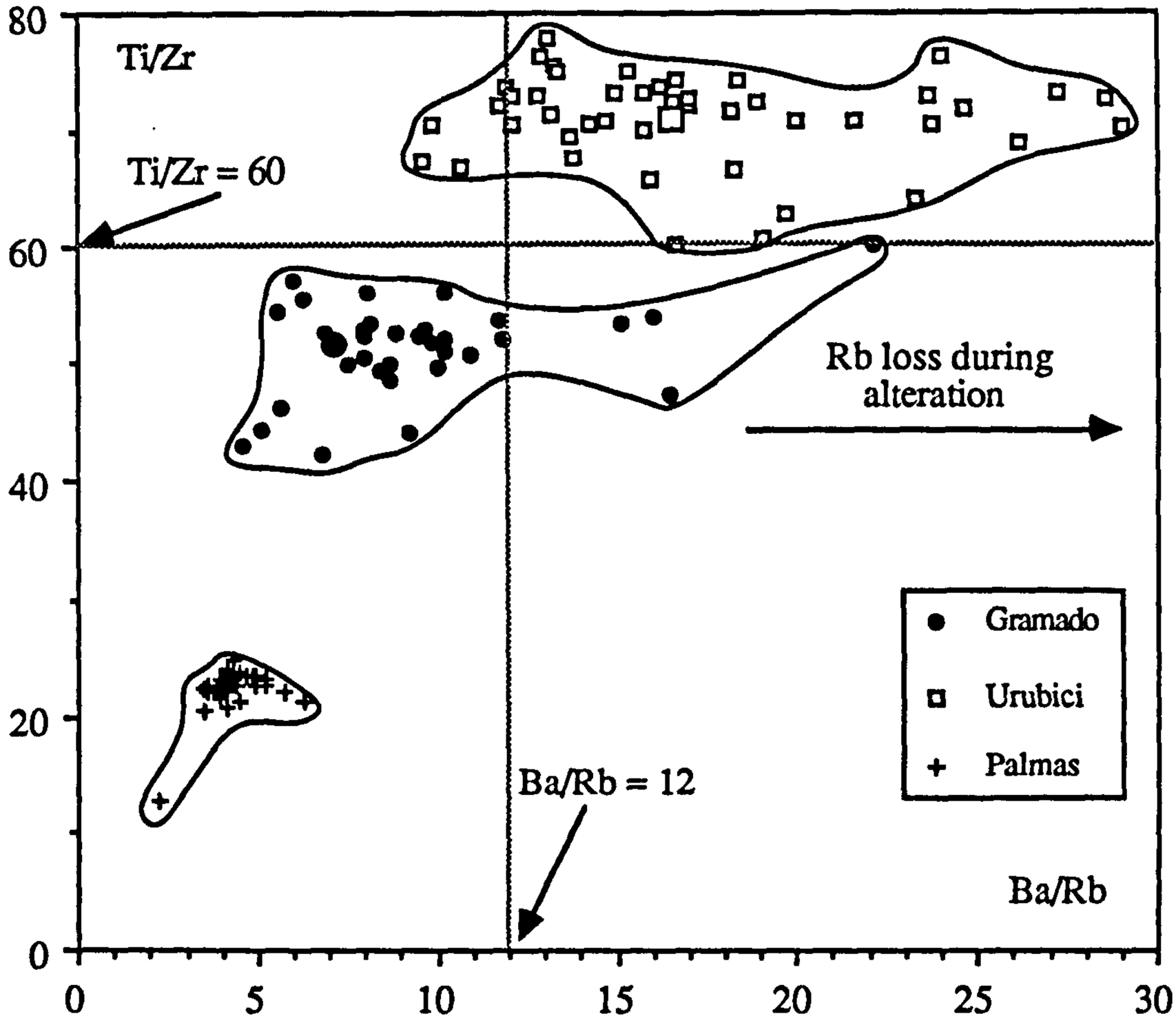

Figure 5.8 Variation of Ba/Rb vs. Ti/Zr between the Gramado and Urubici magma types. During partial melting, Ti/Zr and Ba/Rb are expected to remain virtually constant. Large symbols represent average composition for each magma type.

uncontaminated Gramado-type composition yet recognised (SJ in table 4.1) still has a comparatively low Ti/Zr of 60.

A similar argument can be developed for the behaviour of Ba and Rb, since their similar bulk distribution coefficients (table 5.3) mean that Ba/Rb should remain constant during melting. Instead, Ba/Rb is consistently lower in the Gramado-type magmas than in the Urubici-type magmas. This can be seen in figure 5.8 which illustrates the difference in both Ba/Rb and Ti/Zr between the two magma types. The majority of the Gramado-type samples (89 %) have Ba/Rb < 12 whereas the vast proportion (92 %) of the Urubici-type samples lie at higher Ba/Rb > 12. The scatter in the Ba/Rb ratio within each magma-type and the displacement of several samples to high Ba/Rb most likely reflects Rb mobilisation and loss during post-eruptional alteration and weathering. Figure 5.7(b) has demonstrated that both magma types had similar Rb contents, and field observations have shown that the

lava flows of the two magma types are interbedded. Therefore this secondary process is unlikely to have been the cause of the difference in Ba/Rb between the Urubici and Gramado magma types, since it would have to have been a highly selective process, removing Rb from the Urubici-type flows in preference to the Gramado-type flows.

These trace element anomalies all seem to preclude the possibility of deriving primary magmas for the Urubici and Gramado magma types from a common mantle source by different degrees of melting.

5.5 Discussion of partial melting versus source heterogeneities.

5.5.1 A possible role for crustal interaction ?

The two proposals that have been made in order to account for the high-Ti / low-Ti division displayed by the Urubici and Gramado magma types are;

(i) varying degrees of partial melting of a homogeneous mantle source.

(ii) heterogeneous mantle and a distinct source region to each magma type.

Although the trace element and isotopic evidence outlined in the previous sections has strongly favoured the latter option of source mantle heterogeneities, some consideration should be given to the objections to this model stated by Fodor (1987). He attributed any discrepancies between observed and calculated values of trace element composition in the partial melting models solely to contamination by crust, and suggested that this would also account for the isotopic differences between the Urubici and Gramado magma types. Thus this means that the trace element and isotopic features of the 'parental' Gramado-type magma considered in chapter four are not representative of the mantle source, and have been modified from the values implied by the composition of the Urubici magma type, due to the addition of crustal material. This component must have been relatively enriched in Rb and K, and depleted in Ti, to cause the ratios Ti/Zr, Ti/K and Ba/Rb to be lower than expected in the Gramado magma type. The shift in isotopic composition from the values in

the Urubici magma type to the 'parental' Gramado-type magma requires an increase in $(^{87}Sr/^{86}Sr)_i$ from about 0.7048 to 0.7075, a slight decrease in $(^{143}Nd/^{144}Nd)_i$, and an increase in $^{206}Pb/^{204}Pb$ from 17.5-18.3 to 18.5-19.0. Qualitatively these variations are broadly consistent with the involvement of crustal material, although this is unlikely to be lower crustal in origin. The composition of average lower crust given by Taylor and McLennan (1985) is too depleted in Rb and K relative to Ba and Ti, and has Ba/Rb ~ 28 and Ti/K ~ 1.56 (*c.f.* Urubici - Rb/Ba ~18, Ti/K ~1.7; Gramado Rb/Ba ~8, Ti/K ~0.9).

Chapter four has already demonstrated that the compositional variations within the Gramado-type samples are caused by two separate processes: the trends are dominated by the effects of assimilation and fractional crystallisation involving a crustal component compositionally similar to the Palmas rhyolites, and this was superimposed on an earlier mixing event that produced a regional variation within the magma type and which could not be extrapolated back to Urubici-type compositions. Geochemical arguments have further shown that the parental Gramado-type magma input into the AFC environment already had elevated $(^{87}Sr/^{86}Sr)_i$ of 0.707-0.709 and therefore the contamination event proposed by Fodor (1987) must have occurred prior to the AFC. It also cannot be related to the mixing event that was responsible for the small-scale regional variation within the Gramado magma type because Ba/Nb is similar in both the Urubici magma type and the Gramado-type samples from the São Joaquim area. It is interesting to note that over the whole of the southern Paraná region, no low-Ti magma samples have been found which have trace element and isotope ratios similar to the Urubici magma type. The Esmeralda-type samples which do have lower $(^{87}Sr/^{86}Sr)_i$ (down to 0.7059), have similar $^{206}Pb/^{204}Pb$ to the Gramado-type samples, and different trace element ratios and much higher $(^{143}Nd/^{144}Nd)_i$ to the Urubici magma type. Therefore if this additional contamination event was affecting the Gramado-type magmas, it must have been remarkably consistent in its effects so that no intermediaries were erupted.

Thus, if everything is to be attributed to interaction with crustal material, we are faced with a situation that requires three distinct crustal mixing events in order to account for the compositions displayed by the Gramado magma type: (i) AFC with crustal material

similar to Palmas rhyolites, (ii) mixing event (either source- or magma- mixing) controlling regional variation, best shown by Ba/Nb, $^{87}Sr/^{86}Sr$, and SiO_2 (see figures 4.19 and 4.21), and (iii) early contamination event necessary to displace incompatible trace element and isotope ratios from the values in the Urubici magma type. This appears to be a rather unlikely explanation, and these data are more plausibly reconciled if the difference between the Urubici and Gramado magma types was a source feature. Therefore the trace element and isotope evidence argues strongly for major source mantle heterogeneity beneath Brazil, as was originally suggested by Bellieni *et al.*, (1984a) and Mantovani *et al.*, (1985a). The same conclusion was also reached by Duncan *et al.*, (1988) for the Tafelberg (low-Ti) and Khumib (high-Ti) magma types from the Etendeka, based on similar trace element and isotope observations.

5.5.2 High- and Low-Ti geochemical provinces within Gondwana.

The surface distribution of the different magma types can shed further light over the problem of interpreting the fundamental high-Ti / low-Ti geochemical variation in terms of partial melting differences versus distinct mantle sources. A dominant feature of the Paraná lava field is the simple geographical division into two geochemical provinces, initially recognised by Bellieni *et al.*, (1984a), with high-Ti magmas concentrated in the northern half of the basin and low-Ti varieties largely confined to the south. This requires a systematic north / south variation in the degree of melting if it is to be in keeping with the partial melting hypothesis.

Fodor (1987) suggested that the Tristan da Cunha hot-spot had been the driving force behind the Paraná CFB magmatism, and that melting conditions would be controlled by the position of the source region relative to the hot-spot. In this scenario, a hot-spot impinging on the base of the lithosphere would set up lateral temperature gradients producing a variation in the percentage of melting with distance from the plume axis. Directly above the plume, mantle decompression arising from doming and stretching of the crust, plus the higher mantle temperature, leads to a large degree of melting, consistent with the low-Ti magma type. These effects would then have less influence towards the

flanks of the plume where lower degree melts, enriched in incompatible elements, would be expected, equivalent to the high-Ti magmas. The Tristan da Cunha hot-spot is thought to have been located at about 150 Ma, prior to the initiation of the South Atlantic ocean, beneath the Torres-Posadas syncline, which is onshore of the present day Rio Grande Rise (Neill, 1976). This is where the low-Ti magmas are concentrated, with the high-Ti magmas further to the north. One consequence of this model is that there should be a similar transition to high-Ti magmas to the south, perhaps in northern Argentina, but this has not been recognised at present. The plausibility of this model is brought into question in view of the more complex lava field stratigraphy revealed by the borehole study, and this is discussed later in section 5.7.4 in the context of the Paranapanema magma type. This model is also in conflict with more recent geophysical ideas of the thermal structure and effect of mantle plumes (*e.g.* White and McKenzie, 1989) which do not predict any marked regional variations in the degree of melting (see discussion in chapter six).

Both Bellieni *et al.*, (1984a) and Mantovani *et al.*, (1985a), who had argued that the trace element and isotope differences between the low-Ti and high-Ti magma types were not compatible with an origin involving variable melting of a single mantle source, took the view that the geochemical provinces formed by these magma types was further evidence in support of lateral compositional variations within the upper mantle beneath the Paraná lava field.

This geochemical division into high-Ti and low-Ti provinces is not restricted to the Paraná lavas of South America but is a more widespread feature found in the Mesozoic CFB provinces right across Gondwana. It is best demonstrated in the Karoo lavas of southern Africa where Cox *et al.*, (1967) first delineated the existence of two major geochemical provinces; a 'northern K-rich' (and high-Ti) province in the Nuanetsi - North Lebombo area, which was enriched in incompatible trace elements relative to the 'southern K-poor' (and low-Ti) province in the Lesotho - South Lebombo area. The presence of both high-Ti and low-Ti magmas has also been noted among the Coats Land and Dronning Maud Land tholeiites of Antarctica (Brewer *et al.*, 1987). The high-Ti / low-Ti transition was reviewed by Erlank *et al.*, (1988), who used the available geochemical data on the

Paraná and Karoo lavas in order to distinguish areas of high-Ti or low-Ti magmas. From this, it was suggested that a boundary zone separating regions of dominantly high-Ti basalts to the north from exclusively low-Ti basalts to the south could be extrapolated east-west across southern Africa into South America. This is illustrated on figure 5.9, which has been adapted from figure 6 of Erlank *et al.*, (1988) to include the new data obtained on the Paraná lavas in this study. The position of this boundary, which is defined as the southernmost limit of the high-Ti magmas, is only approximate, largely because of the poor sample coverage in many areas and the lateral overlapping of the high-Ti and low-Ti magma types. In the Lebombo, the change occurs over a distance of about 60 km (Erlank *et al.*, 1988), while the borehole results in chapter two showed that for the Paraná, this transition zone was at least 200 km wide. Nonetheless, a few anomalies to the overall pattern do exist, such as the low-Ti Ribeira-type of the northern Paraná and the low-Ti basalts of the northern Karoo in Malawi and Zambia. The remarkably consistency of this

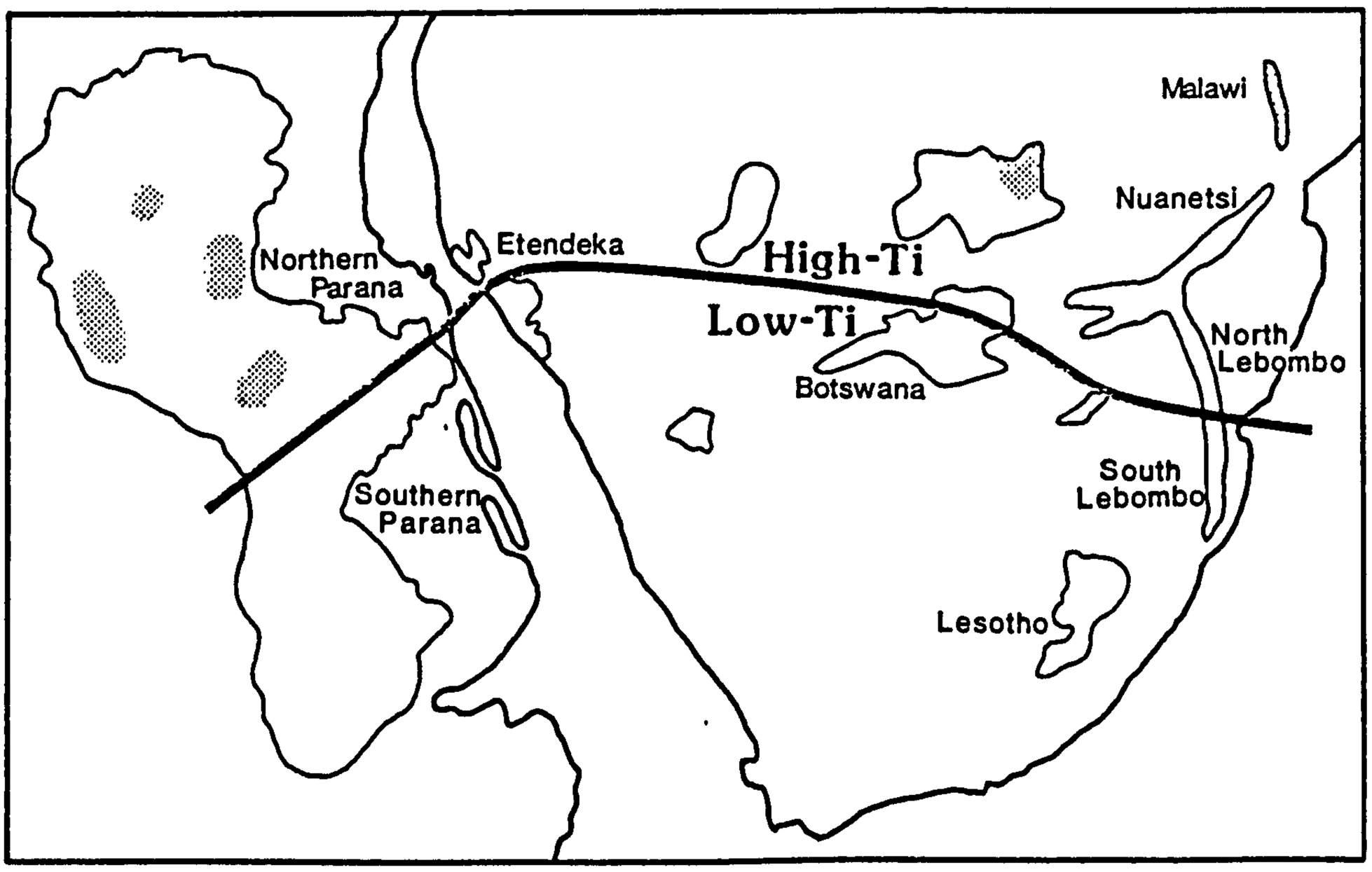

Figure 5.9 High-Ti and low-Ti geochemical provinces within the magmas of the Paraná and Karoo CFB (adapted after Bellieni *et al.*, 1984a and Erlank *et al.*, 1988). Note that the boundary marks the southern limit of high-Ti magmas, and within the Paraná extensive low-Ti magmas underlie the high-Ti types for at least 200 km north of this line. The stippled areas within the high-Ti province denote the few anomalous areas of low-Ti magmas; for the Paraná CFB this represents the Ribeira magma type (see Petrini *et al.*, 1987).

geochemical boundary over such a large geographical distance (> 3000 km) seems difficult to reconcile with any systematic variation in degree of melting, especially if this is to be related to underlying mantle plumes in the manner suggested by Fodor (1987). The Paraná and Karoo CFB provinces differ in age by about 60 Myrs and are therefore unlikely to have been affected by the same mantle plume. Erlank *et al.*, (1988) carried out numerical modelling involving different degrees of partial melting of a garnet lherzolite mantle source in an attempt to explain the high-Ti and low-Ti magmas of the Lebombo but was forced to conclude that such a mechanism could not satisfactorily account for both high-Ti and low-Ti magma types. The high-Ti varieties could be generated by about 10 % partial melting but this would then require the low-Ti magmas to be produced by unreasonably large (~50 %) degrees of melting. Thus, in common with many other studies of the Karoo magmatism {Cox 1983, 1988; Hawkesworth *et al.*, 1983, 1984b; Duncan *et al.*, 1984; Marsh, 1987,...}, Erlank *et al.*, (1988) suggest that the high-Ti / low-Ti divide reflects the existence of large-scale source mantle heterogeneities. The boundary between the high-Ti and low-Ti provinces, marked on figure 5.9, is therefore thought to represent the surface expression of a major laterally extensive geochemical discontinuity in the sub-continental lithospheric mantle of Gondwana.

5.5.3 Summary of evidence for distinct 'high-Ti' and 'low-Ti' mantle source regions.

The previous sections of this chapter have already mentioned several lines of evidence which have pointed to the necessity for distinct mantle source regions to the main Paraná magma types, and these were;

(i) trace element data difficult to reconcile with different degrees of partial melting of a homogeneous source.

(ii) differences in radiogenic isotope compositions that are not attributable to crustal contamination.

(iii) the scale and geographical distribution of distinct 'high-Ti' and 'low-Ti' geochemical provinces.

It has also been shown (*e.g.* Hawkesworth *et al.*, 1983, 1984b; Duncan *et al.*, 1984, etc.) that mantle heterogeneity on several length scales was a major control on the compositional diversity of the flood basalts in the Karoo province. Heterogeneity on a 1000 km length scale is demonstrated by the presence of high- and low-Ti geographical provinces (Cox *et al.*, 1967; Erlank *et al.*, 1988). On a more local scale, Marsh and Eales (1984) proposed a heterogeneous source for the various minor magma types in the Central Area in order to account for differences in their incompatible trace element ratios. Similarly, the two primitive end-member compositions deduced for the Nuanetsi / North Lebombo picrites by Cox, (1983) could not be related by different degrees of melting of a common source, and required separate mantle sources.

This implies the existence of large-scale mantle heterogeneities not just beneath the Paraná region of South America, but as a widespread feature right across the former Gondwana supercontinent. Two main questions still remain to be answered;

(i) Where are the locations of these source regions ?

(ii) What is the origin of their distinct geochemical characteristics ?

5.6 Possible involvement of continental mantle lithosphere in the Paraná CFB magmatism.

The location of the source regions to the Paraná flood basalts, as with all CFB magmatism, is still a contentious issue. The controversy over the origin of the geochemical signature of CFB in general, *viz.* asthenosphere vs. lithosphere, arises because of the perceived problems in melting the lithospheric mantle directly, and the possibility of crustal contamination, which could obscure many of the trace element and isotopic characteristics of the mantle source as inherited by the melt,.

The most striking isotopic feature of the Paraná CFB is that the main magma types, the Urubici (high-Ti) and Gramado (low-Ti), lie within the 'enriched' quadrant on an ε_{Sr}-ε_{Nd} diagram (see figure 5.7), having positive ε_{Sr} and negative ε_{Nd}. Significantly, they are

displaced from the 'asthenospheric' MORB / OIB data which fall mainly in the 'depleted' quadrant (negative ε_{Sr}, positive ε_{Nd}). This requires an origin for the Paraná CFB from source regions which had time-integrated high Rb/Sr, low Sm/Nd ratios relative to bulk earth estimates (and MORB / OIB also), or at least a contribution from such old, trace element enriched material. Traditionally, this 'enriched' component would be placed within the crustal portion of the lithosphere since the continental crust was considered to be the complementary global reservoir to MORB, characterised by old, high Rb/Sr and low Sm/Nd ratios and hence a source of high $^{87}Sr/^{86}Sr$ and low $^{143}Nd/^{144}Nd$ material. Therefore the isotopic characteristics of the Paraná lavas would be attributed to contamination of asthenospheric melts by different crustal materials during ascent. The Urubici-type magmas, which have low ε_{Sr}, would reflect assimilation of low Rb/Sr lower crustal granulite-facies rocks, whereas the higher ε_{Sr} Gramado-type rocks could have assimilated high Rb/Sr upper crustal material (*c.f.* Carter *et al.*, 1978). It has been argued that it is unlikely that the prominent major and trace element differences between the Gramado and Urubici magma types could result from assimilation of crustal material with different compositions. Following on from this, it is difficult to envisage why an Urubici-type magma should be contaminated exclusively within the lower crust, and similarly for a Gramado-type magma within the upper crust.

However, studies of mantle xenoliths (Menzies and Murthy, 1980; Erlank *et al.*, 1987) and inclusions in diamonds (Richardson *et al.*, 1984) have demonstrated that segments of the sub-continental lithospheric mantle are both old (Proterozoic and Archaean) and have variable Rb/Sr and Sm/Nd which with time have generated a wide range of $^{87}Sr/^{86}Sr$ and $^{143}Nd/^{144}Nd$, including values that had previously been regarded as typical of the continental crust. Thus we face the dilemma of the 'enriched' component within the Paraná magmas being potentially contributed by either the crustal or mantle portions of the continental lithosphere.

The effects of crustal assimilation on the Paraná lavas have been extensively investigated in this study. For the Urubici magma type, it was concluded earlier that their isotopic ratios have not been affected significantly by crustal contamination *en route* to the

surface. The situation is more complex for the Gramado magma type, but it has been argued in chapter four that uncontaminated Gramado-type magmas probably had ε_{Sr} ~40 and ε_{Nd} ~2.5. The conclusion therefore is that the isotopic signature of the Paraná basalts reflects a role for the continental mantle lithosphere in the CFB magmatism.

Further evidence for the involvement of continental mantle lithosphere is the presence of distinct geographical high- and low-Ti provinces within the Paraná-Etendeka province and the older Karoo event. The extent of melting required by CFB magmatism and the geographical distribution of these geochemical provinces imply long-lived large-scale heterogeneities within the mantle. It is unlikely that such major heterogeneities could persist within the asthenosphere, especially over the timescale necessary, since the stirring effects of mantle convection will act to erase such features within a few hundred Myrs (Hoffman and McKenzie, 1985). Similarly, the trace element and isotopic features of the Gondwana CFB magmas are different from those derived from the oceanic mantle. This is especially true for the low-Ti magmas (*e.g.* Gramado magma type, Tasmanian dolerites), since comparable low-Ti samples, even with low ε_{Sr}, have yet to be observed among MORB and OIB. Their significantly lower Ti, Ta, Zr, P and high LIL abundances are more akin to those of recent island arc rocks (see section 5.7.2).

Hawkesworth *et al.*, (1986) used Pb isotope data to infer a possible age for the source region to the Urubici magma type. Since the Urubici-type magmas exhibited no clear signs of crustal contamination, the array of data on a $^{207}Pb/^{204}Pb$ vs. $^{206}Pb/^{204}Pb$ diagram can plausibly be interpreted as an inherited secondary isochron from the mantle source region. They obtained an apparent age of about 1.8 ± 0.4 Ga which was similar to a Pb-Pb age of 2.18 ± 0.18 Ga reported by Mantovani *et al.* (1986) for nine composite samples of regional basement rocks. The simplest interpretation of these data was that a major crust-forming event took place in this region at about 2.2 Ga, during the Transamazonian event). In the ensuing 200-300 Myrs, upper mantle material was stabilised within the continental lithosphere, and was subsequently remobilised during the Paraná CFB magmatic event. Hawkesworth *et al.*, (1988) noted that there was a general consistency in the inferred sources ages of the Mesozoic CFB across Gondwana, with a

range of 1.1 to 1.8 Ga (Brooks *et al.*, 1976; Hawkesworth *et al.*, 1986, 1988), and the fact that such ages are often similar to those in the overlying crust suggested that the CFB magmatism was remobilising mantle lithosphere which had formed soon after the stabilisation of the local crust.

All the evidence above suggests that Paraná CFB magmas contain an isotopic and trace element geochemical signature that was derived from the continental mantle lithosphere. This strong lithospheric influence seems to be a feature of almost all of the Mesozoic Gondwana CFB (*e.g.* Hawkesworth *et al.*, 1984b, 1988; Kyle *et al.*, 1980; Hergt *et al.*, 1989), which is in marked contrast to many other CFB provinces such as the Deccan and Columbia River. This is illustrated in figure 5.10 which compares the range in Sr and Nd isotopic compositions of the world's major CFB provinces. The Gondwana CFB {Paraná, Karoo, Tasmania-Antarctica} are virtually restricted to the 'enriched' quadrant (positive ε_{Sr}, negative ε_{Nd}) on figure 5.10, whereas the uncontaminated Columbia River and Deccan samples lie in the 'depleted' quadrant', coincident with the MORB / OIB field, which indicates a ultimate derivation from an asthenospheric source.

The exact nature of how the lithosphere is remobilised during the generation of CFB magmatism is still not well understood. Its participation in the Paraná magmatism could have been achieved in two ways; either the Paraná (and Karoo) CFB represent asthenospheric melts that have assimilated low melting temperature lithospheric components, or they are the products of wholesale melting of lithospheric mantle.

Thompson and Morrison (1988) invoked the first of these possibilities to account for the incompatible trace element variation still present in samples from Skye and Mull (British Tertiary province) which on isotopic grounds were considered not to have been affected by contamination within the crust. They considered that the flow regime would be turbulent for a large and fast-moving magma batch within a lithospheric dyke and, as described for the crustal environment by Huppert and Sparks (1985){see chapter four}, this would lead to efficient heating of the lithospheric wall-rock, allowing the magma to

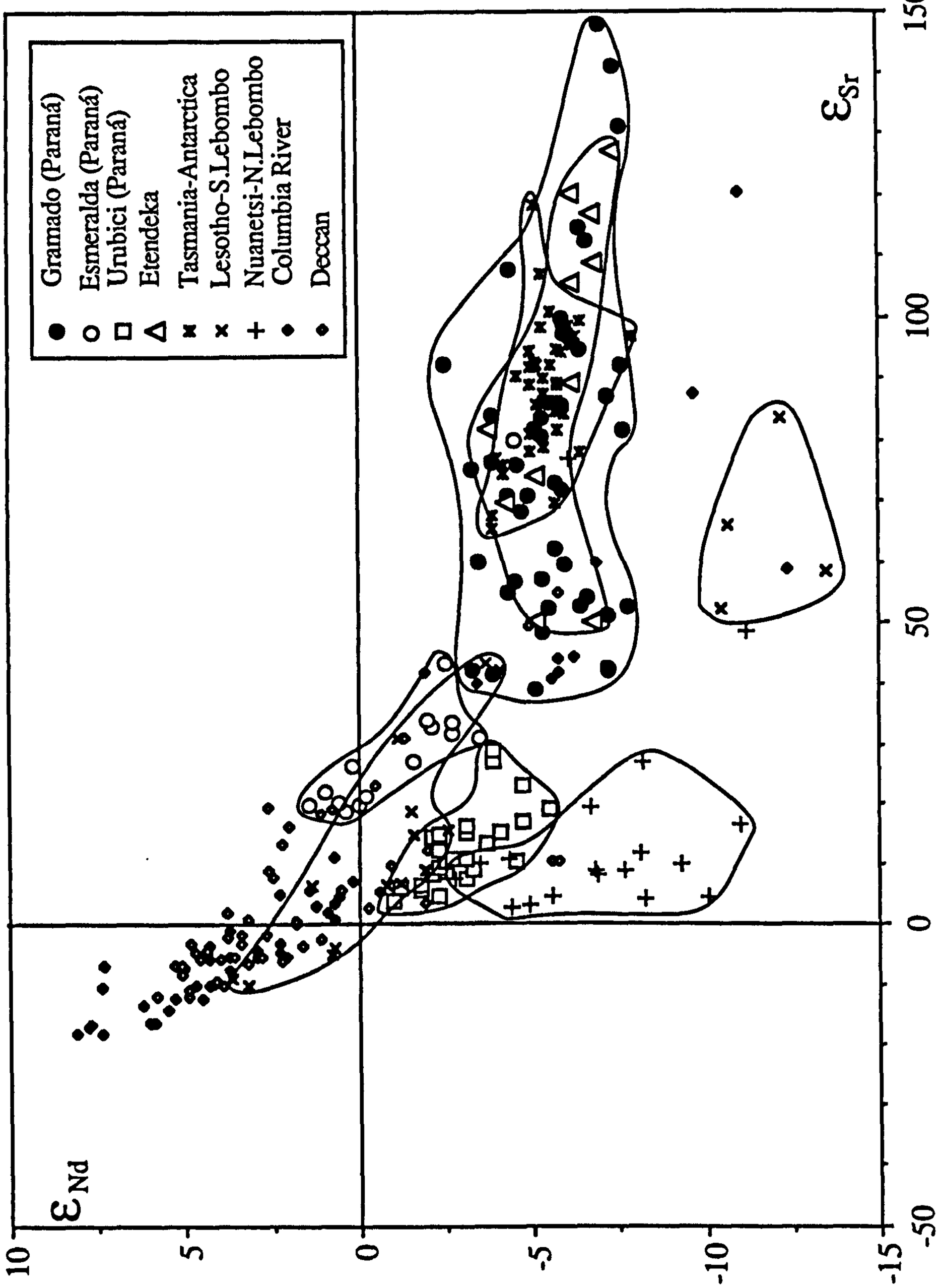

Figure 5.10 Comparison of Sr and Nd isotope variation between CFB provinces. Note the virtual restriction of samples from the Mesozoic CFB of Gondwana to the 'enriched' quadrant, implying a significant contribution from lithospheric material. This is in marked contrast to the Deccan and Columbia River basalts which lie predominantly within the 'depleted' quadrant, consistent with a derivation from an OIB-type asthenospheric source. Data sources - *Paraná* (Gramado, Esmeralda, Urubici) - this study; Hawkesworth *et al.*, (1986, 1988): *Karoo* (Lesotho - South Lebombo, Nuanetsi - North Lebombo) - Hawkesworth *et al.*, (1984b); Ellam and Cox (1989): *Tasmania* and *Antarctica* - Hergt *et al.*, (1989): J.M. Hergt, pers. comm., (1989): *Columbia River* - compilation in Hooper (1988): *Deccan* - Lightfoot (1985).

selectively incorporate the relatively fusible components from the lithospheric mantle. Another possibility suggested, was that the transfer of heat from the asthenosphere to the cooler lithosphere above, by the multiple injection of a closely spaced series of dykes, might itself be sufficient to cause partial melting of the lithospheric mantle on a local scale. The strongly developed lithospheric signature displayed by the Paraná magmatism (and likewise in the Karoo, Antarctican and Tasmanian provinces) suggests that this lithospheric scavenging must therefore have been the dominant process acting on the ascending melts during the evolution of the province. The only magmas that show any convincing evidence for an asthenospheric component are those of the Esmeralda magma type in the Paraná, the Horingbaai dolerites in Etendeka, and the Rooi Rand dolerites of the Karoo. In all three examples, they form just a minor late-stage feature relative to the main lithospheric-dominated CFB magmatism, and it has been argued (*e.g.* Marsh, 1987) that they were erupted only during the more advanced stages of lithospheric attenuation. Thus it is difficult to imagine how this lithospheric mantle assimilation could be maintained to such an extent throughout the whole period of magmatism.

On the other hand, the traditional objections to extracting basaltic melts directly from the continental mantle lithosphere have been that it is cold, and highly depleted in the necessary major element 'basaltic' components (low Al_2O_3, FeO and CaO relative to MgO), as inferred from xenolith data. However, the highly depleted xenoliths appear to be largely confined to Archaean areas, and are believed to represent the residue after removal of large degree komatiite melts (Richter, 1988; Hawkesworth *et al.*, in prep.). Hawkesworth *et al.*, (in prep.) have shown that xenoliths from Proterozoic and younger terrains are generally less depleted in major elements. Thus it appears that the post-Archaean lithospheric mantle is probably sufficiently fertile to generate CFB melts, and this is consistent with the Proterozoic source ages inferred for many of the Mesozoic Gondwana CFB magmas (Brooks *et al.*, 1976; Hawkesworth *et al.*, 1984b, 1986).

Therefore in conclusion, the evidence above has indicated that at least the minor and trace elements in the Paraná CFB magmas were derived from the lithospheric mantle, and futhermore it is suggested that the main Paraná high-Ti and low-Ti magma types were

probably derived from distinct Proterozoic source regions within the continental mantle lithosphere.

5.7 Origins of source mantle characteristics.

5.7.1 Causes of mantle heterogeneity.

Mantle heterogeneity will develop in response to a variety of processes which can cause a redistribution of minor and trace elements, and these are often referred to by the non-specific term of 'mantle enrichment processes'. Two phenomena can play a role in creating a diversity of trace element abundances and isotope ratios within the upper mantle: (i) chemical processes (*e.g.* melt migration, fluid metasomatism) can fractionate parent / daughter ratios, and the effect on the isotopic composition of the daughter element will be amplified through time by radioactive decay, provided that the trace element heterogeneity is stored within an isolated (*i.e.* non-convecting) reservoir, and (ii) mixing between isotopically-distinct components (*e.g.* subducted sediments) derived from different reservoirs that have been physically isolated for geologically long periods of time and which have experienced different histories of trace element enrichment or depletion.

Incompatible trace elements (by definition) are not readily accommodated within the crystal lattices of the common mantle mineral phases and thus they are susceptible to scavenging and mobilisation by small volume fluid or melt phases. The behaviour of a particular trace element will depend on its bulk distribution coefficient between the mantle matrix and the fluid or melt phase. Since bulk distribution coefficients vary as a function of the residual phase assemblage and the nature of the liquid phase, then a wide spectrum of possible styles of mantle enrichment / depletion is expected. This chemical modification of the mantle can be achieved either; (i) by the bulk addition of a small degree melt or fluid, or (ii) by a more complex open-system process in which material is added/removed from percolating melts/fluids. The term 'metasomatism' is generally given to the chemical changes associated with interaction between a fluid or melt, and matrix, whether as contact

effects around the margins of veins or via a pervasive infiltration of H_2O-CO_2-rich fluids (Hawkesworth *et al.*, 1987). Textural, mineralogical and geochemical evidence from mantle xenolith suites (*e.g.* Harte, 1983; Erlank *et al.*, 1982, 1987, etc.) has furnished the most convincing demonstration for the variety of mantle enrichment processes.

The continental mantle lithosphere is relatively rigid and forms a constituent part of the mobile lithospheric plate. It is believed to be physically separate from the underlying asthenospheric regions of active convection, and to have been stabilised shortly after the last major orogenic episode in the overlying crust (Jordon 1978, 1988; Oxburgh and Parmentier, 1978). This tectonic stability and long term isolation from the convecting asthenospheric mantle makes the continental mantle lithosphere a unique reservoir, capable of preserving the effects of a long complex history of mantle enrichment events. It is likely to be sufficiently old under many continental areas (Proterozoic / Archaean) for ancient trace element heterogeneities to be mirrored by variations in radiogenic isotopes.

The continental mantle lithosphere is sampled directly as xenoliths in kimberlite pipes and alkali basalts (*e.g.* Menzies and Murthy, 1980; Erlank *et al.*, 1982, 1987) and, via partial melting, in continental magmatism. This latter conjecture is most convincing in the case of kimberlites and lamproites which have been widely interpreted as small degree lithospheric melts. They are characterised by highly enriched incompatible trace element contents (notably Ba, Sr, Th, LREE) and an extreme range of radiogenic isotopic compositions {ε_{Sr} -16 to +226, ε_{Nd} +1 to -26, $^{206}Pb/^{204}Pb$ 16.02-19.27}(*e.g.* Fraser *et al.*, 1985). The mantle xenolith and kimberlite/lamproite data together, provide a window on the compositional characteristics of the continental mantle lithosphere, and allow a geochemical assessment of trace element enrichment processes in the mantle. The lamproite and kimberlite data on figure 5.11 demonstrates the extreme diversity of Sr and Nd isotopic compositions that can be generated within the continental mantle lithosphere. The extent to which the geochemical characteristics of the mantle lithosphere can be inferred from the characteristics of CFB magmatism is a more contentious issue as we have already seen, especially because of their large volume and because they reflect much larger degrees of

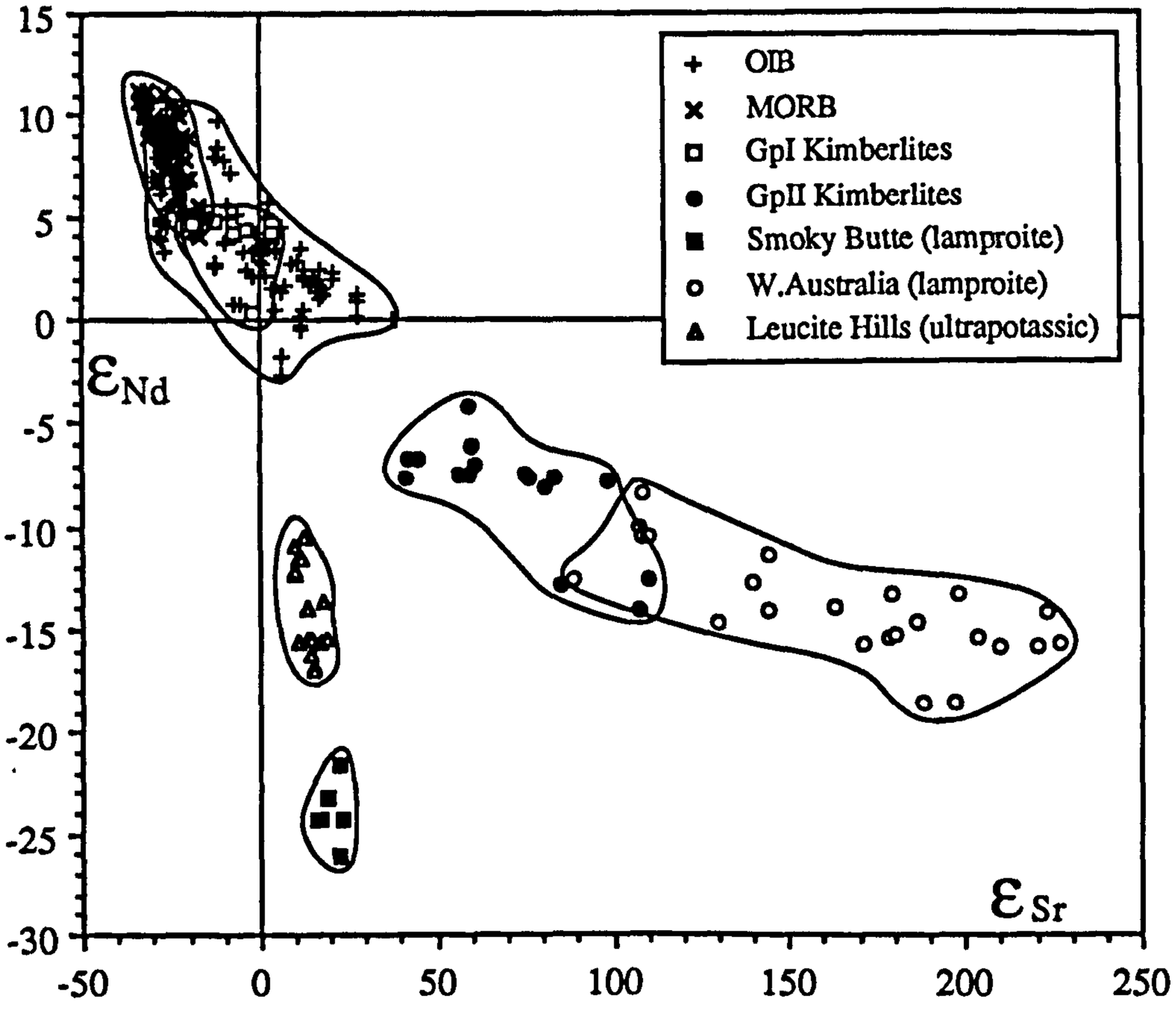

Figure 5.11 ε_{Sr} vs. ε_{Nd} diagram for lamproites and kimberlites, illustrating the wide diversity of possible Sr and Nd isotope compositions that can be generated within the continental mantle lithosphere. Fields for MORB and OIB are also shown to indicate compositions more typical of the asthenospheric mantle. Data sources - Group I kimberlites (Smith 1983); group II kimberlites (Smith, 1983; Fraser *et al.*, 1985); Leucite Hills (Vollmer *et al.*, 1984); Western Australia lamproites (McCulloch *et al.*, 1983; Fraser *et al.*, 1985); Smoky Butte (Fraser *et al.*, 1985).

melting. An encouraging feature though, is the recognition of consistent trends in minor/trace element and Sr and Nd isotope composition between mantle xenoliths, lamproites and kimberlites, and continental flood basalts, which have been attributed to different mantle enrichment processes (Hawkesworth *et al.*, 1984a/b, in prep.; Fraser *et al.*, 1985).

A review of the evidence for mantle enrichment processes from both xenoliths and continental magmas was carried out by Hawkesworth *et al.*, (1984a). They distinguished two dominant styles of trace element enrichment, both producing LREE enrichment (*i.e.* low Sm/Nd) but accompanied by either low or high Rb/Sr ratios. With time, these would

generate two distinct trends on an ε_{Sr} vs. ε_{Nd} diagram (see figures 5.10 and 5.11); a 'steep' trend to low ε_{Nd}, high ε_{Sr}, and a 'shallow' trend towards low ε_{Nd}, low ε_{Sr} respectively. It was suggested that these trends were controlled by distinct trace element enrichment processes within the mantle.

(i) The apparently more common 'steep' trend, characterised by low Rb/Sr and low K/Ti, is believed to reflect enrichment by the migration of small volume 'basanitic' silicate melts, and this conclusion is based on several lines of evidence: (a) many of the low Ti/K basalts have trace element patterns qualitatively similar to those of basinites (see figure 5.12), and such patterns can be modelled as small volume partial melts in equilibrium with garnet-peridotite (Frey *et al.*, 1978), (b) this style of trace element enrichment is the most frequently encountered in spinel peridotite xenoliths where it has been observed to be melt-related (*e.g.* Hawkesworth *et al*, 1984a), and (c) experimental data suggests that the HFS elements are relatively immobile in hydrous fluids.

(ii) The 'shallow' trend, which has high Rb/Sr and high K/Ti, is best demonstrated by the K-richterite- and phlogopite-bearing, garnet-free peridotite (PP and PKP) xenoliths from Kimberley (Erlank *et al.*, 1982). The mineral assemblages in these xenoliths have been ascribed to the effects of pervasive metasomatism and infiltration of H_2O-rich fluids.

These two styles are not necessarily the only trace element enrichment processes that will have occurred within the mantle, although they are probably the most easily detectable. More recent work (*e.g.* Hawkesworth *et al.*, in prep.) has attempted to assess the more subtle geochemical effects of enrichment processes in the presence of other residual phases, such as amphibole and phlogopite, and different fluid phases (*e.g.* CO_2-rich).

The fundamental geochemical division of the Paraná (and most of the other Mesozoic CFB of Gondwana) into high-Ti and low-Ti magma types is noteworthy in the context of these enrichment styles. The high-Ti magmas (*e.g.* Urubici-type) have low Rb/Sr, low ε_{Sr}, low K/Ti, whereas the low-Ti magmas (*e.g.* Gramado-type) have high

Rb/Sr, high ε_{Sr}, high K/Ti. The next sections will consider what constraints can be placed on the nature of the source region to each of these distinctive compositions.

5.7.2 The 'high-Ti' source region.

The Urubici magma type composition shows many of the geochemical characteristics that typify within-plate basalts (*e.g.* Pearce and Cann, 1973); *viz.* low Sm/Nd, low Rb/Sr, low ratios of LIL- to HFS- elements, and high abundances of HFS elements (*i.e.* Ti, Zr, Nb). This is a feature common to the high-Ti magmas throughout Gondwana and suggests that a similar process was involved in producing the high-Ti source regions. Such trace element signatures are conventionally attributed to source enrichment by migration of small volume 'basanitic' mantle melts (see figure 5.12). It has been suggested (Menzies and Wass, 1983) that metasomatism by CO_2-rich fluids can also

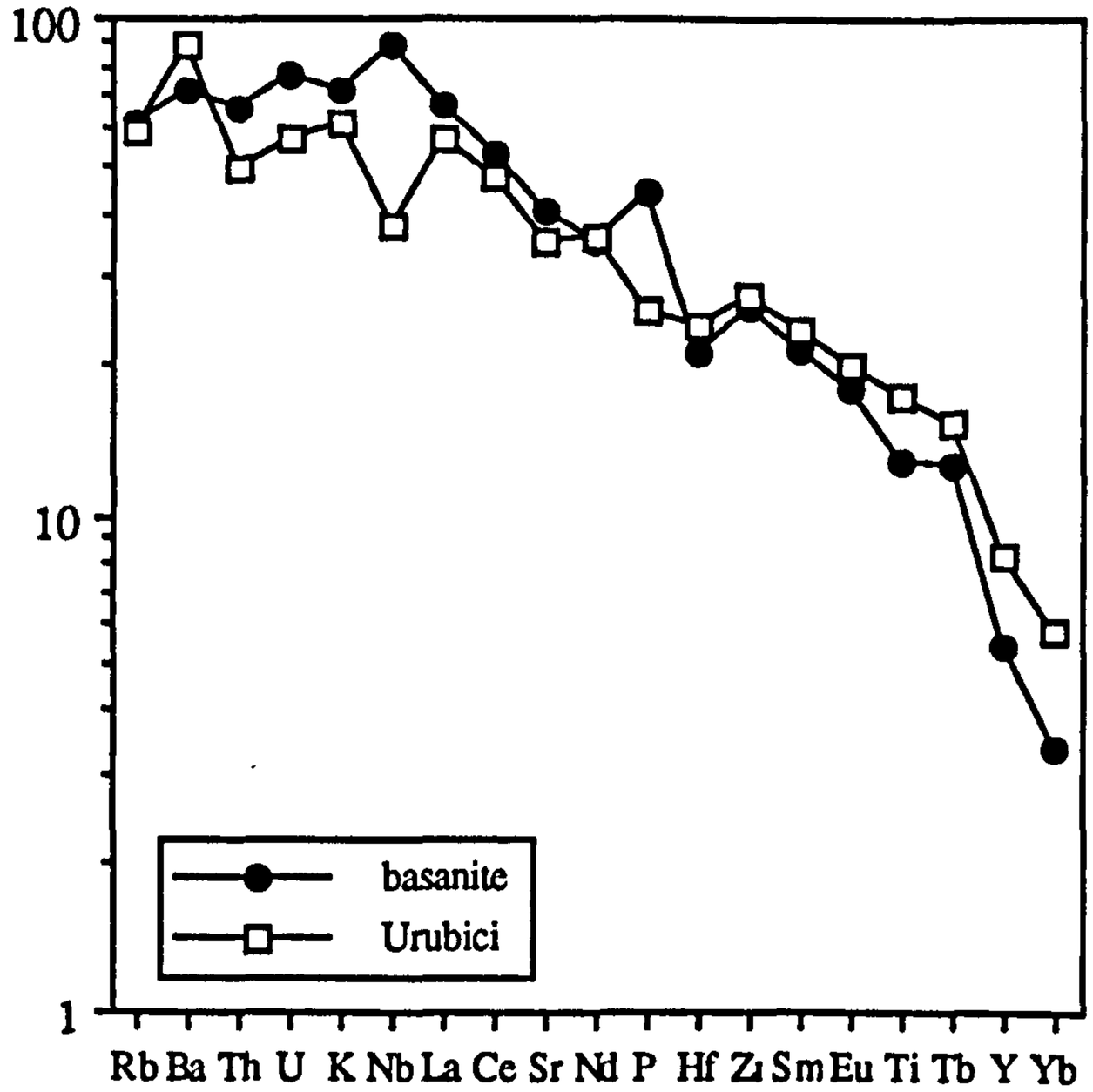

Figure 5.12 'Primitive mantle'-normalised trace element abundance diagram showing the qualitative similarity in pattern between an average Urubici-type composition and a typical basanite (from Frey *et al.*, 1978).

lead to similar trace element characteristics as melt enrichment, but it is possible that the main role of CO_2 is simply to reduce the viscosity of the melt and thus increase its ease of extraction and mobility (Hawkesworth *et al.*, in prep.). This suggests that variable influx of small volume partial melts was probably an important factor in the development of the Urubici source region.

Evidence for a melt-related enrichment process can be found from the observed isotopic features of the Urubici-type (and other high-Ti CFB) magmas, which are consistent with our current understanding of the fractionation of parent / daughter trace element ratios during partial melting processes. Allègre *et al.*, (1986) introduced the

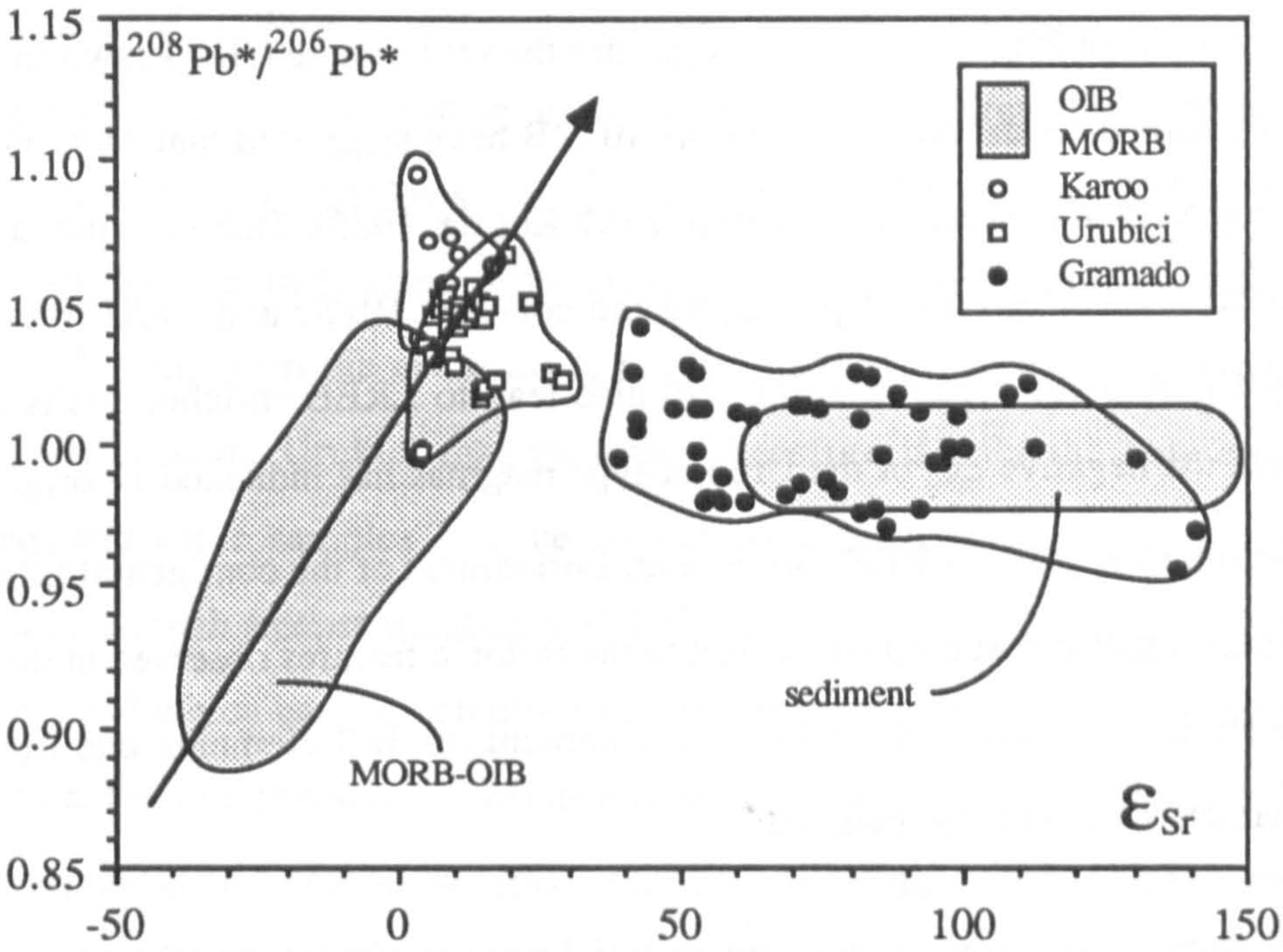

Figure 5.13 Variation of $^{208}Pb^*/^{206}Pb^*$ vs. ε_{Sr} for the Paraná and Karoo CFB. 'High-Ti' magmas from the Paraná (Urubici magma type) and Karoo (Nuanetsi picrites; Ellam and Cox, 1989) lie on an extension of the MORB / OIB trend suggesting a similar, but either more extreme or older, Rb/Sr - Th/U fractionation. 'Low-Ti' magmas from the Paraná (Gramado magma type) are displaced from the MORB / OIB / High-Ti CFB trend towards the sediment field. MORB / OIB and sediment fields are from Allègre *et al.*, (1987).
$^{208}Pb^*/^{206}Pb^*$ is a measure of the time-integrated Th/U ratio (see Allègre *et al.*, 1987) and is defined as;

$$^{208}Pb^*/^{206}Pb^* = \frac{(^{208}Pb/^{204}Pb)_{measured} - (^{208}Pb/^{204}Pb)_{Canyon\ Diablo}}{(^{206}Pb/^{204}Pb)_{measured} - (^{206}Pb/^{204}Pb)_{Canyon\ Diablo}}$$

where $(^{206}Pb/^{204}Pb)_{Canyon\ Diablo} = 9.307$ and $(^{208}Pb/^{204}Pb)_{Canyon\ Diablo} = 29.476$.

concept of $^{208}Pb^*/^{206}Pb^*$ as a measure of the time-integrated Th/U ratio (see caption to figure 5.13 for definition), and the variation of $^{208}Pb^*/^{206}Pb^*$ with ε_{Sr} for MORB / OIB and CFB is illustrated in figure 5.13. The MORB and OIB data define a positive correlation between $^{208}Pb^*/^{206}Pb^*$ and ε_{Sr}, and this indicates that there is a coherent fractionation in Rb/Sr and Th/U in the establishment of upper mantle heterogeneities (Allègre *et al.*, 1986). The Urubici-type magmas, and high-Ti samples from the Karoo (Ellam and Cox, 1989), lie on an extension of this MORB / OIB trend but at higher $^{208}Pb^*/^{206}Pb^*$ and ε_{Sr}, which suggests a similar but more extreme Rb/Sr-Th/U fractionation. It has already been shown (see section 5.4.1) that the Urubici-type magmas also lie on an extension of the MORB / OIB 'mantle-array' on an ε_{Sr} vs. ε_{Nd} diagram (figure 5.2), suggesting a similar coherence with Sm/Nd fractionation. Small volume (*i.e.* F << 1 %) melts, in the absence of residual phlogopite, will have Rb/Sr ratios slightly greater than the source (Hawkesworth *et al.*, in prep.). Th-isotope disequilibrium studies on MORB have suggested that Th/U ratios will similarly be greater in the melt than the source (McKenzie, 1985). Therefore partial melting appears to be a viable means of producing the coherent Rb/Sr and Th/U fractionation implied by figure 5.13. Partial melting will also lead to LREE enriched melts (*i.e.* low Sm/Nd), and the negative ε_{Nd} of the Urubici-type magmas has indicated an origin from a source with time integrated LREE enrichment. Enrichment of the continental lithospheric mantle by such melts can subsequently lead to the isotopic features observed in the high-Ti CFB, as well as introducing the relative enrichment in HFS elements and other trace element characteristics of these magmas.

Evidence for the timing of this source enrichment can be inferred from isotopic data on the Urubici-type magmas. Brooks *et al.*, (1976) suggested that basalts derived from a lithospheric source should define a 'mantle isochron' with an apparent age corresponding to the time of stabilisation of the source. This will only occur if the erupted magmas inherit both the isotope and parent / daughter trace element ratios of their sources, and many factors during CFB petrogenesis {*e.g.* fractional crystallisation, partial melting, magma mixing, crustal contamination} will often act to obscure any such relationships. In terms of both Sr and Nd isotope compositions, the Urubici-type basalts do not preserve an

isochronous relationship between either Rb/Sr and $(^{87}Sr/^{86}Sr)_i$, or Sm/Nd and $(^{143}Nd/^{144}Nd)_i$. An alternative method is to calculate Nd model ages (T_{DM}) which represent the age of isolation of the source from the convecting, depleted mantle. The Urubici-type basalts have an average T_{DM} of 1.3 ± 0.1 Ga, but this must be regarded as a minimum age for the source region since it is likely that Sm/Nd has been fractionated from its ratio in the source during partial melting (see section 5.4.2).

Hawkesworth *et al.*, (1986) interpreted the linear relationship shown by the Urubici-type samples on a $^{207}Pb/^{204}Pb$ vs. $^{206}Pb/^{204}Pb$ diagram in terms of a source-inherited secondary isochron and obtained an age of about 1.8 Ga. A similar age of 1.9 Ga is produced if all the new analyses generated in this study are included with the data of Hawkesworth *et al.*, (1986), a total of 29 samples. However, the story changes slightly if a more rigorous screening of the samples is carried out. It was argued in chapter three that the samples from the evolved flows with > 55 wt% SiO_2 (DSM24 and DSM04/08) showed evidence for having interacted with crustal material, and similarly the samples DSM05b/07/09, all from the same flow, had anomalous trace element contents when compared to the main Urubici magma type. Therefore if only the new analyses are considered, and these samples just mentioned are removed, leaving a data set of 14 samples, then a much steeper trend on a $^{207}Pb/^{204}Pb$ vs. $^{206}Pb/^{204}Pb$ diagram is produced (see figure 5.14) which has a much older apparent age of 2.6 Ga. This bring us to the old dilemma over the interpretation of linear arrays on a diagram such as figure 5.14, which can either represent an isochron or a mixing array. The samples on this steeper trend cover a range in $(^{87}Sr/^{86}Sr)_i$ of 0.7048 to 0.7057 and Th/Ta of 2.1 to 2.8 that in chapter three was attributed to the effects of contamination, and this would imply a mixing relationship. It is worth pointing out though that these samples form a coherent variation on Figure 5.13 of $^{208}Pb^*/^{206}Pb^*$ and ε_{Sr}, lying on the line of the marked arrow. This would suggest that any high ε_{Sr} crustal material would also have to have $^{208}Pb^*/^{206}Pb^*$ of about 1.1 or greater, which is certainly different to that affecting the Gramado magma type. This leaves open the possibility that this might be a mantle rather than a crustal feature. It is possible to

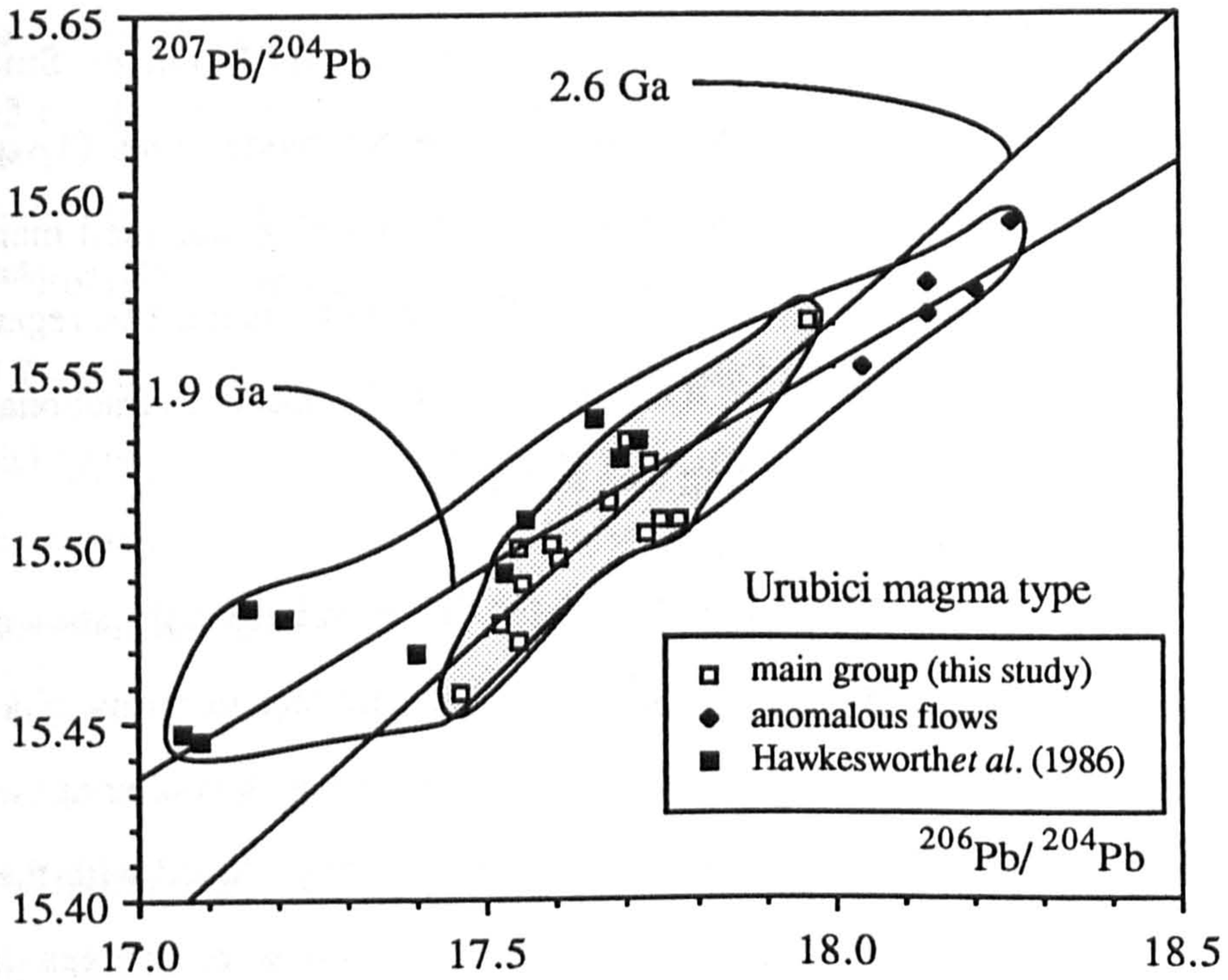

Figure 5.14 $^{207}Pb/^{204}Pb$ vs. $^{206}Pb/^{204}Pb$ diagram for the Urubici magma type. If the linear array is interpreted as a secondary isochron then an apparent source age of 1.9 Ga is obtained from the whole data set {this study; Hawkesworth *et al.*, 1986}. The shaded area represents just data from this study, minus the anomalous flows (DSM24, DSM04/08, DSM05b/07/09), and this gives a Pb-Pb age of 2.6 Ga.

calculate a model Pb age {from the Stacey and Kramers (1975) two-stage Pb ore growth curve) for the possible end-member composition if the data is interpreted as a mixing array. For the least radiogenic Urubici-type composition, this produces a model age of about 2.2 Ga, which is more in keeping with the age of major crust generation in this region of southern Brazil (Mantovani *et al.*, 1986).

5.7.2 The 'low-Ti' source region.

The Gramado magma type of the southern Paraná forms part of a large 'low-Ti' geochemical province stretching right across the former Gondwana landmass from South America to Tasmania (see figure 5.15). These low-Ti basalts have minor and trace element compositions significantly different to OIB, with relatively low HFS- and high LIL-element abundances. In fact they have many geochemical features reminiscent of recent subduction-related basalts; *viz.* high Ba/Nb and low Ti/Y, and despite an obvious 'within-

plate' tectonic setting, most low-Ti CFB magmas would actually classify on tectonic discriminant diagrams as calc-alkaline basalts (see Duncan, 1987). This not surprisingly has led to the suggestion that previous subduction episodes had contributed to the development of the low-Ti source region, although the exact nature of this 'subduction component' and the timing of its enrichment of the source region are uncertain. Duncan (1987) addressed the various possibilities available for the development of the southern Karoo low-Ti source region: either it was in some way related to the Devonian / Recent subduction that was taking place along the Pacific margin of Gondwana (*e.g.* Cox 1978) (see figure 5.15), or it reflected the effects of a much earlier Proterozoic subduction episode(s) (*e.g.* Hawkesworth *et al.*, 1984b).

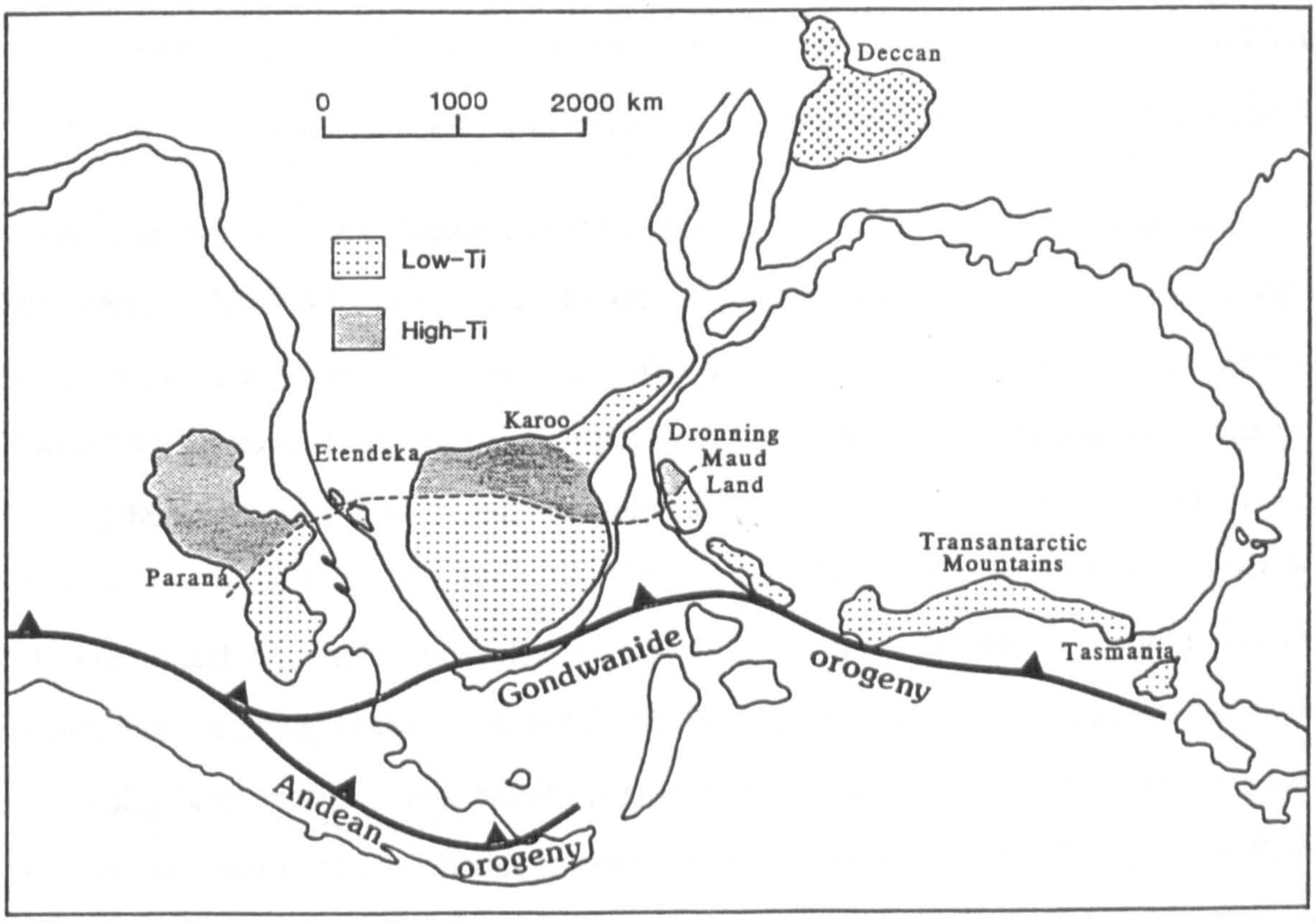

Figure 5.15 Map of the reconstructed Gondwana super-continent showing the vast extent of the 'low-Ti' geochemical province within the Mesozoic CFB lavas, and its spatial relationship to the Devonian/Recent subduction along the Pacific margin.

Geochemical relationships

The effects of source modification by H_2O-rich fluids can be seen from the PP/PKP xenoliths from Kimberley (Erlank *et al.*, 1982), which have low Sm/Nd and high Rb/Sr, K/Ti (and thus with time, high ε_{Sr}, low ε_{Nd}), and these features are also characteristic of the low-Ti Mesozoic Gondwana CFB magmas. Inferences about the source region characteristics of the low-Ti magmas has always been difficult because of the influence of crustal contamination during their magmatic evolution, but the best estimates for 'uncontaminated' basalts (*e.g.* see chapter four for the Gramado magma type) have low Ti, high LIL/HFS element ratios, high Rb/Sr and relatively high ε_{Sr}. Although these first two features suggest a link with subduction processes, the high Rb/Sr required in the source is not a feature of recent subduction-related magmas (Ellam and Hawkesworth, 1988). Instead this is thought to represent a contribution from subducted sediment, consistent with the similar geochemical features displayed by the potassic volcanics of the Italian province where the role of sediment subduction has been demonstrated (Rogers *et al.*, 1987). The trend of the Gramado magma type data, included on figure 5.13 ($^{208}Pb^*/^{206}Pb^*$ vs. ε_{Sr}) would also be consistent with sediment involvement (see Hawkesworth *et al.*, in prep.).

Hergt *et al.*, (1989) have recently outlined such a model to account for the marked crustal geochemical characteristics of the low-Ti Tasmanian dolerites. Among the Gondwana low-Ti magmas, the Tasmanian dolerites have some of the more extreme minor and trace element, and isotopic features; the TiO_2 contents are much lower (< 0.65 wt%) than in the most primitive Gramado-type samples, and they have a more 'enriched' Sr and Nd isotopic signature, with $(^{87}Sr/^{86}Sr)_{175\ Ma}$ of 0.7095 to 0.7125 and ε_{Nd} of -5.0 to -6.5. It was not found possible to reconcile feasibly the trace element and isotope data for models involving crustal assimilation. Alternatively, Hergt *et al.*, (1989) argued that the strong crustal signature of these magmas could be imparted to the source by the introduction of a small quantity (≤ 3 %) of sediment via some process of subduction. The mantle source was inferred to be relatively depleted so that its trace element signature would be dominated by the high elemental abundances in the introduced crustal material.

If sediment subduction is the main control on producing the geochemical characteristics of the low-Ti source region, then it is interesting to speculate on the possible

causes for the variation within the uncontaminated low-Ti magmas across Gondwana. The difference between the source regions to the Gramado magma type in the Paraná and the Tasmanian region could be accounted for in a number of ways with this model;

(i) the composition of sediment and/or the amount added was regionally variable.

(ii) the process of sediment introduction and the sediment composition remained roughly similar over this area, but the initial mantle source showed variable depletion. In this case, the Gramado mantle source must have been initially less depleted in trace elements than the Tasmanian mantle source, so that the added effects of the sediment characteristics were partially masked by its already higher trace element abundances.

To resolve these possibilities in the future will require a comparison of the low-Ti magmas throughout Gondwana, after careful consideration first of the effects of higher level crustal contamination (*sensu stricto*). It was demonstrated in chapter four that the Gramado magma type shows a pronounced regional variation over the southern Paraná area and, moving south, there is an increase in SiO_2, Ba/Nb, and $(^{87}Sr/^{86}Sr)_i$. Maybe on this more local scale, it is easier to envisage the variable addition of a high Ba/Nb component, which plausibly could be sediment, to the source region. If this is the case, then it is more difficult to constrain the timing of the enrichment of the low-Ti Gramado source since the high ε_{Sr} might reflect the addition of a high $^{87}Sr/^{86}Sr$ component (*i.e.* sediment) rather than *in situ* decay within a high Rb/Sr source region.

5.8 The magma types of the northern Paraná.

5.8.1 Introduction.

Most of the discussions in this chapter, and in the previous two chapters, have been biased towards dealing with the magma types of the southern half of the lava field. The elemental and isotopic characteristics of these magma types {the Urubici, Gramado and Esmeralda magma types} have been clearly established, and the petrogenetic origins of the

geochemical variations displayed within each magma type are, broadly speaking, reasonably well understood. In contrast, the trace element and isotopic compositions of the northern magma types {the Pitanga, Paranapanema and Ribeira magma types} are still poorly constrained. The aim of this section is to use the available data to provide a brief description of the relationships between these northern magma types, and suggest how they might fit into the emerging picture of the Paraná magmatism. It is largely confined to defining several problems posed by the northern magma types, and introducing possible ideas as a means of explanation. Much future work on the northern magma types is required before these issues can be resolved.

5.8.2 The Paranapanema magma type.

The status of the Paranapanema magma type has suffered from its general inclusion with the Pitanga magma type as part of a single 'northern high-Ti' magma type in the literature. The marked compositional differences that distinguish the Paranapanema magma type from the other truly high-Ti magma types {Urubici and Pitanga} were outlined in chapter two. Many minor and trace elements have abundances in the Paranapanema magma type that are intermediate to the two extremes of the low-Ti magma types and the other high-Ti magma types, and this is best shown by their TiO_2 contents; the Paranapanema-type samples have 2-3 wt% TiO_2 compared with < 2 wt% and > 3 wt% for the low-Ti and high-Ti magmas respectively. Not much attention has been paid as to how the Paranapanema magma type fits into the general petrogenetic scheme for the Paraná magmatism, and it is uncertain whether this magma type has a closer affinity with the low-Ti magmas or the other high-Ti magmas. The 'intermediate' nature of its elemental abundances has led to speculation as to whether it represents an intermediate degree of partial melting to the low-Ti and high-Ti magmas (Fodor, 1987) or instead is related to the low-Ti and high-Ti magmas by some type of mixing process (Piccirillo *et al.*, 1988a).

Fodor (1987) argued that the majority of the Paraná lavas were the product of variable degrees of partial melting, governed by their position relative to the Tristan da Cunha hot-spot. The inferred percentage melting for the low-Ti and high-Ti magmas were

25 % and 11 % respectively. This model did not rule out the existence of magmas derived by intermediate degrees of melting, and Fodor (1987) suggested that the Paranapanema-types samples mentioned by Piccirillo *et al.*, (1988a) could represent the products of about 20 % melting. This would be consistent with the view of Piccirillo *et al.*, (1988a) that the Paranapanema magma type was largely restricted to the central region of the lava field, lying in a transition zone between the high-Ti magmas of the north and low-Ti magmas of the south. Unfortunately this conflicts with the picture of the regional lava stratigraphy revealed by the borehole studies in chapter two, which does not show a simple succession from low-Ti {Gramado} to intermediate-Ti {Paranapanema} to high-Ti {Urubici, Pitanga} magma types, or *vice versa*. Instead, the Paranapanema magma type occurs as the last major geochemical unit over most of the north and west of the lava field, overlying the Pitanga magma type.

Geochemical considerations also rule out the possibility of the suggestion of Fodor (1987). The limited REE available for the Paranapanema magma type (10 borehole samples) indicate that it has the same $(Tb/Yb)_N$ of 1.2-1.5 as found in the Gramado magma type (*c.f.* 1.2-1.4). This is markedly different from the higher values that characterise both the Urubici and Pitanga magma types (2.0-2.4 and 1.5-1.9). Using the same arguments marshalled earlier for the behaviour of (Tb/Yb) during melting, this leaves a situation where this variety of magma types cannot be reconciled by variable degrees of melting of the same mantle source. Even though this model cannot be the explanation for all the magma types, a melting relationship might exist between any two of these magma types.

Piccirillo *et al.*, (1988a) showed that the compositional variation within the Paranapanema magma did not define a mixing array between a low-Ti and a high-Ti composition, but the parental magma to the Paranapanema magma type could be a mixture between primitive low-Ti and high-Ti compositions. This latter suggestion can now also be ruled out with reference to figure 5.16 of $(Tb/Yb)_N$ vs. Ti/Tb. Any mixing curve on this diagram will be linear because the denominator of both plotted elemental ratios is the same (Langmuir *et al.*, 1978). Because the Paranapanema and Gramado magma types have the

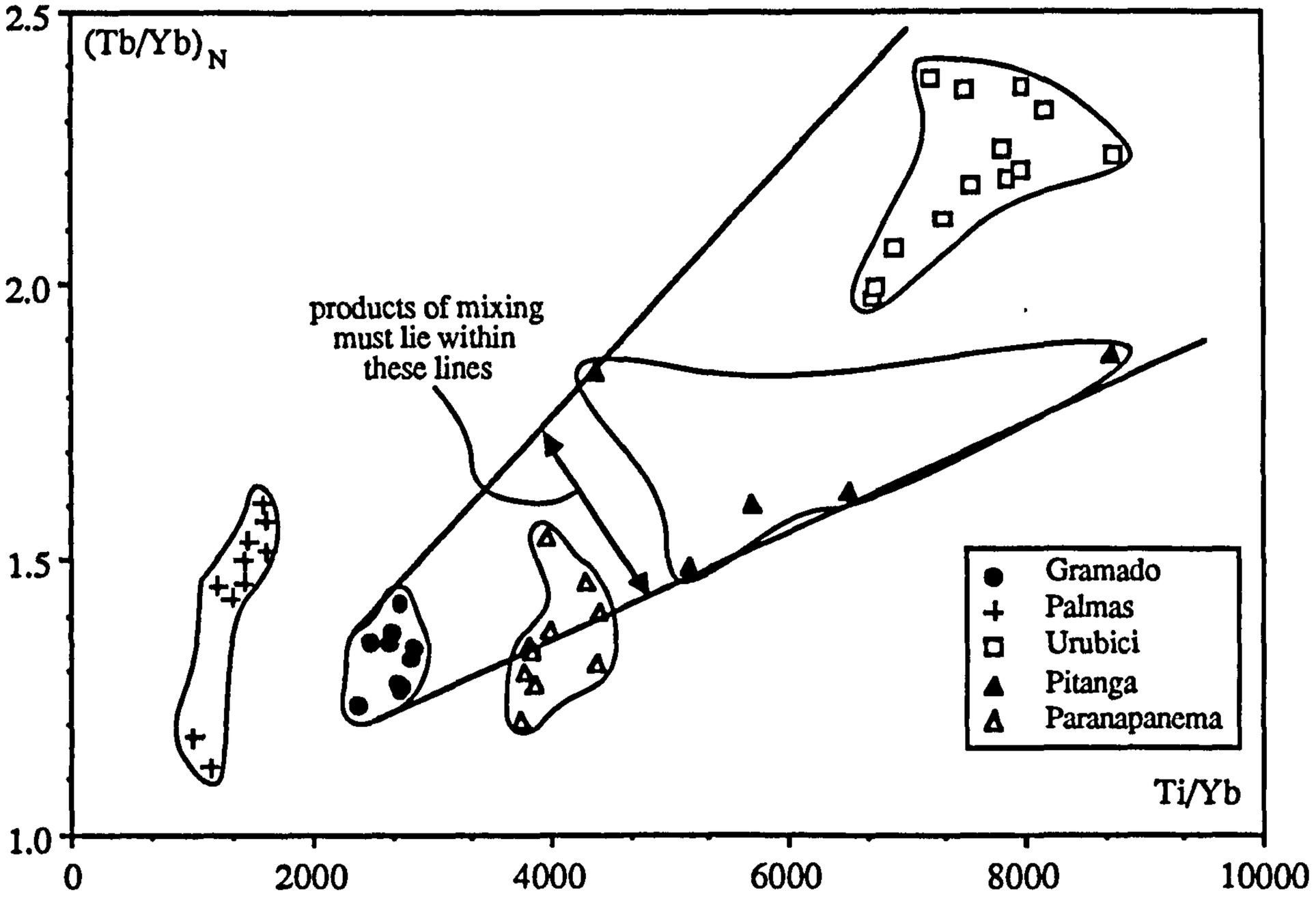

Figure 5.16 Variation of $(Tb/Yb)_N$ vs. Ti/Yb for Paraná magma types. Products of mixing between a Gramado-type magma and either an Urubici-type or a Pitanga-type are constrained to lie within the two lines drawn. Half of the Paranapanema-type samples fall outside these lines, indicating that they are not a result of mixing between high-Ti and low-Ti magmas.

same $(Tb/Yb)_N$ ratio of about 1.2-1.4, this must also be true of any 'enriched' (*i.e.* Ti/Yb > 5000) mixing end-member, and this not consistent with either the Urubici or Pitanga magma types.

The borehole samples have provided a good impression of the major and trace element variations within the Paranapanema magma type (once samples with L.O.I. > ~1.5 wt% have been eliminated), preserving quite tight data arrays. Another, still unaccounted for, feature of the Paranapanema magma types is the range of $(^{87}Sr/^{86}Sr)_i$ of 0.7055 to 0.7078 (see chapter two), and this requires further investigation. It is hoped that the fresh surface samples of this magma type collected recently in Paraguay and northern Argentina will form the basis of a future detailed geochemical study of the Paranapanema magma type.

5.8.3 Ribeira and Pitanga magma types: a possible role for partial melting variations ?

It has already been established that the large-scale north-south divide into high-Ti and low-Ti geochemical provinces in general reflects fundamental compositional differences in the respective mantle source regions. The lavas of the northern half of the Paraná basin, though, are not exclusively of high-Ti affinity, and scattered low-Ti samples, assigned to the Ribeira magma type (see chapter two), have been reported by Petrini *et al.*, (1987). Petrini *et al.*, (1987) argued that the Ribeira-type lavas were compositionally distinct from the more southerly low-Ti varieties (*viz.* Gramado and Esmeralda magma types), and for samples with similar MgO and $(^{87}Sr/^{86}Sr)_i$ (< 0.706), the Ribeira-type were relatively enriched in SiO_2 and incompatible elements (K, P, Sr, Ba, Rb, La, Zr, etc.). The enrichment of Sr along with other incompatible elements, accompanied by almost no variation in Sr isotopic composition, is not readily compatible with any crustal assimilation processes, and the conclusion was that the main north-south difference among low-Ti magmas could only be reconciled by appealing to systematic regional heterogeneities within the mantle source, although with the effects of crustal contamination superimposed on many of the southern low-Ti lavas.

It is important to note that although there is some disagreement among workers as to the composition of the 'uncontaminated' low-Ti parental magmas of southern Paraná (see chapter four), nobody disputes that the Ribeira magma type is distinct. The preferred choice given in chapter four for the Sr and Nd isotopic composition of uncontaminated parental liquid to the main southern low-Ti magma type (*i.e.* Gramado) was $(^{87}Sr/^{86}Sr)_i$ ~0.7075 and $(^{143}Nd/^{144}Nd)_i$ ~0.5123, whereas Petrini *et al.*, (1987) suggested a uncontaminated parental magma composition of $(^{87}Sr/^{86}Sr)_i$ ~0.7046 and $(^{143}Nd/^{144}Nd)_i$ ~0.5126 based on Esmeralda-type magmas. In contrast to both of these, according to Petrini *et al.*, (1987) the Ribeira magma type has $(^{87}Sr/^{86}Sr)_i$ ~0.7058 and $(^{143}Nd/^{144}Nd)_i$ ~0.5122-3, assuming Sm/Nd ~0.23 (Marques, 1988).

Geochemical relationships

It is interesting that, within the northern region, the low-Ti Ribeira magma type and the genuinely high-Ti (*i.e.* > 3 wt% TiO_2) Pitanga magma type share many geochemical features. The Ribeira and Pitanga magma types have similar primitive mantle-normalised trace element abundance patterns, as was noted by Marques *et al.*, (1988), and this is illustrated on figure 5.17 where average compositions for the two magma types have been plotted. The average composition for the Pitanga magma type is taken from table 2.4. The major element and XRF-determined trace element data for the Pitanga magma type are based on 53 borehole samples, but only four of these have been analysed by INAA for REE, Th, U, Ta, Hf. Average data for the Ribeira type (n=19) are given in Petrini *et al.*, (1987), and a few (n=10) REE analyses are available in Marques (1988). The plotted average Pitanga composition has an MgO content of 4.4 wt%, and is quite evolved in comparison to the average Ribeira composition that has 5.4 wt% MgO. The only major

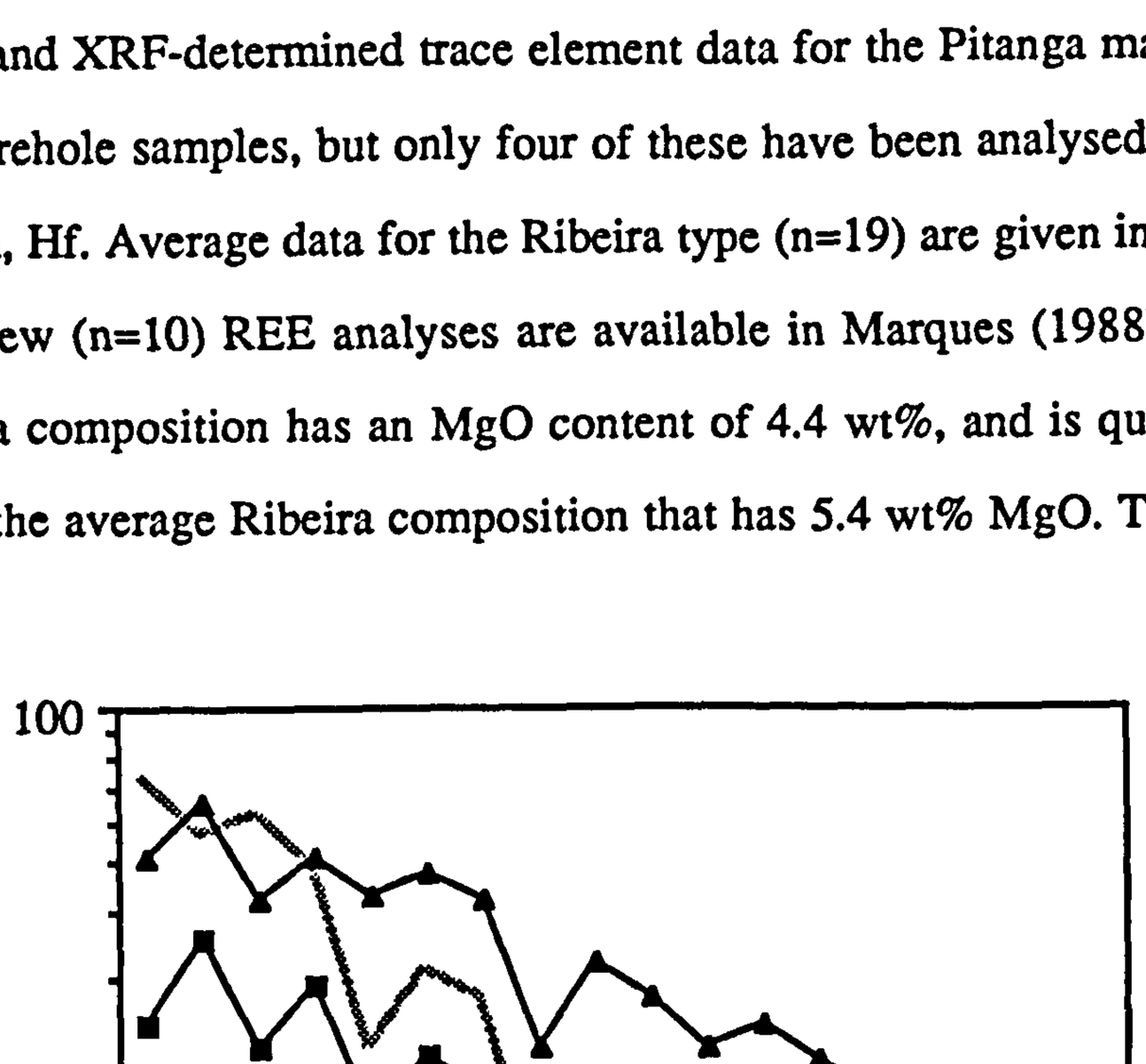

Figure 5.17 'Primitive-mantle'-normalised plot of average compositions of Ribeira and Pitanga magma types, showing the similarity in trace element patterns. The average Gramado-type composition is included for comparison. Data sources - (Pitanga, Gramado - this study: Ribeira - Petrini *et al.*, 1987; Marques 1988).

discrepancies between the two patterns are the marked negative Sr-anomaly in the Pitanga magma type, which perhaps reflects plagioclase fractionation, and the variable enrichment at the less incompatible end of the diagram (*i.e.* Ti to Yb) which results in variable LREE/HREE enrichments between the two magma types {*e.g.* $(La/Lu)_N$ Pitanga 7.4 ± 0.3 vs. Ribeira 3.8 ± 0.3; Marques *et al.*, (1988)}.

Table 5.4 shows the good agreement for several incompatible trace element ratios between the two magma types. As was noted above, good quality trace element data on these northern magma types are rather sparse within the literature, and this is also true for isotopic data with only a handful of Sr and Nd analyses and no Pb isotopic data presently available. It appears that the geochemical similarity also extends to their Sr and Nd isotopic compositions, since the Pitanga magma type has $(^{87}Sr/^{86}Sr)_i$ of 0.7055-60 (borehole samples, this study; Piccirillo *et al.*, 1987) and $(^{143}Nd/^{144}Nd)_m$ of 0.51238-46 (Cordani *et al.*, 1988) which compares with the isotopic values given by Petrini *et al.*, (1987) for the Ribeira magma type of $(^{87}Sr/^{86}Sr)_i$ 0.7055-60 and $(^{143}Nd/^{144}Nd)_m$ 0.51240-48. The restricted isotopic range in both magma types suggests that crustal interaction has not played a major role in their evolution.

	Ti/Zr	Ti/K	Rb/Sr	Rb/Ba	$(^{87}Sr/^{86}Sr)_i$
Ribeira	80	1.6	0.07	0.046	0.7055-0.7060
Pitanga	76	1.8	0.07	0.055	0.7055-0.7060

Table 5.4 Similarities of incompatible trace element and initial Sr isotopic ratios between the Pitanga and Ribeira magma types. Data sources - {Pitanga - this study, Picirillo *et al.*, 1987; Ribeira - Petrini *et al.*, 1987).

The reasonable agreement of incompatible trace element and isotopic ratios between the Ribeira and Pitanga magma types strongly suggests that both could be produced from varying degrees of partial melting of a single, homogeneous mantle source. At present there have been no detailed investigations of the petrogenetic processes that operated during

the individual evolution of the Ribeira and Pitanga magma types, and a better understanding of the compositional variations found within each magma type will be required before any detailed evaluation of the partial melting hypothesis can be carried out. It is equally important to establish the stratigraphical relationship between these two magma types. Chapter two showed that no Ribeira-type samples had been been encountered in any of the sampled boreholes. This, together with their surface distribution reported by Petrini *et al.*, (1987), suggests that the Ribeira magma type may overlie both the Pitanga and Paranapanema magma types and be exposed around the extreme north-east and north-west margins of the lava field.

Thus it appears that for the northern half of the Paraná CFB province there may be less need to invoke mantle heterogeneities to produce the low-Ti / high-Ti distinction since it could plausibly be controlled, at least on a local scale, by variations in the extent of melting of a single mantle source. This may also have implications for the 'northern low-Ti' region (Cox, 1988) of the Karoo CFB province. In Zambia and Malawi there is a similar, but relatively minor, transition back to low-Ti magmas, which are not geochemically well known. This transition might not be related to the large-scale mantle heterogeneity that has been postulated to explain the dominant high-Ti / low-Ti geochemical provinciality further to the south. An alternative suggestion is that it might be the result of local partial melting variations of a source that also yielded the high-Ti rocks of Nuanetsi and north Lebombo, and therefore these low-Ti magmas might have no connection with the dominant Lesotho low-Ti magma type of the south.

5.8.4 Pitanga and Urubici magma types: geographical distinctions within the High-Ti magmas.

Bellieni *et al.*, (1984a) first noticed the distinction in composition of the high-Ti (> 3 wt% TiO_2) between the north and south of the province. This difference was reviewed in chapter two (see section 2.4.3), where it was discussed in terms of two distinct magma types; the Urubici magma type in the south and the Pitanga magma type in the north. For a similar MgO content, the Urubici-type magmas are enriched in SiO_2 and most incompatible

elements (*e.g.* K, Sr, Ba, Rb, Th) relative to the Pitanga-type magmas, and have lower Fe_2O_3(t). The trace element abundance patterns for the Urubici and Pitanga magma types in general share similar features, just at different absolute abundances, except for the least incompatible elements Y and Yb whose content is similar in both magma types.

The geographical variation is also shown in the available isotopic data. Lavas of the Urubici magma type have a range in $(^{87}Sr/^{86}Sr)_i$ of 0.7048 to 0.7062, with the majority (> 70%) of samples lying between 0.7048 and 0.7053, and $(^{143}Nd/^{144}Nd)_i$ is generally between 0.51220 and 0.51242. $(^{87}Sr/^{86}Sr)_i$ within the Pitanga magma type, on the other hand, is about 0.7055 to 0.7060, with $(^{143}Nd/^{144}Nd)_i$ in the range 0.51216 to 0.51227, assuming an Sm/Nd ratio of 0.22 (Piccirillo *et al.*, 1987; Cordani *et al.*, 1988). This implies that the Urubici magma type has a more 'depleted' isotopic signature {*i.e.* lower $(^{87}Sr/^{86}Sr)_i$ and higher $(^{143}Nd/^{144}Nd)_i$} relative to the Pitanga magma type, and this is illustrated on figure 5.18. No Pb isotope data are available on samples of the Pitanga

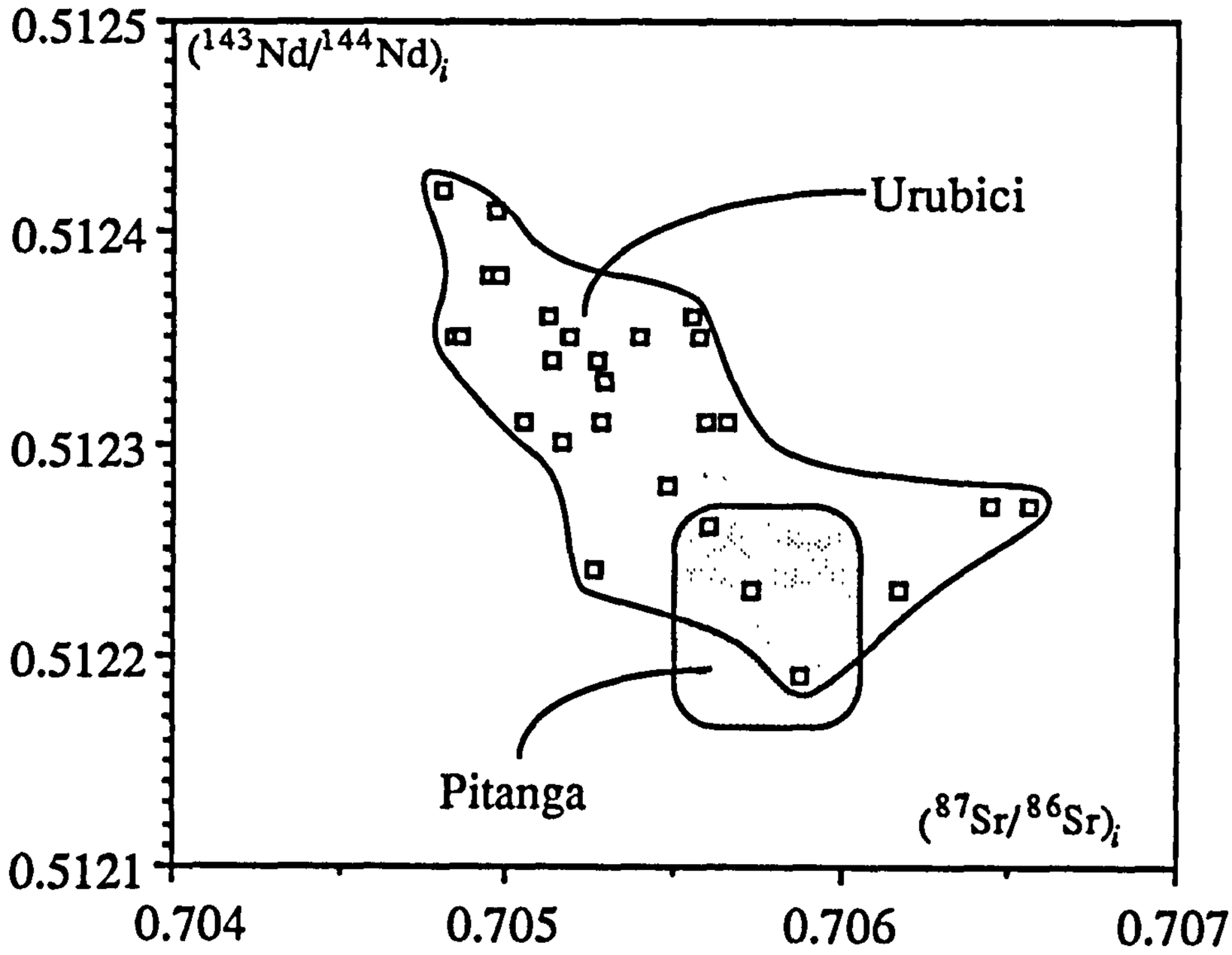

Figure 5.18 Sr and Nd isotopic variation for the Urubici (open squares) and Pitanga (shaded area) magma types, showing that the Pitanga magma type has a more 'enriched' isotopic signature to the majority of the Urubici-type samples. Pitanga data - {Piccirillo *et al.*, 1987; Cordani *et al.*, 1988}.

magma type to enable any comparison with the Urubici-type magmas.

To put these two magma types into some perspective, it was argued in chapter two that volumetrically the Pitanga magma type dominates over the Urubici-type. The Urubici magma type is apparently restricted to the eastern margin of the lava field (east of ~52° W) between latitudes 25° S and 29° S. The Pitanga magma type occurs extensively throughout the lava field to the north of this, and also towards the west in Paraguay and Argentina north of about 27° S. The quantity of trace element and isotope data on the Urubici magma type is disproportionate to its spatial extent, which is a reflection of its better exposure at the northern end of the coastal Serra Geral escarpment. In contrast, despite its size, the Pitanga magma type is still relatively unconstrained in terms of many trace element abundances (*e.g.* REE, Th, Ta, Hf etc.) and its isotopic composition, especially Pb ratios.

It is difficult, on several grounds, to ascribe the difference between the Urubici and Pitanga magma types to crustal interaction. The elevated trace element contents of the high-Ti magmas (*e.g.* Sr > 400 ppm) makes it more difficult for crustal contamination to have any detectable effect on the erupted lava compositions. The evolution of the Urubici magma type was discussed in chapter three and although several features were attributed to crustal interaction, this was not the dominant control on the magmatic composition. The Urubici-type samples that showed any signs of assimilating crustal material did not have compositions approaching that of the Pitanga magma type. The increase in Sr content coupled with the enrichment in other incompatible elements such as the LIL elements, suggests the involvement of a process in the absence of plagioclase, which is more likely to be a mantle rather than a crustal feature.

One possibility for this could be to invoke partial melting differences within a single 'high-Ti' mantle source region, with the enriched levels of trace elements in the Urubici being a consequence of a lower degree of partial melting than that required to produce the less enriched Pitanga-type lavas. The limited REE data available on the Pitanga magma type apparently indicate a difference in HREE patterns between the two magma types with $(Tb/Yb)_N$ of 1.5-1.9 for the Pitanga magma type compared with 2.0-2.4 in the Urubici

magma type. For a partial melting scenario, this would suggest a role for garnet in the residual source mineralogy. The Sr and Nd isotopic variation between the Urubici and Pitanga magma types demonstrates that the situation can not be this straightforward, involving just variations in the degree of partial melting. The isotope data argue instead for a distinct parental magma to each magma type. This might be solely a feature of the mantle source region, although the otherwise consistent similarities in trace element patterns suggests the involvement of either source- or magma- mixing. The isotope difference between the two magma types either developed in response to an ancient trace element enrichment event that had modified the respective source regions to varying extents, or reflected the addition of a component with a different isotopic composition during some unspecified mixing process. Assessment of these various possibilities awaits new trace element and isotopic data on the Pitanga magma type.

5.9 Geochemical conclusions and future work.

Although shallow level processes such as fractional crystallisation and crustal assimilation were the dominant controls on the geochemical variation displayed within each magma type, these were not the cause of the compositional diversity between magma types as illustrated by the two main southern Paraná magma types, Urubici (high-Ti) and Gramado (low-Ti). It has been argued that distinct parental magmas were required for the Urubici and Gramado magma types, and these could either be a result of different degrees of partial melting of a single homogeneous source or be derived from two different mantle source regions. Trace element and isotope data on these two magma types have strongly favoured the latter possibility of mantle source heterogeneity. The broad division of the Paraná lavas into distinct 'high-Ti' and 'low-Ti' geographical provinces is further evidence in support of this, especially since a similar geochemical division forms a major feature of the earlier Karoo lavas in southern Africa, and together, these are therefore thought to represent the surface expression of a major lateral geochemical discontinuity within the sub-continental lithospheric mantle of Gondwana.

Geochemical relationships

The trace element and isotope characteristics of 'uncontaminated' Urubici- and Gramado- type magmas are notably different to typical asthenospheric magmas (*i.e.* MORB and OIB), and it is concluded that at least the minor and trace elements (and therefore the isotope characteristics as well) of the Paraná CFB were derived from 'enriched' lithospheric mantle sources. This marked lithospheric signature seems to be a common feature to almost all of the Mesozoic CFB of Gondwana (Paraná, Karoo, Antarctica, Tasmania). Xenolith data have suggested that the Proterozoic lithospheric mantle is likely to be more fertile for basalt generation than the more depleted Archaean lithosphere, which would generally be consistent with the inferred source ages for these CFB provinces, and in the case of the Paraná lavas, they appear to have remobilised lithospheric mantle that stabilised shortly after the Transamazonian event (1.8-2.2 Ga). The Urubici magma type shows geochemical characteristics consistent with a derivation from a lithospheric mantle source region that had undergone enrichment by the migration of small volume partial melts. The origin of the source region characteristics inherited by the Gramado magma type is more contentious. It is thought to reflect a contribution from a 'subduction-related' component, either metasomatism by hydrous fluids or via the introduction of subducted sediment.

There are several areas of the Paraná CFB magmatism that still require clarification and further investigation, and these include:

(i) There is scope for a Hf isotope study of the Gramado and Urubici magma types, which might be able to clearly resolve the debate over partial melting differences versus source heterogeneity. In contrast to Nd, where both the Urubici and Gramado magma types have similar Sm/Nd and $(^{143}Nd/^{144}Nd)_i$, Lu/Hf is markedly different between the Urubici (Lu/Hf ~0.06) and Gramado (~0.125) magma types, and if this is a source feature then the difference in Lu/Hf should be detectable in the $(^{176}Hf/^{177}Hf)$ ratio provided the source is old enough.

(ii) Little attention has been paid so far to the northern magma types (Paranapanema, Pitanga, and Ribeira). The scant available data has highlighted several tantalising problems, and a full trace element and isotopic study of these magma types is

urgently required in order to resolve how they fit into the overall petrogenetic scheme of the Paraná CFB magmatism.

(iii) This thesis has not tackled the regional aspects of the Paraná CFB magmatism in the context of the magmatism of the South Atlantic ocean (*e.g.* Tristan da Cunha, Gough, Walvis ridge, Rio Grande Rise). These ocean islands define the DUPAL anomaly of Hart (1984), being displaced to higher $^{207}Pb/^{204}Pb$ and $^{208}Pb/^{204}Pb$ relative to most MORB and OIB for a similar $^{206}Pb/^{204}Pb$. Trace element and Pb isotope data strongly suggest a genetic link between the high-Ti Paraná CFB and the magmas of the DUPAL anomaly, and the geographical restriction (in the South Atlantic region) of the DUPAL anomaly to the area between the Paraná and Etendeka provinces is striking. Hawkesworth *et al.*, (1986) suggested that material from the lithospheric mantle, remobilised during the Paraná event, could become detached and contribute to oceanic volcanism as the ocean basin develops. The Tristan da Cunha hot-spot has been suggested as a possible driving force for the Paraná CFB magmatism and future investigation should consider to what extent (if at all) such a plume signature is seen in the products of the Paraná event.

Chapter 6
Geodynamics and concluding remarks.

6.1 Introduction.

The underlying tectonic factors that lead to the initiation of continental flood basalt magmatism are still poorly understood, especially as to what physical process(es) could produce such large-scale melting events, although there appears to be some relationship with continental rifting processes and the presence of mantle plumes. As Cox (1988) pointed out, "every CFB province has its own particular flavour", and the contrasts in the nature of the magmatism and local tectonic regime between different CFB provinces is probably reflected in the wide variety of geodynamical models that have been proposed to explain CFB. The global applicability of individual models (see summary in chapter one) to account for all CFB provinces is more problematical. Aside from explaining the geochemical signatures of the magmatic products, any geodynamical model should also be able to predict the general layout and internal structure of each province, and this should provide a means of assessing the viability of the various postulated models. Stratigraphical studies of the lava sequences have proved invaluable in this regard, especially in the Columbia River and Deccan provinces, by outlining the sequential development of the lava pile and perhaps indicating the area(s) where the feeder zones to the lava flows are situated. More importantly, they should reveal any migration in the locus of magmatism which might be linked to a change in the regional tectonic environment, perhaps variation within a rifting episode or movement relative to an underlying mantle plume. The connection with tectonics is important since this is what controls access to the various mantle source regions during the evolution of the province.

Any discussion concerning the geodynamic controls on Paraná magmatism must be based within the context of its wider tectonic setting, namely its association with the break-

up of the Gondwana supercontinent and the initiation of the South Atlantic ocean, and studies of the earlier Karoo magmatism of southern Africa are pertinent in developing a geodynamic framework for the Paraná-Etendeka magmatic event.

6.2 Temporal relationship of the Paraná-Etendeka magmatism and the opening of the South Atlantic ocean.

An important aspect is the relative timing of the CFB magmatism found on both continental margins of the South Atlantic ocean to the onset of sea-floor spreading. Independent evidence on the possible age of the South America - Africa rift episode can be obtained from sea floor magnetic anomalies, although there is considerable controversy regarding both their identification and geochronological calibration in this region (Duncan *et al.*, 1984). Austin and Uchupi (1982) suggested that the rift propagation that eventually led to the South Atlantic ocean proceeded from south to north, and the oldest sea floor magnetic anomaly that they could recognise with any certainty off-shore of the Paraná-Etendeka CFB volcanism was anomaly M4 off the Namibian coast. This corresponds to a range in possible ages from 122-127 Ma depending on the choice of timescale used. Evidence for the age of the Paraná and Etendeka magmatism was summarised earlier in chapter one and, although the majority of the Paraná lavas have yielded K-Ar ages in the range 115-135 Ma (*e.g.* Melfi, 1967), the overall conclusion reached for both provinces favoured 130 Ma as a minimum age. From this, Duncan *et al.*, (1984) concluded that the magmatism probably predated the main rifting episode, but there was still a margin of doubt regarding the relative ages of these two events.

Direct geological observations to assess the nature of the association of the lavas with the rifting are sparse in Brazil, largely as a result of the vegetation cover that obscures most of the coastal regions. The Etendeka region on the other hand shows extensive coast-parallel extensional faulting within a 30 km wide zone along the coast, where the lavas are faulted and tilted towards the coast by up to 20°. Rhyolite samples have also been recovered in dredge hauls from the off-shore linear ridges parallel to the coastline that

represent the top edges of fault blocks (S. Milner, pers. comm., 1988). Stratigraphical considerations suggested that the faults were active before, during and after the magmatism (Erlank *et al.*, 1984). This is consistent with the local extrusion of lavas being closely linked with the main episode of continental rifting and suggests that any ideas for the evolution of the Paraná-Etendeka CFB province should be evaluated in the context of a developing continental rift that eventually led to an ocean basin. It is important to bear in mind the caveat that since there might have been a migration of volcanism from west to east within the Paraná lava field towards the future continental margin (see section 1.4.2), the rhyolite-dominated sequences of the Etendeka that were largely contemporaneous with the main rifting event might therefore only represent a later phase of the overall CFB magmatism.

6.3 Location of the flood basalts and rhyolites relative to the incipient South Atlantic rift.

The flood basalts are found over a wide area, but their distribution was not controlled by the location of the eventual plate separation but apparently by the position of the pre-existing Paraná sedimentary basin. This has resulted in the marked asymmetry of the Paraná-Etendeka province with respect to the opening of the South Atlantic, with the Paraná lavas covering an area in excess of 1.2×10^6 km^2. This area is over fifteen times larger than the present day extent of the Etendeka lava remnants that were stranded on the African plate margin. However, in contrast to the basalts, the later silicic volcanics are preferentially located adjacent to the continental margins both in south-east Paraná and in Etendeka, and this is illustrated in figure 6.1. There appears to be a general consensus among workers (*e.g.* Cordani *et al.*, 1980; Erlank *et al.*, 1984; Hawkesworth *et al.*, 1988) that the rhyolites of the Paraná and Etendeka originated via a crustal anatexis process. This would require elevated temperatures at or near the base of the crust, localised along the developing plate boundary. Moreover, the disparity between the distribution of acidic and basaltic lavas indicates that the higher crustal temperatures were not simply the result of

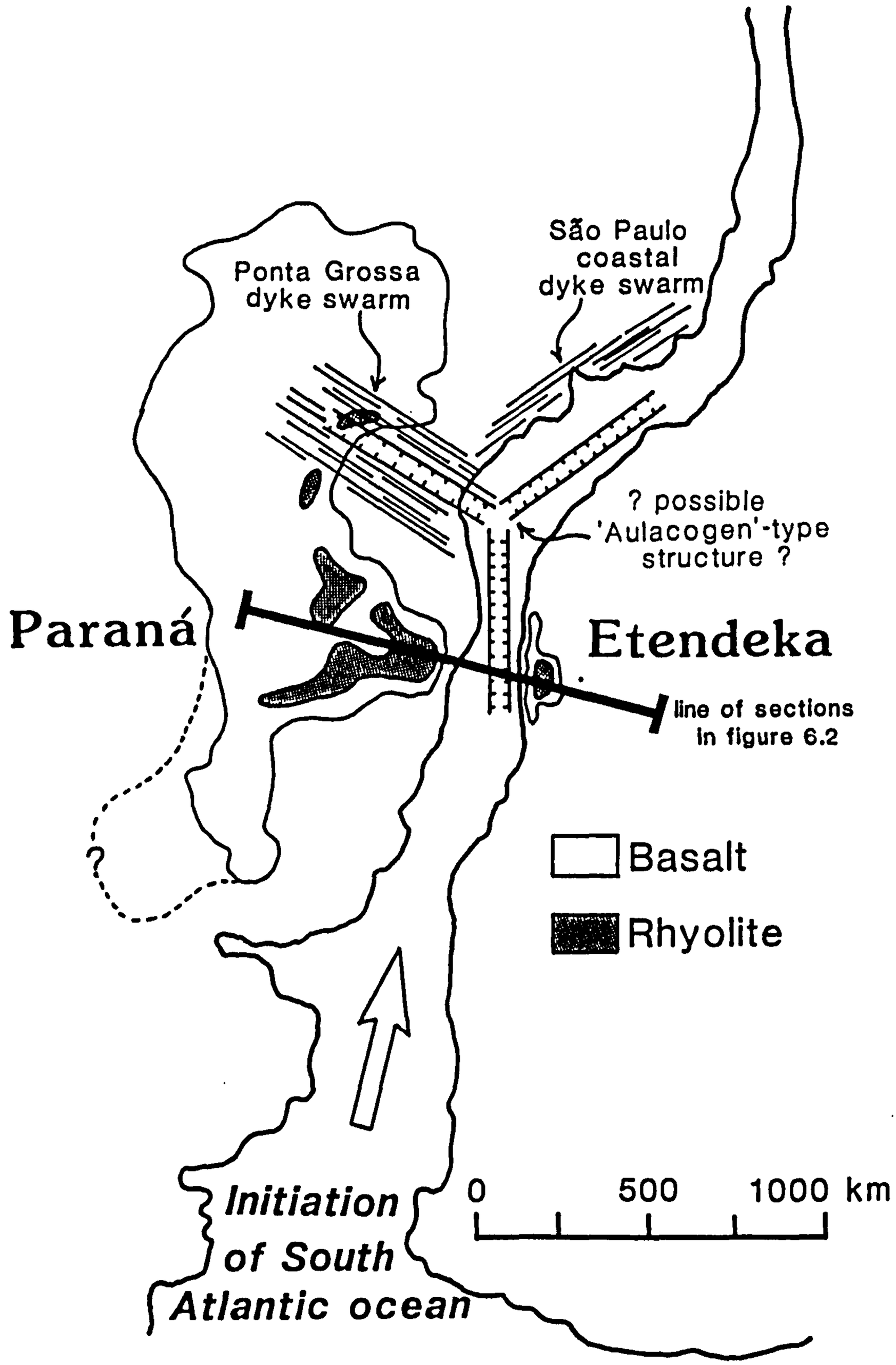

Figure 6.1 Simplified map of the relative distribution of basaltic and rhyolitic products of the Paraná - Etendeka CFB province. The basalts have a pronounced asymmetrical distribution and occur almost exclusively to the South American side of the developing South Atlantic rift zone, whereas the rhyolites are concentrated near to this rift. The dotted line represents the inferred subsurface extent of the basalts. The two major dyke swarms of the Paraná, *viz.* Ponta Grossa and coastal areas of São Paulo, lie in the northern half of the basin, and have a geometrical 120° relationship with the regional coastline suggestive of an 'aulacogen'-type structure (Burke and Dewey, 1973).

intrusion of basic magmas (Duncan *et al.*, 1984), and the additional thermal input needed could have come from the rising asthenosphere accompanying the incipient rifting process. Rhyolite production in the Paraná and Etendeka appears to have been directly related to the rifting episode and the scenario envisaged for this is akin to that outlined by Cleverly *et al.*, (1984) to account for the Lebombo rhyolites of the Karoo that were similarly restricted to a developing plate margin. In this model, crustal thinning or attenuation led to 'necking' of the crust which could have caused the base of the crust to be uplifted by up to 20 km. This decompression would be sufficient to raise any lower crustal material above its solidus and thus initiate melting to form rhyolitic magmas. Since the Lebombo rhyolites shared similar isotope compositions to the earlier basalts, this indicated that both had probably been ultimately derived from the same mantle source. Cleverly *et al.*, (1984) proposed that the source for the Lebombo rhyolites could have been basic material within deep crustal sill complexes that had been emplaced near the crust - mantle boundary during the main phase of flood basalt activity, in the manner suggested by Cox (1980) and Ewart *et al.*, (1980). For the Paraná-Etendeka province, partial melting of underplated basaltic material in this fashion might be viable for the Chapecó rhyolites but the more dominant Palmas rhyolites have apparently been derived from older crustal material with higher $^{87}Sr/^{86}Sr$.

The final stages of magmatic activity within the Paraná-Etendeka province were marked by the intrusion or eruption of basic magmas which showed more 'depleted' (*i.e.* asthenospheric) trace element and isotopic characteristics than the more volumetrically significant earlier basalts. In Namibia these magmas are represented by the Horingbaai dolerites, a suite of late-stage dykes and sills intruding the Etendeka lavas, which geochemically have a convincing MORB-like asthenospheric signature (Erlank *et al.*, 1984). In Brazil, the Esmeralda magma type forms the uppermost lava flows over much of the south-east corner of the Paraná, including numerous intrusives that cross-cut the lava pile, and chapter four has shown that this magma type also carries a strong asthenospheric component. Fodor and Vetter (1984) have also documented the transition from CFB to MORB-like compositions within basalts sampled off-shore of the south-east Brazilian continental margin. Continuation of the lithospheric extension that was responsible for the

generation of the rhyolites, would have led to extensive attenuation and/or rupture of the lithosphere which would then have allowed direct access to magmas derived from the upwelling asthenosphere. The Esmeralda magma type seems to represent a more intermediate stage to the true asthenospheric Horingbaai dolerites, and their interaction with evolved and already contaminated Gramado-type magmas (see chapter four) suggests that such 'contamination' was quite a high-level mixing feature.

Thus the Paraná-Etendeka province preserves the association of flood basalts, rhyolites and late-stage 'depleted' dykes that according to Marsh (1987) are characteristic of the CFB activity which occurs within many rift or thinned lithosphere environments (*e.g.* Lebombo monocline of the Karoo; the British Tertiary volcanic province). Marsh (1987) suggests that the derivation of the earlier 'enriched' basalts involved sources in the sub-continental lithosphere whereas the later 'depleted' basalts were essentially of asthenospheric origin. The series of successive schematic cross sections illustrated in figure 6.2 outline the general scenario for the possible development of the Paraná-Etendeka CFB in the context of a rift or thinned lithosphere environment, as also envisaged by Marsh (1987).

6.4 Possible causes of the asymmetrical distribution of the Paraná - Etendeka CFB.

The gross asymmetrical distribution of lavas between the Paraná and Etendeka provinces, as illustrated in figure 6.1, has been an intriguing feature of this magmatic event. This leads to the question as to whether there is any link between what controlled the location of the flood basalts and the eventual location of the South Atlantic ocean, *i.e.* the basalts might not have been a direct consequence of the disruption of Gondwana although a common process could have been responsible for both events (as was concluded for the Karoo province by Duncan *et al.*, 1984). The schematic cross-sections of figure 6.2 show the westward shift in the locus of magmatism between the initial flood basalts {figure 6.2(a)} and the later rhyolites {figure 6.2(b)}. The underlying cause of this shift in the

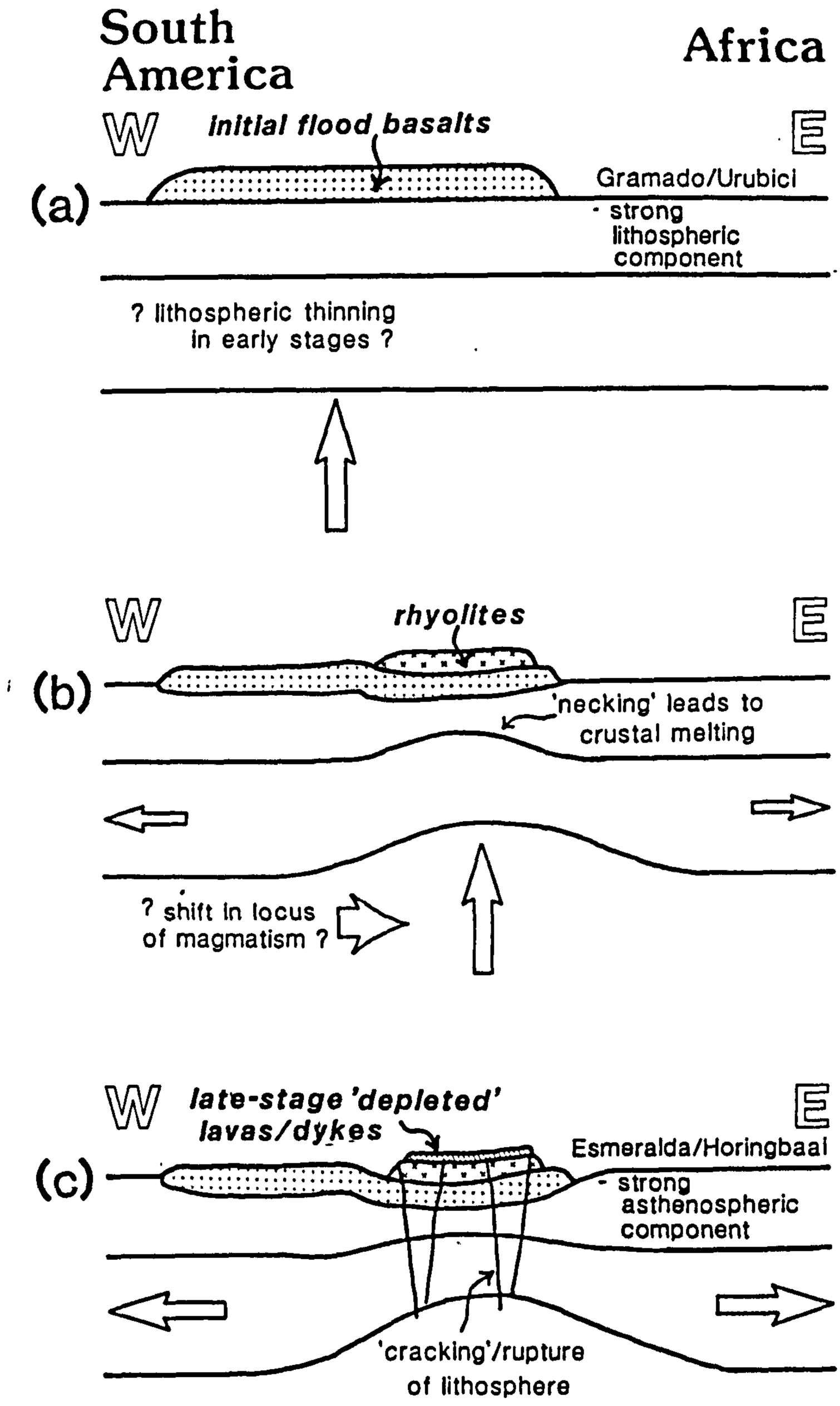

Figure 6.2 Progressive series of schematic cross sections through the Paraná-Etendeka CFB province during its evolution. The approximate line of section is marked on figure 6.1. The location and extent of early lithospheric thinning accompanying the initial flood basalts is uncertain (and for convenience is not illustrated). Sections (a) and (b) shows the west to east shift in the locus of magmatism between the flood basalts and the rhyolites (possible reasons for this are discussed in the text). The rhyolites are generated within the rift zone by crustal melting in response to crustal thinning. During the advanced stages of extension, section (c), 'cracking' of the lithosphere allows direct access to asthenospheric material (*e.g.* Horingbaai dolerites) which can also interact with the earlier formed magmas (*e.g.* late stage 'depleted' lavas/dykes of the Esmeralda magma type show evidence of mixing between Gramado magma type and an asthenospheric component).

magmatic locus is problematical and could owe its origin to several processes. It could be just a shallow feature with the lava distribution controlled by the surface topography, or alternatively it might be related to asymmetrical continental extension during the opening of the South Atlantic ocean. An additional possibility is that it could have been in response to lithospheric movement relative to an underlying thermal mantle plume, and the link between flood basalts and hot-spots will be developed separately in the next section.

In the model for CFB magmatism postulated by White and McKenzie (1989), it is suggested that flood basalts occur when a rift develops above a mantle plume or hot spot, and it is assumed that the lavas were fed directly from fissures located in the central rift zone. Since this rifted region has generally been uplifted, typically by 1-2 km, this might have assisted the outward flow of the lavas, and in the case of the Paraná-Etendeka CFB province, White and McKenzie (1989) considered that the asymmetry of the lavas had been controlled by pre-existing topography. According to Eales *et al.*, (1984), the Etendeka lavas overstepped on to the Pre-Cambrian basement which suggested the existence of considerable relief at the onset of volcanism, and it was this topographic relief that White and McKenzie (1989) believed had prevented the widespread flow of lavas eastwards onto the African plate. The Paraná basin was probably already a low-lying and still subsiding area, and so the lavas could flow to the west and infill the sedimentary basin virtually unhindered, although the stratigraphical data in chapter two has also hinted at the presence of a certain amount of pre-existing relief within the coastal Serra Geral region of southern Brazil. Another problem with this model is the extensive sill complexes intruded into the Paraná basin sediments. Borehole data have shown that the sills reached a maximum total thickness of about 1 km, and this coincided with the location of the thickest and deepest part of the Paraná lavas. This might suggest that magma had been intruded from beneath this area rather than having travelled laterally from the rift zone. To reach the most westerly lava outcrops in Argentina for example from the incipient Atlantic rift zone would have required the lavas to have flowed over 750 km laterally. Extensive lava flows, although not quite of this length scale, have been documented from within the well studied Columbia River CFB province, and Hooper (1982) cites one example, the Pomona flow within the

Saddle Mountains Formation, for which there is good evidence that it had travelled at least 550 km from its fissure source. The northern half of the Paraná province is complicated by the presence of the extensive Ponta Grossa dyke swarm. These are the most likely candidates for the feeders to the northern lavas to which they are compositionally similar. The coincidence of the dyke swarm with the sudden change in direction of the Brazilian coastline near São Paulo (see figure 6.1) indicates that it might represent a possible 'aulacogen' or failed rift arm structure as suggested by Burke and Dewey, (1973), and this could have resulted in a different tectonic environment to that further south.

Several models have been developed which give rise to asymmetrical continental extension (*e.g.* Wernicke, 1985; Coward, 1986) as opposed to the symmetrical homogeneous pure-shear lithospheric thinning outlined by McKenzie (1978). In the 'Wernicke'-model, major detachment zones (low-angle normal faults) transfer extension laterally from the upper crust in one region to the lower crust or lithospheric mantle elsewhere. Importantly, this means that the zone of upwelled asthenosphere does not lie beneath the main zone of upper crustal extension {see figure 6.3(a)}. To explain the Paraná-Etendeka asymmetry in terms of this model, the bulk of the flood basalts must have been erupted above the region of thinned lithospheric mantle, with the rhyolites restricted to the area of crustal rifting. If this model is continued to its logical conclusion, the development of a passive margin, the part of the crust lying above the detachment zone would probably form a submerged continental fragment. The São Paulo plateau that marks the wide continental shelf off-shore of southern Brazil between Florianopolis and Rio de Janeiro is known on geophysical grounds to be underlain by continental crust and, additionally, sub-aerial lava samples compositionally similar to the Paraná CFB have been recovered from up to 200 km off-shore of São Paulo (Fodor and Vetter, 1984).

An alternative model has recently been proposed by Braun and Beaumont (in press) primarily to explain the occurrence of rift flank basins, but it is suggested here that this might also represent a plausible scenario to invoke for the South Atlantic rift episode. In contrast to the 'Wernicke'-type model above, the main rift is established above the locus of lithospheric mantle extension. Pre-existing crustal weaknesses which are laterally offset

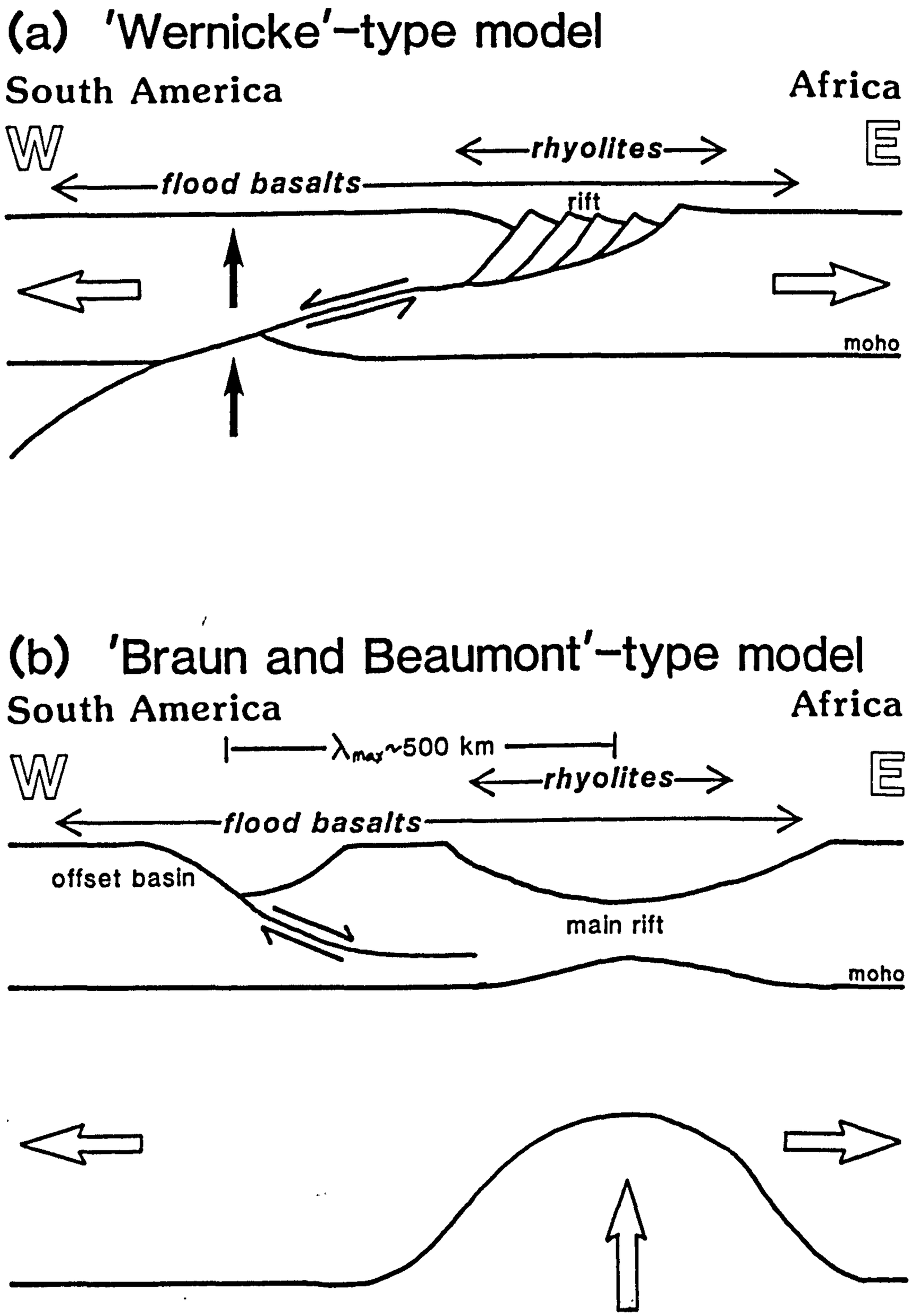

Figure 6.3 Possible application of asymmetrical stretching models to the Paraná-Etendeka magmatism.
(a) 'Wernicke'-type model. - the flood basalts occur above the deeper zone of upwelled asthenosphere, with the rhyolites displaced to the east and asssociated with the main zone of crustal extension.
(b) 'Braun and Beaumont'-type model - during the initial stages of rifting, extension is transferred to a laterally offset pre-existing crustal weakness (Paraná basin), and the flood basalts can exploit the resultant shear zone as a conduit to the surface. As lithospheric thinning becomes more intense, the shear zone becomes abandoned and crustal extension is concentrated in the main rift zone above the deeper lithospheric mantle extension. This is accompanied by crustal anatexis and results in rhyolite magmas concentrated in the main rift zone.

from the main rift axis can be reactivated to form offset or rift flank basins, with the transfer of lithospheric extension being accommodated along deep crustal shear zones. These basins are predicted only to be active during the initial stages of rifting, probably on a time scale of less than 10 Myrs, since subsequent thermal weakening of the crust directly above the main zone of lithospheric mantle thinning should lead to the abandonment of the shear zone in favour of the localisation of crustal extension at the centre of the main rift. The most critical parameter in determining the maximum offset distance over which the lithospheric extension can be transferred to a crustal weak zone (λ_{max}) is the viscosity of the shear zone which itself is strongly temperature dependent, and increasing the temperature of the shear zone will increase λ_{max}. Realistic estimates for crustal mineralogy and thermal structure produced a modelled range in λ_{max} of 50-300 km.

This model is preferable to that of Wernicke (1985) as it can more easily explain the two sites of magmatism within the Paraná-Etendeka province {see figure 6.3(b)}. The Paraná sedimentary basin is a likely zone of crustal weakness that is offset from the eventual plate boundary between South America and Africa. The early flood basalts might have been able to exploit the connecting crustal shear zone as a conduit to the surface. The locus of the flood basalt magmatism is displaced on the order of 500 km from the main rift, which is slightly more than the maximum estimates given by Braun and Beaumont (in press). This might be a consequence of the higher temperatures along the shear zone caused by the input of mantle-derived magmas which would act to increase λ_{max}. The initial marginal zones became abandoned as the lithospheric extension continued, and with more extensive thinning of the crust, crustal anatexis resulted in the production of rhyolite magmas concentrated in the main rift zone. Confirmation of this model will require more extensive geophysical studies, especially deep seismic surveys that might be able to pick up evidence for a deep crustal shear zone.

A common feature to all these models is their restriction to crustal level processes in order to control the asymmetrical Paraná-Etendeka lava distribution. Thus they are largely independent of whatever mechanism is proposed for the actual process of magma generation within the mantle.

6.5 Geodynamic mechanisms to account for CFB magmatism.

6.5.1 General background.

A characteristic feature of CFB magmatism appears to be the generation of large amounts of melt over a relatively short time span, which must have important consequences for the nature of the melting regime. Any models proposed for the driving mechanism behind the production of CFB must offer some explanation as to the thermal cause of this extensive melting, in addition to accounting for the other major features, namely the overall structure of the province and the geochemical signatures of the erupted magmas. One drawback to the development of any geodynamic model for CFB magmatism is the lack of consensus as to the actual site of melt generation, whether this is within the lithosphere or the asthenosphere. The argument over whether the 'enriched' isotope and trace element signature of many CFB, widely believed to be a characteristic of the sub-continental mantle lithosphere, was acquired via scavenging by an asthenospheric melt during its passage through the lithosphere, or was inherited directly as a result of lithospheric melting, is still an unresolved question. The spectrum of published models for CFB generation were introduced in chapter one, and this section will discuss what evidence is available in order to assess their viability for the Paraná-Etendeka event.

6.5.2 The 'Hot-spot' connection.

The link between CFB magmatism and mantle hot-spots, as suggested originally by Duncan (1978) and Morgan (1981), is quite appealing. For each of the major CFB provinces there is evidence for the presence of a hot-spot beneath, or close to, the province at the time of its eruption. In the case of the Paraná-Etendeka province, there is a close association with the hot-spot or mantle plume presently underlying the island of Tristan da Cunha. This plume was active throughout the history of the South Atlantic ocean, and its effects can be traced back to the continental margins of South America and Africa (and hence the Paraná and Etendeka lavas) via the two aseismic ridges; the Rio Grande Rise and the Walvis ridge (see figure 6.4). Several mechanisms have been proposed to suggest how

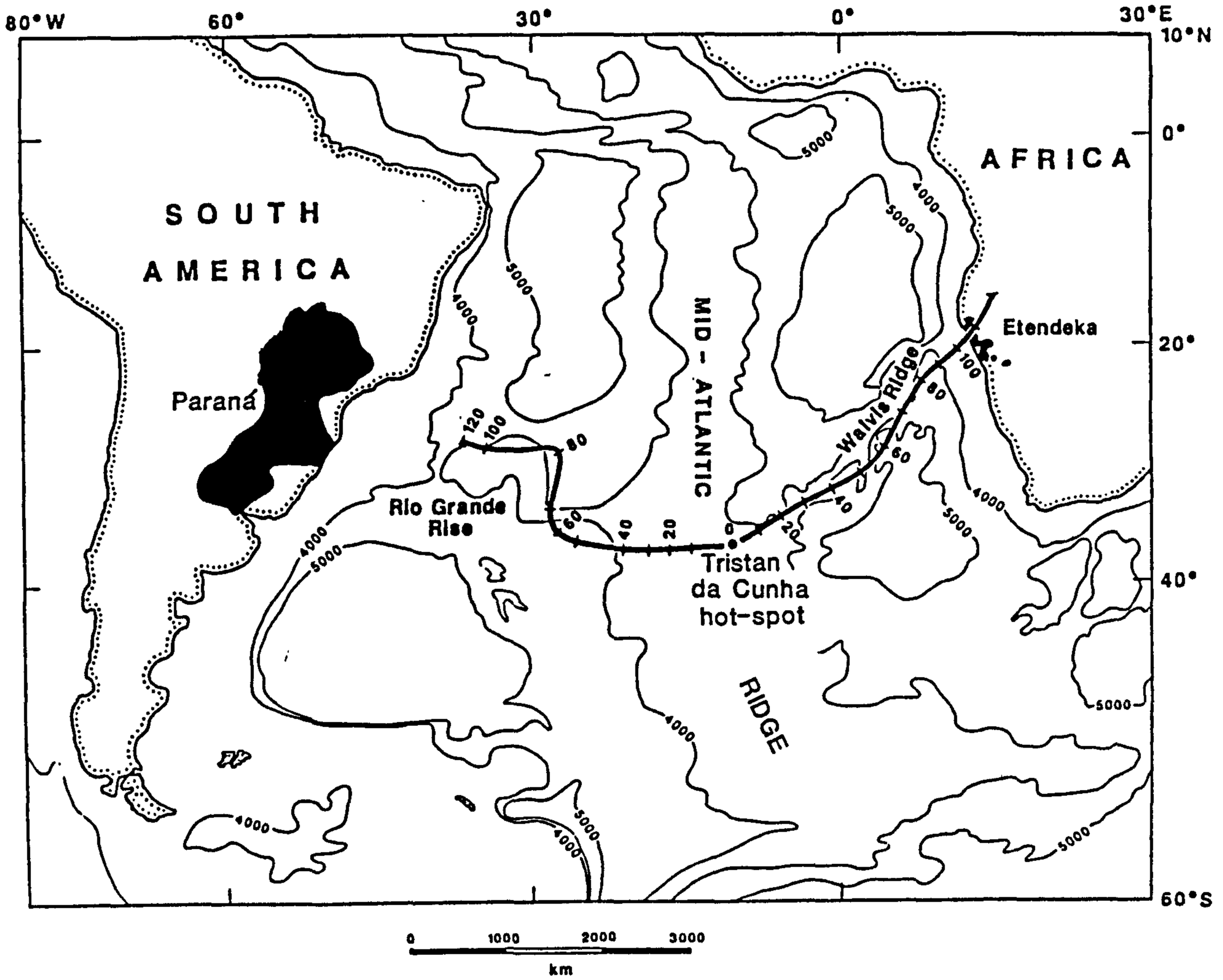

Figure 6.4 Present day configuration of the South Atlantic Ocean (taken from White and McKenzie, 1989) showing the relationship of the Tristan da Cunha plume to the thick aseismic ridges of the Rio Grande Rise and the Walvis Ridge, produced above the mantle plume as the ocean opened. The hot-spot track (tick marks at 10 Ma age intervals) is from Duncan (1981). Note the location of the Paraná and Etendeka lava fields, at the landward extensions of the Rio Grande Rise and the Walvis Ridge respectively.

the thermal anomaly caused by a mantle plume can induce the melting event responsible for CFB magmatism.

(i) Morgan (1981) considered that initiation of a hot-spot beneath the continental interior would produce a gradual heating of the sub-continental mantle lithosphere over a period of 10-30 Myrs and result in CFB magmatism once the hot-spot moved away, *i.e.* there will be a time delay between when the hot-spot was beneath the region and the subsequent CFB magmatism. A similar model was considered by Fodor (1987) specifically for the Paraná CFB province. In this, he related the geographical position of

the high-Ti and low-Ti geochemical provinces to variations in melting degree arising from their location relative to the plume axis. Higher degrees of melting would occur directly over the rising plume as a result of the higher mantle temperature and decompression caused by uplift and stretching of the crust. Away from the plume, these effects would be less well developed, producing lower degrees of melting. In their models, both authors consider the influence of the hot-spot to be a relatively narrow feature, in contrast to the view taken by White and McKenzie (1989) below.

(ii) White and McKenzie (1989) combined a geophysicists view of the thermal structure of a mantle plume with recent models (McKenzie and Bickle, 1988) for the volume of melt generated by asthenosphere during decompression. The thermal structure assumed for a mantle plume in this paper was based on results from modelling geophysical observations of the Cape Verde plume, and this is illustrated in figure 6.5. In general, hot-spots are expected to have a narrow (150-200 km) central plume of hot mantle rising upwards, which is deflected laterally by the overlying lithospheric plate to form a mushroom-shaped head of anomalously hot asthenosphere some 1500 km across. Hence the thermal effect on the base of the lithosphere is not localised in a restricted area or 'hot-spot', a common misconception, and can still be an important feature at distances greater than 1000 km from

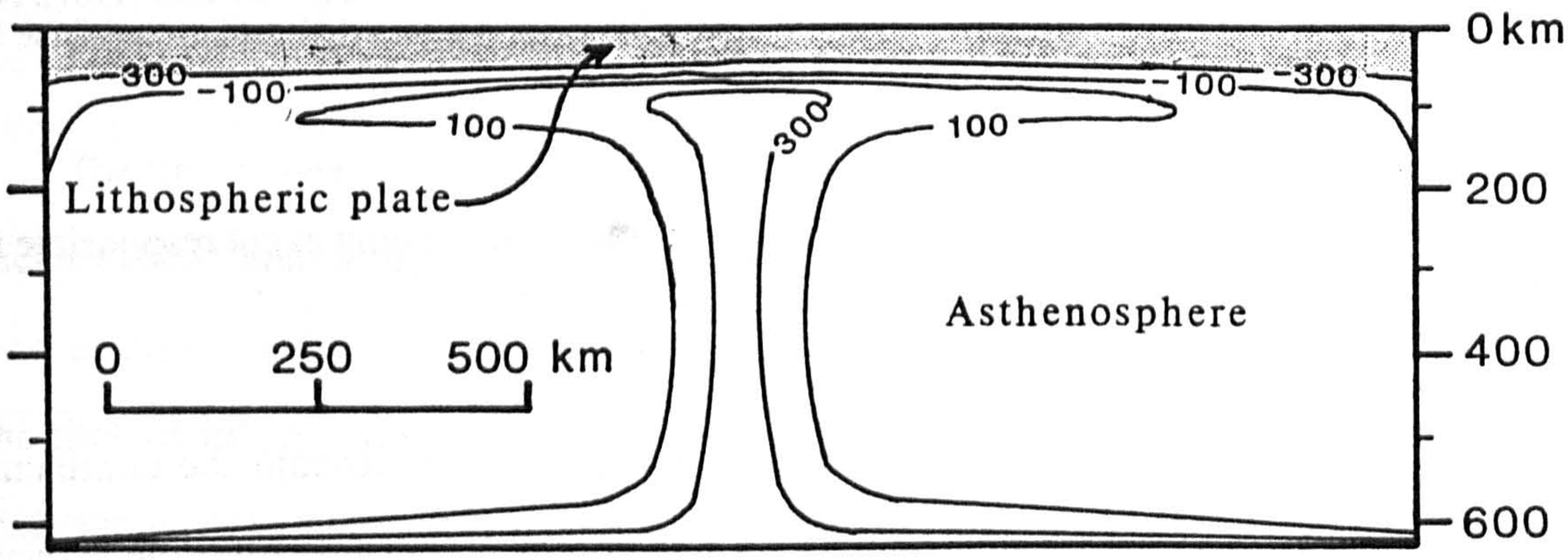

Figure 6.5 Thermal structure of a mantle plume, in cross section, based on the oceanic Cape Verde plume (after White and McKenzie, 1989). Temperature anomalies relative to the mean asthenospheric temperature are shown in 200 °C intervals. The important features are; (i) the narrow central rising plume, and (ii) the broad mushroom-shaped head of hot material deflected laterally by the overlying lithospheric plate.

the plume axis. If the continental lithosphere is rifted above this thermal anomaly created by a mantle plume, passive upwelling of abnormaly hot asthenosphere to fill the space createdwill undergo extensive decompression melting and produce massive amounts of magma. Part of this magma can reach the surface, covering the adjacent continental areas with flood basalt magmatism, and the remainder is accreted beneath, or intruded into, the thinned continental crust. Continuation of the rifting will lead to the emplacement of huge quantities of magma onto the developing continental margins, which show up on seismic sections as seaward-dipping reflectors, a characteristic of many volcanic passive margins such as the northern North Atlantic (White *et al.*, 1987).

Figure 6.6 (after White and McKenzie, 1989) illustrates the application of this mantle plume model to the Paraná-Etendeka CFB province. The shaded area around the Tristan da Cunha hot-spot represents the estimated extent of the thermal anomaly created by the plume, and has a radius of 1200 km. White and McKenzie (1989) suggested that this anomaly was probably of comparable magnitude to that created by the Iceland hot-spot because of the similarity in structure of the Rio Grande Rise / Walvis Ridge and the Iceland-Faeroes ridge. The location of off-shore seaward-dipping reflectors reported by Hinz (1981), Gerrard and Smith (1982) and Austin and Uchupi (1982) are also shown, since these features are believed to represent basaltic flows erupted onto the continental margins during rifting (White *et al.*, 1987).

If there is a relative motion during the evolution of the CFB province between the lithospheric plate onto which the flood basalts are erupted, and the underlying mantle plume, then this should be recorded in the structure and layout of the lava pile. For example, the north-south structure in the Western Ghats region of the Deccan CFB province, which has a sequence of southwardly dipping units, has been interpreted in terms of the progressive southward migration of the volcanic source as India moved northwards over the Reunion hot-spot (Devey and Lightfoot, 1986; Watts and Cox, 1989).

Is there any evidence for the involvement of a hot-spot in the Paraná magmatic event similarly preserved within the lava stratigraphy ? The regional stratigraphy of the

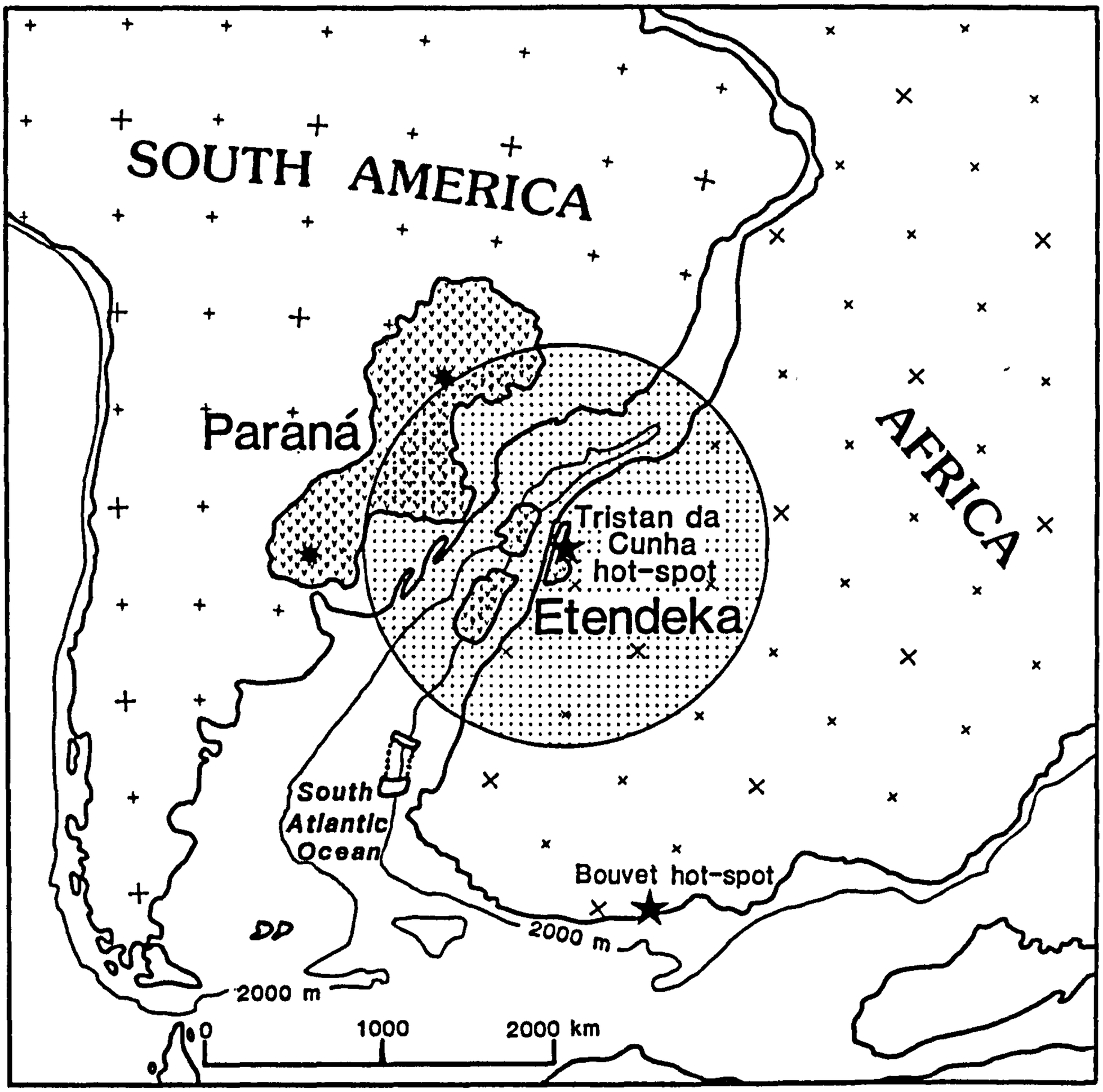

Figure 6.6 Reconstruction of South Atlantic at anomaly M4 time (~120 Ma) shortly after onset of sea-floor spreading (after White and McKenzie, 1989). The position of the Tristan da Cunha (and Bouvet) hot-spots at that time are shown by the star symbols. The extent of the mushroom-shaped head of abnormally hot asthenosphere around the Tristan da Cunha plume at the time of rifting is indicated by the circular shaded area (radius 1200 km). The areas with v-ornament represent extrusive basalts: the Paraná and Etendeka CFB provinces, and off-shore seaward dipping reflectors reported by Hinz (1981), Gerrard and Smith (1982) and Austin and Uchupi (1982). The asterisks mark the two thickest parts (> 1 km) of the Paraná lavas.

Paraná lava pile as revealed by the borehole studies, was summarised in chapter two. It consists of a sequence of northwardly dipping geochemical units, and this could be interpreted in terms of a northward migration of the magmatic source. If this is an analogous situation to that proposed for the Deccan province, then the Tristan da Cunha hot-spot must have been moving northwards relative to the South American lithospheric

plate. In order to verify this idea, an understanding of the position of the Tristan da Cunha hot-spot and its motion relative to the South American and African plates is required for the time period from about 150 Ma to 100 Ma.

The extrapolation of hot-spot locations with any certainty prior to 80 Ma is fraught with difficulties, especially in light of recent studies (*e.g.* Molnar and Stock, 1987) which have shown that hot-spots are not fixed in position relative to each other as was previously thought. Relative motions of 1-3 $cm.yr^{-1}$ have occurred between hot-spots and this will lead to uncertainties in calculations of their palaeo-positions. The detailed location of the Tristan da Cunha hot-spot with respect to the Paraná-Etendeka lava field is therefore poorly known. The age and shape of the Rio Grande Rise and Walvis Ridge, which represent the hot-spot track (see figure 6.4), can provide some constraint on the behaviour of the Tristan da Cunha hot-spot. The reconstructions of Morgan (1981), which were based on a fixed hot-spot reference frame, placed the Tristan da Cunha hot-spot beneath Brazil from about 160 Ma to 130 Ma when it crossed into the future African plate. Figure 6.4, which uses the reconstruction of Duncan (1981), shows the Tristan da Cunha hot-spot clearly beneath the African plate at 120 Ma. This would be consistent with the poor initial development of the Rio Grande Rise and the fact that the excessive magmatism of the aseismic ridges was largely concentrated on the African plate to form the Walvis ridge (Neill, 1976). Thus Morgan (1981) suggested that the hot-spot had already left the region of magmatism before the main peak of volcanic activity, although it is important to bear in mind that there is no direct evidence for the existence of the Tristan da Cunha plume prior to about 120 Ma. Neill (1976) investigated the landward extension of the Rio Grande Rise and concluded that it was aligned with the Torres-Posadas syncline in the south-east corner of the Paraná lava field, coincident with the exposures of the Serra Geral escarpment considered in this study. Despite the limitations of the hot-spot reconstructions, they all show a general north-west to south-east motion for the Tristan da Cunha hot-spot beneath the Paraná province prior to its eruption and further imply that during the flood basalt eruption the hot-spot was probably beneath Africa. This eastward hot-spot motion, from the Southern Paraná to the Rio Grande Rise off-shore might account for the shift in locus of magmatism on figure 6.2

but it is difficult to reconcile with the observed regional lava stratigraphy which required a northward migration beneath the volcanic province. Thus an alternative explanation is required.

If the mantle plume model of White and McKenzie (1989) is considered, then the exact position of the central plume axis is not important in governing the location of magmatism. The mantle plume has a passive role in the melt generation process, and is only required as a means of raising the ambient asthenospheric temperature. The melt is generated by decompression melting of anomalously hot asthenosphere accompanying an episode of lithospheric stretching, and not by the mantle plume directly. Flood basalt magmatism will be produced in association with a developing rift provided that the rift zone intersects the wide 'mushroom-head' thermal anomaly caused by the mantle plume, and therefore the position of the rift controls the geographical location of magma generation. This would imply that the rifting process would probably have more influence on the structural evolution of a CFB province than any plate motion relative to an underlying hot-spot.

The rifting that eventually gave rise to the South Atlantic ocean is known to have propagated from south to north (Austin and Uchupi, 1982). Sea floor spreading between Africa and South America started in the southern Cape basin at about the time of anomaly M9 {130 Ma - Harland *et al.*, 1982 timescale; 126 Ma - van Hinte *et al.*, 1976 timescale}. As mentioned previously, the earliest recognised magnetic anomaly off Walvis Bay, over 1000 km to the north, is anomaly M4 which is about 3-4 Myrs younger than M9 {127 Ma - Harland *et al.*, 1982 timescale; 122 Ma - van Hinte *et al.*, 1976 timescale}. These figures imply a rate of rift propagation on the order of 30-35 $cm.yr^{-1}$ (*c.f.* typical plate motions relative to the hot-spot reference frame which are probably of the order of 5 $cm.yr^{-1}$ or less). Hence this might provide an alternative to the hot-spot model above, in explaining the observed lava stratigraphy. The northward shift in the locus of the Paraná magmatism, as implied by the lava stratigraphy, could possibly be governed by this relatively rapid northward propagation of the South Atlantic rifting. The developing rift will control the surface access to the untapped magmas below, and in the specific case of the White and

McKenzie model, it will control the location of passive asthenospheric upwelling and melt generation. The Deccan province therefore, appears to be a special case where the observed stratigraphical pattern of the lava units is consistent with being controlled by the underlying motion of a hot-spot. This might have arisen because of the rather unusual behaviour of the Indian plate, which apparently had a particularly rapid northwards motion (15-20 $cm.yr^{-1}$ - Patriat and Achache, 1984) relative to the Reunion hot-spot.

The detailed geodynamic mechanism for the origin of CFB magmatism developed by White and McKenzie (1989) offers several means by which the viability of the model for individual CFB provinces can be tested, and these include the timing of the volcanic activity and the regional geometry of the feeder dyke systems. The timing of the magmatism is a key aspect of the White and McKenzie (1989) model, because the magmatism is expected to be essentially simultaneous with the main rifting episode. It is important in two respects; (i) the time span of the magmatism, and (ii) the relative timing of the magmatism and rifting. The timing of the surface volcanism will depend on the time and rate of lithospheric thinning (which governs the extent of asthenospheric decompression) and on the time taken for melt migration from the melting zone to the surface. The asthenospheric melts formed by decompression will separate out from the mantle matrix very rapidly, and the bulk of the magmas should reach the surface less than 1 Myr after their formation (McKenzie, 1985). Although continental break-up may involve a long precursory period of small-scale rifting, perhaps with minor volcanism, the main phase of rifting which is accompanied by CFB magmatism is usually rapid (McKenzie, 1978). Therefore the time span for the main episode of CFB activity is expected to be of relatively short duration, 1-2 Myrs or less.

Available radiometric ages for the Paraná and Etendeka lavas are not sufficiently precise to test this assertion, but there is a hint from palaeomagnetic studies (see summary in chapter one) that the period of lava eruption was less than a few million years. Evidence for the relative timing of the Paraná-Etendeka flood basalt eruptions with respect to the onset of the main continental rifting event was reviewed earlier in this chapter (section 6.2). It was concluded that the magmatism probably just predated the main rifting episode,

although the two events are not easily resolvable with the present data. The Karoo province poses more of a problem to this model because Duncan *et al.*, (1984) took the view that the Karoo volcanism (175-195 Ma) substantially predated continental break-up. The oldest identifiable Indian ocean crust along the eastern continental margin of Africa is about 140 Ma, although there is a possibility that older crust than this might exist and is either obscured by sedimentary cover or not recognised through problems associated with the Cretaceous magnetic quiet zone.

Another important constraint on possible geodynamic models might come from the geometry of the regional dyke swarms. The feeder dykes are expected to be either concentrated in dense swarms linked to the rift system, as implied by White and McKenzie (1989), or to form a diffuse network of dykes over a large area which might suggest a more pervasive regional availability of magma. The northern region of the Paraná province contains two major dyke systems which lie along the Ponta Grossa arch and along the Rio de Janeiro - São Paulo coastline. Dykes further to the south are scarce, and the location of the feeder zones to the southern magma types is not known. The picture is partly obscured by the lack of deep erosion through the Paraná lava pile and by the extensive forest cover around the margins of the lava field. Within the Karoo province, most of the dykes occur in swarms scattered throughout the province, although some of the lavas (*e.g.* Lesotho) appear to have been erupted from more diffuse zones of narrow dykes (Eales *et al.*, 1984) suggesting a more pervasive style of feeder dykes. This might have implications for the Paraná province if the more extensively eroded Karoo province is used a model for the deeper structure of the Paraná.

The hot-spot model of White and McKenzie (1989) neatly accounts for most of the features seen in the North Atlantic CFB province (the province for which this model was developed) as well as the Deccan CFB province. The uncontaminated magmas in both of these provinces have trace element and isotopic signatures that are are compatible with a derivation from a sub-lithospheric OIB-type mantle source (*e.g.* Thompson *et al.*, 1983; Mahoney, *et al.*, 1982, Lightfoot 1985). It is the Mesozoic Gondwana CFB provinces {*i.e.* Paraná, Karoo, Antarctica, Tasmania} that do not conform as nicely to this model.

Several of the problems posed by the Paraná-Etendeka province in relation to this model have been discussed in section 6.4 earlier in this chapter; *viz.* the marked asymmetry of the lava field with respect to the South Atlantic rift, and the large distances required for lava to have flowed from this central rift. An important feature of the Karoo, Antarctica, and Tasmanian provinces is that they are all closely spaced in time, with ages in the relatively restricted range of 170 Ma to 190 Ma. The magmatism during this period forms an almost continuous belt of activity from southern Namibia to Australia, a distance of about 8000 km (see figure 6.7), which is unlikely to have been the consequence of a single mantle plume. Morgan (1981) and White and McKenzie (1989) have proposed the involvement of the Crozet hot-spot at least for the Karoo flood basalts, including the dolerites of Dronning Maud Land and the Theron Mountains in Antarctica, but this magmatism still covers an excessively large area compared to the typical size of a plume-driven thermal anomaly. There were no suitable candidates for a plume to explain the remainder of the Antarctican and Australian magmatism.

A notable geochemical feature of all these provinces compared, for example, to the Deccan, North Atlantic, and Columbia River provinces, is that they all carry a strong lithospheric signature. The exact mechanism by which the sub-continental mantle lithosphere contributes to CFB magmatism is still a controversial subject. One possibility is that if the temperature of the lithospheric mantle has been raised closer to its solidus as a result of a previous thermal event, then it might be more easily mobilised by decompression melting connected with an episode of lithospheric thinning or rifting. This initial thermal episode might be provided by a mantle plume, but the sheer scale of the Gondwana magmatism from the Karoo to the Tasmanian province is difficult to reconcile with the White and McKenzie (1989) mantle plume origin, and instead this suggests an extensive linear zone of mantle melting. Numerous alternatives for the cause of this thermal anomaly have been proposed for the Gondwana CFB, involving insulation within a supercontinent or a connection with subduction processes, and these will be discussed in the following section.

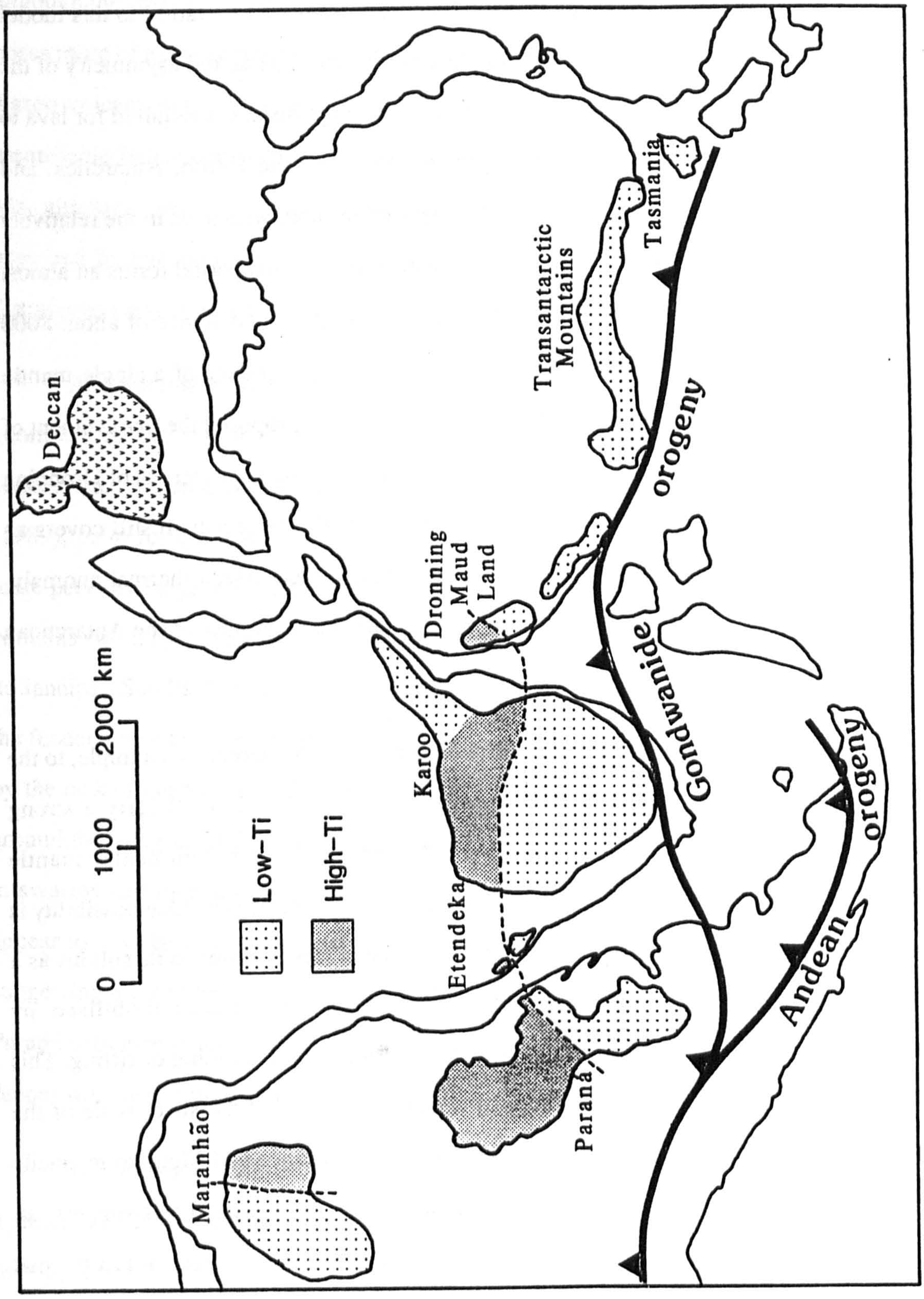

Figure 6.7 Distribution of the Mesozoic CFB provinces within a reconstructed Gondwana supercontinent, and the geochemical division into 'high-Ti' and 'low-Ti' geochemical provinces {adapted from Cox (1980), Piccirillo and Melfi (1989), and J.M. Hergt (pers. comm., 1989)}. The Andean and Gondwanide orogenic belts along the Pacific margin represent the sites of subduction since the Devonian to the present day.

Thus, in conclusion, it appears that CFB provinces can be divided into two separate groups. Many of the CFB provinces {*e.g.* Deccan, North Atlantic, Ethiopia, Columbia River} show fairly convincing evidence for a plume-generated origin and, furthermore, uncontaminated magmas from each area have geochemical signatures consistent with an asthenospheric OIB-type mantle source. In contrast, the group of CFB provinces specific to the Mesozoic era in Gondwana {Paraná, Karoo, Antarctica, Tasmania} are quite distinct. Geochemically the magmas all show a strong lithospheric influence, and the large magnitude of each event has been difficult to reconcile with a plume model. It is interesting to speculate whether or not all CFB provinces share the same ultimate mechanism of generation. Either the marked difference in character of these two groups of CFB provinces suggests that there is not really a single fundamental mechanism behind all CFB magmatism, or instead the Mesozoic CFB of Gondwana require the operation of an additional process which has perhaps been superimposed on the plume activity that is common to all regions.

6.5.3 'Insulation-melting' or 'subduction-related' as alternatives.

Marsh (in prep.) also considered the Mesozoic CFB of Gondwana to be distinct from other CFB provinces, and a study of the distribution of dolerite sills and dykes with the Karoo, Antarctica and Tasmanian gave the impression that the surface volcanism was fed via a diffuse network of dykes rather than from a limited number of linear feeder systems associated with areas of continental rifting. Furthermore, the contemporaneous and extensive belt of activity from southern Africa, right across the Antarctica continent and into Tasmania, as well as the vast spatial extent of each province suggested an origin from a large zone of melting rather than a mantle plume. These provinces are all associated with the former position of the Pangaea super-continent, and Anderson (1982) argued that the stable presence of this large super-continent for a period greater than 100 Myrs would have had an insulating effect on the underlying mantle, because there were no nearby mid-ocean ridges where the heat could be dissipated. The key point is at what depth such 'insulation' would cause melting; whether this would lead to the initiation of shallow plumes or hot-spots as envisaged by Anderson (1982), or instead cause melting within the lithospheric

mantle. This 'insulation' mechanism would produce an increase in the temperature of the sub-continental lithosphere and could lead to a pervasive style of melting of the lithospheric mantle which Marsh (in prep.) believed was more consistent with the large scale extent of these CFB provinces. Uplift of the region caused by thermal expansion and partial melting would ultimately result in break-up and dispersal of the super-continent. As soon as continental rifts and sea-floor spreading are established, the magmatism of the continental interior will decrease and become concentrated at the rift zone, due to the increased role for the asthenospheric mantle in convecting the heat away through the mid-ocean ridges.

Several authors {Elliot (1975); Cox (1978); Froidvaux and Nataf (1981)} have proposed that the generation of the Mesozoic Gondwana CFB was in some way related to subduction processes. They all noted the alignment of the Paraná, Karoo, Antarctican and Tasmanian CFB provinces forming a broad band parallel to the Pacific margin of a reconstructed Gondwana, along which subduction had occurred at least since Devonian times (see figure 6.7). The relationship is not restricted to geometrical considerations, and chapter five has already discussed the many geochemical characteristics that the low-Ti magmas have in common with subduction-related magmas. It should also be noted that the areas of low-Ti magmatism all lie on the proposed subduction zone side of the CFB provinces. The CFB magmatism was generated in response to the development of an extremely widespread zone of mantle melting, the exact cause of which is still in some doubt, but there are two means by which subduction processes could have been involved. Both Elliot (1975) and Cox (1978) proposed that the CFB were formed in a back-arc spreading type of tectonic environment, although on a larger scale for the Columbia River province which has also been linked to a back-arc setting (*e.g.* Hooper, 1982). However, such an environment is believed to be restricted to within a few hundred kilometres of the subduction zone whereas the flood basalts are positioned a few thousand kilometres away from the subduction zone. In a review of the Karoo magmatism, Duncan *et al.*, (1984) favoured the alternative model as suggested by Froidvaux and Nataf (1981). They had shown that large convective 'rolls' will develop within the asthenospheric mantle on the continental side of a subduction zone. The upwelling limbs of these subduction-induced

'rolls' would produce widespread heating of the sub-continental lithosphere within an area of about 3000-4000 km inland of the subduction zone. Such 'rolls' would take about 200 Myrs to establish, consistent with the age and location of the Mesozoic Gondwana CFB provinces. One problem with this model is that it does not explain the substantially younger age of the Paraná CFB (about 130 Ma) compared with the Karoo, Antarctican and Tasmanian CFB (about 170-190 Ma). It might well be a plausible solution for these other provinces, where any relationship with mantle plumes and/or rifting episodes is somewhat tenuous, but the timing of the Paraná magmatism seems to have been more closely connected with the rifting event that led to the initiation of the South Atlantic ocean.

6.6 Tectonic summary and future work.

The precise cause of the extensive melting that typifies the generation of continental flood basalts is still not clearly understood, and much will depend on whether or not future geochemical arguments can resolve the questions over the site of melt generation, *i.e.* lithospheric melting versus lithospheric contamination of asthenospheric melts. As with many geological controversies, there is probably an element of truth in most of the geodynamic mechanisms proposed for the origin of flood basalts. The suggested scenario for the Paraná-Etendeka province is one which involves lithospheric thinning and rifting above the thermal influence of the Tristan da Cunha mantle plume, in the manner of White and McKenzie (1989). If the plume was acting on an already 'warm' lithosphere, perhaps having been pre-heated either by the effect of a subduction-related conductive 'roll' within the asthenospheric mantle (Froidvaux and Nataf, 1981) or by the mechanism of continental insulation (Marsh, in prep.), this would enhance the likely participation of the lithospheric mantle in the Paraná-Etendeka CFB magmatism.

Some reservations have been made in this chapter regarding the applicability of the White and McKenzie (1989) model to the Paraná CFB province as well as the other Mesozoic Gondwana CFB. Notably these include; (a) the pronounced asymmetrical distribution of the Paraná-Etendeka province relative to the main rifting, and the presence of extensive sills within the sedimentary sequences of the Paraná basin, which both count

against all the magmas being fed from the central rift, (b) the possibility (admittedly not well constrained at present) from K-Ar dates of a west to east migration of volcanism within the Paraná sequences, from the plate interior towards the rift, (c) the suggestion for the Paraná (and more pronounced for the Karoo) that magmatism predated the main rifting episode, (d) the vast extent of the Paraná-Etendeka province and the combined Karoo / Antarctica / Tasmania province, which both appear to be excessively large to be related to the influence of individual plumes. However, it seems more likely that the surface distribution of the lavas would be more strongly influenced by the exact mechanism of continental stretching and rifting rather than by any deep-seated phenomenon. The White and McKenzie (1989) model has an additional advantage, at least over the other proposed models, in that it provides testable predictions for many aspects of a flood basalt province. The most important future constraints will probably come from improved estimates for the duration of the magmatism, and clarification of the relative ages of the flood basalts and the initial episode of South Atlantic rifting, which might also establish whether or not there was any west to east migration in the volcanism. The early history of rifting between South America and Africa and its relationship to the flood basalt magmatism is not well constrained at present, and geophysical studies, especially deep seismic sections across the Brazilian (or Namibian) continental margin, would be helpful in this regard.

The dominant feature of the observed regional stratigraphy within the Paraná lava pile is an overlapping sequence of geochemical units dipping towards the north, and this suggested a northward migration of the magmatic source. This south to north structure within the lavas was most likely controlled by the rapid northward propagation of the rifting of the South Atlantic ocean and thus is largely independent of the actual nature of the deeper mechanism of melt generation.

6.7 Concluding Remarks.

" The outcome of any serious research can only be to make two questions grow where only one grew before " Thorstein Veblen, 1919.

The Paraná continental flood basalt province of South America has proved a fruitful place in which to study many diverse aspects of CFB magmatism, and this thesis is submitted as a contribution to our ever-increasing understanding of these immense magmatic events. While the original study aims, as outlined in chapter one, have been largely fulfilled, another important (and inevitable) feature of any thesis is to highlight the topics that require further investigation. For the Paraná CFB province, these can be broken down into three main areas; (i) petrogenesis, (ii) lava stratigraphy, and (iii) tectonics / geodynamics.

The biggest gap in our knowledge of the petrogenesis of the Paraná CFB lavas concerns the magma types of the northern Paraná basin {Ribeira, Paranapanema, Pitanga} for which there is little trace element and isotope data available, and this is where any future efforts should be concentrated.

One of the main achievements of this study has been to put the various geochemical groups within the Paraná lavas on a surer footing, by defining a range of geochemical criteria which can be used to classify flows to a specific magma type. This has provided a basic foundation onto which any future stratigraphical studies can build on. The lack of deeper level erosion of the Paraná lava field has been partly remedied through access to borehole samples. Further unravelling of the lava stratigraphy, especially in order to place east-west constraints on the emerging picture of the internal structure of the lava pile, will inevitably involve a continuation of this work, provided that the samples are made available. The next step is to set up a computer-based classification system to cope with the new data base of ~1500 analyses in Piccirillo and Melfi (1988), which can then be integrated with the borehole results to produce maps of the geographical and stratigraphical distribution of each magma type. For several areas of the Paraná lava field, there is only

sparse geochemical information available, notably the south-western extremities in northern Argentina which are largely obscured by Tertiary/Quaternary sediments but represent one of the thickest portions of the Paraná lava pile, and the distant outliers (Tapirapuã and Anari Formations) close to the Brazilian-Bolivian border.

As has just been stressed in the tectonic summary above, probably the single most important study that is now required on the Paraná lavas is a detailed $^{40}Ar/^{39}Ar$ age survey, based within the available stratigraphical framework. This should lead to improved estimates for the duration of the magmatism and its timing relative to the initiation of the South Atlantic ocean, and thereby place constraints on the various geodynamic mechanisms proposed for the Paraná CFB magmatism.

References.

Abbey S. (1983). 'Studies in 'standard' samples of silicate rocks and minerals, 1969-1982'. *Geol. Surv. Canada*, paper 83-15.

Albarède F. (1983). 'Inversion of batch melting equations and the trace element pattern of the mantle'. *J. geophys. Res.*, **88**, 10573-10583.

Allègre C.J. and Minster J.F. (1978). 'Quantitative models of trace element behaviour in magmatic process'. *Earth Planet. Sci. Lett.*, **38**, 1-25.

Allègre C.J., Dupré B. and Lewin E. (1986). 'Thorium/Uranium ratio of the earth'. *Chem. Geol.*, **56**, 219-227.

Allègre C.J., Dupré B., Richard P. and Rousseau D. (1982). 'Subcontinental versus suboceanic mantle, II. Nd-Sr-Pb isotopic comparison of continental tholeiites with mid-ocean ridge tholeiites, and structure of the continental lithosphere'. *Earth Planet. Sci. Lett.*, **57**, 25-34.

Allègre C.J., Hamelin B., Provost A. and Dupré B. (1987). 'Topology in isotopic multispace and origin of mantle chemical heterogeneities'. *Earth Planet. Sci. Lett.*, **81**, 319-337.

Allègre C.J., Treuil M., Minster J-F., Minster J.B. and Albarède F. (1977). 'Systematic use of trace element in igneous processes. part I: Fractional crystallization processes in volcanic suites'. *Contrib. Mineral. Petrol.*, **60**, 57-75.

Allsopp H.L., Bristow J.W., Logan C.T., Eales H.V. and Erlank A.J. (1984b). 'Rb-Sr geochronology of three Karoo-related intrusive complexes'. *Spec. Publ. geol. Soc. S. Af.*, **13**, 281-288.

Allsopp H.L., Matton W.I., Bristow J.W. and Erlank A.J. (1984a). 'Rb-Sr geochronology of Karoo felsic volcanics'. *Spec. Publ. geol. Soc. S. Af.*, **13**, 273-280.

Amaral G., Cordani U.G., Kawashita K. and Reynolds J.H. (1966). 'Potassium-argon dates of basaltic rocks from southern Brazil'. *Geochim. Cosmochim. Acta*, **30**, 159-189.

Anderson A.T. and Greenland L.P. (1969). 'Phosphorus fractionation as a quantitative indicator of crystallization differentiation of basaltic liquids'. *Geochim. Cosmochim. Acta*, **33**, 493-505.

Anderson D.L. (1982). 'Hotspots, polar wander, Mesozoic convection and the geoid'. *Nature*, **297**, 391-393.

Asmus H.E. and Baisch P.R. (1983). 'Geological evolution of the Brazilian continental margin'. *Episodes*, **4**, 3-9.

Austin J.A. and Uchupi E. (1982). 'Continental-oceanic crustal transition off south-west Africa'. *Am. Assn. Petrol. Geol. Bull.*, **66**, 1328-1347.

Baker C.L. (1923). 'The lava field of the Paraná basin, South America'. *J. Geol.*, **31**, 66-79.

References

Baksi A.K., Barman T.R., Paul D.K. and Farrar E. (1987). 'Widespread Early Cretaceous flood basalt volcanism in eastern India: geochemical data from the Rajmahal-Bengal-Sylhet traps'. *Chem. Geol.*, **63**, 133-141.

Barbieri M., Beccaluva L., Brotzu P., Conte A., Garbarino C., Gomes C.B., Loss E., Macciotta G., Morbidelli L., Scheibe L.F., Tamura R.M. and Traversa G. (1987). 'Petrological and geochemical studies of alkaline rocks from southern Brazil: 1. The phonolite suite from Piritini, RS'. *Geochim. Brasil.*, **1**, 109-138.

Basaltic Volcanism Study Project. (1981). 'Basaltic volcanism on the terrestrial planets', Pergamon Press, Inc., New York, pp 1286.

Beane J.E. (1988). 'Flow stratigraphy, chemical variation and petrogenesis of Deccan flood basalts from the western Ghats, India'. Ph.D. thesis (unpubl.), Washington State University, pp 576.

Beane J.E., Turner C.A., Hooper P.R., Subbarao K.V. and Walsh J.N. (1986). 'Stratigraphy, composition and form of the Deccan basalts, Western Ghats, India'. *Bull. Volcanol.*, **48**, 61-83.

Bellieni G., Brotzu P., Comin-Chiaramonti P., Ernesto M., Melfi A.J., Pacca I.G. and Piccirillo E.M. (1984c). 'Flood basalt to rhyolite suites in the southern Paraná plateau (Brazil): palaeomagnetism, petrogenesis and geodynamic implications'. *J. Petrol.*, **25**, 579-618.

Bellieni G., Brotzu P., Comin-Chiaramonti P., Ernesto M., Melfi A.J., Pacca I.G., Piccirillo E.M. and Stolfa D. (1983). 'Petrological and palaeomagnetic data on the plateau basalt to rhyolite sequences of the southern Paraná basin (Brazil)'. *An. Acad. bras. Ciênc.*, **55**, 355-383.

Bellieni G., Cavazzini G., Comin-Chiaramonti P., Laurenzi M., Melfi A.J., Nardy A.J.R., Petrini R., Piccirillo E.M. and Sial A.N. (1988). 'Triassic - Lower Cretaceous tholeiitic magmatism from NE Brazil (Maranhão basin): petrogenetic aspects and tectonic significance' (abstr.). *"Geochemical evolution of the continental crust", conference abstracts vol., Poços de Caldas, Brazil*, 42-44.

Bellieni G., Comin-Chiaramonti P., Marques L.S., Melfi A.J., Piccirillo E.M. and Stolfa D. (1984b). 'Low pressure evolution of basalt sills from boreholes in the Paraná basin'. *Tschermaks Min. Petr. Mit.*, **33**, 25-47.

Bellieni G., Comin-Chiaramonti P., Marques L.S., Melfi A.J., Nardy A.J.R., Papatrechas C., Piccirillo E.M., Roisenberg A. and Stolfa D. (1986b). 'Petrogenetic aspects of acid and basaltic lavas from the Paraná plateau (Brazil): mineralogical and petrochemical relationships'. *J. Petrol.*, **27**, 915-944.

Bellieni G., Comin-Chiaramonti P., Marques L.S., Martinez L.A., Melfi A.J., Nardy A.J.R., Piccirillo E.M. and Stolfa D. (1986a). 'Continental flood basalts from the central-western regions of the Paraná plateau (Paraguay and Argentina): petology and petrogenetic aspects'. *N. Jb. Miner. Abh.*, **154**, 111-139.

Bellieni G., Comin-Chiaramonti P., Marques L.S., Melfi A.J., Piccirillo E.M., Nardy A.J.R. and Roisenberg A. (1984a). 'High- and low-Ti flood basalts from the Paraná plateau (Brazil): petrology and geochemical aspects bearing on their mantle origin'. *N. Jb. Miner. Abh.*, **150**, 273-306.

Ben Othman D., Polvé M. and Allègre C.J. (1984). 'Nd-Sr isotopic composition of granulites and constraints on the evolution of the lower continental crust'. *Nature*, **307**, 510-515.

References

Bernasconi A. (1987). 'The major precambrian terranes of eastern South America: a study of their regional and chronological evolution'. *Precambrian Res.*, **37**, 107-124.

Betton P.J. and Cox K.G. (1979). 'Production of rhyolites at continental margins: an example from the Lebombo monocline (abstr.)'. *18th Congress Geol. Soc. S. Afr. Abstracts Volume* , part 1, 29-32.

Bowen N.L. (1928). "The evolution of igneous rocks", Princeton University Press, Princeton, N.I., pp 332.

Braun J. and Beaumont C. (1989). 'Dynamical models of the role of crustal shear zones in asymmetric continental extension'. *Earth Planet. Sci. Lett.*, (in press.).

Brewer T.S., Palacz Z. and Hawkesworth C.J. (1987). 'Mesozoic tholeiites from Coats Land and Dronning Maud Land, Antarctica: further pieces in the Gondwanaland jigsaw (abstr.)'. *Terra Cognita*, **7**, 604.

Bristow J.W. (1988). 'Flood basalts in new perspective'. *Nuclear Active*, **39**, 26-36.

Bristow J.W., Allsop H.L., Erlank A.J., Marsh J.S. and Armstrong R.A. (1984). 'Strontium isotope characterization of Karoo volcanic rocks'. *Spec. Publ. geol. Soc. S. Af.*, **13**, 295-330.

Brooks C., James D.E. and Hart S.R. (1976). 'Ancient lithosphere: its role in young continental volcanism'. *Science*, **193**, 1086-1094.

Burke K. and Dewey J.F. (1973). 'Plume-generated triple junctions: key indicators in applying plate tectonics to old rocks'. *J. Geol.*, **81**, 406-433.

Campbell I.H. (1985). 'The difference between oceanic and continental tholeiites: a fluid dynamic explanation'. *Contrib. Mineral. Petrol.*, **91**, 37-43.

Carlson R.W., Lugmair G.W. and MacDougall J.D. (1981). 'Columbia River volcanism: the question of mantle heterogeneity of crustal contamination'. *Geochim. Cosmochim. Acta*, **45**, 2483-2499.

Carter S.R., Evensen N.M., Hamilton P.J. and O'Nions R.K. (1978). 'Nd- and Sr-isotopic evidence for crustal contamination of continental volcanics'. *Science*, **202**, 743-747.

Cleverly R.W. Betton P.J. and Bristow J.W. (1984). 'Geochemistry and petrogenesis of the Lebombo rhyolites'. *Spec. Publ. geol. Soc. S. Af.*, **13**, 171-194.

Comin-Chiaramonti P., Gomes C.B., Piccirillo E.M. and Rivalenti G. (1983). 'High-TiO_2 basaltic dykes in the coastline of São Paulo and Rio de Janeiro states (Brazil)'. *N. Jb. Miner. Abh.*, **146**, 133-150.

Comte D. and Hasui Y. (1971). 'Geochronology of eastern Paraguay by the potassium-argon method'. *Rev. Bras. Geoc.*, **1**, 33-43.

Cordani U.G. and Vandoros P. (1967). 'Basaltic rocks of the Paraná basin' in "Problems in Brazilian Gondwana geology", eds. J.J. Bigarella, R.D. Becker and J.D. Pinto, 207-231.

Cordani U.G., Civetta L., Mantovani M.S.M., Petrini R., Kawashita K., Hawkesworth C.J., Taylor P., Longinelli A., Cavazzzini G. and Piccirillo E.M. (1988). 'Isotope geochemistry of flood volcanics from the Paraná basin (Brazil)', in "The Mesozoic flood volcanism of the Paraná basin: petrogenetic and geophysical aspects", eds. E.M. Piccirillo and A.J. Melfi, IAG-USP press, São Paulo, 157-178.

References

Cordani U.G., Sartori P.L.P. and Kawashita K. (1980). 'Geoquimica dos isotopos de estrôncio e a evolução da atividade vulcânica na bacia do Paraná (Sul do Brasil) durante o Cretáceo'. *An. Acad. bras. Ciênc.*, **52**, 811-818.

Courtillot V., Besse J., Vandamme D., Montigny R., Jaeger J.-J. and Cappetta H. (1986). 'Deccan flood basalts at the Cretaceous/Tertiary boundary ?'. *Earth Planet. Sci. Lett.*, **80**, 361-374.

Coward M.P. (1986). 'Heterogeneous stretching, simple shear and basin development'. *Earth Planet. Sci. Lett.*, **80**, 325-336.

Cox K.G. (1980). 'A model for flood basalt vulcanism'. *J. Petrol.*, **21**, 629-650.

Cox K.G. (1988). 'The Karoo province', in "Continental Flood Basalts" ed. J.D. MacDougall'. Kluwer academic publishers, 239-271.

Cox K.G. (1978). 'Flood basalts, subduction and the break-up of Gondwanaland'. *Nature*, **274**, 47-49.

Cox K.G. (1983). 'The Karoo province of southern Africa: origin of trace element enrichment patterns', in "Continental basalts and mantle xenoliths", eds. C.J. Hawkesworth and M.J. Norry, Shiva Press, 139-157.

Cox K.G. and Hawkesworth C.J. (1984). 'Relative contribution of crust and mantle to flood basalt magmatism, Mahabaleshwar area, Deccan traps'. *Phil. Trans. R. Soc. Lond.*, **A310**, 627-641.

Cox K.G. and Hawkesworth C.J. (1985). 'Geochemical stratigraphy of the Deccan traps at Mahabaleshwar, Western Ghats, India, with implications for open system magmatic processes'. *J. Petrol.*, **26**, 355-377.

Cox K.G., Macdonald R. and Hornung G. (1967). 'Geochemical and petrographic provinces in the Karoo basalts of southern Africa'. *Am. Miner.*, **52**, 1451-1474.

Creer K.M. (1962). 'Palaeomagnetism of the Serra Geral formation'. *Geophys. J. R. astr. Soc.*, **7**, 1-22.

Creer K.M., Miller J.A. and Smith A.G. (1965). 'Radiometric age of the Serra Geral formation'. *Nature*, **207**, 282-283.

DePaolo D.J. (1981). 'Trace element and isotopic effects of combined wallrock assimilation and fractional crystallisation'. *Earth Planet. Sci. Lett.*, **53**, 189-202.

DePaolo D.J. and Wasserburg G.J. (1976). 'Nd isotopic variations and petrogenetic models'. *Geophys. Res. Lett.*, **3**, 249-252.

Derby O.A. (1878). 'A geologia da região diamantifera da Provincia do Paraná no Brasil'. *Arq. Mus. Nac., Rio de Janeiro*, **3**, 89-96.

Devey C.W. and Cox K.G. (1987). 'Relationships between crustal contamination and crystallisation in continental flood basalt magmas with special reference to the Deccan traps of the Western Ghats, India'. *Earth Planet. Sci. Lett.*, **84**, 59-68.

Devey C.W. and Lightfoot P.C. (1986). 'Volcanological and tectonic control of stratigraphy and structure in the western Deccan traps'. *Bull. Volcanol.*, **48**, 195-207.

Dickin A.P. (1981). 'Isotope geochemistry of Tertiary igneous rocks from the Isle of Skye, N.W. Scotland'. *J. Petrol.*, **22**, 155-189.

Du Toit, A.L. (1937). "Our wandering continents", Oliver and Boyd, Edinburgh, pp 366.

References

Duncan A.R. (1987). 'The Karoo igneous province - a problem area for inferring tectonic setting from basalt geochemistry'. *J. Volcanol. Geotherm. Res.* , **32**, 13-34.

Duncan A.R., Erlank A.J. and Marsh J.S. (1984). 'Regional geochemistry of the Karoo igneous province'. *Spec. Publ. geol. Soc. S. Af.*, **13**, 355-388.

Duncan A.R., Marsh J.S., Milner S.C. and Erlank A.J. (1988). 'Distribution and petrogenesis of the basic rocks of the Etendeka Formation of northwestern Namibia' (abstr.). *"Geochemical evolution of the continental crust", conference abstracts vol., Poços de Caldas, Brazil*, 10-18.

Duncan R.A and Pyle D.G. (1988). 'Rapid eruption of the Deccan flood basalts at the Cretaceous/Tertiary boundary'. *Nature*, **333**, 841-843.

Duncan R.A. (1978). 'Geochronology of basalts from the Ninetyeast Ridge and continental dispersion in the eastern Indian Ocean'. *J. Volcanol. Geotherm. Res.* , **4**, 283-305.

Duncan R.A. (1981). 'Hot-spots in the southern oceans - an absolute frame of reference for motion in the Gondwana continents'. *Tectonophysics*, **74**, 29-42.

Dupuy C. and Dostal J. (1984). 'Trace element geochemistry of some continental tholeiites'. *Earth Planet. Sci. Lett.*, **67**, 61-69.

Eales H.V., Marsh J.S. and Cox K.G. (1984). 'The Karoo igneous province: an introduction'. *Spec. Publ. geol. Soc. S. Af.*, **13**, 1-26.

Ellam R.M. and Cox K.G. (1989). 'A Proterozoic lithospheric source for Karoo magmatism: evidence from the Nuanetsi picrites'. *Earth Planet. Sci. Lett.*, **92**, 207-218.

Ellam R.M. and Hawkesworth C.J. (1988). 'Is average continental crust generated at subduction zones ?'. *Geology*, **16**, 314-317.

Elliot D.H. (1975). 'Tectonics of Antarctica: a review'. *Am. J. Sci.*, **275a**, 295-307.

Emery K.O. and Uchupi E. (1984). "The geology of the Atlantic ocean", Springer-Verlag, New York, pp 1050.

Erlank A.J., Duncan A.R., Marsh J.S., Sweeney R.J., Hawkesworth C.J., Milner S.C., Miller R.McG. and Rogers N.W. (1988). 'A laterally extensive geochemical discontinuity in the sub-continental Gondwana lithosphere' (abstr.). *"Geochemical evolution of the continental crust", conference abstracts vol., Poços de Caldas, Brazil*, 1-10.

Erlank A.J., Allsopp R.S., Hawkesworth C.J. and Menzies M.A. (1982). 'Chemical and isotopic characterisation of upper mantle metasomatism in peridotite nodules from the Bulfontein kimberlite'. *Terra Cognita*, **2**, 261-263.

Erlank A.J., Marsh J.S., Duncan A.R., Miller R.McG., Hawkesworth C.J., Betton P.J. and Rex D.C. (1984). 'Geochemistry and petrogenesis of the Etendeka volcanic rocks from SWA/Namibia'. *Spec. Publ. geol. Soc. S. Af.*, **13**, 195-246.

Erlank A.J., Waters F.G., Hawkesworth C.J., Haggerty H.L., Allsopp R.S., Rickard R.S. and Menzies M.A. (1987). 'Evidence for mantle metasomatism in peridotite nodules from the Kimberley pipes, South Africa', in "Mantle metasomatism", eds. M.A. Menzies and C.J. Hawkesworth. Academic press, London, 221-311.

Ernesto M., Hiodo F.Y. and Pacca I.G. (1979). 'Estudo paleomagnético de seqüência de derrames basálticos da formação Serra Geral em Santa Catarina'. *An. Acad. bras. Ciênc.*, **51**, 327-332.

References

Ewart A., Baxter K. and Ross J.A. (1980). 'The petrology and petrogenesis of the Tertiary anorogenic mafic lavas of southern and central Queemsland, Australia - possible implications for crustal thickening'. *Contrib. Mineral. Petrol.*, **75**, 129-152.

Faure G. (1986). "Principles of Isotope Geology", 2nd edition, John Wiley and Sons, New York, pp 590.

Fitch F.J. and Miller J.A. (1984). 'Dating Karoo igneous rocks by the conventional K-Ar and $^{40}Ar/^{39}Ar$ age spectrum methods'. *Spec. Publ. geol. Soc. S. Af.*, **13**, 247-266.

Fitton J.G. and Dunlop H.M. (1985). 'The Cameroon line, West Africa, and its bearing on the origin of oceanic and continental alkali basalt'. *Earth Planet. Sci. Lett.*, **72**, 23-38.

Fodor R.V. (1987). 'Low- and high-TiO_2 flood basalts of southern Brazil: origin from picritic parentage and a common mantle source'. *Earth Planet. Sci. Lett.*, **84**, 423-430.

Fodor R.V. and Vetter S.K. (1984). 'Rift-zone magmatism: Petrology of basaltic rocks transitional from CFB to MORB, southeastern Brazil'. *Contrib. Mineral. Petrol.*, **88**, 307-321.

Fodor R.V., Corwin C. and Roisenberg A. (1985a). 'Petrology of Serra Geral (Paraná) continental flood basalts, southern Brazil: crustal contamination, source material, and South Atlantic magmatism'. *Contrib. Mineral. Petrol.*, **91**, 54-65.

Fodor R.V., Corwin C. and Sial A.N. (1985b). 'Crustal signatures in the Serra Geral flood basalt province, southern Brazil: O- and Sr-isotope evidence'. *Geology*, **13**, 763-765.

Fraser K.J., Hawkesworth C.J., Erlank A.J., Mitchell R.H. and Scott-Smith B.H. (1985). 'Sr, Nd and Pb isotope and minor element geochemistry of lamproites and kimberlites'. *Earth Planet. Sci. Lett.*, **76**, 57-70.

Frey F.A., Green D.H. and Roy S.D. (1978). 'Integrated models of basalt petrogenesis: A study of quartz tholeiites to olivine melilitites from south eastern Australia utilising geochemical and experimental petrological data'. *J. Petrol.*, **19**, 463-513.

Froidevaux C. and Nataf H.C. (1981). 'Continental drift: what driving mechanism ?'. *Geol. Rdsch.*, **70**, 166-176.

Geikie, A. (1903). "Textbook of Geology", 4th edition, Macmillan, London, 344 pp.

Gerrard I. and Smith G.C. (1982). 'Post-Palaeozoic succession and structure of the southwestern African continental margin', in "Studies in continental margin geology", ed. J.S. Watkins and C.L. Drake, *Am. Assn. Petrol. Geol. Mem.*, **34**, 49-76.

Gidskehaug A., Creer K.M. and Mitchell J.G. (1975). 'Palaeomagnetism and K-Ar ages of the South West African basalts and their bearing on the timing of initial rifting of the South Atlantic ocean'. *Geophys. J. R. astr. Soc.*, **42**, 1-20.

Gomes C.B., Barbieri M., Beccaluva L., Brotzu P., Conte A., Garbarino C., Macciotta G., Melluso L., Morbidelli L., Ruberti E., Scheibe L.F., Tamura R.M. and Traversa G. (1987). 'Petrological and geochemical studies of alkaline rocks from continental Brazil: 2. The Tunas massif, state of Paraná'. *Geochim. Brasil.*, **1**, 201-234.

Grove T.L. and Baker M.B. (1984). 'Phase equilibrium controls on the tholeiitic versus calc-alkaline differentiation trends'. *J. geophys. Res.*, **89**, 3253-3274.

Hanan B.B., Kingsley R.H. and Schilling J-G. (1986). 'Pb isotope evidence in the South Atlantic for migrating ridge-hotspot interactions'. *Nature*, **322**, 137-144.

Harland W.B., Cox A.V., Llewellyn P.G., Pickton C.A.G., Smith A.G. and Walters R. (1982). "A geologic time scale", Cambridge University Press, pp.131.

Hart S.R. (1984). 'A large-scale isotope anomaly in the southern hemisphere mantle'. *Nature*, **309**, 753-757.

Harte B. (1983). 'Mantle peridotites and processes-the kimberlite sample', in "Continental basalts and mantle xenoliths", eds. C.J. Hawkesworth and M.J. Norry, Shiva Press, 46-91.

Harvey P.K. and Atkins B.P. (1982). 'Automated X-ray fluorescence analysis', in "Sampling and analysis for the mining industry", IMM, London, 17-26.

Hawkesworth C.J. and Morrison M.A. (1978). 'A reduction in $^{87}Sr/^{86}Sr$ during basalt alteration'. *Nature*, **276**, 381-383.

Hawkesworth C.J., Erlank A.J., Marsh J.S., Menzies M.A. and van Calsteren P. (1983). 'Evolution of the continental lithosphere: evidence from volcanics and xenoliths' in southern Africa, in "Continental basalts and mantle xenoliths", eds. C.J. Hawkesworth and M.J. Norry, Shiva Press, 111-138.

Hawkesworth C.J., van Calsteren P.W., Rogers N.W. and Menzies M.A. (1987). 'Isotope variation in revent volcanics: a trace element perspective', in "Mantle metasomatism", eds. M.A. Menzies and C.J. Hawkesworth. Academic press, London, 365-388.

Hawkesworth C.J., Kempton P.D., Rogers N.W., Ellam R.M. and van Calsteren P.W. (in prep.). 'Continental mantle lithosphere, and shallow level enrichment processes in the Earth's mantle'.

Hawkesworth C.J., Mantovani M.S.M. and Peate D.W. (1988). 'Lithosphere remobilisation during Paraná magmatism', in "Oceanic and continental lithosphere: similarities and differences", eds. K.G. Cox and M.A. Menzies, *J. Petrol.*, **Spec. Vol.**, 205-223.

Hawkesworth C.J., Mantovani M.S.M., Taylor P.N. and Palacz Z. (1986). 'Evidence from the Paraná of south Brazil for a contribution to Dupal basalts'. *Nature*, **322**, 356-359.

Hawkesworth C.J., Marsh J.S., Duncan A.R., Erlank A.J. and Norry M.J. (1984b). 'The role of continental lithosphere in the generation of the Karoo volcanic rocks: evidence from combined Nd- and Sr-isotope studies'. *Spec. Publ. geol. Soc. S. Af.*, **13**, 341-354.

Hawkesworth C.J., Rogers N.W., van Calsteren P.W. and Menzies M.A. (1984a). 'Mantle enrichment processes'. *Nature*, **311**, 331-335.

Henderson P. (1982). "Inorganic Geochemistry", Pergamon Press, Oxford, pp 353.

Hergt J.M., Chappell B.W., McCulloch M.T., McDougall I. and Chivas A.R. (1989). 'Geochemical and isotopic constraints on the origin of the Jurassic dolerites of Tasmania'. *J. Petrol.*, (in press).

Hinz K. (1981). 'A hypothesis on terrestrial catastrophes: wedges of very thick oceanward dipping layers beneath passive continental margins - their origin and palaeoenvironmental significance'. *Geol. Jahrb. Reihe E, Geophys.*, **22**, 3-28.

Hofmann A.W. and Feigenson M.D. (1983). 'Case studies on the origin of basalt, I. Theory and reassessment of Grenada basalts'. *Contrib. Mineral. Petrol.*, **84**, 382-389.

References

Hoffman N.R.A. and McKenzie D.P. (1985). 'The destruction of mantle heterogeneities by differental fluid motions during mantle convection'. *Geophys. J. R. astr. Soc.*, **82**, 163-206.

Hooper P.R. (1982). 'The Columbia River basalts'. *Science*, **215**, 1463-1468.

Hooper P.R. (1988). 'The Columbia River Basalt', in "Continental Flood Basalts" ed. J.D. MacDougall. Kluwer academic publishers, 1-33.

Huene F.v. (1933). 'Zur stratigraphie Brasiliens'. *Zentralbl. f. Min. Geol. Palaeont. Abt. B.*, **7**, 418-423.

Huppert H.E. and Sparks R.S.J. (1985). 'Cooling and contamination of mafic and ultramafic magmas during ascent through continental crust'. *Earth Planet. Sci. Lett.*, **74**, 371-386.

Jaques A.L. and Green D.H. (1980). 'Anhydrous melting of peridotite at 0-15 Kb pressure and the genesis of tholeiitic basalts'. *Contrib. Mineral. Petrol.*, **73**, 287-310.

Jolly W.T. (1987). 'Lithophile elements in Huronian low-Ti continental tholeiites from Canada, and evolution of the Precambrian mantle'. *Earth Planet. Sci. Lett.*, **85**, 401-415.

Jordan T.H. (1978). 'Composition and development of the continental tectosphere'. *Nature*, **274**, 544-548.

Jordan T.H. (1988). 'Structure and formation of the continental tectosphere', in "Oceanic and continental lithosphere: similarities and differences", eds. K.G. Cox and M.A. Menzies. *J. Petrol.*, **Spec. Vol.**, 11-37.

Kent D.V. and Gradstein F.M. (1985). 'A Cretaceous and Jurassic geochronology'. *Bull. Geol. Soc. Am.*, **96**, 1419-1427.

Kyle P.R. (1980). 'Development of heterogeneities in the subcontinental mantle: evidence from the Ferrar group, Antarctica'. *Contrib. Mineral. Petrol.*, **73**, 89-104.

Kyle P.R., Elliot D.H. and Sutter J.F. (1981). 'Jurassic Ferrar supergroup tholeiites from the Transantarctic Mountains, Antarctica, and their relation to the initial fragmentation of Gondwana', in "Gondwana Five", eds. M. Cresswell and P. Vell, A.A. Balkema Rotterdam ', 283-287.

Kyser T.K., O'Neill J.R. and Carmichael I.S.E. (1982). 'Genetic relations among basic lavas and ultramafic nodules: evidence from oxygen isotopic compositions'. *Contrib. Mineral. Petrol.*, **81**, 88-102.

Langmuir C.H., Bender J.F., Bence A.E.,Hanson G.H. and Taylor S.R. (1977). 'Petrogenesis of basalts from the Famous area: mid-Atlantic'. *Earth Planet. Sci. Lett.*, **36**, 133-156.

Langmuir C.H., Vocke R.D.Jr., Hanson G.H. and Hart S.R. (1978). 'A general mixing equation with applications to Icelandic basalts'. *Earth Planet. Sci. Lett.*, **37**, 380-392.

Leinz V., Bartorelli A. and Isotta C.A.L. (1968). 'Contribuição ao estudo do magmatismo basáltico Mesozóic da bacia do Paraná '. *An. Acad. bras. Ciênc.*, **40**, 167-181.

Leinz V., Bartorelli A., Sadowiski G.R. and Isotta C.A.L. (1966). 'Sobre o compartamento especial do trapp basáltico da Bacia do Paraná'. *Bol. Soc. Bras. Geol.*, **15**, 79-91.

Lighfoot P.C. (1985). 'Isotope and trace element geochemistry of the South Deccan lavas, India'. Ph.D. Thesis (unpubl.), Open University, pp 589.

Lightfoot P.C., Hawkesworth C.J. and Sethna S.F. (1987). 'Petrogenesis of rhyolites and trachytes from the Deccan trap: Sr, Nd and Pb isotope and trace element evidence'. *Contrib. Mineral. Petrol.*, **95**, 044-054.

Long P.E. (1978). 'Characterization and recognition of intraflow structures, Grande Ronde Basalt'. RHO-BWI-LD-10, Rockwell Handford Operations, Richland, Washington, pp 74.

Long P.E. and Wood B.J. (1986). 'Structures, textures, and cooling histories of Columbia River basalt flows'. *Bull. Geol. Soc. Am.*, **97**, 1144-1155.

Maack R. (1952). 'Die Entwicklung der Gondwana-Schichten Suedbrasiliens und ihre Beziehungen zur Karru-formation Suedafrikas'. *Int. Geol. Congr. Algiers*, **19**, 339-372.

Macdougall J.D. (1988). 'Continental flood basalts and MORB: a brief discussion of similarities and differences in their petrogenesis', in "Continental Flood Basalts" ed. J.D. Macdougall. Kluwer academic publishers, 331-341.

Mahoney J.J., Macdougall J.D., Lugmair G.W., Murali A.V., Sankar Das M. and Gopalan K. (1982). 'Origin of the Deccan Trap flows at Mahabaleshwar inferred from Nd and Sr isotopic and chemical evidence'. *Earth Planet. Sci. Lett.*, **60**, 47-60.

Mangan M.T., Wright T.L., Swanson D.A. and Byerly G.R. (1986). 'Regional correlation of Grande Ronde flows, Columbia River basalt group, Washington, Oregon and Idaho'. *Bull. Geol. Soc. Am.*, **97**, 1300-1318.

Mantovani M.S.M. and Hawkesworth C.J. (in press). 'An inversion approach to assimilation and fractional crystallisation processes'. *Contrib. Mineral. Petrol.*

Mantovani M.S.M. and Hawkesworth C.J. (1988). 'Crustal contamination inverted: some preliminary results'. *Rev. Bras. Geoc.*, **18**, 27-32.

Mantovani M.S.M., Cordani U.G. and Roisenberg A. (1985b). 'Geoquímica isotópica em vulcânicas ácidas da bacia do Paraná, e implicações genéticas associadas'. *Rev. Bras. Geoc.*, **15**, 061-065.

Mantovani M.S.M., Marques L.S., De Sousa M.A., Civetta L., Atalla L. and Innocenti F. (1985a). 'Trace element and strontium isotope constraints on the origin and evolution of Paraná continental flood basalts of Santa Catarina state (southern Brazil)'. *J. Petrol.*, **26**, 187-209.

Mantovani M.S.M., Hawkesworth C.J., Taylor P.N. and Palacz Z. (1986). *Abstr. Vol.* IAVCEI New Zealand, 181.

Mantovani M.S.M., Peate D.W. and Hawkesworth C.J. (1988). 'Geochemical stratigraphy of Paraná continental flood basalts: a contribution from borehole samples, in "The Mesozoic flood volcanism of the Paraná basin: petrogenetic and geophysical aspects", eds. E.M. Piccirillo and A.J. Melfi', IAG-USP press, São Paulo, 15-24.

Marimon M.P.C., Moreira M.L.D. and Ayala L. (1983). 'Formação Serra Geral no Sul do Brasil: novos dados de razões isotopicas $^{87}Sr/^{86}Sr$ e implicações com a gêese das rochas desta formação'. *Atas do Iº Simpósio Sul-Brasileiro de Geologia, Porto Alegre, RS*, 69-81.

Marques L.S. (1988). 'Caracterização geoquímica das rochas vulcânicas da bacia do Paraná: implicações petrogenéticas'. Ph.D. Thesis (unpubl.), University of São Paulo.

References

Marques L.S., Piccirillo E.M., Melfi A.J., Comin-Chiaramonti P. and Bellieni G. (1988). 'Geochemistry and REE distribution of flood basalt - rhyolite suites from the Paraná basin (Brazil) (abstr.)'. *"Geochemical evolution of the continental crust", conference abstracts vol., Poços de Caldas, Brazil*, 70-79.

Marsh J.S. (1973). 'Relationships between transform directions and alkaline igneous rock lineaments in Africa and South America'. *Earth Planet. Sci. Lett.*, **18**, 317-323.

Marsh J.S. (in prep.). 'Very large continental flood basalt provinces: emplacement and possible origin'.

Marsh J.S. (1987). 'Basalt geochemistry and tectonic discrimination within continental flood basalt provinces'. *J. Volcanol. Geotherm. Res.* , **32**, 35-49.

Marsh J.S. and Eales H.V. (1984). 'The chemistry and petrogenesis of igneous rocks of the Karoo central area, southern Africa'. *Spec. Publ. geol. Soc. S. Af.*, **13**, 27-68.

McCulloch M.T., Jaques A.L., Nelson D.R. and Lewis J.D. (1983). 'Nd and Sr isotopes in kimberlites and lamproites from Western Australia: and enriched mantle origin'. *Nature*, **302**, 400-403.

McDougall I. and Rüegg N.R. (1966). 'Potassium-argon dates on the Serra Geral formation of South America'. *Geochim. Cosmochim. Acta*, **30**, 191-195.

McKenzie D.P. (1978). 'Some remarks on the development of sedimentary basins'. *Earth Planet. Sci. Lett.*, **40**, 25-32.

McKenzie D.P. (1984). 'The generation and compaction of partially molten rock'. *J. Petrol.*, **25**, 713-765.

McKenzie D.P. (1985). '^{230}Th-^{238}U disequilibrium and the melting process beneath ridge axes'. *Earth Planet. Sci. Lett.*, **72**, 149-157.

McKenzie D.P. (1987). 'The compaction of igneous and sedimentary rocks'. *J. Geol. Soc*, **144**, 299-307.

McKenzie D.P. and Bickle M.J. (1988). 'The volume and composition of melt generated by extension of the lithosphere'. *J. Petrol.*, **29**, 625-679.

Melfi A.J. (1967). 'Potassium-argon ages for core samples of basaltic rocks fron southern Brazil'. *Geochim. Cosmochim. Acta*, **31**, 1079-1089.

Menzies M.A. and Murthy V.R. (1980). 'Enriched mantle: Nd and Sr isotopes in diopsides from kimberlite nodules'. *Nature*, **283**, 634-636.

Menzies M.A. and Wass S.Y. (1983). 'CO_2 and LREE-rich mantle below eastern Australia: a REE and isotopic study of alkaline magmas and apatite rich mantle xenoliths from the Southern Highland Province, Australia'. *Earth Planet. Sci. Lett.*, **74**, 634-636.

Milner S.C. (1986). 'The geological and volcanological features of the quartz latites of the Etendeka formation'. *Communs. geol. Surv. S.W. Africa/Namibia*, **2**, 109-116.

Milner S.C. and Duncan A.R. (1987). 'Geochemical characterisation of quartz latite units in the Etendeka formation'. *Communs. geol. Surv. S.W. Africa/Namibia*, **3**, 83-90.

Milner S.C., Duncan A.R., and Erlank A.J. (1988). 'The geochemical characteristics and petrogenesis of the quartz latites of the Etendeka Formation, Namibia'. *"Geochemical evolution of the continental crust", conference abstracts vol., Poços de Caldas, Brazil*, 19-25.

Milner S.C., Duncan A.R., Marsh J.S. and Erlank A.J. (1988). 'Field excursion guide to the Etendeka volcanics and associated intrusives, N.W. Namibia', *unpublished*, pp 90.

Minioli B., Ponçano W.L. and De Oliveira S.M.B. (1971). 'Extensão geográfica do vulcanismo basáltico do Brasil meridional'. *An. Acad. bras. Ciênc.*, **43**, 433-437.

Minster J.F. and Allègre C.J. (1978). 'Systematic use of trace element in igneous processes. part III: Inverse problem of batch partial melting in volcanic suites'. *Contrib. Mineral. Petrol.*, **68**, 37-52.

Molnar P. and Stock J. (1987). 'Relative motions of hotspots in the Pacific, Atlantic and Indian oceans since late Cretaceous times'. *Nature*, **327**, 587-591.

Morgan W.J. (1981). 'Hotspot tracks and the opening of the Atlantic and Indian oceans', in "The Sea: vol. 7, The oceanic lithosphere", ed. C. Emiliani, Wiley, New York, 443-487.

Murata K.J., Formoso M.L.L. and Roisenberg A. (1987). 'Distribution of zeolites in lavas of southestern Paraná basin, state of Rio Grande do Sul, Brazil'. *J. Geol.*, **95**, 455-467.

Mysen B.O. (1976). 'Rare earth partitioning between crystal and liquid in the upper mantle'. *Carnegie Inst. Wash. Yb.*, **75**, 656-659.

Mysen B.O. and Kushiro I. (1977). 'Compositional variations of coexisting phases with degrees of melting of peridotite in the upper mantle'. *Am. Mineral.*, **62**, 843-865.

Nakamura N. (1974). 'Determination of REE, Ba, Fe, Mg, Na and K in carbonaceous and ordinary chondrites'. *Geochim. Cosmochim. Acta*, **38**, 757-775.

Nardy A.J.R. (1988). 'Petrologia e paleomagnetismo das rochas vulcânicas da região centro-sul do estado do Paraná: Formação Serra Geral'. Ph.D. Thesis (unpubl.), University of São Paulo, pp 186.

Nathan H.D. and Van Kirk C.K. (1978). 'A model of magmatic crystallisation'. *J. Petrol.*, **19**, 66-94.

Neill W.M. (1976). 'Mesozoic epeirogeny at the South Atlantic margin and the Tristan hot spot'. *Geology*, **4**, 495-498.

Nicholls J. and Stout M.Z. (1982). 'Heat effects of assimilation, crystallisation and vesiculation in magmas'. *Contrib. Mineral. Petrol.*, **81**, 328-339.

Nielsen R.L. (1988). 'A model for the simulation of combined major and trace element liquid lines of descent'. *Geochim. Cosmochim. Acta*, **52**, 27-38.

O'Hara M.J. and Mathews R.E. (1981). 'Geochemical evolution in an advancing, periodically replenished, periodically tapped, continuously fractionated magma chamber'. *J. Geol. Soc*, **138**, 237-277.

Oliveira A.I. (1956). 'Brazil', in "Handbook of South American geology". *Mem. Geol. Soc. Amer.*, **65**, 1-62.

Oxburgh E.R. and Parmentier E.M. (1978). 'Thermal processes in the formation of continental lithosphere'. *Phil. Trans. R. Soc. Lond.*, **A288**, 415-429.

Pacca I.G. and Hiodo F.Y. (1976). 'Palaeomagnetic analysis of mesozoic Serra Geral basaltic lava flows in southern Brazil'. *An. Acad. bras. Ciênc.*, **48**, 207-214.

References

Palmieri J.H. and Velázquez J.C. (1982). 'Geologia del Paraguay'. *Serie Ciencias naturales, ediciones NAPA*, , pp 165.

Patchett P.J. (1980). 'Thermal effects of basalt on continental crust and crustal contamination of magmas'. *Nature*, **283**, 559-561.

Patriat P. and Achache J. (1984). 'India-Eurasia collision chronology has implications for crustal shortening and driving mechanisms for plates'. *Nature*, **311**, 615-621.

PAULIPETRO (1982). 'Geologia da Bacia do Paraná: reavaliação da potentialidade e prospectividade em hidrocarbonetos'. *Consórcio CESP/IPT*, pp 198.

Pearce J.A. and Cann J.R. (1973). 'Tectonic setting of basic volcanic rocks determined using trace element analyses'. *Earth Planet. Sci. Lett.*, **19**, 290-300.

Pearce J.A. and Norry M.J. (1979). 'Petrogenetic implications of Ti, Zr, Y and Nb variations in volcanic rocks'. *Contrib. Mineral. Petrol.*, **69**, 33-47.

Pearce J.A., Harris N.B.W. and Tindle A.G. (1984). 'Trace element discrimination diagrams for the tectonic interpretation of granitic rocks'. *J. Petrol.*, **25**, 956-983.

Peate D.W., Hawkesworth C.J. and Mantovani M.S.M. (1988a). 'Lithospheric to asthenospheric transition within the coastal margin CFB of the Paraná province' (abstr.). *"Geochemical evolution of the continental crust", conference abstracts vol., Poços de Caldas, Brazil*, 80-83.

Peate D.W., Mantovani M.S.M. and Hawkesworth C.J. (1988b). 'Geochemical stratigraphy of Paraná CFB: borehole evidence'. *Rev. Bras. Geoc.*, **18**, 212-221.

Piccirillo E.M. and Cox K.G. (1988). 'Origins of variation in the mafic rocks of the S. Paraná basin' (abstr.). *"Geochemical evolution of the continental crust", conference abstracts vol., Poços de Caldas, Brazil*, 83-89.

Piccirillo E.M. and Melfi A.J. (1988). "The Mesozoic flood volcanism of the Paraná basin: petrogenetic and geophysical aspects", IAG-USP press, São Paulo, pp 600.

Piccirillo E.M., Melfi A.J., Comin-Chiaramonti P., Bellieni G., Ernesto M., Marques L.S., Nardy A.J.R., Pacca I.G., Roisenberg A. and Stolfa D. (1988a). 'Continental flood volcanism from the Paraná basin (Brazil)' in "Continental flood basalts" ed. J.D. MacDougall, Kluwen academic publishers, 195-238.

Piccirillo E.M., Melfi A.J., Roisenberg A., Ussami N., Ernesto M. and Pacca I.G. (1988b). 'The Paraná basin magmatism', field guide for international conference - "Geochemical evolution of the continental crust", Poços de Caldas, Brazil, 43-107.

Piccirillo E.M., Raposo M.I.B., Melfi A.J., Comin-Chiaramonti P., Bellieni G., Cordani U.G. and Kawashita K. (1987). 'Bimodal fissural volcanic suites from the Paraná basin (Brazil): K-Ar age, Sr-isotopes and geochemistry'. *Geochim. Brasiliensis.*, **1**, 053-069.

Potts P.J., Thorpe O.W. and Watson J.S. (1981). 'Determination of the rare-earth element abundances in 29 international rock standards by instrumental neutron activation analysis: a critical appraisal of calibration errors'. *Chem. Geol.*, **34**, 331-352.

Potts P.J., Thorpe O.W., Isaacs M.C. and Wright D.W. (1985). 'High precision instrumental neutron-activation analysis of geological samples employing simultaneouus counting with both planar and coaxial detectors'. *Chem. Geol.*, **48**, 145-155.

Potts P.J., Webb P.C. and Watson J.S. (1984). 'Energy dispersive x-ray fluorescence analysis of silicate rocks for major and trace elements'. *X-ray Spectrom.*, **13**, 2-15.

Powell R. (1984). 'Inversion of the assimilation and fractional crystallization (AFC) equations; characterization of contaminants from isotope and trace element relationships in volcanic suites'. *J. Geol. Soc*, **141**, 447-452.

Prinzhofer A. and Allègre C.J. (1985). 'Residual peridotites and the mechanics of partial melting'. *Earth Planet. Sci. Lett.*, **74**, 251-265.

Rayleigh J.W.S. (1896). 'Theoretical considerations respecting the separation of gases by diffusion and similar processes'. *Philos. Mag.*, **42**, 77-107.

Richardson S.H., Gurney A.J., Erlank A.J. and Harris K.W. (1984). 'Origin of diamonds in old enriched mantle'. *Nature*, **310**, 198-202.

Richter F.M. (1986). 'Simple models for trace element fractionation during melt segregation'. *Earth Planet. Sci. Lett.*, **77**, 333-344.

Richter F.M. (1988). 'A major change in the thermal state of the Earth at the Archaean-Proterozoic boundary: consequences for the nature and preservation of continental lithosphere', in "Oceanic and continental lithosphere: similarities and differences", eds. K.G. Cox and M.A. Menzies, *J. Petrol.*, **Spec. Vol.**, 39-52.

Roden M.F., Murthy V. R. and Gaspar J.C. (1985). 'Sr and Nd isotopic composition of the Jacupiranga carbonatite'. *J. Geol.*, **93**, 212-220.

Roeder P.L. and Emslie R.F. (1970). 'Olivine-liquid equilibrium'. *Contrib. Mineral. Petrol.*, **29**, 275-289.

Rogers N.W., Hawkesworth C.J., Mattey D.P. and Harmon R.S. (1987). 'Sediment subduction and the source of potassium in orogenic leucites'. *Geology*, **15**, 451-453.

Sanford R.M. and Lange F.W. (1960). 'Basin-study approach to oil evaluation of Paraná miogeosyncline, south Brazil'. *Amer. Ass. Petrol. Geol.*, **44**, 1316-1370.

Sartori P.L., Filho C.M. and Menegotto E. (1975). 'Contribuição ao estudo das rochas vulcânicas da bacia do Paraná na região de Santa Maria, RS'. *Rev. Bras. Geoc.*, **5**, 141-159.

Schmitt P.W. and McDougall I. (1977). 'Paleomagnetic and potassium-argon dating studies of the Tasmanian dolerites'. *J. Geol. Soc. Aust.*, **25**, 321-328.

Schobbenhaus C., Almeida Campos D. de, Derze G.R. and Asmus H.E. (1984). 'Geologia do Brasil: texto explicativo do mapa geológico do Brasil e da área oceânica adjacente incluindo depósitos minerais; escala 1:2,000,000'. DNPM, Brasilia.

Shaw D.M. (1970). 'Trace element fractionation during anatexis'. *Geochim. Cosmochim. Acta*, **34**, 237-243.

Siedner G. and Miller J.A. (1968). 'K-Ar age determinations on basaltic rocks from South West Africa, and their bearing on continental drift'. *Earth Planet. Sci. Lett.*, **4**, 451-458.

Siedner G. and Mitchell J.G. (1976). 'Episodic mesozoic volcanism in Namibia and Brazil: a K-Ar isochron study bearing on the opening of the South Atlantic'. *Earth Planet. Sci. Lett.*, **30**, 292-302.

Smith C.B. (1983). 'Pb, Sr and Nd isotopic evidence for sources of southern African Cretaceous kimberlites'. *Nature*, **304**, 51-54.

Stacey J.S. and Kramers J.D. (1975). 'Approximation of terrestrial lead isotope evolution by a two-stage model'. *Earth Planet. Sci. Lett.*, **26**, 207-221.

Sun S.-S. and McDonough W.D. (1988). 'Chemical and isotopic systematics of oceanic basalts: implications for mantle composition and processes', in "Magmatism in the ocean basins", eds. A.D. Saunders and M.J. Norry. *Spec. Publ. Geol. Soc Lond.*, **42**.

Swanson D.A. and Wright T.L. (1980). 'The regional approach to studying the Columbia River basalt group'. *Mem. Geol. Soc. India*, **3**, 58-80.

Swanson D.A., Wright T.L. and Helz R.T. (1975). 'Linear vent systems and estimated rates of magma production and eruption for the Yakima basalt on the Columbia plateau'. *Am. Jour. Sci.*, **275**, 877-905.

Swanson D.A., Wright T.L., Hooper P.R. and Bentley R.D. (1979). 'Revisions in stratigraphic nomenclature of the Columbia River Basalt Group'. *U.S. Geol. Surv. Bull.*, **1457-G**, G1-G59.

Takahashi E. and Kushiro I. (1983). 'Melting of a dry pridotite at high pressures and basalt magma genesis'. *Am. Mineralogist*, **68**, 859-879.

Taylor H.P. (1980). 'The effects of assimilation of country rocks by magmas on $^{18}O/^{16}O$ and $^{87}Sr/^{86}Sr$ systematics in igneous rocks'. *Earth Planet. Sci. Lett.*, **47**, 243-254.

Taylor S.R. and McLennan S.M. (1985). "The continental crust: its composition and evolution", Blackwell, Oxford, pp 312.

Thirlwall M.F. and Jones N.W. (1983). 'Isotope geochemistry and contamination mechanics of Tertiary lavas from Skye, northwest Scotland', in "Continental basalts and mantle xenoliths", eds. C.J. Hawkesworth and M.J. Norry, Shiva Press, 186-208.

Thompson R.N. (1977). 'Columbia/Snake River - Yellowstone magmatism in the context of Western U.S. Cenozoic geodynamics'. *Tectonophysics*, **39**, 621-636.

Thompson R.N. and Morrison M.A. (1988). 'Asthenospheric and lower-lithospheric mantle contributions to continental extensional magmatism: an example from the British Tertiary province'. *Chem. Geol.*, **68**, 1-15.

Thompson R.N., Dickin A.P., Gibson I.L. and Morison M.A. (1982). 'Elemental fingerprints of isotopic contamination of Hebridean Palaeocene mantle-derived magmas by Archaean sial'. *Contrib. Mineral. Petrol.*, **79**, 159-168.

Thompson R.N., Morrison M.A., Dickin A.P. and Hendry G.L. (1983). 'Continental flood basalts ... arachnids rule OK ?', in "Continental basalts and mantle xenoliths", eds. C.J. Hawkesworth and M.J. Norry, Shiva Press, 158-185.

Treuil M. and Varet J. (1973). 'Critères volcanologiques, pétrologiques et géochemiques de la genèses et de la différenciation des magmas basaltiques" exemple de l'Afar '. *Bull. Soc. Geol. France, 7eme series*, **15**, 401-644.

Tyrrell G.W. (1937). 'Flood basalts and fissure eruption'. *Bull. Volcan.*, **1**, 89-111.

Ulbrich H.H.G.J. and Gomes C.B. (1981). 'Alkaline rocks from continental Brazil'. *Earth Sci. Rev.*, **17**, 135-154.

van Hinte J.E. (1976). 'A Cretaceous time scale'. *Am. Assn. Petrol. Geol. Bull.*, **60**, 498-516.

Vanderos P., Rüegg N.R. and Cordani U.G. (1966). 'On potassium-argon age measurements of basaltic rocks from southern Brazil'. *Earth Planet. Sci. Lett.*, **1**, 449-452.

Vollmer R., Ogden P., Schilling J.-G., Kingsley R.H. and Waggoner D.G. (1984). 'Nd and Sr isotopes in ultrapotassic rocks from the Leucite Hills, Wyoming'. *Contrib. Mineral. Petrol.*, **87**, 359-368.

Walker G.P.L. (1972). 'Compound and simple lava flows and flood basalts'. *Bull. Volcanol.*, **35**, 579-590.

Watson E.B. (1982). 'Basalt contamination by continental crust: some experiments and models'. *Earth Planet. Sci. Lett.*, **80**, 73-87.

Watts A.B. and Cox K.G. (1989). 'The Deccan traps: an interpretation in terms of progressive lithospheric flexure in response to a migrating load'. *Earth Planet. Sci. Lett.*, **93**, 85-97.

Weaver B.L. and Tarney J. (1983). 'Chemistry of the sub-continental mantle: inferences from Archaean and Proterozoic dykes and continental flood basalts', in "Continental basalts and mantle xenoliths", eds. C.J. Hawkesworth and M.J. Norry, Shiva Press, 209-229.

Wernicke B. (1985). 'Uniform-sense normal simple shear of the continental lithosphere'. *Can. J. Earth Sci.*, **22**, 108-125.

White I.C. (1908). 'Relatório final da Commissão das Minas de Carvão de Pedra do Brasil'. Imprensa Nacional, Rio de Janeiro, pp 617.

White R.S. and McKenzie D.P. (1989). 'Magmatism at rift zones: the generation of volcanic continental margins and flood basalts'. *J. geophys. Res.*, **94**, (in press).

White R.S., Spence G.D., Fowler S.R., McKenzie D.P., Westbrook G.K. and Bowen A.N. (1987). 'Magmatism at rifted continental margins'. *Nature*, **330**, 439-444.

Wilkinson J.F.G. and Binns R.A. (1977). 'Relatively iron-rich lherzolite xenoliths of the Cr-diopside suite: a guide to the primary nature of anorogenic tholeiitic andesite magmas'. *Contrib. Mineral. Petrol.*, **65**, 199-212.

Wood B.J. and Fraser D.G. (1977). "Elementary thermodynamics for geologists", Oxford University Press, Oxford, pp 303.

Wood D.A. (1979). 'A variably veined suboceanic upper mantle - genetic significance for mid-ocean ridge basalts from geochemical evidence'. *Geology*, **7**, 499-503.

Wood D.A., Gibson I.L. and Thompson R.N. (1976). 'Element mobility during zeolite facies metamorphism of the Tertiary basalts of Eastern Iceland'. *Contrib. Mineral. Petrol.*, **55**, 241-255.

Woodworth J.B. (1912). 'Geological Expedition to Brazil and Chile, 1908-1909'. *Bull. Mus. Comp. Zool.*, **56**, 1-137.

Wright T.L. and Doherty P.C. (1970). 'A linear programming and least squares computer method for solving petrologic mixing problems'. *Bull. Geol. Soc. Am.*, **81**, 1995-2008.

Zalan P.V, Wolff S., Conceição J.C.J., Astolfi M.A.M., Vieira I.S., Appi V.T., Zanotto O.A. and Marques A. (1987). 'Tectonics and sedimentation of the Paraná basin'. *Anais do VII sympósio do Gondwana*, pp 35.

References

Zambrano J.J. and Urien C.M. (1974). 'Pre-Cretaceous basins in the Argentine continental shelf' in "The geology of continental margins", eds. C.A. Burke and C.L. Drake, New York, Springer-Verlag, 463-470.

Appendix A
Geochemical Data Tables.

A.1 General Information.

Geochemical analyses on whole rock samples from the São Joaquim road sections and road profiles in Paraguay and Argentina, as well as on drillcore chippings from the central Paraná boreholes, are presented below in tables A.2 and A.3. Table A.2 gives the XRF major and trace element data for each sample, and is divided into two sections. The data on the road section flows and other miscellaneous surface samples are listed in the first half, followed by the borehole analyses. Each sample is accompanied by a road section or borehole name, a sample elevation (where available) and an assigned magma type name. The major element data have been normalised to 100 % on a volatile-free basis, with total iron expressed as Fe_2O_3(t). The major element data for which the total is only quoted to one decimal place were obtained by WD-XRF at Southampton University, and all other major element data were acquired on the ED-XRF at the Open University (see appendix B). The table also indicates which samples have also been analysed by INAA or for Sr, Nd or Pb isotope compositions, and these data are then listed separately in table A.3.

A.2 Sample locality information.

The road section localities have been illustrated earlier on figure 2.11, and details of the borehole locations are given in appendix C (table C.2) and also shown in figure 2.20. The samples prefixed by the letters PAR were collected from roadside exposures and quarries in Paraguay and Argentina and their localities are listed below in table A.1.

Geochemical data tables

sample n°	Lat. (°S)	Long. (°W)	sample n°	Lat. (°S)	Long. (°W)
PAR-01	25.46	54.67	PAR-15	29.13	58.32
PAR-02	26.00	54.84	PAR-16	27.61	55.82
PAR-03	26.22	54.85	PAR-17	27.11	55.30
PAR-04	26.26	54.88	PAR-18	27.11	55.30
PAR-05	26.33	54.91	PAR-19	27.11	55.30
PAR-06	26.51	54.98	PAR-20	27.11	55.30
PAR-07	26.48	55.06	PAR-21	26.82	54.95
PAR-08	26.60	55.17	PAR-22	26.77	54.88
PAR-09	26.72	55.29	PAR-23	26.74	54.83
PAR-10	29.80	58.16	PAR-24	26.69	54.76
PAR-11	29.80	58.16	PAR-25	25.84	54.56
PAR-12	29.80	58.16	PAR-26	25.91	54.53
PAR-13	29.13	58.32	PAR-27	25.96	54.53
PAR-14	29.13	58.32			

Table A.1 Sample localities (Latitude and Longitude) for surface flows sampled in Paraguay and Argentina.

- - - -

sample n°	DSM37	DSM36	DSM35	DSM34	DSM33	DSM31	DSM30	DSM29	DSM27	DSM41	DSM40	DSM24	DSM22	DSM21	DSM19	DSM18	DSM17a	DSM17b	DSM16	DSM15	DSM14
road section	SM	SM	SM	SM	SM	SM	SM	SM	SM	SM	SM	SM	SM	SM	SM	SM	SM	SM	SM	SM	SM
altitude	1235	1260	1275	1300	1305	1325	1350	1375	1390	1400	1405	1420	1445	1450	1470	1515	1540	1540	1570	1590	1620
description	flow	flow	flow	flow	flow	flow	flow	flow	flow	flow	flow	flow	flow	flow	flow	flow	flow	flow	flow	flow	flow
magma type	Urubici	Urubici	Urubici	Urubici	Urubici	Urubici	Urubici	Urubici	Urubici	Urubici	Urubici	Urubici	Urubici	Urubici	Gramado	Gramado	Urubici	Urubici	Urubici	Gramado	Gramado
SiO2	52.53	52.48	51.61	51.48	50.44	51.84	51.74	51.41	52.64	51.87	51.66	54.93	51.34	51.49	53.44	52.67	51.83	52.35	51.28	54.49	54.50
TiO2	3.52	3.52	3.39	3.40	3.44	3.60	3.61	3.57	3.76	3.88	3.62	2.95	4.23	4.21	1.65	1.47	4.16	4.15	3.88	1.45	1.34
Al2O3	13.49	13.42	13.46	13.75	14.13	13.43	13.22	13.43	12.91	13.48	13.27	13.94	13.14	13.17	13.65	13.95	13.07	13.10	13.33	13.67	13.93
Fe2O3(t)	12.68	12.81	12.67	13.25	12.97	12.61	12.87	12.63	13.09	12.98	13.13	11.53	13.40	13.43	13.59	13.36	13.39	13.36	13.36	12.60	12.22
MnO	0.16	0.17	0.17	0.19	0.18	0.19	0.17	0.17	0.15	0.16	0.17	0.17	0.16	0.17	0.20	0.20	0.16	0.17	0.17	0.20	0.19
MgO	4.53	4.51	5.38	4.67	4.86	4.96	5.01	5.14	4.50	4.60	4.71	3.18	4.35	4.32	4.56	5.18	4.12	4.06	4.45	4.68	4.90
CaO	7.55	7.69	8.53	8.32	8.86	8.32	8.28	8.38	8.48	8.33	8.42	6.44	7.87	7.27	8.54	9.37	7.62	7.85	8.18	8.58	8.80
Na2O	3.08	2.99	2.74	3.08	2.91	2.89	2.89	3.17	2.23	2.41	2.79	3.29	2.89	3.05	2.58	2.74	2.91	2.50	3.17	2.84	2.62
K2O	1.90	1.88	1.56	1.38	1.20	1.64	1.71	1.57	1.72	1.77	1.72	2.86	2.03	2.29	1.56	0.80	2.11	1.84	1.64	1.27	1.28
P2O5	0.57	0.53	0.49	0.47	0.48	0.53	0.49	0.55	0.52	0.53	0.49	0.70	0.59	0.60	0.24	0.24	0.61	0.62	0.57	0.22	0.23
L.O.I.	0.26	0.06	0.70	0.85	1.06	1.10	0.26	0.96	1.21	1.54	0.69	0.50	0.83	1.76	0.14	0.45	0.91	0.91	0.62	1.47	1.07
Total	98.76	98.08	98.35	97.98	99.88	100.61	98.26	102.33	98.94	100.10	98.74	99.27	99.43	97.87	98.24	99.99	99.40	97.86	99.19	100.31	100.09
Mg#	45.4	45.1	49.7	45.1	46.6	47.8	47.6	48.7	44.5	45.2	45.5	39.1	43.1	42.8	43.9	47.5	41.8	41.5	43.7	46.4	48.3
XRF-O.U.																					
Ni	49	48	97	57	63	60	65	52	67	51	61	25	54	58	40	44	51	55	64	40	35
Cu	132	126	151	166	159	136	102	152	185	179	136	72	188	190	166	162	169	181	165	181	134
Zn	103	118	108	108	109	110	104	115	121	118	124	134	126	132	124	107	114	116	111	108	104
Ga	25	23	26	23	26	22	27	26	25	26	21	26	27	24	16	22	24	24	26	20	20
Rb	43	44	32	30	19	31	36	34	39	48	38	73	48	60	45	20	43	32	37	69	52
Sr	642	620	694	835	881	706	661	703	969	1091	784	564	718	613	252	332	789	885	879	292	229
Y	41	40	38	35	37	38	38	36	38	46	36	50	40	39	38	34	40	42	38	39	32
Zr	318	322	278	280	289	283	289	291	301	326	311	397	348	347	187	164	345	354	321	160	153
Nb	26.8	26.9	24.4	25.5	26.4	22.9	24	23.6	25.2	26.9	26	37.7	32.7	32.1	16.2	13.4	30	29.8	27.4	12.5	11.5
XRF-Notts																					
Ni	50	49	100	50	56	59	58	55	60	53	59	25	53	52	36	31	50	56	60	28	29
Cr	77	83	315	57	76	155	118	313	83	70	81	38	217	190	39	178	297	54	56	167	41
Co	36	41	42	37	43	36	38	43	n/a	40	35	n/a	38	39	n/a	39	39	39	38	33	n/a
V	331	344	343	314	365	347	360	355	337	342	357	257	393	379	340	322	370	358	349	283	293
Zn	103	115	99	95	108	116	104	106	113	100	112	139	123	127	116	103	114	106	107	95	100
Rb	44	40	29	28	19	31	35	32	36	42	34	70	45	57	40	18	43	30	36	64	46
Sr	632	605	654	805	845	705	653	694	933	1009	743	540	696	603	242	310	789	873	858	275	210
Y	38	40	37	32	36	39	35	35	36	41	36	46	37	42	36	32	39	39	38	37	30
Zr	301	304	257	263	264	273	268	272	298	288	288	385	324	331	181	153	341	347	303	147	148
Nb	29	29	23	28	30	25	26	24	25	27	29	39	33	34	15	13	33	33	27	13	11
Ba	785	701	503	709	736	743	551	550	519	670	600	776	615	727	358	321	707	738	630	385	359
INAA		-	√	√			√		√			√	-		√			√		√	√
isotopes		√	√	√			√		√			√	√		√			√		√	√

sample n°	DSM12	DSM11	DSM13	DSM10	DSM09	DSM07	DSM05b	DSM04	DSM08	DSM05a	DSM03a	DSM02	DSM06	DSM23	DSM01	DSM20	DSM25	DSM26	DUP46	DUP44	DUP43
road section	SM	SM	SM	SM	SM	SM	SM	SM	SM	SM	SM	SM	SM	SM	SM	SM	SM	SM	UP	UP	UP
altitude	1675	1685	1650	1720	1755	1755	1755	1765	1765	1775	1795	1815	1750	1435	1820	1440	1435	1435	1190	1220	1225
description	flow	flow	flow	flow	flow	flow	flow	flow	flow	flow	flow	flow	sill	sill	sill	dyke	dyke	dyke	flow	flow	flow
magma type	Gramado	Gramado	Gramado	Urubici	Urubici	Urubici	Urubici	Urubici	Urubici	Esmeralda	Esmeralda	Esmeralda	Esmeralda	Esmeralda	Esmeralda	Esmeralda	Esmeralda	Urubici	Urubici	Urubici	Urubici
SiO2	54.48	54.26	54.08	51.25	51.43	51.61	51.56	59.78	59.96	52.86	51.08	51.52	51.16	51.04	51.10	51.66	51.72	52.10	51.40	51.51	50.99
TiO2	1.34	1.73	1.74	3.66	3.49	3.48	3.51	2.01	2.03	2.16	2.13	1.86	1.38	1.38	1.37	1.39	1.64	3.41	3.46	3.36	3.34
Al2O3	13.78	13.36	13.27	13.71	13.32	13.32	13.24	14.06	13.86	12.66	13.20	13.70	13.70	13.88	13.87	13.75	13.78	13.89	12.93	13.19	13.30
Fe2O3(t)	12.26	14.29	14.25	13.20	14.05	14.15	13.87	9.20	9.38	15.30	16.11	14.50	13.53	13.32	13.40	13.44	13.30	12.18	12.86	12.93	12.89
MnO	0.19	0.22	0.21	0.17	0.17	0.17	0.19	0.14	0.15	0.21	0.23	0.19	0.20	0.20	0.20	0.21	0.21	0.17	0.16	0.19	0.17
MgO	5.01	3.97	3.89	4.56	4.37	4.21	4.30	2.05	1.92	4.11	4.63	4.87	6.06	6.11	6.09	5.85	5.75	4.39	4.41	5.30	5.33
CaO	8.69	8.18	8.26	8.40	8.04	7.93	8.01	4.11	4.11	7.71	8.54	8.95	10.82	10.65	10.64	9.86	9.64	8.39	7.77	8.49	9.29
Na2O	2.82	2.06	2.76	2.95	2.94	2.72	3.01	3.84	3.89	3.23	2.73	3.16	2.44	2.70	2.62	2.82	2.81	2.77	3.64	2.89	2.78
K2O	1.17	1.61	1.26	1.54	1.71	1.87	1.80	4.12	4.01	1.44	0.87	0.96	0.54	0.51	0.50	0.76	0.89	1.87	1.83	1.68	1.43
P2O5	0.24	0.32	0.29	0.55	0.50	0.53	0.51	0.70	0.69	0.32	0.30	0.30	0.18	0.19	0.21	0.21	0.27	0.46	0.51	0.45	0.47
L.O.I.	0.94	1.94	1.26	0.73	0.86	1.65	0.75	0.87	0.88	0.75	1.94	1.98	0.86	-0.06	1.39	0.33	1.05	1.40	0.82	0.91	0.56
Total	99.74	99.58	99.82	99.62	99.18	99.91	99.54	100.92	100.35	99.86	99.58	101.58	97.77	99.79	100.94	99.58	101.49	100.05	98.32	97.72	98.63
Mg#	48.8	39.3	38.9	44.6	42.0	40.9	41.9	34.2	32.3	38.5	40.1	43.9	51.1	51.7	51.4	50.4	50.2	45.7	44.4	48.9	49.1
XRF-O.U.																					
Ni	34	22	17	47	40	37	39	n/d	n/d	40	40	42	58	67	57	61	48	66	48	95	83
Cu	94	205	202	152	165	200	188	39	43	158	251	128	169	180	168	188	178	182	152	124	148
Zn	98	123	110	125	117	123	107	109	115	112	122	113	92	93	95	100	106	107	98	102	108
Ga	19	22	22	26	27	26	27	27	27	22	21	22	21	17	21	18	20	23	22	22	23
Rb	42	52	61	60	43	48	46	116	111	55	50	22	20	19	18	28	29	39	43	42	24
Sr	240	243	264	840	692	699	706	698	609	244	198	215	165	173	166	166	236	785	633	672	734
Y	31	41	40	36	37	40	37	50	50	45	45	43	29	32	31	34	35	37	40	38	35
Zr	151	187	183	312	269	283	276	490	510	202	180	167	101	102	103	116	137	294	311	279	280
Nb	11.4	15.0	13.6	29	23.4	24	24.7	44.7	46.7	12.4	12.4	11.5	6.4	6.0	6.5	7.1	9.9	24.4	25.7	23.6	24.1
XRF-Notts																					
Ni	32	22	18	61	37	30	34	4	0	25	30	47	61	60	60	60	60	63	45	89	73
Cr	277	32	19	263	73	22	211	7	16	256	248	160	101	219	109	116	122	78	82	357	458
Co	n/a	37	41	n/a	37	n/a	32	n/a	n/a	42	47	n/a	n/a	n/a	n/a	n/a	n/a	n/a	33	41	34
V	281	384	353	378	407	373	387	119	130	396	469	369	323	307	313	319	324	345	330	339	365
Zn	90	110	103	119	108	124	103	106	116	104	116	110	92	89	76	95	101	97	93	95	99
Rb	39	49	58	56	39	46	44	111	108	52	48	20	18	18	18	27	28	39	43	38	21
Sr	223	224	251	812	652	681	695	678	593	239	192	200	161	167	160	163	234	781	604	632	687
Y	29	36	37	35	35	38	37	47	47	45	43	40	28	29	30	33	34	35	38	40	34
Zr	143	172	170	300	249	280	268	480	502	193	166	157	97	102	102	115	139	295	290	259	258
Nb	11	15	13	28	24	25	23	49	50	13	12	11	6	6	5	7	10	26	28	23	25
Ba	344	324	367	592	563	570	595	1137	1139	358	323	294	183	183	179	219	196	579	457	794	437
INAA	√	√		√		√	√	√	√	√	-	√	√	√	√	√	√	√			
isotopes	√	√		√		√	√	√	√	√	√	√	√	√	√	√	√	√			

sample n°	DUP42	DUP40	DUP38	DUP37	DUP35	DUP36	DUP34	DUP33	DUP32	DUP31	DUP30	DUP29	DUP28	DUP27	DUP26	DUP25	DUP01	DUP02	DUP03	DUP04	DUP05
road section	UP	UP	UP	UP	UP	UP	UP	UP	UP	UP	UP	UP	UP	UP	UP	UP	PE	PE	PE	PE	PE
altitude	1270	1290	1325	1345	1365	1405	1420	1435	1450	1465	1485	1505	1520	1530	1555	1570	1185	1220	1220	1230	1235
description	flow	flow	flow	flow	flow	flow	flow	flow	flow	flow	flow	flow	flow	flow	flow	flow	flow	flow	flow	flow	flow
magma type	Urubici	Urubici	Gramado	Urubici	Urubici	Urubici	Urubici	Urubici	Urubici	Urubici	Gramado	Urubici	Urubici	Gramado	Gramado	Gramado	Urubici	Urubici	Urubici	Urubici	Urubici
SiO2	51.79	52.04	56.14	52.93	53.01	52.27	52.85	52.35	51.51	51.23	50.89	51.44	51.42	53.77	54.01	52.84	51.57	50.53	50.29	53.00	52.20
TiO2	3.33	3.50	1.68	3.55	3.76	3.75	3.80	3.79	4.12	4.15	0.95	4.20	4.20	1.74	1.64	1.61	3.89	3.89	3.95	3.51	3.55
Al2O3	13.42	13.16	13.19	13.02	12.86	13.16	13.12	12.96	12.74	12.96	14.92	12.91	12.92	13.49	13.38	13.78	13.14	13.48	13.20	13.38	13.39
Fe2O3(t)	12.63	12.80	13.54	12.50	12.68	13.10	13.01	13.25	13.93	14.02	10.34	13.57	13.49	14.05	13.69	13.62	13.33	13.60	14.03	12.76	13.09
MnO	0.17	0.18	0.19	0.16	0.19	0.17	0.19	0.16	0.20	0.18	0.17	0.19	0.17	0.21	0.18	0.21	0.18	0.18	0.18	0.16	0.18
MgO	4.89	5.05	3.26	4.81	4.34	4.65	4.36	4.50	4.52	4.53	7.99	4.29	4.42	4.20	4.31	4.99	4.80	4.87	4.99	4.01	4.35
CaO	8.71	8.85	6.39	8.20	8.30	7.93	8.31	8.38	7.59	8.67	11.61	8.24	8.33	8.29	8.77	8.92	9.15	8.90	8.86	7.39	8.05
Na2O	2.69	2.50	2.81	2.63	2.57	2.66	2.70	2.68	2.69	2.62	2.44	3.25	2.98	3.19	2.64	2.97	2.50	2.85	2.60	3.06	2.68
K2O	1.91	1.46	2.57	1.70	1.70	1.80	1.11	1.35	2.14	1.08	0.51	1.31	1.47	0.79	1.12	0.81	0.93	1.19	1.39	2.13	1.92
P2O5	0.46	0.47	0.24	0.50	0.58	0.51	0.56	0.59	0.55	0.55	0.16	0.60	0.59	0.27	0.26	0.25	0.54	0.52	0.51	0.60	0.60
L.O.I.	0.27	1.08	0.44	1.00	0.26	0.57	1.05	1.06	0.10	1.10	0.90	0.96	0.72	1.21	1.40	1.05	1.39	1.98	1.80	0.87	0.75
Total	96.14	98.60	98.11	98.74	98.63	97.93	98.17	99.42	97.16	97.71	100.27	98.12	98.03	99.00	98.87	100.27	97.90	97.96	97.20	98.87	97.55
Mg#	47.4	47.9	35.9	47.3	44.4	45.3	43.9	44.2	43.1	43.0	64.3	42.4	43.3	41.1	42.3	46.1	45.6	45.5	45.3	42.3	43.6
XRF-O.U.																					
Ni	68	69	19	53	60	56	64	58	70	73	105	62	54	40	36	55	57	60	55	39	35
Cu	142	158	61	145	267	134	182	182	160	196	99	191	185	170	117	153	171	185	175	134	118
Zn	111	108	109	114	108	112	113	116	124	124	75	117	114	106	104	101	122	121	117	130	123
Ga	23	25	22	28	26	30	29	26	27	26	17	22	30	23	19	23	26	25	25	25	24
Rb	40	21	91	49	30	42	48	21	45	21	11	49	43	59	47	43	11	28	26	36	32
Sr	679	828	217	767	777	702	898	847	748	900	226	956	890	305	273	272	926	1006	869	730	850
Y	34	34	42	37	38	41	38	41	41	42	24	40	38	40	37	36	40	44	39	41	38
Zr	280	287	228	296	319	324	323	324	338	341	95	356	340	212	198	184	331	339	335	348	333
Nb	24.3	25.1	15.9	25.1	26.6	26.2	28	27.9	30.7	31.5	8.6	31.3	31.5	20.3	17	15.2	27.8	28.2	27.5	32.4	31.6
XRF-Notts																					
Ni	64	64	13	50	55	51	58	54	59	57	93	56	44	31	27	33	57	60	63	37	37
Cr	310	390	54	88	75	60	78	85	154	100	307	59	202	36	164	51	84	87	143	98	257
Co	45	39	41	35	36	36	35	36	45	38	44	39	36	42	33	39	38	42	40	38	32
V	336	358	317	349	343	324	326	358	398	371	221	361	362	330	287	294	354	371	370	323	323
Zn	105	97	100	103	106	98	110	112	118	113	68	102	106	100	96	97	111	116	107	111	109
Rb	36	20	81	45	29	36	46	19	43	21	8	43	38	54	42	40	10	26	25	31	32
Sr	648	790	205	722	750	644	865	811	726	868	206	904	860	296	265	259	862	947	791	663	814
Y	34	34	45	34	39	38	38	40	40	41	21	40	37	37	36	36	38	42	38	38	38
Zr	261	263	211	271	295	285	295	299	314	314	89	322	319	198	185	168	295	310	292	304	303
Nb	27	27	16	25	27	27	29	28	35	33	9	40	33	20	17	16	29	29	27	33	31
Ba	525	572	461	574	600	576	682	609	673	684	243	718	715	499	470	416	592	732	562	686	746
INAA	-		√	√	√				√		√			-		√		√		-	
isotopes	√		√	√	√				√		√			√		√		√		√	

sample n°	DUP06	DUP07	DUP08	DUP09	DUP10	DUP11	DUP12	DUP13	DUP14	DUP15	DUP16	DUP17	DUP18	DUP20	DUP21	DUP22	DUP24	DUP19	DUP23	DGB01	DGB05
road section	PE	PE	PE	PE	PE	PE	PE	PE	PE	PE	PE	PE	PE	PE	PE	PE	PE	PE	PE	GB	GB
altitude	1235	1240	1300	1315	1335	1375	1385	1420	1450	1460	1470	1475	1500	1495	1520	1540	1565	1490	1560	765	810
description	flow	flow	flow	flow	flow	flow	flow	flow	flow	flow	flow	flow	flow	flow	flow	flow	flow	sill	sill	flow	flow
magma type	Urubici	Urubici	Gramado	Gramado	Gramado	Urubici	Urubici	Urubici	Gramado	Gramado	Gramado	Gramado	Gramado	Urubici	Gramado	Gramado	Gramado	Esmeralda	Esmeralda	Gramado	Gramado
SiO2	53.52	49.73	52.66	54.25	54.49	51.20	51.08	51.38	54.28	51.74	53.24	53.13	54.46	51.23	52.41	53.86	53.27	51.23	50.91		54.29
TiO2	3.56	3.74	1.37	1.35	1.36	4.13	3.72	4.16	1.58	1.67	1.61	1.61	1.60	4.33	1.83	1.65	1.62	1.39	1.40		1.47
Al2O3	13.26	13.92	14.34	14.14	13.85	12.98	13.13	12.71	13.52	14.09	13.66	13.61	13.38	13.13	14.05	13.58	13.63	13.56	13.80		13.91
Fe2O3(t)	12.87	13.45	12.42	11.83	11.95	14.16	14.04	13.94	13.25	14.24	13.54	13.59	13.47	13.50	14.45	13.46	13.65	13.77	13.77		12.98
MnO	0.17	0.16	0.19	0.19	0.18	0.17	0.17	0.19	0.17	0.23	0.21	0.20	0.20	0.17	0.23	0.19	0.21	0.20	0.22		0.20
MgO	4.06	4.93	5.60	5.23	5.09	4.50	4.65	4.35	4.55	4.94	4.92	4.77	4.42	4.39	4.59	4.38	4.95	5.99	6.09		4.35
CaO	7.45	8.93	9.22	9.03	8.67	8.99	8.23	8.37	8.73	9.32	8.65	9.02	7.81	8.07	8.94	7.99	8.68	10.53	10.54		8.16
Na2O	2.49	2.69	2.82	2.54	2.75	2.30	2.56	3.13	2.38	2.57	2.58	2.71	2.65	2.72	2.39	2.95	2.56	2.62	2.58		2.74
K2O	2.06	1.95	1.14	1.22	1.42	1.00	1.83	1.21	1.30	0.97	1.36	1.16	1.78	1.88	0.84	1.64	1.21	0.56	0.55		1.68
P2O5	0.54	0.50	0.23	0.21	0.23	0.58	0.59	0.56	0.24	0.25	0.23	0.22	0.22	0.58	0.28	0.31	0.23	0.16	0.16		0.21
L.O.I.	0.86	1.65	0.88	0.86	0.73	1.94	0.94	1.26	1.07	1.47	0.62	0.91	0.45	0.33	1.76	0.83	0.50	0.14	-0.06		0.45
Total	97.06	98.40	99.67	99.17	99.64	98.14	98.36	98.02	98.54	98.81	98.63	98.44	98.53	97.62	98.57	99.90	98.70	98.15	99.27		100.3
Mg#	42.4	46.1	51.2	50.8	49.8	42.6	43.6	42.1	44.5	44.7	45.9	45.0	43.3	43.1	42.5	43.1	45.8	50.3	50.8		43.8
XRF-O.U.																					
Ni	32	55	31	39	31	45	38	47	39	35	43	54	41	67	52	50	40	81	88	49	31
Cu	125	84	117	114	106	201	177	170	153	173	167	154	151	192	167	145	151	178	173	87	61
Zn	124	113	91	92	92	113	132	118	98	115	105	118	115	136	117	112	112	94	97	105	117
Ga	27	32	21	21	20	29	25	32	19	23	21	24	19	20	24	21	19	21	22	22	22
Rb	35	49	30	40	38	22	44	41	49	38	41	40	50	43	26	54	28	22	22	42	58
Sr	682	759	294	363	303	860	737	902	327	308	273	276	223	854	378	260	300	168	169	271	236
Y	40	42	30	32	31	41	39	45	36	41	41	36	39	43	45	40	35	30	30	33	37
Zr	341	318	153	155	160	342	330	337	183	198	186	184	192	360	232	204	182	103	105	171	201
Nb	31.7	28.5	13	12.4	14	32.3	29.8	31.6	16.3	17.6	15.4	16.9	15.7	33.9	21.4	18.2	15.2	6.1	6.3	12.5	14.3
XRF-Notts																					
Ni	43	57	31	34	30	57	46	50	41	35	38	41	31	51	32	27	36	55	57	37	25
Cr	64	84	65	225	266	61	138	54	45	200	67	60	259	137	52	37	81	329	94	147	42
Co	35	40	39	39	37	39	40	40	42	42	42	44	39	45	40	36	46	42	39	40	36
V	332	354	298	286	288	364	379	341	300	354	313	324	313	375	366	344	303	325	332	223	235
Zn	111	111	88	81	81	104	118	110	90	110	93	110	103	121	107	105	99	88	91	98	104
Rb	32	10	26	37	34	20	38	37	46	32	34	36	46	42	24	49	24	21	17	37	55
Sr	640	862	279	340	285	820	674	881	315	289	252	258	214	812	356	243	287	161	161	261	227
Y	38	38	30	28	31	39	36	46	35	40	41	32	37	40	44	38	35	31	29	32	36
Zr	303	295	144	141	151	314	291	315	175	181	170	172	181	327	212	182	171	98	98	163	188
Nb	32	29	12	15	12	34	31	33	17	17	14	16	17	35	23	18	15	7	6	12	15
Ba	690	592	353	317	389	628	608	753	483	417	419	354	436	732	429	471	423	208	187	483	536
INAA			√																		
isotopes			√										√					√			

sample n°	DGB08	DGB09	DGB36	DGB31	DGB30	DGB27	DGB25	DGB21	DGB20	DGB19	DGB18	DGB17	DGB15	DGB14	DGB13	DGB11	DGB10	DGB49	DGB46	DGB45	DGB62
road section	GB	GB	GB	GB	GB	GB	GB	GB	GB	GB	GB	GB	GB	GB	GB	GB	GB	GB	GB	GB	GB
altitude	885	905	1030	1105	1110	1140	1175	1205	1225	1245	1280	1290	1310	1320	1325	1350	1365	1405	1480	1485	1425
description	flow	flow	flow	flow	flow	flow	flow	flow	flow	flow	flow	flow	flow	flow	flow	flow	flow	flow	flow	flow	flow
magma type	Gramado	Urubici	Urubici	Urubici	Gramado	Gramado	Urubici	Gramado	Gramado	Gramado	Gramado	Gramado	Gramado	Gramado	Gramado	Gramado	Gramado	Gramado	Gramado	Gramado	Gramado
SiO2	52.61	52.55	52.01	50.07	54.72	54.77	53.74	53.21	53.62	52.96	55.80	57.64	57.18	54.52	52.87	51.48	53.96		53.15	51.22	53.99
TiO2	1.04	3.59	3.67	4.00	1.71	1.65	3.68	1.82	1.70	1.63	1.76	1.66	1.73	1.80	1.43	1.34	1.40		1.44	1.45	1.37
Al2O3	15.77	13.74	13.48	14.12	13.53	13.36	12.94	13.34	13.67	13.80	13.63	13.35	13.59	14.40	14.40	14.45	13.95		14.16	15.09	14.31
Fe2O3(t)	11.63	12.48	13.14	14.00	13.61	13.49	12.94	14.72	13.97	13.74	13.03	12.17	12.50	13.10	13.26	13.51	13.04		13.14	13.56	12.74
MnO	0.17	0.15	0.17	0.16	0.18	0.19	0.18	0.19	0.20	0.21	0.18	0.16	0.19	0.22	0.22	0.20	0.18		0.21	0.24	0.24
MgO	5.37	4.22	4.49	4.61	3.91	4.26	3.73	4.32	4.31	4.73	3.60	3.03	3.18	3.71	5.13	5.76	4.86		4.82	5.56	4.98
CaO	9.56	7.73	8.30	9.25	8.07	8.32	7.26	8.34	8.37	8.86	6.26	5.57	6.43	6.56	8.85	10.29	8.73		8.95	9.39	8.77
Na2O	2.48	2.78	2.49	2.20	2.76	2.48	2.66	2.84	2.89	2.69	3.04	3.16	2.63	2.31	2.65	2.36	2.52		3.23	2.24	2.47
K2O	1.24	2.24	1.76	1.03	1.26	1.22	2.31	0.96	1.02	1.14	2.42	2.99	2.29	3.09	1.02	0.43	1.18		0.70	1.06	0.93
P2O5	0.12	0.52	0.47	0.56	0.24	0.24	0.56	0.26	0.24	0.23	0.28	0.28	0.28	0.29	0.18	0.19	0.18		0.20	0.18	0.19
L.O.I.	0.33	0.56	0.93	2.31	1.53	1.16	0.48	1.48	1.16	0.94	0.56	0.61	1.09	3.58	1.29	1.7	1.01		1.24	3.39	1.54
Total	100.3	100.3	100.2	100.8	100.1	100.9	99.8	100.5	100.7	100.6	100.8	100.4	100.2	100.9	100.6	99.6	100.7		100.9	100.83	100.5
Mg#	51.8	44.1	44.4	43.4	40.1	42.4	40.2	40.6	41.8	44.5	39.2	36.7	37.2	39.8	47.4	49.8	46.5		46.1	48.9	47.7
XRF-O.U.																					
Ni	66	57	50	42	40	26	53	39	43	55	30	26	29	28	44	50	48	56	29	34	48
Cu	74	147	136	154	144	160	163	150	162	155	87	107	110	111	173	171	139	141	168	169	140
Zn	89	117	117	117	120	107	128	106	104	121	110	116	114	115	103	87	97	93	101	106	104
Ga	21	25	25	27	22	23	27	20	22	19	19	18	22	21	20	17	21	21	24	21	20
Rb	42	60	35	39	40	32	49	41	54	41	88	112	73	119	28	11	35	15	18	37	40
Sr	228	668	801	735	290	285	754	296	266	268	177	162	194	434	280	219	234	239	226	148	220
Y	26	36	36	44	36	34	40	37	38	35	42	43	45	45	35	30	32	34	34	36	36
Zr	125	320	312	313	195	177	368	210	202	186	228	237	245	251	159	134	149	124	157	160	157
Nb	7.9	27	28.3	27.5	15.9	15.3	33.9	20.4	17.2	15.5	16.5	18.3	17.9	18.5	12.7	10.4	10.9	10	12.3	12.9	12.8
XRF-Notts																					
Ni	52	47			20	22	40	25	28	38	22		16	21		39	31				
Cr	52	256			45	32	70	200	34	233	42		50	30		59	41				
Co	40	31			36	38	35	41	35	37	33		30	33		40	35				
V	216	336			359	330	344	303	308	317	285		298	302		282	293				
Zn	84	100			94	94	117	102	98	105	104		105	100		81	86				
Rb	39	53			32	30	45	40	48	36	84		65	102		8	31				
Sr	215	629			256	267	713	286	254	249	176		180	386		204	224				
Y	26	37			36	33	38	37	37	34	44		43	44		28	32				
Zr	122	290			165	164	333	197	192	169	217		225	218		126	139				
Nb	8	29			15	15	34	20	19	15	16		18	18		11	11				
Ba	316	573			388	259	816	486	431	388	494		500	544		336	357				
INAA	√	-																			
isotopes	√	√																			

sample n°	DGB61	DGB60	DGB59	DGB58	DGB03	DGB70	DGB34	DRR02	DRR03	DRR04	DRR05	DRR06	DRR07	DRR10	DRR12	DRR18	DRR22	DRR23	DRR25	DAB01	DAB03
road section	GB	GB	GB	GB	GB	GB	GB	RR	RR	RR	RR	RR	RR	RR	RR	RR	RR	RR	RR	AB	AB
altitude	1430	1445	1475	1495		1295		1535	1505	1490	1485	1465	1445	1390	1355	1245	1535	1535	1535	1200	1200
description	flow	flow	flow	flow	dyke	sill	dyke	flow	flow	flow	flow	flow	flow	flow	flow	flow	flow	flow	flow	dyke?	dyke?
magma type	Palmas	Palmas	Palmas	Palmas	Gramado	Esmeralda	Gramado	Gramado	Gramado	Gramado	Gramado	Urubici	Gramado	Gramado	Urubici	Urubici	Gramado	Gramado	Gramado	Urubici	Urubici
						* 12km E of Bom Jardim															
SiO2	69.21		67.44	67.52	52.01	50.66		54.69	54.62		52.83	53.09	51.76	53.48	51.13	51.84	55.53	54.28	54.53	51.40	
TiO2	0.88		0.99	0.98	1.78	1.38		1.44	1.48		1.62	4.04	1.70	1.64	4.20	3.61	1.45	1.49	1.47	3.67	
Al2O3	12.73		13.29	13.29	12.98	14.00		13.98	14.19		13.97	12.64	14.21	13.71	13.27	13.31	13.88	14.16	14.12	13.52	
Fe2O3(t)	5.66		6.39	6.37	15.44	13.89		12.86	12.86		13.60	13.00	14.33	13.90	13.92	13.02	12.56	13.02	12.77	13.02	
MnO	0.10		0.11	0.11	0.25	0.22		0.19	0.19		0.21	0.16	0.23	0.21	0.17	0.17	0.18	0.19	0.19	0.17	
MgO	1.22		1.37	1.33	4.73	6.13		4.14	4.25		4.80	4.03	4.77	4.45	4.42	4.88	4.14	4.31	4.19	4.63	
CaO	2.53		3.76	3.64	9.32	10.59		7.51	7.64		8.78	7.27	8.40	8.53	8.32	8.00	7.76	7.87	7.02	7.48	
Na2O	2.47		3.50	3.58	2.73	2.53		3.13	2.75		3.08	2.82	3.10	3.00	2.55	2.68	2.51	2.73	3.25	3.53	
K2O	4.95		2.88	2.92	0.52	0.48		1.87	1.81		0.88	2.36	1.26	0.84	1.44	2.02	1.80	1.76	2.26	2.05	
P2O5	0.26		0.27	0.26	0.23	0.14		0.20	0.21		0.23	0.60	0.24	0.23	0.58	0.49	0.20	0.20	0.20	0.51	
L.O.I.	0.72		2.28	2.21	0.7	0.05		0.22	0.25		0.86	0.49	0.74	1.14	0.72	0.13	0.28	1.24	0.32	1.36	
Total	100.8		100.7	100.4	100.2	101.8		101.6	101.1		101.9	101	101.3	100.9	100.3	100.3	100.8	100.9	101	100.7	
Mg#	33.4		33.3	32.8	41.7	50.7		42.9	43.5		45.1	41.9	43.7	42.7	42.5	46.6	43.4	43.5	43.3	45.3	
XRF-O.U.																					
Ni	10	8	8	8	35	56		26	43	38	35	47	33	39	50	72	36	24	25	54	23
Cu	53	54	77	72	221	201		141	150	176	165	165	176	174	196	187	137	155	140	152	214
Zn	72	78	78	81	123	98		110	105	126	104	133	126	116	130	120	107	108	101	130	144
Ga	19	17	19	18	18	18		21	19	23	23	25	26	21	27	23	22	19	21	26	28
Rb	188	236	162	171	16	18		68	66	16	38	42	28	43	20	37	52	56	83	49	52
Sr	113	163	160	164	357	173		220	213	290	283	691	280	276	960	658	250	219	186	857	690
Y	44	44	42	42	40	33		36	35	38	36	41	37	36	42	38	46	36	34	39	48
Zr	256	267	262	265	172	100		171	172	190	186	361	198	190	345	288	170	175	174	325	400
Nb	21.5	21.6	21	21.4	11.4	6.4		14.3	13.9	17.3	15.0	32.7	17.9	16.3	32.4	25.1	14.3	14.9	14.1	27.1	33.4
XRF-Notts																					
Ni			2		31	63	35					43									
Cr			3		62	205	147					42									
Co			n/a		42	n/a	n/a					n/a									
V			42		391	303	394					353									
Zn			n/a		110	n/a	n/a					n/a									
Rb			152		11	18	54					39									
Sr			152		332	158	174					633									
Y			42		37	28	41					36									
Zr			248		159	89	173					331									
Nb			20		12	5	11					32									
Ba			573		313	150	307					691									
INAA	-		-			-						-									
isotopes	√		√			√						√									

sample n°	DAB06	DAB15	DAB14	DAB16	DW11	DW12	DW13	DW14	DW15	DW16	DW17	DW18A	DW18B	DW19	DW20	DW21	DW24	DW23	DW25	DW22	SC-06
road section	AB	AB	AB	AB	RA	RA	RA	RA	RA	RA	RA	RA	RA	RA	RA	CO	CO	CO	CO	Aiure	
altitude	1160	1210	1230	1155												1275	1295	1210	~1180	~200	
description	flow	flow	flow	dyke	flow	flow	flow	flow	flow	flow	flow	flow	flow	flow	flow	flow	flow	dyke	dyke	dyke	flow
magma type	Urubici	Urubici	Gramado	Esmeralda	Palmas	Palmas	Palmas	Palmas	Palmas	Palmas	Esmeralda	Palmas	Palmas	Palmas	Palmas	Urubici	Urubici	Esmeralda	Esmeralda	Urubici	Chapecó
SiO2	51.67	51.65	53.76		67.44	67.36		67.80	67.83	67.53	53.06	67.66	67.68	67.21	68.18	52.00	51.79	47.66	50.59	50.86	66.96
TiO2	3.63	3.61	1.71		0.95	1.07		1.07	1.09	1.06	1.91	1.06	1.09	1.12	1.05	3.62	3.74	1.69	1.84	3.55	0.99
Al2O3	13.73	13.72	12.87		13.30	13.00		12.97	13.07	13.10	12.53	13.17	13.05	13.36	12.64	13.11	13.54	15.20	16.25	13.15	12.66
Fe2O3(t)	13.20	13.21	15.61		6.10	6.47		6.45	6.49	6.63	15.97	6.90	6.90	6.74	6.47	12.86	13.45	12.78	14.37	14.45	7.89
MnO	0.17	0.17	0.22		0.10	0.13		0.12	0.09	0.08	0.24	0.07	0.07	0.13	0.09	0.16	0.19	0.58	0.25	0.19	0.10
MgO	4.39	4.38	3.60		1.41	1.45		1.32	0.95	1.13	4.01	0.75	0.72	1.44	1.19	4.83	4.48	5.80	4.35	4.44	1.61
CaO	7.87	7.83	7.98		3.40	2.99		2.99	2.96	2.69	8.19	2.71	2.69	2.48	2.88	8.15	8.02	12.29	9.10	8.00	3.17
Na2O	2.82	2.96	3.06		3.41	3.44		3.28	3.52	3.72	2.79	3.78	3.89	3.53	3.61	3.10	2.61	3.67	2.67	3.01	3.10
K2O	1.98	1.93	0.97		3.60	3.76		3.69	3.67	3.75	1.10	3.57	3.60	3.67	3.57	1.69	1.68	0.16	0.40	1.78	3.20
P2O5	0.54	0.55	0.23		0.30	0.34		0.32	0.32	0.32	0.25	0.32	0.30	0.32	0.32	0.48	0.49	0.21	0.17	0.56	0.31
L.O.I.	0.15	-0.01	0.7		2.09	0.92		0.99	0.77	0.98	0.66	0.85	0.88	1.29	0.94	0.49	0.63	3.41	5.84	0.39	1.43
Total	100.8	100.8	101.1		100.74	100.64		100.31	100.46	100.75	97.76	99.60	99.90	99.65	96.99	98.09	100.4	99.47	100	98.36	
Mg#	43.7	43.6	34.9		35.0	34.3		32.3	25.4	28.4	36.9	20.2	19.6	33.2	30.0	46.7	43.7	51.4	41.4	41.7	32.3
XRF-O.U.																					
Ni	40	42	23	61	n/d	n/d	8	n/d	n/d	10	36	n/d	9	n/d	12	66	66	75	64	48	n/d
Cu	145	154	223	181	57	103	108	88	103	106	217	83	79	104	80	135	140	242	270	138	156
Zn	124	117	124	94	75	83	81	78	77	77	123	94	91	72	73	100	122	122	136	125	154
Ga	24	27	20	22	17	17	17	15	18	17	24	17	16	17	15	23	25	25	25	25	27
Rb	43	39	54	17	164	159	173	165	165	168	49	159	155	158	147	38	25	3	13	56	88
Sr	708	735	326	190	154	128	116	126	138	134	204	142	141	105	130	611	858	227	253	601	540
Y	42	44	45	30	43	69	48	55	69	59	44	50	53	69	52	36	39	37	42	39	69
Zr	321	313	182	102	264	274	282	267	277	281	183	288	283	282	268	288	312	120	133	291	550
Nb	28.5	27.5	11.7	7.3	21.3	20.8	20.9	21	21.5	21.2	11.9	22.4	22.2	21.6	20.1	23.5	28.3	7.0	7.4	26.9	44.9
XRF-Notts																					
Ni					5	4	3	2	3	2	28	2	5	4	3	59	55	61		42	4
Cr					0	180	114	209	204	20	131	120	218	4	253	157	125	130		78	165
Co					10	13	10	10	11	11	39	13	11	9	10	33	42	48		34	n/a
V					77	82	79	78	74	76	418	88	84	78	82	344	358	394		387	57
Zn					66	74	69	73	69	64	116	87	86	69	65	91	115	100		112	n/a
Rb					157	157	165	162	160	159	48	144	143	151	143	34	23	2		54	87
Sr					146	130	116	130	138	129	198	138	136	106	126	592	806	204		574	540
Y					42	69	49	55	67	58	43	49	53	64	52	34	37	35		37	72
Zr					241	267	266	261	264	263	170	266	270	264	255	270	284	108		266	558
Nb					22	23	26	24	23	24	10	24	22	23	23	24	28	6		28	48
Ba					646	779	687	679	696	667	343	655	653	703	635	502	615	152		630	1064
INAA				-							√							-			√
isotopes				√							√							√			√

sample n°	RS-67	PR-01	DRG-1	DRG-6	PAR-1	PAR-2	PAR-3	PAR-4	PAR-5	PAR-6	PAR-7	PAR-8	PAR-9	PAR-10	PAR-11	PAR-12	PAR-13	PAR-14	PAR-15	PAR-16	PAR-17
road section			S of Rancho	Aiure	see p316	see p316	see p316	see p316	see p316	see p316	see p316	see p316	see p316	see p316	see p316	see p316	see p316	see p316	see p316	see p316	see p316
altitude			Queimado	~200																	
description	flow	flow	dyke	dyke	flow	flow	flow	flow	flow	flow	flow	flow	flow	flow	flow	flow	flow	flow	flow	flow	flow
magma type	Chapecó	Chapecó	?	Urubici?	Parana'ma	Parana'ma	Parana'ma	Parana'ma	Parana'ma	Parana'ma	Parana'ma	Pitanga	Parana'ma								
SiO2	65.22	65.48	48.19	50.55	50.08		50.51	50.15	50.26		50.37	51.26	49.81								
TiO2	1.23	1.18	2.50	3.66	2.83		2.81	2.29	2.34		2.16	3.30	2.36								
Al2O3	12.74	12.87	16.12	13.19	13.46		13.11	13.61	13.57		13.90	12.88	13.64								
Fe2O3(t)	7.91	7.61	12.72	14.84	14.64		15.58	14.97	14.79		14.15	15.21	14.95								
MnO	0.12	0.15	0.20	0.19	0.20		0.23	0.21	0.20		0.20	0.24	0.21								
MgO	1.78	1.86	6.37	4.50	5.32		4.51	5.48	5.43		5.69	4.14	5.47								
CaO	3.84	3.45	8.58	7.67	9.43		8.81	9.55	9.65		9.88	8.17	9.75								
Na2O	3.30	3.26	2.72	2.90	2.45		2.53	2.48	2.49		2.45	2.74	2.53								
K2O	3.49	3.80	2.20	1.97	1.17		1.34	1.02	1.01		0.95	1.58	1.03								
P2O5	0.37	0.33	0.41	0.53	0.40		0.57	0.26	0.27		0.26	0.47	0.26								
L.O.I.	1.67	1.39	1.73	0.38	0.27		0.24	-0.01	0.02		0.29	0.25	-0.03								
Total			100.1	99.9	99.1		101.3	101.4	101.4		101.2	101.4	101.2								
Mg#	34.4	36.3	53.8	41.4	45.9		40.3	46.0	46.1		48.4	38.8	46.0								
XRF-O.U.																					
Ni	n/d		36	39	53	40	42	67	67	64	61	54	40								
Cu	80		22	139	161	130	232	245	253	187	223	180	196								
Zn	128		115	123	108	117	122	105	106	102	102	116	115								
Ga	25		25	25	21	25	24	17	23	22	21	24	20								
Rb	100		264	55	28	28	35	25	24	26	24	41	25								
Sr	488		451	577	410	516	413	380	384	404	427	913	489								
Y	71		38	40	36	38	43	31	32	30	30	39	32								
Zr	571		228	296	199	243	223	164	167	163	157	353	171								
Nb	47.3		15.2	27.7	18.9	20.5	19.4	15.0	15.6	14.2	13.3	32.5	14.9								
XRF-Notts																					
Ni	2				22	13	17	64	34	32	64	32	57	28	28	26	60	36	46	58	56
Cr	155				311	153	405	158	195	237	235	47	205	108	264	282	123	47	89	373	261
Co	n/a				n/a	n/a	n/a	n/a	n/a	n/a	n/a	n/a	n/a	n/a	n/a	n/a	n/a	n/a	n/a	n/a	n/a
V	52				395	345	379	317	372	352	337	340	396	412	438	406	341	462	302	364	373
Zn	n/a				n/a	n/a	n/a	n/a	n/a	n/a	n/a	n/a	n/a	n/a	n/a	n/a	n/a	n/a	n/a	n/a	n/a
Rb	94				63	78	66	24	37	32	20	33	24	29	30	31	26	27	31	20	24
Sr	471				213	202	205	401	419	422	406	418	457	424	410	423	378	488	387	353	357
Y	73				39	43	39	27	39	40	30	38	29	37	40	38	33	37	46	30	30
Zr	562				170	201	185	145	256	243	130	254	153	228	234	224	180	216	198	153	153
Nb	48				13	15	14	13	26	22	11	25	13	17	19	20	17	19	17	15	14
Ba	1165				356	412	391	339	505	491	300	502	327	415	462	439	349	625	436	314	318
INAA	√	-			-	-	-	-	-	-	-	-	-								
isotopes	√	√			√	√	√	√	√	√	√	√	√								

sample n°	PAR-18	PAR-19	PAR-20	PAR-21	PAR-22	PAR-23	PAR-24	PAR-26	PAR-27
road section	see p316	see p316	see p316	see p316	see p316	see p316	see p316	see p316	see p316
altitude									
description	flow	flow	flow	flow	flow	flow	flow	flow	flow
magma type									
SiO2									
TiO2									
Al2O3									
Fe2O3(t)									
MnO									
MgO									
CaO									
Na2O									
K2O									
P2O5									
L.O.I.									
Total									
Mg#									
XRF-O.U.									
Ni									
Cu									
Zn									
Ga									
Rb									
Sr									
Y									
Zr									
Nb									
XRF-Notts									
Ni	64	39	26	75	61	63	60	60	68
Cr	122	59	180	174	182	108	141	267	194
Co	n/a	n/a	n/a	n/a	n/a	n/a	n/a	n/a	n/a
V	328	350	348	352	369	330	391	332	291
Zn	n/a	n/a	n/a	n/a	n/a	n/a	n/a	n/a	n/a
Rb	25	34	34	22	23	26	40	25	26
Sr	372	451	410	361	370	370	349	360	366
Y	27	36	41	32	30	28	32	34	32
Zr	144	232	258	151	157	148	148	157	161
Nb	13	21	22	13	14	11	12	14	14
Ba	310	482	520	265	311	359	302	303	325
INAA									
isotopes									

sample n°	CB234	CB249	CB276	CB381	CB441A	CB441B	CB555	CB621	CB648	CB657
borehole	CB	CB	CB	CB	CB	CB	CB	CB	CB	CB
depth	234	249	276	381	441	441	555	621	648	657
elevation	162	147	120	15	-45	-45	-159	-225	-252	-261
magma type	Parana'ma	Parana'ma	Parana'ma	Parana'ma	Parana'ma	Parana'ma	Parana'ma	Parana'ma	Parana'ma	Parana'ma
SiO2	51.09	48.72	50.79	49.39	51.39	50.62	50.97	50.47	49.88	51.09
TiO2	2.65	2.71	3.17	2.42	2.18	2.34	2.16	2.37	2.27	2.17
Al2O3	12.90	13.44	11.80	13.38	12.61	12.78	12.83	12.10	12.88	12.88
Fe2O3	14.75	16.25	17.03	16.09	15.42	16.79	15.19	15.80	15.00	15.06
MnO	0.22	0.22	0.26	0.22	0.23	0.24	0.22	0.21	0.21	0.22
MgO	5.05	4.02	4.06	5.20	4.75	5.06	5.21	5.22	5.24	5.27
CaO	9.53	8.91	8.02	9.48	9.09	8.16	9.21	7.17	9.03	9.41
Na2O	2.66	3.47	2.77	2.63	3.07	4.39	2.93	5.56	4.14	2.66
K2O	0.80	1.89	1.72	0.90	1.01	0.39	0.99	0.77	1.03	0.95
P2O5	0.37	0.36	0.38	0.28	0.26	0.28	0.29	0.33	0.35	0.30
LOI	0.17	0.86	0.37	0.96	0.21	1.26	0.21	2.28	1.11	0.13
Total	98.76	99.14	99.66	99.37	99.48	98.97	100.78	99.75	100.21	99.88
*Mg**	44.4	36.6	35.7	43.0	41.8	41.3	44.4	43.5	44.9	44.9
XRF-O.U.										
Ni	28	49	36	51	26	50	48	55	41	52
Cu	212	220	206	179	128	269	182	196	188	247
Zn	124	148	125	116	112	137	133	141	121	119
Ga	21	22	15	17	18	22	20	20	21	22
Rb	17	36	35	14	24	7	26	17	21	23
Sr	364	265	204	250	249	274	313	225	306	274
Y	45	55	47	39	36	42	38	47	36	36
Zr	218	247	228	172	163	187	178	201	176	165
Nb	16.6	19	18	15	14	17	16	17	14.7	13.5
XRF-Notts										
Ni	37	49	35	49	34	40	42	52	43	47
Cr	200	165	180	124	80	188	82	255	114	119
Co	42	n/a	n/a	n/a	n/a	n/a	n/a	n/a	36	n/a
V	403	479	459	432	394	443	374	399	430	385
Zn	108	127	128	116	115	119	118	124	122	109
Rb	14	31	37	15	25	7	22	14	19	22
Sr	289	231	208	259	245	239	274	181	266	266
Y	44	45	48	36	37	37	33	38	36	33
Zr	199	221	236	177	164	170	165	172	169	164
Nb	16	18	19	16	13	14	14	14	17	13
Ba	245	290	369	207	279	248	288	203	324	307
INAA	√		√						√	
isotopes	√		√						√	

sample n°	CB747	CB807	CB846	CB954	CB975	CB1002	CB1047	CB1110	CB1140A	CB1140B	CB1170	CB1218A	CB1218B	CB1335	CB1350	CB1362	CB1392	CB1446	CB1461	CB1488	CB1518
borehole	CB	CB	CB	CB	CB	CB	CB	CB	CB	CB	CB	CB	CB	CB	CB	CB	CB	CB	CB	CB	CB
depth	747	807	846	954	975	1002	1047	1110	1140	1140	1170	1218	1218	1335	1350	1362	1392	1446	1461	1488	1518
elevation	-351	-411	-450	-558	-579	-606	-651	-714	-744	-744	-774	-822	-822	-939	-954	-966	-996	-1050	-1065	-1092	-1122
magma type	Parana'ma	Parana'ma	Pitanga	Parana'ma	Parana'ma	Parana'ma	Pitanga	Pitanga	Pitanga	Pitanga	Pitanga	Pitanga	Pitanga	Pitanga	Pitanga	Pitanga	Pitanga	Pitanga	Pitanga	Pitanga	Pitanga
SiO2	49.87	49.42	49.75	50.24	49.40	50.70	50.64	51.27	50.93	50.77	48.98	50.65	50.88	51.01	50.73	49.79	50.43	50.99	51.30	51.25	49.88
TiO2	1.94	2.06	3.15	2.30	2.85	2.75	3.29	3.35	3.32	3.42	3.40	3.53	3.42	3.66	3.70	3.66	3.75	3.64	3.56	3.87	3.54
Al2O3	13.14	13.54	13.09	13.22	13.17	12.81	12.97	12.70	12.78	12.84	12.47	12.96	12.47	12.78	12.55	12.84	12.67	12.42	12.56	12.20	12.90
Fe2O3	14.28	14.31	15.31	14.72	16.07	15.43	15.11	14.96	15.11	15.66	15.09	14.94	15.06	14.80	15.13	15.22	15.24	15.44	14.91	15.06	15.06
MnO	0.19	0.21	0.23	0.21	0.24	0.22	0.20	0.23	0.22	0.23	0.22	0.22	0.22	0.21	0.22	0.21	0.22	0.23	0.22	0.22	0.21
MgO	6.45	5.77	4.92	5.54	4.47	4.39	4.15	4.34	4.54	4.20	4.60	4.58	4.11	4.36	4.38	4.75	4.55	3.90	4.17	3.93	4.76
CaO	7.75	11.14	9.34	9.78	8.38	8.60	8.01	8.56	8.30	8.35	8.22	8.94	8.15	8.37	8.28	9.13	8.68	8.13	8.14	7.98	8.93
Na2O	5.75	2.78	2.50	2.61	3.77	3.00	3.71	3.02	2.85	3.07	5.05	2.77	3.57	2.68	2.90	3.18	2.66	3.13	2.96	3.01	2.96
K2O	0.40	0.60	1.25	1.03	0.99	1.44	1.54	1.05	1.50	1.01	1.50	1.03	1.39	1.57	1.57	0.74	1.39	1.38	1.49	1.79	1.30
P2O5	0.24	0.23	0.48	0.35	0.66	0.65	0.39	0.54	0.46	0.46	0.45	0.47	0.44	0.57	0.55	0.47	0.42	0.73	0.71	0.69	0.46
LOI	2.76	1.34	0.54	0.40	0.88	0.49	0.47	1.04	0.23	0.88	1.18	0.92	0.57	0.14	0.12	0.73	0.46	0.96	0.93	0.79	0.87
Total	100.57	98.20	98.13	99.89	98.94	99.67	100.07	98.31	100.39	100.2	100.92	98.48	99.80	98.79	98.91	99.40	98.69	98.70	98.31	98.73	100.3
*Mg**	51.3	48.4	42.8	46.7	39.3	39.9	39.0	40.3	41.2	38.5	41.5	41.7	38.9	40.7	40.3	42.1	41.0	37.1	39.5	37.8	42.4
XRF-O.U.																					
Ni	79	73	27	61	41	32	36	18	30	34	50	20	18	21	34	22	32	26	16	27	56
Cu	152	148	282	215	302	191	131	140	126	125	134	135	79	206	207	199	167	223	226	153	210
Zn	106	123	90	103	140	125	124	137	125	136	132	131	118	106	141	137	126	125	134	134	129
Ga	16	25	24	19	21	22	21	26	22	22	21	27	21	25	27	23	23	24	23	29	23
Rb	8	18	29	22	21	42	32	31	31	27	30	28	26	37	38	29	29	25	33	39	28
Sr	175	432	392	326	348	403	407	469	408	455	403	497	452	503	508	521	438	494	504	517	518
Y	28	32	37	32	48	48	39	39	40	40	40	37	36	38	43	36	35	45	43	47	40
Zr	136	156	209	155	241	247	238	262	237	253	251	259	246	272	296	250	229	309	317	320	265
Nb	12.4	14.3	18.7	14.0	22.6	22.2	22.8	23.1	21.1	24.4	22.7	22.4	23.3	22.7	27.2	22.8	20.9	26.9	27.2	28.8	22.7
XRF-Notts																					
Ni	77	64	37	60	34	33	37	21	29	24	37	25	19	30	28	28	33	23	22	23	44
Cr	340	121	76	135	225	66	482	46	51	233	88	85	86	58	56	86	106	100	46	68	184
Co	n/a	n/a	38	n/a	n/a	n/a	n/a	34	n/a	n/a	n/a	39	n/a	38	n/a	41	n/a	n/a	n/a	n/a	n/a
V	358	382	367	364	350	281	438	405	398	414	428	429	378	377	419	462	492	386	392	325	410
Zn	98	100	92	103	141	108	115	126	126	127	125	127	116	99	118	129	122	126	122	125	111
Rb	8	17	27	25	21	36	31	29	29	26	29	24	27	34	32	27	31	27	30	37	25
Sr	170	374	389	343	336	365	375	449	403	426	373	459	455	486	440	485	433	479	479	484	453
Y	25	24	38	32	43	43	33	40	40	37	35	36	36	39	36	34	35	43	41	43	35
Zr	138	140	198	166	237	232	229	242	243	245	234	232	255	250	263	220	228	308	305	305	242
Nb	12	11	19	16	21	20	22	23	22	23	21	24	24	26	26	22	22	28	29	28	23
Ba	136	226	454	333	330	481	441	465	453	441	429	440	488	540	508	381	432	577	553	570	434
INAA	√		√			√		√				-				√					
isotopes	-		√			-		√				√				√					

sample n°	CB1542A	CB1608	CB1668	CB1695	CB1734	CB1776	CB1842	CB1863A	CB1902	AV702	AV816	AV1104	AV1251	AV1470	AN306	AN378	AN516	AN585	AN657	AN783	AN900
borehole	CB	CB	CB	CB	CB	CB	CB	CB	CB	AV	AV	AV	AV	AV	AN	AN	AN	AN	AN	AN	AN
depth	1542	1608	1668	1695	1734	1776	1842	1863	1902	702	816	1104	1251	1470	306	378	516	585	657	783	900
elevation	-1146	-1212	-1272	-1299	-1338	-1380	-1446	-1467	-1506	-185	-299	-587	-734	-953	104	32	-106	-175	-247	-373	-490
magma type	Pitanga	Pitanga	Pitanga	Pitanga	Pitanga	Votu'va?	Votu'va?	Votu'va?	Votu'va?	Parana'ma	Pitanga	Pitanga	Pitanga	Pitanga	Parana'ma	Parana'ma	Parana'ma	Parana'ma	Parana'ma	Parana'ma	Parana'ma
SiO2	50.46	51.04	49.83	52.42	50.10	49.75	52.13	54.55	49.27	49.25	51.17	51.19	50.79	50.77	50.40	49.96	51.35	50.41	50.43	50.42	50.48
TiO2	3.77	3.79	3.32	2.89	3.08	3.88	3.59	3.08	3.91	2.19	3.36	3.45	3.74	3.87	2.72	2.55	2.45	2.47	2.39	1.82	2.38
Al2O3	12.59	13.01	13.09	13.10	12.91	14.39	13.16	13.47	12.81	13.84	12.45	13.11	12.67	12.99	12.75	12.74	12.68	13.00	13.06	13.82	13.29
Fe2O3	15.11	14.29	14.83	13.68	14.60	13.97	14.03	12.85	14.79	14.53	16.03	15.16	15.69	15.06	16.08	15.72	15.58	15.51	15.23	13.45	14.01
MnO	0.21	0.22	0.22	0.20	0.21	0.17	0.19	0.18	0.19	0.21	0.23	0.22	0.22	0.23	0.23	0.23	0.24	0.21	0.23	0.20	0.20
MgO	4.44	4.23	5.26	4.32	5.42	4.17	3.70	2.83	5.75	6.14	3.93	4.01	3.86	3.84	4.44	4.53	4.59	4.45	4.82	6.06	5.42
CaO	8.75	8.21	8.68	8.18	9.25	7.83	7.08	6.37	8.46	10.66	8.02	8.43	8.08	7.42	8.82	8.36	9.07	8.47	9.21	10.60	7.35
Na2O	3.20	2.85	3.12	3.14	3.03	3.11	3.48	3.52	2.83	2.39	2.82	2.98	3.03	3.21	2.83	4.77	3.17	3.69	3.22	2.63	5.48
K2O	0.94	1.67	1.25	1.61	1.10	2.16	2.10	2.52	1.51	0.59	1.29	0.98	1.18	2.09	1.34	0.85	0.68	1.46	1.06	0.80	1.12
P2O5	0.53	0.68	0.39	0.45	0.34	0.55	0.53	0.63	0.49	0.21	0.69	0.46	0.72	0.52	0.39	0.33	0.32	0.31	0.31	0.20	0.31
LOI	1.27	1.03	1.62	0.71	0.08	1.43	0.95	0.85	0.58	0.33	0.76	1.22	1.08	0.65	0.45	1.92	0.78	0.34	0.81	0.56	2.26
Total	100.01	98.07	100.7	99.92	99.58	98.09	98.91	98.93	97.35	100.1	100.3	100.8	100	100.5	97.71	98.93	98.03	98.46	97.43	96.52	102.90
*Mg**	40.6	40.8	45.3	42.4	46.4	41.0	38.1	33.9	47.5	49.6	36.4	38.2	36.4	37.3	39.2	40.2	40.7	40.1	42.4	51.2	47.4
XRF-O.U.																					
Ni	33	14	70	42	54	31	40	17	80	63	24	24	28	<16	25	29	25	19	37	63	49
Cu	159	110	193	162	196	71	139	156	170	206	194	100	246	33	186	177	306	205	126	102	309
Zn	131	136	126	123	114	134	111	106	103	109	162	123	121	160	139	120	138	140	132	102	108
Ga	23	28	26	29	26	29	29	27	22	22	25	26	24	27	24	17	20	22	21	19	18
Rb	24	34	26	45	26	48	62	71	44	8	39	24	28	43	32	17	27	34	27	20	23
Sr	513	495	436	474	478	635	493	447	555	377	397	527	544	492	278	258	375	288	299	353	223
Y	39	42	38	43	33	34	43	48	31	28	56	40	45	43	45	42	40	38	36	23	29
Zr	265	328	242	286	201	297	305	361	223	137	289	273	316	303	226	202	212	204	181	133	163
Nb	24.2	28.2	21.1	22.8	15.9	23.9	26.8	30.7	21.0	12.3	28.4	24.3	27.5	25.6	16.1	17.1	18	16	14.8	11.6	14.3
XRF-Notts																					
Ni	27	20	55	40	60	41	32	20	74	61	23	15	26	7	38	37	27	29	35	59	49
Cr	143	29	122	176	286	84	290	350	264	260	39	23	29	28	110	105	57	54	132	126	194
Co	n/a	35	n/a	n/a	n/a	n/a	n/a	n/a	48	40	39	34	38	35	44	36	41	37	38	51	37
V	432	403	405	317	368	381	353	267	375	389	310	366	386	396	423	460	434	374	383	340	433
Zn	122	120	116	100	111	127	95	96	88	93	131	109	111	133	130	115	128	130	125	93	102
Rb	25	33	23	36	23	44	56	66	41	8	33	23	28	38	28	15	25	34	24	14	19
Sr	492	460	382	411	461	599	457	448	523	353	343	488	521	444	266	246	353	274	288	346	220
Y	35	43	33	37	32	35	40	45	29	27	52	42	46	42	43	40	41	37	37	25	30
Zr	262	293	219	254	204	283	291	349	205	135	255	245	303	273	208	186	195	188	169	127	160
Nb	23	30	18	20	16	23	27	30	21	11	25	23	28	23	17	18	19	17	16	11	16
Ba	445	568	445	453	397	802	647	742	534	255	431	480	554	425	368	269	340	414	355	299	303
INAA						√			√						-		-	√	√	√	-
isotopes						√			√						√		√	√	√	√	√

sample n°	AN1047	AN1128	AN1254	RO57	RO78	RO192	RO255	RO381	RO414	RO465	RO561	RO657	RO714A	RO714B	RO735	RO759	RO804A	RO840	RO930	RO1023	RO1185
borehole	AN	AN	AN	RO	RO	RO	RO	RO	RO	RO	RO	RO	RO	RO	RO	RO	RO	RO	RO	RO	RO
depth	1047	1128	1254	57	78	192	255	381	414	465	561	657	714	714	735	759	804	840	930	1023	1185
elevation	-637	-718	-844	691	670	556	493	367	334	283	187	91	34	34	13	-11	-56	-92	-182	-275	-437
magma type	Pitanga	Pitanga	Pitanga	Parana'ma	Parana'ma	Parana'ma	Parana'ma	Parana'ma	Pitanga	Pitanga	Pitanga	Pitanga	Pitanga	Pitanga	Pitanga	Pitanga	Pitanga	Pitanga	Pitanga	Gramado	Urubici?
SiO2	49.94	50.35	50.23	50.27	50.10	50.20	49.86	49.51	49.80	50.87	50.86					52.43		51.74	50.31		
TiO2	3.56	3.90	3.24	2.01	1.76	2.18	1.91	2.34	3.86	3.60	3.53					3.28		3.65	3.01		
Al2O3	12.66	12.75	12.92	13.56	13.94	13.45	13.95	13.52	12.79	12.45	12.90					12.33		12.81	13.13		
Fe2O3	15.27	15.11	14.59	13.99	13.47	13.87	14.40	14.29	15.82	15.03	14.84					15.05		14.77	14.17		
MnO	0.22	0.21	0.20	0.22	0.20	0.22	0.19	0.22	0.22	0.21	0.23					0.22		0.19	0.19		
MgO	4.85	4.45	5.06	6.28	6.82	5.38	6.31	5.27	4.34	4.28	4.06					3.17		4.21	5.46		
CaO	9.07	8.64	9.02	10.35	10.58	10.42	10.45	9.66	8.37	8.32	8.69					7.44		7.88	9.45		
Na2O	2.91	2.79	2.78	2.34	2.23	2.70	2.41	3.34	2.70	2.91	3.34					3.14		3.12	2.79		
K2O	1.08	1.36	1.44	0.65	0.70	0.93	0.32	1.50	1.54	1.58	0.86					2.04		1.70	1.10		
P2O5	0.45	0.46	0.52	0.32	0.20	0.27	0.28	0.36	0.57	0.74	0.70					0.92		0.55	0.39		
LOI	0.81	0.60	0.23	0.72	0.21	1.05	1.59	0.75	0.36	0.29	1.55					1.11		0.31	0.79		
Total	97.09	98.43	97.40	99.74	100.4	99.55	99.05	99.29	100.9	98.35	98.25					98.71		98.82	99.78		
*Mg**	42.5	40.7	44.7	51.1	54.1	47.5	50.5	46.2	39.0	39.9	38.9					32.9		39.9	47.3		
XRF-O.U.																					
Ni	36	16	50	74	98	62	69	60	27							n/d		23	65		
Cu	129	115	140	99	183	206	189	191	199	187	80					242		57	183		
Zn	111	127	116	111	96	105	131	126	128	126	137					130		131	103		
Ga	26	26	23	19	20	20	22	21	19	21	22					24		25	22		
Rb	26	31	33	11	16	26	9	38	38	39	19					42		38	28		
Sr	494	525	494	292	273	286	381	300	418	428	509					531		478	494		
Y	35	37	33	32	28	29	33	34	42	42	43					52		41	30		
Zr	241	256	250	153	129	167	157	178	252	261	281					380		294	207		
Nb	21.5	23	20.8	12.3	12.0	14.1	12.3	15.7	23.8	25.0	24.7					30.5		22.0	16.0		
XRF-Notts																					
Ni	39	21	41	66	91	52	65	58		21	11	44	46	49	46	14	26	24	55	47	23
Cr	101	49	300	205	417	253	162	136		33	27	437	252	308	148	24	204	64	186	72	184
Co	42	37	37	39	45	39	n/a	43		31	32	n/a	n/a	n/a	n/a	31	n/a	32	34	n/a	n/a
V	394	403	396	320	330	376	325	357		349	347	436	446	438	419	259	402	356	326	368	332
Zn	97	117	104	98	87	96	119	112		114	119	n/a	n/a	n/a	n/a	119	n/a	127	90	n/a	n/a
Rb	23	26	30	10	15	21	8	34		35	17	29	19	22	26	39	36	35	26	30	48
Sr	458	499	473	267	258	355	267	329		414	471	464	495	478	488	493	409	451	464	229	751
Y	35	39	32	32	27	28	30	31		41	40	32	35	36	35	49	42	39	31	35	38
Zr	213	229	226	145	127	150	142	163		240	245	251	234	238	233	336	289	265	189	147	280
Nb	22	23	23	14	9	15	10	15		25	26	21	19	21	21	31	23	23	16	10	27
Ba	446	467	440	285	202	346	185	364		534	554	431	338	336	415	685	459	485	370	304	682
INAA				√			-	√								√			-		
isotopes				√			√	√								√			√		

sample n°	CS66	CS258	CS348	CS384	CS417	CS447	CS480	CS531	CS657	CS783	CS843	CS900	CS2532	RS57A	RS57B	RS72A	RS120	RS147	RS189	RS234	RS252A
borehole	CS	CS	CS	CS	CS	CS	CS	CS	CS	CS	CS	CS	CS	RS	RS	RS	RS	RS	RS	RS	RS
depth	66	258	348	384	417	447	480	531	657	783	843	900	2532	57	57	72	120	147	189	234	252
elevation	847	655	565	529	496	466	433	382	256	130	70	13	-1619	790	790	775	727	700	658	613	595
magma type	Parana'ma	Pitanga	Pitanga	Pitanga	Pitanga	Pitanga	Pitanga	Pitanga	Gramado	Gramado	Gramado	Gramado	Pitanga	Pitanga	Pitanga	Pitanga	Pitanga	Chapecó	Chapecó	Gramado?	Gramado?
SiO2	50.22	49.91	51.07	51.16	49.76	50.04	49.96	51.61	50.41	52.18	53.22	54.58	46.84	52.13	48.78	51.52	47.30		66.46	51.46	50.15
TiO2	2.36	3.37	3.91	3.66	3.40	3.39	3.66	3.77	1.47	1.95	1.31	1.41	3.13	3.39	3.67	3.56	4.01		1.52	1.65	1.37
Al2O3	13.43	11.92	12.67	12.53	13.17	13.19	13.09	12.81	13.93	13.18	14.09	13.95	12.95	13.28	13.45	12.48	13.93		12.93	13.81	14.06
Fe2O3	14.39	15.77	14.64	15.83	14.93	14.54	15.44	14.19	14.41	15.00	12.75	12.14	16.78	15.10	17.44	15.64	16.42		7.34	14.33	13.30
MnO	0.18	0.22	0.23	0.22	0.20	0.20	0.21	0.20	0.22	0.22	0.18	0.20	0.20	0.30	0.20	0.21	0.21		0.13	0.20	0.21
MgO	5.61	5.77	4.32	3.66	5.16	4.95	4.64	4.25	5.83	4.65	5.35	4.96	6.16	3.18	4.22	3.52	5.20		1.24	5.60	7.33
CaO	10.00	9.18	8.31	7.76	9.52	9.16	8.79	8.03	10.38	8.78	9.03	8.75	10.64	5.98	6.18	7.49	8.86		2.15	9.10	10.09
Na2O	2.36	2.26	2.66	3.11	2.65	2.95	2.73	2.90	2.51	2.70	2.64	2.76	2.40	2.86	2.86	2.86	2.67		3.56	2.90	3.08
K2O	1.11	1.26	1.62	1.32	0.84	1.16	1.06	1.71	0.68	1.03	1.23	1.33	0.68	2.76	2.11	1.94	0.94		4.25	0.75	0.29
P2O5	0.36	0.45	0.57	0.76	0.38	0.45	0.43	0.54	0.16	0.30	0.19	0.21	0.24	1.03	1.08	0.79	0.46		0.40	0.20	0.12
LOI	0.96	0.93	0.25	1.31	1.06	0.68	0.94	0.47	0.29	0.56	0.43	0.40	0.15	1.2	1.8	0.84	1.53		1.19	1.56	3.58
Total	98.83	96.97	97.75	101.1	101.1	98.96	101.1	98.20	101.1	98.83	100.3	99.93	100.99	101	100.2	100.9	101.7		100.1	99.4	100.7
*Mg**	47.6	46.0	40.7	35.0	44.6	44.2	41.2	41.1	48.5	41.9	49.4	48.8	46.1	32.9	36.1	34.4	42.5		28.3	47.7	56.2
XRF-O.U.																					
Ni	57	51	19	22	64	38	46	13	47	36		39	82	<16	<17	<16	39		<8	47	78
Cu	224	143	198	306	211	134	146	40	146	193		123	494	281	290	242	164		7	176	158
Zn	118	131	124	124	112	114	117	121	92	116		93	92	218	170	136	117		106	114	102
Ga	20	23	23	29	25	22	23	24	21	25		20	21	27	29	31	30		26	21	20
Rb	27	31	37	35	14	17	18	40	21	36		49	20	44	47	47	10		102	25	8
Sr	354	434	495	547	503	543	550	484	182	237		224	447	541	583	538	640		271	189	128
Y	31	33	38	49	35	30	37	41	29	37		33	24	63	64	53	39		66	37	30
Zr	166	224	278	342	223	244	263	293	111	173		148	128	423	439	357	286		663	142	85
Nb	14.8	20.5	24.9	30.0	20.0	20.3	21.8	22.8	7.3	12.4		11.9	10.1	36.5	38.8	30.9	23.8		54.4	10.1	5.3
XRF-Notts																					
Ni	65	43	32	17	50	38	38	19	46	40	38	38	85	6	14	15		3	7	58	85
Cr	153	69	50	31	75	86	41	34	53	66	179	42	82	11	102	29		196	34	362	187
Co	40	38	38	33	41	42	40	30	45	43	n/a	n/a	50	28	39	33		n/a	6	40	42
V	400	460	440	303	410	399	388	389	318	421	276	295	645	263	287	302		64	57	344	317
Zn	111	118	118	110	92	103	96	108	84	109	79	91	83	181	129	116		n/a	92	100	83
Rb	26	28	36	31	12	15	19	34	18	34	42	48	17	38	41	43		109	101	26	6
Sr	355	416	489	514	473	530	513	469	176	234	211	215	424	493	518	490		202	268	179	116
Y	30	34	39	48	36	33	36	40	29	37	28	30	23	59	62	48		65	72	37	28
Zr	159	211	259	315	215	231	244	271	106	172	134	150	118	380	386	325		685	664	134	86
Nb	14	19	24	29	19	21	19	24	7	13	8	11	11	37	36	30		57	61	8	3
Ba	341	440	506	596	355	464	457	484	217	333	327	365	250	636	660	607		1117	987	147	108
INAA	-								-	-		-	√								
isotopes	√								√	√		√	-								

sample n°	RS264	RS306	RS336	RS378	RS396	RS438	RS474	RS489	RS531	RS561	RS606	RS660	RS696A	RS696B	RS720	GO102	GO114	GO120	GO141	GO180A	GO180B
borehole	RS	RS	RS	RS	RS	RS	RS	RS	RS	RS	RS	RS	RS	RS	RS	GO	GO	GO	GO	GO	GO
depth	264	306	336	378	396	438	474	489	531	561	606	660	696	696	720	102	114	120	141	180	180
elevation	583	541	511	469	451	409	373	358	316	286	241	187	151	151	127	814	802	796	775	736	736
magma type	Pitanga	Pitanga	Gramado	Gramado	Gramado	Gramado	Gramado	Gramado	Gramado	Gramado	Gramado	Gramado	Gramado	Gramado	Gramado	Parana'ma	Pitanga	Pitanga	Pitanga	Pitanga	Pitanga
SiO2		49.80						55.11	54.00			53.62	53.15	53.04	53.05	49.98	50.28	50.18	50.23	47.63	47.75
TiO2		3.65						1.70	1.87			1.41	1.54	1.53	1.52	2.36	3.62	3.68	3.79	3.72	3.65
Al2O3		12.31						13.29	13.91			14.35	14.04	14.06	13.99	13.38	12.66	12.71	12.73	13.04	13.13
Fe2O3		15.77						14.19	14.91			13.25	13.41	13.51	13.48	14.75	15.79	16.04	15.62	17.23	16.96
MnO		0.24						0.20	0.17			0.15	0.19	0.20	0.21	0.20	0.23	0.20	0.23	0.25	0.27
MgO		4.05						3.24	3.49			6.43	4.87	4.88	4.88	5.52	4.03	4.18	4.09	5.30	4.89
CaO		5.90						6.68	6.80			6.84	8.55	8.62	8.57	9.89	8.40	8.60	8.34	9.24	8.95
Na2O		4.27						3.05	2.87			2.87	2.78	2.71	2.74	2.56	2.74	3.01	2.81	2.47	2.76
K2O		2.30						2.28	1.69			0.90	1.27	1.25	1.33	1.05	1.67	0.84	1.56	0.62	1.12
P2O5		1.71						0.26	0.29			0.18	0.20	0.20	0.21	0.32	0.57	0.57	0.60	0.50	0.51
LOI		3.18						0.59	2.34			3.68	0.83	0.87	0.57	0.28	0.74	1.29	0.55	1.6	1.22
Total		100.2						101.1	101.2			101	100.4	101.2	101.1	100.3	100.60	101.4	100.9	100.2	100.1
*Mg**		37.4						34.8	35.3			53.1	45.8	45.7	45.8	46.6	37.3	37.8	37.9	41.8	40.2
XRF-O.U.																					
Ni		<16		48				<15	<16			38	32	23	<15	69	21	30	37	21	32
Cu		47		143				250	256			165	133	178	153	193	196	217	190	196	178
Zn		170		98				96	138			104	90	115	104	111	126	121	115	149	139
Ga		23		16				22	23			19	19	24	21	21	25	21	23	27	28
Rb		83		13				95	76			27	35	40	46	28	42	33	40	9	16
Sr		225		201				167	187			194	232	259	251	376	427	437	452	479	482
Y		68		30				45	50			32	33	35	36	34	43	41	44	42	45
Zr		390		127				218	235			147	153	169	170	168	254	253	264	288	291
Nb		37.1		9.0				16.8	17.8			12.1	13.6	15.3	13.8	15.1	25.2	24.2	25.0	27.4	28.8
XRF-Notts																					
Ni	2	4	36		68	64	33			32	39										
Cr	12	9	107		282	272	153			149	120										
Co	n/a	33	n/a		n/a	n/a	n/a			n/a	n/a										
V	153	157	347		276	307	336			515	291										
Zn	n/a	148	n/a		n/a	n/a	n/a			n/a	n/a										
Rb	52	72	42		19	28	58			45	41										
Sr	497	199	179		186	189	167			159	207										
Y	59	64	35		29	28	38			44	29										
Zr	322	340	149		105	117	161			200	121										
Nb	32	36	9		7	6	12			11	10										
Ba	568	405	268		220	245	328			315	300										
INAA																					
isotopes																					

sample n°	GO183A	GO198	GO441A	GO441B	GO456A	GO513	GO516	GO519	GO522	GO525	GO528	GO564	GO585	GO603	GO741A	GO876	GO1062	SE72	SE117A	SE117B	SE120A
borehole	GO	GO	GO	GO	GO	GO	GO	GO	GO	GO	GO	GO	GO	GO	GO	GO	GO	SE	SE	SE	SE
depth	183	198	441	441	456	513	516	519	522	525	528	564	585	603	741	876	1062	72	117	117	120
elevation	733	718	475	475	460	403	400	397	394	391	388	352	331	313	175	40	-146	604	559	559	556
magma type	Pitanga	Pitanga	Gramado	Gramado?	Gramado	Gramado	Gramado	Gramado	Gramado	Gramado	Gramado	Gramado?	Gramado	Gramado?	Gramado	Gramado?	Gramado	Esmeralda?	Esmeralda	Esmeralda	Esmeralda
SiO2	48.71	49.67	50.63	50.40		59.03						51.05	54.13	52.61		50.65	52.05	51.63	51.23	51.31	51.18
TiO2	3.54	3.46	1.45	1.96		1.42						1.83	1.75	1.82		1.47	1.53	1.82	1.36	1.38	1.38
Al2O3	13.27	13.27	14.29	13.58		13.28						13.73	13.06	13.02		13.93	14.36	13.96	13.62	13.76	13.56
Fe2O3	16.27	15.68	13.00	14.22		10.40						13.66	14.54	15.80		13.86	13.75	15.86	14.19	13.69	14.28
MnO	0.21	0.19	0.19	0.21		0.17						0.20	0.21	0.23		0.21	0.21	0.23	0.21	0.22	0.22
MgO	4.91	4.20	6.75	6.03		3.88						6.10	4.16	4.27		5.84	5.15	4.55	5.64	5.77	5.68
CaO	9.05	7.68	9.69	9.91		6.94						9.85	8.24	8.48		10.31	8.91	8.11	10.05	10.19	10.02
Na2O	2.47	2.86	3.41	2.61		2.84						2.52	2.80	2.73		3.17	2.64	2.58	2.55	2.66	2.60
K2O	1.05	2.47	0.44	0.87		1.82						0.87	0.90	0.83		0.41	1.21	0.97	0.99	0.86	0.93
P2O5	0.51	0.50	0.14	0.22		0.21						0.20	0.22	0.22		0.15	0.20	0.28	0.17	0.16	0.16
LOI	1.37	0.94	0.66	0.08		1.64						0.41	1.26	0.68		1.61	3.65	1.32	0.28	0.2	0.12
Total	100.5	100.5	100.6	101		100.6						100.6	100.7	101.2		101.2	100.7	100.6	100.6	100.7	100.4
*Mg**	41.3	38.4	54.8	49.7		46.5						51.0	40.0	38.6		49.5	46.6	40.1	48.1	49.6	48.1
XRF-O.U.																					
Ni	20	<16	66	84	85	47	40	75	74	81	29	62	27	34	75	47	44	38	38	46	37
Cu	237	230	239	132	238	124	110	215	213	227	93	213	196	198	207	177	142	207	157	172	170
Zn	148	138	103	94	106	94	85	91	93	100	99	101	121	122	103	98	112	134	93	103	106
Ga	25	21	18	19	22	20	17	15	17	21	20	20	22	26	20	18	20	23	23	21	19
Rb	26	85	22	16	22	118	137	19	19	23	257	26	57	27	22	14	47	27	33	24	28
Sr	468	429	337	155	343	225	200	304	306	344	205	310	206	206	319	309	285	182	195	194	198
Y	43	44	29	31	30	40	42	27	26	30	56	29	42	42	27	33	36	45	33	32	35
Zr	289	282	151	97	155	220	226	132	131	150	307	145	181	169	143	123	161	213	129	130	134
Nb	28.5	26.5	12.8	6.3	12.8	17.9	18.5	11.3	11.4	13.0	23.5	12.2	13.1	11.4	12.4	8.8	11.7	17.8	10.0	10.3	9.9
XRF-Notts																					
Ni																		17	35	50	40
Cr																		108	153	269	67
Co																		42	43	45	42
V																		415	302	336	332
Zn																		120	72	91	84
Rb																		23	29	22	23
Sr																		171	184	184	178
Y																		45	31	30	33
Zr																		201	127	125	123
Nb																		16	8	9	8
Ba																		351	276	198	284
INAA																					
isotopes																					

sample n°	SE120B	SE192	ES66	ES87	ES105	ES123	ES135	ES150	ES216A	ES216B	ES240	ES273	ES312	ES345	ES537	ES957
borehole	SE	SE	ES	ES	ES	ES	ES	ES	ES	ES	ES	ES	ES	ES	ES	ES
depth	120	192	66	87	105	123	135	150	216	216	240	273	312	345	537	957
elevation	556	484	875	854	836	818	806	791	725	725	701	668	629	596	404	-16
magma type	Esmeralda	Esmeralda	Esmeralda	Palmas	Palmas	Palmas	Palmas	Palmas	Palmas	Palmas	Palmas	Palmas	Palmas	Palmas	Urubici	Gramado
SiO2	51.31	52.61	50.46	67.61	67.80	68.33		67.83	67.80	69.65		66.99	67.15			
TiO2	1.37	2.00	1.33	1.05	1.06	1.03		1.07	1.08	1.00		1.07	0.98			
Al2O3	13.77	12.84	14.26	12.77	12.83	12.72		12.86	12.90	12.12		13.31	14.02			
Fe2O3	13.78	16.12	13.28	6.39	6.42	6.08		6.36	6.43	6.03		6.56	5.86			
MnO	0.22	0.23	0.22	0.12	0.11	0.09		0.12	0.11	0.10		0.12	0.12			
MgO	5.73	3.69	6.40	1.17	1.10	1.11		1.04	0.81	0.86		1.31	1.83			
CaO	10.18	8.02	10.84	3.18	3.30	3.29		3.19	3.01	2.99		4.12	3.76			
Na2O	2.62	3.19	2.41	3.19	3.41	3.34		3.48	3.26	3.20		3.41	2.69			
K2O	0.85	1.06	0.64	4.22	3.67	3.70		3.75	4.28	3.75		2.78	3.27			
P2O5	0.17	0.24	0.16	0.31	0.32	0.31		0.31	0.32	0.31		0.34	0.31			
LOI	0.22	0.29	0.47	0.52	0.48	0.69		0.48	0.47	0.47		2.56	2.39			
Total	101.2	100.5	101.2	99.9	100.9	100.1		100.6	100.8	100.9		100.5	100.4			
*Mg**	49.2	34.8	52.9	29.9	28.4	29.8		27.6	22.6	24.9		31.7	42.0			
XRF-O.U.																
Ni	51	29	80	10	9	<8	13	<8	<9	<8		<8	<8			
Cu	166	228	139	104	110	86	96	98	96	96		116	54			
Zn	97	132	95	82	76	76	67	72	77	68		92	93			
Ga	20	22	19	19	20	19	17	14	17	18		16	22			
Rb	23	46	24	175	158	166	158	160	170	147		114	75			
Sr	199	206	193	131	147	149	144	148	145	135		175	160			
Y	33	47	30	45	46	47	45	46	47	44		47	46			
Zr	131	190	112	260	265	269	258	269	280	253		278	278			
Nb	9.6	13.5	9.0	20.1	20.9	21.3	20.7	21.4	22.5	20.2		21.9	23.3			
XRF-Notts																
Ni	42	22	74								<2		3	54	41	
Cr	71	38	394								48		3	70	211	
Co	43	45	n/a								n/a		n/a	n/a	n/a	
V	328	445	332								75		79	349	267	
Zn	80	109	n/a								n/a		n/a	n/a	n/a	
Rb	21	42	21								155		181	43	40	
Sr	189	189	182								144		135	792	215	
Y	31	44	31								43		39	38	33	
Zr	131	175	110								264		247	321	147	
Nb	9	11	7								22		21	28	11	
Ba	270	315	238								589		609	674	373	
INAA			-													
isotopes			√													

	DUP30 Gramado	DSM19 Gramado	DUP25 Gramado	DSM15 Gramado	DUP27 Gramado	DSM11 Gramado	DUP08 Gramado	DSM14 Gramado	DUP18 Gramado	DSM12 Gramado	DGB08 Gramado	DUP38 Gramado	DGB61 Palmas	DGB59 Palmas	DSM01 Esmeralda	DSM25 Esmeralda	DSM02 Esmeralda	DW17 Esmeralda
Rb	11	45	43	69	59	52	30	52	50	42	42	91	188	162	18	29	22	49
Sr	226	252	272	292	305	243	294	229	223	240	228	217	113	160	166	236	215	204
La	10.6	26.7	25.9	21.5		24.7	20.4	19.6		20.1	15.7	32.2			8.6	14.6	19.7	21.4
Ce	22.9	59.7	52.5	46.2		51.5	43.2	43.0		45.9	32.0	66.3			21.8	35.9	44.6	46.4
Nd	12.8	29.7	27.8	25.0		29.5	25.7	22.9		24.1	19.7	35.9			14.3	21.1	27.0	27.5
Sm	3.18	6.34	6.34	5.42		6.77	5.42	5.05		5.19	4.11	7.94			4.02	5.20	6.02	6.31
Eu	1.11	2.00	1.79	1.63		1.85	1.48	1.53		1.61	1.27	1.92			1.46	1.72	1.96	1.93
Tb	0.63	1.21	1.07	1.06		1.13	0.91	0.97		0.97	0.68	1.29			0.93	0.99	1.21	1.31
Yb	2.09	3.60	3.38	3.64		3.76	2.91	3.04		3.00	2.28	4.03			2.95	3.30	3.91	3.97
Lu	0.35	0.54	0.53	0.58		0.60	0.46	0.47		0.47	0.39	0.65			0.48	0.54	0.62	0.65
Th	2.04	6.02	5.41	5.68		6.12	5.24	5.21		5.52	3.86	9.00			1.81	3.10	4.75	5.32
U	n/d	1.37	1.68	1.62		1.83	1.70	1.47		1.76	0.99	2.23			0.61	0.66	1.52	1.43
Ta	0.50	1.10	1.06	0.90		1.00	0.87	0.85		0.83	0.52	1.12			0.38	0.66	0.78	0.84
Hf	2.15	4.76	4.51	3.97		4.70	3.79	3.70		3.76	2.88	5.84			2.65	3.56	4.45	4.71
Cs	0.77	n/d	1.46	2.65		1.38	0.46	1.67		1.95	0.64	0.93			n/d	n/d	1.34	5.00
Sc	40	38	30	36		37	31	36		37	39	32			42	40	41	41
Co	45	n/d	43	40		44	42	39		n/d	46	42			n/d	n/d	n/d	46
Rb	18	56	38	68		52	30	52		44	47	88			19	32	25	51
Pb-ID	3.39	8.11	7.49	8.72				7.90			5.82	11.90			2.87	4.57	6.73	7.37
Sr 87/86	0.707781	0.708904	0.709071	0.709505	0.709291	0.709552	0.709076	0.710568	0.710720	0.710477	0.711420	0.713754	0.728767	0.723331	0.706620	0.706585	0.708133	0.711462
Nd143/144	0.512415	0.512312	0.512308	0.512298	0.512246	0.512366	0.512349	0.512343	0.512326	0.512364	0.512310	0.512274	0.512174	0.512241	0.512608	0.512600	0.512456	0.512358
Pb 6/4	18.596	18.392	18.730	18.787	18.372	18.808	18.904	18.827	18.579	18.849	18.586	18.810			18.708	18.624	18.644	18.514
Pb 7/4	15.647	15.575	15.652	15.665	15.608	15.658	15.671	15.667	15.641	15.687	15.679	15.680			25.657	15.623	15.652	15.658
Pb 8/4	38.807	38.679	38.870	38.861	38.777	38.794	38.888	38.828	38.876	38.888	38.977	39.075			38.745	38.642	38.764	38.937
@130 Ma																		
Sr 87/86	0.70752	0.70795	0.70823	0.70824	0.70826	0.70841	0.70853	0.70935	0.70952	0.70954	0.71043	0.71151	0.71985	0.71791	0.70604	0.70593	0.70759	0.71018
Nd143/144	0.51230	0.51220	0.51219	0.51219	0.51214	0.51225	0.51224	0.51223	0.51222	0.51225	0.51220	0.51216	0.51207	0.51214	0.51246	0.51247	0.51234	0.51224

	DSM05a Esmeralda	DSM03a Esmeralda	DAB16 Esmeralda	DSM23 Esmeralda	DSM06 Esmeralda	DW23 Esmeralda	DSM20 Esmeralda	ES66 Esmeralda	DGB70 Esmeralda	DUP19 Esmeralda	DUP37 Urubici	DSM30 Urubici	DSM35 Urubici	DSM27 Urubici	DSM34 Urubici	DSM05b Urubici	DSM26 Urubici	DSM07 Urubici
Rb	55	50	17	19	20	3	28	24	18	22	49	36	32	39	30	46	39	48
Sr	244	198	190	173	165	227	166	193	173	168	767	661	694	969	835	706	785	699
La	24.1			8.2	8.4		10.4				37.1	37.2	37.8	38.0	39.2	39.8	39.9	40.7
Ce	53.5			21.0	20.8		25.1				79.4	83.3	80.4	83.2	79.3	87.5	93.1	88.5
Nd	29.8			14.1	14.5		14.9				45.9	46.3	49.3	47.7	43.7	49.0	51.7	50.8
Sm	7.05			3.94	3.97		4.31				10.4	9.81	10.5	10.2	9.26	10.3	10.8	10.2
Eu	2.26			1.36	1.41		1.42				3.21	3.38	3.19	3.43	2.91	3.41	3.56	3.37
Tb	1.34			0.89	0.90		0.91				1.40	1.47	1.44	1.51	1.23	1.47	1.59	1.45
Yb	3.82			2.83	2.92		3.16				2.71	2.77	2.95	2.76	2.33	3.12	2.83	3.11
Lu	0.65			0.47	0.47		0.52				0.42	0.44	0.46	0.41	0.38	0.47	0.44	0.48
Th	5.16			1.73	1.75		2.80				3.62	3.77	4.16	3.86	4.49	5.02	4.47	5.20
U	1.34			0.66	0.71		0.84				1.27	0.98	1.77	0.76	1.04	1.08	1.40	1.37
Ta	0.99			0.38	0.37		0.50				1.68	1.75	1.71	1.78	1.70	1.89	1.90	1.91
Hf	5.22			2.63	2.71		2.97				7.18	7.55	7.08	7.61	6.67	7.30	7.59	7.44
Cs	0.84			n/d	n/d		0.77				1.25	n/d	0.42	1.23	1.24	0.62	n/d	0.62
Sc	38			41	42		41				20	26	34	25	24	27	25	27
Co	44			n/d	n/d		n/d				38	40	46	38	42	40	n/d	41
Rb	59			25	23		24				46	36	32	45	31	48	40	53
Pb-ID	7.71						4.21					5.67	5.58		6.81	7.31		7.35
Sr 87/86	0.708136	0.708113	0.706868	0.706519	0.706611	0.706159	0.707356	0.707390	0.706416	0.706654	0.705631	0.705455	0.705727	0.705200	0.705853	0.705916	0.705381	0.705914
Nd143/144	0.512494	0.512448	0.512617	0.512681	0.512636	0.512662	0.512541	0.512427	0.512631		0.512446	0.512411	0.512388	0.512487	0.512415	0.512456	0.512463	0.512461
Pb 6/4	18.608	18.631	18.693	18.694	18.720	18.730	18.822			18.712	17.519		17.553	17.545	17.702	18.138	17.674	18.137
Pb 7/4	15.637	15.639	15.621	15.648	15.645	15.650	15.659			15.636	15.477		15.488	15.498	15.529	15.574	15.511	15.565
Pb 8/4	38.713	38.698	38.680	38.712	38.721	38.731	38.800			38.697	38.033		38.186	38.091	38.288	38.476	38.255	38.450
@130 Ma																		
Sr 87/86	0.70693	0.70676	0.70639	0.70593	0.70596	0.70609	0.70645	0.70673	0.70586	0.70595	0.70529	0.70516	0.70548	0.70498	0.70566	0.70557	0.70512	0.70555
Nd143/144	0.51237	0.51233	0.51248	0.51250	0.51250	0.51252	0.51239	0.51229	0.51249		0.51233	0.51230	0.51228	0.51238	0.51231	0.51235	0.51236	0.51236

	DSM10 Urubici	DUP35 Urubici	DUP02 Urubici	DSM17b Urubici	DUP32 Urubici	DSM22 Urubici	DRR06 Urubici	DUP42 Urubici	DUP04 Urubici	DSM36 Urubici	DGB09 Urubici	DSM24 Urubici	DSM08 Urubici	DSM04 Urubici	SC-06 Chapecó	RS-67 Chapecó	PR-01 Chapecó	PAR-1 Parana'ma
Rb	60	30	28	32	45	48	42	40	36	44	60	73	111	116	88	100		28
Sr	840	777	1006	885	748	718	691	679	730	620	668	564	609	698	540	488		410
La	42.0	42.5	43.2	48.6	49.0							60.5	81.1	79.6	78.8	83.1		
Ce	92.7	90.4	93.8	110	108							126	180	173	175	175		
Nd	51.6	54.3	50.8	62.4	60.6							63.5	85.6	82.6	92.7	91.7		
Sm	10.6	11.6	11.2	13.0	12.8							12.6	15.9	15.3	19.3	19.6		
Eu	3.53	3.53	3.58	4.02	3.98							4.03	4.65	4.42	5.36	5.34		
Tb	1.44	1.54	1.59	1.74	1.83							1.72	2.00	1.85	2.56	2.49		
Yb	2.76	2.99	3.18	3.12	3.29							3.66	3.92	3.63	5.15	5.32		
Lu	0.42	0.44	0.50	0.49	0.49							0.56	0.56	0.55	0.81	0.84		
Th	4.78	4.25	4.71	5.11	5.20							7.39	12.8	12.1	8.52	9.29		
U	1.13	1.34	1.15	1.86	1.36							2.01	2.71	3.00	1.80	1.97		
Ta	2.03	1.92	1.98	2.35	2.30							2.53	3.20	3.32	3.12	3.22		
Hf	7.78	7.97	8.12	9.30	8.70							9.32	12.3	12.4	13.7	14.1		
Cs	1.66	0.33	0.51	1.13	0.48							0.60	1.83	1.80	1.26	1.29		
Sc	25	29	27	25	33							20	14	14	13	13		
Co	40	40	47	40	48							28	16	17	6	5		
Rb	60	33	31	31	44							77	117	119	85	99		
Pb-ID	6.49										7.51	9.48		14.2	10.3	10.5		
Sr 87/86	0.705576	0.705253	0.705421	0.705137	0.705183	0.705164	0.705287	0.705700	0.705849	0.706257	0.706049	0.706422	0.707445	0.707411	0.706447	0.706708	0.706798	0.706058
Nd143/144	0.512460	0.512415	0.512457	0.512490	0.512460	0.512526	0.512516	0.512452	0.512417	0.512293		0.512336	0.512365	0.512368				
Pb 6/4	17.967	17.464	17.604	17.749	17.776		17.728	17.545	17.733		17.591	18.045	18.208	18.259	18.150	18.171	18.228	17.979
Pb 7/4	15.563	15.458	15.495	15.506	15.506		15.502	15.472	15.522		15.499	15.550	15.572	15.591	15.539	15.545	15.577	15.525
Pb 8/4	38.412	38.026	38.163	38.171	38.250		38.164	38.077	38.276		38.179	38.413	38.580	38.657	38.433	38.483	38.606	38.404
@130 Ma																		
Sr 87/86	0.70519	0.70505	0.70527	0.70494	0.70486	0.70481	0.70496	0.70539	0.70559	0.70588	0.70557	0.70573	0.70656	0.70644	0.70562	0.70590	0.70569	0.70569
Nd143/144	0.51235	0.51231	0.51234	0.51238	0.51235	0.51242	0.51241	0.51235	0.51231	0.51219		0.51223	0.51227	0.51227				

	PAR-2 Parana'ma	PAR-3 Parana'ma	PAR-4 Parana'ma	PAR-5 Parana'ma	PAR-6 Parana'ma	PAR-7 Parana'ma	PAR-8 Urubici?	PAR-9 Parana'ma	CB234 Parana'ma	CB276 Parana'ma	CB648 Parana'ma	CB747 Parana'ma	CB846 Pitanga	CB1002 Parana'ma	CB1110 Pitanga	CB1218A Pitanga	CB1362 Pitanga	CB1776 Pitanga
Rb	28	35	25	24	26	24	41	25	17	35	21	8	29	42	31	28	29	48
Sr	516	413	380	384	404	427	913	489	364	204	306	175	392	403	469	497	521	635
La									21.1	26.3	19.9	17.4	29.1	34.5	33.4		29.4	37.3
Ce									50.0	61.8	46.6	40.1	62.2	73.9	76.3		71.0	90.2
Nd									29.6	35.6	26.2	24.0	34.2	43.0	48.0		43.2	46.4
Sm									6.54	8.25	5.59	5.19	7.12	9.44	n/d		n/d	n/d
Eu									2.24	2.45	1.98	1.71	2.52	2.95	2.94		2.82	3.56
Tb									1.29	1.56	1.13	0.93	1.28	1.51	1.34		1.29	1.56
Yb									3.98	4.94	3.56	2.70	3.65	4.15	3.53		3.36	2.90
Lu									0.66	0.84	0.58	0.46	0.58	0.72	0.59		0.48	0.39
Th									2.60	3.33	2.59	2.27	3.31	4.31	3.67		3.42	4.25
U									0.53	n/d	0.67	1.71	1.16	1.47	1.00		n/d	n/d
Ta									1.10	1.48	0.97	0.88	1.49	1.57	1.58		1.65	2.03
Hf									5.30	6.29	4.60	3.65	5.39	5.83	7.13		6.34	7.78
Cs																		
Sc																		
Co																		
Rb																		
Pb-ID																		
Sr 87/86	0.705912	0.706381	0.706157	0.706180	0.706273	0.706520	0.705973	0.707110	0.706156	0.706448	0.706075		0.706162		0.705803	0.705837	0.705793	0.706002
Nd143/144																		
Pb 6/4	17.807	18.011			18.058				17.842	17.908	17.829		17.942		17.791	17.703	17.687	17.814
Pb 7/4	15.503	15.533			15.562				15.526	15.517	15.535		15.550		15.513	15.516	15.514	15.541
Pb 8/4	38.271	38.445			38.519				38.300	38.381	38.101		38.269		38.186	38.023	37.928	38.081
@130 Ma																		
Sr 87/86	0.70562	0.70593	0.70581	0.70585	0.70593	0.70622	0.70573	0.70684	0.70591	0.70553	0.70571		0.70577		0.70545	0.70554	0.70550	0.70560
Nd143/144																		

	CB1902 Pitanga	AN306 Parana'ma	AN516 Parana'ma	AN585 Parana'ma	AN657 Parana'ma	AN783 Parana'ma	AN900 Parana'ma	RO57 Parana'ma	RO255 Parana'ma	RO381 Parana'ma	RO759 Pitanga	RO930 Pitanga	CS66 Parana'ma	CS657 Gramado	CS783 Gramado	CS900 Gramado	CS2532 Gramado?
Rb	44	32	27	34	27	20	23	11	9	38	42	28	27	21	36	49	20
Sr	555	278	375	288	299	353	223	292	381	300	531	494	354	182	237	224	447
La	34.1			23.9	21.7	16.4		17.5		21.4	47.8						13.2
Ce	71.7			56.0	50.5	38.2		41.1		52.9	112						26.8
Nd	42.2			30.8	28.3	22.1		23.0		29.4	54.3						17.9
Sm	6.79			6.33	5.86	4.29		4.92		5.97	n/d						n/d
Eu	2.69			2.13	2.05	1.61		1.75		2.04	4.10						1.37
Tb	1.19			1.15	1.16	0.82		0.92		0.99	1.95						0.58
Yb	2.69			3.82	3.78	2.47		3.21		3.19	4.48						1.81
Lu	0.47			0.63	0.62	0.40		0.53		0.53	0.64						0.31
Th	4.34			3.11	2.84	2.09		2.48		6.05	5.14						1.52
U	1.10			1.29	1.62	n/a		0.66		0.67	1.21						n/d
Ta	1.66			1.13	1.04	0.81		0.83		1.01	2.44						0.57
Hf	5.92			5.24	4.90	3.47		3.80		4.44	9.14						3.05
Cs																	0.90
Sc																	36
Co																	50
Rb																	24
Pb-ID																	
Sr 87/86	0.706616	0.706579	0.706860	0.706451	0.706317	0.706161	0.706504	0.705884	0.706257	0.706226		0.706011	0.706408	0.707075	0.708128	0.710206	
Nd143/144																	
Pb 6/4		17.769	17.783	17.646	17.817		17.977	17.538	17.898	17.755	17.613	17.650	17.994				
Pb 7/4		15.504	15.559	15.500	15.542		15.586	15.524	15.595	15.557	15.568	15.537	15.556				
Pb 8/4		38.049	38.162	37.557	37.902		38.127	37.435	38.087	37.877	37.769	37.778	38.306				
@130 Ma																	
Sr 87/86	0.70618	0.70596	0.70647	0.70582	0.70583	0.70586	0.70595	0.70568	0.70613	0.70555		0.70571	0.70600	0.70646	0.70732	0.70904	
Nd143/144																	

Appendix B
Analytical Techniques.

B.1 Sample preparation.

Within the road sections, to ensure that a representative sample of each flow was obtained, at least 1 kg of material was collected; the worst of the weathered surfaces being trimmed whilst in the field. Back at the Open University, the remainder of the weathering was removed using a hydraulic splitter, reducing the sample to matchbox-sized fragments which were then fed into a hardened steel jaw crusher and crushed to approximately 5 mm chips. A split of the crushed basalt of about 100 g was taken by 'cone and quartering' and finely ground to -200 mesh in an agate tema swing mill.

B.2 X-Ray Fluorescence (XRF) techniques.

B.2.1 Sample preparation.

(i) *major elements.*

Major elements were determined by XRF analysis on glass discs prepared at the Open University. The rock powder was dried in an oven at 110 °C overnight. 0.4 g of the sample was thoroughly mixed in a 1:6 ratio with Spectroflux 100B (a 4:1 lithium metaborate-tetraborate mixture; Johnson Matthey chemicals Ltd.). The rock:flux ratio was corrected to allow for flux weight loss on ignition and was carried out for each batch of 16 samples. This mixture was fused in a Pt/5%Au crucible in a muffle furnace for 12-15 mins. Careful mixing of sample and flux before, and during, fusion was necessary to ensure melt homogeneity. The melt was poured onto a heated brass platen and pressed to form a glass disc, which was then allowed to cool slowly. Loss on ignition (L.O.I.) data were

determined by igniting 1-2 g of sample powder in a pre-ignited silica crucible for 20 mins at 1000 °C.

(ii) *Trace elements.*

Trace element analyses were performed on pressed powder pellets. 6-8 g of finely ground rock powder were thoroughly mixed with 6-12 drops of a PVP binding agent (Polyvinylpyrrolidine / methyl cellulose; Moviol) in an agate pestle and mortar. The sample was compressed at 10 ton.in^{-2} into a 3 cm diameter disc using a hydraulic press, and then baked overnight at 110 °C.

B.2.2 Energy-dispersive XRF analysis.

The majority of samples in this study were analysed for both major elements and selected trace elements {Rb, Sr, Y, Zr, Nb, Ni, Cu, Zn, Ga} at the Open University using energy-dispersive x-ray fluorescence (ED-XRF) techniques. The analytical data were obtained on a Link Systems Meca 10-44 ED-XRF spectrometer and analysis system which employed a low-power (max. 49 W) silver side-window X-ray tube operated in pulsed mode. A Si(Li) detector with a 6 μm beryllium entrance window was used, which gave a resolution of 165 eV at 5.9 keV. It was coarsely collimated and viewed ~200 mm^2 of the fluoresced area of the 3 cm diameter samples. The ED-XRF system was computer controlled and could automatically analyse samples in batches of 19 under a vacuum of < 0.5 torr. It was calibrated using a selection of international standards covering a wide compositional range. For major elements, the glass discs were fluoresced at 10 kV, 0.2 mA with no primary beam filter and counted for 500 s twice. For trace elements, the pressed powder pellets were counted twice for 800 s at 45 kV, 0.3 mA with a 127 μm silver primary beam filter and then an additional spectrum obtained at 10 kV, 0.1 mA and without a beam filter was used to provide rough major element data for the matrix correction procedure. Any instrumental drift in peak intensities was monitored by comparison of spectra obtained on a standard sample several times during each run; USGS AGV-1 for major elements, USGS GSP-1 for trace elements. Two international rock standards were included in each sample

Major elements.

	W-2 Abbey (1983)	this study n=6 mean	s.d.	C.V.		QAB-1 this study n=6 mean	s.d.	C.V.
SiO_2	52.81	52.16	0.15	0.29		46.91	0.21	0.45
TiO_2	1.06	1.07	0.01	0.76		1.53	0.01	0.79
Al_2O_3	15.49	15.23	0.03	0.20		15.60	0.14	0.88
$Fe_2O_3(t)$	10.86	10.76	0.04	0.34		12.64	0.08	0.64
MnO	0.17	0.17	0.00	2.43		0.18	0.00	0.00
MgO	6.39	6.37	0.07	1.02		7.00	0.17	2.39
CaO	10.89	10.93	0.04	0.37		10.20	0.06	0.55
Na_2O	2.21	2.32	0.10	4.17		2.55	0.17	6.79
K_2O	0.63	0.62	0.02	3.04		0.41	0.01	2.93
P_2O_5	0.14	0.21	0.02	7.90		0.27	0.01	4.54
	GSP-1 Abbey (1983)	this study n=9 mean	s.d.	C.V.		**QAB-2** this study n=9 mean	s.d.	C.V.
SiO_2	67.32	66.96	0.28	0.41		46.67	0.19	0.41
TiO_2	0.66	0.67	0.01	0.99		1.52	0.02	1.04
Al_2O_3	15.28	15.26	0.16	1.03		15.31	0.16	1.02
$Fe_2O_3(t)$	4.30	4.31	0.02	0.52		12.82	0.11	0.84
MnO	0.04	0.04	0.00	0.00		0.19	0.00	0.00
MgO	0.97	1.03	0.07	6.67		6.81	0.14	2.10
CaO	2.03	2.00	0.01	0.53		10.16	0.07	0.74
Na_2O	2.81	2.96	0.16	5.29		2.47	0.26	10.54
K_2O	5.51	5.50	0.03	0.59		0.42	0.01	2.33
P_2O_5	0.28	0.30	0.02	6.35		0.22	0.02	8.32

Trace elements.

	BHVO-1 Abbey (1983)	this study n=19 mean	s.d.	C.V.	G-2 Abbey (1983)	this study n=13 mean	s.d.	C.V.
Ni	120	118	6.9	5.9	3.5	7	0.6	8.3
Cu	140	139	6.9	5.0	10	11	3.0	27.6
Zn	105	105	3.1	2.9	84	85	3.0	3.6
Ga	21	21	1.7	8.0	23	23	1.2	5.4
Rb	10	11	1.3	11.4	170	168	2.9	1.7
Sr	420	403	5.9	1.5	480	477	5.2	1.1
Y	27	27	1.1	4.0	11	11	0.8	6.7
Zr	180	178	2.3	1.3	300	300	3.8	1.3
Nb	19	18	0.6	3.4	13	12	0.4	3.3

Table B.1 Major and trace element data on standards for ED-XRF analysis at the Open University. The coefficient of variation, C.V.=100 x s.d./mean.

batch to be analysed as unknowns, and the results obtained during this study are given in table B.1 together with the values quoted in Abbey (1983). Further details of the Open University ED-XRF system are given in Potts *et al.*, (1984) which provides additional information on data acquisition and processing, spectral interferences, calibration, precision and detection limits.

B.2.3 Wavelength-dispersive XRF analysis.

The same powder pellets were also analysed for a selection of trace elements {Rb, Sr, Y, Zr, Nb, Ba, V, Ni, Co, Cr, Zn} by wavelength dispersive x-ray fluorescence (WD-XRF) techniques at the University of Nottingham. The WD-XRF analytical data were obtained on a Phillips PW 1400 spectrometer controlled by an Intel 8080A microprocessor, using a rhodium x-ray tube. The choice of collimator setting, type of diffracting crystal and type of detector used, as well as the excitation conditions of the X-ray tube, was varied for the different elements to ensure optimum operating conditions (see table B.2). Mass absorption corrections were made using a Compton scatter technique. Further details of the Nottingham University WD-XRF system can be found in Harvey and Atkins (1982).

element	line	kV	mA	crystal	coll.	det.	CT(peak)	CT(background)
Rb	Kα	75	40	LiF220	F	S	10	8
Sr	Kα	75	40	LiF220	F	S	16	8
Y	Kα	75	40	LiF220	F	S	20	16
Zr	Kβ	75	40	LiF220	F	S	20	20
Nb	Kα	75	40	LiF220	F	S	10	8
Ba	Lα	50	60	LiF220	C	S	20	10
V	Kα	40	70	LiF220	F	F	20	10
Ni	Kα	70	40	LiF200	C	FS	10	4
Co	Kα	60	50	LiF220	F	F	20	20
Cr	Kα	50	60	LiF200	F	F	20	8
Zn	Kα	75	40	LiF220	F	S	20	10

Table B.2 Operating conditions for the WD-XRF system at University of Nottingham. Coll.=collimator (F=fine, C=coarse), Det.= detector (S=scintillation counter, F=gas flow proportional counter). CT(peak)=normal counting time on peak (s). CT(background)=normal counting time on background (s).

Over 150 samples were analysed for trace elements at both Nottingham and the Open University, and several trace elements {Rb, Sr, Y, Zr, Nb, Ni, Zn} were thus determined on both machines. There was a good agreement for these elements between the WD-XRF and ED-XRF techniques, and this is illustrated by the correlation equations given in table B.3.

	Ni	Zn	Rb	Sr	Y	Zr	Nb
gradient - 'm'	0.805	0.921	0.958	0.959	0.946	0.926	1.078
intercept - 'c'	5.377	0.125	-1.721	-1.781	1.000	0.702	-0.931
correlation coefficient - 'r'	0.923	0.941	0.995	0.997	0.975	0.994	0.987

Table B.3 Comparison between ED-XRF (Open University) and WD-XRF (Nottingham University) for selected trace elements. The table gives the coefficients for a linear regression equation through the data and these are related by: $[element]_{Nottingham} = m.[element]_{O.U.} + c.$

Problems with the Open University's ED-XRF machine in 1988 meant that the later batches of major element glass discs were analysed at Southampton by WD-XRF techniques similar to those employed at Nottingham University.

B.3 Instrumental Neutron Activation analysis (INAA).

REE (La, Ce, Nd, Sm, Eu, Tb, Yb, Lu) and several trace element (Th, U, Ta, Hf, Sc, Co) abundances were determined on selected samples by Instrumental Neutron Activation analysis (INAA). Full details of the analytical technique employed at the Open University are described in Potts *et al.*, (1981, 1985).

The rock powders were dried overnight at 105 °C, and a 300 mg aliquot of each sample was weighed into a polyethylene vial which was then heat-sealed by soldering. Batches of eleven individual vials were stacked into an outer polyethylene tube and each batch included two standard powders that were placed halfway along the tube. The standards used were an irradiation calibration standard AC(OURS), Ailsa Craig microgranite, as well as an internal standard WS, Whin Sill dolerite, analysed as an

unknown. The neutron flux was monitored via weighed discs of pure iron foil placed between each capsule in the tube. These were coated with laquer prior to use in order to prevent corrosion during irradiation.

Samples were irradiated in the 270° core tube facility at the University of London Reactor centre, Ascot, in a thermal neutron flux of 5×10^{12} n.cm^{-2}.s^{-1} for 24-30 hours of reactor time. After one week of 'cooling' to allow short-lived isotopes (predominantly ^{24}Na) to decay, samples were counted at the Open University using two detectors simultaneously; a planar low-energy photon spectrometer (LEPS) and a coaxial Ge(Li) detector. Samples were mounted onto an automatic sample-changing wheel for analysis. The counting procedure involved three separate stages carried out over a period of a month.

(i) For the initial set of counts ('short counts') each sample was counted for between 600 and 8000 s.

(ii) Each sample was then recounted for between 6 and 10 hours ('long counts') two to four weeks after irradiation in order to improve precision on the longer-lived isotopes.

(iii) The iron foils were counted on just the coaxial detector for 1000 s each. The measured activity induced in ^{59}Fe gave an estimate of the neutron flux variation over the length of each individual batch and allowed a subsequent flux correction to be made to each sample.

Potts *et al.*, (1985) gives more complete details of the data acquisition and processing procedures, peak fitting and interferences, etc. Table B.4 shows seven analyses of the WS standard obtained during this study, and the observed mean and standard deviation are compared with those quoted in Potts *et al.*, (1985). Sm in WS from the second batch was 6.74 ppm, noticably lower than expected and thought to have been the result of the count times being too short, and so the Sm contents for the samples in this batch were normalised to an Sm content in WS of 7.2 ppm.

	Whin Sill (WS) #1	#2	#3	#4	#5	#6	#7	observed mean	C.V.(%)	expected mean	C.V.(%)
La	25.3	24.2	25.2	25.8	26.9	25.4	25.0	25.4	3.3	25.5	2.6
Ce	58.7	57.6	56.7	57.4	58.4	58.0	57.8	57.8	1.1	57.5	3.1
Nd	33.4	33.2	31.8	35.1	33.0	33.9	34.2	33.5	3.1	32.9	3.5
Sm	7.24	6.74	7.16	7.54	7.22	7.21	7.29	7.20	1.9	7.27	2.1
Eu	2.29	2.26	2.31	2.30	2.29	2.25	2.36	2.29	1.6	2.25	3.9
Tb	1.08	1.05	1.18	1.16	1.16	1.17	1.17	1.14	4.7	1.09	3.9
Yb	2.55	2.53	2.52	2.70	2.61	2.43	2.60	2.56	3.3	2.54	3.1
Lu	0.40	0.40	0.39	0.41	0.41	0.41	0.42	0.41	2.4	0.39	1.7
Th	3.10	3.10	3.08	3.06	3.15	2.96	3.14	3.08	2.0	3.05	4.3
U	0.94	0.81	0.76	0.94	1.15	0.99	1.13	0.96	15.3	0.90	26.5
Ta	1.27	1.30	1.30	1.30	1.32	1.27	1.31	1.30	1.5	1.26	4.7
Hf	4.91	4.99	4.99	5.04	5.06	4.89	4.79	4.95	1.9	4.93	3.0
Rb	36.0	43.6	36.1	39.5	35.8	33.3	33.5	36.8	9.8	35.3	11.0
Cs	1.09	1.00	0.99	0.99	1.03	1.09	1.03	1.03	4.2	1.03	9.5
Co	n/d	47.9	47.8	48.6	49.4	49.1	47.2	48.3	1.8	47.4	3.1
W	53	49	52	56	68	58	84	60	20	-	-
Fe_2O_3	12.71	13.02	12.62	12.83	12.78	13.80	11.98	12.82	4.2	12.62	3.1

Table B.4 INAA determinations for the Whin Sill (WS) standard (this study). Expected values for WS are from Potts *et al.*, (1985). C.V. is the coefficient of variation (=100 x s.d./mean). Because of the low abundance of Sc and Cr in AC(OURS), these elements are calibrated against their concentrations in WS, defined as Sc - 29 ppm and Cr - 75 ppm.

B.4 Mass Spectrometric Techniques.

B.4.1 Chemistry.

(i) *General.*

The laboratory environment at the Open University, where all chemical preparation and analysis were performed, had a small positive pressure generated by an air circulation unit equipped with particle filters. All reagents were of Analar grade but their purity was improved as follows: HCl and HNO_3 were double-distilled using quartz stills and then further purified in sub-boiling teflon stills (TD); HF and HBr were cleaned up by just using the teflon two-bottle stills. A Millipore™ reverse osmosis system was used to supply (RO) water, though for Pb chemistry this was also double-distilled in a teflon still.

All sample digestions and subsequent evaporations were perfomed in teflon beakers (Sr and Nd) or teflon Sevalex™ screw-top bombs (Pb) within laminar-flow 'fume'

cupboards. Evaporations were carried out within a teflon evaporation hood with air circulation under a thermal lamp. The routine for cleaning the teflon beakers was as follows: (i) thorough rinsing with RO H_2O until visibly clean; (ii) add ~ 5 ml 1.5M HNO_3, leave standing overnight; (iii) soak in hot (~80 °C) concentrated HNO_3 for at least 24 hours; (iv) soak in RO H_2O for 24 hours; (v) add ~ 10-15 ml 6M HCl, heat under lamps for ~ 15 mins. After each stage in the cleaning procedure, the beaker was rinsed with RO H_2O.

Before loading samples for the mass spectrometer, filaments had to be made and outgassed. Filament assemblies were first cleaned, boiled in RO H_2O and then dried in a vacuum oven. The filaments were prepared by welding a strip of Ta or Re ribbon across pins mounted in the filament housing, and these were then outgassed, in batches of eight, for 5 mins at 4.5 A in a vacuum of $< 2 \times 10^{-5}$ torr.

(ii) *Sr and Nd chemistry, and loading.*

100-150 mg of rock powder was weighed into a teflon beaker. About 2 ml 15M TD HNO_3 followed by ~ 8 ml 40% TD HF were added and the sample was left to digest overnight, prior to evaporating to dryness. A further 2 ml 15M TD HNO_3 was added and evaporated, followed by the addition of 2 ml 6M TD HCl, checking to ensure complete dissolution before evaporating. The sample was then redissolved in 2 ml 2.5M HCl and centrifuged to remove any residue. 1 ml of this solution was loaded onto a preconditioned cation exchange column containing 10 ml Bio-Rad AG 50 Wx8, 200-400 mesh resin. The sample was washed in with 2 x 1 ml 2.5M HCl and then eluted with 43 ml 2.5M HCl. Sr was then collected with a further 10 ml 2.5M HCl in a clean teflon beaker and evaporated to dryness, ready for loading. Nd (when required) was obtained by further washing with 1 ml RO H_2O and eluting 21 ml 3M HNO_3. An additional 20 ml 3M HNO_3 was then collected and this contained the Nd along with the other MREE and Ba. After evaporating to dryness, the extract was dissolved in 1 ml 0.25M HCl and left standing overnight in a covered beaker. This was then loaded onto a preconditioned ion-exchange reverse chromatatography column which was prepared by mixing 1 g of teflon powder (Voltalef 300LD PL micro) with 100 mg HD-EHP {Di(2-ethylhexyl)orthophosphoric acid}. The

sample was washed in with 2 x 1 ml 0.25M HCl and then eluted with a further 8 ml 0.25M HCl. Nd was then collected with 4 ml 0.25M HCl in a clean teflon beaker and evaporated to dryness, ready for loading.

Sr and Nd were loaded in a filtered loading bay, and laboratory coat and gloves were worn throughout. Sr was dissolved in a drop of TD H_2O and loaded bit-by-bit onto a 'single' Ta filament onto which a drop of H_3PO_4 had been placed. A current of ~0.8-1.0 A was passed through the filament to slowly dry the sample, and then gradually increased (max. ~2.1 A) until the H_3PO_4 fumed off and the filament glowed dull red. Nd was dissolved in a drop of TD H_2O and loaded onto a 'double' Ta filament on which a small 'nick' had been made in order to concentrate the Nd in the centre of the filament. The sample was gently dried out, using a current of ~1.0 A. The total procedure blanks for Sr and Nd analyses during this study were < 5 ng and < 1 ng respectively which are negligible against the sample studied.

(iii) *Pb chemistry, and loading.*

All chemical separations of Pb including sample loading were carried out in a laminar-flow cupboard in a separate low blank laboratory. A laboratory coat, hat and gloves were worn at all times to avoid contamination by the high levels of Pb inherent in todays modern society, as contributed largely by car drivers thoughtlessly persisting in the use of leaded petrol. The cleaning procedure for the screw-top teflon Sevalex™ bombs was similar to that outlined for the teflon beakers except that the RO H_2O wash was in a separate pyrex beaker in the Pb lab. They were finally cleaned by adding ~3 ml 16M TD HNO_3 and standing on a hot plate, with the lids firmly screwed down, for 24 hours. Prior to use, they were rinsed in TD H_2O and dried. A separate dissolution was performed for Pb extractions. About 100-150 mg of sample was digested overnight in 1ml 16M TD HNO_3 and 3 ml TD HF and then evaporated to dryness. 2-3 ml 16M TD HNO_3 was then added and evaporated, and this process was repeated with 2-3 ml 6M HCl. Finally, 1 ml 1M HBr was added and the sample left to stand overnight. If there is any residue, the HBr should efficiently leach any Pb from it.

Analytical techniques

1 ml polypropylene disposable pipette tips with a small teflon frit at the tip were used as separation columns. These were stored in 6M HCl and washed with 0.5 cv (column volume) 16M TD HNO_3, 1 cv RO H_2O, 1 cv 6M HCl, 1 cv RO H_2O, prior to adding 10-15 µl (2-3 drops) of Bio-Rad 1x8 200-400 mesh anion exchange resin. The resin was pre-conditioned by washing with 1 cv 6M HCl, 1 cv TD H_2O, 1 cv 6M HCl, 1 cv TD H_2O and then 0.5 cv 1M HBr. The HBr containing the sample was loaded dropwise onto the resin. The column procedure was changed early in the course of this study because of problems of Pb yield. The original procedure involved washing samples in with 0.5 cv 1M HBr and then eluting with 3 x 1 cv 1M HBr. The Pb was collected in 2-3 ml TD H_2O. Recovery tests showed that significant Pb losses occured in the HBr washes after the second 1 ml wash and also that HCl was much more efficient in stripping Pb off the resin. The new procedure adopted used less reagents but required a second column pass, though not to the detriment of blank levels (see table B.4). The sample was washed in with 0.5 ml 1M HBr followed by another 1 ml (=0.75 cv) 1M HBr wash. The Pb fraction was collected in 1 ml 6M TD HCl. 3-4 drops 16M TD HNO_3 were added to remove any HBr (liberating Br_2) before evaporating to dryness. The sample was then redissolved in 1 ml 1M HBr and the column procedure was repeated. While the sample solution was on the column, the bomb was rinsed in RO H_2O, filled with 6M HCl, sealed and put on the hot plate (~80 °C). Before Pb collection, the acid was thrown away and the bomb rinsed with TD H_2O.

Except for one early minor hiccup, all Pb total procedure blanks (table B.5) were less than 1.5 ng which, with the change in column procedure improved to well below 1 ng.

Aug 1986	1.51 ng	May 1988	0.19 ng
Jan 1987	5.14 ng	June 1988	0.84 ng
Jan 1987	1.40 ng	Sept 1988	0.76 ng
Nov 1987	0.85 ng	Sept 1988	0.85 ng
May 1988	0.49 ng		

Table B.5 Pb total procedure blanks run during this study.

The silica gel method was used for loading Pb, though the exact technique used was modified slightly whilst I served out my sentence in the Pb lab. Initially the technique involved placing a large drop of silica gel onto a 'single' Re filament and using a current of ~0.8-0.9 A to evaporate the gel until it was almost (but not quite) dry. The Pb sample extract, dissolved a small drop of H_3PO_4, was added to this and evaporated down. The current was then increased, driving off white fumes of H_3PO_4, and then turned off as soon as a faint red glow from the filament was detected. During the second half of my incarceration, the procedure was changed to enable loading to be carried out in a single step. A small drop (~1 µl) H_3PO_4 was added, after the second column pass, to the collected 1 ml 6M HCl Pb solution which was then evaporated. The H_3PO_4 did not evaporate, efficiently concentrating the Pb extract, and this was 'picked-up' with 1-2 µl silica gel and loaded onto a Re filament as above.

B.4.2 Isotope measurements.

Isotope Dilution.

All isotope dilution samples (Pb contents and Sr, Nd, Pb procedure blanks) were analysed on a Vacuum Generators Isomass 54E thermal ionisation single-collector mass spectrometer, in batches of six. Samples were run automatically by software developed at the Open University by D.W. Wright and P.W.C. van Calsteren, using a HP 9845T computer. All elements were analysed at a vacuum < 10^{-7} torr and an accelerating potential of 8 kV.

Isotope Ratios.

Sr, Nd and Pb isotopic ratios were all analysed on the newly acquired (Dec 1985) Finnigan MAT261 multi-collector mass spectrometer. My laboratory work coincided with the machine set-up and subsequent development of both hardware and software. Samples run prior to summer 1988 were controlled automatically using Finnigan software on a HP

9836 computer. Since then, in-house software, again developed by D.W. Wright and P.W.C. van Calsteren, was used - a marked improvement.

Appendix C
Miscellany.

C.1 Altimetry.

Altimetry was a vital part of sample collection in an effort to find as accurately as possible the height of all flow contacts and sample localities. This was approached in two ways.

(i) During the first field season in 1985, a 'primitive' altimeter was used in a relative manner either between trigonometric 'spot' heights marked on the road or using assumed heights derived from the topographic maps (see table C.1)

(ii) In 1986 a different method was tried with a new type of altimeter. This involved using four altimeters; two stationary at a base station and two mobile. Results were corrected for latitude, humidity and machine drift, and gave an 'absolute' height once they had been adjusted to a point of known altitude. The agreement between the two methods was reasonably good.

On the sections 'GB' and 'SM', where the recent road improvements had provided numerous spot heights, altitudes are probably accurate to ± 2-3 m. On the other sections where no spot heights were found, relative heights within the sequence are probably within ± 5 m but the whole sequence could be out from the true height by ± 5-10 m. The lavas are subhorizontal with flow contacts generally showing up to 1-2 m of surface relief and this, coupled with the lack of extensive lateral exposure, ruled out determining the dip of the basalt layers by direct field observations. The regional dip of the basalts causes further complications as it is probably only of the order of 0.5° or less and, since several of the road sections extend for about 10 km horizontally, even a dip of 0.5° will affect the altitude of a flow by up to 80 m if it is to be extrapolated back to give a true vertical profile.

Topographic maps

IBGE 1:50,000 sheets

sheet name	sheet number	year issued	sheet name	sheet number	year issued
Urupema	SG-22-Z-C-VI-3	1980	Aguas Brancas	SH-22-Z-C-VI-4	1980
Bom Retiro	SG-22-Z-D-IV-3	1976	Pericó	SH-22-X-A-III-1	1976
Urubici	SH-22-X-A-III-2	1976	Aiurê	SH-22-X-B-I-1	1976
São Joaquim	SH-22-X-A-III-3	1976	Bom Jardim da Serra	SH-22-X-A-III-4	1976
Orleães	SH-22-X-B-I-3	1976	Silveira	SH-22-X-A-VI-1	1976
São Bento Baixo	SH-22-X-A-VI-2	1976	Jacinto Machado	SH-22-X-A-VI-3	1976
Turvo	SH-22-X-A-VI-4	1976			

Geological maps

DNPM 1:1,000,000 sheets

sheet name	sheet number	year issued	sheet name	sheet number	year issued
Curitiba	SG-22	1974	Pôrto Alegre	SH-22	1974
Asunción	SG-21	1974	Uruguaiana	SH-21	1974

DNPM 1:2,500,000 sheets

South-West quadrant 1981
North-West quadrant 1981

Table C.1 Topographic and geological maps used during this study.

C.2 Borehole information.

Borehole	CB	TI	AV	AN	RO
Well identifier	2-CB-1-SP	1-TI-1-SP	1-AV-1-PR	2-AN-1-PR	1-RO-1-PR
Location	Cuiabá Paulista	Tarabai	Agua de Valenca	Altônia	Roncador
State	São Paulo	São Paulo	Paraná	Paraná	Paraná
Latitude	22° 18' 11.9" S	22° 21' 07" S	23° 05' 36.2" S	23° 51' 16" S	24° 36' 33" S
Longitude	52° 02' 21.6" W	51° 40' 28" W	51° 54' 46.5" W	53° 48' 27" W	52° 14' 48" W
Elevation (a.s.l)	396m	393m	517m	410m	748m
Thickness					
Bauru Fm	207m	184m	100m	262m	absent
Serra Geral Fm	1723m	1537m	1664m	1072m	1248m

Borehole	CS	RS	GO	SE	ES
Well identifier	1-CS-2-PR	1-RS-1-PR	1-GO-1-SC	1-SE-1-SC	1-ES-1-RS
Location	Chapeu do Sul	Rio Segredo	Galvão	Seara	Esmeralda
State	Paraná	Paraná	Sta. Catarina	Sta. Catarina	R.Grande do Sul
Latitude	24° 58' 50" S	25° 42' 09.4" S	26° 22' 58" S	27° 08' 39" S	28° 05' 36.3" S
Longitude	51° 56' 35" W	52° 06' 59.8" W	52° 42' 35" W	52° 18' 04" W	51° 09' 13.8" W
Elevation (a.s.l.)	913m	847m	916m	676m	941m
Thickness					
Bauru Fm	absent	absent	absent	absent	absent
Serra Geral Fm	933m	741m	1235m	642m	1000m

Table C.2 Locality details of boreholes studied.

C.3 Partition coefficient data.

Partition coefficient data are given below for selected trace elements between various minerals {olivine, augite, plagioclase, magnetite} and a basaltic liquid, suitable for low-pressure conditions of magmatic evolution. The value given in brackets for Y in augite is suitable for more intermediate compositions.

	olivine	*augite*	*plagioclase*	*magnetite*
Ti	0.02 (i)	0.3 (i)	0.04 (i)	7.5 (i)
Zr	0.01 (i)	0.1 (i)	0.01 (i)	0.1 (i)
Nb	0.01 (i)	0.1 (i)	0.01 (i)	0.4 (i)
Y	0.01 (i)	0.5 (1.5) (i)	0.03 (i)	0.2 (i)
Rb	0.01 (ii)	0.04 (ii)	0.02 (ii)	0.01 (ii)
Ba	0.01 (ii)	0.07 (ii)	0.23 (ii)	0.01 (ii)
Sr	0.01 (ii)	0.14 (ii)	1.8 (ii)	0.01 (ii)
Ni	14.0 (ii)	2.6 (ii)	0.01 (ii)	10.0 (ii)
Cr	2.1 (ii)	8.4 (ii)	0.01 (ii)	>10.0 (ii)
V	0.01 (iii)	2.0 (iii)	0.01 (iii)	5.0 (iii)
Cu	0.36 (iii)	2.0 (iii)	0.01 (iii)	n/a
Zn	0.7 (ii)	0.41 (ii)	0.01 (ii)	12.0 (ii)

Data sources;
(i) Pearce and Norry (1979).
(ii) Henderson (1982).
(iii) Erlank *et al.*, (1984).
N.B. - reference (iii) gives magnetite/liquid K_D for Nb of 2.3.

C.4 REE chondritic normalising values.

REE data are normalised to the chondritic ppm (parts per million) values of Nakamura, (1974).

La	0.328	Eu	0.077
Ce	0.865	Tb	0.052
Nd	0.630	Yb	0.220
Sm	0.203	Lu	0.034

C.5 Primitive mantle normalising values.

Trace element abundance diagrams in this thesis have been normalised to the primitive mantle values (in ppm) taken from Sun and McDonough (1989).

Rb	0.65	Nd	1.413
Ba	7.23	P	92
Th	0.092	Hf	0.32
U	0.022	Zr	11.6
K	230	Sm	0.456
Ta	0.042	Eu	0.172
Nb	0.738	Ti	1300
La	0.732	Tb	0.098
Ce	1.896	Y	4.7
Sr	21.8	Yb	0.498

C.6 Mg number.

Mg number, denoted by Mg# in this thesis, is defined as the atomic ratio 100 x $Mg/(Mg+Fe^{2+})$. The XRF technique is not able to distinguish ferrous from ferric iron, and so the total iron content is expressed as $Fe_2O_3(t)$ in wt% (weight percent). An arbitrary choice of the Fe_2O_3/FeO ratio must be made to determine the Fe^{2+} content, and conventionally this ratio is set at 0.15 which implies that 85% of the total Fe is Fe^{2+}.

Mg# can be calculated from the weight percent oxide values using the formula;

$$Mg\# = \frac{100 \times \left(\frac{MgO}{40.304}\right)}{\left(\frac{MgO}{40.304}\right)+\left(\frac{Fe_2O_3(t)}{93.936}\right)}$$

Appendix D

Magma type classification procedure.

D.1 Background.

The purpose of this short appendix is to provide a more detailed appraisal of the magma type classification scheme proposed in chapter two, and to outline a suggested strategy to follow in trying to assign any unknown flow to one of the defined magma types. The general methodology behind the classification has been discussed more thoroughly in section 2.4.1 and will not be repeated here except for a few comments pertinent to this discussion. Because there is a certain amount of overlap in many elemental abundances and trace element ratios between the various magma types, the magma types can only be resolved through a judicious combination of several geochemical criteria. The expected range in values of selected geochemical variables have been listed in table 2.2 for each of the main recognised magma types. Ideally this table should allow any Paraná lava sample to be classified into one of these magma types, however several important points must be borne in mind before arriving at a final decision.

(i) Although the geochemical criteria given in table 2.2 were deliberately selected only from those elements routinely determined by the XRF method {*i.e.* major elements + Rb, Ba, Sr, Zr, Y, Ni, Cu, Zn}, some magma types can be more clearly distinguished using other trace element or isotope criteria, and these might have been employed during the initial recognition of a group of samples as being distinct from the rest. For example, the initial distinction between the Esmeralda and Gramado magma types was made on the basis of their Ti/Nb ratios, but unfortunately many laboratories do not analyse for Nb. If information on other trace elements or isotopes is available then this can help in resolving borderline cases between two magma types.

(ii) Some of the geochemical criteria are more diagnostic in distinguishing between particular magma types than others, and so their relative importance in the characterisation of individual magma types must be emphasised. For example, Urubici-type samples can be separated from the mélange of other Paraná magma types solely on the basis of Sr and $Fe_2O_3(t)$ content.

D.2 Classification procedure.

The Paraná suite of volcanics is strongly bimodal in terms of SiO_2, and there is a pronounced 'silica-gap' between 61wt% and 64 wt% SiO_2. Piccirillo and Melfi (1988) have used 63 wt% as marking the divide between basalts (*s.l.*) and rhyolites (*s.l.*), and this value will also be adopted here, as the first filter in the classification procedure.

Rhyolite is used here as a general term for any sample with $SiO_2 > 63$ wt%. The rhyolites can be clearly resolved into two dominant groups, the Palmas and Chapecó magma types, purely on the basis of their Sr and Zr contents. Palmas rhyolites have Sr < 170 ppm and Zr < 400 ppm whereas the Chapecó type have Sr > 250 ppm and Zr > 500 ppm. Within each of these magma types there is considerable regional compositional variation, and a more detailed consideration of this might allow a future sub-division into smaller stratigraphically distinct sub-units.

The situation is more complex for the basalts (*s.l.*), not least because there are at least six possible magma types to be considered. The problem comes from the overlap in many criteria between these basaltic magma types. An initial division can be made on TiO_2 content by selecting samples with greater than or less than 2.3 wt% TiO_2. Although it was stated earlier (section 2.4.2 and table 2.1) that low-Ti magmas have less than 2 wt% TiO_2, this is not strictly true as some Esmeralda and Ribeira samples can have up to 2.2 wt% TiO_2; hence the choice of 2.3 wt% as a discriminant. Samples with $TiO_2 > 2.3$ wt% can classify only as either Urubici-, Pitanga- or Paranapanema-type, and those with $TiO_2 < 2.3$ wt% potentially can belong to the Gramado, Esmeralda, Ribeira or Paranapanema magma

type. Note that the Paranapanema magma type must be considered as a possibility for samples of either group.

If the 'high-Ti group' of samples (*i.e.* TiO_2 > 2.3 wt%) is dealt with first, all the Urubici-type flows can be selected by choosing all samples with *both* $Fe_2O_3(t)$ < 14.5 wt% and Sr > 550 ppm. The remainder must therefore belong to either the Pitanga or the Paranapanema magma type. These two magma types can be resolved largely by their differing TiO_2 contents {Paranapanema 1.8 - 3.2 wt% vs. Pitanga 2.9 - 4.0 wt%} although any samples that fall within the overlap in TiO_2 content between the two (*i.e.* with TiO_2 2.9 - 3.2 wt%) require further attention. These samples will either be primitive Pitanga-type samples (*i.e.* high MgO ~5 - 6 wt%) or evolved Paranapanema-type (*i.e.* low MgO ~3 - 4 wt%), and their classification can be confirmed by resorting to some of the other criteria listed in table 2.2. If Zr/Y > 6 or Zr > 250 ppm or Sr > 430 ppm or Ba > 410 ppm then the sample concerned is Pitanga-type; otherwise it is Paranapanema-type.

The distinctions between the magma types available to samples of the 'low-Ti group' (*i.e.* TiO_2 < 2.3 wt%) are less clear cut that those just discussed for the 'high-Ti group'. It is best to further subdivide the samples of this group and treat each sub-group separately. Samples with TiO_2 between 1.8 wt% and 2.3 wt% could belong to either the Paranapanema, Ribeira or Esmeralda magma types, and those with TiO_2 < 1.8 wt% are potentially Gramado-, Esmeralda- or Ribeira-type. Within the latter sub-group, samples of the Gramado magma type are generally quite distinctive, and any with SiO_2 > 53 wt% or with Ti/Zr < 60 will classify as Gramado-type. The Ribeira magma type can be distinguished from the Esmeralda magma type by its higher Ti/Y (> 300 vs. < 300), Sr/Y (> 8 vs. < 7) and Sr content (> 250 vs. < 250). Within the sub-group with the higher TiO_2 contents (*i.e.* 1.8 - 2.3 wt%), the Esmeralda-type samples can be recognised since they have Ti/Y < 300 and Sr/Y < 7. This just leaves the problem of distinguishing the Paranapanema and Ribeira magma types; Paranapanema-type samples have lower Al_2O_3 contents (< 14 wt%) than the Ribeira-type samples (>14 wt%).

The final step in the procedure should be to check all samples against the full list of geochemical variables as a precaution against any anomalous samples that might have slipped through the net.

D.3 Final remarks.

Each group of samples that were used in the initial recognition of a particular magma type were chosen from a relatively restricted area of the lava field. During the subsequent assignment of new analyses to these magma types, some account was taken of their geographical and stratigraphical position, especially in the cases that had rather borderline compositions. Ideally, any future attempts to classify unknown samples should, at least in the first instance, be carried out independently of any positional infomation so that they are not blinkered by any prior prejudices about the geographical distribution of each magma type.

It is worth checking the success rate of the above procedure in correctly classifying the samples given in appendix A if it is assumed that they are of unknown magma type. Some of these samples have not yet been analysed for major elements (the reasons for this would take up a whole appendix) and, while the trace element data by themselves can give a reasonable indication of the likely magma type membership, the major elements (especially Ti, Si and Fe) are required for a more rigorous classification. Of the 274 samples which have both major and trace element analyses, only 13 samples were problematical for the classification procedure. These fell into three distinct groups; (i) the distinctive evolved Urubici-type flow, DSM04/08, which has 60 wt% SiO_2 but only 2.0 wt% TiO_2, (ii) the 'Votuverava-type' flows at the base of the CB borehole which, as mentioned in chapter two, are distinct from the Pitanga magma type in several respects, although one sample would have classified as an Urubici-type flow, (iii) eight 'low-Ti' samples which had borderline characteristics between the Gramado and Esmeralda magma types. Therefore the classification procedure proved to be about 95 % successful for the samples analysed in this thesis.

It is hoped that the classification outlined in this thesis will account for the bulk of Paraná lava flows, and it now needs to be tested on the ~1500 samples in Piccirillo and Melfi (1988). There are numerous reasons why some samples might lie outside the bounds of this scheme. The anomalous characteristics might be a particular feature of that magma, perhaps produced by mixing between magmas of different magma types, or alternatively it may be just a single flow with a unique composition generated by purely local conditions. One important consideration must be the state of alteration of the samples, which from a published geochemical analysis can be inferred from the L.O.I. (loss on ignition) value. The expected effects of weathering have already been discussed at length in earlier chapters (see sections 2.5.2 and 2.7.2) to which the reader is referred. In an ideal situation there should be an initial screening of samples on their L.O.I. value by perhaps eliminating all samples with L.O.I. > 2 wt%. The reluctance to employ such a filter for the Paraná data set unless the alteration is excessively bad (*i.e.* L.O.I. >> 3 wt%) stems from the general state of most of the Paraná lavas; almost 25 % of the now available geochemical analyses have L.O.I. > 2 wt%. Of course, as a final resort it might be concluded that the unknown flow genuinely belongs to a previously unrecognised magma type, especially if several samples have been found with similar compositional characteristics.

There is still some uncertainty about the basin-wide applicability of the magma type definitions, and some geographical variation might exist within each magma type. Because of this, and the fact that the samples initially used to define a magma type might not be representative of its true compositional range, the criteria given in table 2.2 will certainly need to be reviewed in the future in light of any new data.